AMN-2 Second International Conference on Advanced Materials and Nanotechnology

DISTRIBUTION STATEMENT A
Approved for Public Release
Distribution Unlimited

THIS DOCUMENT CONTAINED
BLANK PAGES THAT HAVE
BEEN DELETED

6 - 11 February 2005, Queenstown, New Zealand

www.macdiarmid.ac.nz/amn-2

The MacDiarmid Institute
for Advanced Materials and Nanotechnology

REPORT DOCUMENTATION PAGE

Form Approved
OMB No. 0704-0188

Public reporting burden for this collection of information is estimated to average 1 hour per response, including the time for reviewing instructions, searching existing data sources, gathering and maintaining the data needed, and completing and reviewing this collection of information. Send comments regarding this burden estimate or any other aspect of this collection of information, including suggestions for reducing this burden to Department of Defense, Washington Headquarters Services, Directorate for Information Operations and Reports (0704-0188), 1215 Jefferson Davis Highway, Suite 1204, Arlington, VA 22202-4302. Respondents should be aware that notwithstanding any other provision of law, no person shall be subject to any penalty for failing to comply with a collection of information if it does not display a currently valid OMB control number. **PLEASE DO NOT RETURN YOUR FORM TO THE ABOVE ADDRESS.**

1. REPORT DATE *(DD-MM-YYYY)*	2. REPORT TYPE	3. DATES COVERED *(From - To)*
	FINAL	

4. TITLE AND SUBTITLE
AMN-2: Second International Conference on Advanced Materials And Nanotechnology. Held in Queenstown, New Zealand on 6-11 February 2005. Programme and Abstract Book.

5a. CONTRACT NUMBER

5b. GRANT NUMBER

5c. PROGRAM ELEMENT NUMBER

6. AUTHOR(S)

5d. PROJECT NUMBER
CSP 051022

5e. TASK NUMBER

5f. WORK UNIT NUMBER

7. PERFORMING ORGANIZATION NAME(S) AND ADDRESS(ES)

Conference Secretariat
Centre for Continuing Ed
University of Canterbury
Private Bag 4800
Christchurch, New Zealand

8. PERFORMING ORGANIZATION REPORT NUMBER

9. SPONSORING / MONITORING AGENCY NAME(S) AND ADDRESS(ES)
US AFSOR/AOARD

10. SPONSOR/MONITOR'S ACRONYM(S)

11. SPONSOR/MONITOR'S REPORT NUMBER(S)

12. DISTRIBUTION / AVAILABILITY STATEMENT
A: Public Release

13. SUPPLEMENTARY NOTES Copyright 2004, The MacDiarmid Institute. **US Government purpose rights.** All other rights reserved by the publisher.

14. ABSTRACT
AMN-2, Second International Conference on Advanced Materials and Nanotechnology http://www.elec.canterbury.ac.nz/AMN-2/ , will be held at the Millennium Hotel in Queenstown, New Zealand from 6-11 February 2005. The purpose of the conference is to promote international collaborations in the broad areas of advanced materials and nanotechnology, with a particular emphasis on new and emerging technologies. Technical symposia will include biomolecular assembly, conducting polymers, functional materials, nanoengineered materials and devices, nanolithography, nanoscale optics, nanotube growth and device concepts, novel semiconductor materials, physics of clusters and cluster-based devices, and properties of superconducting materials

15. SUBJECT TERMS

16. SECURITY CLASSIFICATION OF:			17. LIMITATION OF ABSTRACT	18. NUMBER OF PAGES	19a. NAME OF RESPONSIBLE PERSON
a. REPORT	b. ABSTRACT	c. THIS PAGE			19b. TELEPHONE NUMBER *(include area code)*
U	U	U	U		

Contents

20050812 086

AQ F05-08-3397

Welcome

E nga manuhiri tuarangi, tena koutou, tena koutou, tena koutou katoa. E korero ana ahau mo te taha ki Te Komiti Whakahaere o Te AMN-2, Te Huinga-a-Taiao Tuarua mo Nga Hihiri Whatutoto me Te Hangarau Iti Rawa: nau mai, haere mai ki te roto tino ataahua o Wakatipu, Aotearoa New Zealand.

On behalf of the organising committee of AMN-2, Second International Conference on Advanced Materials and Nanotechnology, it is my pleasure to welcome you to beautiful Queenstown, New Zealand.

The AMN conference series is hosted by the MacDiarmid Institute for Advanced Materials and Nanotechnology, a New Zealand National Centre of Research Excellence (CoRE). This Institute is hosted by Victoria University of Wellington, in partnership with the University of Canterbury, Industrial Research Ltd., Massey University, Otago University and the Institute of Geological and Nuclear Sciences. We are very fortunate this year to have many generous sponsors, including the Foundation for Research, Science and Technology, Raith, Industrial Research Ltd., AFOSR/AOARD/ARO, and the Royal Society of New Zealand. Without their financial support this conference would not be possible.

It is a privilege to acknowledge the participation of Nobel laureates Alan MacDiarmid and Klaus von Klitzing, who so willingly agreed to make time in their busy schedules to attend. Their presence raises the international profile of the conference and their presentations are eagerly anticipated.

The conference technical sessions run for five days, with plenary sessions on Monday to Wednesday, and poster and parallel oral sessions on Thursday and Friday. Wednesday afternoon has been kept free for you to catch your breath and enjoy some of the most spectacular scenery that Aotearoa New Zealand has to offer in the Queenstown Lakes region. There are a number of organised excursion options, or you may simply opt to relax by the lakeshore or enjoy a leisurely walk in the botanical gardens.

I would like to take this opportunity to thank the many people who have helped in the planning and organisation of this conference. First and foremost, Richard Blaikie has put in countless hours assembling what has proven to be an impressive technical programme spanning a broad range of topics in materials science and nanotechnology. His efforts have been above and beyond the call of duty, and no programme chair has ever worked harder. Kate McGrath has worked tirelessly (and relentlessly) securing external sponsorship so critical to the success of this conference. Mark Waterland has cheerfully taken on the role of coordinating the two poster sessions, each of which includes a buffet-style breakfast – intended as a gentler way to start what promises to be a busy set of technical sessions. Shaun Hendy took care of many of the publicity issues surrounding this conference, which has been much appreciated. Paul Callaghan and Margaret Brown have been working quietly behind the scenes to finalise arrangements with our distinguished speakers, and organise media releases. I have enjoyed working with them all very much.

All of the above deserve the credit for making AMN-2 what it is, along with the members of the technical programme committee, and my heartfelt gratitude goes to each of them for serving on the committee with such enthusiasm and energy, and for giving so generously of their time. I would also like to acknowledge the hard work of the University of Canterbury Conference Management Office team comprised of Margaret Brown, Merrin McAuley, Angela Armstrong and Claire McConchie. Every conference should be so fortunate.

Finally, thank you, the delegates from throughout New Zealand and around the world, for participating in AMN-2, and making this conference series such a success.

Sincerely,

Steven M. Durbin
General Chair

Organising Committee

Committee Chairman:	Steven M. Durbin	University of Canterbury
Programme Chairman:	Richard Blaikie	University of Canterbury
	Margaret Brown	Victoria University of Wellington
	Paul Callaghan	Victoria University of Wellington
	Shaun Hendy	Industrial Research Ltd
	Kathryn McGrath	Victoria University of Wellington
	Rebecca Munro	University of Canterbury
	Roger Reeves	University of Canterbury
	Mark Waterland	Massey University

Programme Committee Members

New Zealand Committee Members

Programme Chairman:	Richard Blaikie	University of Canterbury
	Steven M. Durbin	University of Canterbury
	Andrew Abell	University of Canterbury
	Maan Alkaisi	University of Canterbury
	Simon Brown	University of Canterbury
	Paul CallaghanAlison	Victoria University of Wellington
	Downard	University of Canterbury
	Pablo Etchegoin	Victoria University of Wellington
	Keith Gordon	University of Otago
	Shaun Hendy	Industrial Research Ltd
	Alan Kaiser	Victoria University of Wellington
	Andreas Markwitz	Geological & Nuclear Sciences
	Kathryn McGrath	Victoria University of Wellington
	Jim Metson	Auckland University
	David Officer	Massey University
	Roger Reeves	University of Canterbury
	John Spencer	Victoria University of Wellington
	Joe Trodahl	Victoria University of Wellington
	Jeff Tallon	Industrial Research Ltd
	Mark Waterland	Massey University

International Committee Members

	Lynn Gladden	Cambridge University
	Chennupati Jagadish	Australian National University
	Michael Kelly	Cambridge University
	Hiroshi Mizuta	Tokyo Institute of Technology
	Ed Samulski	University of North Carolina
	Henry Smith	Massachusetts Institute of Technology
	Mark Warner	Hitachi Cambridge
	David Williams	Hitachi Cambridge

Conference Secretariat

	The Conference Office	University of Canterbury

AMN-2 Sponsors

The organisers wish to thank the following for their contribution to the success of this conference:

Gold Sponsors

Foundation for Research, Science and Technology
Raith

Silver Sponsor

Industrial Research Limited

Bronze Sponsors

AFOSR/AOARD/ARO
Air Force Office of Scientific Research (AFOSR)
Asian Office of Aerospace Research and Development (AOARD)
US Army Asian Research Office (ARO)
Disclaimer: AFOSR/AOARD support is not intended to express or imply endorsement by the U.S. Federal Government.
The Royal Society of New Zealand

Contributing Sponsors

AJ Park
Baldwins
Biolab Ltd
BOC Edwards
Canesis Network Ltd
European Commission
JEOL (Australasia) Pty Ltd
Millennium Hotel Queenstown
Ministry of Research, Science & Technology
Quantum Design, Inc.
Shotover Jet Queenstown
TA Instruments

Satchel Inserts

Advent Research Materials Ltd
Baldwins
Canesis Network Ltd
Coherent Scientific
E-Science, Inc
Group Scientific Pty Ltd
Hoare Research Software
Institute of Physics
JEOL (Australasia) Pty Ltd
k-Space Associates, Inc.
Quantum Design, Inc.
Raith
Scitek Australia Pty Ltd
TA Instruments/Alphatech Systems

Exhibiting Companies

The trade exhibition is from 5.00pm Sunday 6th February until 12noon Wednesday 9th February on the conference floor, level five of the Millennium Hotel.

- Canesis Network Ltd
- Group Scientific Pty Ltd
- Quantum Design, Inc.
- Raith
- TA Instruments/Alphatech Systems

Conference Venue

AMN-2 is being held at the Millennium Hotel in Queenstown, phone 03 441 8888. On Thursday and Friday sessions will also be held at the Copthorne Lakefront Hotel across the road from the Millennium.

Millennium Hotel
Galaxy rooms I, II and III, level 5
Meeting room V, level 2
Meeting room for email facilities is on level 2

Copthorne Lakefront Hotel
Copthorne rooms I, II and III

Conference Information

Audio Visual for Presenters

Technical assistance is available in each room; please take your presentation to the room in which you are scheduled to present during the break prior to your presentation. If you are scheduled before morning tea please see the technician before sessions commence.

If you have any technical concerns please see the technicians who will be on-site throughout the conference.

Catering

Catering will be held in the hotel restaurant and on the conference floor, level 5 of the Millennium Hotel.

Email

Email facilities are available in a meeting room on level 2 of the Millennium Hotel.

Messages

Please see the conference registration desk in hotel lobby.

Name Badges

Entry to sessions and catering is by name badge only. Please wear your name badge at all times. If your name badge is lost please see the registration desk.

Posters

Poster sessions will be held on the Thursday and Friday mornings from 8.00-10.00am. For those presenting posters, all posters are numbered. Your number may be found on the poster list for Thursday from page 63 and Friday from page 247.

Thursday poster presenters may put their poster up from 6.00-7.00pm on Wednesday or between 7.00-7.45am on Thursday. Your poster must be removed by the conclusion of afternoon tea at 3.30pm on Thursday.

Friday poster presenters may put their poster up between 5.00-6.00pm on Thursday or between 7.00-7.45am on Friday. Your poster must be removed by 5.30pm on Friday.

Breakfast will be provided in the poster area for conference registrants between 8.00-10.00am.

Social Programme

Sunday 6 February

Welcome Function *sponsored by JEOL (Australasia) Pty Ltd*
The registration function will be held on level five of the Millennium Hotel between 6.00-7.30pm. A Maori cultural group will perform during this time. Light refreshments will be served.

Tuesday 8 February

Conference Banquet *sponsored by Industrial Research Limited*
Venue is the Skyline Gondola. Dinner commences at 7.30pm.

Enjoy a wide variety of dishes and stunning panoramic views, complemented by a special performance by one of New Zealand's leading contemporary groups, Goldenhorse. Accommodation for Goldenhorse is *sponsored by Millennium Hotel Queenstown.*

The Conference Banquet is optional and pre-purchased tickets will be found in your registration envelope. Transfers to and from the Millennium are included; please see your ticket for further information. Please wear your name badge to the dinner.

Thursday 10 February

Cocktail Function *sponsored by European Commission*
Further details will be provided during the conference.

Half Day and Full Day Excursions

For those who have pre-purchased tickets they are to be found in your registration envelope. Details about meeting points are on your ticket.

General Information

Banking

ASB Bank	24 Camp St
ANZ Bank	81 Beach St
Bank of New Zealand	11-13 Rees Street
National Bank	7-9 Ballarat Street
Westpac Trust	59 Beach Street

Cell Phones

You are kindly requested to have your cell phone turned off while in any of the conference sessions.

Pharmacy

Queenstown Medical Centre and Pharmacy
Open 7 Days cnr Brecon & Isle Sts 03 441 0590

Taxis

A A Taxis	03 441 8222
Alpine Taxi	03 442 6666
Taxis Queenstown Ltd	03 442 7788
SuperShuttle	03 442 3639

Conference Programme

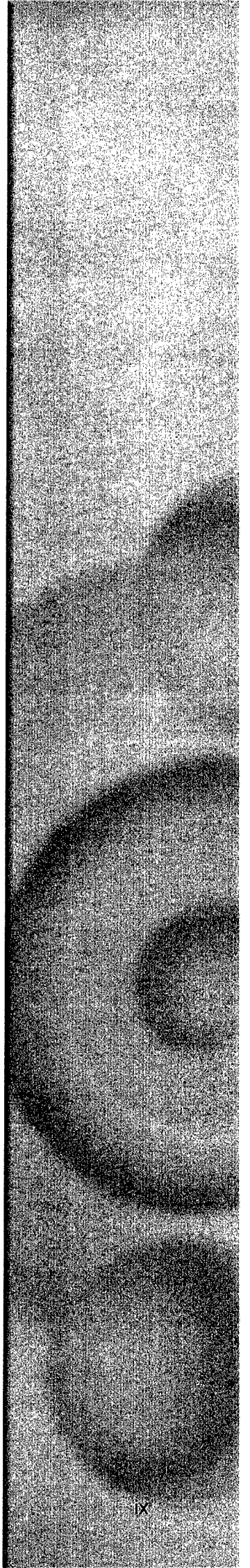

Sunday 6 February

Monday 7 February

Tuesday 8 February

Galaxy Ballroom	**0840-1000**
Session Tu 1	**Keynote Session II** **29**
08:40	Introduction for Prof von Klitzing
08:45	25 years of the quantum Hall effect – a special field of nanoscience
09:20	Introduction for Prof Tallon
09:25	Novel and (by now) not so novel electronic materials
Morning Tea	**1000-1030**
Galaxy Ballroom	**1030-1210**
Session Tu 2	**Plenary Session IV** **33**
10:30	Fluoropolymers for use in next generation photolithography, soft lithography, microfluidics and proton exchange membranes
10:55	The path toward fabricating complex nanoscale assemblies in 2 and 3 dimensions
11:20	Controlling the flow of colour: photonic systems in Lepidoptera
11:45	Structural colour from natural and nanoengineered circular Bragg resonators
Lunch	**1210-1320**
Galaxy Ballroom	**1320-1500**
Session Tu 3	**Plenary Session V** **39**
13:20	NMR of electronic inhomogeneities in cuprate superconductors
13:45	Seeing materials in new light – x-ray absorption spectroscopies in materials characterisation
14:10	Shear banding and non-linear dynamics in complex fluids
14:35	Resonance Raman probe of solvent effects in charge-transfer processes
Afternoon Tea	**1500-1530**
Galaxy Ballroom	**1530-1645**
Session Tu 4	**Plenary Session VI** **45**
Session sponsored by European Commission	
15:30	The European strategy for nanotechnology
15:45	Overview of the European Commission's new thematic call for nanotechnology-related research proposals
Skyline Gondola	
Conference Banquet *sponsored by Industrial Research Limited* ..... **vii**	

Wednesday 9 February

Galaxy Ballroom **0830-1000**

Session We 1 **Keynote Session III** **51**

Session sponsored by Foundation for Research, Science and Technology and The Ministry of Research, Science and Technology

08:30	Introduction for Prof Dowling
08:35	Responsible development of nanotechnologies
09:10	On the nature of our tenuous, metals based civilization
09:35	Putting nanomaterials to work: the design, construction and operation of synthetic nanmotors

Morning Tea **1000-1030**

Galaxy Ballroom **1030-1210**

Session We 2 **Plenary Session VII** **55**

Session sponsored by AJ Park

10:30	Nanotube devices in micro and nanoelectronics
10:55	Determination of chiral indices and electronic transition energies in carbon nanotubes
11:20	Nanoscience in the discovery of porosome: a new cellular structure
11:45	Small scale technologies: directions for Victoria

Lunch **1210-1320**

Half Day Excursions ..... **viii**

Thursday 10 February

Galaxy II and III **0800-1000**

Breakfast will be provided in the poster area for conference registrants between 8.00-10.00am.

Morning Tea **1000-1030**

Galaxy I **1030-1210**

Session Th A1 **Semiconductor Growth and Characterisation I** 131

10:30	Effects of electron-phonon interaction on the electronic band structure of semiconductors
10:55	Indium nitride: towards an understanding of the bandgap
11:10	Zinc oxide for optoelectronic device applications: opportunities and challenges
11:25	Scanning ion probe studies of processing–induced point defect distributions on the surface of gallium nitride
11:40	Effects of growth templates on ZnO grown by RF-PAMBE
11:55	Nucleation and growth kinetics of ZnO layers deposited on 6H-SiC substrates

Meeting Room V **1030-1210**

Session Th B1 **Bio-MEMS and Bio-Cell Imaging** 139

10:30	High speed single particle analysis and sorting bio-chips
10:55	Cell isolation and growth in electric-field defined micro-wells
11:10	The self-assembly of keratin intermediate filaments into macrofibrils: is this process mediated by a mesophase?
11:25	Multiscale conformal structures: a biomimetic chip integrated adhesive
11:40	Analysis of dielectrophoretically trapped biological cells by atomic force microscopy using a biochip platform
11:55	Femtogram mass biosensor using a self-sensing cantilever for resonance frequency shift

Copthorne I **1030-1210**

Session Th C1 **Polymer Nanofibres and Nanotubes** 147

10:30	One-dimensional transport in polymer nanofibers
10:55	A lithographic processing technique for conducting polymers on the micro- (and nano-)metre Scale
11:10	Enhanced electrical properties of a RAFT polymerised MWCNT/polystyrene nanocomposite
11:25	Atomic force spectroscopy as a tool to study the electrical conductivity of polyaniline and derivatives
11:40	Characterisation of cut single-walled carbon nanotubes and their functionalisation for controlled attachment
11:55	Study on the structure behavior of gel spun ultra-high molecular weight polyethylene/carbon nanotube fiber

Galaxy I	**1320-1500**
Session Th A2	**Semiconductor Growth and Characterisation II 173**
13.20	Ultrafast spectroscopy of carrier dynamics in III-N epilayers and heterostructures
13.45	Optical and electrical properties of GaN nanowires synthesized with N_2-quenched pulsed laser ablation
14.00	Optoelectronics of highly disordered gallium nitride
14.15	TEM characterisation of GdN thin films
14.30	Persistent photo-effects in nitride-based electronic devices
14.45	Silicon vacancy annealing and the D_I luminescence in 6H-SiC
Meeting Room V	**1320-1500**
Session Th B2	**Nanoscale Optics 181**
13.20	Plasmonic nanophotonics
13.45	Plasmon resonances of silver colloids aggregates studied by surface enhanced raman spectroscopy
14.00	Towards nonlinear left-handed metamaterials
14.15	A comparison of near-field lithography and planar lens lithography through simulation and experiment.
14.30	Bending light with photonic crystals
14.45	Sculpturing thin films for DUV wavelengths
Copthorne I	**1320-1500**
Session Th C2	**Nanotubes 189**
13.20	Phase behaviour of carbon nanotube dispersions: percolation and nematic states
13.45	Peculiarities in the synthesis of carbon nanotubes from Müller clusters
14.00	Field emission from carbon nanotubes produced on a substrate treated by arc-discharge
14.15	Manipulation and purification of multiwalled carbon nanotubes by dielectrophoresis within a large array
14.30	CNTs for field emission applications: use of nanoimprint lithography and PE CVD techniques
14.45	Synthesis of nano-magnets and nano-tubes using high magnetic fields
Copthorne II	**1320-1500**
Session Th D2	**Materials Characterisation Techniques 197**
13.20	Anisotropy in the optical response of metal surfaces and interfaces
13.45	Stretching single polysaccharide molecules using AFM
14.00	TEM investigation of hydrogen-implanted and annealed single-crystal $SrTiO_3$
14.15	Predicting non-linear optical properties in push-pull molecules using vibrational spectroscopy and density functional theory
14.30	Neutron irradiation effect of poly-$Si_{1-x}Mn_x$ semiconductors grown by MBE
14.45	Atomic force microscopy on adsorbed organics
Copthorne III	**1320-1500**
Session Th E2	**Catalysis, Corrosion and Capillarity 205**
13.20	Electrochemistry in nanometer-scale domains
13.45	Chemistry in really hot water
14.00	Towards electrocatalysis of fuel oxidation using non-noble materials
14.15	Control of microfluidic flows using surfaces with switchable wettability
14.30	Multiscale computer simulation of pit propagation in stainless steels
14.45	TBA
Afternoon Tea	**1500-1530** *sponsored by European Commission*

Friday 11 February

Galaxy II and III **0800-1000**

Poster Session 2 ..... **247**

Breakfast will be provided in the poster area for conference registrants between 8.00-10.00am.

Morning Tea **1000-1045**

Galaxy I **1045-1200**

Session Fr A1 **Nanostructured Semiconductors** **317**

10.45 Dielectric transition of nano-diamond and nano-silicon

11.00 Field emission properties of self-assembled silicon nanostructures formed by electron beam annealing

11.15 InGaN nanostructures: a combined AFM and TEM study

11.30 Investigating the fabrication of SiC nanoboulders *on* Si (100) surface by ^{12}C implantation and electron beam annealing

11.45 Field-effect transistor and field emission display devices using nanoporous inorganic semiconductor C12A7:*e*-

Meeting Room V **1045-1200**

Session Fr B1 **Superconducting and Ferroelectric Ceramics** **323**

10.45 Oxygen loading in second-generation high-temperature superconductor tapes

11.00 The effect of substituents on magnetic order and superconductivity in $RuSr_2R_{2-x}Ce_xCu_2O_{10-a}$ (R=Gd,Eu)

11.15 Scattering effects in single crystal cuprate superconductors

11.30 Epitaxial growth of the ferroelectric $Pb(Zr_{0.2}Ti_{0.8})O3$ thin films grown on $SrRuO_3/SrTiO_3$ for nano-data storage application

11.45 Effects of uniaxial stress on dielectric properties of ferroelectric ceramics

Copthorne I **1045-1200**

Session Fr C1 **Surface and Interface Phenomena** **329**

10.45 Changing the pattern of surface chemistry

11.00 Semiconductor surface optical response upon organic functionalization: first-principles study of a π-conjugated molecular monolayer on Si(001)

11.15 Delving into the nanostructure of self assembled porphyrin monolayers

11.30 STM on self-organised supramolecular assembly

11.45 Effects of metal-molecule interface conformations on the electronic conductance of single molecules

Copthorne II	**1045-1200**
Session Fr D1	**NMR Studies and Techniques 335**
Session sponsored by Biolab Ltd	
10.45	NMR studies on ion diffusion in the lithium salt doped room temperature ionic liquids
11.00	Boomerang: The path to sensitive magnetic resonance on small samples
11.15	A study of water diffusion in lyotropic liquid crystals using a novel two-dimensional NMR technique
11.30	Diffusion measurement in a Couette flow using multi-double PGSE NMR sequences
11.45	Characterisation of the rheology of worm-like micelles using diffusing wave spectroscopy
Copthorne III	**1045-1215**
Session Fr E1	**Quantum-Effect Electronic Devices 341**
10.45	Observation of interdot coupling phenomena in nanocrystalline silicon point-contact structures
11.00	The role of confinement on fractal interference phenomena in nanoscale ballistic devices
11.15	Semiconductor structures for quantum information processing.
11.30	InAlN/GaN HFET layer characterization and transistor performance
11.45	Thin-film field-effect transistor of layered tungsten oxide system
12.00	Selective reduction of intersubband relaxation in doped multi-quantum wells due to a magnetic field applied perpendicularly to the wells layers
Lunch	**1200-1320** *sponsored by BOC Edwards*

Abstracts

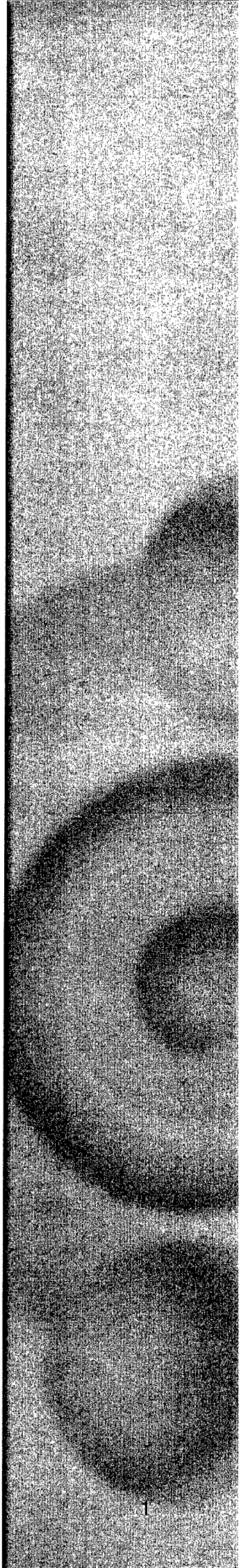

Monday 7 February

Galaxy Ballroom **0840-1000**
Session Mo 1 **Keynote Session I** **5**
Session sponsored by Foundation for Research, Science and Technology

---

Galaxy Ballroom **1030-1210**
Session Mo 2 **Plenary Session I** **9**

Galaxy Ballroom **1320-1500**
Session Mo 3 **Plenary Session II** **15**
Session sponsored by Baldwins

Galaxy Ballroom **1530-1710**
Session Mo 4 **Plenary Session III** **21**
Session sponsored by Quantum Design, Inc.

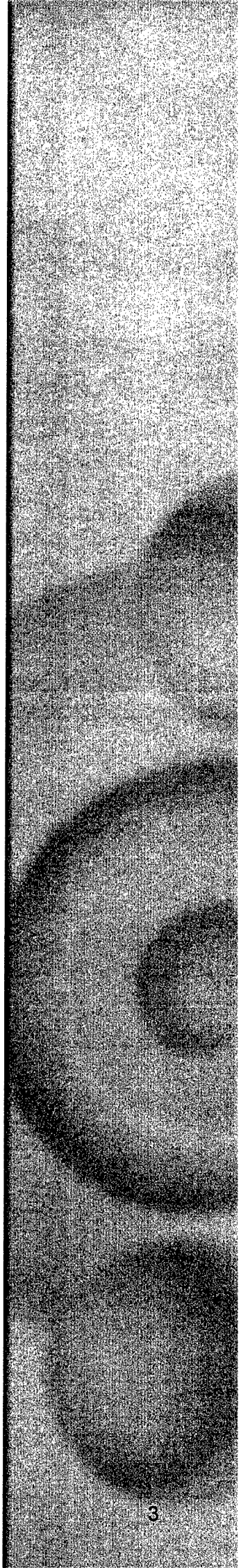

SESSION Mo 1
KEYNOTE SESSION I

Session sponsor: Foundation for Research, Science and Technology

Monday 7 February 2005 **0840–1000**

Galaxy Ballroom

Session Chairs **Steve Durbin, University of Canterbury, NZ**
Richard Blaikie, University of Canterbury, NZ

08:40 **Overview of AMN-2 by the Conference Chair**
S.M. Durbin
University of Canterbury, Christchurch, NZ

08:50 **Overview of the Programme by the Programme Chair**
R.J. Blaikie
University of Canterbury, Christchurch, NZ

09:00 **Overview of the MacDiarmid Institute and introduction for Prof MacDiarmid**
P.T. Callaghan
Victoria University of Wellington, Wellington, NZ

09:20 **Electronic polymers and nanoscience**
Mo 1.1 A.G. MacDiarmid
(Keynote Speaker)
University of Pennsylvania, Philadelphia, USA
University of Texas at Dallas, Richardson, USA
Jilin University, Changchun, China

Electronic Polymers and Nanoscience

Alan G. MacDiarmid*

Department of Chemistry, University of Pennsylvania, Philadelphia, USA, Department of Chemistry, University of Texas at Dallas, Richardson, USA and Jilin University, Changchun, China

A nanomaterial is commonly defined as a solid which has at least one dimension of 100 nm or less. A basic present purpose of this research is to blend the now well-established field of electronic/conducting polymers with the new, emerging field of nanoscience, to produce the hybrid field of "organic nanoelectronics" involving organic fibers, junctions and devices significantly smaller than the diameter of a human hair (~50,000 nm). It is first desirable to find a method to conveniently and reproducibly synthesize nanostructures of electronic polymers. Of particular interest are factors controlling the morphology of polyaniline (nanofibers, nanotubes, nanospheres) and of all electronic (and conventional!) polymers. Our recent studies suggest the pH of the (aqueous) polymerization system may have influence on the resulting nano-morphology and indeed on the actual chemical composition of the polymer of aniline produced.

Acknowledgement: This study was financially supported by the US Office of Naval Research and by the University of Texas at Dallas.

*e-mail address: macdiarm@sas.upenn.edu

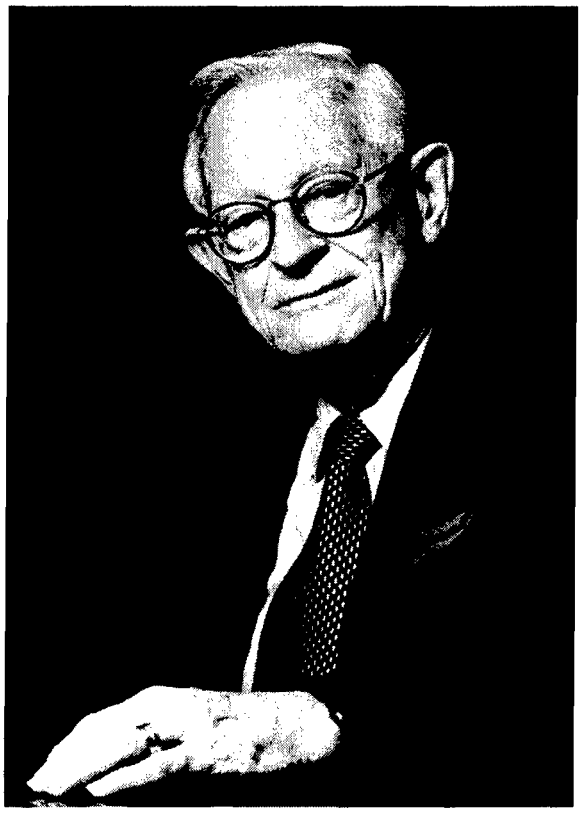

ALAN G. MACDIARMID

Alan MacDiarmid was the chemist responsible in 1977 for the initial synthesis and chemical and electrochemical doping of polyacetylene, $(CH)_x$, the prototype conducting polymer, and the "rediscovery" of polyaniline, now probably the foremost industrial conducting polymer.

In 1973, he began research on $(SN)_x$, an unusual polymeric material with metallic conductivity. His interest in organic conducting polymers began in 1975 when he was introduced to a new form of polyacetylene by Dr. Hideki Shirakawa at the Tokyo Institute of Technology. The ensuing collaboration between MacDiarmid, Shirakawa and Alan Heeger (then at the Department of Physics at the University of Pennsylvania) led to the historic discovery of metallic conductivity in an organic polymer thus introducing and establishing the field of conducting polymers (electronic polymers). In 2000 these three collaborators received the Nobel Prize in Chemistry for this pioneering research.

This initial discovery and ensuing studies permitted MacDiarmid, in collaboration with Shirakawa, to attempt the first chemical doping of $(CH)_x$ and to collaborate on detailed physics studies with Heeger. That an organic polymer could be readily doped to the metallic regime introduced a phenomenon, completely new and unexpected to both the chemistry and physics communities.

His current scientific interests are centered around the technologically important conducting polymers, polyaniline, and poly(ethylenedioxy thiophene) and their use in conducting polymer nanofibers (diameter <100 nm) and inexpensive, disposable plastic and paper electronic circuits. He has recently extended his activities to include carbon nanotubes as possible analogs of conducting polymers.

MacDiarmid's most recent research has created electronic organic fibers with a diameter of ~ 4 nanometers. A nanomaterial is a material consisting of a substance or structure which has at least one dimension less than 100 nm (the diameter of a human hair is approximately 50,000 nm). His objective is to combine the fields of electronic organic polymers and electronic nanofibers to develop a new field of "nanoelectronics".

He is also actively involved in the establishment of a new institute (The Jilin MacDiarmid Institute) of organic nanomaterials at Jilin University, Changchun, China, opened in November 2001 and a new Institute (MacDiarmid Institute of Materials Science and Nanotechnology) at Victoria University of Wellington, New Zealand.

MacDiarmid has recently accepted the James Von Ehr Distinguished Chair in Science & Technology, and also the position of Professor of Chemistry and Physics at the University of Texas at Dallas while maintaining his Blanchard Chair in Chemistry, at a reduced level of input, at the University of Pennsylvania. He has also very recently been appointed as Professor of Chemistry at Jilin University, Changchun, P.R. China.

MacDiarmid was born in New Zealand 77 years ago and after obtaining his higher education at the University of New Zealand, University of Wisconsin and Cambridge University he joined the faculty of the University of Pennsylvania in 1955. He is author/coauthor of over 600 research papers and approximately 25 patents. He is also the recipient of numerous awards and honorary degrees both nationally and internationally.

SESSION Mo 2
PLENARY SESSION I

Monday 7 February 2005 **1030–1210**

Galaxy Ballroom

Session Chairs **David Williams, Hitachi Cambridge Laboratory, UK**
Yung Woo Park, Seoul National University, Korea

10:30 **Electronics and optoelectronics with single carbon nanotubes**
Mo 2.1 P. Avouris
(Invited Talk)
IBM Research Division, T.J. Watson Research Center, Yorktown Heights, USA

10:55 **Electronic conduction in materials with nanoscale or microscale structure**
Mo 2.2 A.B. Kaiser[1], S.K. Goh[1], S.W. Lee[2], D.S. Lee[2], H.Y. Yu[2] and Y.W. Park[2]
(Invited Talk)
[1] *Victoria University of Wellington, Wellington, NZ*
[2] *Seoul National University, Seoul, Korea*

11:20 **Novel silicon-based materials and nanotechnology applications**
Mo 2.3 J.S. Williams, J.E. Bradby, J. Wong-Leung and M.J. Conway
(Invited Talk)
Australian National University, Canberra, Australia

11:45 **Silicon-based quantum computing using buried donor architectures**
Mo 2.4 A.S. Dzurak
(Invited Talk)
University of New South Wales, Sydney, Australia

Electronics and Optoelectronics with Single Carbon Nanotubes

Phaedon Avouris
IBM Research Division, T. J. Watson Research Center, P.O. Box 218, Yorktown Heights, NY 10598, USA.

Carbon nanotubes (CNTs) are 1-dimentional nanostructures with unique properties that recommend them for applications in nanoelectronics and optoelectronics. [1] I will discuss the electronic structure and electrical properties of semiconducting carbon nanotubes and the fabrication and performance of nanotube field-effect transistors (CNTFETs). The results of experiments and theoretical calculations will be used to discuss the transport properties of CNTs, evaluate the switching mechanism of CNTFETs, their scaling behavior and the role of nanotube-metal interactions and of the ambient environment on CNTFET performance. [2] I will then discuss how these findings can be utilized to produce p- and n-type nanotube field-effect transistors (CNTFETs) and logic circuits. In general Schottky barriers (SB) tend to form at the CNT-metal interfaces which affect the properties of CNTFETs. SB-CNTFETs are characterized by large subthreshold swings that are undesirable. Moreover, CNTFETs with very thin gate insulator films become ambipolar. In these devices, depending on the applied gate bias, both electrons and holes can be involved in electrical transport. This is also an undesirable property. I would present new results on how to eliminate these last remaining problems of CNTFETs. This is achieved by using two approaches: (a) electrostatic doping of the contact regions in double-gate CNT devices, and (b) chemical doping through charge-transfer interactions with adsorbed molecules. The resulting unipolar CNTFETs have outstanding operational characteristics exceeding those of the state-of-the art silicon devices.

While ambipolar FET behavior is undesirable in logic applications, it can be ideal for photonic applications. [1] We have used ambipolar CNTFETs to simultaneously inject electrons (e) and holes (h) from the opposite terminals of the FET. When these confined carriers recombine, a fraction of the encounters release the recombination energy in the form of light. Using this scheme we produced an electrically excited and controlled light emitter involving a single nanotube molecule. [3] The radiative recombination nature of the emission was confirmed by measurements of its spectrum, its polarization, and the dependence of its intensity on applied bias. The lineshape of the emission depends on the length of the CNT channel and the magnitude of the current. From it the energy distribution of the hot carriers can be obtained. Unlike conventional p-n diodes the ambipolar CNTFETs do not have dopands and it is not clear where in the nanotube the emission originates. By spatially resolving the light emission as a function of the applied bias we found that the emission originates from a spot that propagates along the length of the CNT as the gate voltage is scanned. This allows us to determine the location of the boundaries of the e- and h-currents, the emission intensity provides information on the magnitude of the minority currents, and the shape of the emitting spot gives their recombination length. Stationary light spots also present that identify defect sites. Finally, we will demonstrate the reverse process of recombination, i.e. the photogeneration of e-h pairs in the single CNT channel with a high yield. The observed resonances in the photoconductivity spectra of individual CNTs correspond to the exciton states of the CNT. Thus, a single device, a CNT-FET, can act, depending on the applied biases, as a switch (transistor), a light emitter or a light detector.

References

1. For recent reviews see: Ph. Avouris , MRS Bulletin 29, 403 (2004): *Proc. of IEEE* **91**, 1772 (2003).
2. J. Appenzeller, J. Knoch, V. Derycke, R. Martel, S. Wind, Ph. Avouris, *Phys. Rev. Lett.* **89**, 126801 (2002); S. Heinze, J. Tersoff, R. Martel. V. Derycke, J. Appenzeller, Ph. Avouris, *Phys. Rev. Lett.* **89**, 106801 (2002); R. Martel, V. Derycke, C. Lavoie, J. Appenzeller, K. Chen, J. Tersoff, Ph. Avouris, *Phys. Rev. Lett.* **87**, 256805 (2001); M. Radosavljevic, S. Heinze, J. Tersoff, Ph. Avouris, *Appl. Phys. Lett.* **83**, 2435 (2003); J. Appenzeller, M. Radosavljevic, J. Knoch and Ph. Avouris, *Phys. Rev. Lett.* (2003).
3. J. A. Misewich, R. Martel, Ph. Avouris, J. C. Tsang, S. Heinze, J. Tersoff, *Science* **300**, 783 (2003); M. Freitag, J. Chen, J. Tersoff, J. Chiang, Q.Fu , J. Liu, Ph. Avouris, Phys. Rev. Lett.93, 076807 (2004).

---

* e-mail: avouris@us.ibm.com

Electronic conduction in materials with nanoscale or microscale structure

Alan B. Kaiser*[1], S.K. Goh[1], S.W. Lee[2], D.S. Lee[2], H.Y. Yu[2] and Y.W. Park[2]
[1] *MacDiarmid Institute for Advanced Materials and Nanotechnology, SCPS, Victoria University of Wellington, P O Box 600, Wellington, NEW ZEALAND*
[2] *School of Physics and Nano Systems Institute - National Core Research Center, Seoul National University, Seoul 151-747, KOREA*

The nanoscale or microscale structure of materials often has a profound effect on their properties, and for example can lead to a similarity in their electronic transport properties. We point out a striking similarity in the measured current-voltage (I-V) characteristics of a variety of nanostructured materials despite the different conduction mechanisms expected in different materials (e.g. see Fig. 1 below). Materials that we investigate include single-wall carbon nanotubes and nanotube networks, vanadium pentoxide nanofibres, conducting polymers (nanofibres, microlines and thin films), and half-metallic materials such as granular Sr_2FeMoO_6 (which are of interest for spintronics as a source of spin-polarized tunnelling currents).

We propose a generic expression for the nonlinear conductance based on our numerical calculations for fluctuation-assisted tunnelling and thermal activation, and show that this expression gives a very good description of the observed nonlinear I-V characteristics in many materials (see examples in Fig. 1). Our calculations (extending the Sheng model) are particularly appropriate for quasi-1D conduction interrupted by small conduction barriers, although it appears that the main features have wider application.

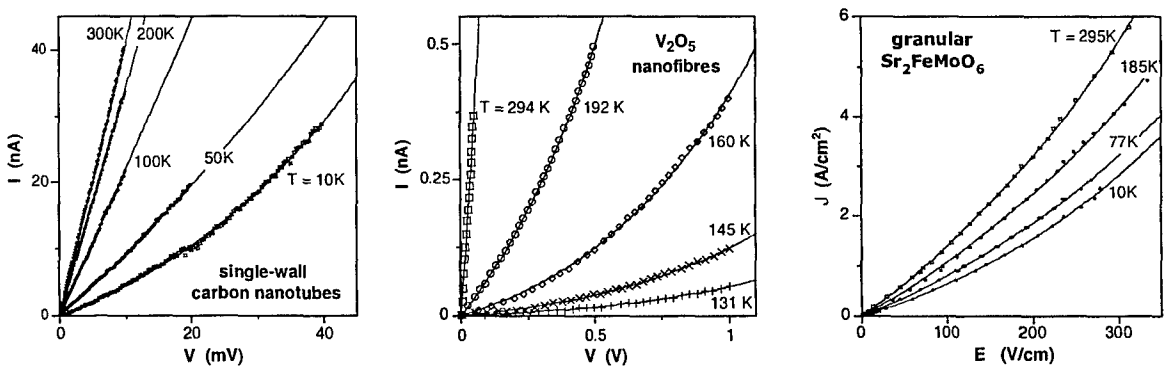

Fig. 1. Current-voltage (I-V) characteristics at different temperatures T of single-wall carbon nanotubes [1], vanadium pentoxide nanofibres [2], and half-metallic granular Sr_2FeMoO_6 [3], with fits to our expression for fluctuation-assisted tunnelling and thermal activation (lines).

In some cases, more exotic behaviour can be seen, for example quantized one-dimensional conductance, Coulomb blockade and Luttinger liquid behaviour in carbon nanotubes. In polyacetylene nanofibres at temperatures below 10 - 30 K, we find highly nonlinear temperature-independent I-V characteristics that we showed are consistent with field-driven tunnelling of the conjugated-bond pattern along a single chain [4]. Such single-chain conduction might be realized along a polyacetylene chain inside a nanotube: McIntosh et al. [5] calculated that this configuration is stable for a (6,6) single-wall carbon nanotube.

We thank Bertina Fisher and Gregory McIntosh for helpful discussions and Ben Chapman and Simon Rogers for research assistance.

References

[1] S. W. Lee, D. S. Lee, H. Y. Yu, E. E. B. Campbell, Y. W. Park, App. Phys. A **78**, 283 (2004).
[2] G. T. Kim, J. Muster, V. Krstic, J. G. Park, Y. W. Park, S. Roth, M. Burghard, Appl. Phys. Lett. **76**, 1875 (2000).
[3] B. Fisher, K. B. Chashka, L. Patlagan, G. M. Reisner, Phys. Rev. B **68**,134420 (2003).
[4] A. B. Kaiser and Y. W. Park, Synth. Met. **135**, 245 (2003).
[5] G. C. McIntosh, D. Tomanek and Y. W. Park, Phys. Rev. B **67**, 125419 (2003).

* Contact author: Alan.Kaiser@vuw.ac.nz

Novel Silicon-based Materials and Nanotechnology Applications

J. S. Williams, J. E. Bradby, J. Wong-Leung and M. J. Conway
Department of Electronic Materials Engineering, Research School of Physical Sciences and Engineering, Australian National University, Canberra, ACT 0200, AUSTRALIA

This presentation will review two novel aspects of silicon-based materials research at the Australian National University. The first involves the ability to form and manipulate nanocavities in silicon by ion bombardment, as well as subsequent experiments that have explored an array of interesting properties that these nanocavities can exhibit. The second area involves nanoindentation of silicon, whereby intriguing phase transformations can occur in extremely small volumes under the indenter and these regions can exhibit interesting properties.

Nanocavities can be formed in silicon by one of two ion beam processes. Under specific irradiation conditions, a vacancy excess can be generated at about half the ion's range, which, upon annealing, can lead to an array of small voids. An easier method is to implant hydrogen or helium ions into silicon to high concentrations. Upon annealing gas bubbles are formed and further annealing expels the gas, leaving cavities. It is possible to 'shrink' cavities by further ion bombardment in which silicon interstitials are injected into them or, alternatively, the region around the cavities is amorphised. In this way it is possible to tailor the size of nanocavities. A particularly interesting property of cavities is their ability to 'getter' or trap fast-diffusing (often metallic) impurities. A range of interesting trapping and precipitation behaviour can occur, whereby some elements preferentially decorate cavity walls and the cavities can also act as preferential precipitation sites for a range of interesting phases. This presentation reviews this behaviour, in particular the ability of cavities to remove extremely small fractions of metal impurities from the surrounding silicon matrix and the interest in using this process in silicon device processing. The ability to form novel nanoparticles in silicon by precipitation at cavities is also reviewed.

Nanoindentation of silicon has generated much interest in recent years as a result of a number of pressure-induced phase transformations that can occur under the indenter. For example, diamond-cubic silicon can transform into a metallic phase at a pressure of 11.5 GPa and, on pressure release, to a number of other possible phases. We have studied this intriguing behaviour in considerable detail using an array of analysis methods, including micro-Raman, transmission electron microscopy, atomic force microscopy and in-situ electrical measurements. We have found that it is possible to control the end phases by controlling the indentation conditions. For example, we are able cycle between crystalline and amorphous phases of silicon by controlling the unloading rate for room temperature indentation. Noting that the different end phases exhibit very different properties, particularly electrical conductivity, nanoindentation opens up prospects for selective 'processing' of silicon. This presentation reviews the science and potential applications of nanoindentation of silicon.

Silicon-based quantum computing using buried donor architectures

Andrew S. Dzurak*

Centre for Quantum Computer Technology, School of Electrical Engineering & Telecommunications, University of New South Wales, Sydney 2052, Australia

Quantum computers have the potential to unveil a new paradigm of information processing via the coherent control of quantum bits (qubits). Solid-state implementations based on superconductors and semiconductors are particularly promising due to the prospect of producing large numbers of qubits via integrated circuit fabrication technology. Of these, the Kane Si:P scheme [1] has generated great interest because of the long coherence times of spins in silicon. This and related Si schemes (such as the Si:P *charge* qubit [2]) require the positioning of single phosphorus atoms in silicon, registered to surface control gates with high precision, together with an ability to read out a single spin or charge. Important strides in construction of atomically-precise P atom arrays in Si have been demonstrated over the past few years using a bottom-up assembly approach [3], while controlled single ion implantation [4] has recently been used to construct Si:P qubit test devices with a *precise number* of P atoms using more conventional top-down nanotechnologies. This presentation will discuss the challenges of fabricating, controlling and measuring such single donor qubits, in particular those constructed via single ion implantation. Experimental results showing the gate-controlled transfer of single electrons between two buried Si:P quantum dots, each containing ~ 600 phosphorus atoms, with *non-invasive* detection using rf single electron transistors (SETs) will be presented [5], together with recent data on devices with only a few (less than ten) phosphorus donors.

References

[1] B.E. Kane, *Nature* **393**, 133 (1998).

[2] L.C.L. Hollenberg, A.S. Dzurak, C. Wellard, A.R. Hamilton, D.J. Reilly, G.J. Milburn and R.G. Clark, *Phys. Rev. B* **69**, 113301 (2004).

[3] J.L. O'Brien, S.R. Schofield, M.Y. Simmons, R.G. Clark, A.S. Dzurak, N.J. Curson, B.E. Kane, N.S. McAlpine, M.E. Hawley and G.W. Brown, *Phys. Rev. B* **64**, R161401 (2001); S.R. Schofield, N.J. Curson, M.Y. Simmons, F.J. Ruess, T. Hallam, L. Oberbeck and R.G. Clark, *Phys. Rev. Lett.* **91**, 136104 (2003).

[4] R.P. McKinnon, F.E. Stanley, E. Gauja, L.D. Macks, M. Mitic, V. Chan, K. Peceros, T.M. Buehler, A.S. Dzurak, R.G. Clark, C. Yang, D.N. Jamieson and S.D. Prawer, *Smart Mat. and Struct.* **11**, 735 (2002).

[5] T.M. Buehler, V. Chan, A.G. Ferguson, A.S. Dzurak, F.E. Stanley, D.J. Reilly, A.R. Hamilton, R.G. Clark, D.N. Jamieson, C. Yang, C.I. Pakes and S. Prawer, in preparation.

* Contact email: a.dzurak@unsw.edu.au

SESSION Mo 3
PLENARY SESSION II

Session Sponsor: Baldwins

Monday 7 February 2005 **1320–1500**

Galaxy Ballroom

Session Chairs **Andy Edgar, Victoria University of Wellington, NZ**
Richard Haverkamp, Massey University, NZ

13:20 **Advances in the science and technology of direct conversion x-ray image detectors for digital radiography**

Mo 3.1 S.O. Kasap[1] and J.A. Rowlands[2]
(Invited Talk)
[1] *University of Saskatchewan, Saskatoon, Canada*
[2] *University of Toronto, Toronto, Canada*

13:45 **Geopolymers: nanoparticulate, nanoporous ceramics fabricated under ambient conditions**

Mo 3.2 W.M. Kriven, M. Gordon and J.L. Bell
(Invited Talk)
University of Illinois at Urbana-Champaign, Urbana, USA

14:10 **Smartening-up carbon: towards chemically well-defined interfaces through attachment of molecular layers**

Mo 3.3 A.J. Downard
(Invited Talk)
University of Canterbury, Christchurch, NZ

14:35 **Atomic force microscopy and organic films - from a chemical probe to a mechanochemical tool in nanochemistry**

Mo 3.4 T. Rayment
(Invited Talk)
University of Cambridge, Cambridge, UK

Advances in the Science and Technology of Direct Conversion X-ray Image Detectors for Digital Radiography

S.O. Kasap[1,*] and J.A. Rowlands[2]
[1] *Department of Electrical Engineering, University of Saskatchewan, Saskatoon, S7N 5A9, Canada*
[2] *Sunnybrook and Women's College Health Sciences Centre, University of Toronto, Toronto, M4N 3M5, Canada*

Although the world has become digital, today's x-ray imaging, by and large, is still mainly based on the antiquated old film technology. In the last ten to fifteen years, however, much progress has been made towards transforming medical imaging into the digital era. In particular, advances in active matrix array flat panels for displays over the last decade have lead to the development of flat panel x-ray image detectors [1]. Flat panel x-ray image detectors have been shown to be highly suitable for replacing the conventional x-ray film/screen cassettes used in medical radiography. They are capable of capturing and displaying the x-ray image digitally immediately after the x-ray exposure, which will permit a convenient clinical transition to digital radiography. There are two general approaches to the flat panel x-ray detector technology: *direct* and *indirect conversions*. The present paper reviews the operating principles for direct conversion detectors, and formulates and reviews the required x-ray photoconductor properties for enabling a successful direct conversion detector. Two important photoconductor requirements are discussed in detail: the x-ray sensitivity and dark current, both of which are topical current research areas in seeking the best photoconductor amongst a number of candidate semiconductors. The science and technology of the state of the art flat panel direct conversion x-ray image detectors are discussed in detail, and the scientific advances behind their development are highlighted. The requirements of medical fluoroscopy (real time imaging at very low exposure levels) is challenging this technology and demanding even higher x-ray sensitivity. Although the technology has advanced enormously, there is still much fundamental work left to be done in understanding the technology and its limitations; we identify some of these fundamental scientific issues.

References

[1] S.O. Kasap and J.A. Rowlands, *Proceedings of the IEEE*, **90,** 591, 2002.

* Contact author: sok533@engr.usask.ca

Geopolymers: Nanoparticulate, Nanoporous Ceramics Fabricated under Ambient Conditions

W. M. Kriven*, M. Gordon and J.L. Bell
Dept. of Materials Science and Engineering, University of Illinois at Urbana-Champaign, Urbana, IL, USA

Geopolymers are a ceramic-like, inorganic polymer made from aluminosilicates crosslinked with alkai metal ions. A nominal composition of 4 SiO_2•Al_2O_3•M_2O can be assigned to such a material, in which M is an alkali metal, such as Na, K or Cs.[1] The material is made by dissolving as much silica as possible in highly caustic hydroxide solution, forming "waterglass" (in the case of sodium metasilicate) or its K or Cs analogues. This clear solution is then mixed with a mineral source of alumino-silicate such as metakaolin containing equimolar SiO_4 and AlO_4 tetrahedral units, and having been calcined at ~700°C for 2 h. Geopolymers have also been made from other aluminosilicate minerals such as feldspars, mullite, andalusite, bentonite, or smectite,. Only a limited amount of water is used for the inorganic reaction, such that the molar ratios are $SiO_2/Al_2O_3 = 4$, $M_2O/ SiO_2 =$ 0.25-0.3, and $H_2O/M_2O = 10$ where M = Na, K, or Cs. Because of the low water content, the metastable, amorphous geopolymer results, rather than crystalline zeolites. Therefore geolymers may be thought of as metastable zeolites made with insufficient water.

In the SEM, the microstructure is nanoparticulate resulting from numerous nuclei precipitated from solution. The XRD is pattern is amorphous, with a maximum at ~22 ° in 2θ. Upon geopolymerization, however, the amorphous hump migrates to ~28° in 2θ. In the TEM it is seen that the microstructure has particulate features and pores which are of the order of 5-10 nm. The EDS spectra taken in TEM indicate an intrinsic composition of $4SiO_2 : Al_2O_3$ plus the alkali metal oxide. Upon further heating to ~1000°C or above, the equilibrium ceramic phases of nephtheline, kalsilite, leucite or pollucite form, depending on the nature of the cross-linking alkali. The fact that these materials can be formed as a room temperature paste, and can incorporate a large variety of filler phases, opens the door to a versatile ceramic processing method, based on the geopolymer behaving as a refractory adhesive or transient sintering aid.

Recently, potassium cross-linked geopolymer made from synthetic metakaolin (SynMK) was prepared and contrasted to a similar geopolymer derived from natural metakaolin (NatMK).[2] X-ray diffraction (XRD) showed that the SynMK was a high purity analog of NatMK that exhibited no crystallinity and had a diffraction "halo" similar to that of the NatMK at 23° 2-theta. The SynMK had a surface area of 166 m^2/g and reacted rapidly with a potassium silicate solution to form a synthetic geopolymer. XRD of the resulting geopolymers, based on NatMK and SynMK, showed that the diffraction "halo" of the starting metakaolins at 23° 2-theta shifted to 28° 2-theta after reaction with alkali-silicate solutions. SEM micrographs of the geopolymer based on SynMK revealed a uniform and dense microstructure with no unreacted aluminosilicate particles present. Bright field TEM of the synthetic geopolymer showed a 2-phase microstructure, similar to naturally based geopolymers described in literature. Fig. 1 below TEM micrograph of geopolymer made from synthetic Al_2O_3•SiO_2 showing characteristic nano microstructure

Acknowledgement: This work was supported by the AFOSR, under STTR Grant F49620-02 C-010.

References

1. W. M. Kriven, J. L. Bell and M. Gordon, *Ceramic Trans.*, American Ceramic Soc. Publ. **153** 227-252 (2003).
2. M. Gordon, J. Bell and W. M. Kriven, Ceramic Transactions, ed. by J. P. Singh, N. P. Bansal and W. M. Kriven, in press

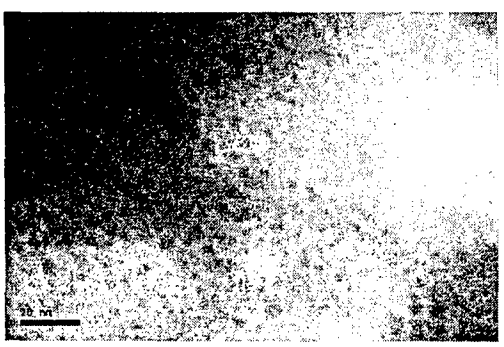

Bar = 20 nm

* Kriven@uiuc.edu

Smartening-up carbon: towards chemically well-defined interfaces through attachment of molecular layers

Alison J. Downard*
MacDiarmid Institute for Advanced Materials and Nanotechnology
Department of Chemistry, University of Canterbury, Christchurch, NEW ZEALAND

Modification of interfaces with synthetic and biological molecules leads to potential applications in sensing, nanofabrication, separation science and molecular diagnostics. To perform such functions at the molecular scale, surfaces must be chemically well-defined. A chemically well-defined surface is one for which the placement, patterning, orientation and packing of chemical functional groups is tightly controlled.

This talk will describe our research aimed at forming chemically well-defined surfaces on carbon substrates using electrochemically-assisted grafting methods. Carbon is a low-cost, versatile material with high mechanical stability and good conductivity. The electrochemically-assisted grafting methods result in very stable surface coatings, attached by strong C-C or C-N covalent bonds.

We have deposited thin organic films (thickness less than 15 nm) on bulk glassy carbon and pyrolysed photoresist films (PPFs). PPF is fabricated in-house and is glassy carbon-like but with near atomic smoothness. Combining electrochemical and AFM techniques affords insights into the electrochemical film formation mechanism and film structure.

Covalent and non-covalent interactions have been exploited to assemble further layers on the modified surfaces. Examples include the covalent attachment of molecular species and nanoparticles, and the assembly of nanoparticles, proteins and protein-nanoparticle bioconjugates via non-covalent interactions.

The possibility of patterning modifiers on the carbon surface has also been explored and nanoscale patterning has been demonstrated using an AFM method.

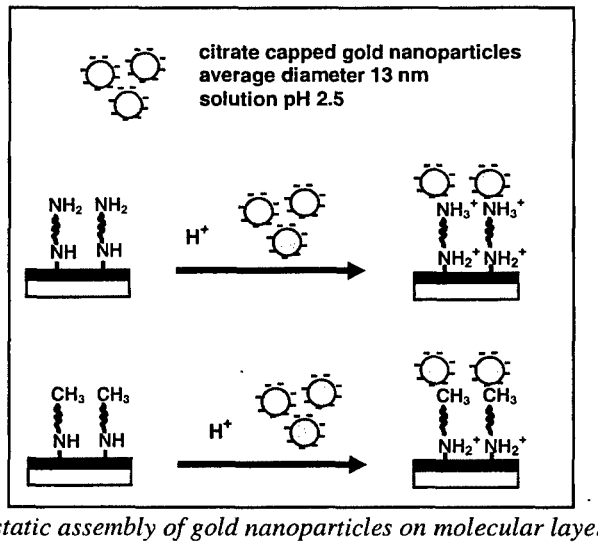

Electrostatic assembly of gold nanoparticles on molecular layers on carbon

* Contact author: alison.downard@canterbury.ac.nz

Atomic Force Microscopy and organic films - from a chemical probe to a mechanochemical tool in nanochemistry.

Dr Trevor Rayment*

Department of Chemistry, Lensfield Road, Cambridge, CB2 1EW, United Kingdom

Since their inception, scanned probes have been used for imaging surfaces and as active tools for nanoscale manipulation. In both cases, the mechanism for imaging and manipulation rests upon the interaction between the local probe and the surface and for more than a decade chemists have sought control of these interactions by deliberate modification of the surface chemistry of the probe. However, in many cases, it is not clear how much 'chemistry' is added by this functionalisation. Perhaps the only situation where solely chemical interactions are observed is for chiral surfaces with a chiral probe [1]. We will describe recent experimental work in this area on nanoscale chirality and illustrate the challenges that face computer simulations of chiral systems [2].

Nanografting, whereby adsorbed molecules are displaced from the surface by a probe and replaced by others is one of the more recent manifestation of use of AFM to prototype nanoscale manipulation. We will describe applications of this approach for the detection of attomolar quantities of DNA in nanoscale features [3], the selective oriented deposition of active enzymes [4] and the growth of 3-dimensional nanoscale features on a surface.

References

1. *Chiral discrimination by chemical force microscopy*, R McKendry,., M. E. Theoclitou, T. Rayment, and C. Abell, *Nature*, **391**, 566-568, (1998)
2. *Chiral discrimination of basic and hydrophobic molecules by chemical force microscopy*, M. Mahapatro, C .Gibson, C .Abell, T .Rayment, *Ultramicroscopy* **97**, 297-301 (2003)
3. *Label-free detection of DNA hybridisation at the nanoscale: a highly sensitive and selective approach using atomic force microscopy*, D.J. Zhou, K .Sinniah, .Abell, T .Rayment, *Angew. Chem. Int. Edit.* **42**, 4934-493, (2003)
4. *Electrostatic Orientation of Enzymes on Surfaces for Ligand Screening Probed by Force Spectroscopy*, X.Z. Wang, D.J. Zhou, K. Sinniah, C. Clarke, L. Birch, T. Rayment, and C. Abell, submitted to *Angew. Chem. Int. Edit.*, 2004

*Contact author tr22@cam.ac.uk

SESSION Mo 4
PLENARY SESSION III

Session Sponsor: Quantum Design, Inc.

Monday 7 February 2005 **1530–1710**

Galaxy Ballroom

Session Chairs **Joe Trodahl, Victoria University of Wellington, NZ**
Manuel Cardona, Max Planck Institute, Germany

15:30 **The magnetic and transport properties of (Ga,Mn)As ferromagnetic semiconductors**
Mo 4.1 K.W. Edmonds, K.Y. Wang, A.D. Giddings, R.P. Campion, T. Jungwirth, C.T. Foxon and B.L. Gallagher
(Invited Talk)
University of Nottingham, Nottingham, UK

15:55 **Spin-dependent electron interferometers**
Mo 4.2 U. Zülicke
(Invited Talk)
Massey University, Palmerston North, NZ

16:20 **Nuclear magnetic resonance measurements on the electron-doped high temperature superconductors**
Mo 4.3 G.V.M. Williams[1], J. Haase[2], M.-S. Park[3], C.U. Jung[3] and S.-I. Lee[3]
(Invited Talk)
[1] *Industrial Research Ltd., Lower Hutt, NZ*
[2] *IFW, Dresden, Germany*
[3] *Pohang University of Science and Technology, Pohang, Korea*

16:45 **Luminescence of rare earth ions in epitaxial fluoride superlattices**
Mo 4.4 R.J. Reeves[1] S.V. Gastev[2], S.J. Choi[1], K.R. Hoffman[3], A.V. Krupin[2], and N.S. Sokolov[2]
(Invited Talk)
[1] *University of Canterbury, Christchurch, NZ*
[2] *Ioffe Institute of Russian Academy of Sciences, St. Petersburg, Russia*
[3] *Whitman College, Walla Walla, USA*

The Magnetic and Transport Properties of (Ga,Mn)As Ferromagnetic Semiconductors

K.W. Edmonds*, K.Y. Wang, A.D. Giddings, R.P. Campion, T. Jungwirth, C.T. Foxon, and B.L. Gallagher
School of Physics and Astronomy, University of Nottingham, Nottingham NG7 2RD, United Kingdom

There is currently much interest in combining the properties of ferromagnetic materials with semiconductors, for new electronics architectures utilising the spin degree of freedom. Observations of ferromagnetism in III-V semiconductors doped with Mn have therefore attracted considerable attention [1]. For the arsenide ferromagnetic semiconductors, it is well-established that the magnetic order is intrinsic to the host semiconductor, and is related to the shallow-acceptor nature of the Mn dopant leading to a spin-polarised valence band. Intensive efforts by several groups across the world have resulted in substantial enhancement of the ferromagnetic transition temperature (up to 173K at the time of writing) as well as an impressive range of prototype devices based on these materials.

This presentation will summarise our recent work on characterising the electronic, magnetic and magnetotransport properties of the (Ga,Mn)As system. A complex temperature-dependent magnetic anisotropy is observed, resulting from the large spin-orbit coupling within the host semiconductor valence bands. The films also show a rich assortment of low-field magnetoresistance effects, which are clearly correlated with the magnetic behaviour, and can be quantitatively understood within a mean field description including quasiparticle scattering [2]. The non-linear dependence of the Curie temperature, hole density, and saturation magnetisation on the Mn concentration are discussed in terms of the occurrence of Mn on both interstitial and substitutional sites. Transport measurements at high temperatures give evidence that annealing-induced changes in these properties are due to diffusion of interstitial Mn to the free surface [3]. Finally, the transport properties of small devices based on (Ga,Mn)As will be presented.

References

[1] H. Ohno *et al.*, Appl. Phys. Lett. **69,** 363 (1996).
[2] T. Jungwirth *et al.*, Appl. Phys. Lett. **83**, 320 (2004); K.Y. Wang *et al.*, J. Appl. Phys. **95**, 6512 (2004).
[3] K.W. Edmonds *et al.*, Phys. Rev. Lett. **92**, 037201 (2004).

* Contact author: kevin.edmonds@nottingham.ac.uk

Spin-dependent electron interferometers

U. Zülicke*
Institute of Fundamental Sciences, Massey University, Palmerston North, NEW ZEALAND

The wave nature of electrons in semiconductor nanostructures results in spatial interference effects similar to those exhibited by coherent light. In complete analogy to the fringes seen in optics experiments, oscillatory modulations of conductances signify electronic interference phenomena in small conductors. These have been observed recently, e.g., in electronic double-slit [1] and Mach-Zehnder [2] interferometers.

The presence of spin-orbit coupling renders interference in spin space and in real space interdependent, making it possible to manipulate the electron's spin state by addressing its orbital degree of freedom. For example, the experimentally demonstrated [3-5] ability to tune the strength of spin-orbit coupling due to structural inversion asymmetry (SIA) [6] forms the basis for the blueprint of a spin-dependent field-effect transistor [7]. Furthermore, designs for spin-dependent electronic ring resonators have been proposed recently [8, 9]. We are motivated by these developments to consider spin-dependent analogs of quantum-optics experiments in nanostructures.

We have studied theoretically the effect of spin splitting on the conductance modulation in electronic interferometers [10]. The interplay between interference and spin precession results in peculiar transport properties that are very interesting from a fundamental-science point of view and are also useful for the design of new spintronics devices. As an example, we discuss the setup of an electronic Mach-Zehnder interferometer in a spin-split two-dimensional electron system. (See the figure below for an illustration.) We have obtained its spin-resolved transport coefficients analytically for the case of quasi-onedimensional interferometer arms. Tunability of the spin splitting by external gate voltages enables switching between complete transmission and reflection, realizing a spin-dependent field-effect switch without magnetic contacts or magnetic fields. In a different configuration, the spin-dependent Mach-Zehnder interferometer acts as a quantum logical gate. In contrast to other recently suggested spin-precession-based quantum gates, this one performs the operation also on incoming electrons that are in spin-split eigenstates and would not precess in a purely onedimensional device.

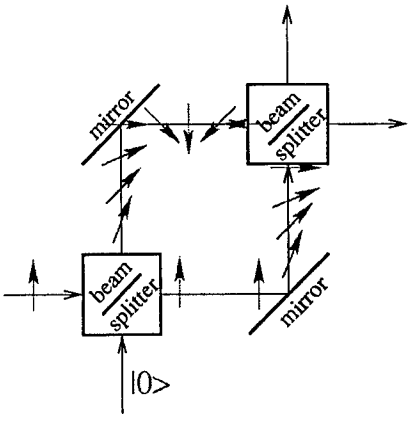

Figure: *Schematic setup of the spin-dependent electronic Mach-Zehnder interferometer. The spin state of electron waves is indicated by short arrows. An electron incoming at the lower-left beam splitter with spin as indicated will give rise to a reflected partial wave whose spin precesses while continuing to propagate in the interferometer. The transmitted partial wave travels the finite distance to the next mirror without precessing but acquires a spin-dependent dynamical phase. An intriguing interplay between spin precession and interference at the second beam splitter results in surprising transport effects that can be manipulated by external gate voltages.*

References

[1] A. Yacoby, M. Heiblum, V. Umansky, H. Shtrikman, and D. Mahalu , Phys. Rev. Lett. **73**, 3149 (1994).
[2] Y. Ji, Y. Chung, D. Sprinzak, M. Heiblum, D. Mahalu, and H. Shtrikman, Nature **422**, 415 (2003).
[3] J. Nitta, T. Akazaki, H. Takayanagi, and T. Enoki, Phys. Rev. Lett. **78**, 1335 (1997).
[4] G. Engels, J. Lange, T. Schäpers, and H. Lüth, Phys. Rev. B **55**, R1958 (1997).
[5] Y. Sato, T. Kita, S. Gozu, and S. Yamada, J. Appl. Phys. **89**, 8017 (2001).
[6] R. Winkler, Phys. Rev. B **62**, 4245 (2000).
[7] S. Datta and B. Das, Appl. Phys. Lett. **56**, 665 (1990).
[8] J. Nitta, F.E. Meijer, and H. Takayanagi, Appl. Phys. Lett. **75**, 695 (1999).
[9] A.A. Kiselev and K.W. Kim, J. Appl. Phys. **94**, 4001 (2003).
[10] U. Zülicke, Appl. Phys. Lett. **85**, in press (2004).

* Contact email address: u.zuelicke@massey.ac.nz

Nuclear Magnetic Resonance Measurements on the Electron-Doped High Temperature Superconductors

G. V. M. Williams[1,*] J. Haase[2], Min-Seok Park[3], C. U. Jung[3], and Sung-Ik Lee[3]
[1] *Industrial Research, P.O. Box 31310, Lower Hutt, NEW ZEALAND*
[2] *IFW, P.O. Box 270116, Dresden, GERMANY*
[3] *National Creative Research Initiative Center for Superconductivity and Department of Physics, Pohang University of Science and Technology, Pohang 790-784, REPUBLIC OF KOREA*

The observation of a similar antiferromagnetic spin fluctuation spectrum in the electron-doped high temperature superconducting cuprates (HTSC's) and the hole-doped HTSC's [1,2] has provided support for spin-fluctuation mediated pairing in the HTSC's. However, there are a number of other models to account for superconductivity in the HTSC's, and the most prominent of these is the "stripes" model [3]. This model is based on calculations that show that dynamic phase separation into antiferromagnetic domains is possible where the conductivity occurs in the domain walls. Support for a dynamic spin and charge density modulation has been provided by Cu NMR measurements on some underdoped and hole-doped HTSC's, where a temperature-dependent wipe-out of the Cu NMR signal is observed [4].

It is not known if there is also a temperature-dependent wipe-out of the Cu NMR signal in the electron-doped HTSC's that could indicate the presence, and slowing down, of dynamic spin and charge density modulations. For this reason we have performed ^{63}Cu NMR measurements on the electron-doped HTSC, $Sr_{0.9}La_{0.1}CuO_2$, and report the results from temperature-dependent measurements of the Cu NMR intensity.

We have also measured the Cu NMR linewidth anisotropy and the frequency-dependence of the Cu spin-lattice relaxation rate in $Sr_{0.9}La_{0.1}CuO_2$ and $Pr_{2-x}Ce_xCuO_4$. We show that the results can be interpreted in terms of an inhomogeneous electronic state that exists for temperatures up to room temperature. The results are discussed in relation to similar measurements on the hole-doped HTSC, $La_{2-x}Sr_xCuO_4$ [5,6].

References

[1] G. V. M. Williams, S. Krämer, R. Dupree, A. Howes, H. J. Trodahl, C. U. Jung, Min-Seok Park and Sung-Ik Lee, Phys. Rev. B **65**, 224520 (2002).
[2] G. V. M. Williams, S. Krämer, R. Dupree, A. Howes, Phys. Rev. B **69**, 134504 (2004).
[3] V. J. Emery, S. A. Kivelsen and H. Q. Lin, Phys Rev. Lett. **64**, 475 (1990).
[4] A. W. Hunt, P. M. Singer, K. R. Thurber and T. Imai, Phys. Rev. Lett. **82**, 4300 (1999).
[5] J. Haase, C. P. Slichter and C. T. Milling, J. Supercond. **15**, 339 (2002).
[6] P. M. Singer, A. W. Hunt and T. Imai, Phys. Rev. Lett. **88**, 47602 (2002).

* Contact author: g.williams@irl.cri.nz

Luminescence of rare earth ions in epitaxial fluoride superlattices

Roger J. Reeves[1], S. V. Gastev[2], S. J. Choi[1], K. R. Hoffman[3], A. V. Krupin[2], N. S. Sokolov[2]

[1] *MacDiarmid Institute for Advanced Materials and Nanotechnology, Department of Physics and Astronomy, University of Canterbury, PB 4800 Christchurch, New Zealand*
[2] *Ioffe Physico-Technical Institute of RAS, 26 Politechnicheskaya, 194021 St. Petersburg, Russia*
[3] *Department of Physics, Whitman College, Walla Walla, WA 99362, USA*

For many decades the precision of molecular-beam-epitaxial growth has generated a wonderous array of semiconductor nanostructures. For example, multiple period superlattices (SL's) in the AlGaAs family underly many devices in optoelectronics as well as providing platforms in fundamental science. Less well studied have been SL's of insulating materials. In addition to their fundamental interest, such structures have possible roles in spintronic applications as templates for magnetic layers or as insulating barriers. Because of their very-wide band gap, insulating SL's do not easily reveal their intrinsic optical properties. However, often they can be doped with optically active impurity ions. The spectroscopy of such ions is sensitive to crystalline enviroment and thus an indirect measurement can be obtained.

We have developed a sensitive combined excitation-emission spectroscopy (CEES) technique that incorporates tunable laser excitation with simultaneous CCD detection of emission to study rare-earth ions in fluoride SL's. In particular to be discussed in this talk are the electronic transitions of Eu^{2+}/Eu^{3+} ions in [CdF_2/CaF_2:Eu (0.1 mol %)] SL's grown on Si(111). Under UV excitation it is revealed that the Eu^{2+} photoluminescence (PL) intensity fades away through a spontaneous tunneling of the electron from $4f^6 5d$ of the Eu^{2+} excited state to the conduction band of the neighbouring CdF_2 layer. The CdF_2 conduction band offset traps the electron and Eu^{3+} ions subsequently appear during this process.

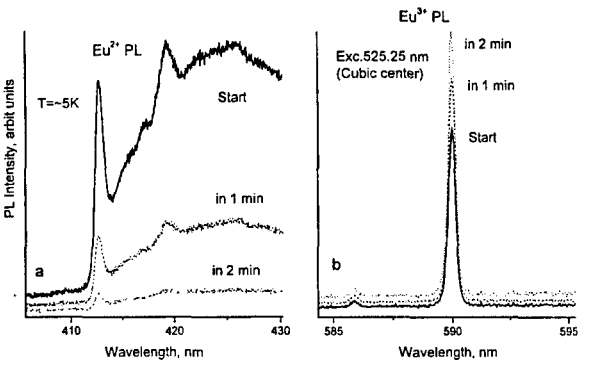

Fig.1 The Eu^{2+} (a) and Eu^{3+} (b) PL behaviour under nitrogen laser (337 nm) irradiation

Temporal behaviour of the Eu^{2+} and Eu^{3+} PL intensities during nitrogen laser radiation of the SL with CaF_2 layer thickness of 20 monolayers (ML) is presented in Fig. 1. One can show that such observations allow calculation of the tunneling mechanism parameters.

The CEES experiment shows that Eu^{3+} ions in cubic crystalline symmetry are dominant in thick SL's while a novel interface Eu^{3+} center is revealed in the thinner SLs. Figure 2 shows the cubic and interface (I-centre) centres in SL's with 5 and 3 ML layer thickness. Analysis of the temperature dependence of the PL for the two centres shows the I-centre results from a Coulomb interaction of the interface Eu^{3+} ions with a free electron in CdF_2 layer of the SL.

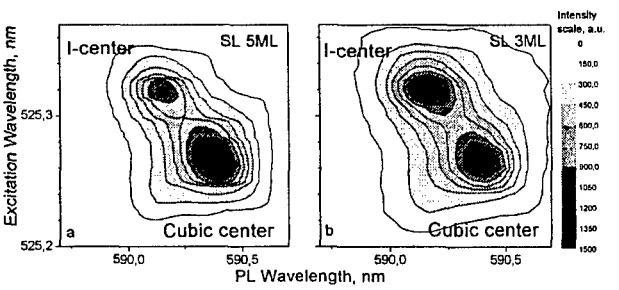

Fig.2 Contour plot of CEES measurements on Eu^{3+} in SLs with the 5 ML (a) and 3 ML (b) layer thickness at T=5K

Tuesday 8 February

SESSION Tu 1
KEYNOTE SESSION II

Tuesday 8 February 2005 **0840–1000**

Galaxy Ballroom

Session Chairs **Simon Brown, University of Canterbury, NZ**
Hiroshi Mizuta, Tokyo Institute of Technology, Japan

08:40 **Introduction for Prof von Klitzing**
H. Mizuta
Tokyo Institute of Technology, Tokyo, Japan

08:45 **25 years of the quantum Hall effect – a special field of nanoscience**
Tu 1.1 K. von Klitzing
(Keynote Speaker)
Max-Planck-Institut für Festkörperforschung, Stuttgart, Germany

09:20 **Introduction for Prof Tallon**
S.A. Brown
University of Canterbury, Christchurch, NZ

09:25 **Novel and (by now) not so novel electronic materials**
Tu 1.2 J. Tallon
(Keynote Speaker)
Industrial Research Ltd., Lower Hutt, NZ

25 Years of the Quantum Hall Effect – a Special Field of Nanoscience

Klaus von Klitzing

Max-Planck-Institut für Festkörperforschung,
Heisenbergstr.1, D-70569 Stuttgart, Germany

The quantum Hall effect (QHE) is well known for his application as a resistance standard based on fundamental constants but the combination of electrical charges with magnetic fields has connections to nearly all fields in physics.

The talk summarizes the most interesting aspects of the QHE since his discovery 25 years ago with the focus on fundamental experiments related to nanoscience like new band structure phenomena in modulated two-dimensional systems (Hofstadter butterfly, magnetic breakthrough), ballistic transport of composite fermions or new interaction phenomena between electrons in a double layer system with separations in the nanometer range.

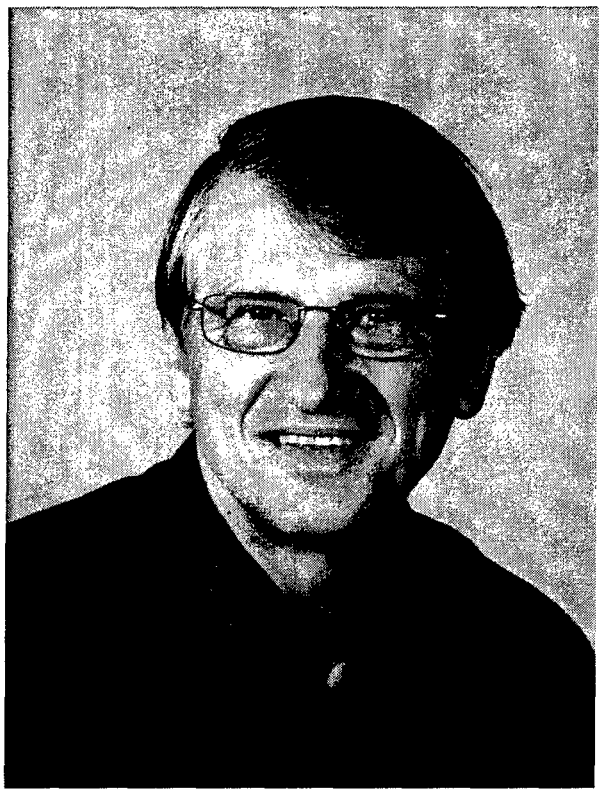

KLAUS VON KLITZING

Klaus von Klitzing was awarded the Nobel Prize for Physics in 1985 for his discovery that under appropriate conditions the resistance offered by an electrical conductor is quantized. Klitzing demonstrated this by using the Hall effect in the two-dimensional electron system formed at the inversion layer of a silicon field-effect device. When the magnetic field is very strong and the temperature very low, the Hall resistance varies only in the discrete jumps first observed by Klitzing and co-workers. The size of those jumps is directly related to the fine-structure constant, which defines the mathematical ratio between the motion of an electron in the innermost orbit around an atomic nucleus to the speed of light.

The significance of Klitzing's discovery, made in 1980, was immediately recognized. His experiments enabled other scientists to study the conducting properties of electronic components with extraordinary precision. His work also aided in determining the precise value of the fine structure constant and in establishing convenient standards for the measurement of electrical resistance. As a result, the fundamental constant h/e^2 is now known as the von Klitzing constant.

At the end of World War II, Klitzing was taken by his parents to live in West Germany. He attended the Technical University of Brunswick, graduating in 1969, and then earned a doctorate in physics at the University of Wurzburg in 1972. In 1980 he became a professor at the Technical University of Munich, and in 1985 he became director of the Max Planck Institute for Solid State Physics in Stuttgart, Germany, his current position.

The main topics of von Klitzing's group currently include the electronic properties of heterostructures, quantum wells, superlattices, and molecular systems, in particular the influence of quantum phenomena on the transport and optical response. Optical and transport measurements in magnetic fields up to 20 Tesla and temperatures down to 20 mK are used to characterize the systems. The quantum Hall effect is studied by analysing the electrical breakdown, the time-resolved transport, the edge channels and the behaviour of composite fermions. Electron-phonon interactions and the phonon transmission through interfaces are investigated with ballistic phonon-techniques. Time-resolved photoconductivity, luminescence, and Raman measurements in magnetic fields are also used for characterising these low dimensional electronic systems. A strong current interest is the preparation of nanostructures either by self organised growth or by lithographic and synthetic routes (nanotubes and other synthetic nanoparticles) and the investigation of coupled two- and zero-dimensional electronic systems (electron drag, Kondo resonance, single electron transistor). The experiments are supported within the group by theoretical investigations of the transport and dynamic response of these low-dimensional electronic systems.

Klitzing is a member of 3 German Academies of Sciences, Academia Europaea, the National Academy of Sciences of the United States of America, the Russian Academy of Sciences and the Russian Metrological Academy. He is a Fellow of The American Physical Society, Ehrenmitglied Deutsche Physikalische Gesellschaft, Ehrenmitglied Nepal German Academic Association, an Honorary Foreign Member of the Korean Academy of Science and Technology, an Honorary Fellow of The Institute of Physics UK, and a foreign member of The Royal Society.

Novel and (by now) not so novel electronic materials

Jeffery Tallon

MacDiarmid Institute for Advanced Materials and Nanotechnology
Industrial Research Ltd and Victoria University
P.O. Box 31310, Lower Hutt, New Zealand.

Industrial Research Ltd has established an internationally prominent research programme in strongly-correlated materials such as superconductors, magnets and hybrid materials. This talk will discuss some of the important materials that have been developed within this programme over the past 18 years including the only high temperature superconductor currently used for magnets, motors and cables. Recent progress includes the development of hybrid materials that combine magnetism and superconductivity or that combine organic and inorganic structures. It is a story of fascinating science, extended patent battles and fitful business development.

Jeff Tallon is joint Professor of Physics at Victoria University and Distinguished Scientist at Industrial Research Ltd. He is an internationally leading researcher in superconductivity who has discovered a number of new superconductors and progressively advanced their understanding over many years. Prof Tallon is a Fellow of the Royal Society of New Zealand and a Visiting Fellow, Trinity College, Cambridge University. He has received a number of awards for his contributions to science including: the Mechaelis Medal for Physics, the 1990 Sesquicentennial Commemoration Medal, a James Cook Fellowship, the Hector Medal and the Rutherford Medal.

SESSION Tu 2
PLENARY SESSION IV

Tuesday 8 February 2005 **1030–1210**

Galaxy Ballroom

Session Chairs **Maan Alkaisi, University of Canterbury, NZ**
Vladimir Shalaev, Purdue University, USA

10:30 **Fluoropolymers for use in next generation photolithography, soft lithography, microfluidics and proton exchange membranes**
Tu 2.1 J.M. DeSimone
(Invited Talk)
University of North Carolina at Chapel Hill; North Carolina State University, Chapel Hill, USA

10:55 **The path toward fabricating complex nanoscale assemblies in 2 and 3 dimensions**
Tu 2.2 H.I. Smith
(Invited Talk)
Massachusetts Institute of Technology, Cambridge, USA

11:20 **Controlling the flow of colour: photonic systems in Lepidoptera**
Tu 2.3 P. Vukusic
(Invited Talk)
University of Exeter, Exeter, UK

11:45 **Structural colour from natural and nanoengineered circular Bragg resonators**
Tu 2.4 I.J. Hodgkinson
(Invited Talk)
University of Otago, Dunedin, NZ

Fluoropolymers for use in Next Generation Photolithography, Soft Lithography, Microfluidics and Proton Exchange Membranes

Joseph M. DeSimone
Department of Chemistry, University of North Carolina at Chapel Hill; Department of Chemical Engineering, North Carolina State University, NC 27599, USA

This presentation will focus on the synthesis of three different classes of fluoropolymers that could impact several advanced technology applications. Two classes of these materials have potential application in lithography, one for next generation photolithography (193 nm, 157 nm, and immersion lithography) and the other for use in soft lithographic techniques. The third class of fluoropolymers is targeted for use as next generation proton exchange membranes in fuel cells.

Photolithography is the current technology used for fabricating microelectronic devices. Responding to the increasing demands for smaller features on microchips, which equates to faster and cheaper integrated circuits, researchers are trying to develop materials that can be used in systems which utilize shorter wavelengths of light in order to create smaller features. We will present the environmentally friendly synthesis of a range of resist materials that were made in supercritical carbon dioxide. The targeted materials have potential application in traditional 193 nm and 157 nm lithography as well as use in immersion 193nm and 157 nm lithography. Moreover, the materials are being chemically and physically characterized with the potential to process (coat and develop) using dry techniques based on CO_2.

We will also present an approach to using fluoropolymers in novel solvent-compatible microfluidic devices based upon the use of perfluoropolyether (PFPE)-based elastomers. Devices made using this approach show remarkable resistance to organic solvents and as such open up entirely new uses for microfluidic devices. Specifically, this work has the potential to expand the field of microfluidics to many novel applications involving micro- and nano-chemistry platforms. In addition, we have shown the utility of PFPE-based materials to be used as molds in soft lithographic imprint techniques. The materials show ideal properties for imprinting and molding techniques to generate isolated objects that are uniform in size and dimensionality down to the sub 100-nm regime.

This presentation will also cover the synthesis of variants of Nafion™. The advancement of fuel cell technology hinges on robust, high performance PEMs. We are attempting to build on the well-established chemical and thermal stability of fluorinated polymers to develop a family of new materials with superior properties. Specifically we are attempting to prepare new PEM materials by terpolymerization of perfluoro(4-methyl-3,6-dioxa-7-octene-1-sulfonyl fluoride) (PSEPVE) with other monomers to make new materials. An interesting aspect of this work involves the merging of soft lithographic methods with PEMs to make patterned, high surface area PEMs. The goals of this research are to increase mechanical stability, reduce methanol permeability, to improve the power density, and to further integrate fuel cell concepts into more functional systems and materials.

*Contact author: desimone@unc.edu

The Path Toward Fabricating Complex Nanoscale Assemblies in 2 and 3 Dimensions

Henry I. Smith
Dept. Electrical Engineering & Computer Science, MIT, Cambridge, MA 02139, USA

An ability to reliably fabricate structures at the nanoscale, in 2 and 3 dimensions, and with nanoaccuracy, will be essential to future science, engineering, and economic development. In living systems and in semiconductor chips it is the information content, encoded in structures, that determines functionality. At present, lithography is the only synthetic means we have of putting information into nanoscale assemblies. For this reason lithography will continue to play a role, but issues of cost, area coverage, nanoscale accuracy and manufacturability must be addressed. To enable the assembly of structures at the molecular scale, new techniques that bridge the gap between lithography and the molecular domain will need to be invented. Templated Self Assembly (TSA) is a small step in that direction, but to date it has not enabled an increase complexity. Hence, information content is limited to that achieved with lithography. How to go beyond this limit remains a major challenge and opportunity.

"Controlling the flow of colour: photonic systems in Lepidoptera"

P. Vukusic
School of Physics. University of Exeter, Exeter, UK.

A broad range of structural architecture may be found in natural systems. This structure has developed for a variety of reasons, under the influence of many different ecological and physiological selection pressures: however, when its dimensions range from tens to hundreds of nanometers, it invariably results in strong optical phenomena.

There is evidence that optics R&D in Nature ostensibly existed since the *Cambrian explosion*; this signifies the start of the Cambrian period over 500 million years ago which heralded the first sudden and vast development of different life forms [1,2]. Here, co-development of many species' visual systems, concurrently with their external colouration, led to a massive growth in the evolution of life forms. The principle selection pressure responsible for the subsequent development of all life is believed photonics-driven; it has created the remarkably diverse range of colour we observe in the living world today.

Studies of iridescence in terrestrial systems, such as those associated with brightly coloured insects [3-7] and birds, have seen significant advances in recent years. Complex partial photonic bandgap structures in the elytra of Colepotera [4] and the scales of Lepidoptera [5,6] suggest broad innovation in nature's use of materials and manipulation of incident light [7]. The existence of an analogue of optically active cholesteric liquid crystalline structure has been shown responsible for the circularly polarised reflection from certain beetles' exocuticle [4]. In other insecta, principally certain butterflies, ultra-long-range visibility of up to one half-mile is attributed to photonic structures that are formed by discrete multilayers of cuticle and air [5]. This contrasts, in other butterfly species, to photonic structures designed more for crypsis and which not only produce strong polarisation effects but also colour stimulus synthesis using a doubly periodic multilayered photonic structure [6].

Optical systems also exist that employ remarkable 3D photonic crystals of cuticle to produce partial PBGs, with the effect that bright colour is reflected over a broad angle range. From the perspective of modern optical technology, this indicates an evolutionary step further along the photonic road, since in principle, 3D periodicity potentially manipulates the flow of light in all directions. In certain beetles, the 3D structure is an analogue of the construction of gem opal; comprising in the beetle's case, close-packed sphere-arrays of cuticle. In certain butterflies the 3D structure is termed inverse-opal and comprises hollow voids surrounded by a honeycomb of cuticle. The physical structure of this inverse-opal photonic crystal, while varying somewhat between examined species, appears consistently as a minor variation of tetrahedral. Interestingly, band gap calculations indicate that a perfect tetrahedral configuration offers the highest reflectivity over the broadest angle range for a given refractive index contrast between component media. Given constraints associated with cuticular morphology and the ecological and intraspecific selection pressures thought to exist, it appears the physical design of this photonic structure has converged towards one of the most optically efficient configurations.

Numerous studies, many of them very recent, have sought to discover and characterise the photonics associated with a diverse range of natural specimens. Many of them have revealed system designs that have evolved and existed naturally for millennia and that were, until their discovery in nature, thought to have been the recent product of technological innovation.

References

1. A.R. Parker, "Colour in Burgess shale animals and the effect of light on evolution in the Cambrian", *Proc Roy Soc Lond B* **265**: 967-972, (1998).
2. A.R. Parker **"**In the Blink of an Eye**"** *Perseus Publishing, 2003*.
3. P. Vukusic, "Natural Coatings" in *Optical Interference Coatings*. (eds Kaiser, N. & Pulker, H. K.) Springer Series in Optical Sciences 88, (2003).
4. A.C. Neville and S. Caveney "Scarabeid beetle exocuticle as an optical analogue of cholesteric liquid crystals". *Biol Rev* **44**: 531-562 (1969).
5. P. Vukusic, J.R. Sambles, C.R. Lawrence & R.J. Wootton Quantified interference and diffraction in single *Morpho* butterfly scales. *Proc Roy Soc B* **266**: 1403-1411 (1999).
6. P. Vukusic, J.R. Sambles, C.R. Lawrence "Structural colour: Colour mixing in wing scales of a butterfly" *Nature* **404**: 457 (2000).
7. P. Vukusic and J.R. Sambles, "Photonic structures in Biology" *Nature* **424**, 852-855 (2003).

Structural Colour from Natural and Nanoengineered Circular Bragg Resonators

Ian Hodgkinson[1]
Department of Physics, University of Otago, PO Box 56, Dunedin, New Zealand

Nanostructures observed in nature are inspiring optical engineers to fabricate or initiate the self-assembly of similar elements for use in applications such as photonics [1,2]. Here we resolve the structural basis for wide-angle reflection of circularly-polarized green light from the New Zealand manuka beetle [3] Pyronota festiva and trace a path to fabrication of inorganic Bragg media for circularly and elliptically polarized light. Potential applications of the handed materials include twist-defect filters [4] for mode and polarization selection in laser devices [5].

The manuka beetle appears green when it is illuminated with unpolarized white light and black when a right-circular filter is used. Selective reflection of handed light is known for many scarab beetles [6,7] and has been related to helicoidal layers of microfibrils [8] that behave in a similar way to cholesteric liquid crystals. A reflectance spectrum recorded from a small area of the manuka beetle shows a left-handed Bragg resonance at about 540nm that makes a major contribution to the green colour, and a larger resonance in the far red. Tilting the beetle causes the Bragg peaks to move to smaller wavelengths, an effect that is indicative of interference rather than diffraction [6]. Observation of the elytra of the manuka beetle using a standard optical microscope showed that the surface is not a uniform reflector, but rather light is returned from an array of chiral micro-mirrors. Using depth-sensitive fluorescent confocal microscopy we were able to establish the structure of the micro-mirrors as curved pits and troughs filled with contouring chiral material. A solution of fluorescein applied to the elytra didn't penetrate the surface, and established that the top surface of the micro-mirror is nearly flat.

At normal incidence light reflected from the bottom of a typical pit appeared yellow. Greenish-yellow contours were seen when a ring illuminator was used to provide obliquely incident light, and a connected network of blueish-green thin lines was observed at the boundaries of the micro-mirrors when normal illumination was used. In each case the reflected light was observed to be left handed. We conclude that the observed green colour of the beetle results from colour mixing of light remitted from multiple paths, similar to that reported for the butterfly Papilo palinunus [2]. At the boundaries of the micro-mirrors where chiral layers meet we observed apparent mixing of chiral mediums.

Our observations of manuka beetles have inspired us to study the optical properties of mixed chiral materials. We have found that a medium in which a chiral material threads through a birefringent material with fixed axes behaves as a Bragg medium for elliptically polarized light [9]. By depositing alternately thin layer components of chiral titanium oxide and birefringent titanium oxide [10] we have fabricated such a medium. Lakshman De Silva, John Leader, Petra Murray, Qi hong Wu, Matthew Arnold and Andrew McNaughton made significant contributions to this project which is supported financially by the New Zealand New Economy Research Fund contract CO8X0206, and by the MacDiarmid Institute for Advanced Materials and Nanotechnology.

References

[1] Parker, A.R., McPhedran, R.C., McKenzie, D.R., Botten, L.C. and Nicorovici, N-A.P. Nature 409, 36-37 (2001).
[2] Vukusic, P. and Sambles, J.R. Nature 424, 852-855 (2003).
[3] Crowe, A. Which New Zealand Insect? (Penguin Books, Auckland, 2002).
[4] Hodgkinson, I.J., Wu, Q.H., De Silva, L., Arnold, M.D., McCall, M.H. and Lakhtakia, A. Phys. Rev. Lett. 91, 223903, (2003).
[5] Schmidtke, J., Stille, W. and Finkelmann, H. Phys.Rev. Lett. 90, 83902 (2003).
[6] Neville, A.C. and Caveny, S. Biol. Rev. 44, 531-562 (1969).
[7] Srinivasarao, M. Chem. Rev. 99, 1935-1961 (1999).
[8] Neville, A.C. Biology of Fibrous Composites: Development beyond the cell membrane, (Cambridge University Press, 1993).
[9] Hodgkinson, I.J., Wu, Q.H., De Silva, L. and Arnold, M. SPIE 5508, 47-56 (2004).
[10] Hodgkinson, I.J. and Wu, Q.H. Adv. Mater. 13, 889-987 (2001).

[1]Contact author: ijh@physics.otago.ac.nz

SESSION Tu 3
PLENARY SESSION V

Tuesday 8 February 2005 **1320–1500**

Galaxy Ballroom

Session Chairs **Jeff Tallon, Industrial Research Ltd., NZ**
Lynn Gladden, Cambridge University, UK

13:20 **NMR of electronic inhomogeneities in cuprate superconductors**
Tu 3.1 J. Haase[1], G.V.M. Williams[2] and O. P. Sushkov[3]
(Invited Talk)
[1] *Leibniz Institute of Solid State and Materials Research Dresden, Germany*
[2] *Industrial Research Ltd., Lower Hutt, NZ*
[3] *University of New South Wales, Sydney, Australia*

13:45 **Seeing materials in new light – x-ray absorption spectroscopies in materials characterisation**
Tu 3.2 J.B. Metson
(Invited Talk)
University of Auckland, Auckland, NZ

14:10 **Shear banding and non-linear dynamics in complex fluids**
Tu 3.3 P.D. Olmsted
(Invited Talk)
University of Leeds, Leeds, UK

14:35 **Resonance Raman probe of solvent effects in charge-transfer processes**
Tu 3.4 M.R. Waterland
(Invited Talk)
Massey University, Palmerston North, NZ

NMR of Electronic Inhomogeneities in Cuprate Superconductors

J. Haase[1,*], G.V.M. Williams[2] and O. P. Sushkov[3]
[1] *Leibniz Institute of Solid State and Materials Research Dresden, GERMANY*
[2] *Industrial Research, Lower Hutt, NEW ZEALAND*
[3] *Department of Physics, University of New South Wales, Sydney, AUSTRALIA*

Nuclear Magnetic Resonance (NMR) investigates the nuclear spin level splitting and dynamics. Since the nuclei couple through electric and magnetic hyperfine interactions with the electrons NMR can investigate the electronic properties of materials with atomic scale resolution at particular sites in the unit cell. The electric quadrupole moment of the nucleus (present for nuclei with spin larger than 1/2, e.g. ^{63,65}Cu, ^{17}O) gives rise to its interaction with a local electric field gradient. While the nuclear magnetic dipole moment interacts with a local magnetic field. The latter interaction is, e.g., responsible for the peculiar NMR shift and relaxation of metals (temperature-independent Knight shift, Heitler-Teller relaxation) and conventional superconductors (disappearance of the Knight shift below the transition temperature T_c, Hebel-Slichter peak in the nuclear relaxation rate near T_c and vanishing relaxation at lower temperature), as it is dominated by the excitations near the Fermi surface. Consequently, most of the NMR work on the cuprates focused on the magnetic interaction which, e.g., shows a change in the shift and an additional decrease in the nuclear relaxation rate already well above T_c (which is a manifestation of the pseudogap).

It is well documented, that the NMR data of cuprate superconductors also reveal a distinct relationship between the electric field gradient at planar Cu and O (but not apical O) and the doping level of the material [1]. Moreover, these field gradients are intimately related to the magnetic shift above T_c, a very unusual property [2] that still awaits a theoretical explanation. These findings suggest that the electric field gradient, while notoriously difficult to calculate, must relate to the doping level that in turn dictates the magnetic properties.

In a recent report [3] we have introduced a powerful, new NMR approach that quantitatively measures the hole concentration at planar Cu and O. Utilizing novel data from atomic spectroscopy that relate the electric hyperfine interaction to the various ionic states of Cu and O, we were able to calibrate the NMR quadrupole splitting and use it together with a simple model for a hybridized Cu-O_2 plane to follow the process of doping. We find that upon doping the holes predominantly occupy O $2p_\sigma$ orbitals. Counting the holes at Cu and O we can actually measure the phase diagram of the cuprates (with the published T_c data). Thus, with the achieved calibration of the NMR data we can also estimate the hole variation in the cuprates by measuring the distribution of electric field gradients. Depending on the particular cuprate we deduce charge density variations in the Cu-O_2 plane that are as large as ±70% of the doped carriers in optimally doped $La_{2-x}Sr_xCuO_4$. More examples will be discussed. We will demonstrate that this charge density variation is always correlated with a spin shift variation that is in agreement with a local hole variation of similar extent. By analyzing the distributions in various materials we can estimate the extent of the local hole variation.

In our presentation, we will also discuss our recent progress with performing NMR in pulsed, rather than static magnets. This allowed us to observe the nuclear precession at very high magnetic fields (60 T).

References

[1] S. Ohsugi, J. Phys. Soc. Jap. **64**, 3656 (1995).

[2] J. Haase, C. P. Slichter, and C. T. Milling, J. Supercond. **15**, 339 (2002).

[3] J. Haase, O. P. Sushkov, P. Horsch, G.V.M. Williams, Phys. Rev. B **69**, 094504 (2004).

* Contact author: j.haase@ifw-dresden.de

Seeing Materials in New Light – X-ray Absorption Spectroscopies in Materials Characterisation.

J. B. Metson*
Department of Chemistry, The University of Auckland, Auckland, NEW ZEALAND
and MacDiarmid Institute for Advanced Materials and Nanotechnology
Private Bag 92019, Auckland, New Zealand

The advent of high brightness synchrotron light sources has significantly widened the range and power of techniques for materials characterisation [1]. The synchrotron offers the capacity to do some existing experiments with much higher sensitivity and resolution, for example powder and single crystal x-ray diffraction, but more importantly introduces a range of methods, such as the x-ray absorption and emission spectroscopies, simply not accessible with any other radiation source. Both the Extended x-ray Absorption Fine Structure (EXAFS) and X-ray Absorption Near Edge Spectroscopy (XANES) offer very powerful tools for the detailed elemental, chemical, and structural analysis of materials, in the latter case particularly utilising the softer absorption edges between 100 and 2000 eV.

Recent examples from our own work include examining the speciation of S in carbon based electrodes [2] and of N in nitride thin films [3,4]. In the latter case is that the 70 meV resolution obtained in the N K-edge XANES spectrum allows the vibrational spectrum of the nitrogen molecule trapped in the solid to be resolved. The sulfur spectra provide an interesting test case in that the oxidation state based chemical shifts of a variety of compounds are well resolved in the K-edge spectra just below 2500 eV, while not surprisingly, but with more technical difficulty, the fingerprinting of individual compounds is far better resolved at the less shielded sulfur L-edge around 164 eV. For layered oxide structures for Li ion battery cathodes, the K and L-edge spectra have been used to elucidate the role of transition metals with cycling of the cathode in test cells [5].

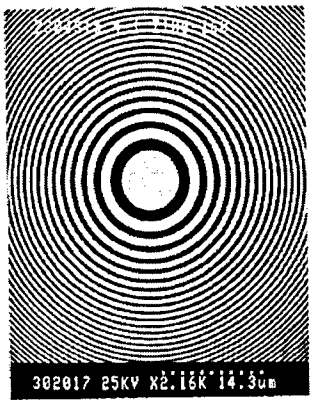

In addition to the extreme brightness of the synchrotron source, several developments are changing the accepted boundaries of spatial resolution. The increasing use of Kirkpatrick-Baez grazing incidence mirrors and especially Fresnel Zone Plates for X-ray focussing (Figure 1) coupled with the rapid evolution of detector technologies customised for area detection of X-rays are opening new horizons in areas from materials science to medical imaging. Some of these developments will be reviewed, particularly in the light of applications in nano-technology and the progress of the Australian Synchrotron.

Figure 1. Image of an x-ray focussing Zone Plate manufactured by Xradia (gold relief on a SiN membrane support) and used in synchrotron imaging - in this case an x-ray tomography instrument [6]. The specified resolution of this instrument is currently 60 nm.

References

1. Synchrotron Radiation Sources a Primer. H. Winick (ed). World Scientific, Singapore (1994).
2. S.J. Hay, J.B. Metson, M. M. Hyland. Sulfur Speciation in Aluminium Smelting Anodes. *Industrial and Engineering Chemical Research*, **43**(7) 1690-1700 (2004).
3. J.B. Metson, B.J.Ruck, U.D.Lanke, F.Budde, H.J.Trodahl and A.Bittar. Characterisation of Amorphous GaN Films. *Applied Surface Science* (Accepted for publication)
4. B.J.Ruck, A.Koo, U.D.Lanke, F.Budde, H.J.Trodahl, G.V.M.Williams, A.Bittar, J.B.Metson, E.Nodwell and T.Tiedje. Filled and Empty States of Disordered GaN Studied by X-ray Absorption and Emission. *Applied Physics Letters* - Accepted for Publication
5. B. Ammundsen, J. Desilvestro, T. Groutso, D. Hassell, J.B. Metson, E. Regan, R. Steiner and P. J. Pickering, *Formation and Structural Properties of Layered $LiMnO_2$ Cathode Materials*, J.Electrochemical Soc. **147**(11) 4078-4082, (2000)
6. www.xradia.com

* Contact author: j.metson@auckland.ac.nz

Shear banding and non-linear dynamics in complex fluids

P. D. Olmsted[1,*]
[1] *School of Physics and Astronomy, University of Leeds, Leeds LS2 9JT, UNITED KINGDOM*

"Shear banding", *i.e.* macroscopic flow-induced phase coexistence or apparent "phase transitions" between different steady state microstructures, has been observed in many complex fluids, including wormlike micelles, lamellar systems, associating polymers, and liquid crystals. In this talk I will review this behaviour, and discuss a general phenomenology for understanding shear banding and flow-induced phase separation in complex fluids, at a thermodynamic level (as opposed to a statistical mechanics level). An accurate theory must include the relevant microstructural order parameters, with which one must construct the fully coupled spatially-dependent hydrodynamic equations of motion. Although this has been successfully done for very few model fluids, we have nonetheless obtained general rules for the phase behaviour of complex fluids in shear flow. Perhaps surprisingly, the interface between coexisting phases plays a crucial role in determining the steady state behaviour [1], and is much more important than its equilibrium counterpart. I will discuss recent work addressed at the kinetics and morphology of wormlike micellar solutions [2], and touch on models for more complex oscillatory and possibly chaotic systems [3].

References

[1] C.-Y. D. Lu, P. D. Olmsted, and R. C. Ball , "Effects of Non-local Stress on the Determination of Shear Banding Flow", Physical Review Letters **84**. 642 (2000).

[2] O. Radulescu, P. D. Olmsted, J. P. Decruppe, S. Lerouge, J. F. Berret, G. Porte, "Timescales in shear banding of wormlike micelles", Europhysics Letters **62**, 230 (2003).

[3] S. M. Fielding and P. D. Olmsted, "Spatio-temporal oscillations and rheochaos in a simple model of shear banding", Physical Review Letters **92,** 084502 (2004).

* Contact author: p.d.olmsted@leeds.ac.uk

Resonance Raman probe of solvent effects in charge-transfer processes

M. R. Waterland
Institute of Fundamental Sciences, Massey University, Palmerston, NEW ZEALAND
MacDiarmid Institute for Advanced Materials and Nanotechnology

Resonance Raman Intensity Analysis is a powerful technique for determining detailed information regarding the nuclear motions that are coupled to electronic excitation immediately following photoexcitation.[1] By measuring the absolute resonance Raman intensity, reorganization energies are obtained for both the internal modes of the chromophore and the surrounding solvent modes that are coupled to the electronic transition. It can be shown that the same molecular and solvent modes that couple to the optical transition probed by resonance Raman spectroscopy also promote thermally or electrically driven charge transfer.[2]

At the molecular level electron-transfer or charge-transfer has been successfully described using the Marcus-Hush Theory.[3] The Marcus-Hush theory highlights the importance of solvent or environmental effects on the rates of thermal electron-transfer. The large majority of studies of solvent effects on electron-transfer have been performed in the liquid phase, with solvent effects accounted for via a simple dielectric continuum. Many advanced materials such as oLEDs, organic electro-optic switches and plastic solar cells incorporate solid solutions of chromophores that undergo charge-transfer processes.

From a solvation point of view the polymer matrix presents an environment that is fundamentally different from a liquid environment because a large majority of the translational motions available to a liquid are frozen out in the polymer matrix. Only solvent motions that are rapid on the charge-transfer timescale will dynamically control the rate of charge-transfer.[3] Solvent motions that are very slow or static on this time-scale will result in an inhomogeneous broadening of the solute energy levels. A central question is then: How do the solvent motions partition between motions that are rapid on the transition time-scale (i.e. homogeneous broadening) and motions that are slow on the transition time-scale (i.e. inhomogeneous broadening). The use of absolute resonance Raman intensities and the time-dependent theory of Raman scattering allows a coarse determination of this partitioning to be made.

This paper presents some initial studies of the intramolecular charge-transfer transition of Disperse Red (shown below) in solution phase and it will outline the connection between resonance Raman spectroscopy and thermal electron-transfer.

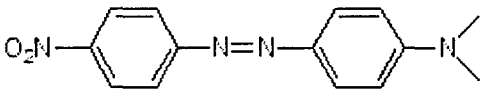

Disperse Red

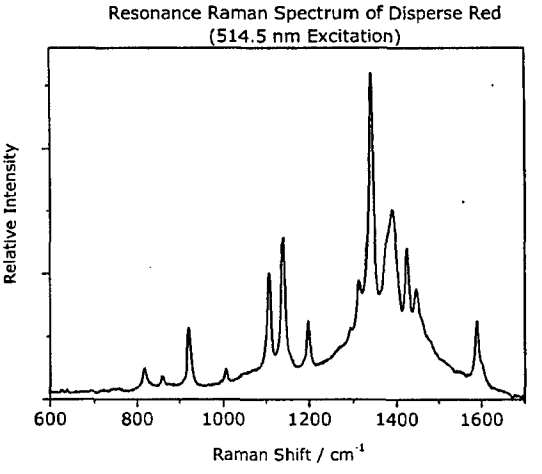

References

1. A. B. Myers, Chem. Rev. **96**, 911 (1996)
2. B. Li, A. E. Johnson, S. Mukamel, and A. B. Myers, J. Am. Chem. Soc. **116**, 11039 (1994)
3. P. F. Barbara, T. J. Meyer, and M. A. Ratner, J. Phys. Chem. **100**, 13148 (1996)

SESSION Tu 4
PLENARY SESSION VI

Session sponsor: European Commission

Tuesday 8 February 2005 **1530–1645**

Galaxy Ballroom

Session Chairs **TBA**
Prof Alan MacDiarmid

15:30 **The European strategy for nanotechnology**
Tu 4.1 E. Andreta
(Invited Talk)
Director of DG Research Nanotechnology and Advanced Materials Directorate
European Commission, Brussels, Belgium

15:45 **Overview of the European Commission's new thematic call for nanotechnology-related research proposals**
Tu 4.2 R. Tomellini
(Invited Talk)
Head of Nanotechnology Unit
European Commission, Brussels, Belgium

The European Strategy for Nanotechnology

E. Andreta
Director of Industrial Technologies Directorate, Directorate-General for Research, European Commission, Brussels, BELGIUM

In this session Dr Ezio Andreta will discuss the European strategy for nanotechnology outlined by the European Commission in its May 2004 publication "Towards a European Strategy for Nanotechnology" and the implications of this strategy for the European and international research communities.

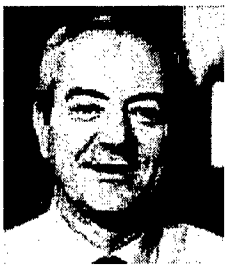

Ezio Andreta graduated in Political Sciences and Economics at the Universities of Genoa and Lyon. He did post-graduate studies in Industrial and Monetary issues at the London School of Economics; and obtained a Doctorate in International Relations at the University of Genoa. He started his career as Assistant Professor in Economics. Since 1995 he is Director at the European Commission in the Directorate-General for Research. Under the 6th framework programme (FP6), he is responsible for the Priority on Nanotechnologies, multifunctional materials and new production processes. He is also Professor of knowledge management at the PhD school of Politecnico di Torino

Overview of the European Commission's New Thematic Call for Nanotechnology-related Research Proposals

R. Tomellini*
Head of Unit for Nanosciences and Nanotechnologies, Industrial Technologies Directorate, Directorate-General for Research, European Commission, Brussels, BELGIUM

In this session Dr Renzo Tomellini will overview the European Commission's new thematic call for research proposals in the area of 'Nanotechnologies and nanosciences, knowledge-based multifunctional materials and new production processes and devices'. The topic areas and funding instruments will be explained and areas in which international cooperation is sought highlighted.

Born in 1960. Graduated in chemistry "cum laude" in Rome in 1986. After a period as visiting researcher in Germany and France, he worked in Italy as a researcher at the Centro Sviluppo Materiali [1]. His further education included one course in management and business administration, and one in European law and regulations.

In 1991 he joined the European Commission in Brussels, where was scientific/technical responsible for ECSC [2] steel research projects. Between 1995 and 1999 he was managing the ECSC-Steel research and technological development programme. In 1999 he became the assistant to the director of "Industrial Technologies" in the Research Directorate-general of the European Commission. Amongst others, he prepared for the provisions to bring to its end the ECSC Treaty and to launch the new research fund for coal and steel (see the Nice Treaty). Meanwhile, since 1999 he promoted initiatives in nanotechnology and in 2003 became the Head of the newly-created Unit "Nanosciences and Nanotechnologies".

He deposited 4 patent applications (a new source for atomic spectroscopy and some innovative sensors), published some 50 articles, drafted 4 standards on analysis and measurements, edited 11 books, created one newsletter and 2 web pages, and realised 3 films on science and research issues.

[1] Centre for development of materials
[2] European Coal and Steel Community (historically, the first of the European Communities)

* renzo.tomellini@cec.eu.int

Wednesday 9 February

Galaxy Ballroom **0830-1000**

Session We 1 **Keynote Session III.....51**

Session sponsored by Foundation for Research, Science and Technology and The Ministry of Research, Science and Technology

---

Galaxy Ballroom **1030-1210**

Session We 2 **Plenary Session VII 55**

Session sponsored by AJ Park

SESSION We 1
KEYNOTE SESSION III

Session Sponsor: Foundation for Research, Science and Technology and The Ministry of Research, Science and Technology

Wednesday 9 February 2005 0830–1000

Galaxy Ballroom

Session Chairs **Paul Callaghan, Victoria University of Wellington, NZ**
TBA

08:30 **Introduction for Prof Dowling**
P.T. Callaghan
Victoria University of Wellington, Wellington, NZ

08:35 **Responsible development of nanotechnologies**
We 1.1 A. Dowling
(Keynote Speaker)
University of Cambridge, Cambridge, UK

09:10 **On the nature of our tenuous, metals based civilization**
We 1.2 D.D. Macdonald
(Invited Talk)
Pennsylvania State University University Park, USA

09:35 **Putting nanomaterials to work: the design, construction and operation of synthetic nanmotors**
We 1.3 C. Regan and A. Zettl
(Invited Talk)
University of California at Berkeley, Berkeley, USA

Responsible development of nanotechnologies

Professor Ann Dowling CBE FREng FRS

Professor of Mechanical Engineering, University of Cambridge
Cambridge, UK

This presentation summaries the key findings and recommendations of the Royal Society/Royal Academy of Engineering Report on Nanotechnology. The report is enthusiastic about the great potential benefits of nanotechnologies. Uncertainties associated with the health and environmental impacts of free manufactured nanoparticles and nanotubes are discussed. It recommends research to understand better their toxicology and exposure pathways, and actions to restrict exposure of humans and the environment to free manufactured nanoparticles and nanotubes until they are better understood. The report makes recommendations to ensure that regulations account for the potentially different properties of chemicals in nanoparticle form. The need for public dialogue about the development of nanotechnologies is highlighted.

Ann Dowling is a Fellow of the Royal Society, Royal Academy of Engineering (Vice-President 1999-2002) and is a Foreign Associate Member of the French Academy of Sciences. She serves on a number industry and government advisory committees, and has recently chaired the Royal Society/Royal Academy of Engineering study on nanotechnology. She is a member of the Council of the Engineering and Physical Sciences Research Council (EPSRC), chairing their Technical Opportunities Panel. She is a non-executive director of the Cambridge-MIT Institute, a Trustee of the National Museum of Science and Industry and was appointed CBE for services to Mechanical Engineering in the Queen's 2002 Birthday Honours List.

On the Nature of Our Tenuous, Metals Based Civilization

Digby D. Macdonald
Center for Electrochemical Science and Technology
Department of Materials Science and Engineering
Pennsylvania State University
University Park, PA 16802

The phenomenon of passivity has enabled the development of our metals-based civilization, because it is the protective nature of the nano-scale oxide films that form on surfaces that allows the use of reactive metals in contact with oxidizing environments [1]. These films form as meta-stable phases, with their continued existence and ability to protect the underlying reactive metal from explosive reaction with the environment depending entirely upon an appropriate relationship between the rate of formation and the rate of dissolution. Under certain circumstances, the "passivating" films (a term apparently coined by Faraday) break down locally, resulting in rapid dissolution to form corrosion pits, stress corrosion cracks, etc. The resulting damage has been estimated to cost an industrial nation about 4.5 % of the GNP, or about $540 billion per year in the US alone. This enormous cost amounts to nearly $2000 per year for every man, women, and child in the country.

Extensive work over the past one hundred and seventy years has demonstrated that passive films posses a multi-layer structure, with the defective, nano scale oxide barrier layer forming directly from the metal and the outer layers forming via the hydrolysis and precipitation of oxides, hydroxides, and/or oxyhydroxides from cations that are transmitted through the barrier layer or via restructuring the barrier layer itself. The barrier layer is typically several nanometers thick, but the outer layer may grow to be many hundreds of micrometers thick, as in the rusting of iron. The exact mechanisms involved in the growth and breakdown of passive films on metals and alloys has been hotly debated, but the lack of experimental techniques with sub-nanometer resolution completely hampered advancement of the field until the development of high resolution techniques a couple of decades or so ago. Thus, high resolution (angle resolved) XPS, XAFS, SEXAFS, analytical STEM, AES, and various scanning "microscopies" (STM, AFM, ECSM) have been able to discern the morphology at the nano-scale, defect structure, and electronic structure of passive films on metal surfaces. These techniques, and other methods, have confirmed that the barrier layer is highly defective, that the barrier layer grows into the substrate metal, and that the outer layer(s) grow by precipitation from solution.

Over the past two decades, the author and his colleagues have developed a comprehensive theory in the form of the Point Defect Model (PDM) [1] for the growth and breakdown of passive films on metal surfaces. This analytical model provides quantitative relationships between dependent and independent variables that are subject to experimental test, and to the author's knowledge the PDM has withstood the test of time. Furthermore, the PDM provides an analytical relationship between the rate of film growth and the film thickness, thereby permitting a phase space analysis of film stability. From this analysis, it is concluded that the passive films are only meta stable, clearly demonstrating the tenuous nature of our metals-based civilization. The PDM also forms the basis of Damage Function Analysis (DFA) [2], which is now being developed and used to predict localized corrosion damage deterministically in real structures (e.g., in low pressure steam turbines and in nuclear power reactors). In particular, unification of the DFA and Extreme Value Statistical (EVS) methods for predicting the accumulation of localized corrosion damage has circumvented one of the most difficult problems in the field; the calculation of the shape and location parameters in the Gumbel Type II (EVS) distribution function. Values for these parameters can now be calculated from "first principles", thereby rendering EVS truly "predictive". The development of DFA represents the first, deterministically predictive philosophy for projecting damage into the future for complex industrial systems. The successful development of DFA potentially has enormous economic consequences, because it would enable operators of complex industrial systems to avoid or minimize costly unscheduled downtime.

1. D. D. Macdonald, Pure Appl. Chem., 71, 951 (1999)
2. G. Englehardt and D. D. Macdonald, Corrosion Science, **46**, 2755 (2004).

Putting Nanomaterials to Work: the Design, Construction, and Operation of Synthetic Nanomotors

B. C. Regan* and A. Zettl
Department of Physics, University of California at Berkeley,
Materials Sciences Division, Lawrence Berkeley National Laboratory &
Center of Integrated Nanomechanical Systems
Berkeley, CA 94720 USA

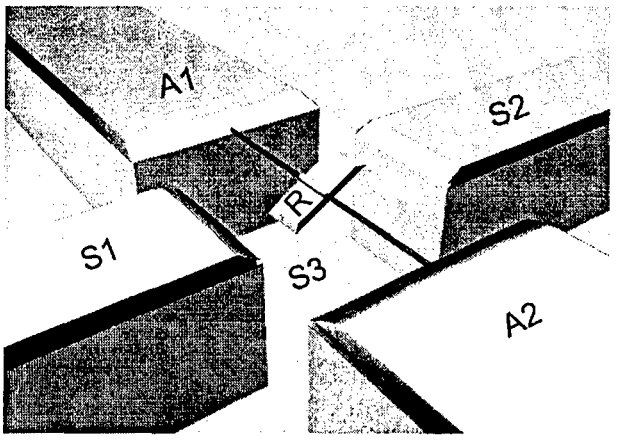

Figure 1. Rotational nanomotor. A gold rotor paddle (R) is attached to the outer walls of a MWCNT suspended from two anchor pads (A1, A2). Electrostatic fields applied through three stator electrodes (stator pads S1 & S2 and the back gate S3) can control the orientation of the paddle.

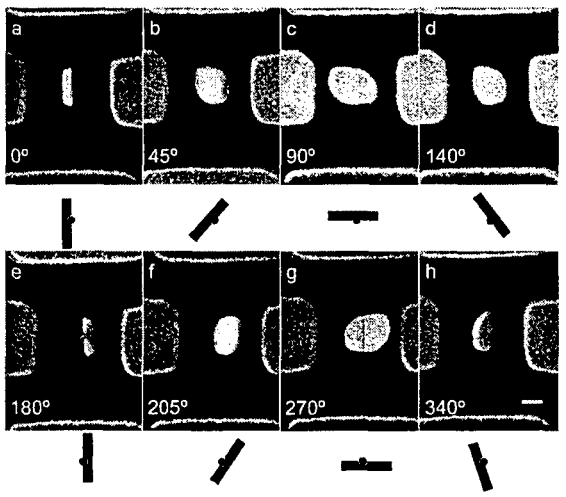

Figure 2. Scanning electron micrographs of a nanomotor stepped through 360°. The scale bar is 300 nm.

I will discuss recent advances at Berkeley in the design, construction, and operation of electrically-driven molecular actuators and motors using carbon nanotubes as integral components. One design [1] uses a multiwall carbon nanotube (MWCNT) as a rotational bearing, allowing low-level voltages to fully control the angular position of a metal plate rotor. This motor, of size ~200 nm on a side, is integrated on a silicon chip. Aligned arrays of such motors have been produced. Another successful design concerns a linear molecular motor driven by a newly-discovered mass conveyance process [2], whereby individual metal atoms can be electrically driven back and forth along a nanotube. In the linear motor configuration both carbon nanotubes and metal nanocrystals play central functional roles. I will address the novel underlying physics of these exciting new devices.

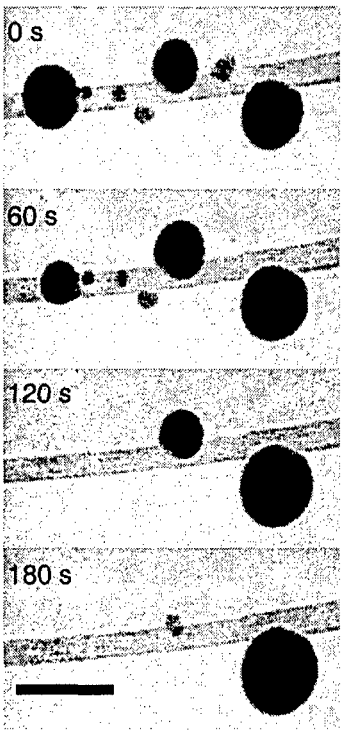

Figure 3. Atomic mass conveyor. As electrical current is driven through the MWCNT from left to right, metal atoms move from particle to particle along the nanotube. The scale bar is 100 nm.

References

[1] A. M. Fennimore, T.D. Yuzvinsky, Wei-Qiang Han, M.S. Fuhrer, J. Cumings and A. Zettl, Nature **424**, 408 (2003).
[2] B. C. Regan, S. Aloni, R.O. Ritchie, U. Dahmen, and A. Zettl, Nature **428**, 924 (2004).

* Contact author: regan@physics.berkeley.edu

SESSION We 2
PLENARY SESSION VII

Session Sponsor: AJ Park

Wednesday 9 February 2005 1030–1210

Galaxy Ballroom

Session Chairs **David Officer, Massey University, NZ**
Katie Robinson, A J Park Patent Attorneys, NZ

10:30 **Nanotube devices in micro and nanoelectronics**
We 2.1 S. Roth
(Invited Talk)
Max Planck Institute for Solid State Research, Stuttgart, Germany

10:55 **Determination of chiral indices and electronic transition energies in carbon nanotubes**
We 2.2 C. Thomsen
(Invited Talk)
Technische Universität Berlin, Berlin, Germany

11:20 **Nanoscience in the discovery of porosome: a new cellular structure**
We 2.3 B.P. Jena
(Invited Talk)
Wayne State University, Detroit, USA

11:45 **Small scale technologies: directions for Victoria**
We 2.4 G. Tegart
Victoria University, Melbourne, Australia

Dr. Siegmar Roth
Max Planck Institute
for Solid State Research

06.09.2004

Nanotube Devices in Micro and Nanoelectronics

Carbon Nanotubes are seamless tubes of graphitic carbon, about 1nm in diameter and up to several µm in length. Depending on the diameter and helical pitch, the tubes can be metallic or semiconducting. Depending on the production process, there can be single-walled, double-walled, few-walled and multi-walled tubes.

Electron transport in perfect metallic tubes is ballistic, i.e. the electrons move without collisions and hence without losses. In real tubes there are losses, but the resistance is low and very high current densities are achieved, up to ~10^9 A/cm, i.e. several orders of magnitude higher than in copper. In addition, the covalent chemical bonds of the graphite lattice are much stronger than metallic bonds in copper, so that carbon nanotubes are less effected by electromigration. Consequently metallic carbon nanotubes are ideal candidates for vias and interconnects in VLSI silicon technology.

Semiconducting nanotubes can be p and n doped, and they can be used to prepare nanoscale transistors. In the simple case a nanotube is adsorbed on the native oxide layer of a silicon chip and gold leads are applied as source and drain contacts by electron beam lithography. The bulk of the silicon chip server as a gate and varying the gate voltage the current through the tube can be changed by several orders of magnitude.

In more sophisticated carbon nanotube field effect transistors a top gate can be used in connection with a high–kappa gate dielectric. The ultimate device is the all carbon transistor, where the gate is another carbon nanotube and a heteroatomic linker molecule server as a "gate dielectric".

The contribution will give a short introduction into the physics of carbon nanotubes and summarize the state of the art of application of nanotubes as interconnects and as transistors.

Determination of Chiral Indices and Electronic Transition Energies in Carbon Nanotubes

Christian Thomsen
Institut für Festkörperphysik, Technische Universität Berlin, Hardenbergstr. 36, 10623 Berlin, GERMANY

Resonant Raman scattering has recently allowed the investigation of electronic transitions in carbon nanotubes. We show that the Raman resonances of the radial breathing mode can be used for the assignment of the chiral indices. Different from luminescence measurements [1] the chirality of both semiconducting and metallic nanotubes can be investigated. Our assignment is based on a comparison of the resonance maxima for the radial breathing modes as a function of the laser excitation energy versus inverse frequency of the radial breathing mode. These maxima are seen to shift through the spectra in *laola*-like waves and may be compared to a theoretical plot of this relationship based on the third-nearest neighbor tight-binding approximation in a so-called Kataura plot. From a comparison of 50 different-chirality nanotubes we are able to derive the parameters of the well-known inverse relationship between the breathing-mode frequency ω_{RBM} of a nanotube and its diameter d, independent of any prior assumptions about these constants [2]. We find ω_{RBM}=214 cm^{-1} nm / d + 19 cm^{-1}.

References:

[1] S. M. Bachilo *et al.*, Science **298**, 2361 (2002)
[2] H. Telg, J. Maultzsch, S. Reich, F. Hennrich, and C. Thomsen, Phys. Rev. Lett., in print (2004)

Contact: thomsen@physik.tu-berlin.de

Nanoscience in the Discovery of Porosome: a New Cellular Structure

Bhanu P. Jena
Department of Physiology, Wayne State University School of Medicine, 5245 Scott Hall, 540 E. Canfield Avenue, Detroit, Michigan 48201–4177, USA

Throughout history, the development of new technologies and imaging tools have provided new insights into our perceptions of the living world, which has profoundly impacted human health. The invention of the light microscope more than 300 years ago enabled discovery of the unit of life the cell, and some of its organelles. With the birth of the electron microscope in the last century, dawned a new era in biology and medicine. Electron microscopy enabled the identification of a number of subcellular structures and determination of their function. Despite the capability of electron microscopes to image biological samples at near nanometer resolution, sample processing, results in morphological alterations and therefore have always been a major concern. The invention of the atomic force microscope (AFM)[1] in the mid 80's has help overcome both limitations of the light and electron microscopies, and has further extended our perception of the living world to the near atomic relm of a few angstroms. For the first time, the AFM has enabled the determination of the position and dynamics of single biomolecules in living cells. This unique capability of the AFM has thus given rise to the new discipline of nanobioscience, and heralds a new era in biology and medicine. Using nanoscience in combination with conventional tools and techniques, this past decade has witnessed major advances in our understanding of cell secretion[1-6] and membrane fusion[7-9]. AFM applications on live cells have revealed a new cellular structure[1] called porosome or fusion pore, where secretory vesicles dock and fuse to release their contents. Secretion and membrane fusion are fundamental cellular processes regulating ER-Golgi transport, plasma membrane recycling, cell division, sexual reproduction, acid secretion, and the release of enzymes, hormones and neurotransmitters, to name just a few. It is therefore no surprise that defects in secretion and membrane fusion give rise to diseases like diabetes, Alzheimer's, Parkinson's, acute gastroduodenal diseases, gastroesophageal reflux disease, intestinal infections due to inhibition of gastric acid secretion, biliary diseases resulting from malfunction of secretion from hepatocytes, polycystic ovarian disease as a result of altered gonadotropin secretion, and Gitelman disease associated with growth hormone deficiency and disturbances in vasopressin secretion, are only a few examples. Understanding cell secretion and membrane fusion is therefore critical not only to advance our understanding of these vital cellular and physiological processes, but in the development of drugs to help ameliorate secretory defects, provide insight into our understanding of cellular entry and exit of viruses and other pathogens, and in the development of smart drug delivery systems. Thus the role of secretion and membrane fusion in health and disease is profound, and nanobioscence has greatly contributed to the field.

References

1. Hörber JKH, Miles MJ. Scanning probe evolution in biology. Science 2003;302:1002-1005.
2. Schneider SW, Sritharan KC, Geibel JP, Oberleithner H, Jena BP. Surface dynamics in living acinar cells imaged by atomic force microscopy: identification of plasma membrane structures involved in exocytosis. Proc.Natl.Acad.Sci.USA. 1997;94:316–321.
3. Cho, SJ, Quinn AS, Stromer MH, et al, Structure and dynamics of the fusion pore in live cells. Cell Biol.Int. 2002; 26:35–42.
4. Jeremic A, Kelly M, Cho SJ, Stromer MH, Jena BP. Reconstituted Fusion Pore. Biophys. J. 2003;85:2035-2043.
5. Cho SJ, Jeftinija K, Glavaski S, Jena BP, Anderson LL. Structure and dynamics of the fusion pore in live GH-secreting cells revealed using atomic force microscopy. Endocrinology. 2002;143:1144-1148.
6. Cho WJ, Jeremic A, Rognlien KT, Zhvania MG, Lazrishvili I, Tamar B, Jena BP. Structure, isolation, composition and reconstituted of the neuronal fusion pore. Cell Biol. Int. 2004; (published on-line, Aug. 25, 2004).
7. Cho SJ, Kelly M, Rognlien KT, Cho J, Hoerber JKH, Jena BP. SNAREs in opposing bilayers interact in a circular array to form conducting pores. Biophys.J. 2002;83:2522–2527.
8. Jeremic A, Kelly M, Cho J, Cho SJ, Hoerber JKH, Jena BP. Calcium drives fusion of SNARE-apposing bilayers. Cell Biol. Int. 2004;28:19–31.
9. Jeremic A, Cho WJ, Jena BP. Membrane fusion: what may transpire at the atomic level. J. Biol. Phys. & Chem.. 2004; (in press).
Corresponding author. E-Mail:bjena@med.wayne.edu

Small Scale Technologies: Directions for Victoria

Greg Tegart
Centre for Strategic Economic Studies, Victoria University, Melbourne, Australia

Small scale technologies are already having a significant economic and social impact. Over the next two decades they will have profound effects on industrial products and processes, on the lives of individuals and on the nature of human society. The term small scale technologies refers to technologies with feature line sizes less than 100 nanometers; this covers both microtechnology and nanotechnology since they are often used in industry in combination with each other. The latter will become increasingly dominant over the next two decades.

The State of Victoria in Australia has a population of over 4 million with strong traditional industries in food processing based on agricultural production , pharmaceuticals, metal manufacturing, and building and construction. It has a strong research base particularly in medicine, molecular biology and materials. The paper will reflect the findings of a recent report to the Victorian Government on the potential for application of small scale technologies in existing industries and for development of new industries based on these technologies. A review was carried out of health care industries, food and agriculture, transport indistries, energy and mining, computing and communications, environmental industries, chemicals and materials, building and construction, and security and defence.

Arising from this review, six main areas were identified where policy initiatives are required to make Victoria a leading centre for exploitation of small scale technologies. These are: facilitating infrastructure, raising awareness and demonstrating applications, building the skills base, encouraging commercial applications, facilitating alliances and networks, and strengthening social and ethical reflection .Initiatives are already underway in some of these areas.

Thursday 10 February
Poster Session One

Galaxy II and III **0800-1000**

POSTER GROUP 1	Ceramic Materials
POSTER GROUP 2	Hybrid and Nanocomposite Materials
POSTER GROUP 3	Materials Modelling
POSTER GROUP 4	Nanofibres and Nanotubes
POSTER GROUP 5	Molecular Materials and Devices
POSTER GROUP 6	Clusters, Quantum Dots and Nanoparticles
POSTER GROUP 7	Photo-Active and Radiation-Sensitive Materials
POSTER GROUP 8	Nanoscale Optics

POSTER SESSION 1

Thursday 10 February 2005 0800–1000

Galaxy Ballrooms II and III

POSTER GROUP 1 CERAMIC MATERIALS

PG1.1 **Mechanical properties and crack growth behavior in unpoled and poled ferroelectric PMN-PZT ceramics**
S. Jiansirisomboon, K. Songsiri and T. Tunkasiri

PG1.2 **Piezoelectric property of (*1-x*) $Pb(Zr_{1/2}Ti_{1/2})O_3$ -*x*$Pb(Zn_{1/3}Nb_{2/3})O_3$ ceramics prepared by columbite-(wolframite) precursor method**
N. Vittayakorn, G. Rujijanagul, X. Tan and D.P. Cann

PG1.3 **Phase formation and transitions in the lead magnesium niobate-lead zirconate titanate system**
S. Ananta, R. Tipakontitikul and R. Yimnirun

PG1.4 **Pyroelectric properties of Bi_3TiNbO_9-based ceramics at high temperature**
J. Barrel, K. MacKenzie and E. Stytsenko

PG1.5 **Structural investigation of the double Perovskites $(Sr,Ba)_2FeMoO_6$**
E.K. Hemery, J. Crisford, M.J. Dalley, G.V.M. Williams and H.J. Trodahl

PG1.6 **Preparation and characterization of barium iron niobate ($BaFe_{0.5}Nb_{0.5}O_3$) ceramics**
T. Tunkasiri, U. Intatha, S. Eitssayeam and K. Pengpat

PG1.7 **Effect of excess PbO on microstructure and mechanical properties of $(Pb_{0.975}Ba_{0.025})ZrO_3$ ceramics**
T. Bongkarn and G. Rujijanagul

PG1.8 **Fabrication and characterization of zirconia-baria solid solutions**
A. Udomporn, R. Paisan and L. Portia

POSTER GROUP 2 HYBRID AND NANOCOMPOSITE MATERIALS

PG2.1 **Carboxylic acids as crystal modifiers: the role of the hydrophobic chain**
G.E. Henderson, B.J. Murray and K.M. McGrath

PG2.2 **Flame retardant polymer nanocomposites**
F. Au, W. Gao and N.R. Edmonds

PG2.3 **Mechanical properties evaluation of PZT/Al_2O_3 composites prepared by a simple solid-state mixed oxide method**
C. Puchmark, S. Jiansirisomboon and G. Rujijanagul

PG2.4 **High energy milled nano-structured Ti-Al-oxide composite powders for plasma spray coatings**
J. Liang, Z. Li, K. Zhang, D. Zhang and W. Gao

PG2.5 **The dominant of CH bonding in a-C: H thin films grown by DC-PECVD at various chamber pressures**
Y.B. Wahab, S.A. Bakar and S. Sakrani

PG2.6 **Study on the properties of coal-tar-based carbon foam**
Y C. Zhang, X. Wang, J. Tian and Y. Wang

PG2.7 **Wollastonite fibre reinforced polyethylene composites in rotational moulding**
X.W. Yuan, D. Bhattacharyya and A.J. Easteal

PG2.8 **Spectroscopic properties of oxygen- and nitrogen-doped a-C:H : a nanostructural model**
S. Petrie, V.I. Grishko, W.W. Duley, and P. Bernath

PG2.9 **Study on thermal properties of energy storage fiber concrete**
W. Kong and L. Zou

PG2.10 **Atom ingress from synthetic biological fluid into nanoporous layers formed in titanium by helium ion-implantation**
P.B. Johnson, C.R. Varoy, V.J. Kennedy and A. Markwitz

POSTER GROUP 3 MATERIALS MODELLING

PG3.1 **Mechanistic modeling using AC impedance**
M. Urquidi-Macdonald

PG3.2 **Multi-scale modelling of ZnO nanorod formation and growth by electrochemical deposition**
J.R. Mackay, S. Hendy and M.P. Ryan

PG3.3 **Periodic ab initio study of silico-erionite**
C. Samaniego, D.H. Galván, A. Posadas-Amarillas and V.P. Petranovskii

PG3.4 **Si(001) c(4x2)-p(2x2) surface phase transitions induced by electric fields and doping**
W.G. Schmidt, K. Seino and F. Bechstedt

POSTER GROUP 4 NANOFIBRES AND NANOTUBES

PG4.1 **Growth and characterization of cubic hafnium oxide single crystal fibers**
A. Watcharapasorn, R.C. DeMattei, R.S. Feigelson, K.C. Chen and D. Krommenhoek

PG4.2 **Templated photofunctional nanotube arrays**
T. Kemmitt, M.E. Bowden and I.W.M. Brown

PG4.3 **Effect of arc parameters on CNT growth using a continuous reactor**
H.M. Yusoff and J. Abrahamson

PG4.4 **Carbon covalent-bonded nanotube junctions: structures, formation mechanism and transport properties**
L. A. Chernozatonskii, A.N. Andriotis, M.Menon, E. Mikheeva, D. Srivastava

PG4.5 **Temperature dependence of the thermal conductivity in chiral carbon nanotubes**
N.G. Mensah, G. Nkrumah ,S.Y. Mensah and F.K. Allotey

PG4.6 **Preparation and electrochemical characterisation of carbon nanotube microelectrodes**
N. Yahya, G.Z. Chen, G.A. Snook, V.P. Kotzeva and Derek J. Fray

PG4.7 **Bundles of boron-carbide nanotubes: effects of doping by Li and Cu**
O. Ponomarenko, M.W. Radny and P. V. Smith

PG4.8 **Self consistent calculation of nonlinear capacitance and its corresponding relaxation time in doped nanotube junctions**
K. Esfarjani, A.A. Farajian, Y. Kawazoe and S.T. Chui, K. Mehrany

POSTER GROUP 5 MOLECULAR MATERIALS AND DEVICES

PG5.1 **NMR T_2-relaxation dispersion of polymeric materials under shear**
A. Gottwald and P. T. Callaghan

PG5.2 **Substitution of dipyrido[3,2-*a*:2',3'-*c*]phenazine: an attempt to produce highly emissive materials**
A.G. Blackman, K.C. Gordon and N.J. Lundin

PG5.3 **Photoexcitation in metal polypyridyl OLED complexes: a spectroscopic and density functional theoretical study**
P.J. Walsh, K.C. Gordon and N.J. Lundin

PG5.4 **Transport studies of silver based fast ion conducting glassy system for battery applications**
Y. Chakravarthi and V.Chandramouli

PG5.5 **Towards smart membranes and surfaces for sensors and catalytic applications**
T.H. Lim, T. Borrmann, R. Batchelor, J.H. Johnston and J.L. Spencer

PG5.6 **Process of novel hydrothermal flow-reactor with adiabatic expansion cooling: toward production of functional biopolymer**
T. Goto, Y. Futamura, Y. Yamaguchi and K. Yamamoto

PG5.7 **Possible separation of an optical isomer from a racemic amino acid by kaolinite**
A H. Hashizume

PG5.8 **Measurement of polymer shear modulus using thickness shear acoustic waves**
G.J.Gouws, R.C.Holt and J.Zhen

PG5.9 **Regiospecificity in σ-dimerisation of terthiophenes: a density functional theory study**
T.M. Clarke and K.C. Gordon

PG5.10 **Study of plasma-polymerized tetraethylorthosilicate thin film**
M.A. Badsha, F. Ahmed, A.B.M.O. Islam and A.H. Bhuiyan

PG5.11 **Electrical properties in fuel cell based on DNA film**
Y. Matsuo, G. Kumasaka, J. Hatori, K. Saito and S. Ikehata

PG5.12 **Polymer films and LEDs: how to realise ultra low-cost and low-power chemical sensing platforms**
D. Diamond

PG5.13 **Novel buckyball functionalised terthiophene and polyterthiophenes - electrochemistry, synthesis, characterisation and applications**
J. Chen, G. Tsekouras, D.L. Officer, P. Wagner, C.Y. Wang, C.O. Too and G.G. Wallace

PG5.14 **Photovoltaic and electrochromic properties of poly(3-alkylthiophenes) and poly(3,3"-didecyloxyterthiophenes)**
G. Tsekouras, C. O. Too, G. G. Wallace, S. Gambhir, K. Wagner and D.L. Officer

POSTER GROUP 6 CLUSTERS, QUANTUM DOTS AND NANOPARTICLES

PG6.1 **High-density assembly of nanocrystalline silicon quantum dots**
A. Tanaka, Y. Tsuchiya, K. Usami, H. Mizuta and S. Oda

PG6.2 **Quantum dots conjugated with captopril while remained effective *in vivo***
N. Manabe, A. Hoshino, Y.-q. Liang, T. Goto, N. Kato and K. Yamamoto

PG6.3 **Charging effect of gold(Au) nano-particles embedded in SiO_2**
J.H. Kim, E.K. Kim and W.M. Kim

PG6.4 **Electrochemical detection of DNA hybridization amplified by CdS nanoparticles**
H. Peng, C. Soeller and J. Travas-Sejdic

PG6.5 **Fundamental and applied directions of field emission electronics using nanocluster carbon materials**
Yu.V. Gulyaev and S.A.Nikitov

POSTER GROUP 7 PHOTO-ACTIVE AND RADIATION-SENSITIVE MATERIALS

PG7.1 **Local field effects on the radiative lifetimes of Ce^{3+} in different hosts**
C.-K. Duan and M. F. Reid

PG7.2 **Advanced materials for dosimeter applications**
G.V.M. Williams, C. Dunford, S. Schweizer, J.–M. Spaeth, B. Henke, M. Secu and U. Rogulis

PG7.3 **Optical scattering in glass ceramics**
A. Edgar, R. Tilley, A. Bittar and G.V.M. Williams

PG7.4 **Simulation of the photoluminescence process of Er^{3+} and Si nanocrystal co-doped in silica**
C.-K. Duan

PG7.5 **The dynamics of crystalline structure formation in lumogen optical coatings**
A. Deslandes, A.B. Wedding, and J.S. Quinton

PG7.6 **Microstructure and optical study of Al implanted ZnO thin films**
J. Lee, C. Depagne, J. Metson, P. Evans and D. Bhattacharyya

PG7.7 **First principles calculations of the $4f^n \rightarrow 4f^{n-1}5d$ absorption spectra of Ce^{3+}, Pr^{3+}, Nd^{3+} in CaF_2, SrF_2, and BaF_2 crystals**
K. Ogasawara, T. Ishii, M.G. Brik and I. Tanaka

POSTER GROUP 8 NANOSCALE OPTICS

PG8.1 **Sub-wavelength localization of plasmon resonances evidenced by surface enhanced Raman spectroscopy**
E.C. Le Ru and P.G. Etchegoin

PG8.2 **Asymptotic behaviour of subwavelength nano-layer space charge toward conducting interface**
K. Mehrany and B. Rashidan

PG8.3 **Control of the optical transmission of metal films via excitation of surface plasmons**
L. Lin,S.J. Drake, R.J. Reeves and R.J. Blaikie

PG8.4 **Two-dimensional bandgap in a one-dimensional negative-index periodic structure**
I.V. Shadrivov, A.A. Sukhorukov and Y.S. Kivshar

PG8.5 **Light propagation through patterned nanoscale metallic polarisers**
A.T. Chin and R.J. Blaikie

Mechanical Properties and Crack Growth Behavior in Unpoled and Poled Ferroelectric PMN-PZT Ceramics

S. Jiansirisomboon*, K. Songsiri and T. Tunkasiri

Department of Physics, Faculty of Science, Chiang Mai University, Chiang Mai, 50200, THAILAND

Mechanical properties in terms of hardness and fracture toughness of unpoled and poled ferroelectric Lead Magnesium Niobate - Lead Zirconate Titanate (PMN-PZT) ceramics were investigated as well as their crack growth behaviors. Firstly, the ceramics with the formula $x\mathrm{Pb}(\mathrm{Mg}_{1/3}\mathrm{Nb}_{2/3})\mathrm{O}_3 - (1-x)\mathrm{Pb}(\mathrm{Zr}_{0.52}\mathrm{Ti}_{0.48})\mathrm{O}_3$ where x = 0.0, 0.2, 0.4, 0.6, 0.8 and 1.0 were fabricated using a conventional mixed-oxide method. Basic physical properties, i.e. density and volume shrinkage, and microstructure of the ceramics were observed. The densest ceramics of different PMN-PZT compositions were selected and some samples were subjected to electrical poling before mechanical investigation by indentation technique. The values of Vickers hardness (H_V), Knoop hardness (H_K), Young's modulus (E) and fracture toughness (K_{IC}) were compared between unpoled and poled ceramics. In the poled ceramics, the growth of radial crack was found to be dependent on the orientation of ferroelectric domains with respect to the poling direction. The crack length then showed significant anisotropy in the direction parallel and perpendicular to the poling which affected the K_{IC} values. However, the domain reorientation had no effect on H_V, H_K and E values. These values trended to reduce as increasing the mole ratio of PMN in PMN-PZT ceramics. Microstructure of fracture surfaces also revealed changes of mainly intergranular fracture mode in the monolithic PMN and PZT ceramics to a mixed mode of inter/trangranular fracture in PMN-PZT ceramics.

References

[1] S.L. Swartz, T.R. Shrout, Mater. Res. Bull., **17** (1982) 1245.
[2] F. Guiu, B.S. Hahn, H.L. Lee, M.J. Reece, J. Euro. Ceram. Soc., **17** (1997) 505.
[3] K. Mehta, A. Virkar, J. Am. Ceram. Soc., **73** (1990) 56.
[4] K. Okazaki, Bull. Am. Ceram. Soc., **63**[9] (1984) 1150.
[5] G.G. Pisarenko, V.M. Chushko, S.P. Kovalev, J. Am. Ceram. Soc., **68**[5] (1985) 259.
[6] J.M. Calderon-Moreno, F. Guiu, B. Jimenez, M.J. Reece, K.S. Sohn, Ferroelectrics, **228** (1999) 111.

* Contact author: sukanda@chiangmai.ac.th

Piezoelectric property of $(1-x)$ $Pb(Zr_{1/2}Ti_{1/2})O_3$ -$xPb(Zn_{1/3}Nb_{2/3})O_3$ ceramics prepared by columbite-(wolframite) precursor method.

Naratip Vittayakorn*, Gobwute Rujijanagul

Department of Physics Faculty of Science
Chiang Mai University
Chiang Mai 50200
THAILAND

Xiaoli Tan and David P. Cann

Materials Science and Engineering Department
Iowa State University
Ames, IA 50011 USA

Abstract – The solid solution of perovskite structure $xPb(Zn_{1/3}Nb_{2/3})O_3$–$(1-x)Pb(Zr_{1/2}Ti_{1/2})O_3$ with x = *0.1 - 0.5* has been synthesized via columbite-(wolframite) precursor method. Columbite structure $ZnNb_2O_6$ and wolframite structure $ZrTiO_4$ has been prepared for precursors. Phase development of calcined powder precursor was analyzed by x-ray diffraction. The phase-pure perovskite phase of PZN–PZT ceramics was obtained over a wide compositional range. Microstructure and piezoelectric properties were characterized by means of scanning electron microscopy (SEM), d_{33} meter and Impedance Analyzer. It has been found that Ultra-high piezoelectric properties were observed in composition close to MPB. The maximum value of d_{33}(690pC/N) and the highest k_p(0.7) were recorded for composition x = 0.3. Furthermore another composition that observed high value of d_{33}(600) and k_p(0.67) were x = 0.5. Both compositions closed to MPB of this system.

Phase Formation and Transitions in The Lead Magnesium Niobate-Lead Zirconate Titanate System

S. Ananta*, R. Tipakontitikul, R. Yimnirun
Department of Physics, Faculty of Science, Chiang Mai University, Chiang Mai, Thailand.

Lead-based complex perovskite compounds are among the most important smart materials for applications in electronics and microelectronics owing to their excellent ferroelectric, piezoelectric, and dielectric properties [1]. They are widely used as the main constituent in many types of applications such as capacitors, actuators, transducers and electro-optic devices [2]. The investigation of phase formation and transitions are believed to have significance from both theoretical and practical view points. However, studies on these aspects in the PMN-PZT system are rarely reported.

In the present work, phase formation and transition characteristics of smart materials in the $(1-x)Pb(Mg_{0.33}Nb_{0.67})O_3 - xPb(Zr_{0.52}Ti_{0.48})O_3$, $(1-x)$PMN-xPZT system prepared by a modified mixed-oxide synthetic route have been investigated by varying the chemical compositions and calcination conditions. Lattice parameters and crystallite size changes were examined as a function of composition. The results show that complete solid solutions of perovskite-like phase in the $(1-x)$PMN-xPZT system were obtained. With increasing PZT content, the degree of tetragonality and the optimum firing temperature increased continuously. The perovskite phases undergo the transitions pseudocubic => rhombohedral => coexistence of rhombohedral and tetragonal => tetragonal in the x value range 0.0-1.0.

References

[1] A.J. Moulson and J.M. Herbert, *Electroceramics*, 2nd ed., (Wiley-Interscience, New York, 2003).
[2] K. Uchino, *Piezoelectrics and Ultrasonic Applications* (Kluwer, Deventer, 1998).

* Contact author: suponananta@yahoo.com

Pyroelectric properties of Bi_3TiNbO_9-based ceramics at high temperature

Jeremie Barrel[1], Kenneth MacKenzie[1,2], Eugene Stytsenko[2]
[1]*MacDiarmid Institute for Advanced Materials and Nanotechnology, Victoria University of Wellington, P.O. Box 600 Wellington*
[2]*NZ Institute for Industrial research and Development, Lower Hutt*

The pyroelectric properties of bismuth niobate titanate doped with acceptor ions (Sr_{Bi}, Ca_{Bi}, Pb_{Bi} and Fe_{Ti}), donor ions (Nb_{Ti} and W_{Ti}) and isovalent ions (Y_{Bi} and Zr_{Ti}) have been studied. The ceramics were prepared by solid state reaction and hot-pressed sintering to achieve grain orientation. Their crystal structures were investigated by X-ray diffractometry.

The pyroelectric coefficient ρ, dielectric constant ε, loss tangent tan δ and Curie temperature was measured at 900°C to evaluate the effect of composition and grain orientation on the figures of merit F_V and F_D to identify the most suitable Bi_3TiNbO_9-based ceramic for high-temperature pyrosensor applications.

Structural Investigation of the Double Perovskites $(Sr,Ba)_2FeMoO_6$

E.K. Hemery[1], J. Crisford[2], M.J. Dalley[1], G.V.M. Williams[2] and H.J. Trodahl[1]
[1] *School of Chemical and Physical Sciences, Victoria University of Wellington, NEW ZEALAND*
[2] *Industrial Research Ltd., Lower Hutt, NEW ZEALAND*

Several double perovskites are thought to have half metallic ground states, with the magnetic order persisting to well above ambient temperature [1], and they have consequently gained attention recently for their potential as a source of spin polarized electrons for spintronics device injection. The most heavily studied in this context has been Sr_2FeMoO_6 (SFMO), though more recently attention has also been afforded other members of the class, including Ba_2FeMoO_6 (BFMO) [2,3] and various mixed and oxygen deficient double pervoskites. The IRL-VUW group has undertaken a study of several of these materials as part of an ongoing programme on strongly correlated transition metal oxides, particularly conducting oxides. This paper focuses on studies of the polycrystalline ceramic materials prepared in a solid-state reaction, and particularly the nature of the crystallite surfaces.

Although the main thrust of our research in these materials is toward their half metallicity, it is interesting that at the present the most advanced proposals for their exploitation is associated with a very strong low-field *negative* magnetoresistance. It is found in ceramic polycrystalline material, and is clearly associated with a field-sensitive tunnelling between grains, through a non-conducting $SrMoO_4$ film that forms on their interfaces. The magnetoresistance has potential for sensing elements in magnetic read heads.

Stoichiometric SFMO and BFMO ceramic samples were prepared from the corresponding oxides and nitrides after decomposing at 700 °C for 60 minutes. The powder was then pressed into pellets and sintered in air at 1200 °C for 5 hours. This was followed by sintering at 1100 °C in $4\%H_2/96\%N_2$ gas for 800 minutes.

This poster will present SEM, EDS, Raman spectroscopy and XRD results on as-prepared and aged ceramic pellets. Although immediately after reaction the material appears to be very close to phase pure, there is a development over several months in air of both a surface layer with a composition that differs significantly from the parent material, and a coarser phase separation locating significant Fe in separate islands easily seen in SEM and even conventional optical microscopy. These developments have been studied by their Raman signatures as well as by elemental EDS analysis.

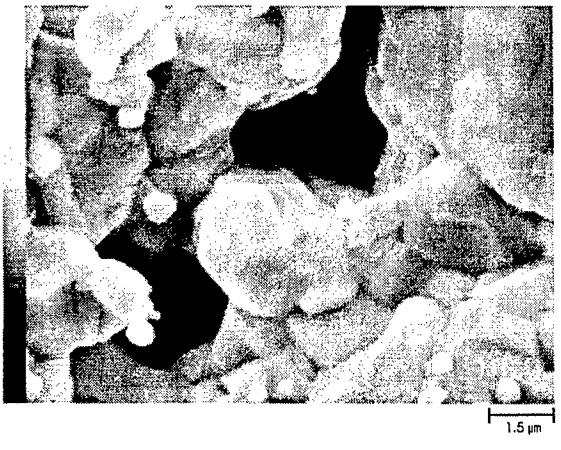

Figure 1. Scanning electron microscope image of an aged BFMO sample. EDS analysis showed that the majority of the sample has kept its initial stoichiometric values. However the distribution is not uniform; in particular the bright spots with diameters of about 0.5 µm are composed of mainly Fe and O.

References

[1] K.I. Kobayashi, T. Kimura, H. Sawada, K. Terakura, Y. Tokura, Nature **395**, 677 (1998).
[2] N. Nguyen, F. Sirti, C. Martin, F. Bourée, J.M. Grenèche, A. Ducourt, F. Studer, B. Raveau, J. Phys. Condens. Matter **14**, 12629 (2002).
[3] Z. Szotek, W.M. Temmerman, A. Svane, L. Petit, G.M. Stocks, H. Winter, J. Magn. Magn. Mater. **272-276**, 1816 (2004).

Preparation and Characterization of Barium Iron Niobate ($BaFe_{0.5}Nb_{0.5}O_3$) Ceramics

T. Tunkasiri*, U. Intatha, S. Eitssayeam and K. Pengpat
Department of Physics, Faculty of Science, Chiang Mai University, Chiang Mai 50200, THAILAND

Barium Iron Niobate ($BaFe_{0.5}Nb_{0.5}O_3$: BFN) is a relaxor ferroelectric material that has a diffuse phase transition (DPT) with a broad maximum in the temperature dependence of the dielectric constant. This ceramic is useful for high voltage capacitors and other applications. In this research, ceramic powder of BFN was synthesized by the solid state reaction technique and calcined at 800 - 1200°C for 4 hrs with 5°C/min heating and cooling rate. The phase identification of calcined powders was performed using X-ray diffraction technique (XRD). The XRD patterns show that pure cubic BFN powder could be obtained at 1200°C. The powder was then pressed into disc shape which were subsequently sintered at 1250 - 1400°C for 4 hrs with 5°C/min heating and cooling rate. Densities of the sintered discs were determined by Archimedes principle. The microstructure of the ceramics were examined by the scanning electron microscopy (SEM). The frequency and temperature dependence of dielectric constant were presented.

References:

[1] M.A. Subramanian, D. Li, N. Duan, B.A. Reisner and A.W. Sleight, J. Solid State Chem. **151**, 323 (2000).
[2] C.C. Homes, T. Vogt, S.M. Shapiro, S. Wakimoto and A.P. Ramirez, Science. **293**, 673 (2001).
[3] J.B. He, ,J.B. Neaton, M.H. Cohen, D. Vanderbilt and C.C. Homes, Phys. Rev. *B.* **65**, 214112 (2002).
[4] D.C. Sinelair, T.B. Adams, F.D. Morrison and A.R. West, Appl. Phys. Lett. **80**, 2153 (2002).
[5] I.P. Raevski *et al.*, J. Appl. Phys, **93**, 4130 (2003).
[6] S. Saha and T.P. Sinha, J. Phys.: Condens. Matter, **14**, 249 (2002).

* Contact author: tawee@chaingmai.ac.th

Effect of Excess PbO on Microstructure and Mechanical Properties of $(Pb_{0.975}Ba_{0.025})ZrO_3$ ceramics

T. Bongkarn* and G. Rujijanagul
Department of Physics, Faculty of Science, Chiang Mai University, Chiang Mai, 50200, THAILAND

$(Pb_{0.975}Ba_{0.025})ZrO_3$ (PBZ) ceramics were fabricated from their oxide mixture via the solid state reaction method. Excess PbO (1, 3, 5 and 10 wt%) was added together with starting materials to compensate for PbO loss from evaporation during calcination and sintering. The phase structure was analyzed by XRD. Pure PBZ phase was observed in any of the PBZ samples. Density, dielectric and mechanical properties were measured. The experimental results suggest that 1% excess PbO is the optimize level to obtain the best properties of the ceramics. The results were discussed in terms of the mechanisms of densification.

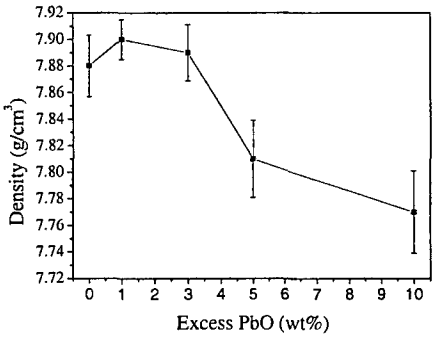

Fig. 1. Variation of density of sintered pellets as a function of starting Pb excess.

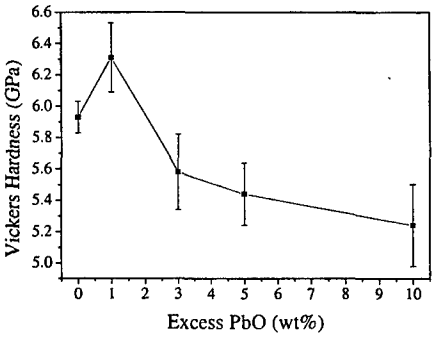

Fig. 2. Variation of Vickers hardness of sintered pellets as a function of starting PbO excess.

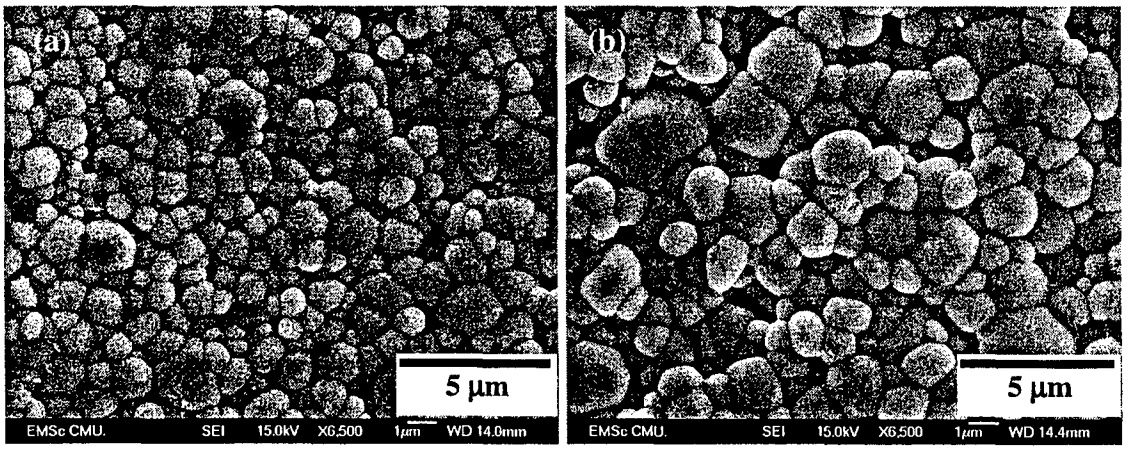

Fig. 3. SEM micrograph of as-sintered pellet made from starting powders with different PbO content: (a) no excess PbO and (b) excess PbO 3 wt%.

Acknowledgement

This work was supported by The Thailand Research Fund (TRF).

References

[1] I.H. Ismailzade, O.A. Samedovert, Phys. Stat. Sol. (a) **90**, 445 (1985).
[2] B.P. Pokharel, M.K. Datta, D. Pandey, J. Mater. Sci. **34**, 691 (1999).
[3] B.P. Pokharel, D. Pandey, J. Appl. Phys. **88**, 5365 (2000).

* Contact author: researchcmu@yahoo.com

Fabrication and Characterization of zirconia-baria Solid Solutions

A. Udomporn*, R. Paisan and L. Portia
Department of Physics, Faculty of Science, Mahasarakham University, Mahasarakham, Thailand

Zirconia, ZrO_2, ceramics is member of structural ceramics. They exhibit phase transformation as follow: monoclinic ← 1170° → tetragonal ← 2370° → cubic ← 2760 →melt.[1] The monoclinic to tetragonal phase transformation is likely martenstic in nature. This transformation has generated great interest among scientist and technologist because it contributes to the toughening of ceramic.[2] In this study, two major aspects have been carried out in order to determine the relationship between preparation condition and structural characteristic of the barium additions on sintering of ZrO_2. It has been found that zirconia-baria powders were successfully obtained for calcination conditions of 1100 °C/min for 3 h with heating/cooling rates of 20 °C/min. $Zr_{(1-x)}Ba_xO_2$ ceramics have been fabricated by sintering $Zr_{(1-x)}Ba_xO_2$ powders via a normal sintering method. It has been observed that $Zr_{(1-x)}Ba_xO_2$ ceramics of high density and optimised phase may be produced by use of a straightforward sintering conditions, i.e. 1450 °C for 2 h with heating/cooling rate of 15 °C/min. The ratios of tetragonal to monoclinic phase in $Zr_{(1-x)}Ba_xO_2$, where x between 0.05 to 0.10, were investigated by x-ray diffraction patterns. The results indicated maximum content of tetragonal phase obtained under content of barium at 0.10 mol%.

References

1. Stevens, R., Introduction to Zirconia, Magnesium Elektron LTD., Manchester, U.K.(1986).
2. Mashino, S. et al., *J. Euro. Ceram. Soc*, 24: 2241-2246, (2004).

*Contact author: au_wow@yahoo.com

Carboxylic Acids as Crystal Modifiers: The Role of the Hydrophobic Chain

G. E. Henderson[1], B. J. Murray[2]and K. M. McGrath[2,*]
[1] *Department of Chemistry, University of Otago, POBox 56, Dunedin, NEW ZEALAND*
[2] *School of Chemical and Physical Sciences, Victoria University of Wellington, POBox 600, Wellington, NEW ZEALAND*

Composite materials are a common occurrence in modern life. The classification of composites can be thought to encompass materials spanning from alloys, comprising a blend of at least two metals or a metal and a non-metal, to biominerals, which meld together an inorganic material with organic components such as proteins. Whatever the example used to describe them, one feature that distinguishes composites and highlights their importance, as a class is that their physical properties, such as tensile strength, are superior to those of their integral components. The technology however is not new. Metal alloys have been known since 2000 BC and biominerals have existed for at least 550 million years. For the case of biominerals, however, the secret of their manufacture is locked in the organisms that synthesize them.

Biomaterials, fabricated by flora and fauna, include as their base inorganic the widely spread calcium phosphates and carbonates (e.g. human bones, egg shells and gravity receptors), silicates (skeletal plant material) and iron oxides (magnetic field receptors) through to the rarities of materials such as strontium sulphate (marine organism skeleton). Irrespective of the inorganic material used as the final biomineral, its nucleation and growth are manipulated by organic molecules or matrices present in the growth medium leading to enhanced physicochemical properties, highly specific nucleation and growth, which differs markedly from the parent inorganic material, and hierarchical patterning on length scales ranging from nanometres to metres. That is, biological organisms decide not only what inorganic material they will deposit, thereby controlling chemical reactivity and response, but also the precise morphological form and three-dimensional connectivity of the material, aiding in the manipulation and control of this reactivity and the material's physical characteristics.

The manipulation of biomineralization processes is an increasingly widely investigated discipline, with one aim being the generation of biomineral-like materials with readily manipulated physicochemical properties through hierarchical patterning that can be controlled over a wide range of length scales. Acidic glycoproteins are often found as occlusions in biominerals [1]. Calcium carbonate crystal growth studies have shown that the presence of these proteins controls both the polymorph that is nucleated and also the final crystal habit [2,3]. These proteins consist of carboxylic acid functionalities and saccharide residues in addition to the amino acid residues making up the polymer backbone. Here we have investigated the role of the carboxylic acid moiety and its inherent hydrophilicity as a component of a wider study aimed at understanding the role of each of the principle functionalities in the protein in the biomineralization mechanism.

Calcium carbonate growth could be manipulated with a molecule as small as acetic acid when coupled to varying environmental pH and carbon dioxide availability. This manipulation of the calcium carbonate crystal growth could be modified by varying the inherent hydrophobicity of the carboxylic acid through the length of the hydrocarbon chain, indicating that hydrophilic/hydrophobic pockets on the protein coupled with the presence of the carboxylic acid moiety could be important in controlling biomineralization *in vivo*.

References

[1] S. Albeck, L. Addadi, and S. Weiner, Conn. Tissue Res. **35**, 365 (1996).
[2] S. Albeck, S. Weiner, and L. Addadi, Chem.-A Eur. J. **2**, 278 (1996)
[3] C. R. MacKenzie, S. M. Wilbanks, and K. M. McGrath, J. Mater. Chem. **14**, 1238(2004).

* kathryn.mcgrath@vuw.ac.nz

FLAME RETARDANT POLYMER NANOCOMPOSITES

F. Au [1]*, W. Gao [1] and N.R. Edmonds [2]
[1]*Department of Chemical and Materials Engineering,* [2]*Department of Chemistry,*
The University of Auckland, New Zealand

Industries have been using halogenated organic compounds as flame retardants for many polymers. However, halogenated organic compounds are non-recyclable and not environmentally friendly, as dense smoke, toxic and corrosive compounds are formed as by-products in a fire. Therefore there is an increasing interest in the development of halogen-free flame retardants, and polymer nanocomposites are the latest development.

Flame retardants function by several mechanisms; the removal of heat or oxygen from combustible materials, the absorption or restriction of flammable gases from joining the fire, the coupling with active radicals that propagate the fire, and prevention of the polymer from flowing after it has been melted [1]. Synthetic polymers have no natural flame retardant capacity with the exceptions of some linear polymers like the Teflon family and polymers with aromatic structures. During a fire they melt, drip, evolve flammable gases, and leave no carbonaceous residue. Flame retardants have proven to be effective in reducing the flammability of polymers.

For the last decades, plastics industries have shown great interest in using nano-particle fillers in polymers. There are many advantages of using nano-structured fillers rather than conventional reinforcement additives such as glass fibres and talc. Nanocomposites exhibit unparalleled mechanical and barrier properties at low loadings (3–5% compared to 30-40% using conventional fillers).

By mixing clay nanocomposites with a thermoplastic polymer, flammability is lowered without sacrificing the mechanical properties. This is an advantage over the existing condensed-phase flame retardants. Polymer nanocomposites are also more environmentally friendly as layers of char are formed when the nanocomposites are exposed to flame.

Several mechanisms have been suggested as to how layered silicate has improved the flame retardancy of nanocomposites. Firstly, there is an increase in char layers formed when the nanocomposites were exposed to flame. This layer inhibits oxygen transport to the flame front and therefore reduces the heat release rate of the burning polymer. Another possible mechanism is the catalytic ability of the layered silicates. At higher temperatures, the inorganic nanoclay has the ability to act as radical sink due to absorption of Lewis acid sites. This interrupts the burning cycle as radical species are needed to break polymer chain to the oligomer fuel. The disordered nanocomposites also inhibit oxygen and combustible oligomer transfer by increasing the path length of these species to the flame front [2].

The polymer nanocomposites prepared can be characterized using X-Ray Diffraction (XRD) and Transmission electron Microscopy (TEM). Heat deflection temperature (HDT) is also used to measure the extent of intercalation in the nanocomposites system. Cone calorimeter tests are used to measure the heat release rate and analyze the gas given out when the sample is exposed to flame. This paper presents our research results for the processing, composition, microstructure and properties of polymer-clay nanocomposites.

References

[1] G. Amarasinghe et al, *Non-Halogenated Flame Retardants for Polyolefins*

[2] K.A. Beall, *Annual Conference on Fire Research,* **1998, 39**

[1]* Contact author: F. Au, email: franau@hotmail.com

Mechanical Properties Evaluation of PZT/Al_2O_3 Composites Prepared by a Simple Solid-State Mixed Oxide Method

C. Puchmark*, S. Jiansirisomboon, and G. Rujijanagul
Department of Physics, Faculty of Science, Chiang Mai University, Chiang Mai, 50200, THAILAND.
T. Comyn and S. J. Milne.
Institute for Materials Research, University of Leeds, Leeds, LS2 9JT, UK.

A ferroelectric lead zirconate titanate (PZT) based composites contained nano-particles of Al_2O_3 were prepared by a simple solid-state mixed oxide method. Sintering procedure was carried out at 1200°C for 2h with a heating/cooling rate of 5°C/min. Phase formation and microstructure were fully examined by XRD and SEM, respectively. In this study, composite ceramics with high density were simply achieved through a normal mixed oxide procedure. Effects of Al_2O_3 additive on mechanical properties were investigated. Mechanical properties in terms of hardness and fracture toughness were determined using a Vickers indentation technique and were evaluated as a function of Al_2O_3 volume fraction between 0-2%. The hardness of the composites tended to improve with an addition of the nano-particles, while the fracture toughness tended to reduce. The maximum hardness and minimum toughness were received at PZT/1vol%Al_2O_3. The mechanical results were related to the microstructure and compared with the previous result reported earlier by the others.

Acknowledge
This work was supported by The Thailand Research Fund (TRF).

References
[1] K. Tajima, H. Hwang, M. Sando, *J. Am. Ceram. Soc.* **83**, 651 (2000).
[2] K. Tajima, H. Hwang, M. Sando, *J. Eur. Ceram. Soc.***19**, 1179 (1999).
[3] M. Sternitzke, *J. Eur. Ceram. Soc.* **17**, 1061 (1997).

* Contact author: kungmic2002@yahoo.com

High Energy Milled Nano-Structured Ti-Al-Oxide Composite Powders for Plasma Spray Coatings

Jing Liang [1*], Zhengwei Li [1], Kai Zhang [1], Deliang Zhang [2] and Wei Gao [1]
[1] *Dept of Chemical & Materials Engineering, the University of Auckland, New Zealand*
[2] *Dept of Materials and Processing Engineering, the University of Waikato, New Zealand*

Abstract

Ti-Al-oxide composite powders were produced by high energy mechanical ball milling, sintering and grinding. The as-milled powders were characterized as a TiO_2/Al composite with particle size around 200 nm, shown in Fig 1. The as-heat treated powder was identified as a intermetallic based composite consisting of Ti-Al(O) and Al_2O_3 phases. Plasma spraying was used to coat these powders onto Ti-6Al-4V alloy samples. High temperature oxidation and hot corrosion behaviour of the composite coatings was studied in dry air and Na_2SO_4 + NaCl vapour. The results showed that Ti-Al-oxide composite coatings have a much improved oxidation and hot corrosion resistance compared to the substrate Ti-6Al-4V alloy, shown in Fig 2. The oxide scales have excellent adhesion to the coatings, showing superior scale spallation resistance. The mechanisms with which the coatings improved the oxidation resistance were studied based on microstructural analysis. It is believed that these types of composites can provide a new generation of coatings to the Ti based alloys which will be able to raise the application temperature of Ti alloys from 650°C to 800-900°C.

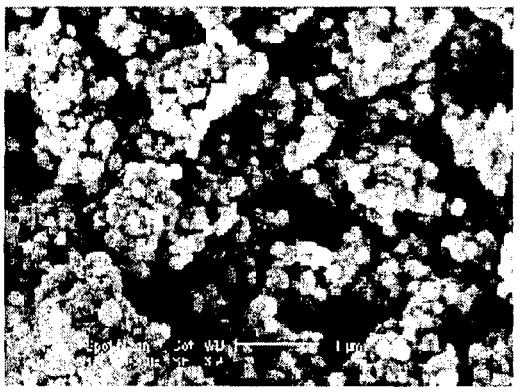

Fig 1. Morphology of as-milled composite powder particles.

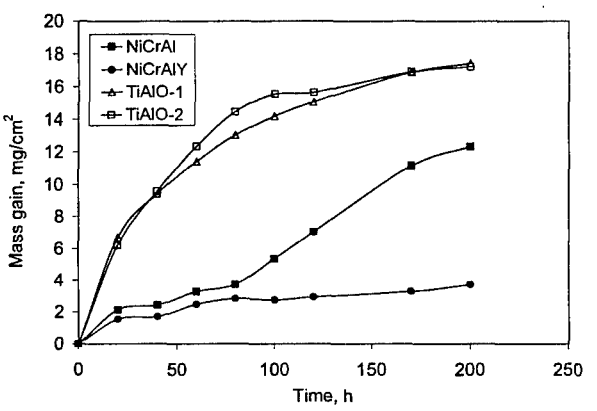

Fig.2 The Kinetics of the hot corrosion test in the Na_2SO_4 + NaCl vapour at 800°C.

Keywords: Ti-Al intermetallic compounds, nano-structured composites, ball milling, plasma spray coatings, high temperature oxidation

* Presenting Author: Dr. Jing Liang, email: jlia010@ec.auckland.ac.nz

The Dominant of CH Bonding in a-C: H Thin Films Grown by DC-PECVD at Various Chamber Pressures

Y. B. Wahab, S. A. Bakar and S. Sakrani

Nanostructure and Nanophysics Laboratory
Ibnu Sina Institute for Fundamental Science Studies
Universiti Teknologi Malaysia
81310 UTM Skudai, Johor
Tel:607-5534094 Fax: 607-5536080
E-mail: ybw@ utm.my

Hydrogenated amorphous carbon thin films (a-C: H) have been of great scientific interest since their advent for mechanical, chemical, optical and electrical applications, owing to their flexible properties depending on specific deposition conditions. Their final resulting properties seem to be determined from their microscopic structure compromised by the local bonding configuration among carbon-carbon and carbon hydrogen atoms in the film matrix, which can be varied by choosing the appropriate external deposition parameters. In this work the bonding configurations of PECVD's deposited a-C: H films are studied using infrared analysis under varying deposition pressures of 0.1- 0.8 torr or an equivalent electrical power between 0.30 – 0.16 W. Other fixed parameters were 5 sccm CH_4 flow rate, 2.5 cm electrode spacing, and room temperature deposition for the periods of 5 hrs. It was observed that, form IR Spectroscopy the relevant CH bonding in the stretching frequency range, 2700 - 3200 cm^{-1} appeared to be dominant if compared to those of CC bonding. Essentially, the stretching of the measured spectrums seemed to be in wavy-like curves associated with sp^mCH_n configurations with m, n = 1-3, and this trend was gradually disappearing with an increase of pressure up to 0.8 torr. The curve measured at 0.2 torr indicated marked changes with detectable infrared absorption rates in a-C: H at 2959 cm^{-1}, 2934 cm^{-1} and 2872 cm^{-1}, which were corresponded to the presence of sp^3CH_3 (both symmetric and asymmetric) and sp^3CH_2 (asymmetric). A further investigation using XRD analysis confirmed the amorphous of the as-prepared a-C: H thin films.

Study on the properties of coal-tar-based carbon foam

Changxing Zhang*, Xinying Wang, Jing Tian and Yimin Wang
College of Material and Engineering, DongHua University, Shanghai, CHINA

Abstract A novel process for the preparation of coal-tar pitch based carbon foam was introduced. Infrared Ray (IR) and Wide angle X-ray diffraction (WAXD) were used for the characterization of the properties of coal-tar mesophase pitch. Scanning electron microscope (SEM) was used for the morphological study of resulted carbon foam, and the thermal properties and mechanical properties were also measured. The results showed that the carbon foam with pore size from 300~500μm, density from 0.2~0.5g/cm-3 and high thermal conductivity could be successfully obtained for different applications.

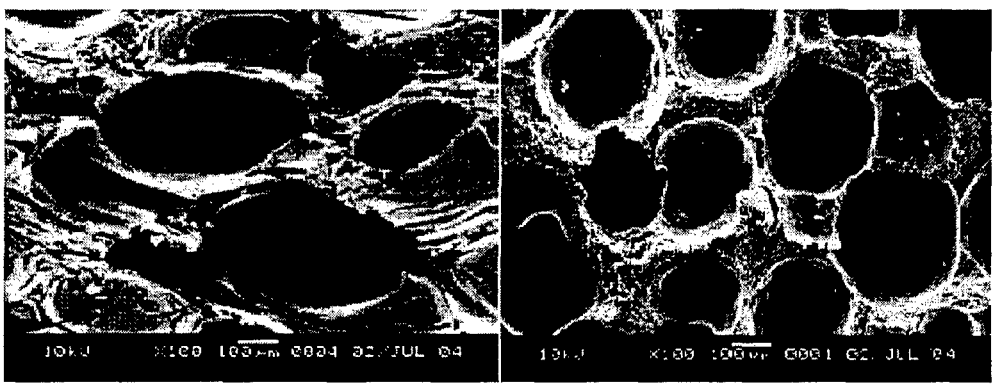

Fig.1 SEM pictures of coal-tar-pitch derived foam

References

[1] Nidia C.Gallego and James W.Klett, Carbon, B41, 1461 (2003).
[2] White,J.L. and P.M.Scheaffer, Carbon, B27, 697 (1989)
[3] Klett JW. US patent 6033506, (2000)
[4] James Klett, Rommie Hardy and Ernie Romine, Carbon, B38, 953 (2000).
[5] Koichi Kanno, Hirotaka Tsuruya and Takeshi Koshikawa, US patent 6689336 B2, (2004).
[6] Murdie, Neil (South Bend, IN), Pigford and James F., US Patent 6,315,974, (2001).
[7] Kim CJ., Ryu S. K. and Bhee B.S., Carbon, B31, 833 (1993).

*Contact author: yd_zh78@163.com

Wollastonite Fibre Reinforced Polyethylene Composites in Rotational Moulding

X. W. Yuan[1*], D. Bhattacharyya [1] and A. J. Easteal [2]
Centre for Advanced Composite Materials
[1] *Department of Mechanical Engineering, University of Auckland, Auckland*
[2] *Department of Chemistry, University of Auckland, Auckland*

The rotational moulding industry has achieved a growth rate of more than 10% per annum over the last decade. As a manufacturing process it involves charging a metal mould with powdered polymer, then heating the mould while it is slowly rotated about two perpendicular axes so that the polymer melts to form a coating on the inside of the mould. Rotational moulding has significant advantages over other methods such as injection moulding and blow moulding for the production of large hollow plastic parts but at the same it is limited by its dependence on the dominant use of polyethylene as the base polymer [1,2]. Polyethylene is suited because of its thermal stability, low cost and the low melting point but its low mechanical strength and stiffness must be often improved to meet the product requirements.

Wollastonite is a naturally-occurring calcium silicate mineral with the molecular formula $CaSiO_3$, usually formed from the reaction of calcium carbonate and silica under intense heat and pressure. Its calcium silicate structure grows naturally as a chain, resulting in needle-like crystals [3]. The high aspect ratio needles in wollastonite are retained by appropriate milling, or broken into lower aspect ratio fragments as required for particular applications. For the reinforcement of plastics, smaller and higher aspect ratio particles expose greater surface area to better intercept stress propagation [4,5]. The addition of micro- to nano-size fillers to polymeric materials has been observed to significantly influence the mechanical properties of polymeric materials such as modulus, yield stress, and strain to fracture, which have a strong bearing on the resistance to mechanical deformation [6,7]. As a natural mineral, wollastonite is readily available in the market for commercial applications, and is considerably less expensive than other synthetic fibres. It has, therefore, the potential for developing high performance polyethylene products.

In the present study the process of creating wollastonite-polyethylene composites involved blending, compounding by extrusion and then rotational moulding. Prior to the incorporation into a polymer matrix, wollastonite micro-fibres were characterised in terms of morphology and aspect ratio using scanning electron microscopy (SEM). The three point bending, tensile and impact tests were used to characterise the wollastonite reinforced polyethylene composites. The effects of filler volume fraction, varied from 5 to 40 vol%, and the compatibilisers of silane and maleated polyethylene (MAPE) on the flexural modulus and strength, tensile strength, elongation, Young's modulus, and impact strength were investigated. Morphological observations of the fracture surface of wollostonite-polyethylene composites were performed by SEM. Increasing the filler content caused an increase in Young's modulus and flexural strength, and decreased elongation and impact strength. Incorporation of MAPE provided a better overall balance of stiffness and impact strength. The effects of the aspect ratio of wollastonite are also discussed and it is proposed that small size with high aspect ratio fillers (such as wollastonite) provide a large interfacial area between the filler and the polymer matrix and influence the mobility of the molecular chains [8].

References

[1] R.J. Crawford, *Rotational moulding of plastics (second edition)*, (Research Studies Press LTD, 1996).
[2] R.J. Crawford and A. Robert, in *Proceedings of the Third Asian-Australasian Conference on Composite Materials (ACCM-3), Auckland, 2002*, edited by D. Bhattacharyya, et al.
[3] P.A.Ciullo, *Wollastonite A Versatile Functional Filler*, in *Paint & Coating Industry Magazine*. 2002.
[4] S. Ahmed and F.R. Jones, J. Mater. Sci. **25,** 4933 (1990).
[5] C.J.R. Verbeek, Materials Letters. **57,** 1919 (2003).
[6] Z.J. Gao and A.H. Tsou, J. Poly. Sci. Part B-Polymer Physics. **37**(2), 155 (1999).
[7] C.B. Ng, et al., Advanced Composites Letters. **10**(3), 101 (2001).
[8] A. Dasari, S. Sarang, and R.D.K. Misra, Mater. Sci. Eng. **A368,** 191 (2004).

Spectroscopic Properties of Oxygen- and Nitrogen-Doped a-C:H : A Nanostructural Model

S. Petrie,[1] V. I. Grishko,[2] W. W. Duley,[2,*] and P. Bernath[2,3]
[1] *Chemistry Department, the Faculties, the Australian National University, Canberra ACT 0200, Australia*
[2] *Department of Physics, University of Waterloo, ON N2I 3G1, Canada*
[3] *Department of Chemistry, University of Waterloo, ON N2I 3G1, Canada*

Laser ablation of graphite, in the presence of H_2 and/or other gases, yields heteroatom-doped hydrogenated amorphous carbon (a-C:H). We have previously reported the near- and mid-IR emission and absorption spectra of such N- and O-doped material,[1] prepared using N_2, NH_3, O_2 or CO. Doping of a-C:H in this manner is seen to result in markedly different spectra than those obtained from 'standard' a-C:H. Here we report measurements on the far-IR spectra of O-doped a-C:H. Density functional calculations on relevant model compounds are also presented.

Our density functional theory calculations were performed at the B3-LYP/4-31G level of theory, which has been identified [2] as a highly efficient and reliable method for obtaining spectra of larger molecules. This level of theory permitted the geometry optimization and calculation of vibrational frequencies for a series of O-doped model compounds including PAHs, adamantane-like structures and 'locally aromatic polycyclic hydrocarbons' (LAPHs). We have proposed [3] that the latter class of hydrocarbons provide an excellent 'model in miniature' for the structural and spectroscopic properties of a-C:H. Calculations performed for the present work encompassed species containing between 20 and 40 carbon atoms.

In our B3-LYP/4-31G calculations, a range of O-containing functional groups (carbonyl, carboxylic, ether, and hydroxyl groups) were variously embedded in our 'model compounds'. Substantially the best match with the experimentally observed far-IR features (a strong, broad, and modulated band covering $\nu \sim 450$ to 200 cm^{-1}) is provided by the intense torsional modes associated with OH groups, which dominate the calculated emission spectrum below 400 cm^{-1}. Quantum chemical calculations on such low-frequency modes are subject to comparatively large errors, and so the far-IR frequencies obtained in our B3-LYP/4-31G calculations are not expected to be highly reliable. On the other hand, there is fair to good overlap between calculated and observed features, and none of the other functional groups explored yield any comparably bright low-frequency modes. We therefore assign the strong, broad, far-IR band seen in the lab spectra to OH torsional modes in the O-doped a-C:H. (Our analysis does not preclude the occurrence of other O-containing functional groups, e.g. ketone or ether functions, in the lab samples; we merely note that the latter groups appear incapable of reproducing the observed intense far-IR band). It is likely also that the dominant far-IR bands seen in N-doped a-C:H spectra arise from analogous modes involving torsional motion of amine ($-NH_2$) groups.

Hydrogenated amorphous carbon, from laser ablation of graphite, is widely regarded as a convenient model for both the soot particles which form in fuel-rich flames and for the carbonaceous material produced in various astrophysical environments. Since such environments are invariably subject to contamination by elements other than H and C, an understanding of the spectroscopic implications of heteroatom doping of a-C:H should allow a more complete interpretation of the astrophysically-observed spectra. We propose also that the intense low-frequency torsional modes in such material provide a particularly effective mechanism for the radiative cooling of such particles. Other implications, for the chemistry and physics of carbonaceous material in flames, in astrophysical plasmas, and in other environments, are likely to follow from the derivatization of a-C:H by highly polar OH (and NH_2) groups.

References

[1] V.I. Grishko and W.W. Duley, Astrophys. J. **568**, 448 (2002).
[2] C.W. Bauschlicher and S.R. Langhoff, Spectrochim. Acta A **53**, 1225 (1997).
[3] S. Petrie, R. Stranger and W. W. Duley, Astrophys. J. **594**, 869 (2003).

* Contact author: wwduley@sciborg.uwaterloo.ca

Study on thermal properties of energy storage fiber concrete

Weijuan Kong , Liming Zou*

State Key Laboratory for Modification of Chemical Fibers and Polymer Materials,

Donghua University, Shanghai, 200051, China

Abstract

In order to solve the poor thermal insulation and heat preservation properties of ordinary concrete block, a new kind of fiber concrete brick with thermal energy storage was made by impregnating phase changing materials (PCMs). The thermal performance of PCMs mixtures was characterized by means of Differential Scanning Calorimetry (DSC) and appropriate PCMs within human comfort temperature range was chosen to incorporated into hollow fiber. Several fiber concrete specimens were manufactured and their thermal conductivities and compressive strengths were measured.

Keywords: Concrete block; phase change material; thermal conductivity; compressive strength

References

[1] T. Lee, D. W. Hawes, D. Banu, and D. Feldman, Solar Energy Materials & Solar Cells **62**, 217 (2000).

[2] Amar M. Khudhair and Mohammed M. Farid, Energy Conversion and Management **45**, 263 (2004).

[3] Dong Zhang, Zongjin Li, Jianmin Zhou and Keru Wu, Cement and Concrete Research **34**, 927(2004).

*

* Corresponding author. lmzou@dhu.edu.cn

Atom ingress from synthetic biological fluid into nanoporous layers formed in titanium by helium ion-implantation

P. B. Johnson [1,3], C. R. Varoy [1], V. J. Kennedy[2,3], A. Markwitz [2,3,*]

1 School of Chemical and Physical Sciences, Victoria University of Wellington, P O Box 600, Wellington, New Zealand
2 Rafter Research Centre, Institute of Geological and Nuclear Sciences, P.O. Box 31-312, 30 Gracefield Road, Lower Hutt, New Zealand
3 The MacDiarmid Institute for Advanced Materials and Nanotechnology, Victoria University of Wellington, New Zealand

Helium ion-implantation can be used to form nanoporous cavity structures in Ti [1]. This offers the potential of diffusing dopant atoms, of interest for biomedical applications, into a Ti surface. A Ti foil was implanted with He to form a buried nanoporous layer. Disc specimens were taken from the foil and a small spot in the centre was eroded, each disc to a different depth. They were subsequently treated with synthetic biological fluid in a bath under controlled conditions of temperature and pH.

IBA techniques including RBS, NRA and PIXE, were used to determine the uptake of specific elements in two regions: the central eroded spot and an outer (un-eroded) region [2,3]. The most significant effect was for oxygen. A small amount of prior erosion resulted in a *threefold* increase in the oxygen in *both* regions. For greater erosion, the uptake in the centre was less than for no erosion. However, the threefold enhancement in the *outer* region remained a striking feature. This observation suggests the nanoporous layer allows oxygen to move laterally through relatively large distances from the eroded central spot during the bath treatment to heavily oxidize the un-eroded surrounding area. This may offer a technique for intimate bonding of an oxide-based intermediate layer to Ti surfaces for biomedical applications.

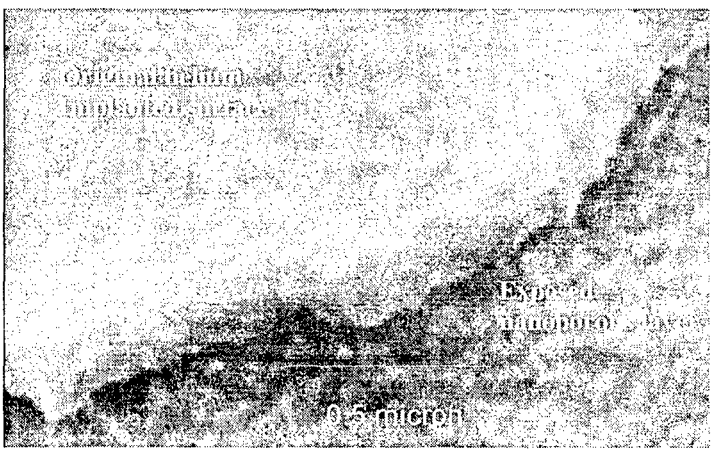

Figure 1: SEM image of the originally helium implanted surface and the exposed nanoporous layer.

[1] P.B. Johnson, "Bubble Lattices in Metals", in Fundamental Aspects of Inert Gases in Solids; eds. J.H. Evans, S.E. Donnelly (Plenum, New York, 1991) 167
[2] P. B. Johnson, V. J. Kennedy, A. Markwitz, C. Varoy, N. Dytlewski and K. T. Short, "Uptake of light elements of nanoporous layers formed by helium ion implantation", Nucl. Instr. and Meth. in Phys. Res. B206 (2003) 1051
[3] V. J. Kennedy, P. B. Johnson, A. Markwitz, C. R. Varoy and K. T. Short, "Microprobe analysis of light elements in nanoporous surfaces produced by helium ion implantation", Nucl. Instr. and Meth. in Phys. Res. B210 (2003) 543

* presenting author

Mechanistic Modeling Using AC Impedance

M. Urquidi-Macdonald*
Pennsylvania State University, University Park, PA, 16802, USA

AC impedance can be used to learn about corrosion activity in systems for which corrosion is not exposed to readily available inspection. A good example of this kind of system is metal reinforced rebar in concrete structures, such as buildings, bridges, etc., or electrical conductive nano-tubes in contact with an electrolyte.

The development of efficient methods for determining the nature of the processes happening at the interfaces will have a major impact in understanding the phenomena to be studied. AC impedance spectroscopy is a powerful tool to learn about the kinetics of mechanisms occurring at interfaces (i.e., metal or metal-alloy/electrolyte). However, the interpretation of AC impedance data has been largely limited to a "circuit theory" interpretation, which only correctly interprets those mechanisms for which unabsorbed species occur on the interface and for reactions that are kinetically controlled (slow reactions). Other mechanistic reactions sets will not conform with an "electrical circuit" picture and valuable information on the type of mechanisms occurring and how to control or reverse those mechanisms is left out of the data and not interpreted.

The equations to describe possible sets of mechanisms are developed from the electrochemical and chemical reactions produced during the different phenomena and summarized elsewhere. Those equations were used to produce a table of possible sets of AC impedance signatures in the Nyquist and Bode diagrams. Each of the AC signatures can be assigned to more than one set of mechanistic reactions happening at the metal interface. The values and shapes of the AC impedance signatures obtained with the model are dependent on the relative values adopted by the rate-constants of the reactions describing the mechanism being studied.

A Neural network pattern recognition tool was developed to map the collected AC signatures to the most probable mechanisms that may originate that signature. The tool developed not only selects the best set of mechanisms that originate the AC impedance signature, but also gives a qualitative value of the rate constants involved in the mechanism.

* Contact author: mumesm@engr.psu.edu

Multi-Scale Modelling of ZnO Nanorod Formation and Growth by Electrochemical Deposition

J. R. Mackay[1,2,*], S. Hendy[1,2,3] and M. P. Ryan[4]
[1] *The MacDiarmid Institute for Advanced Materials & Nanotechnology, NEW ZEALAND*
[2] *Victoria University, Wellington, NEW ZEALAND*
[3] *Industrial Research Limited, Lower Hutt, NEW ZEALAND*
[4] *Department of Materials, Imperial College, Prince Consort Road, London SW7 2BP, UK*

ZnO has an extraordinarily rich family of nanostructures and associated properties [1]. It provides a unique opportunity for the development of a multi-scale growth model that includes a variety of morphological outcomes. Such a model will have the potential for transference to a number of different materials.

Electrochemical methods show good potential as a simple and cheap method for the synthesis of nano-structured materials. We have recently begun investigation into the growth and properties of ZnO nano-rods formed by cathodic deposition [2].

We will present work on the development of a multi-scale model of the electrochemical growth of ZnO nano-rods on polycrystalline Zn foil. Hexagonal nano-rods with a range of diameters (60-140 nm) and heights (1-2 μm) have been grown under a variety of conditions [3]. The nano-rod size, shape, spatial distribution, and alignment were found to depend on the nature and condition of the substrate, pH, concentration of aqueous zinc ions, type of counter-ion, presence of oxygen, temperature, and the applied potential.

Multi-scale modelling resolves material behaviour at multiple length and time scales by linking atomistic models with continuum models. The scales can be linked by calculating effective material parameters from atomistic models and using the results in continuum models, or, by coupling atomistic simulations with continuum models into a hybrid scheme. Implementation of our model involves dividing the system into three different regions.

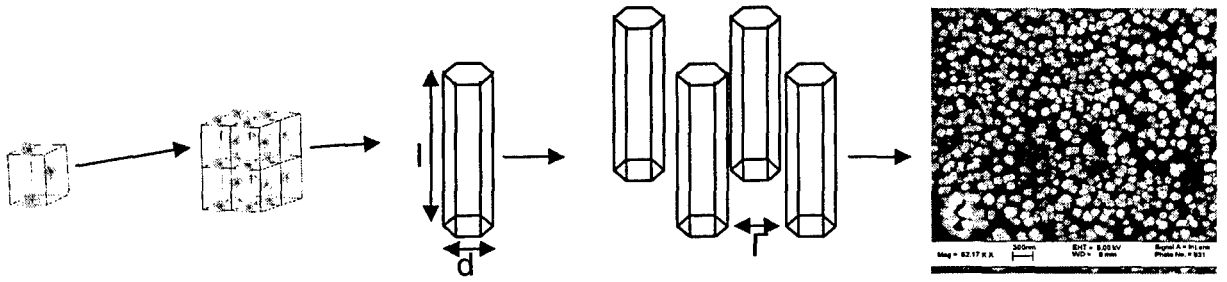

FIG 1. Schematic illustrating nano-rod growth at a variety of scales.

We have chosen to divide the system into 'nucleation and growth', 'electrochemical transport', and 'interfacial dynamics'. *Ab initio* methods will be used to find parameters (for example diffusion, surface energy, electrostatic field strength, and surface band structure) to be coupled with Interface and electrochemical transport models. The processes within each sub-model will be updated using either Finite Elements or Kinetic Monte Carlo methods.

The model will consolidate our understanding of the relationship between growth conditions and nano-rod growth behaviour. We can gain extra insight by calculating parameters that cannot be investigated experimentally (due to cost, time, or technological limits). Once an acceptable model for this system is developed, transfer to other similar oxide systems will be comparatively rapid.

References

[1] Z. L. Wang, J. Phys: Condes. Matter **16,** 829 (2004).
[2] M. H. Wong, A. Berenov, X. Qi, M. J. Kappers, Z. H. Barber, B. Illy, Z. Lockman, M. P. Ryan and J. l. MacManus-Driscoll, Nanotechnology **14,** 968 (2003).
[3] *Ibid.*

* Contact author: mackayjade@student.vuw.ac.nz

Periodic ab initio study of silico-erionite

Cuauhtémoc Samaniego[1*], Donald H. Galván[1], A. Posadas -Amarillas [2] and Vitalii P. Petranovskii[1]
[1] *Centro de Ciencias de la Materia Condensada-UNAM, A. Postal 2681, 22800 Ensenada, B.C., México*
[2] *Departamento de Investigación en Física, Universidad de Sonora, Hermosillo, Sonora, México*

Zeolites are crystalline aluminosilicates with an open framework structure and extraframework intercalated cations. The zeolites framework is built by combination of corner shared TO_4 tetrahedra, where T is either an Si or an Al atom. Extraframework cations are requiered to compensate the charge deficiency produced by inclusion of an Al^{3+} ion in a 4-fold coordinated position. The zeolite framework presents multidimensional channels and cavities throughout the crystal, the effective pore diameters being generally lower than 7-8 Å. The resulting microporosity is exploited by using zeolites as "molecular sieves". This feature, together with the presence of framemork or extraframework active centers, makes zeolites attractive catalysts.

In this work we use ab initio quantum mechanical methods to study the electronic structure of silico-erionite. Silico-erionite is the pure silica analogue of the above mentioned familiy of zeolites. Si-erionite belongs to the P63/mmc space group [1] (hexagonal family with a (Å)=13.252(2) and c(Å)=14.810(1)); the primitive cell contains 108 atoms, only eigth of which belong to the asymmetric unit. Calculations were performed within the linear combination of atomic orbitals periodic Hartree-Fock (**PHF**) fromalisim as implemented in **CRYSTAL98** code [2]. The role of electron-correlations effects were studied by employing periodic Density Functional Theory (**PDFT**) and using the **B3LYP** functional [3,4]. The following split valence basis sets : 6-21G** [5] and 6-31G**[6,7] were investigated.

The electrostatic potential maps and the electron density in selected regions have been calculated from the density matrix and use to qualitatively investigate the catalytic activity ocurring inside the channels and cavities.

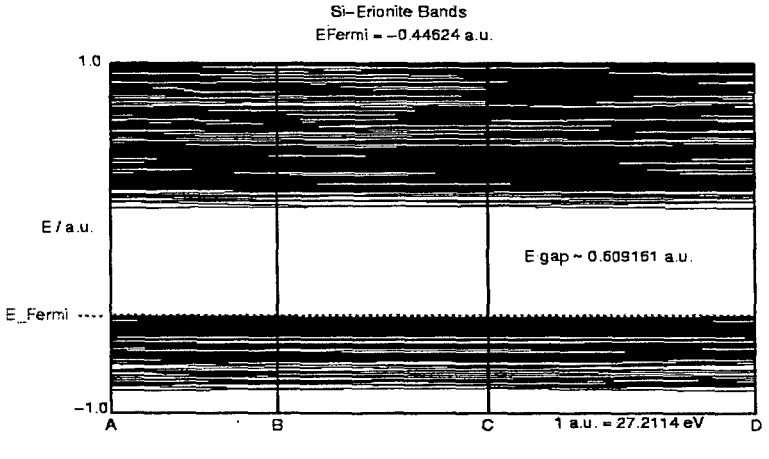

References

[1] J.L. Schlenker, J.J. Pluth and J.V. Smith, Acta Crystallogr. **B33**, 3265 (1977).
[2] **CRYSTAL98** User's Manual, R. Dovesi, V. R. Saunders, C. Roetti, M. Causa, N. M. Harrison, R. Orlando and C. M. Zicovich-Wilson, Theoretical Chemistry Group-University of Tornio, Torino-Italy, September (2000).
[3] A. D. Becke, J. Chem. Phys. **88**, 2547 (1988).
[4] C. Lee and W. Yang and R. G. Parr, Phys. Rev. **B37,** 785 (1988).
[5] J. S. Binkley and J. A. Pople and W. J. Hehre, J. Am. Chem. Soc. **102**, 939 (1980).
[6] W. J. Hehre and R. Ditchfield and J. A. Pople J. Chem. Phys. **56**, 2257 (1972).
[7] J. D. Dill and J. A. Pople J. Chem. Phys. **62,** 2921 (1975).

* Contact author: jsam@ccmc.unam.mx

Si(001) c(4x2)-p(2x2) surface phase transitions induced by electric fields and doping

W. G. Schmidt*, K. Seino, and F. Bechstedt
Institut für Festkörpertheorie und -optik,
Friedrich-Schiller-Universität, Max-Wien-Platz 1, 07743 Jena, Germany

For semiconductor devices, Si(001) is by far the most important surface. Therefore, and because of its apparent simplicity, it is a textbook example for semiconductor surfaces. Numerous studies have established the surface to show a c(4x2) reconstruction formed by asymmetric dimers. Recently, however, the true ground state of the Si(001) surface has become a matter of debate. A single p(2x2) phase, a phase never observed before, was detected at temperatures below 40 K [1]. At 4.2 K even a phase manipulation between c(4x2) and p(2x2) has been performed, using the STM [2]. Similar results were reported for Ge(001) [3]. These observations are very exiting, because they point out a relatively simple way of rewritable nanopatterning, possibly applicable for nanometer-scale memory devices. At the same time, the findings contradict the common knowledge about Si(001) surfaces and are not understood at all.

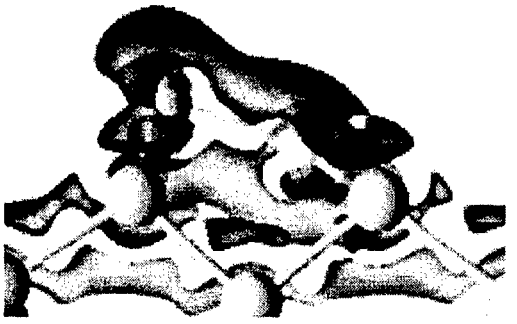

Figure: Calculated charge density difference induced by an electric field along the surface normal for the Si(001) surface. Red (dark) and blue (light) isosurfaces represent charge accumulation and depletion regions, respectively.

We perform first-principles calculations of the Si(001) surface energetics. The calculations are performed within the gradient-corrected density functional theory (DFT-GGA) as implemented in the VASP package [4]. In agreement with previous first-principles calculations, it is found that asymmetric dimers arranged in c(4x2) symmetry represent the surface ground state. Our work goes beyond previous studies by exploring the effects of electric fields and charging on the surface stability. This allows us to identify two mechanisms which shift the surface energy balance in favour of the formation of p(2x2) reconstructions: (i) external electric fields pointing along the surface normal and (ii) electrons inserted into surface states. The outcome of the total-energy calculations are analysed in terms of interacting surface dipoles and surface strain and deliver a natural and intuitive explanation of the low-temperature STM results [5].

* Email: W.G.Schmidt@ifto.physik.uni-jena.de

References

[1] K. Hata, S. Yoshida, and H. Shigekawa, Phys. Rev. Lett. **89**, 286104 (2002).
[2] K. Sagisaka, D. Fujita, and G. Kido, Phys. Rev. Lett. **91**, 146103 (2003).
[3] Y. Takagi *et al.*, J. Phys. Soc. Jpn., **72**, 2425 (2003).
[4] G. Kresse and J. Furthmüller, Comp. Mat. Sci. **6**, 15 (1996).
[5] K. Seino, W.G. Schmidt, and F. Bechstedt, Phys. Rev. Lett. **93**, 036101 (2004).

Growth and Characterization of Cubic Hafnium Oxide Single Crystal Fibers

A. Watcharapasorn[1,*], R. C. DeMattei[2], R. S. Feigelson[3], K.C. Chen[4] and D. Krommenhoek[4]
[1] *Department of Physics, Faculty of Science, Chiang Mai University, Chiang Mai, 50200, THAILAND*
[2] *Geballe Laboratory for Advanced Materials, Stanford University, Stanford, CA, 94305, USA*
[3] *Department of Materials Science and Engineering, Stanford University, Stanford, CA, 94305, USA*
[4] *Quantum Group, Inc., San Diego, CA, 92121, USA*

This paper describes the growth and characterization of cubic hafnium oxide single crystal fibers. The typical solid-state synthesis technique was employed to prepare rare-earth oxide (Yb_2O_3, Er_2O_3 and/or Tm_2O_3) doped hafnium oxide powder. X-ray diffraction analysis on the powder showed that the amount of pure/mixed rare-earth oxide used was enough to produce hafnium oxide having a cubic structure as compared with the usual monoclinic structure of pure hafnium oxide. The powder was isostatically pressed at room temperature and then sintered at high temperature to make dense ceramic. The ceramic was cut into small rods, which were used for single crystal fiber growth. In this case, the laser-heated pedestal growth (LHPG) method was used to grow cubic hafnium oxide in the form of single crystalline fiber. It was found that a number of single crystal fibers of rare-earth oxide doped hafnium oxide with an average diameter of ~400 μm and length ranging from 1-4 cm were successfully grown using the LHPG method. All grown fibers were transparent which make them suitable for high-temperature optical applications. Some physical properties of these fibers were also measured and discussed.

References

[1] F.M. Spiridonov, L.N. Komissarova, A.G. Kocharov and V.I. Spitsyn, Zh. Neorg. Khim. **14**, 9, 2535 (1969); Russ. J. Inorg. Chem. **14**, 9, 1332 (1969)
[2] V.P. Gorelov, Tr. Inst. Elektrokhim., Ural. Nauchn. Tsentr, Akad. Nauk SSSR **26**, 69 (1978)
[3] V.I. Aleksandrov, V.V. Osiko, A.M. Prokhorov and V.M. Tatarintsev, *Current Topics in Materials Science*, edited by E. Kaldis (North-Holland, Amsterdam, 1978), Vol. 2, p. 421
[4] R.S. Feigelson, *Crystal Growth of Electronic Materials*, edited by E. Kaldis (North-Holland, Amsterdam, 1985), p. 127
[5] D.K. Smith and C.F. Cline, J. Amer. Ceram. Soc. **45**, 249 (1962)
[6] R.P. Ingel, D. Lewis, B.A. Bender and R.W. Rice, Ceram. Eng. Sci. Proc. **3**, 577 (1982)
[7] S.L. Dole, R.W. Scheidecker, L.E. Shiers, M.F. Berard ad O. Hunter, Jr., Mater. Sci. Eng. **32**, 277 (1978)
[8] F.J. Ritzert, H.M. Yun and R.V. Miner, J. Mater. Sci. **33**, 5339 (1998)

* Contact author: anucha@stanfordalumni.org

Templated Photofunctional Nanotube Arrays

T. Kemmitt[1*], M.E. Bowden[1], and I.W.M. Brown[1],
[1]*MacDiarmid Institute for Advanced Materials and Nanotechnology, Industrial Research, PO Box 31-310, Lower Hutt, NEW ZEALAND*

Anodic aluminium oxide has been identified as a versatile porous template material having high pore density, (up to 10^{10} cm^{-2}), controllable channel length and monodisperse pore diameter within the range 20-250 nm [1,2]. In order to take advantage of the porous structure and high surface area, we have coated the internal surfaces of the pores with photoactive anatase TiO_2 nanocrystallites. Field emission SEM clearly shows a titania layer coating the internal surfaces of the porous substrate.

Grafting of TiO_2 surfaces onto nanoporous surfaces has been demonstrated previously using sol-gel techniques [3], however the resulting amorphous TiO_2 surface would require additional thermal processing for applications in photocatalysis. Our method uses a novel route to prepare an aqueous, colloidal sol, wherein the titania particles have been hydrothermally processed in the presence of oxalic acid to form nanocrystallites (20-120nm) requiring only processing at low temperature or low level UV exposure to exhibit useful photoactivity [4]. Platinum doping on the crystallite surfaces creates a 'photochemical diode' whereby the Pt acts as an electron absorber, enhancing the photoefficiency [5].

Formation of photoactive nanotubes within the self-supporting template allows a flow-through arrangement to be adopted, whereby reactants can be carried to the photoelectrochemical electrode in a gaseous or liquid carrier fluid. This permits efficient presentation of the target molecules to the catalyst surface, reducing the usual difficulties associated with mass transport, frequently observed in photocatalytic reactor systems. Thus photochemical oxidations of organic and inorganic molecules can be carried out within the nanotube arrays. Photocatalytic oxidation of model organic pollutants has been demonstrated, and comparisons can be drawn with photocatalysts presented on planar substrates. Our longer term interest is in promoting advances toward efficient conversion of solar energy into chemical energy, thus we will describe progress toward photogeneration of hydrogen gas from liquid or vapour phase water and alcohol mixtures.

References

[1] H. Masuda and K. Fukuda, Science, **268**, 1466 (1995).
[2] W. Lee, H.-I. Yoo, and J.-K. Lee, Chem. Commun., 2530 (2001).
[3] M. Widenmeyer, S. Grasser, K. Köhler, and R. Anwander, Micropor. Mesopor. Mater., **44-45**, 327 (2001).
[4] N.I. Al-Salim and T. Kemmitt, J. Mater. Chem., to be published.
[5] E. Sanchez and T. Lopez, Mater. Lett., **25**, 271 (1995).

* Contact author: t.kemmitt@irl.cri.nz

Effect of Arc parameters on CNT growth using a continuous reactor

H. M. Yusoff* and J. Abrahamson
Chemical and Process Engineering Department, School of Engineering, University of Canterbury, NEW ZEALAND

A new continuous method for producing carbon nanotube (CNT) has been developed using the arc discharge method in which carbon substrate was used as a carbon source. In the process, carbon nanotubes grew on the surface of the carbon substrate during the arc discharge. A method used is differed from the conventional arc discharge method *i.e.* low current - less than 20 Amps and inter electrode gap more than 5 mm.

The aim of this work is to study the effect of the physical parameters of the arc on CNT growth. In this work, the effects of arc gap, substrate surface temperature and carbon density, were investigated. The experimental investigation done showed that the growth of carbon nanotube using arc discharge method is dependent on the technical parameters such as type of background gas used, inert gas concentration[1] , arc current[2] and inter electrode gap[3] . However, the influence of these parameters to the physical parameters in the arc is not well understood.

An optical pyrometric technique was used to determine the surface temperature of the substrate where nanotubes were growing. Other studies showed that carbon evaporation rate depended on the surface temperature[4] . Therefore, substrate surface temperature is one of the significant factors influencing the first stage of carbon nanotube formation. It is found that carbon nanotube growth is favourable over a certain temperature range. This temperature range provides maximum potential productivity and defines method scalability. In addition, a spectroscopic method was used to study the arc plasma. Carbon plasma emission spectroscopy allows the determination of temperature in the arc and density of carbon vapour in the arc zone where carbon nanotubes are formed.

References

1 S. Farhat, I. Hinkov, and C. D. Scott, Journal of Nanoscience and Nanotechnology **4**, 377 (2004).

2 M. Cadek, R. Murphy, B. McCarthy, et al., Carbon **40**, 923 (2002).

3 H. Lange, P. Baranowski, and A. Huczko, Review of Scientific Instruments [H.W. Wilson - AST] **68**, 3723 (1997).

4 J. Abrahamson, Carbon **12**, 111 (1974).

* Contact author: hyu17@student.canterbury.ac.nz

Carbon covalent-bonded nanotube junctions: structures, formation mechanism and transport properties

L. A. Chernozatonskii[1,*], A.N. Andriotis[2], M.Menon[3], E. Mikheeva[1], D. Srivastava[4]
[1] *Institute of Biochemical Physics, Russian Academy of Sciences, 119991 Moscow, RUSSIA*
[2] *Institute of Electronic Structure and Laser, P.O. Box 1527, 71110 Heraklio Crete, Greece*
[3] *Department of Physics and Astronomy, University of Kentucky, Lexington, KY 40506-0055, USA*
[4] *NASA Ames Research Center, CSC, Mail Stop T27-A1, MoÆett Field, CA 94035-1000ex, USA*

In recent time the building of "nanonet" from nanotubes have been very important in nanoelectronics [1]. Process of nanotube's covalent binding is one of resources of the building of junction new types. The experimantal observation of rectification properties in carbon nanotube Y-junctions has provided additional support for realizing their device potential [2]. Theoretical calculations have confirmed the rectification behavior for the Y-junctions [3,4].

Covalent-junction combinations from single-wall nanotubes (SWNT) with various types of electronic properties (metallic and semiconducting) are considered. The mechanism of formation X-,Y- and T-types of covalent junctions are investigated, defined potential barriers and P-T phase diagrams. The simulation use molecular dynamics method with empirical bond-order potential that was parameterized by Brenner [5] including long-range interaction [6], and tight-binding molecular dynamics scheme [7]. The energy simulation has shown that the investigated structures are stable.

It was demonstrated [4] that the intrinsic symmetry of the structural nature at the junction and the external asymmetric conditions imposed by the bias voltage play a significant role in deciding the rectification behavior of the junction. In the present work various forms of the spacer region, the latter formed by one or more pairs of 2+2 cycloaddition bonds which include sp3 bonded C-atoms are considered. We investigate the effect of the spacer-symmetry on the transmission function and the I-V characteristics of the tube junctions. The results are compared with the previous results for all sp2 junctions - they cofirm our earlier findings that structural symmetry is a necessary condition for rectification and switching properties.

References

[1] *Synthesis, Structure, Properties and Applications,* ed. by M.S. Dresselhaus et al., Springer, 2001.
[2] J. Li, C. Papadopoulos, and J. Xu, Nature **402**, 253 (1999).
[3] A. N. Andriotis et al.,, Phys. Rev. Lett. **87**, 066802 (2001).
[4] A. N. Andriotis et al., Phys. Rev. **B 65**, 165416 (2002).
[5] D.W.Brenner et al.,J. Phys.: Condens. Matter **14**, 783 (2002).
[6] Z.Mao et al., Nanotechnology **10**, 273 (1999).
[7] A. N. Andriotis and M. Menon, Phys. Rev. **B 57**, 10069 (1998).

Temperature dependence of the thermal conductivity in chiral carbon nanotubes

N.G. Mensah, G. Nkrumah ,S.Y. Mensah and F.K. Allotey
Department of Mathematics and Statistics, University of Cape Coast,Cape Coast,GHANA

The thermal conductivity of a chiral carbon nanotube (CCNT) is calculated using a tractable analytical approach. This is based on solving the Bolzmann kinetic equation with energy dispersion relation obtained in the tight binding approximation. The results obtained are numerically analysed. Unusually high electron thermal conductivity is observed along the tubular axis. The dependence of thermal conductivity against temperature was plotted. It is noted that thermal conductivity shows a peaking behaviour falling off at higher temperature. Another interesting result obtained is the fact that circumferential electron thermal conductivity appears to be very small

Preparation and Electrochemical Characterisation of *Carbon Nanotube* Microelectrodes

[1]Noorhana Yahya, George Zhen Chen, Graeme A. Snook, Vega P. Kotzeva, Derek J. Fray

[1]*AML, Institute of Advanced Technology, Universiti Putra Malaysia, 43400 Serdang, Selangor, MALAYSIA*
Department of Materials Science and Metallurgy,University of Cambridge, Pembroke Street, Cambridge CB2 3QZ, United Kingdom

Carbon nanotubes (CNTs) have been intensively investigated for their fundamental and technical importance since their discovery made by Iijma in 1991[1].Structural diversities and the related diverse physical properties with large aspect ratio and small diameter and hollowness are fascinating [2]. CNTs are metal, semiconductor or insulator depending on their chirality [3]. This preliminary work was initiated by our interest in looking at the possibility of producing arrays of CNT microelectrodes in a non-conducting polymer, polyvinyldine fluoride (PVDF). Nevertheless, the multiwall CNTs are entangled and the difficulty to disperse them in the polymer is a setback. These entanglements tend to form nucleation points resulting in reduced electrical and mechanical properties. This work reports on an earnest effort of preparing novel *carbon nanotube* and graphite flake microelectrodes. Polyvinyldine Flouride (PVDF) was used as the polymer to fabricate the nanocomposite. The first work premise consists of determination of percolation threshold for the CNTs and graphite filled nanocomposites. We obtained a percolation threshold of 1% and 18% with conductivity of 3.16 S/m and 1.05 S/m respectively, for the CNTs and graphite filled nanocomposites. The second premise deals with changing the sonication time, heat treatment, types of CNTs and average molecular weight of the PVDF to optimize the conductivity of the nanocomposites. Of the four efforts, sonication time is the utmost important route as it not only could enhance the electrical conductivity, but also contribute to the dispersion of the fillers behaving as an individual microelectrode. The third premise was devoted to the construction of 10% and 25% of CNTs and graphite, respectively, as the microelectrodes in the nanocomposite. Preliminary experimental results of cyclic voltammetry demonstrate that there is increase in current after 20 hours toluene etching at room temperature. It could be concluded that the carbon nanotube fillers gave a hemispherical field indicating a microelectrode-like behaviour.

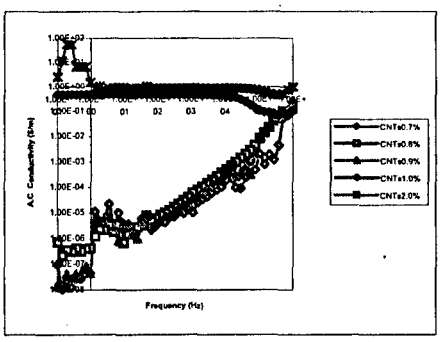

Figure 1: Log-log plot of the conductivity of the nanocomposite as a function of frequency with the changing CNTs loading as parameter

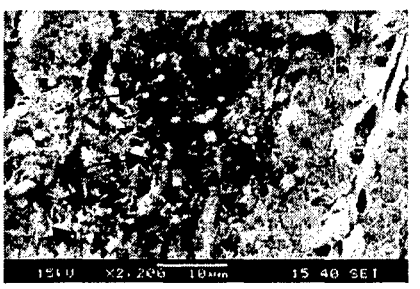

Figure 2: SEM image of the CNTs filled nanocomposite

A clear understanding of the electrical conduction (Figure 1) and the dispersion (Figure 2) of the fillers is an important aspect to build microelectrodes. 40 minutes (Figure 2) and 20 minutes sonication time is sufficient to disperse the entanglement of CNTs and graphite flake, respectively. Slow air cooled after hot press process will ultimately allow heat transfer by the CNTs or graphite to the polymer resulting in an increased crystallinity and thus better electron tunneling. The average molecular weight relating to a crosslinking between two adjacent molecules attaching the filler gave an impact on the conductivity of the nanocomposite. We had developed microelectrodes consisting of individual carbon nanotube due to the above factors.

References

[1] S. Ijima, *Nature*, 1991, 56, 354.
[2] Q. Jiang, M.Z. Qu. G.M Zhou, B.L. Zhang, Z.L. Yu, *Mat. Sc. Letts.*, 2002, 57, 988-991.
[3] R. H. Baughman, A.A. Zakhidov, W.A. de Heer, Science, *2002, 297, 787-792.*
*Contact author : noorhana@fsas.upm.edu.my

Bundles of Boron-Carbide Nanotubes: Effects of Doping by Li and Cu

O. Ponomarenko, M.W. Radny and P. V. Smith*

School of Mathematical and Physical Sciences, The University of Newcastle, Callaghan, Australia 2308

Hole-doping of layered semiconductor LiBC was recently predicted to lead to superconductivity of this material [1]. Calculations by Mehl et al. [2] have also shown that full replacement of Mg by Cu in the novel medium-temperature superconductor MgB_2, and partial replacement of the Boron atoms by Carbon, would increase the critical temperature T_c by up to ~50 K. We have shown that small radius, undoped, single-walled Boron-Carbide (BC) nanotubes are more energetically favourable than the corresponding BC strips, and that doping these small radius BC nanotubes with Li and Cu can significantly enhance the density of states at the Fermi level [3].

It has recently been speculated that a composite based on a two-dimensional nanotubular lattice could provide an ideal high-T_c superconductor [4]. In this paper we present the results of a*b initio* density functional theory calculations of the properties of bundles of clean and metal doped BC tubes. These fully spin polarised calculations are based on the plane wave pseudopotential method (VASP [5]) within the generalized gradient approximation (GGA) for the exchange and correlation energy. Several possible sites for doping by Li and Cu atoms have been examined. The effects of different arrangements of these dopants on the stability and electronic properties of bundles of BC tubes of different helicity and radius will be discussed.

References

[1] H. Rosner, A. Kitaigorodsky and W. E. Pickett, Phys. Rev. Lett. **88**, 127001 (2002).

[2] M. L. Mehl, D. A. Papaconstantopoulus and D. J. Singh, Phys. Rev. B **64**, 140509 (2001).

[3] O. Ponomarenko, M. Radny and P. Smith (to be published).

[4] V. Pokropivny, Physica C **351,** 71 (2001).

[5] G. Kresse and J. Hafner, Phys. Rev. B **47**, 558 (1993); ibid. **49**, 14251 (1994).
G. Kresse and J. Furthmuller, Comput. Mat. Sci. **6**, 15 (1996); Phys. Rev. B **54**, 11169 (1996).

* Contact author: Phil.Smith@newcastle.edu.au

Self Consistent Calculation of Nonlinear Capacitance and Its Corresponding Relaxation Time in Doped Nanotube Junctions

Keivan Esfarjani*
Department of Electrical Engineering, Sharif University of Technology, 11365-9161, Tehran, IRAN

Amir A. Farajian and Yoshiyuki Kawazoe
IMR, Tohoku University, Sendai 980-8577 JAPAN

Siu Tat Chui
BRI, University of Delaware, Newark, DE 19716 USA

The nonlinear capacitance in doped nanotube junctions is calculated self consistently. It decreases as a function of the applied bias when the latter becomes larger than the pseudogap of the nanotube. For this device, one can deduce a relaxation time of about 0.1 femtosecond. Because of its negative differential resistance (NDR), a switching time of less than a femtosecond can also be deduced.

PACS numbers: 72.20.-i Conductivity phenomena in semiconductors and insulators 71.20.Tx Fullerenes and related materials

* Contact author: k1@sharif.edu

NMR T_2-Relaxation Dispersion of Polymeric Materials under Shear

A. Gottwald* and P. T. Callaghan
MacDiarmid Institute for Advanced Materials and Nanotechnology, Victoria University of Wellington, PO Box 600, Wellington, New Zealand

Polymers can be found in materials as diverse as optical fibres or plastic bags. They also form an important part of many pharmaceutical, cosmetic or food substances. Many production processes include strong shearing forces, either for mixing or for transporting the material, and in consequence, the shear rheology of polymers is a subject of some industrial relevance.

Rheo-NMR allows one to examine effects caused by shear at both a macroscopic and a molecular level. For example one may analyse molecular order (orientation) or, by means of NMR microscopy, visualise flow fields. In addition, relatively simple T_2-measurements can be used to indicate changes in molecular mobility due to shear. Single T_2-values are difficult to interpret because several quite different dynamical processes may cause the spins to lose coherence and hence the signal to decay. Therefore it is often helpful to measure T_2-dispersions, i.e. T_2 at different echo spacings in the Carr-Purcell-Meiboom-Gill (CPMG) sequence. While at short spacings the T_2-value can be considered as the inherent relaxation time, the apparent T_2 at longer spacings is also affected by motion through magnetic field gradients. Because shear competes with internal motion, the resulting dispersion can provide some insight regarding the relative influence of each. Furthermore the dispersion may be influenced by magnetic field gradients, either internal and due to structural heterogeneity, or external through the deliberate application of additional magnetic fields. We will discuss such T_2-dispersion experiments on both polymer solutions and melts.

* Contact author: antje.gottwald@vuw.ac.nz

Substitution of Dipyrido[3,2-*a*:2',3'-*c*]phenazine: an Attempt to Produce Highly Emissive Materials

A. G. Blackman, K. C. Gordon, N. J. Lundin*
MacDiarmid Institute for Advanced Materials and Nanotechnology,
Department of Chemistry, University of Otago, Dunedin, NEW ZEALAND

The development of efficient electroluminescent materials is a rapidly expanding field, in part due to their application as dopants in organic light emitting diodes (OLEDs). Many studies of complexes containing dyprido[3,2-*a*:2',3'-*c*]phenazine (dppz) ligands have been undertaken due to its rigid, aromatic structure producing interesting emission properties that are affected significantly by the surrounding environment. For example, the emission intensity of the complex cation $[Ru(1,10\text{-phenanthroline})_2(dppz)]^{2+}$ is highly sensitive to its solvent environment; intense fluorescence is observed in some organic solvents [1] or in the presence of DNA [2] but this is quenched significantly in water. The appendage of electron withdrawing functional groups onto the 11-position of dppz (*Figure 1*) may therefore allow tuning of the electronic properties of the ligand.

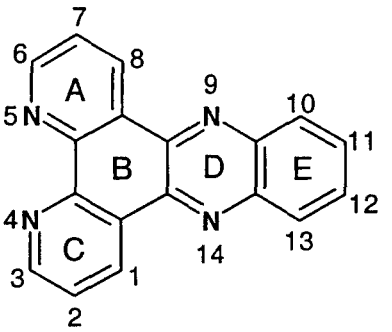

Figure 1. Structure of dppz with ring and atom labels.

Dppz is also of interest to researchers from the perspective of its electronic structure. Dppz has two unoccupied molecular orbitals (MOs) that are similar in energy but are localised over different regions of dppz's aromatic skeleton. The phen MO is localised over the phenanthroline region (rings A, B, C) of the molecule , and can allow intense metal-to-ligand charge transfer (MLCT) transitions to occur in complexes containing dppz due to orbital overlap with dπ MOs of the metal atom. The phz MO is centralised over the phenazine region (rings B, D, E) of dppz and has almost no wavefunction amplitude at the coordinating nitrogen atoms [3]. This results in the phz MO having poor overlap with dπ MOs of the metal atom, and hence a weak MLCT transition. Judicious selection of the metal ion in complexes of dppz can allow the nature of the lowest energy excited state to be tuned from MLCT to a ligand centred transition, due to the phz MO and phen MO being close in energy [4]. Substitution of dppz at the 11-position should also allow the energy of the phz MO to be controlled.

Dppz has been substituted at the 11-position with a bromine atom and ethyl ester group to produce two new ligands. The syntheses of these ligands and their complexes $[Ru(bpy)_2(L)](PF_6)_2$, $[Cu(PPh_3)_2(L)]BF_4$ and $[Re(CO)_3(L)Cl]$ (where bpy = 2,2'-bipyridine, PPh_3 = triphenylphosphine, and L = substituted dppz ligand) are outlined, and crystal structures of both rhenium(I) complexes are presented. Spectroscopic techniques are used to investigate the electronic behaviour of these ligands and complexes, and assess their potential for use as dopants in OLEDs. The ligands appear to have delocalised lowest unoccupied MOs, which is uncommon in dppz-based molecules.

References

[1] C. Turro, *et al.*, J. Am. Chem. Soc. **117**, 9026 (1995).
[2] R. M. Hartshorn and J. K. Barton, J. Am. Chem. Soc. **114**, 5919 (1992).
[3] K. C. Gordon, P. J. Walsh, and E. M. McGale, Curr. Appl. Phys. **4**, 331 (2004).
[4] M. R. Waterland, K. C. Gordon, J. J. McGarvey, and P. M. Jayaweera, J. Chem. Soc., Dalton Trans., 609 (1998).

* Contact author: natashal@alkali.otago.ac.nz

Photoexcitation in metal polypyridyl OLED complexes: a spectroscopic and density functional theoretical study.

P. J. Walsh,* K. C. Gordon, N. J. Lundin
Department of Chemistry, University of Otago, Dunedin, NEW ZEALAND

Complexes of dipyrido[3,2-a:2',3'-c]phenazine (dppz) derivatives are useful as components in organic light emitting devices (OLEDs). A series of detailed photophysical and theoretical studies [1-4] suggest that Re(I) and Ru(II) complexes with dppz involve the presence of two low-lying triplet metal-to-ligand charge transfer (^{3}MLCT) states and a triplet ligand-centred (^{3}LC) state. The dppz ligands may be described as having a phenanthroline (phen) portion and a phenazine (phz) portion. The two ^{3}MLCT states terminate on ligand molecular orbitals (MOs) that are phen- and phz-based respectively. The interplay between these close lying states is a sensitive function of metal ion [5], solvent [5-7] and substitutent [8].

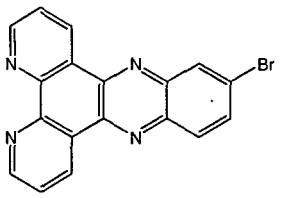

Fig. 1. Schematic of dppz-11-Br.

Understanding of the processes which occur in dppz complexes is vital to development of rationally designed complexes for applications in OLED cells. A resonance Raman (RR) and time-resolved resonance Raman (TR^3) study of the Franck-Condon (FC) and thermally equilibrated excited (THEXI) states provides evidence of both LC and MLCT THEXI states. TR^3 spectra of the substituted dppz ligands have a strong marker band for the ^{3}LC state at 1383 cm^{-1}. TR^3 spectra of Cu(I), Ru(II) and Re(I) complexes of these ligands are spectrally distinct from those of the ligands themselves; indicating the presence of transitions which involve the metal centre. However, the LC marker band is present to varying degrees in the TR^3 spectra of the metal complexes. Density functional theory (DFT) calculations are used to gain insight into the influence of the metal centre on the proportion of LC and MLCT states. Calculated Raman spectra give good agreement with experimental Raman spectra, indicating the validity of the calculations and their usefulness in predicting vibrational mode characteristics, MOs and their energy levels.

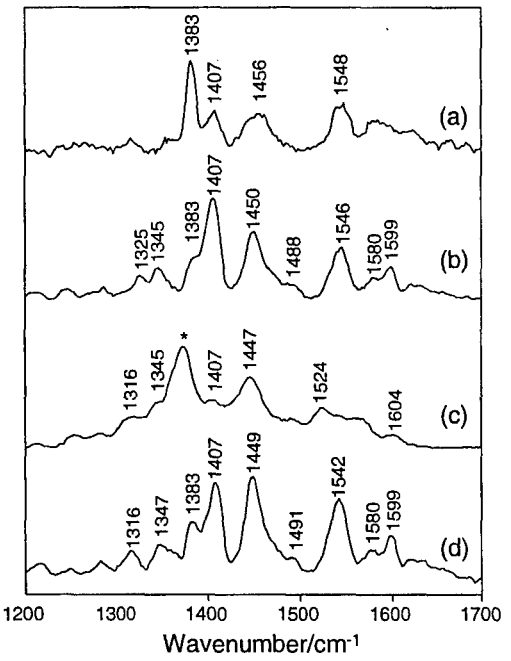

*Fig. 2. TR^3 spectra (λ_{exc} 355 nm) of (a) dppz-11-Br, (b) [Cu(PPH$_3$)$_2$(dppz-11-Br)]BF$_4$, (c) [Ru(bpy)$_2$(dppz-11-Br)](PF$_6$)$_2$, (d) fac-[Re(CO)$_3$Cl(dppz-11-Br)]. Spectra were taken in CDCl$_3$ except for (c) which was taken in CH$_3$CN. * denotes a solvent band.*

References

[1] H. D. Stoeffler, N. B. Thornton, S. L. Temkin, et al., J. Am. Chem. Soc. **117**, 7119 (1995).
[2] J. R. Schoonover, W. D. Bates, and T. J. Meyer, Inorg. Chem. **34**, 6421 (1995).
[3] E. J. C. Olson, D. Hu, A. Hormann, A. M. Jonkman, M. R. Arkin, E. D. A. Stemp, J. K. Barton, P. F. Barbara, J. Am. Chem. Soc. **119**, 11458 (1997).
[4] J. R. Schoonover, G. F. Strouse, R. B. Dyer, et al., Inorg. Chem. **35**, 273 (1996).
[5] D. M. Dattelbaum, K. M. Omberg, P. J. Hay, et al., J. Phys. Chem. A **108**, 3527 (2004).
[6] E. Amouyal, A. Homsi, J. C. Chambron, et al., J. Chem. Soc., Dalton Trans.: Inorg. Chem. (1972-1999), 1841 (1990).
[7] J. R. Schoonover, C. A. Bignozzi, and T. J. Meyer, Coord. Chem. Rev. **165**, 239 (1997).
[8] M. R. Waterland, K. C. Gordon, J. J. McGarvey, et al., J. Chem. Soc. Dalton Trans., 609 (1998).

* Contact author: pennyw@alkali.otago.ac.nz

TRANSPORT STUDIES OF SILVER BASED FAST ION CONDUCTING GLASSY SYSTEM FOR BATTERY APPLICATIONS.

Y.Chakravarthi, Prof.V.Chandramouli
Dept of physics, Osmania University, Hyderabad 500007, India

Agi-Ag_2o-(As_2O_3+Cro_3)(SAC) system prepared by conventional melt quenching technique for fixed dopant salt (Agi=60%) & modifier (M= Ag_2o) to formers (F= As_2o_3+ Cro_3) (M/F=2) ratio at two and varied two formers in steps of 10%.All the prepared compounds were characterized by X-ray diffraction technique. Electrical conductivity measurements were carried out using two probe a.c conductivity bridge (Elico make model CM82T) at room temperature as well as at higher temperature. The highest conductivity ($s = 1.18 \times 10^{-2}$ S/cm) obtained for the formers composition of 60% Agi-26.67% Ag_2o -13.33 %(0.3 As_2O_3+0.7 Cro_3) at room temperature. The temperature dependence of conductivity data plotted as (log sT) vs. 1000/T and all the plots follows the arhenius behavior. Activation energy obtained from the plots and the highest conducting composition found to be minimum (0.21 ev).The observed conductivity discussed base on the available theoretical models (1).

Electronic conductivity was measured by using the Wagner's d.c polarization Technique and found to be an order of 10-8 S/cm. Transport number calculated. Impedance measurements were made in the wide frequency ((5 HZ to 13 MHZ) and temperature (298 to 323k) range using the HP 4192A LF impedance analyzer. A.C. conductivity and dielectric properties were evaluated from the impedance data.

The high ionic conducting SAC formers composition is used for battery studies. Three sets of batteries were constructed with different compositions of iodide, graphite, SAC glass and TMAI. From the first set of batteries the best combination of I:C ratio selected from the discharge characteristics data. SAC glass was added to best I:C percentage and discharge characteristics were made and fixed the best percentage (I+C:SE) cathode composition for the best composition of (I+C:SE) cathode, 10% of tetramethylammoniumiodide added and observed that there is improvement in discharge characteristics. Transport properties and battery performance of SAC system will be presented and discussed.

Acknowledgements: Authors are thankful to Prof.K.shahi, IIT Kanpur for providing impedance facilities.

Reference

(1) Materials for solid state batteries (editors) B.V.R chowadari and S.Radhakrishan, World Scientific, Singapore (1986)

Towards Smart Membranes and Surfaces for Sensors and Catalytic Applications

T. H. Lim, T. Borrmann*, R. Batchelor, J. H. Johnston, J. L. Spencer
School of Chemical and Physical Sciences, Victoria University, P. O. Box 600, Wellington, NEW ZEALAND

Presented in this paper are the results of our preliminary studies leading towards the development of functionalised membranes and surfaces for advanced catalytic and sensor applications. By combining designer organometallic chemistry molecules with inorganic and organic support materials, for example nano-structured calcium silicates and conducting polymers, we hope to develop a suite of new materials and hence opportunities and applications in the field of catalysis and sensors.

Recently we synthesized a novel gold (I) complex utilising a proprietary phosphor nitrogen derivative of a bispidinone ligand. The structure of the complex has been fully characterised using single crystal X-rayanalysis (**Figure 1**) and has appears to have potential in catalytic applications. We have gained insights into the requirements that different metal centres have towards their ligand environment where bispidinone and its derivatives are concerned.

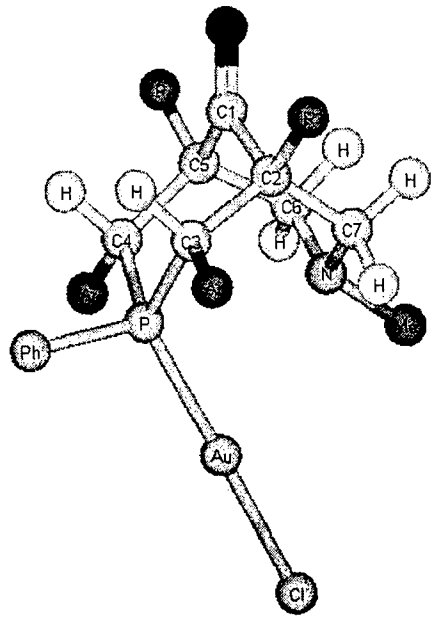

Furthermore, we have worked towards the derivatisation of bispidinone related ligands in order to allow them to be anchored to the surface of a substrate. NMR studies confirm this. The carbonyl group at the top of the ligand can be transformed using standard organic chemistry methods without compromising the backbone structure. Furthermore the side chains R, attached to the carbons C2 and C5, can be modified and allow binding to various substrates. For example, in the complex depicted above these side chains are esters.

It is probable that the catalyst can be linked to a polymer or inorganic support structure, thereby generating a heterogeneous material. Furthermore an exchange of metal centres seems at this stage possible, allowing for a controlled absorption and release of metals into solution.

* Contact author: thomas.borrmann@vuw.ac.nz

Process of Novel Hydrothermal Flow-Reactor with Adiabatic Expansion Cooling: Toward Production of Functional Biopolymer

Tomomasa Goto[1], Yasuhiro Futamura[2,3], Yukio Yamaguchi[1] and Kenji Yamamoto[1,2*]

[1] *Department of Chemical System Engineering, Graduate School of Engineering, The University of Tokyo, 7-3-1, Hongo, Bunkyou-ku, Tokyo, 113-8656, Japan*

[2] *Department of Medical Ecology and Informatics Research Institute, International Medical Center of Japan, 1-21-1, Toyama, Shinjuku-ku. Tokyo 162-8655, Japan*

[3] *Department of Bioactive Molecules, The National Institute of Infectious Diseases, 1-23-1, Toyama, Shinjuku-ku. Tokyo 162-8640, Japan*

The biopolymer has been studied to develop the functional nano-sized device like carbon compounds such as carbon nanotube and fullerene. One of the reasons for this kind of research would be the improvement of the high density and low energy cost device such as functional circuits, memories, and displays, by using the specific character of the biopolymer.

For this purpose we had designed a continuous flow reactor dealing with high temperature and high pressure water to polymerise a monomer such as amino acid and nucleic acid easily[1]. Our reactor made it feasible to heat sample solution quickly before the reaction with the mix of heated water and sample solution in an interflow block, and also to quench it rapidly after the reaction with a needle valve (See Figure (A)). In this reactor the quench method was an adiabatic expansion cooling with Joule-Thomson. On the other hand, in most of previous studies[2-4] the quench method was composed of two steps, cooling and depressurising. Figure (B) shows the comparison of the quench processes between the adiabatic expansion and the two steps. Because we hypothesized that the hydrolysis of products, which had already polymerised in high temperature and high pressure water, was promoted as the cooling speed became slow, the adiabatic expansion cooling was thought to reduce the hydrolysis and dissociation of products.

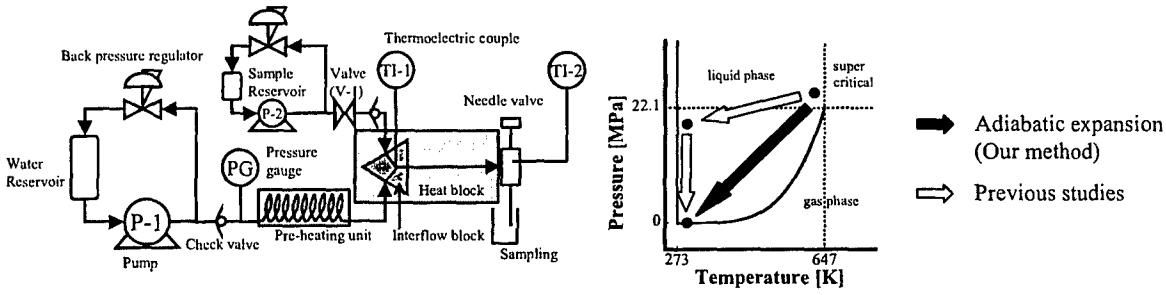

Figure (A) The experimental apparatus adopted for an adiabatic expansion cooling with a needle valve and (B) the comparison of the quench processes between the adiabatic expansion and the two steps.

Glycine reacted with this reactor at 270 °C and 25 MPa. With a high performance liquid chromatography (HPLC) and LC/mass spectrometry we have detected that di-, tri-, tetra-, penta-, hexa-, hepta-, octa-, nona- and decaglycine were produced from glycine in high temperature and high pressure water. We have not confirmed whether undecaglycine or longer peptide was synthesized or not. We are planed to synthesize peptides from amino acids other than glycine to make functional molecule like self-assembling peptides[5,6].

References

[1] Tomomasa Goto *et al.*, Proceedings of the 10th APCChE (APCChE 2004), 3P-03-016 (2004)
[2] Imai E *et al.*, Science **283**, 831 (1999)
[3] Islam M.N., Kaneko T. and Kobayashi K., Bull Chem Soc Jpn **76**, 1171 (2003)
[4] Alargov DK *et al.*, Origins Life Evol. Biosphere **32**, 1 (2002)
[5] Sylvain Vauthey *et al.*, PNAS **99**, 5355 (2002)
[6] Todd C. Holmes *et al.*, PNAS **97**, 6728 (2000)

* Contact author: backen@ri.imcj.go.jp

Possible Separation of an Optical Isomer from a Racemic Amino Acid by Kaolinite.

H. Hashizume*

Ecomaterials Center, National Institute for Materials Science, Tsukuba, Japan.

It is generally difficult to discriminate between optical isomers, such as amino acids, of which the energy difference between dextrorotary (D) and levortatory (L) is very small. It is known that clay minerals adsorb organic matters well. Furthermore, it has been said that an edge of a sheet silicate clay mineral (kaolinite, montmorillonite etc.) may be able to adsorb one optical isomer from racemic body selectively and that one optical isomer may be preferred to another by a structural defect of clay minerals[1,]. For those reasons, it has been investigated that clay minerals discriminate between optical isomers of amino acids. Hashizume and Theng (2002) carried out discrimination between D-alanyl-D-alanine and L-alanyl-L-alanine by allophane which was a hallow spherical clay mineral. Allophane has several perforations which are a structural defect to keep the hallow spherical structure and an adsorption site. Allophane preferred L-alanyl-L-alanine to D-alanyl-D-alanine thought they could not recognize the selectivity of the optical isomer of mono-alanine by allophane [2]. An optical isomer of a particular amino acid may be able to be separated from its racemic body by the structural discontinuous portion (i.e. the edge or the structural defect) in clay minerals. The selective adsorption of an optical isomer by the edge of kaolinite was investigated in this report. Kaolinite was collected particles under 1μm to see an effect of the edge, because it was expected that an area of the edge per unit mass became large by using very fine particle. Nine racemic amino acids, i.e. alanine (ala), valine (val), leucine (leu), isoleucine (ile), proline (pro), phenylalanine (phe), serine (ser), aspartic acid (asp) and glutamic acid (glu), were used.

Kaolinite which was derived from USA (GK) and New Zealand (NZK) was used. Kaolinite was dispersed in water and fractionated under 1μm. Kaolinite collected was treated by 10 % H_2O_2 at 110 °C to remove a natural organic matter. After that, kaolinite was dialyzed and dried by a freeze dryer. 5 mmol/l of an amino acid solution was prepared. 100 mg of kaolinite and 7 ml of the amino acid solution were put into a glass bottle. The bottle was shaken for 65 hours. After that, pH of the solution was measured. The pH was 7 to 8.5. Supernatant was separated from the solution by centrifugation. Supernatant and the starting solution were measured by TOC. Adsorption was estimated to use the carbon contents in supernatant and starting solution. Further, supernatant was analyzed by HPLC with CD detector to find the selective adsorption.

Adsorption of ala, pro, asp and glu by GK and NZK were higher than that of other amino acids. Adsorption of nine amino acids by GK was higher than that by NZK. For the analysis of supernatant by HPLC with CD, D-ala, D-val and D-pro in supernatant existed more than L-ala, L-val and L-pro after adsorption treatment by both kaolinites. For those, it was expected that L-ala, L-val and L-pro was more adsorbed on those kaolinites than D-ala, D-val and D-pro. GK and NZK showed the selective adsorption to a few particular amino acids.

References

[1] E. Friebele, A. Shimoyama, P. E. Hare, and C. Ponnamperuma. Origins Life, **11**, 173 (1981).

[2] H. Hashziume, and B. K. G. Theng. Clay Minerals, **37**, 551 (2002).

---

*Contact author:HASHIZUME.Hideo@nims.go.jp

Measurement of polymer shear modulus using thickness shear acoustic waves.

G.J.Gouws*, R.C.Holt and J.Zhen

The MacDiarmid Institute for Advanced Materials and Nanotechnology, School of Chemical and Physical Sciences, Victoria University Wellington, Wellington 6001, New Zealand.

There is considerable interest in the diffusion of small molecules across polymer membranes, mainly due to the large number of application in which this process plays a role. The use of thickness shear mode (TSM) resonators offers a potential method of studying this diffusion process. This work describes the measurement of polymer viscoelastic properties by this method and in particular the effect of exposure to organic vapours on the observed polymer shear modulus is detail. Two distinct cases are considered, the first when the polymer is a glassy polymer which forms an acoustically thin layer on the resonator and the second when the polymer layer is a rubbery layer that does not move in phase with the resonator surface.

Thin layers of polyethylene oxide (PEO) and polydimethylsiloxane (PDMS) are deposited on TSM resonators with a fundamental frequency of 25 MHz and an impedance analyser is used to measure the impedance and phase around the series resonance point. The resonator response is modeled by the modified Butterworth – Van Dyke equivalent circuit, which is used to calculate the motional parameters of the resonator. The deposition of a polymer layer on the resonator surface introduces an additional motional impedance term in this model and by fitting the modeled impedance spectra to the experimental results, values for the storage modulus G' and the loss modulus G" are calculated.

It is found that the PEO layer has a shear modulus of a value $G = 2.0 \times 10^8 + j1.6 \times 10^6$ Pa. This high value of the storage modulus is indicative of a rigid film. In contrast, the PDMS layers has a typical shear modulus of $1.4 \times 10^6 + j8.1 \times 10^6$ Pa, which is indicative of a polymer in the rubbery state. This difference in viscoelastic properties between the two polymer layers is accentuated when the polymers are exposed to organic vapours. In the case of the PEO player, the resonator shows an increasing drop in resonance frequency with vapour concentration, consistent with that predicted for pure mass loading. In the case of the PEO layer, an anomalous increase in resonance frequency is observed upon exposure to organic vapour. This is explained in terms of the change in viscoelastic properties of this layer due to the further softening from the in-diffusion of the organic molecules. The variation in PDMS shear modulus upon exposure to different concentrations of benzene is shown in figure 1.

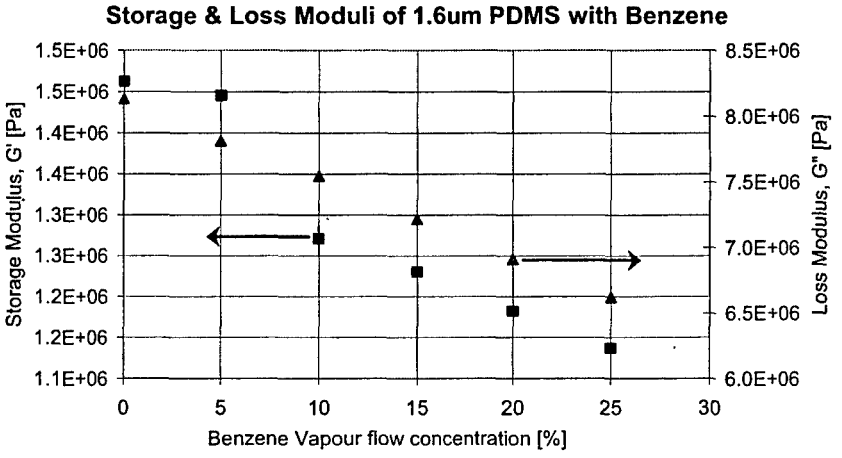

Figure 1: The variation in the storage modulus, G', and the loss modulus, G", of a PDMS layer when exposed to benzene vapour.

* Contact author:gideon.gouws@vuw.ac.nz

Regiospecificity in σ-dimerisation of terthiophenes: a density functional theory study.

T. M. Clarke* and K. C. Gordon
Department of Chemistry, University of Otago, Dunedin, NEW ZEALAND

When an unsymmetrical oligothiophene undergoes a σ-dimerisation reaction, one of three possible regioisomers forms: head-to-head (HH), head-to-tail (HT) or tail-to-tail (TT). This issue of regioregularity has implications for a variety of physical properties of the resulting oligomer or polymer, conductivity in particular.[1] The styryl-substituted terthiophene **I** (Figure 1a) rapidly forms σ-dimers when it is oxidised. Although it has been ascertained that the head-to-head isomer is the sole product of this reaction, it was considered of interest to investigate the structural and vibrational properties of each possible $(\mathbf{I})_2$ isomer (Figure 1b-d) using density functional theory (DFT).

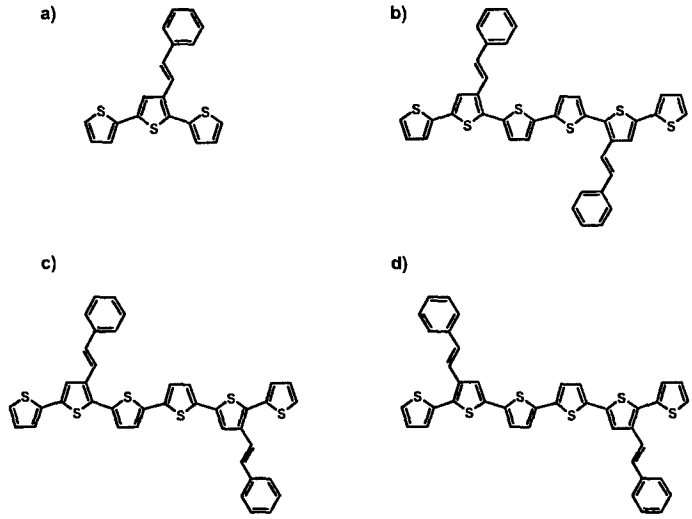

*Figure 1. The structures of **I** (a) and the regioisomers of $(\mathbf{I})_2$: HH (b), HT (c) and TT (d).*

The calculated Raman spectra of neutral HH and HT $(\mathbf{I})_2$ share a number of similar features; however, it is clear that the experimental Raman spectrum of $(\mathbf{I})_2$ more closely matches the spectrum predicted for the HH isomer. The calculated spectrum of TT $(\mathbf{I})_2$ has a very different intensity pattern to that of the other two regioisomers. The Raman spectra of the radical cation and dication were also calculated for each isomer and the spectra in each case are very different. The structures of each isomer's charged species were examined to establish the extent of the polaronic and bipolaronic defects. The HH $(\mathbf{I})_2$ radical cation structure shows its polaronic defect to be strongly confined to the central two thiophene rings. The bipolaron occupies a similar area but the quinoidal nature is more pronounced. In contrast, the TT isomer charged species present more extended defects while the HT charged defects are, not surprisingly, unsymmetrical.

Other parameters such as the relative energies, spin densities, charges and molecular orbital characteristics of the three regioisomers have also been compared. It has been discovered, for instance, that the spin density of the HH $(\mathbf{I})_2$ radical cation is predominantly localised in the centre of the molecule while the spin density of the TT isomer radical cation is delocalised over the thiophene backbone. The molecular orbitals of HT $(\mathbf{I})_2$ and its charged species appear to be a combination of the corresponding molecular orbitals of both the HH and TT isomers.

Reference

[1] H. S. O. Chan and S. C. Ng. Prog. Polym. Sci. **23**, 1167 (1998).

* Contact author: traceyc@alkali.otago.ac.nz

Study of Plasma-polymerized Tetraethylorthosilicate Thin Film

M.A. Badsha[1], F. Ahmed[2], A.B.M.O. Islam[1]* and A.H. Bhuiyan[3]

[1]*Department of Physics, University of Dhaka, Dhaka 1000, Bangladesh*

[2]*Department of Physics, Jahangirnagar University, Savar, Dhaka 1342, Bangladesh*

[3]*Department of Physics, Bangladesh University of Engineering & Technology, Dhaka 1000, Bangladesh*

In recent years, several techniques have been developed for obtaining thin films of organic and inorgancic materials. Of these, plasma polymerization considered a simple yet elegant means to deposit thin films from a wide variety of organic and inorganic monomers. Owing to the wide range of possible technological applications, this technique has been used to prepare organic thin films and cermet thin films and also to modify surface properties etc. In the last few years, there has been increasing interest in the study of the electrical properties of plasma-deposited thin organic films. Although study of the electrical properties of a number of plasma-polymerized organic materials has been carried out, full understanding of the electrical and dielectric behaviour in these materials still requires more investigations, both experimental and theoretical.

In this article, the a.c. conductivity and dielectric response of the as-deposited and heat-treated plasma-polymerized tetraethylorthosilicate (PP-TEOS) films for varied frequency and temperature are examined. The structural investigation has been performed by high-resolution microscopy and infrared (IR) spectroscopy. Films are smooth and pinhole free and observed to be structurally different from TEOS. The a.c. conductivity, dielectric constant, dielectric loss tangent and activation energy of the samples have been measured. The observed data suggest that on heat treatment the PP-TEOS film stabilizes. The dielectric behaviour of the films is discussed in the light of the observed data.[1]

*Corresponding author (A.B.M.O.I): Fax: +880-2-8615583, Email: oislambd@yahoo.com

Electrical Properties in Fuel Cell Based on DNA Film

Y. Matsuo*, G. Kumasaka, J. Hatori, K. Saito and S. Ikehata
Department of Applied Physics, Faculty of Science, Tokyo University of Science, 1-3 Kagurazaka, Shinjyukuku, Tokyo, 162-8601, Japan

Recently, devices based on biomaterials have been investigated with great interest. Especially, considerable efforts have been devoted to the construction of electrical devices based on DNA. The electrical conductivity in the DNA film strongly depends on the atmospheric conditions and increases with the increase of the relative humidity. This increase of electrical conductivity under the humidified condition is caused by the transfer motion of proton that is derived from the breaking of the hydrogen bond formed between oxygen (or nitrogen) in DNA and hydrogen in H_2O molecule, accompanied by the infiltration of the H_2O molecule into the DNA. This result indicates the possibility for the fabrication of fuel cell based on the DNA films under the humidified condition. It is also known that materials used as electrolytes of the fuel cells are very few and therefore the exploitation of new electrolytes of fuel cells is required. Recently, we have tried to fabricate a fuel cell based on the DNA film and have investigated its electrical properties. In the present study, we report the electrical properties of fuel cell based on the DNA film.

Figure 1 shows the relative humidity dependence of the open-circuit voltage in the fuel cell based on the DNA film under the supply of the H_2 gas. We can clearly see that the open-circuit voltage appears under the humidified conditions. This result indicates that the DNA film can be used as the electrolyte of fuel cell under the humidified condition. Moreover as shown in Fig. 1 the open-circuit voltage strongly depends on the relative humidity condition. The open-circuit voltage steeply begins to increase around 14 %, takes a maximum around the 55 % relative humidity condition and thereafter tends to decrease to almost zero. Thus in the fuel cell based on the DNA film the optimum condition, in which the open-circuit voltage becomes a maximum, exists and is achieved under the 55 % relative humidity condition. Figure 2 shows the frequency dependence of ε'' (the imaginary part of dielectric constant) observed under the various relative humidity conditions. It is evident that the behaviour of ε'' strongly depends on the relative humidity. Under the 55 % relative humidity condition, ε'' is approximately inversely proportional to frequency. This result indicates that ε'' mainly consists of the DC conductivity ($\sigma_0 = \omega\varepsilon''\varepsilon_0$). On the other hand, under the 14 % relative humidity condition, in which the open-circuit voltage is almost zero, we can observe not only the decrease in the component of DC conductivity but also the appearance of the component of the dielectric dispersion (for example, $\varepsilon''=(\varepsilon_s-\varepsilon_\infty)\omega\tau/(1+\omega^2\tau^2)$) in the high-frequency region. Under the 85 % relative humidity condition, the behaviour of ε'' is different from those observed in the lower relative humidity region. The imaginary part of dielectric constant ε'' increases compared with those of the 55% and 14 % relative humidity conditions and shows the maximum at approximately 50 kHz. These results indicate that under the high-relative humidity, in which the open-circuit voltage tends to be zero, the new dielectric dispersion related to the reorientational motion of the DNA molecule appears around 50 kHz, although DC conductivity increases. From these results, it is deduced that the optimum conduction of the fuel cell based on the DNA film is closely related not only the proton conductivity but also the existence of the dielectric dispersion.

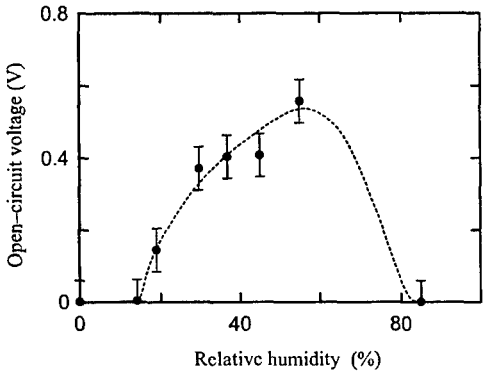

Figure 1 Relative humidity dependence of open-circuit voltage

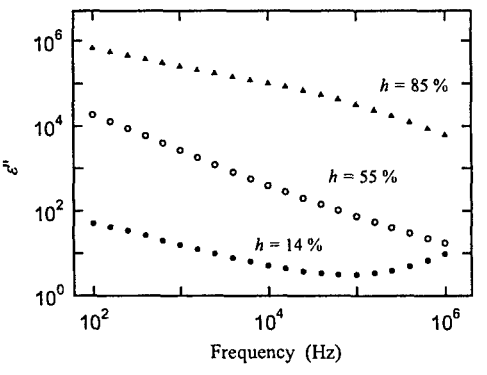

Figure 2 Frequency dependence of ε''

* Contact author: ymatsuo@rs.kagu.tus.ac.jp

Polymer Films and LEDs: How to Realise Ultra Low-Cost & Low-Power Chemical Sensing Platforms

Dermot Diamond[1]
AIC Adaptive Sensors Group, National Centre for Sensor Research, School of Chemcial Sciences, Dublin City University, Dublin 9, Ireland

In order to realise scalability of chemical sensors in extensively deployed wireless sensor networks, considerable materials challenges must be overcome. For example, conventional devices (including sensing film, sampling, transducer, signal capture, digitisation, data storage and communication) are currently far too expensive for massive scale up in numbers, and too unreliable for long-term (months, years) field deployment.[1]

Cost can be driven down by imaginative approaches to transduction and instrument design. For example, we have produced a complete instrument based on LED measurement of colour changes that has sub-micromolar detection limits for a number of heavy metals for around $1.[2] In its current form, the device also has a wireless communications functionality (albeit over relatively short distance, around 1 m), and very low power consumption.

However, chemical sensors capable of long-term reliability will require imaginative solutions to the key issue – how can the sensing films/membranes in chemical sensors maintain unchanging (or predictable) characteristics in long term deployment? In other words, how can a film that must interact chemically with a sample remain unchanged?

The vision of 'internet-scale sensing' will only be realised through advances in materials science, and a complete rethink of how we do chemical sensing. For example, fully autonomous sensing platforms must be completely self-reliant in terms of power, communications, reagents and consumables. The sensor network must be self-sustaining, meaning that as individual nodes become unreliable, new nodes are established, for example through physical replacement or through devices capable of self-repair/regeneration.

In this paper, these issues will be presented, along with some recent advances mentioned above. The importance of close cooperation of researchers working on new materials, innovative approaches to sensing and ultra low-power wireless communications will be an essential strategy for future progress in this exciting area of multidisciplinary research.

References

1 Dermot Diamond, Internet Scale Sensing, Analytical Chemistry A-Section, 76 (2004) 278A-286A.

2 Novel Fused-LED Devices as Optical Sensors for Colorimetric Analysis, King Tong Lau, Susan Baldwin, Roderick L. Shepherd, Paul H. Dietz, William S. Yerazunis, and Dermot Diamond, Talanta 63 (2004) 167–173.

[1] dermot.diamond@dcu.ie

Novel Buckyball Functionalised Terthiophene and Polyterthiophenes - Electrochemistry, Synthesis, Characterisation and Applications

J. Chen[a,b], G. Tsekouras[a,b], D.L. Officer[a,c], P. Wagner[c], C. Y. Wang[b], C.O. Too[a,b], and G.G. Wallace[a,b]*

[a] *ARC Centre for Nanostructured Electromaterials, University of Wollongong, NSW 2522, Australia*
[b] *Intelligent Polymer Research Institute, University of Wollongong, NSW 2522, Australia*
[c] *Nanomaterials Research Centre, Massey University, Private Bag 11222, Palmerston North, New Zealand*

A novel buckyball functionalised terthiophene monomer, TTh-BB has been successfully electropolymerised to form the homopolymer, poly(TTh-BB), and the copolymer with terthiophene (TTh), poly(TTh-BB-co-TTh) using potentiodynamic, potentiostatic and galvanostatic procedures. The polymers have been characterised using cyclic voltammetry (CV), in-situ UV-visible spectroscopy, contact angle measurement, scanning electron microscopy and Raman spectroscopy. It is evident from CV, UV-vis, and Raman spectra that the buckyball has been incorporated into the copolymer, poly(TTh-BB-co-TTh). Preliminary investigation into the potential use of these novel buckyball functionalized polymers in photo-electrochemical cells, capacitors, and cathode materials in polymer batteries have been carried out.

Keywords: Buckyball; Synthesis; Electrochemistry; Terthiophene

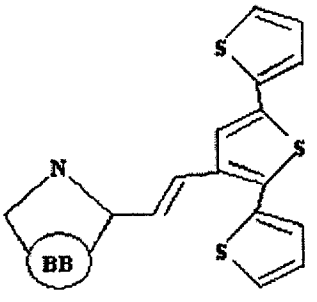

TTh-BB

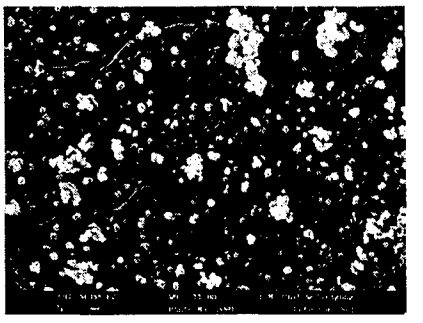

SEM of Poly(TTh-BB)

References:

[1] H.W. Kroto, J.R. Heath, S.C. O'Brien, R.F. Curl, R.E. Smalley, Nature 318 (1985) 162.

[2] E. Frackowiak, S. Gautier, H. Gaucher, H. Bonnany, F. Beguin. Carbon. 37 (1999) 61.

[3] J.P. Ferraris, A. Yassar, D.C. Loveday, M. Hmyene. Optical Materials. 9 (1998) 34.

[4] S. Wang, S.X. Xiao, Y.L. Li, Z.Q. Shi, C. Du, H.J. Fang, D.B. Zhu. Polymer. 43 (2002) 2049.

*Corresponding author: gordon_wallace@uow.edu.au

Photovoltaic and Electrochromic Properties of Poly(3-alkylthiophenes) and Poly(3,3"-didecyloxyterthiophenes)

G. Tsekouras[1], C. O. Too[1], G. G. Wallace[1,*], S. Gambhir[2], K. Wagner[2] and D. L. Officer[2]

[1] *ARC Centre for Nanostructured Electromaterials and Intelligent Polymer Research Institute, University of Wollongong, Northfields Avenue, Wollongong, NSW 2522, Australia.*

[2] *Nanomaterials Research Centre, Massey University, Private Bag 11222, Palmerston North, New Zealand*

Poly(3-hexylthiophene) (P3HT) and poly(3-octylthiophene) (P3OT) were synthesised by oxidative polymerisation using $FeCl_3$. The effects of the order of reactant addition on molecular weight and regioregularity were determined. Photoelectrochemical cells (PECs) based on spin cast P3HT and P3OT showed poor photovoltaic (PV) properties. Blending of P3HT and P3OT with the soluble C_{60} derivative PCBM resulted in greatly enhanced PV properties, as found previously by Camaioni *et al.* [1] P3HT and P3OT also exhibited electrochromism from red to blue when switched between reduced and oxidised states. The 3,3"-didecyloxyterthiophene derivatives **I**, **II** and **III** were readily electropolymerised onto ITO glass. The corresponding homopolymers P(**I**), P(**II**) and P(**III**) showed very stable electrochemical properties. *In-situ* spectroelectrochemistry of P(**I**), P(**II**) and P(**III**) showed a decrease in absorption due to π-π^* transitions and a corresponding increase in absorption at longer wavelengths as the oxidation state was raised. These findings were similar to those observed by Lee *et al* [2] for the polymer based on terthiophene-3'-carboxylic acid and by Ribeiro *et al* [3] for novel polymers based on 3-alkylthiophenes. Accompanying the transition from reduced to oxidised states for all homopolymers was a change from dark violet to transmissive blue.

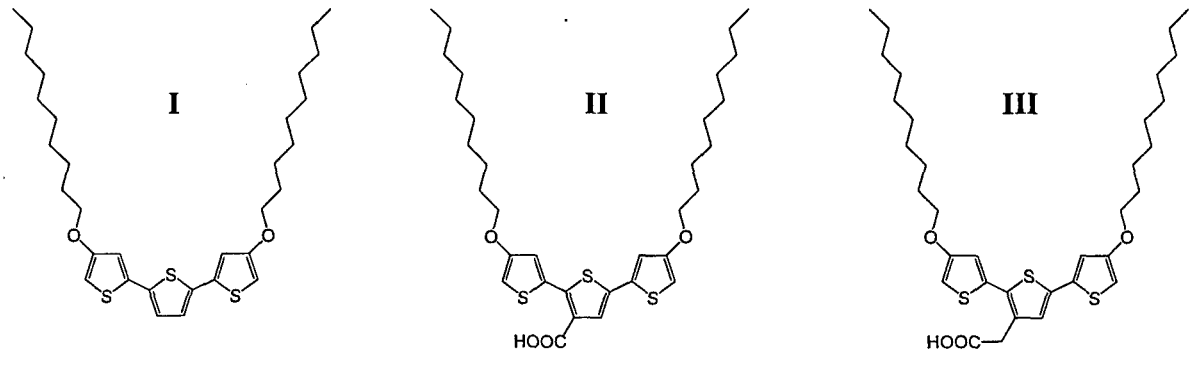

References

1. Camaioni, N., Garlaschelli, L., Geri, A., Maggini, M., Possamai, G. and Ridolfi, G., *Journal of Materials Chemistry*, 12 (2002) 2065-2070.
2. Lee, T.-Y., Shim, Y.-B. and Shin, S.C., *Synthetic Metals*, 126 (2002) 105-110.
3. Ribeiro, A.S., Gazotti, W.A., dos Santos Filho, P.F. and De Paoli, M.-A., *Synthetic Metals*, 145 (2004) 43-49.

* Corresponding author: gordon_wallace@uow.edu.au

High-Density Assembly of Nanocrystalline Silicon Quantum Dots

A. Tanaka[1,3], Y. Tsuchiya[1,3], K. Usami[1,3], H. Mizuta[2,3] and S. Oda[1,3,*]
[1] *Quantum Nanoelectronics Research Centre, Tokyo Institute of Technology, Tokyo, Japan*
[2] *Department of Physical Electronics, Tokyo Institute of Technology, Tokyo, Japan*
[3] *CREST, JST (Japan Science and Technology)*

The bottom-up approach to form nanometer-scaled silicon structures is attracting more attentions as an alternative way of developing future quantum nanoelectronics devices since maintaining the conventional top-down miniaturization trend is getting harder due to fundamental physical and technological limitations as well as of the economical limitation. Nanocrystalline silicon (nc-Si) quantum dots [1,2] are particularly a promising material and various new device applications have been explored based on their unique electronic and photonic properties. In this paper we report on a new bottom-up technique of high-density assembly of the nc-Si quantum dots based on natural aggregation of the dots in the solution. We previously studied how the nc-Si dots deposited on the Si substrate get mobile in the hydrofluoride (HF) solution by simply dipping the substrate with the nc-Si dots on into the HF solutions [3]. We demonstrated the HF solution droplet evaporation method that utilizes aggregation of the dots when we evaporate a solution droplet applied onto the nc-Si dots randomly deposited on the Si substrate. It was shown that the nc-Si dots are assembled in a droplet of the HF solution, resulting in various regular patterns locally on the substrate. In the present study we examined to use various other solvents for making the nc-Si dispersed solution more suitable for achieving highly dense nc-Si assembly.

Nanocrystalline Si dots with a diameter of 8±1 nm were deposited on the Si substrates by using VHF plasma decomposition of pulsed SiH_4 gas supply. The samples were immediately (within one minute) put into pure water, methanol and cyclohexane (C_6H_{12}), and ultrasonic cleaning was conducted for 5 minutes. We then observed by SEM how well the nc-Si dots were come off from the substrate. After that we concentrated the solution by heating and dropped a small volume of condensed solution onto a new substrate as shown in Fig. 1. After drying the solution droplet, we observed the assembled nc-Si dots by using SEM. For all three solvents we observed that the nc-Si dots were removed from the substrate to a large extent. After the drop & evaporation process, we could observe the assembled nc-Si dots only for the methanol solvent. The capillary meniscus interactions [4] are supposed to work between the nc-Si dots immersed partially in the methanol, resulting in the dot aggregation. Figure 2 shows the SEM image of the assembled nc-Si dots. We could achieve the areal dot density of approximately 7 x 10^{11} cm^{-2} which is fairly close to the close packing of the spheres with a diameter of 10 nm. Quasi-regular patterns of the dots are also recognized locally in the assembly (Fig. 2).

References

[1] T. Ifuku, M. Otobe, A. Itoh, and S. Oda, *Jpn. J. Appl. Phys.* **36**, 4031 (1997).
[2] K. Nishiguchi, S. Hara, and S. Oda., *Mat. Res. Soc. Symp. Proc.* **571**, 43 (2000).
[3] Y. Tsuchiya, T. Iwasa, A. Tanaka, K. Usami, H. Mizuta, S. Oda, MRS Spring Meeting, April 2004.
[4] P. A. Kralchevsky, V. N. Paunov, N. D. Denkov, I. B. Ivanov and K. Nagayama, J. Colloid Interface Sci. **155**, 420 (1993).

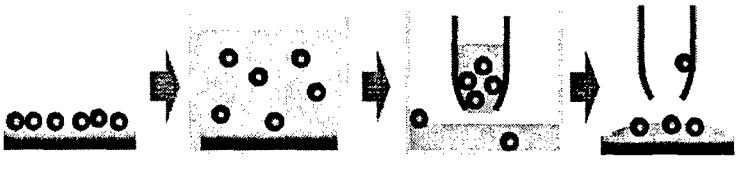

Fig. 1 Nanocrystal Si dots deposition, removal & condensation in the solvent and dripping of the nc-Si solution

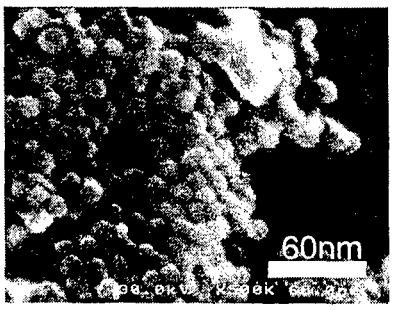

Fig. 2 SEM image of assembled nc-Si dots obtained by using methanol solution drop & evaporation method

Contact author: soda@pe.titech.ac.jp

Quantum dots conjugated with captopril while remained effective *in vivo*

Noriyoshi MANABE[1,*], Akiyoshi HOSHINO[1], Yi-qiang LIANG[2], Tomomasa GOTO[1], Norihiro KATO[2] and Kenji YAMAMOTO[1]

[1]*Department of Medical Ecology and Informatics, Research Institute, International Medical Center of Japan, Tokyo, Japan*

[2]*Department of Gene Diagnostics and Therapeutics, Research Institute, International Medical Center of Japan, Tokyo, Japan*

Inorganic fluorophore quantum dots are nanometer-size probes that have the potential to be applied to the fields of the bio-imaging (1) and the study of the cell mobility inside the body (2). At the same time, on the other hand, quantum dots are expected to carry some kind of molecules to the local organ inside of the animal body, which leads to the expectation that they can be used as a medicine-carrier. For this purpose, we conjugate (2S)-1-[(2s)-2-Methyl-3-sulfanylpropionyl] pyrrolidine-2-carboxylic acid (captopril) with the quantum dots. Captopril has the effect as an anti-hypertension drug, which inhibits angiotensin 1 converting enzyme. We conjugated the quantum dots with captopril by the exchange reaction avoiding the regions that holds medicinal effect. Approximately 180 captopril are coordinating with yellow quantum dots. Quantum dots conjugated with captopril (QD-cap) were 20% brighter than 11-mercaptoundecanoic acid (MUA)-coated quantum dots (QD-MUA) that had the stronger intensity of the fluorescent light than any other our previously works. The wavelength of the QD-cap was slightly shorter than that of the original non-conjugated quantum dot. The particle size of captopril was 1.1nm and that of QD-cap was 12nm. QD-cap was permeated into the HeLa cells, while QD-MUA were taken into the HeLa cells by endocytosis. In addition, no apoptosis was detected against the cells that permeated QD-cap, because there was no damage to DNA. These results indicated that QD-conjugated medicines (QD-medicine) could be safe in the experiment on the level of the cell. More over, when QD-cap was intravenously injected into Stroke-prone Spontaneously Hypertensive Rats (SHRSP), they reduced blood pressure at systole. Therefore, the anti-hypertension effect of captopril remained after conjugated with the quantum dot. Furthermore, 30min after the injecting, almost all of QD-cap existed in the plasma. These results suggested that QD-medicine were effective on the animal level.

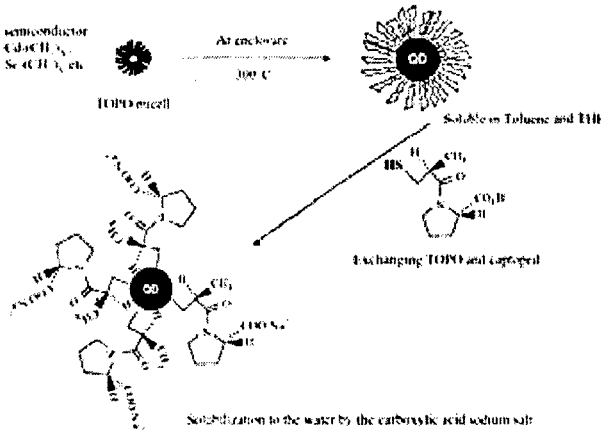

Figure The synthesis of quantum dot conjugated captopril

References

[1] Hanaki K. et al., Biochem. Biophysic. Res. Commun. **302**, 496-501 (2003).

[2] Hoshino A., Hanaki K., Suzuki K. and Yamamoto K., Biochem. Biophysic. Res. Commun. **314**, 46-53 (2004).

*Contact author: backen@ri.imcj.go.jp

Charging Effect of Gold(Au) Nano-particles embedded in SiO_2

Jae Hoon Kim[1], Eun Kyu Kim[1,*] and Won Mok Kim[2]
[1] *Department of Physics, Hanyang University, Seoul 133-791, KOREA*
[2] *Korea Institute of Science and Technology, Seoul 130-650, KOREA*

The optical properties of nano-size particles have studied very actively. But the electrical properties of quantum dots (QDs) are also important, because of its possibility for single-electron memory devices and other useable electronic devices. Especially, applying of electrical charging effect of the nano-particles non-volatile nano floating gate memory (NFGM) device could be made. The NFGM being a kind of non-volatile memory devices has several advantages because the process is alike MOS(metal oxide semiconductor) process and its quantum effective action may use the register memory of quantum information processing[1,2].
The size of gold particles is controlled with thickness of gold metal film. Firstly, the structure is made with metal film as shown in figure 1. And then under thermal annealing at 300 °C, Au nano-particles are formed within SiO_2. SiO_2 is a stable dielectric material, so any charge can pass from Si wafer to the particle by only tunneling. The charging electron in the particle could be retained during enough time, if no bias is added the structure.
In this study, we experienced by mono-layer and double-layers with Au particles structures and the diameters of Au particles are from 0.5 to 3 nm. Figure 2 shows the result of mono-layer with Au particles of 15 nm. Capacitance variance under voltage sweeping looks what of an electrical switching device. We discussed the capacitance-voltage relation for particle size and measuring temperature condition. And double-layers with Au particle structure also discussed on its capacitance-voltage result and charge coupling.

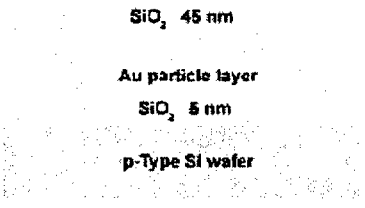

Figure 1. structure of Au particles within SiO_2

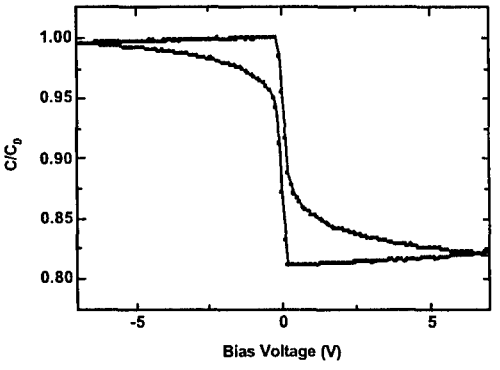

Figure 2. C-V characteristic of mono-layer with Au particles at Room Temp

References

[1] El-Sayed Hasaneen, E. Heller, R. Bansal, W. Huang and F. jain, Sol. Stat. Electron. **48**, 2055 (2004)
[2] J. Ackaert, A. Lowe, S. Boonen, T. Yao, J, Rayhem, B. Desoete, J. Prasad, M. Thomason, J. Van Houdt, R. Degraeve, L. Haspeslaghm and P. Hendrickx, Sol. Stat. Electron. **48**, 1911 (2004)

* Contact author: ek-kim@hanyang.ac.kr

Electrochemical Detection of DNA hybridization Amplified by CdS Nanoparticles

H. Peng,* C. Soeller and J. Travas-Sejdic
Polymer Electronics Research Centre
The University of Auckland, Private Bag 92019, Auckland, New Zealand

The detection and quantification of specific DNA/RNA sequences is of great importance in numerous applications, such as drug research, food technology, forensics and clinical diagnosis. Due to its simplicity and low cost, DNA sensors attract considerable research interest. DNA sensors based on a variety of transduction mechanisms have been developed, such as optical, microgravimetric and electrochemical [1]. Amplified DNA analyses have been reported using specific antibodies [2], labeled proteins [3] and nanoparticles [4]. In the present work, we investigate the amplification of DNA sensing by semiconductor CdS nanoparticles and AC impedance spectroscopy which is an efficient method to probe and model the interfacial characteristics of the transducer.

CdS nanoparticles were synthesized using mercaptoacetic acid as the stabilizer [5]. Oligonucleotide (ODN) probes were covalently immobilized on CdS nanoparticles by using 1-ethyl-3-(3-dimethylaminopropyl)carbodiimide.

The ODNs were immobilized into an electropolymerized polypyrrole film on a gold electrode. Hybridization was carried out by incubating the obtained PPy/ODN film in a PBS solution (pH 7.2) containing ODN labelled CdS nanoparticle probes for 5 h. Fig. 1 shows admittance spectra of PPy/ODN films before and after hybridization. Upon incubation of the PPy/ODN film in CdS-ODN probe solution a significant change in the admittance spectra was observed. The association of negatively charged CdS-ODN complex to the PPy/ODN film as a result of the primary recognition event may have led to the formation of a negatively charged 'micromembrane' interface on the PPy film, which altered the interfacial characteristics of the transducer. In the presence of the negatively charged redox probe $Fe(CN)_6^{3-}$ / $Fe(CN)_6^{4-}$, the electrostatic repulsion hindered the interfacial charge transfer and caused a decrease in admittance of the film.

This sensor showed good selectivity. The obtained sensor responses for one-, two-, and six-point mismatched ODNs were 62.6 %, 55.2 % and 18.7 % of the exact match response, respectively. The sensor signal in the presence of a non-complementary ODN was approximately 12.2 % of the sensor signal obtained with the complementary ODN.

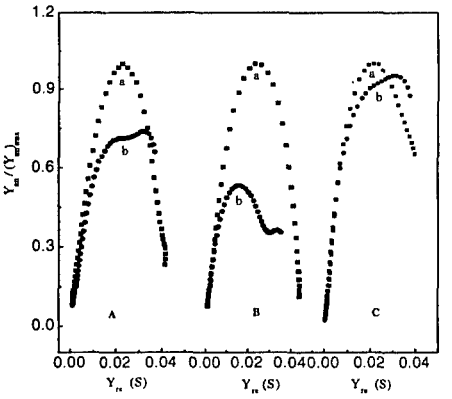

Fig.1 Admittance spectra of Au/PPy/ODN films in PBS solution containing 5.0 mM $Fe(CN)_6^{3-}$ / $Fe(CN)_6^{4-}$ before and after incubation with 20 μg/mL ODN probe or CdS-ODN probe. (A) Au/PPy/complementary ODN film: before (a) and after (b) incubation with ODN probe (B) Au/PPy//complementary ODN film: before (a) and after (b) incubation with CdS-ODN probe. (C) Au/PPy film prepared without ODNs: before (a) and after (b) incubation with CdS-ODN probe.

References

[1] T. G. Drummond, M. G. Hill, J. K. Barton, Nature Biotechnology **21**, 1192 (2003).
[2] A. Bardea, A. Dagan, I. Ben-Dov, B. Amit, I. Willner, Chem. Commun. **7**, 839 (1998).
[3] A. Bardea, F. Patolsky, A. Dagan, I. Willner, Chem. Commun. **1**, 21 (1999).
[4] F. Patolsky, K.T. Ranjit, A. Lichtenstein, I. Willner, Chem. Commun. **12**, 1025 (2000).
[5] L. Jiang, X.Chen,W.S. Yang, L. Jin, B.Q. Yang, L. Xu, T.J. Li, Chem.J.Chin.Univ. **22**,1397 (2001).

Acknowledgement:
The authors greatly thank the University of Auckland VC Development and Staff Research Funds for financial support.

*Contact author: h.peng@auckland.ac.nz

Fundamental and applied Directions of Field Emission Electronics using Nanocluster Carbon Materials

Yu.V. Gulyaev[1*], S.A.Nikitov[1],
[1]Institute of Radioengineering & Electronics, Russian Academy of Sciences, 101999, 11, Mokhovaya St., Moscow, Russia

Fundamental and applied directions of field emission electronics on the base of carbon nanocluster materials are considered. It is shown that these films provide high level of field electron emission and substantional thermal electron emission even at low temperatures. These films exhibit low electron work function and ensure stable field emission under the conditions of operating vacuum.The emission properties of thin films composed of nanotube and nanocluster carbon structures are described. Potentials for their improvement on the path to apply them in various devices are described.

* gulyaev@cplire.ru

Local field effects on the radiative lifetimes of Ce^{3+} in different hosts

C.-K. Duan[1] and M. F. Reid[2*]

[1] *Institute of Applied Physics, Chongqing University of Post and Telecommunications, Chongqing 400065, China, and Department of Physics and Astronomy, University of Canterbury, Christchurch, New Zealand*

[2] *Department of Physics and Astronomy, and MacDiarmid Institute of Advanced Materials and Nanotechnology, University of Canterbury, Christchurch, New Zealand*

It is well known that radiative transition process of emitters in a medium differs from those in vacuum[1]. Because of the fundamental importance and the relevance to various applications in low-dimensional optical materials and photonic crystals, this issue continues to attract both theoretical and experimental attention. Various macroscopic and microscopic theoretical models have been developed to predict, among other optical properties, the spontaneous emission rates or lifetimes[1,2,3]. Different models predict substantially different dependencies of spontaneous emission rates or lifetimes on refractive index.

Various measurements of Eu^{3+} in hosts with variable refractive index appear to favor the real-cavity model [1,4]. However, these measurements are on $f \rightarrow f$ transitions of rare-earth ion Eu^{3+}, which are only weakly electric-dipole allowed due to perturbations of ligands, and therefore the radiative transition rates are very sensitive to the local arrangement of the ligands. This effect is very important but also very difficult to take into account, so is neglected in the analysis. Since $d \rightarrow f$ radiative transitions of rare-earth ions are dominated by allowed electric-dipole transitions, whose line strengths are less perturbed by the ligands, the dependence of $d \rightarrow f$ radiative rates on refractive index is a better test. In this work we analyse the lifetimes of $d \rightarrow f$ Ce^{3+} in hosts of different refractive indices. The results favor the macroscopic model based on Lorentz local field, i.e. the virtual-cavity model [1].

References

[1] D. Toptygin, J. Fluoresc. **13**, 201 (2003) and references therein.
[2] M. E. Crenshaw and C. M. Bowden, Phys. Rev. Lett. **85**, 1851 (2000).
[3] P. R. Berman and P. W. Milonni, Phys. Rev. Lett. **92**, 053601 (2004).
[4] G. M. Kumar, D. N. Rao, and G.S. Agarwal, Phys. Rev. Lett. **91**, 203903 (2003).

* Contact author: Mike.Reid@canterbury.ac.nz

Advanced Materials for Dosimeter Applications

G. V. M. Williams[1,*] C. Dunford[1], S. Schweizer[2], J. –M. Spaeth[2], B. Henke[2], M. Secu[2,3], and U. Rogulis[2,4]
[1] *Industrial Research, Lower Hutt, NEW ZEALAND*
[2] *Department of Physics, Faculty of Sciences, University of Paderborn, GERMANY*
[3] *National Institute of Materials Physics, Bucharest-Magurele, ROMANIA*
[4] *Institute of Solid State Physics, University of Latvia, Riga, LATVIA*

We have recently commenced a New Enterprise Research Fund (NERF) program to study advanced materials and techniques for radiation dosimeters based on optical excitation and emission. The materials that we are studying and the technique of optical read-out represents a departure from current dosimeters based on ionization gauges, solid state or thermo-luminescent devices. The first two methods provide an immediate electronic reading but they are expensive. The last method provides a record of the cumulative dose, but the read-out is destructive because it involves heating to thermally excite the trapped carriers and recording of the resultant thermo-stimulated-luminescence.

The requirements for all-optical dosimeters include the ability to retain a record of the radiation dose for extended periods of time (in excess of two weeks) and the ability to optically erase the dose information. It is expected that a potential application would have the advantage of requiring only one readout device with many different reusable detectors.

It has been known for some time that Mn-doped fluoride compounds are susceptible to radiation damage that can lead to an increase in the optical absorption coefficient in the visible region. Furthermore, a recent study on a Mn-doped fluoroperovskite has shown that there is also an enhanced photo-luminescence, which makes these compounds potentially useful as radiation dosimeters. In this paper we report the preliminary results from long-term stability and Manganese concentration dependent measurements.

References

[1] W. A. Sibley, and N. Koumvakalis, Phys. Rev. B **14**, 35 (1976).
[2] B. Henke, M. Secu, U. Rogulis, S. Schweizer, and J.-M. Spaeth, Phys. Stat. Sol. (in press).

* Contact author: g.williams@irl.cri.nz

Optical Scattering in Glass Ceramics

A. Edgar[1,2*], R.Tilley[1,2], A. Bittar[1,3], G.V.M. Williams[1,3]
[1] *MacDiarmid Institute for Advanced Materials and Nanotechnology*
[2] *School of Chemical and Physical Sciences, Victoria University, Wellington NEW ZEALAND*
[3] *Industrial Research Ltd, Wellington, NEW ZEALAND*

Glass ceramics, comprising nano- or micro-crystals embedded in a glass matrix, have many potential and current optical applications such as fibre lasers and sensors, and imaging plates. Glass ceramics offer the advantages of a transparent medium which can be readily fabricated into shapes such as plates, lenses, and optical fibres, and a crystalline environment for common dopant ions such as those from the rare-earth series.

The optical transparency is critically dependent on particle size, concentration, and refractive index mismatch with the host glass. In the limiting case of a low concentration of particles whose size is much less than the wavelength of light in the medium, the scattering is described by the well known Rayleigh theory, and for larger particles by the theory of Mie. Both of these are single-particle scattering theories, and take no account of multiple scattering or interference effects.

Tick[1] has reported that glass ceramics containing a high concentration of crystals can display ultra-transparency – that is a transparency much higher than expected from Mie scattering theory, and almost as high as the host glass. This would be in accordance with the idea that the material can be described as a single optical medium with a refractive index given by the usual effective medium theories. It would be very useful to have a theory or calculation which fills the gap between Mie/Rayleigh and effective media theory. Earlier attempts at this problem by Hopper[2] and Hendy[3] have been based on the structural model of spinodal decomposition, which is rather different to the usual structure of a glass ceramic, and the calculations do not include multiple scattering effects.

In this paper, we examine the applicability of a model first proposed by Purcell and Pennypacker[4] to calculate the optical scattering for dust grains of arbitrary shape in an astrophysical context. The model is based on an array of polarisable point dipoles, and satisfactorily reproduces the Mie scattering results for spherical particle geometries. However, there is no intrinsic reason why it cannot be extended to particular spatial distributions of point dipoles which represent a glass ceramic. Here we report our preliminary results on simulating the optical absorption and scattering, and confront the results with experimental measurements for fluorozirconate glass ceramics which contain halide nano-crystals. The particle size and distribution are determined using electron microscopy.

The implications for X- and gamma-ray imaging plates are briefly discussed.

References

[1] P. A. Tick, N. F. Borelli, and I. M. Reaney, Optical Materials **15,** 81 (2000).

[2] R. W. Hopper, Journal of Non-Crystalline Solids **49,** 263-285 (1982).

[3] S. C. Hendy, Applied Physics Letters **81,** 1171 (2002).

[4] E. M. Purcell and C. R. Pennypacker, The Astrophysical Journal **186,** 705-714 (1973).

* Contact author: Andy.Edgar@vuw.ac.nz

Simulation of the Photoluminescence Process of Er^{3+} and Si Nanocrystal Co-doped in Silica

C.-K. Duan*

Institute of Applied Physics, Chongqing University of Post and Telecommunications, Chongqing 400065, China, and Department of Physics and Astronomy, University of Canterbury, Christchurch, New Zealand

Er^{3+} and Si nanocrystal (nc-Si) co-doped silica has been attracting strong research interest due to its potential applications in planer-waveguide optical amplifier [1] and electroluminescence devices [2], and its possible integration with current semiconductor processing technologies. Various experiments show that Er^{3+} emission is greatly sensitized by nc-Si [3]. Models have been proposed to simulate the photoluminescent dynamical process and produced PL intensities, lifetimes agreeing with measurements [4]. However, in the simulations, the two very important up-conversion parameters, which should strongly depend on the Er^{3+} concentrations, were chosen fix values. Also, the simulation involves many parameters whose values could not be determined. In this paper, we reanalysis the PL processes by exploring the energy transfer mechanism between nc-Si and Er^{3+}, taking the concentration dependence of up-conversion into account, and reducing the number of parameters by combine several process into one effective process. We also give some predictions to guide further experimental investigation.

References

[1] H. Han, S. Seo, J. Shin, and N. Park, *Appl. Phys. Lett.* **81,** 3720 (2002).
[2] M. E. Castagna, S. Coffa, M. Monaco, L. Caristia, A. Messina, R. Mangano, and C. Bongiorno, *Physica E* **16**, 547 (2003).
[3] M. Wojdak, M. Klik, M. Forcales, O. B. Gusev, T. Gregorkjewicz, D. Pacifici, G. Franzo, F. Priolo, and F. Iacona, *Phys. Rev. B* **69**, 233315 (2004).
[4] D. Pacifici, G. Franzo, F. Priolo, F. Iacona, and L. D. Negro, *Phys. Rev. B* **67**, 245301 (2003).

* Contact author: chang-kui.duan@canterbury.ac.nz

The Dynamics of Crystalline Structure Formation in Lumogen Optical Coatings

A. Deslandes[1], A. B. Wedding[2], and J.S. Quinton*[1]
[1] *School of Chemistry, Physics and Earth Sciences, Flinders University, GPO Box 2100, Adelaide, SA, 5001, Australia.*
[2] *School of Electrical and Information Engineering, University of South Australia, GPO Box 2471, Adelaide, SA, 5001, Australia*

The fluorescent properties of azomethine pigment materials facilitate their use for wavelength converting optical coatings. In this application, the pigment converts ultraviolet radiation to visible light and hence can be used to increase the quantum efficiency (QE) of silicon-based photon detectors such as charge coupled devices (CCDs) [1]. In particular, these coatings are employed for the UV imaging systems of the Hubble Space Telescope and the Cassini-Huygens Spacecraft that reached the Saturnian system in 2004.

Previous reports, however, have shown that as-deposited amorphous Lumogen films exhibit non-uniformity [2], and crystalline growth within the film, if left standing at room temperature for any length of time [3,4]. These properties influence the optical properties and hence affect the performance of these films. In this research area, we are interested in harnessing this behaviour to produce nanocrystalline coatings with controlled optical properties. Using a physical vapour deposition method (PVD) under vacuum, commercial Lumogen® Yellow S0790, an azomethine pigment material with chemical structure as shown in figure 1, was deposited on flat silicon dioxide glass slide surfaces.

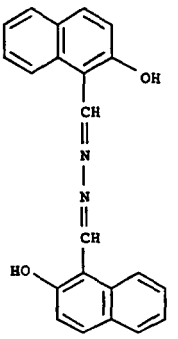

Figure 1. The chemical structure of Lumogen® Yellow S0790

Through the use of techniques such as X-ray Diffraction (XRD), Ultraviolet-Visible Absorption Spectroscopy (UV-vis) and Scanning Electron Microscopy (SEM), the growth kinetics of crystalline structures within the surface film have been studied as a function of time and temperature (ie under refridgeration at 5° C, at room temperature ~ 20° C and at 80° C). Our results demonstrate a significant influence of the storage temperature upon the nucleation and growth of crystals within the film, as well as a difference in the structures that evolve in each case. In addition to studies of the crystal growth mechanisms and annealing temperature, our results further show a strong film crystallinity dependence upon the substrate temperature during deposition. Comparison between UV-vis spectra and XRD results indicates the influence of film structure and morphology upon the resultant optical properties of the film.

Investigation into the structural changes of these films and subsequent changes in their optical properties enables films to be produced with maximum stability and uniformity. In future, the ability to tailor the optical properties of these coatings will enable superior detector technologies.

References

[1] P. F. Morrissey et al., Appl. Opt. **33**, 2534 (1994)
[2] C. L. Butner and W. Viehmann, Appl. Opt. **23**, 2046 (1984)
[3] N. Kristianpoller and D. Dutton, Appl. Opt. **3**, 287 (1964)
[4] J. Janesick, *Scientific Charge Coupled Devices* (SPIE, Bellingham, WA, USA, 2001), p. 179

* Contact Author: Jamie.Quinton@flinders.edu.au

Microstructure and Optical Study of Al Implanted ZnO Thin Films

J. Lee[1], C. Depagne[2], J. Metson[3,*],
P. Evans[2] and D. Bhattacharyya[1]

[1]*Department of Mechanical Engineering, University of Auckland, Private Bag 92019, Auckland, NEW ZEALAND*
[2]*Australian Nuclear Science and Technology Organization, PMB 1, Menai, NSW 2234, AUSTRALIA*
[3]*Department of Chemistry, University of Auckland, Private Bag 92019, Auckland, NEW ZEALAND*

Zinc oxide (ZnO), is a wide band gap semiconductor, displaying interesting photoconducting, piezoelectric, and optical properties. It has a wide range of actual and potential scientific and technological applications in UV light-emitters, varistors, transparent high power electronics, surface acoustic wave devices, piezoelectric transducers, gas-sensing and as a window material for flat panel displays and solar cells [1].

Ion implantation utilizes highly energetic beams of ions to modify surface chemistry, electronic properties and microstructure of materials at low substrate temperatures [2]. For ZnO, n-type conductivity is common in the as prepared material or relatively easy to realize via excess Zn or with Al, Ga, or In doping. Al is frequently used as a dopant to modify the conductivity of ZnO thin films [3]. With respect to p-type doping, ZnO displays significant resistance to the formation of shallow acceptor levels [4]. ZnO thin films deposited by rf magnetron sputtering were implanted with Al in order to study the effects of implantation on their microstructural and optical properties. The implanted films were examined to detect modification of microstructure, optical transparency, and photoluminance, in comparison with unimplanted samples. We have found that implantation without annealing leads to a weaker photoluminance because of the implantation induced structural defects. The reflective index, measured by ellipsometry, film thickness and band gap of Al implanted and unimplanted ZnO thin films have been determined. The micro structural effects of implantation on optical properties will also be discussed.

References

1 S.-Y. Chu, W. Water, and J.-T. Liaw, Journal of the European Ceramic Society 23, 1593-1598 (2003).
2 M. Komatsu, N. Ohashi, I. Sakaguchi, S. Hishita, and H. Haneda, Applied Surface Science 189, 349-352 (2002).
3 J. Lee, Z. Li, M. Hodgson, J. Metson, A. Asadov, and W. Gao, Current Applied Physics 4, 398-401 (2004).
4 S. J. Pearton, D. P. Norton, K. Ip, Y. W. Heo, and T. Steiner, Progress in Materials Science In Press, Corrected Proof.

* Contact author: j.metson@auckland.ac.nz

First principles calculations of the $4f^n \rightarrow 4f^{n-1}5d$ absorption spectra of Ce^{3+}, Pr^{3+}, Nd^{3+} in CaF_2, SrF_2, and BaF_2 crystals

K. Ogasawara[1], T. Ishii[1], M.G. Brik[2], I. Tanaka[3]
[1]School of Science and Technology, Kwansei Gakuin University, 2-1 Gakuen, Sanda, Hyogo 669-1337, Japan
[2]Fukui Institute for Fundamental Chemistry, Kyoto University, 34-4 Takano-Nishihiraki-cho, Sakyo-ku, Kyoto 606-8103, Japan
[3]Department of Materials Science and Engineering, Kyoto University, Sakyo, Kyoto 606-8501, Japan

A lot of studies aimed at high-lying $4f^{n-1}5d$ states of trivalent rare earth (RE) ions [1–3 and references therein] have been published during the last few years. This trend is fully explained by existing of a stable and rapidly increasing strong demand for the luminescent materials and solid-state lasers in the ultraviolet (UV) or vacuum ultraviolet (VUV) regions. In our recent works we reported on the systematic calculations of energy levels and absorption spectra of RE ions in a free state [4] and $LiYF_4$ crystal [5, 6] and extension of the Dieke's diagram to 200000 cm^{-1} and 350000 cm^{-1} for the cases of the $4f^n$ and $4f^{n-1}5d$ electron configurations, respectively. In line with these studies, we present in this paper our new results of calculations of the $4f^n \rightarrow 4f^{n-1}5d$ absorption spectra and complete energy level schemes for Ce^{3+}, Pr^{3+}, and Nd^{3+} in CaF_2, SrF_2, and BaF_2 crystals. The fully-relativistic first-principles many-electron calculations method [7] was used. Its main features are as follows: 1) no fitting parameters are needed to reproduce the absorption spectra fairly well; 2) no restrictions for the symmetry of the impurity center are imposed; 3) molecular orbitals are used to take into account the covalency effects; 4) configuration interaction is considered explicitly. From the results of the calculations, the dependences of the position of the $4f^{n-1}5d$ lowest energetical state and the crystal field splitting of the $5d$ state on the crystal lattice constant for all considered systems were analyzed. Comparison of these trends and calculated absorption spectra with experimental data is discussed.

References:

1. P. Dorenbos, J. Lumin. **91** (2000) 155; ibid, **91** (2000) 91; Phys. Rev. B **65** (2002) 235110.
2. M.F. Reid, L. van Pieterson, R.T. Wegh, and A. Meijerink, Phys. Rev. B **62** (2000) 14744; L. van Pieterson, M.F. Reid, R.T. Wegh, S. Soverna and A. Meijerink, Phys. Rev. B **62** (2000) 045113.
3. Ning L.X., Duan C.K., Xia S.D., Reid M.F., Tanner P.A. J. Alloys Compd. **366** (2004) 34.
4. K. Ogasawara, S. Watanabe, Y. Sakai, H. Toyoshima, T. Ishii, M.G. Brik and I. Tanaka, Jpn. J. Appl. Phys., **43** (2004) L611.
5. T. Ishii, K. Fujimura, K. Sato, M.G. Brik, K. Ogasawara, J. Alloys Compd. **374** (2004) 18.
6. K. Ogasawara, S. Watanabe, H. Toyoshima, T. Ishii, M.G. Brik, H. Ikeno, I. Tanaka, J. Solid State Chem. (article in press).
7. K. Ogasawara, T. Iwata, Y. Koyama, T. Ishii, I. Tanaka and H. Adachi, Phys. Rev. B **64** (2001) 115413.

Sub-wavelength localization of plasmon resonances evidenced by Surface Enhanced Raman Spectroscopy

E. C. Le Ru* and P. G. Etchegoin
The McDiarmid Institute for Advanced Materials and Nanotechnology
School of Chemical and Physical Sciences
Victoria University of Wellington
PO Box 600 Wellington, NEW ZEALAND

Surface enhanced Raman scattering (SERS) [1] is based on single or collective plasmon resonances producing massive amplifications of the laser local field, thus boosting the intensity of the otherwise weak Raman scattering process. The largest SERS signals are believed to come from the so-called hot-spots; spatially localized surface plasmons resonances where the electric field of the laser may reach huge local enhancements. It is believed that hot-spots are responsible for the single-molecule sensitivity of SERS [2]; understanding their physical properties is at the core of many applications of SERS. Reciprocally, SERS can be used as a tool to study these localized plasmon resonances. Although some information on the spatial localization of hot-spots has been obtained in the past with alternative techniques [3,4], a clear-cut experimental demonstration of sub-wavelength localization of hot-spots inferred from the direct monitoring of the Raman signal has not been yet demonstrated.

In this study, we show that localization of plasmon resonances within fractions of the wavelength of the exciting laser can be observed by means of SERS. For this we use a standard Raman spectrometer with a CCD as detector. In a conventional setup, light is dispersed on the CCD, and each column corresponding to a given wavelength is integrated to produce the signal. Here, we show that the second dimension of the CCD array can be used to obtain some spatial information.

We studied the spatial localization of the signal in typical SERS media, such as silver colloids solution with dye, or dry colloids covered with residual amorphous carbon. The usual temporal fluctuations characteristics of SERS are observed but in addition, strong spatial fluctuations are evidenced. For example, different spectra can be observed from two locations separated by a fraction of the wavelength of the laser, close to the diffraction limit.

Our results confirm speculations on sub-wavelength resolution capabilities of SERS, as well as provide a tool to understand highly localized plasmon excitations in disordered metallic nanostructures. It also provides some insight into the nature of hot-spots, believed to be responsible for the huge amplifications seen in single molecule SERS spectroscopy.

References

[1] M. Moskovits, Rev. Mod. Phys. **57**, 783 (1985).
[2] S. Nie and S. R. Emory, Science **275**, 1102 (1997).
[3] D. P. Tsai, J. Kovacs, Z. Wang, M. Moskovits, V. M. Shalaev, J. S. Suh, and R. Botet, Phys. Rev. Lett. **72**, 4149 (1994).
[4] P. Zhang, T. L. Haslett, C. Douketis, and M. Moskovits, Phys. Rev. B **57**, 15513 (1998).

* Contact author: Eric.LeRu@vuw.ac.nz

Asymptotic Behaviour of Subwavelength Nano-Layer Space Charge toward Conducting Interface

K. Mehrany, and B. Rashidian*
Department of Electrical Engineering, Sharif University of Technology, Tehran, IRAN

Recently, interaction of electromagnetic waves with conducting interfaces has been studied and several applications have been proposed [1-3]. For instance, new type of photonic crystals similar to Kronig-Penny electronic crystals has been implemented by using these structures [3]. In these structures a free two dimensional interface charge layer is generated at the dielectric interfaces and interesting phenomena are observed. In this manuscript, the effect of finite charge layer thickness and its asymptotic behavior toward conducting interface, where the thin charge layer is modelled via a surface conductivity σ_s, is thoroughly studied for the first time. Two different regimes are considered: first, propagation of optical waves through sub-wavelength free charge layers and its corresponding reflection and transmission coefficients for both major polarizations TE and TM is considered, second, optical slow waves localized at the interface of two dielectrics with interface charge layer between them and their corresponding effective index of propagation are investigated.

Even though the propagation of electromagnetic waves through the induced interface charge layer depends on the density of induced charge carriers and on the incidence angle of the illuminating wave, the critical value of wavelength over charge layer thickness ratio beyond which the asymptotic behaviour of conducting interfaces can be observed, is usually higher for TM polarized waves than that of TE polarized waves. According to our simulation results, the required value of wavelength over charge thickness ratio beyond which one can observe the asymptotic behaviour of conducting interfaces is about 1000 for TM polarized waves and about 20 for TE polarized waves. Similarly, compared with TE polarized waves, TM polarized optical slow waves localized at the interface of two dielectrics with induced interface charge layer between them demand lower thickness over wavelength ratio to have the effective index of propagation equal to that of the conducting interface. The following figure shows the optical slow wave effective index of propagation at different values of thickness over wavelength ratio for both major polarizations.

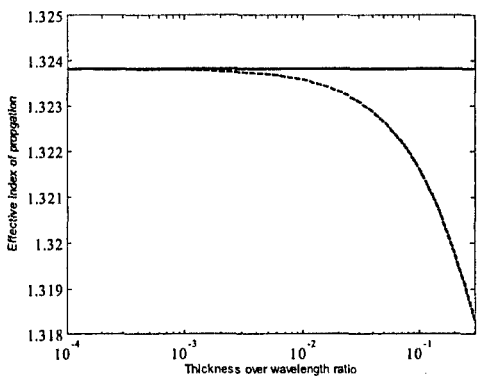

(a) TE effective index of propagation versus thickness over wavelength ratio with host dielectric refractive index of 1.3 and normalized surface conductivity of -0.5: induced charged layer (dashed), conducting interface (solid)

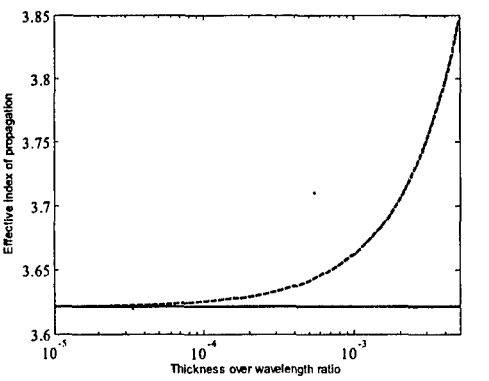

(b) TM effective index of propagation versus thickness over wavelength ratio with host dielectric refractive index of 1.3 and normalized surface conductivity of +1.0: induced charged layer (dashed), conducting interface (solid)

References

[1] K. Mehrany, S. Khorasani, and B. Rashidian, "Novel optical devices based on surface wave excitation at conductive interfaces," *Semi. Science and Technology*, vol. 18, pp. 582-588, June 2003.

[2] K. Mehrany, and B. Rashidian, "Novel optical slow wave structure and surface electromagnetic wave coupler with conducting interfaces," *Semi. Science and Technology, vol. 19, pp. 890-896, May 2004..*

[3] K. Mehrany, and B. Rashidian, "Band structures of coupled electromagnetic slow waves," *Journal of Optics A: Pure and Applied Optics*, vol. 6, pp. 961-970, Nov 2004.

* Contact author: rashidia@sharif.edu

Control of the optical transmission of metal films via excitation of surface plasmons

L. Lin[1*], S.J. Drake[1], R.J. Reeves[2] and R.J. Blaikie[1]
MacDiarmid Institute for Advanced Materials and Nanotechnology,
1. Department of Electrical and Computer Engineering, University of Canterbury, Christchurch, New Zealand
2. Department of Physics and Astronomy, University of Canterbury, Christchurch, New Zealand

Surface-plasmon-enhanced optical transmission through thin metallic films with periodic subwavelegth structures is currently a rapid expanding field of research. It opens possibilities of developing new optical components, as the plasmonic properties of the devices can be manipulated by varying the configuration of the nanostructures associated with the metallic film. We have studied the transmission properties of planar metallic films closely coupled to diffraction gratings, which are used to couple surface plasmons onto the films. The structure of the samples used in this study consist thin silver films vacuum deposited onto glass substrates. A thin layer of SiO_2 is deposited between the silver film and the rectangular transmission gratings, which provides a metal/dielectric interface for generating surface plasmons on the silver. Both Ag and SiO_2 layers have sub-100 nm thicknesses. The incident light gains the required transverse momentum from the gratings to excite surface plasmons. The strength of this surface plasmons field in the interface is strongly enhanced with respect to the exciting optical wave.

In our experimental setup, the interference lithography technique is employed to produce the transmission gratings. The spatial period and the line width of the gratings were controlled by varying the exposure conditions. The minimum spatial period can be achieved in our set-up is ~180nm. Figure 1 shows an example of a 400-nm period grating formed in photoresist using this technique.

The spectral transmission of the samples was analysed in a spectrophotometer at normal incidence. Experimental results indicate that the transmission properties of the gratings, which include the centre wavelength, bandwidth and the intensity of the transmitted light, are strongly affected by the geometrical factors of the gratings, as well as the optical properties and the thickness of the metal and dielectric layers. The details of the fabrication process will be presented, together with experimental results for a series of silver films closely coupled to both metallic and dielectric gratings.

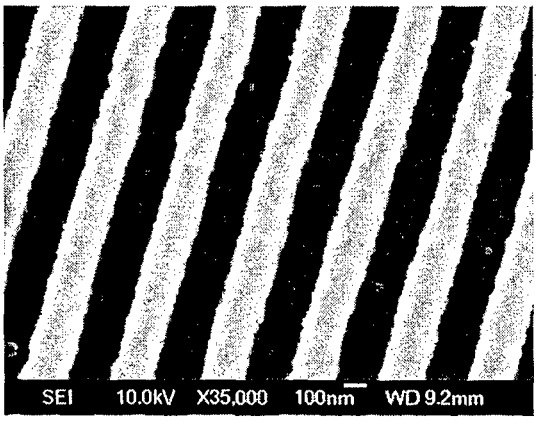

Figure 1: Scanning Electron Microscope (SEM) image of a 400-nm period grating, formed in photoresist using interferometric lithography.

* Electronic mail: lli75@student.canterbury.ac.nz

Two-dimensional bandgap in a one-dimensional negative-index periodic structure

Ilya V. Shadrivov*, Andrey A. Sukhorukov, and Yuri S. Kivshar
Nonlinear Physics Centre, RSPhysSE, Australian National University, Canberra, ACT 0200, AUSTRALIA

Negative-index (or left-handed) metamaterials with simultaneously negative real parts of dielectric permittivity and magnetic permeability were recently realized experimentally for microwaves [1], and it was suggested that specially engineered nano-structured materials may be possible at optical wavelengths [2]. It was shown that anomalous electric and magnetic responses of negative-index materials allow for novel applications, including enhanced sub-wavelength imaging [3].

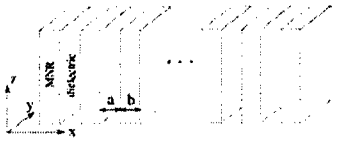

Fig. 1. Schematic of a multilayered structure consisting of slabs with alternating dielectric (or air) and material with negative refraction (MNR)..

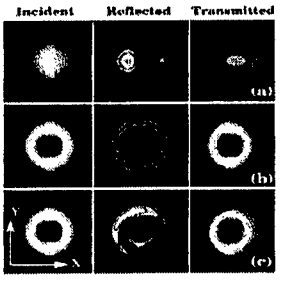

Fig. 2. Cross-section intensity profiles of the incident, reflected, and transmitted beams of various shapes.

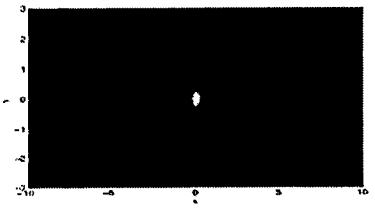

Fig. 3. Green's function demonstrating exponential localization of TE-polarized waves in a plane due to a presence of two-dimensional band-gap.

Here we study the wave transmission and reflectance of a one-dimensional periodic structure made of negative-index material slabs, schematically shown in Fig. 1. Such a structure can reflect waves for certain incident angles [4], and this property can be used to perform tunable beam shaping [5] (see Fig. 2) and bistable transmission [6].

Most remarkably, we find that such a one-dimensional structure can possess a full two-dimensional band-gap that exists if the structural parameters are chosen in a special way. In such a case, TE-polarized waves become fully localized for all propagation angles in a plane, as illustrated by the exponential decay of the Green function (see Fig. 3). The existence of *a one-dimensional structure made of fully transparent materials possessing a two-dimensional band-gap* is a highly nontrivial and unexpected finding, which was not reported in previous studies [4-6]. This is in sharp contrast with the properties of one-dimensional periodic structures made of conventional dielectrics, which can only possess partial band-gaps that provide an omni-directional reflection for a limited range of incident angles [7].

References

[1] R. Shelby, D. R. Smith, and S. Schultz, Science **292**, 77 (2001).
[2] V. A. Podolskiy, A. K. Sarychev, and V. M. Shalaev, Opt. Express **11**, 735 (2003).
[3] J. B. Pendry, Phys. Rev. Lett. **85**, 3966 (2000).
[4] J. Li *et al.*, Phys. Rev. Lett. **90**, 083901 (2003); L. Wu, S. He, and L. Chen, Opt. Express **11**, 1283 (2003).
[5] I. V. Shadrivov, A. A. Sukhorukov, and Yu.S. Kivshar, Appl. Phys. Lett. **82**, 3820 (2003).
[6] M.W. Feise, I.V. Shadrivov, and Yu.S. Kivshar, Appl. Phys. Lett. 85, 1451 (2004).
[7] Y. Fink *et al,* Science **282**, 1679 (1998).

* Contact author: ivs124@rsphysse.anu.edu.au

Light propagation through patterned nanoscale metallic polarisers

A. T. Chin[1] and R. J. Blaikie
MacDiarmid Institute for Advanced Materials and Nanotechnology,
Department of Electrical and Computer Engineering, University of Canterbury, Christchurch, NEW ZEALAND

The optics of polarised light is a mature technology that is widely used, and certain sub-wavelength polarisation effects are well understood—the classical example being a wire-grid polariser. However, what happens when such polarising elements are themselves patterned on a sub-wavelength has not been so widely studied. For visible light this will require that polarising elements are patterned with nanometre-scale dimensions, which is now possible using modern nanofabrication techniques. In this work we have used simulations to investigate the effect of polarised laser focusing onto nanoscale metallic structures. This could give some new ideas for optical communication and optical storage technologies.

This experiment was based on FDTD simulation with the program REMCOM XFDTD v6.1. The light source was set to be a focused Gaussian beam with a wavelength of 650 nm and a variable focal spot size. The samples that have been studied are wire-grid polarisers, both patterned and unpatterned. The laser was set to be polarized either in the E theta or E phi direction, as shown in Fig. 1. The laser spot was defined to be 800 nm in diameter, focused onto a 1×1 $(\mu m)^2$ metal grating. The simulation environment was free space with absorbing boundaries.

Firstly, the experiment investigated the polarising properties as a function of grating size and grating period. Second, the effects of different grating materials were investigated. For the first part of the experiment, perfect conducting material was used for the grating. The result matched the expectation that the E theta polarization laser penetrated the grating and E phi polarization was filtered. The best efficiency occurred when there were 6 gratings (40 nm wide) with 52 nm gaps. In the second part, different metals such as gold, silver, and copper were used as the grating material. These results will be presented, together with simulations for propagation through gratings that are themselves structured at a sub-wavelength scale.

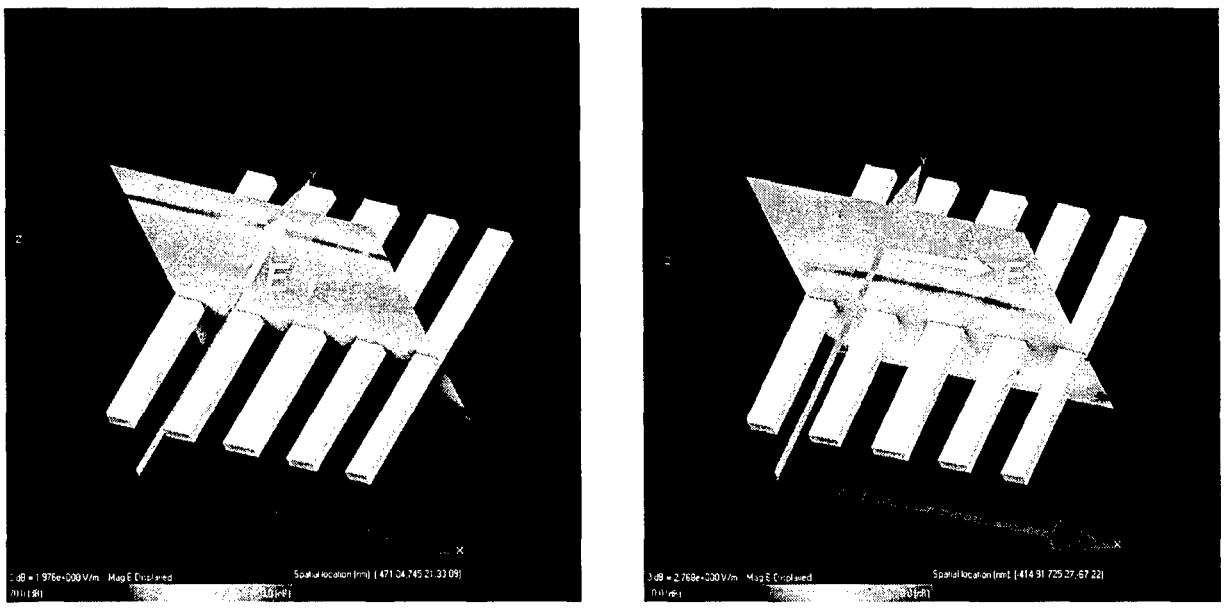

Figure 1. XFDTD simulation results: left, E Phi polarization; right, E Theta polarization.

[1] Contact author: atc24@student.canterbury.ac.nz

Thursday 10 February
Oral Session One

SESSION Th A1
SEMICONDUCTOR GROWTH AND CHARACTERISATION I

Thursday 10 February 2005 1030–1210

Galaxy I

Session Chair **Joe Trodahl, Victoria University of Wellington, NZ**

10:30 **Effects of electron-phonon interaction on the electronic band structure of semiconductors**

Th A1.1 M. Cardona
(Invited Talk)
Max-Planck-Institut für Festkörperforschung, Stuttgart, Germany

10:55 **Indium nitride: towards an understanding of the bandgap**

Th A1.2 R.J. Kinsey[1], P.A. Anderson[1], C.E. Kendrick[1], L.Williams[1], R.J. Reeves[1], Z. Liu[2], S. P. Ringer[2], and S.M. Durbin[1]
[1] *University of Canterbury, Christchurch, NZ*
[2] *University of Sydney, Sydney, Australia*

11:10 **Zinc oxide for optoelectronic device applications: opportunities and challenges**

Th A1.3 V.A. Coleman[1], H.H. Tan[1], C. Jagadish[1], S.O. Kucheyev[2], M.R. Phillips[3] and J. Zou[4]
[1] *Australian National University, Canberra, Australia*
[2] *Lawrence Livermore National Laboratory, Levermore, USA*
[3] *University of Technology Sydney, Sydney, Australia*
[4] *University of Queensland, Brisbane, Australia*

11:25 **Scanning ion probe studies of processing–induced point defect distributions on the surface of gallium nitride**

Th A1.4 G. Parish, R. Stern, H.H. Kwah, B.D. Nener, I. Fletcher, B. Griffin
University of Western Australia, Perth, Australia

11:40 **Effects of growth templates on ZnO grown by RF-PAMBE**

Th A1.5 W.C.T. Lee, E.D. Walsby, M. Kral, P. Miller, R.J. Reeves and S.M. Durbin
University of Canterbury, Christchurch, NZ

11:55 **Nucleation and growth kinetics of ZnO layers deposited on 6H-SiC substrates**

Th A1.6 A.B.M.A. Ashrafi and Y. Segawa
RIKEN Photodynamics Research Centre, Sendai, Japan

Effects of Electron-Phonon Interaction on the Electronic Band Structure of Semiconductors

Manuel Cardona
Max-Planck-Institut für Festkörperforschung
70569 Stuttgart, Germany, European Union

During the past two decades, powerful *ab initio* methods have been developed to calculate the single particle, as well as the electron-hole excitation spectra, of semiconductors. These methods, however, apply to crystals with atoms in their fixed crystallographic positions and thus disregard the effects of the lattice vibrations (i.e., the electron-phonon interaction) which is known to be present even at temperatures T=0 K. Hence, strictly speaking, the experimental excitation spectra cannot be reliably compared with such calculations. In the case of diamond, for instance, the lowest (indirect) absorption edge has been found to be down-shifted by ~ 0.4 eV (by the electron-phonon interaction) with respect to the *ab initio* calculations. A few semi-empirical calculations of these energy gap shifts vs. T are available They can be checked against the measured dependence of optical absorption spectra on temperature and also on the isotopic masses of the constituent atoms: An increase in isotopic mass results in a decrease in the electron-phonon interaction.
The talk will review the progress made in recent years concerning our understanding of such effects, including the widths of optical transitions, in tetrahedral semiconductors. It will be conjectured that the superconductivity recently observed in boron doped diamond [1] is related to the strong electron-phonon interaction mentioned above. Strong electron-phonon effects are observed for all materials containing elements of the first row of the periodic table (e.g. GaN and ZnO). Semi-empirical laws to represent the dependence of excitation energies on temperature and isotopic mass will be presented. It will be theoretically shown that at low T the gap energies vary with T like the vibrational Debye energies, i.e., like T^4. This dependence has been conclusively observed at least in one case which involves the edge luminescence of isotopically pure silicon [2]. It will be shown that in most tetrahedral semiconductors the electron-phonon interaction produces a decrease of the optical gaps with increasing temperature T and, at low T, with decreasing isotopic masses. A few exceptions will be reported. They correspond to the cuprous halides and the copper and silver chalcopyrites. Unfortunately, little detailed information is available for the corresponding effects in semiconductor nanostructures.

References

[1] E.A. Ekimov et al., Nature **428, 542 (2004)**
Y.Takano et al., Cond. Mat. 0406053
[2] M.Cardona, T.A.Meyer, and M.L.W. Thewalt, Phys.Rev.Letters **92**, 196403 (2004)

Indium nitride: towards an understanding of the bandgap

R. J. Kinsey[a *], P. A. Anderson[a], C. E. Kendrick[a], L. Williams[b], R. J. Reeves[b], Z. Liu[c], S. P. Ringer[c] and S. M. Durbin[a]

[a] *Department of Electrical and Computer Engineering, MacDiarmid Institute for Advanced Materials and Nanotechnology, University of Canterbury, Christchurch, NEW ZEALAND*

[b] *Department of Physics and Astronomy, MacDiarmid Institute for Advanced Materials and Nanotechnology, University of Canterbury, Christchurch, NEW ZEALAND*

[c] *Australian Key Centre for Microscopy & Microanalysis, The University of Sydney NSW, 2006, AUSTRALIA*

Semiconducting devices based on the III-nitrides now constitute a significant industry. LEDs, laser diodes and high electron mobility transistors based on the material system are used in multiple applications, including solid state lighting, microwave power amplifiers, high density optical storage and even water purification. The active material in most of these devices is GaN alloyed with a few percent of either InN or AlN to achieve the desired electronic properties. The band structures of GaN and AlN are relatively well understood as their elevated dissociation temperatures (>800 °C) have allowed high quality crystal growth by metal organic chemical vapour deposition (MOCVD) and molecular beam epitaxy (MBE). InN on the other hand dissociates quickly above 550 °C, making high quality growth problematic. The historically accepted bandgap of 1.89 eV was determined by transmission measurements on sputtered films. [1] Recently a number of groups have succeeded in preparing InN films by MOCVD and MBE with optical measurements on these films casting doubt on the previously accepted bandgap and proposing a much narrower bandgap of less than 1 eV. [2]

It is well established that low quality GaN exhibits a very strong 'yellow' defect band which results in a photoluminescence signal much greater than the band edge signal. It has been suggested that a similar mid gap band exists in InN resulting in the 0.7 eV signal. Mie resonances resulting from indium metal precipitates within the film have also been proposed as a source of infrared luminescence. [3] On the other hand, the Moss-Burstein effect, oxygen contamination, deviations from ideal stoichiometry and stress resulting from lattice mismatch have been used to explain the 1.89 eV bandgap. In this study we report on InN grown on a variety of substrates, giving hexagonal, cubic and amorphous templates for growth.

Examination of films grown on single crystal substrates using HRTEM shows them to have a mosaic structure of nanodomains separated by low angle boundaries. Intriguingly there is evidence of the cubic zincblende structure in these nanodomains, despite the hexagonal wurtzite phase being stable; especially when grown on a hexagonal template, such as (0001) sapphire coated with a GaN buffer layer. The existence of multiple phases within the InN films may go some way to explaining why the photoluminescence (PL) signals tend to be unusually broad for a band-end transition and the near degenerate n-type conductivity found in all undoped InN films. InN was grown on cubic (100) yttrium stabilised zirconia (YSZ) in an attempt to isolate the cubic phase, however examination of the film shows that it is also a mix of phases and no clear PL signal from the cubic phase could be obtained. Resolution of this controversy is likely to require a significant improvement in microstructural quality. HRTEM also does not show any evidence of indium metal within the films, casting doubt on the Mie resonances explanation for the infra-red PL signal.

We have also grown polycrystalline InGaN on silica glass, with compositions ranging from InN to GaN. The optical absorption onset for these films were found to move steadily from 0.7 eV to 3.4 eV for varying In:Ga ratios. PL from the films displayed a similar trend but was slightly red shifted from the absorption onset. Our single crystal InN films also all show PL peaks between 0.65 – 0.85 eV and no features in the vicinity of 1.9 eV.

References

[1] T. L. Tansley, C. P.Foley, J. Appl. Phys. **59**, 3241, (1986).
[2] V. Y. Davydov, A. A. Klochikhin, R. P. Seisyan *et al.*, Phys. Stat. Sol. (b) **234**, 787, (2002).
[3] T.V. Shubina, S.V. Ivanov, V. N. Jmerik *et al.*, Phys. Rev. Lett. **92**, 117407, (2004).

* Contact e-mail: Robert.kinsey@elec.canterbury.ac.nz

Zinc Oxide for Optoelectronic Device Applications: Opportunities and Challenges

V. A. Coleman[1], H. H. Tan[1], C. Jagadish[1*], S. O. Kucheyev[2], M. R. Phillips[3] and J. Zou[4]
[1] *Department of Electronic Materials Engineering, The Australian National University, Canberra, ACT 0200, AUSTRALIA*
[2] *Lawrence Livermore National Laboratory, Livermore, CA 94550, USA*
[3] *Mictorstructural Analysis Unit, University of Technology Sydney, Broadway, NSW 2007, AUSTRALIA*
[4] *Division of Materials, School of Engineering, The University of Queensland, Brisbane, AUSTRALIA*

ZnO is increasingly attracting more and more interest as a material for a range of optoelectronic devices including blue and UV light-emitting diodes and laser diodes. With its large exciton binding energy of 60 meV at room temperature, resistance to radiation damage and wide band gap of 3.4 eV [1], it is the perfect candidate for such devices. These properties, combined with the recent advances in the growth of high quality single crystals and epi-layers suggest that ZnO would have advantages over GaN as a light emitter [2]. Such devices have yet to be realized however, because p-type doping of ZnO is still proving to be a major challenge [3]. Currently, there is still much to be understood about the issues of dopant incorporation and activation in ZnO, as well as the underlying cause of the intrinsic n-type doping [4].

Ion implantation is widely used in the microelectronics industry for selective area doping and device isolation [5]. Ion implantation of potential p-type dopants and co-implantation studies are beginning to show promising results for producing p-type ZnO [6]. A thorough understanding of damage accumulation and recrystallization processes is thus important for achieving consistent selective area doping. In this study, high-dose implants and annealing studies were conducted to address some of these issues. Samples were implanted with ~1.4 X 10^{17} As^+/cm^2 at room temperature, using an ion energy of 300 keV. Rapid thermal annealing (RTA) of samples in the range of 900°C to 1200°C was employed to achieve recrystallization of amorphous layers and electrical activation of the dopant. Rutherford backscattering/channeling, transmission electron microscopy and cathodoluminescence spectroscopy were used to monitor damage accumulation and annihilation behavior in the single crystal ZnO. The results of this study have significant implications for p-type doing of ZnO by ion implantation.

References

[1] D. C. Look, Mater. Sci. Eng., **B80**, 383 (2001)
[2] S. J. Pearton, D. P. Norton, K. Ip, Y. W. Heo and T. Steiner, J. Vac. Sci. Technol. B., **22**(3), 932 (2004)
[3] see for example: D. C. Look, B. Clafin, Ya. I. Alivov and S. J. Park, Phys. Stat. Sol. A., **201**, 2203 (2004)
[4] D. C. Look and B. Clafin, Phys. Stat. Sol. B., **241**, 624 (2004)
[5] S. O. Kucheyev, J. S. Williams and C. Jagadish, Vacuum, **73**, 93 (2004)
[6] T. Yamamoto, Thin Solid Films, **420-421**, 100 (2002)

* Contact author: chennupati.jagadish@anu.edu.au

Scanning ion probe studies of processing–induced point defect distributions on the surface of gallium nitride

G. Parish[1,*] R. Stern[2], H.-H. Kwah[1], B. D. Nener[1], I. Fletcher[2], B. Griffin[2]
[1] *School of Electrical, Electronic & Computer Engineering,* [2] *Centre for Microscopy & Microanalysis, The University of Western Australia, Perth, AUSTRALIA*

GaN, and its alloys with InN and AlN, together form a wide-bandgap semiconductor material system with numerous optical and electronic device applications. It is well known that this material system is extremely suited to blue, green, white and UV light-emitting devices, detectors and lasers. With a high breakdown field and large electron saturation velocity, GaN-based materials are also suited for high power, high frequency transistors for microwave applications. Despite commercial realisation of some device applications, there remain significant impediments for the full potential of this material system to be realised. One particular challenge is to understand and minimise processing-induced damage to the material. In many cases this damage is in the form of introduced point defects, both native (for example nitrogen vacancies) and impurity (for example hydrogen). [1,2]

In this study, a CAMECA nanoSIMS 50 ion microprobe, which was recently commissioned at The University of Western Australia as part of the Nanostructural Analysis Network Organisation (NANO) Major National Research Facility development, was used to investigate the impurities in, and stoichiometry of, processed GaN. Processing steps applied to the surface included photolithographic patterning using photoresist polymer, followed by thermal deposition of metal (Pd/Au), selective regions of which were then removed by etching in a potassium iodide/iodine-based (KI/I) solution (after an additional photolithographic patterning step). At various times during processing the surface was also exposed to solvents such as acetone and isopropyl alcohol.

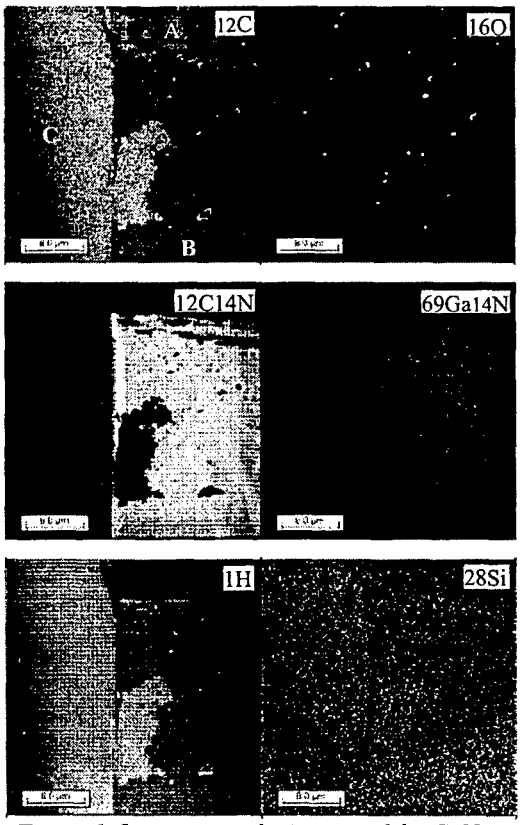

Figure 1. Ion microprobe images of the GaN surface for various ions. Region A - Pd/Au; Region B - Pd/Au etched away; Region C - no Pd/Au

Figure 1 shows an example of the features that were observed at the GaN surface using the nanoSIMS. The images were collected using 1pA Cs^+ ion beam, with 20 minutes acquisition time. To ensure the top surface was imaged, no pre-imaging implantation of Cs^+ was employed.

The results of the imaging were unexpected. It can be seen (region "B") that there is a localised region with higher GaN signal, and higher oxygen, but less hydrogen and carbon (common impurities in GaN). Note that lighter regions correspond to a higher ion signal. For the sample shown this corresponds to a region where the metal was removed by the KI/I etchant. There are also some scratch-type features in which this contrast is enhanced. However, on another sample (not shown), in the regions where the metal was removed there is only a strip along the border of where the metal was removed which exhibits this contrast, and the rest of the surface exhibits no contrast, except for anomalous strips of random orientation with the same characteristics.

As a result of these findings, further samples are being prepared to isolate factors contributing to the contrast. In this paper the full results will be presented, along with theories as to the source of the contrast. The nanoSIMS technique itself will also be discussed - it is clear that nanoSIMS holds much potential for investigation of localised surface effects.

References

[1] S. J. Pearton *et al.*, J. Vac. Sci. Technol. A **14**, 831 (1996).
[2] R. Cheung *et al.*, J. Appl. Phys. **88**, 7110 (2000).

* Contact author: giap@ee.uwa.edu.au

Effects of Growth Templates on ZnO Grown by RF-PAMBE

W. C. T. Lee[1,*], E. D. Walsby[1], M. Kral[2], P. Miller[3], R. J. Reeves[3] and S. M. Durbin[1]
[1] *Department of Electrical and Computer Engineering, University of Canterbury, New Zealand*
[2] *Department of Mechanical Engineering, University of Canterbury, New Zealand*
[3] *Department of Physics and Astronomy, University of Canterbury, New Zealand*

ZnO is a wide bandgap semiconductor with a bandgap of 3.4 eV, and its comparatively large exciton binding energy (60 meV) makes it a desirable material for optoelectronic applications. A considerable number of groups have explored growth of this material, using various growth methods. Currently, the mainstream efforts on ZnO concentrate on the electronic properties and optical properties of epitaxial material – in particular, the origin of the observed n-type doping in as grown samples, as well as fabrication of p-type ZnO. More importantly, however, the actual mechanisms involved in heteroepitaxial growth of ZnO are poorly understood. Before a detailed understanding of defects and impurities in ZnO can be achieved, this more basic issue must be addressed.

In this investigation, ZnO is grown using RF plasma-assisted molecular beam epitaxy (RF-PAMBE). In order to understand the basic growth evolution, different growth conditions along with different growth templates were used to identify factors that affect the surface morphology and microstructures of the grown film. In particular, single crystal ZnO growth on sapphire, GaN, as well as patterned substrates were studied. Preliminary experiments indicate that RF-PAMBE is capable of achieving high quality single crystal growth. Figure 1 shows an SEM image of a typical ZnO film on (0001) sapphire. It can be seen that hexagonal features dominate the surface as expected. Photoluminescence performed at 4 K shows a sharp peak at the bandedge with FWHM of 4meV, indicating the high quality of the material.

As is the case with other II-VI semiconductors, it was observed that the surface morphology is very sensitive to the flux ratio. The size, density and the height of hexagonal features, as well as the rms surface roughness as observed from AFM varies greatly with slight changes in Zn or O flux. Although the photoluminescence generally has a similar shape with the peak position at 3.40 eV corresponding to the free exciton, the sharpness of the donor exciton peak, distinctness of the free exciton peak, and the defect band features differs with varying growth conditions. Growth of ZnO on GaN, proposed by many groups as a potentially viable system, can exhibit interesting surface morphology depending on growth conditions. Being relatively well lattice matched to ZnO, a GaN template theoretically reduces the strain present in the ZnO film. However, SEM images showed the surface of such a film grown at 550°C is characterised by a porous network (Fig. 2), which has not been observed in any of our ZnO on sapphire. It is speculated that a higher growth temperature would eliminate these features giving a smoother surface.

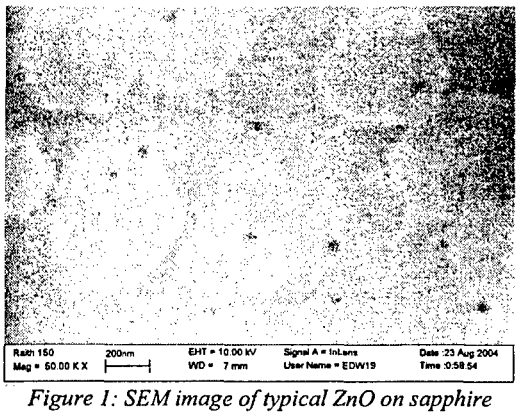

Figure 1: SEM image of typical ZnO on sapphire

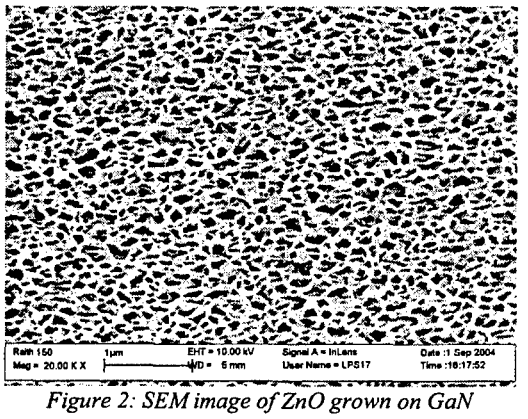

Figure 2: SEM image of ZnO grown on GaN

* Contact author: wcl16@student.canterbury.ac.nz

Nucleation and growth kinetics of ZnO layers deposited on 6H-SiC substrates

A. B. M. A. Ashrafi* and Y. Segawa
Lab for Photophysics, RIKEN Photodynamics Research Center, Sendai 980-0845, Japan

Wide bandgap ZnO material has attracted an attention in research for the fabrication of exciton-based laser and light emitting diodes compared to the GaN. However, there are two big challenges for device fabrication using the ZnO-related materials: control of *p*-type conductivity and high crystalline quality. Considering the crystalline properties, the epitaxial ZnO layers grown on Al_2O_3 substrates are poor due to the larger lattice misfit (f_m) of ~18%. To overcome these basic problems for ZnO material, SiC may be substituted in the Al_2O_3 substrate, where the f_m and k_m (difference in thermal expansion coefficients) are ~5% and 1%, respectively. The f_m and k_m values, in principle, are ¼ times smaller in ZnO/6H-SiC heterostructure than that of the ZnO/Al_2O_3 [1].

Focusing on the smaller f_m and k_m, the key parameters for materials science and engineering, ZnO layers have been grown on 6H-SiC substrates to the first time by metalorganic chemical vapor deposition. We focused on nucleation and growth kinetics of ZnO layers deposited on the thermally treated 6H-SiC substrates. Atomic force microscopy exhibited that ZnO nucleates initially with 2D islands as the S-K growth mode, since the compressive strain is active in the ZnO/6H-SiC heterointerface. However, with the increase of ZnO layer thickness, the 2D islands led to coalescence and grain growths. An analog result was diffracted in transmission electron microscopy (TEM) with columnar growths. The misfit dislocations are extended into the ZnO epilayers to be ≤150 nm. The consistent results were observed in thickness-dependent ZnO layers deposited on 6H-SiC substrates [1].

The biaxial strain ratio (Poisson's ratio) in the ZnO/6H-SiC is estimated to be 0.41, while in ZnO/Al_2O_3 structure has been demonstrated of 0.50 [2]. These different Poisson ratios indicated the role of asymmetric lattice deformation kinetics induced by the different f_m and k_m in the ZnO/6H-SiC and ZnO/Al_2O_3 heterointerfaces [1]. The biaxial strain relaxation rate as a function of ZnO layer thickness exhibited that the ZnO layers grew coherently for the layer thickness ≤6 nm. However, with the increase of ZnO layer thickness, the stress was accounted maximum from ≥7 to ~230 nm under the compressive strain. And, it decreases slowly with the increase of ZnO layer thickness from ≥230 nm to 1.5 μm [1]. This results are consistent with the TEM observations.

It is noted that the maximum strain relaxation in the ZnO/6H-SiC structure is estimated to be ~94% for the layer thickness of 1.5 μm. To make clear on this remaining biaxial strain, however, requires further studies since the *km* are not accounted in these studies. It disclosed that the average strain is almost constant initially and relaxes slowly with the increase of ZnO layer thicknesses. The possible critical thickness of ZnO layer grown on 6H-SiC substrate has been assigned to be 5~7 nm. It has been demonstrated that the critical thickness of II-VI materials for the f_m of ~5% is in the range of 2~6 nm [3].

In addition to these results, $Mg_xZn_{1-x}O$ alloys have been engineered on 6H-SiC substrates. The Vagard's law was employed for Mg composition estimation in $Mg_xZn_{1-x}O$ alloys from $0 \geq x \leq 0.5$ to the first time [4]. It has been demonstrated that the Vagard's law is applicable for material engineering but not for bandgap engineering. The details of these results will be discussed in the Conference.

References

[1] A. B. M. A. Ashrafi, N. T. Binh, B. –P. Zhang, and Y. Segawa, *Appl. Phys. Lett.* **84** (2004) 2814
[2] T. Makino *etal*, Appl. Phys. Lett. **79** (2001) 1282
[3] K. Pinardi, U. Jain, S. C. Jain, R. V. Overstraetem, and M. Willander, *J. Appl. Phys.* **83** (1998) 47
[4] A. B. M. A. Ashrafi, B. –P. Zhang, and Y. Segawa, *Appl. Phys. Lett.* (submitted)

*contact author: ashrafi@postman.riken.jp

SESSION Th B1
BIO-MEMS AND BIO-CELL IMAGING

Thursday 10 February 2004 1030–1210

Meeting Room V

Session Chair **Maan Alkaisi, University of Canterbury, NZ**

10:30 **High speed single particle analysis and sorting bio-chips**
Th B1.1 H. Morgan
(Invited Talk)
University of Southampton, Southampton, UK

10:55 **Cell isolation and growth in electric-field defined micro-wells**
Th B1.2 W. M. Arnold[1,2] and N. R. Franich[1]
[1] *Industrial Research Limited, Lower Hutt, NZ*
[2] *MacDiarmid Institute for Advanced Materials and Nanotechnology, NZ*

11:10 **The self-assembly of keratin intermediate filaments into macrofibrils: is this process mediated by a mesophase?**
Th B1.3 A. J. McKinnon
Canesis Network Limited, Lincoln, NZ

11:25 **Multiscale conformal structures: a biomimetic chip integrated adhesive**
Th B1.4 M. T. Northen and K. L. Turner
UC Santa Barbara, Santa Barbara, USA

11:40 **Analysis of dielectrophoretically trapped biological cells by atomic force microscopy using a biochip platform**
Th B1.5 J. Muys[1], M. M. Alkaisi[1], J. J. Evans[2] and J. Nagase[2]
[1] *University of Canterbury, Christchurch, NZ*
[2] *Christchruch School of Medicine, University of Otago, Christchurch, NZ*

11:55 **Femtogram mass biosensor using a self-sensing cantilever for resonance frequency shift**
Th B1.6 S. Hosaka[1], T. Chiyoma[1], A. Ikeuchi[1], H. Okano[2], H. Sone[1] and T. Izumi[1]
[1] *Gunma University, Kiryu, Japan*
[2] *Tokyo Sokki Kenkyujo Co. Ltd., Gunma, Japan*

High speed single particle analysis and sorting bio-chips

Hywel Morgan
School of Electronics and Computer Science, The University of Southampton
Southampton, SO17 1BJ, England UK

In this paper we describe a micro-chip capable of detecting and counting particles based on their electrical impedance and/or fluorescence emission intensity. Particles are analysed serially at high speed using single particle impedance spectroscopy together with confocal optical analysis. Particles are positioned within the detection volume using a dielectrophoretic focussing technique. High speed particle deflection is accomplished using a combination of hydrodynamic and dielectrophoretic forces. The operating principle of the device is demonstrated by detecting and counting fluorescent latex particles at a rate of 300 particles/sec.

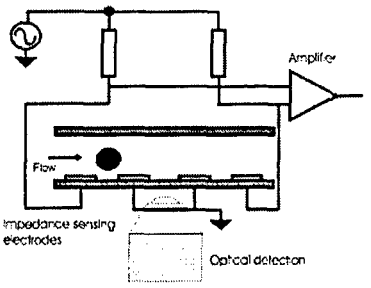

Figure 1, left shows the principle of the detection chip. Particles flow at high speed through two pairs of interdigitated electrodes. The electrodes are configured as a bridge; the small change in channel impedance due to the presence of the particle can be detected and quantified. Concurrently a confocal optical system performs light scattering and three colour fluorescence analysis of the particle. Particle centering within the fluid stream is achieved using dielectrophoretic focussing [1, 2]. This works by energising a set of microelectrodes with high frequency AC voltage, generating a negative dielectrophoretic force that pushes particles into a tight axially centered beam.

Figure 2 (right) is a diagram illustrating the ooperating principle of the chip, showing the focusing and sorting electrodes. Particles are focused into a narrow beam along the axis of the channel. The combination of DEP and hydrodynamic forces at the sorting junction move particles left or right according to the voltage sequence applied to the three sorting electrodes. Sorting has been achieved at several hundred particles per second.

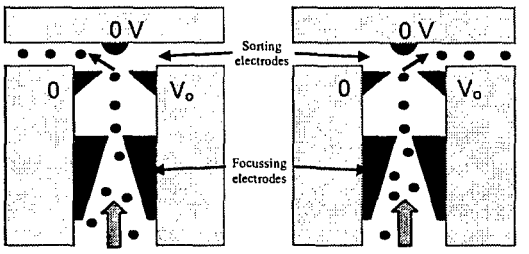

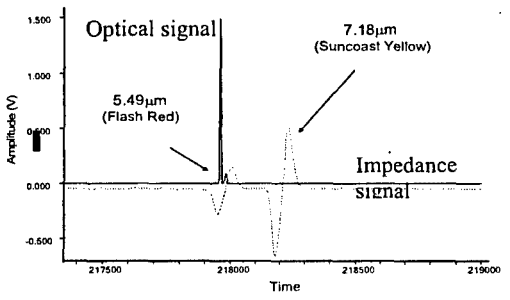

Figure 3, (left) shows an impedance signal from two different sized particles. The channel size in this case was 10µm x 10µm. Also shown is the simultaneous fluorescence signal obtained from one of the particles (red). This device has been used to analyse the properties of blood cells and to detect difference in the properties of latex particles

References

[1] Morgan H., Holmes D and Green N.G. *3-D focussing of nanoparticles in a microfluidics channels.* IEE Proc. Nanobiotechnology 150 76-81 (2003).

[2] Holmes D., Green N.G., and Morgan H. *Dielectrophoretic flow-through separation systems: Comparison of experimental and numerical simulations.* IEEE Eng. Med Biol. **22** 85-90 (2004)

Acknowledgement

This work was funded by EPSRC under project number GR/R28942.

Cell Isolation and Growth in Electric-Field Defined Micro-Wells

W. Mike Arnold[1,2*] and Nick R. Franich[1]
[1]*Industrial Research Limited, PO Box 31-310, Lower Hutt, New Zealand*
[2]*MacDiarmid Institute for Advanced Materials and Nanotechnology, Victoria University of Wellington, P O Box 600, New Zealand*

Biological cells such as those of yeast can be held in electric-field-induced traps produced within and slightly above a horizontal array of planar electrodes. The trapping force is generated by dielectrophoresis [1,2]. When the trap dimension is made slightly larger than one cell diameter, which can be done by lithographic fabrication of a castellated structure [3], then the single cells can be separated out from a low-density suspension. Growth and cell division over several generations can occur within the trap (Fig. 1). In a suitable volume of medium, a convection cell will occur above the array [4]. By use of fields higher than required for trapping, the convection may be accelerated and used to position or concentrate the cells (Fig 2). Despite continuous exposure to RF field strengths of 30-45kV/m, growth and division of *S. cerevisiae* appears to occur normally (or slightly faster than normal), and monitoring of growth at temperatures between 20°C and 30°C shows the expected decrease in cell doubling time.

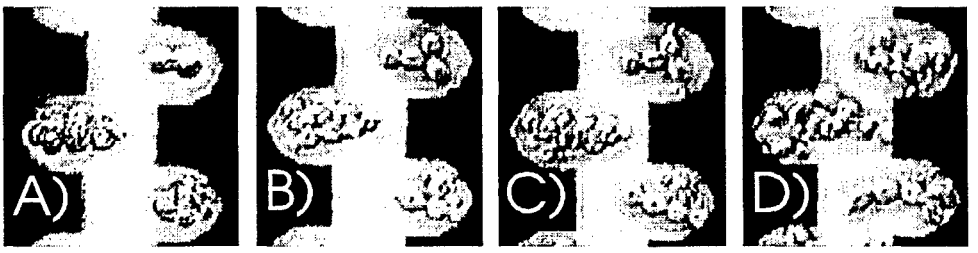

Fig. 1. Growth and division of yeast cells whilst levitated and trapped between interdigitated planar microelectrodes of 20 micron feature size fabricated as described before [3]:
A) (at time 0) shows a doublet cell (post-division) in a trap at top right;
B) (at 1hr 27min) the doublet has now become a quadruplet, still trapped;
C) (at 2hr 0min) further buds are appearing on two of the quadruplets;
D) (after 4hr 29min) shows further division, the group is still trapped.

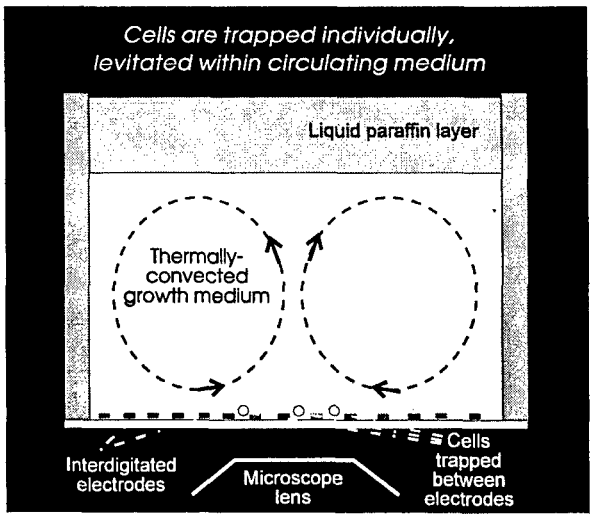

Fig. 2. A vertical cross-section through the levitation apparatus, showing the convection cell [4]. The radius of the liquid cylinder is 4.4 mm. Typically, the depth of the liquid must be less than the radius for stable convection. The convection cell may be inhibited by formation of an aqueous meniscus, therefore a layer of paraffin is used to suppress the meniscus as well as to maintain sterility during prolonged incubation times.

References

[1] Pohl HA (1978) *Dielectrophoresis* (Cambridge, Cambridge University).
[2] Jones TB (1995) *Electromechanics of Particles* (Cambridge, Cambridge University).
[3] Arnold WM and Turner GC (1998) *IEEE Ann.Rep.Conf.Elec.Ins.Diel.Phenom.* pp. 360-363.
[4] Arnold WM and Chapman B (2000) *IEEE Ann. Rep. Conf. Elec. Ins. Diel. Phenom.* pp 752-755.

* Contact author: m.arnold@irl.cri.nz

The Self-assembly of Keratin Intermediate Filaments into Macrofibrils: Is this Process Mediated by a Mesophase?

A J McKinnon*
Canesis Network Ltd, Lincoln, Canterbury, New Zealand

Intermediate filaments of the hard α-keratin class typical of wool and hair (trichokeratins) are complex 32-chain quasi-cylindrical assemblies of diameter some 8 nm consisting of largely α-helical proteins of the keratin intermediate filament (KIF) class [1]. In recent years, filaments have been assembled *in vitro* from bacterially expressed Type I and Type II KIFs, and elegant cross-linking experiments have elucidated the structural arrangements of the sub-elements within the filament, the symmetry of the IF, and the close relationships between the hard (oxidised, crosslinked) IF and the uncrosslinked IF of soft keratins (eg, cytokeratins) [2].

At the next level of hierarchy of structural organisation, the IF are organised into roughly parallel bundles (macrofibrils) of diameter ~200-400 nm, aligned with the fibre axis, which have different morphologies in different cell lines of the fibre cortex. In meso-cortical cells, the IF are arranged in a fairly regular hexagonally close-packed (hcp) array, in the ortho-cortex the filaments exist in a helically wound rope, and in para-cortex there appears to be a disturbed or buckled hcp arrangement. Although our knowledge of the structural details of the macrofibrils has been significantly enhanced by advances in 3D TEM tomographic imaging [3], our understanding of the processes by which these structures form is comparatively poor. Recently a paper appeared which posited a mechanism for macrofibril assembly based on the side-by-side aggregation of IF into sheets, either laminar or curved, to create the hcp or helically wound structures [4]. This model has certain deficiencies in explaining the observed structures, and observational support for the layer structures is not presented.

Surprisingly, given the ubiquity of mesophase development as a key driver in many biological structures [5], nobody has yet seriously proposed that these macrofibrillar structures are initiated by the entropically driven separation, above a certain critical concentration of the rods in the cytoplasm, of liquid crystalline ainisotropic aggregates. This phenomenon is well known in many systems; the statistical mechanics of such phase separations has been developed by Flory and his co-workers [6]. A mesophase-mediated model has many attractive features. The hcp structure is seen to be derived from a nematic mesophase, and the helical rope structure from a twisted nematic mesophase, replicating closely the double-twist structure found in the blue phases of liquid crystals. The provenance of the para-cortex structure is less clear, but is possibly a compression of separate tactoids of a nematic mesophase. The rod-rod separation is then dictated by the statistical mechanics of the phase separation, and not by knob-knob interaction or f-IFAP binding [4]. The mesophase separates at constant composition (rod-rod separation), in a quasi-static sense, creating the opportunity for infill by the later-expressed matrix (IFAP) proteins over an extended period of cell development. The model is consistent with spatial and temporal differences in protein expression in different cell lines, and suggests mechanisms by which parallel or twisted structures may develop. It implies certain experimental findings which are capable of being realised in the near future; these relate to the confirmation of specific IF and/or IFAP proteins in the cell types, and a linear dependence of helix angle on radius in the ortho macrofibrils. The extant literature on IF formation in early-stage differentiating cortical cells provides substantial support for the formation of mesophase structures. The direct observation of tactoids or more extensive phase separation within developing follicle cells is an obvious goal, but challenging given the size and fragility of the substrates.

References

[1] D.A.D. Parry and P.M. Steinert, *Intermediate Filament Structure.* (Springer-Verlag, Heidelberg, 1995).
[2] H Wang et al., J. Cell Biol., **151**, 1459 (2000).
[3] W.G. Bryson, D.N. Mastronarde, J P Caldwell, W G Nelson, and J L Woods, in *Proceedings of 10th International Wool Textile Research Conference, Aachen, 2000,* TP-P3, p1.
[4] R.D.B. Fraser and D.A.D. Parry, J. Struct. Biol., **142**, 319 (2003).
[5] A C Neville. *Biology of Fibrous Composites. Development Beyond the Cell Membrane* (Cambridge Univ. Press, 1993).
[6] P.J. Flory and G. Ronca, Mol. Cryst. Liq. Cryst. **54**, 289 (1979); R R Matheson and P J Flory, Macromolecules **14**, 954 (1981).

* john.mckinnon@canesis.com

Multiscale Conformal Structures: A Biomimetic Chip Integrated Adhesive

M. T. Northen[1*] and K. L. Turner[2]
[1] *Materials Department, UC Santa Barbara, Santa Barbara CA 93106, USA*
[2] *Mechanical and Environmental Engineering Department, UC Santa Barbara, Santa Barbara CA 93106, USA*

A common adhesive system found in nature is the fine hair adhesive motif. This adhesive system can be found in beetles, flies, spiders and geckos[1, 2]. The adhesive relies on a large amount of surface contact between protruding nanofibrils and the adhesion surface to make the operative Van der Waals forces significant[2-4]. To accomplish adhesion biology has developed a multiscale conformal structure consisting of microscale stalks terminating in nanofibers. The nanofibers easily conform to the small scale roughness of the adhesion surface while the microscale stalks conform to larger scale roughness. Thus the adhesive system requires not only nanoconformation abilities but micro and meso scale as well. In this work micro- and nano-fabrication techniques are used to fabricate multiscale conformal structures to mimic the fine hair adhesive motif found in nature.

For meso- to micro-scale conformance 10-200 μm silicon dioxide and polymeric platforms supported by single-high-aspect-ratio-pillar-supports (SHARPS) were fabricated, Figure 1. The pillars are etched out of single-crystal silicon, have heights of 10-50 μm and diameters down to a 0.5 μm. Tests performed using a nanoindenter (Hysitron Triboindenter, Minneapolis, Minnesota) show that the structures are highly compliant [5]. Different platform geometries have been fabricated to increase the structural compliance. To conform to micro- to nano-scale roughness polymer nanorods were fabricated on the surface of platforms. The organic looking polymer nanorods, or "organanorods", were fabricated by spin coating different sized oxide spheres on a polymer surface. The spheres were then directly used as an etch mask in a dry etch process using biased O_2 plasma and produced organanorods varying in diameter from 20-300 nanometers and 0.25 - 4 micrometers in length, Figure 1. Also a modified polymer ashing process has been developed to create organanorods directly from a polymer without an etch mask, Figure 1.

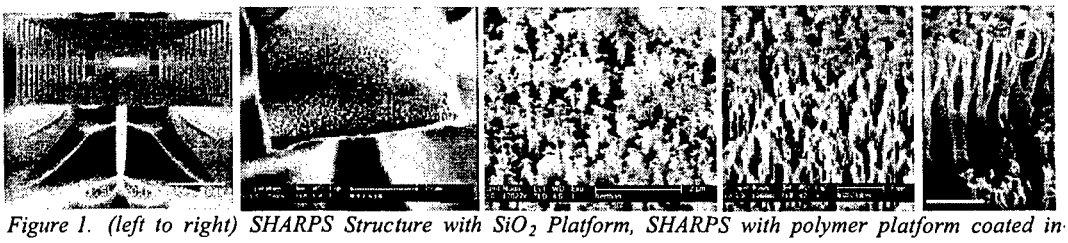

Figure 1. (left to right) SHARPS Structure with SiO_2 Platform, SHARPS with polymer platform coated in organanorods, nanosphere tipped and masked polymer organanorods, high-aspect-ratio polymer organanorods, electron micrograph of gecko adhesive structure (from reference 2).

Adhesion tests were performed using a modified Hysitron Triboindenter by pressing a 1.5 mm diameter polyamide sphere into test surfaces and monitoring the force versus displacement while withdrawing from the surface. Results show improved adhesion with surfaces coated with organanorods and SHARPS structures.

References

1. Russell, A.P., J. Zool. Lond., **176**: p. 437-476 (1975).
2. Arzt E., G.S., Spolenak R., PNAS, **100**(19): p. 10603-10606 (2003).
3. Autumn, K., *et al.*, Nature, **405**(6787): p. 681-5 (2000).
4. Geim, A.K., *et al.*, Nature Materials, **2**: p. 461-463 (2003).
5. Northen, M., Turner, KL, Proceedings. ECS, The 206th Meeting of the Electrochemical Society, In Press (2004).

* Contact author: north@engineering.ucsb.edu

Analysis of dielectrophoretically trapped biological cells by atomic force microscopy using a biochip platform

J. Muys[1,*] M. M. Alkaisi[1] J. J. Evans[2] and J. Nagase[2]
[1] *Department of Electrical and Computer Engineering, University of Canterbury,*
[2] *Christchurch School of Medicine and Health Sciences, University of Otago,*
Christchurch, NEW ZEALAND

The Atomic Force Microscope (AFM) enables imaging of living biological systems and their components at high resolution and in real time. However, the z range imposed by the AFM piezo is a fundamental limitation when investigating biological cells. As shown in Fig. 1, by imbedding cells within cavities which act as incubators, this limitation can be overcome, enabling the cellular structure to be investigated by AFM.
In this work an integrative approach for capturing, trapping and precisely positioning cells at known locations using a biochip has been developed and tested.

Using a method known as dielectrophoresis (DEP), a series of interdigitated micro-electrode structures on the biochip surface generate non-uniform electric field gradients thus inducing polarization in the cell structure. Polarisation causes cell movement either toward (positive DEP) or away (negative DEP) from the intense electric field regions. By fabricating cavities at locations of both intense and weak electric fields, we have successfully trapped and analysed cells by AFM. In Fig. 2, an array of beads that were used to study the field effects on spherical particles, illustrates how the selective response of dielectrophoresis can be used to direct particles towards a series of cavities placed at the electrode edge.

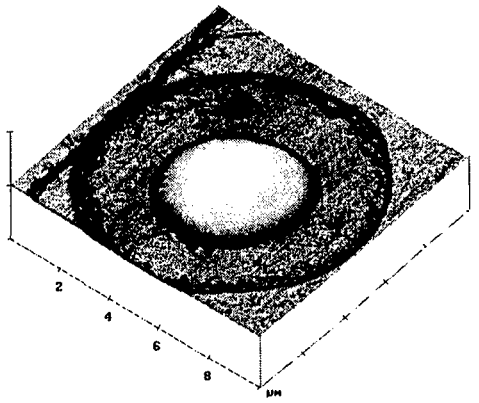

Fig. 1. *AFM image showing the surface topography of a pituitary cell that has been attracted to within a cavity on the biochip by positive DEP.*

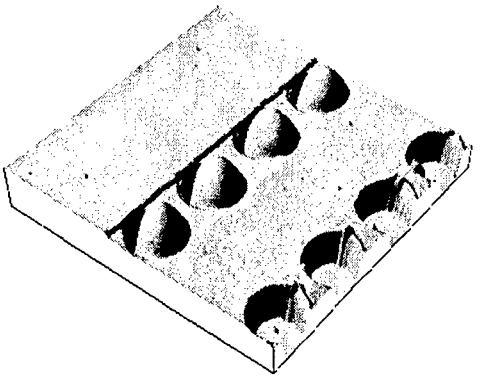

Fig. 2. *AFM image of an array of 10 µm latex beads imbedded within cavities designed to trap material attracted towards the electrode edge of the biochip by positive DEP.*

The aim of combining our biochip platform with the real-time, non-invasive, non-destructive and high resolution capabilities of the AFM is to yield a better understanding into the secretion of hormones at the cell membrane of the pituitary cell. In this work, fabrication of the biochip platform will be outlined and results from AFM imaging of trapped biological cells will be presented.

Funding for this work was provided by the MacDiarmid Institute for Advanced Materials and Nanotechnology, New Zealand.

* Contact author: jmu18@student.canterbury.ac.nz

Femtogram mass biosensor using a self-sensing cantilever for an allergy checker

[a]Sumio Hosaka, [a]Takafumi Chiyoma1, [a]Ayumi Ikeuchi, [b]Haruki Okano, [a]Hayato Sone and [c]Takashi Izumi

[a]Dept. Nano-Material Systems, Graduate Schoo of Eng., Gunma Univ.
1-5-1 Tenjin, Kiryu 376-8515 Japan
[b]Tokyo Sokki Kenkyujo Co., Ltd., 4-247, Aioi, Kiryu, Gunma 376-0011, Japan
[c]Course Medical Sciences, Graduate School of Medicine, Gunma Univ.

A femtogram mass biosensor using a piezoresistive microcantilever has been studied to achieve convenient check system for allergy sensor. The mass detections were done by a resonance frequency shift of the cantilever[1]. The prototyped mass sensor system mainly consists of the cantilever with piezoresistance, piezo actuator, Wheatstone bridge circuits, positive feedback circuits, and a phase-locked loop (PLL) demodulator. In the experiments, we measured the mass change of the adsorbed water molecules and a reaction between antigen and antibody on the cantilever by the resonance frequency shift. We also prototyped the pizoresistive cantilever[2] or used a piezoresistive commercial cantilevers. As experimental results, we could detect water molecule adsorption on the cantilever and a mass change due to antigen-antibody reaction on the cantilever. A mass sensitivity of about 200 fg/Hz was estimated from the antigen- antibody reaction time chart in water.

(1) Principle of Sensor and features of our system[3]

When we vibrate an AFM cantilever using piezoactuator, the resonance frequency f of the cantilever is given by $f=1/2\pi(k/M)^{1/2}$. Where, k is the spring constant and M is the effective mass of a cantilever. When the resonance frequency shift Δf occurs due to molecule adsorption on the cantilever, the mass change Δm is given by $\Delta m=-2(m/f)\Delta f$. From the equation, in order to detect a small Δm, it is necessary to use a micro-cantilever with a small mass and a high resonance frequency and to detect a small resonance frequency shift with a fine resolution. The AFM cantilever is very suitable for the requirements of a small mass and a high resonance frequency. The detection was carried out using the piezoresistive cantilever for self-sensing and the FM demodulator (PLL). When a cantilever with a mass of 45 ng and a resonance frequency of 280 kHz is used, the mass sensitivity .$\Delta m/\Delta f$=320 fg/Hz is obtained. This value is 100 times higher than the sensitivity obtained by the quartz crystal oscillation method.

(2) Experimental results

(a) Water molecule adsorption on the cantilever[2, 3]: We carried out the adsorption on the cantilever in desiccator. We confirmed that the mechanism of water molecular growth on the cantilever consists of 2 modes. At first, island growth occurred and then layer growth occurred.

(b) Antigen-antibody reaction on the cantilever: At first, we dropped antigen of egg albumen with a volume of 10μl. After the mass change was saturated, we dropped immunoglobulin with 10μl. We obtained mass change due to the antigen-antibody reaction. From these mass changes, reacted molecules numbers were estimated. We confirm the antigen-antibody reaction occurred with a binding rate of about 2: 0.8. This means the antibody was covered on the antigen with 80%. The sensor can check the reaction of antigen and antibody for egg allergy.

References

[1] R. Berger, Ch. Gerber, H. P. Lang, and J. K. Gimzewski, Microelectronics Eng. **35**, 373 (1997).
[2] H. Sone, Y. Fujimnuma, and S. Hosaka, Jpn. J. Appl. Phys. **43**, 3648 (2004).
[3] H. Sone, H. Okano, and S. Hosaka, Jpn. J. Appl. Phys. **43**, 4663 (2004).

* Contact author: hosaka@el.gunma-u.ac.jp

SESSION Th C1
POLYMER NANOFIBRES AND NANOTUBES

Thursday 10 February 2005 1030–1210

Copthorne I

Session Chair **Alan Kaiser, Victoria University of Wellington, NZ**

10:30 **One-dimensional transport in polymer nanofibers**
Th C1.1 A.N. Aleshin[1], H.J. Lee[1], Y.W. Park[1] and K. Akagi[3]
(Invited Talk)
[1] *Seoul National University, Seoul, Korea*
[2] *Russian Academy of Sciences, St. Petersburg, Russia.*
[3] *University of Tsukuba, Tsukuba, Japan.*

10:55 **A lithographic processing technique for conducting polymers on the micro-(and nano-)metre Scale**
Th C1.2 P.J.S. Foot[1], J.W. Brown[1], P. Ibison[1], M. Almasri[1], A. Prevost[1] and R. Simon[2]
[1] *Kingston University, Kingston, UK.*
[2] *University of Greenwich, Chatham Maritime, Chatham, Kent, UK.*

11:10 **Enhanced electrical properties of a RAFT polymerised MWCNT/polystyrene nanocomposite**
Th C1.3 A.V.Ellis[1,2], W.T. Wondmagegn[2], J.L.Dewald [2] and S.A. Curran[2]
[1] *Industrial Research Limited, Lower Hutt, NZ.*
[2] *New Mexico State University, Las Cruces, USA.*

11:25 **Atomic force spectroscopy as a tool to study the electrical conductivity of polyaniline and derivatives**
Th C1.4 P.S. de P. Herrmann[1], F. L. Leite[1,2], L. H. C. Mattoso[1,2] and O. N. Oliveira Jr. [2]
[1] *Embrapa Agricultural Instrumentation, São Carlos, Brazil.*
[2] *University of São Paulo , São Carlos, Brazil.*

11:40 **Characterisation of cut single-walled carbon nanotubes and their functionalisation for controlled attachment**
Th C1.5 M. Marshall, S. Popa-Nita, N.T. Baney, J.S. Quinton and J.G. Shapter
Flinders University, Adelaide, Australia.

11:55 **Study on the structure behavior of gel spun ultra-high molecular weight polyethylene/carbon nanotube fiber**
Th C1.6 X. Wang, L. Liang, X. Wang, Y. Wang and Y. Wang.
Donghua University, Shanghai, China.

One-dimensional transport in polymer nanofibers

A. N. Aleshin[1, 2], H. J. Lee[1], Y. W. Park[1 *] and K. Akagi[3]

[1] *School of Physics and Nano Systems Institute - National Core Research Center, Seoul National University, Seoul 151-747, KOREA*

[2] *A. F. Ioffe Physical-Technical Institute, Russian Academy of Sciences, St. Petersburg 194021, RUSSIA*

[3] *Institute of Materials Science and Tsukuba Research Center for Interdisciplinary Materials Science, University of Tsukuba, Tsukuba, Ibaraki 305-8573, JAPAN*

We report the results of transport studies in quasi one-dimensional (1D) conductors - helical polyacetylene fibers doped with iodine and the data analysis for other polymer single fibers and tubes (diameter ~ 15-100 nm). We found that at T = 30-300 K the conductance and the current-voltage characteristics follow the power law: $G(T) \propto T^{\alpha}$ with $\alpha \sim$ 2.2-7.2 and $I(V) \propto V^{\beta}$ with $\beta \sim$ 2-5.7. Both $G(T)$ and $I(V)$ show some features characteristic of 1D systems such as Luttinger liquid or Wigner crystal. The relationship between our results and theories for tunneling in 1D systems is discussed.

* Contact author: ywpark@phya.snu.ac.kr

A Lithographic Processing Technique for Conducting Polymers on the Micro- (and Nano-?) Metre Scale

P. J. S. Foot[1,*], J. W. Brown[1], P. Ibison[1], M. Almasri[1], A. Prevost[1] and R. Simon[2]
[1]Materials Research Group, School of CPS, Kingston University
Penrhyn Road, Kingston, Surrey KT1 2EE (UK)
[2]School of Science, University of Greenwich, Medway Campus
Chatham Maritime, Chatham, Kent ME4 4TB (UK)

A technique will be described which is based on the use of laser alignment to produce conductive microscopic features in an essentially amorphous conjugated polymer.

Liquid crystalline conducting polymers (LCCPs) based on poly(3-substituted pyrrole) or poly(3-substituted thiophene) have been synthesised for more than a decade [1,2], but these early attempts generally produced poor-quality polymers without desirable electronic properties. We have established synthetic routes to comparatively regioregular LCCPs, and produced the first thermoplastic LC polypyrrole [3] and polyaniline [4]. Such polymers are not only capable of being aligned by electric or magnetic fields, but we have shown [5] that they can be laser-aligned to produce high-contrast electronic features on conducting polymer films.

Films of regular polymers, solvent-cast from chloroform, were found to be surprisingly poorly organised and of very low conductivity. On scanning a focused laser beam over the surface, fine lines (1-10 micron wide) were easily drawn, producing highly conductive tracks.

In this work, the technique will be described more fully, and data on the microscopic conductivity will be presented. Structural, electronic and spectroscopic techniques have been used to help understand the mechanism of action of the laser treatment.

Attempts have been made to improve the resolution obtainable from these materials, with a small degree of success so far.

Acknowledgement

We gratefully acknowledge that some of the reported work was funded by the Engineering and Physical Sciences Research Council,, under grant no. GR/J26885.

References

[1] M. R. Bryce, A. D. Chissel, J. Gopal *et al*, Synth. Met. **39**, 397 (1991).

[2] P. J. Langley, F. J. Davis and G. R. Mitchell, Mol. Cryst. Liq. Cryst. **236,** 225 (1993).

[3] L. I. Gabaston, P. J. S. Foot and J. W. Brown, Chem. Commun., 429 (1996).

[4] P. Ibison, P. J. S. Foot and J. W. Brown, Synth. Met. **76**, 297 (1996).

[5] J. W. Brown, P. J. S. Foot, L. I. Gabaston, P. Ibison and A. Prevost, Macromol.Chem. Phys. **205**, 1823 (2004).

Contact author: p.foot@kingston.ac.uk

Enhanced Electrical Properties of a RAFT polymerised MWCNT/Polystyrene nanocomposite

A. V. Ellis,[1,2*] W. T. Wondmagegn,[2] J. L. Dewald,[2] and S. A. Curran[2]
[1] *MacDiarmid Institute for Advanced Materials and Nanotechnology & Industrial Research Ltd, Lower Hutt, NEW ZEALAND*
[2] *New Mexico State University, Department of Physics, Las Cruces, USA*

By controlling the mechanism of polymer-carbon nanotube nanocomposite fabrication we can provide an essential combination to dramatically enhance nanocomposite performance in electronic applications.[1,2] While covalent attachment of polymers to nanotubes has been achieved,[3,4] high loadings with poor nanotube dispersions dominate composite formation and device fabrication.

Due to the limited scope of direct covalent sidewall functionalisation at defect sites,[5] traditional chemical treatments such as wet oxidation in concentrated HNO_3/H_2SO_4 are still in use to oxidize dangling bonds to such groups as hydroxyl (-OH), carboxyl (-COOH) and carbonyl (>C=O) groups.[6,7] Recently carboxyl groups on acid treated single-walled carbon nanotubes (SWCNTs) have been derivatised by thionyl chloride to produce thiols at the ends of the tubes.[8]

In this work we report a unique approach to direct thiation of acid treated oxidised multi-walled carbon nanotubes (MWCNTs) using a mild versatile phosphorus based catalyst. The product being covalently linked nanotubes which are linked together via dithiocarboxyl groups (see Figure 1).

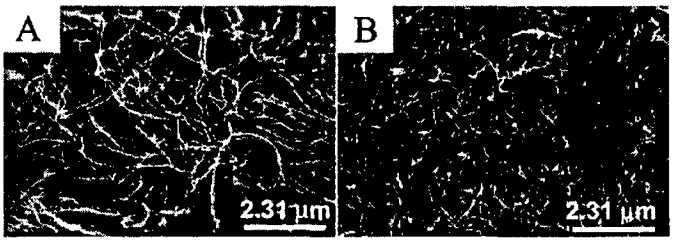

Fig. 1. FESEM images in which A, represents purified pristine arc-discharge MWCNTs and B, represents MWCNTs after 12h acid treatment and thiation.

Using the dithiocarboxylated nanotubes as a chain transfer agent in a Reversible Addition-Fragmentation chain Transfer (RAFT) polymerisation with styrene we have produced a transparent homogeneously dispersed covalently bonded polymer-nanotube thin film nanocomposite. By extensively covalently linking the entire matrix we have achieved conductivity ranges lying between 10^{-9} S/m to 33 S/m at percolation threshold ranges from <0.025% wt/wt to 0.9% wt/wt MWCNT dispersed weight. The film contains covalently linked multi-walled nanotubes that have been controllably cross-polymerized with the polymer to produce highly dispersed films with two percolation thresholds one in the antistatic conductivity range and one in the electromagnetic insulation (EMI) range. Low loadings and simple covalent bonding between MWCNTs and polystyrene results in low cost fabrication of smooth, low melt viscosity and high electrical performance nanocomposites ideal for applications from transparent antistatic coatings to EMI shields for multiple uses, from the telecommunication to semiconductor industry's.

References

[1] M. S. Strano *et al.*, Science **301**, 1519 (2003).
[2] S. A. Curran *et al.*, Adv. Mater. **10**, 1091(1998).
[3] Y. Lin *et al.*, J. Phys. Chem. B **106**, 1294 (2002).
[4] S. Qin *et al.*, Macromolecules **37**, (2004).
[5] Y. Lin, *et al.*, Macromolecules **36**, 7199 (2003).
[6] B. R. Azamian *et al.*, Chem. Comm. 366 (2002).
[7] A. V. Ellis *et al.*, Nano Lett. **3**, 279 (2003).
[8] L. K. Lim *et al.*, Synthetic Met. **139**, 521 (2003).

* Contact author: A.Ellis@irl.cri.nz

Atomic Force Spectroscopy as a Tool to Study the Electrical Conductivity of Polyaniline and Derivatives

P. S. de P. Herrmann[1,*], F. L. Leite[1,2], L. H. C. Mattoso[1,2], O. N. Oliveira Jr.[3]
[1] *Embrapa Agricultural Instrumentation, São Carlos-SP, 13560-970, BRAZIL*
[2] *Graduate Program in Science and Material Engineering, University of São Paulo , São Carlos-SP, 13560-970, BRAZIL*
[3] *Institute* of *Physics – São Carlos, University of São Paulo , São Carlos-SP, 13560, BRAZIL*

An Atomic Force Microscopy (AFM) has been used as force spectrometer to analyze forces generated in a polyaniline and derivatives due the interactions with polyelectrolytes. The surface of PANI films was imaged "as deposited" without any additional surface treatment. And the results from Atomic Force Spectroscopy (AFS) indicate the presence of ionic, steric forces and hydration forces.

Layer-by-layer films (LBL) of POEA and PANI were deposited onto glass substrates, covered by a gold layer. POEA, a derivative of polyaniline, was synthesized according to procedures in [1]. The AFM images (1.5μm x 1.5μm) and AFS measurement were made with a Topometrix Discoverer TMX 2010 in standard contact mode. V-shaped cantilevers were used with nominal spring constants of about 0.32 N/m (Silicon). Images and force curve were recorded in solution, using a fluid cell.

For doped PANI (pH ≤ 3), the double layer appear, and the attractive force decrease. For dedoped PANI (at high pHs), repulsive forces are minimized. Figure 1(a) shows the behavior of the force curves due the degree of doping for PANI, when it was in contact with aqueous solutions of various pHs, and Figure 1(b), (c), (d) e (e) are showing the images of the film obtained in the condition of four different pHs (pH=1.0; 3.0; 5.0 and 9.0). The same experiment was conduct using POEA as film. From the results it was possible to observer that PANI is slightly more doped than POEA in pH=5.0.

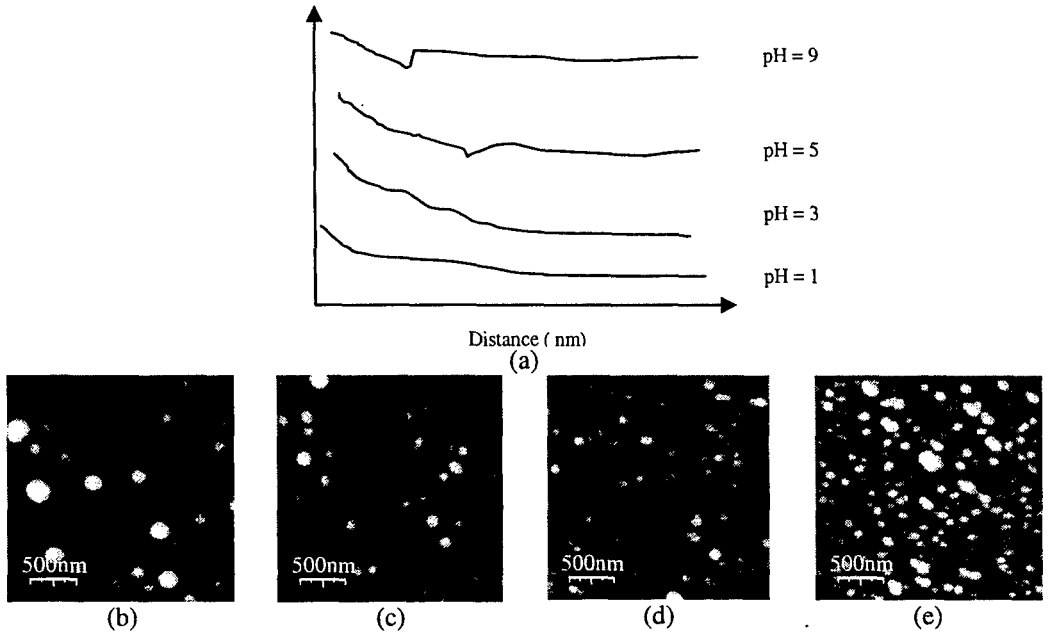

Figure 1 – Dependency of the interactions on a PANI film *vs* pH of the solution (a) and the morphology of the PANI onto the glass to pH=1.0(b); pH=3.0(c); pH=5.0(c) and pH=9.0(d).

Further work will be developing to correlate the different polyelectrolyte with conduction mechanisms in electronically conducting organic polymer.

References

[1] L. H. C. Mattoso, *et al.*, J. Polym. Sci. A 33, 122 (1995).

* Contact author: herrmann@cnpdia.embrapa.br

Characterisation of Cut Single-walled Carbon Nanotubes and their Functionalisation for Controlled Attachment

M. Marshall, S. Popa-Nita*, N.T. Baney, J.S. Quinton† and J.G. Shapter
School of Chemistry, Physics and Earth Sciences, Flinders University, GPO Box 2100, Adelaide, SA, 5001, Australia

Carbon nanotubes are often touted as the next great revolution in material science. While the assembly of nanotubes in an aligned fashion has been demonstrated on a surface in many different ways, such as post-deposition manipulation [1] or self-assembly [2,3], the problem of controlling the orientation of single-walled nanotubes (SWNT) with respect to each other and even other species still remains unsolved. This is largely due to the inertness and low solubility of nanotubes in general. At Flinders, we have used a technique involving the use of strong acidic environment to cut the nanotubes, as well add chemical functionality, in the form of carboxylic acid groups, which terminate the tube ends as shown in figure 1.

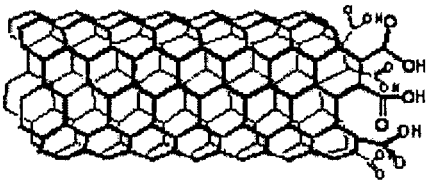

Figure 1.Single walled carbon nanotube, showing carboxylic acid functional groups at tube end

This added functionality subsequently serves two purposes; it greatly enhances nanotube solubility and moreover, enables the controlled attachment of other species. We have successfully illustrated the merit of this method, through the chemical mounting of cut nanotubes on various surfaces. These systems have been characterised by X-ray photoelectron spectroscopy (XPS), atomic force microscopy (AFM) as well as acid-base chemistry. In this presentation, the main focus will be upon the characterisation of cut nanotubes.

The successful attachment of various species to nanotubes in future will enable smarter chemical devices, where only the unique properties of carbon nanotubes, such as superior electron transport properties, will be required for their optimisation.

References

[1] Z. Ren, Z. P. Huang, J. W. Xu, J. H. Wang, P. Bush, M.P. Siegal and P. M. Provencio, Science **282**, 1105 (1998)
[2] S. S. Fan, M. G. Chapline, N. R. Franklin, T. W. Tombler, A. M. Cassell and H. Dai, Science **283**, 512 (1999)
[3] B. Wu, J. Zhang, Z. Wei, S. Cai and Z Liu, J. Phys. Chem. B **105**(22), 5075 (2001)

* On leave from Institut National des Sciences Appliquées de Rennes, 20 avenue des Buttes de Coësmes – CS 14315, 35043 Rennes Cedex (France)
† Presenting Author: Jamie.Quinton@flinders.edu.au

Study on the Structure Behavior of Gel Spun Ultra-High Molecular Weight Polyethylene/Carbon Nanotube Fiber

XinyingWang, Linli Liang, Xinpeng,Wang, Yanping Wang and Yimin Wang*
College of Material Science and Engineering, Donghua University, Shanghai, PRC, 200051

Abstract The ultra-high molecular weight polyethylene (UHMWPE)/carbon nanotubes (CNTs) composite fibers were prepared by gel spinning. TEM, SEM, XRD, IR and Raman were used to characterize the CNTs, its dispersion in the matrix, the functional group changes on the surface of the CNTs and the interaction between the CNTs and the matrix. A peculiar structure, a more regular alignment of the UHMWPE macromolecules was found and a model for restricted PE crystal growing was suggested, in which UHMWPE crystal growing direction was restricted by oriented CNTs.

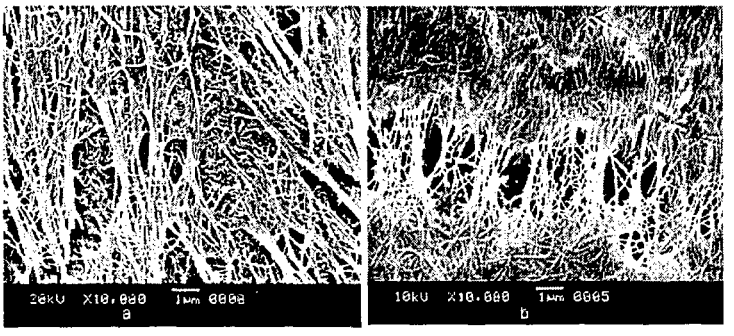

Fig.1 SEM of UHMWPE gel as-spun fibers with (a) and without CNTs (b)

References

[1] Xiaoyi Gong, Jun Liu, Suresh Baskaran, Roger D. Voise and James S. Young, *Chem. Mater.* B12, 1049 (2000).

[2] Andreas, H. *Angew, Chem. Int. Ed.* B41, 1853 (2002).

[3] Boul P.J., Liu, J., Mickelson E.T., Huffman C.B., Ericson L.M., Chiang I.W., Smith K.A., Colbert D.T., Hauge R.H., Margrave J.L., and Smalley R.E., *Chem. Phys. Lett.*, B310, 367 (1999).

[4] Mickelson E.T., Chiang I.W., Zimmerman J.L., Boul P.J., Lozano J., Smalley R.E., Hauge R.H., and Margrave J.L., *J. Phys. Chem. B*, B103, 4318 (1999).

[5] Stephan C, Nguyen TP, Lahr B, Blau W, Lefrant S, and Chauvet O., *Journal of Materials Research*, B17, 396 (2002).

[6] O. Lourie, and H. D. Wagner., *Journal of Materials Research*, B13, 2418 (1998).

*Contact author: ymw@dhu.edu.cn

SESSION Th D1
RADIATION SENSITIVE AND LUMINESCENT MATERIALS

Thursday 10 February 2005 1030–1210

Copthorne II

Session Chair **Martin Spaeth, Universität Paderborn, Germany.**

10:30 **CsBr:Eu2+ based needle image plates: physical mechanisms and present challenges**
Th D1.1 H. von Seggern
(Invited Talk).
Darmstadt University of Technology, Germany

10:55 **Radiative and non-radiative transitions of Eu2+**
Th D1.2 M.F. Reid[1], C-K. Duan[1,2], R.J. Reeves[1], and A. Meijerink[3]
[1] *University of Canterbury, Christchurch, NZ*
[2] *Chongqing University of Post & Telecommunications, Chongqing, China.*
[3] *Utrecht University, Utrecht, The Netherlands.*

11:10 **Lithium borate glasses and glass ceramics as thermal neutron imaging plates**
Th D1.3 G. A. Appleby[1], A. Edgar[1], C. M. Bartle[2], G. V. M. Williams[1,3]
[1] *MacDiarmid Institute, Victoria University of Wellington, NZ*
[2] *Institute of Geological and Nuclear Sciences Limited, Wellington, NZ*
[3] *Industrial Research Ltd., Wellington, NZ*

11:25 **Syntheses and luminescence of rare-earth ion doped nano-insulators**
Th D1.4 P. A. Tanner
City University of Hong Kong, Hong Kong, China.

11:40 **Sensitivity of stabilized a-Se based x-ray photoconductors**
Th D1.5 S.O. Kasap, M.Z. Kabir and M. Yunus
University of Saskatchewan, Saskatoon, Canada.

11:55 **Performance of glass-ceramic x-ray storage phosphors**
Th D1.6 A. Edgar[1,2] G.V.M. Williams[2,3], S. Schweizer[4], J.-M. Spaeth[4]
[1] *MacDiarmid Institute for Advanced Materials and Nanotechnology*
[2] *Victoria University, Wellington NZ*
[3] *Industrial Research Ltd, Lower Hutt, NZ*
[4] *University of Paderborn, Germany.*

$CsBr:Eu^{2+}$ based Needle Image Plates: Physical Mechanisms and Present Challenges

Heinz von Seggern[1]
Institute of Materials Science, Darmstadt University of Technology, 64287 Darmstadt, Germany

Digital x-ray radiography using storage phosphors is widely used nowadays. While commercially available systems are based on granular $BaFBr:Eu^{2+}$ [1], $CsBr:Eu^{2+}$ is an interesting novel storage phosphor with promising properties such as a columnar needle like structure [2] as displayed in Fig.1. This needle structure allows one to avoid the light scattering of the readout beam, which finally limits the spatial resolution and the related photo-stimulated luminescence (PSL) yield. It allows one also to decouple the PSL yield from the obtainable spatial resolution, which now is determined by the laser beam diameter and ultimately by the needle cross-section. This fact makes these materials suitable for high-resolution applications such as mammography.

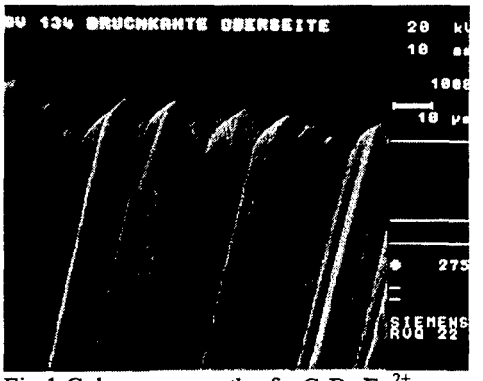

Fig.1 Columnar growth of a $CsBr:Eu^{2+}$

Like in $BaFBr:Eu^{2+}$ electrons and holes are formed by x-ray irradiation and subsequently are stored at different locations in the individual needles. In $CsBr:Eu^{2+}$ electrons are trapped in Br-vacancies forming F-centres with an excitation maximum at 680 nm. Holes are trapped close to Eu^{2+} ions. These stored centres establish a latent image, which can be read out by means of a scanning laser beam. Upon such photo-stimulation electrons are liberated from the F-centres and recombine with the hole centres giving rise to light emission from the Eu^{2+} ions [3,4].

The main disadvantage of present $CsBr:Eu^{2+}$ is, however, its low radiation hardness [5]. This insufficient hardness manifests itself in a loss of PSL yield with accumulated x-ray dose (see Fig. 2). One realizes a strong drop in the PSL yield, which cannot be tolerated in clinical use. In order to understand the physical reason for the low radiation hardness, the photoluminescence (PL) of Eu^{2+} and Eu^{3+} with accumulated radiation dose was monitored and compared to the PSL yield. A proportional decrease of the Eu^{2+} fluorescence and the PSL was observed. At the same time no radiation-induced oxidation to Eu^{3+} was found. Since Europium does not disappear from the sample, the loss in Eu^{2+} PL emission is believed to be due to agglomeration of Eu^{2+} leading to concentration quenching. At the same time the appearance of large F-centre agglomerates can be reported, supporting the idea of the intensive Eu^{2+} ion migration. This agglomeration will be discussed as the reason for the poor radiation hardness and as a possible reason for the formation of a new phase, which is precipitated in the bulk of the needles. Experiments to tackle the problem of the poor radiation hardness will be presented and consequences for the large F-centre agglomerates will be shown.

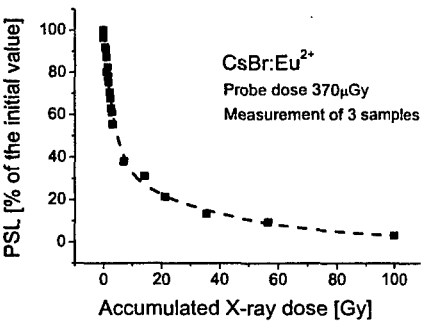

Fig. 2 Loss of PSL yield with accumulated x-ray dose.

References

[1] H. von Seggern, Braz. J. Phys. 29, 254-268 (1999)
[2] B. Schmitt, M. Fuchs, E. Hell, W. Knüpfer, P. Hackenschmied, A. Winnacker, Nucl. Instr. Meth. Phys. Res. B 191, 800-804 (2002)
[3] S. Schweizer, U. Rogulis, S. Assmann, J.-M. Spaeth, Radiation Measurements 33, 483-486 (2001)
[4] P. Hackenschmied, G. Zeitler, M. Batentschuk, A. Winnacker, B. Schmitt, M. Fuchs, E. Hell, W. Knüpfer, Nucl. Instr. Meth. Phys. Res. B 191, 163-167 (2002)
[5] J. Zimmermann, S. Hesse, H. von Seggern, M. Fuchs, W. Knüpfer: *Radiation hardness of $CsBr:Eu^{2+}$*, submitted to J. Luminescence

[1]Corresponding e-mail: seggern@e-mat.tu-darmstadt.de

Radiative and non-radiative transitions of Eu^{2+}

M. F. Reid[1*], C.-K. Duan[2], R. J. Reeves[1], and A. Meijerink[3]

[1] *Department of Physics and Astronomy, and MacDiarmid Institute of Advanced Materials and Nanotechnology, University of Canterbury, Christchurch, New Zealand*

[2] *Institute of Applied Physics, Chongqing University of Post and Telecommunications, Chongqing 400065, China, and Department of Physics and Astronomy, University of Canterbury, Christchurch, New Zealand*

[3] *Debye Institute, Department of condensed Matter, Utrecht University, P.O. Box 80,000, 3508 TA Utrecht, The Netherlands.*

Our work on modelling of $4f^{N-1}5d$ configurations of lanthanide ions in solids has led to detailed calculations of the energy levels of the $4f^{N-1}5d$ configuration, the absorption intensities from the $4f^N$ ground states, and the radiative lifetimes of $4f^{N-1}5d$ states [1]. However, a detailed understanding of non-radiative transitions between the $4f^{N-1}5d$ and $4f^N$ configurations is important to applications developments, such as VUV-excited phosphors. The effect of non-radiative relaxation may be seen in the linewidths of excitation lines [2].

To successfully model non-radiative processes we must take into account the vibrations that mediate the coupling between the configurations. We are currently modelling the line-widths of two-photon absorption transitions between $4f^7$ states in Eu^{2+} [3]. In this paper we will report on our recent progress in this area, which takes into account the symmetry of the vibrations that couple the configurations. We also report on measurement and modelling of the temperature dependence of the radiative lifetime of Eu^{2+}, which gives us further insight into the structure of the excited states [4].

References

[1] L. van Pieterson, M. F. Reid *et al.*, *Phys. Rev. B* 65:045113, 045114, 2002.

[2] L. van Pieterson, M. F. Reid, and A. Meijerink, *Phys. Rev. Lett.*, 88:067405, 2002.

[3] G.W. Burdick, A. Burdick, V. Deev, C.-K. Duan, and M.F. Reid, *Submitted to Phys. Rev. B.*

[4] C.-K. Duan, A. Meijerink, R. J. Reeves, M.F. Reid, *Submitted to Journal of Alloys and Compounds.*

* Contact author: Mike.Reid@canterbury.ac.nz

Lithium Borate Glasses and Glass Ceramics as Thermal Neutron Imaging Plates

G. A. Appleby[1,*], A. Edgar[1], C. M. Bartle[2], G. V. M. Williams[1,3]
[1] *MacDiarmid Institute, Victoria University of Wellington, New Zealand*
[2] *Institute of Geological and Nuclear Sciences Limited, Wellington, New Zealand*
[3] *Industrial Research Limited, Wellington, New Zealand*

Thermal neutron radiography is a powerful method for revealing information about an object's internal structure and is complimentary to the more common X-ray or gamma-ray radiography. Whereas gamma and X-rays are attenuated most strongly by elements with high atomic number, the reverse is generally true for thermal neutrons, meaning that neutron radiography is useful for light elements such as hydrogen or carbon. Hydrogen is a common atomic component of many chemical species of interest such as water, plastics and hydrocarbons. Therefore, there are many applications of thermal neutron imaging, ranging from non-destructive testing to medicine (including cancer treatment), and the detection of explosives (airport security and landmine detection).

Common commercial thermal neutron imaging plates (IPs) produced by Fuji contain a gamma-ray sensitive crystalline imaging plate of $BaFBr:Eu^{2+}$ coated with a Gd_2O_3 layer as a neutron-gamma converter [1]. The basic IP uses the phenomenon of photo-stimulated luminescence (PSL), wherein the recombination energy of radiation-induced trapped electrons and holes is detected optically after stimulation by an incident raster-scanned laser beam. However, the use of high Z elements like Gd and Ba results in a high sensitivity of the IP to the background gamma radiation associated with most thermal neutron sources. The IP is also crystalline in nature, resulting in scattering of the PSL stimulating laser beam and therefore reduced spatial resolution of the image.

We are developing rare-earth doped lithium borate (LiBO) glasses and glass ceramics as thermal neutron IPs, which offer potential advantages over the Fuji IP. These materials have been shown to exhibit both photoluminescence and PSL [2, 3]. When irradiated with thermal neutrons, these IP's make use of the high reaction cross-sections for the $^{10}B(n,\alpha)^7Li$ and $^6Li(n,\alpha)^3H$ reactions, and the secondary alpha particle energy transferred to a rare-earth luminescence centre. The use of the low Z elements Li, B and O result in a gamma half thickness that is about three times greater than that of the Fuji IP, over a range of gamma energies. LiBO glasses are also highly transparent and therefore, in these materials, the laser scattering problem in the Fuji IP will not occur.

We will present details of the structural and optical characteristics of these new IP's, and their responses to neutron and gamma radiation.

References

1. Tazaki, S., et al., *Development of a new type of imaging plate for neutron detection.* Nuclear Instruments and Methods in Physics Research A, 1999. **424**: p. 20-25.

2. Whang, J.H., et al., *Photoluminescence of lithium borate glasses doped by lanthanides.* Functional Materials, 2002. **9**(4): p. 657-660.

3. Qiu, J., et al., *Photostimulated luminescence of Ce^{3+}-doped alkali borate glasses.* Applied Physics Letters, 1997. **71**(1): p. 43-45.

* Contact author: gappleby@paradise.net.nz

Syntheses and Luminescence of Rare-earth Ion Doped Nano-insulators

P. A. Tanner
Department of Biology and Chemistry, City University of Hong Kong, Tat Chee Avenue, Kowloon, Hong Kong S.A.R., P.R. CHINA

The optical applications of rare-earth ions (RE^{3+}) doped into insulators (REDI) include phosphors, solid-state laser materials, upconverters and quantum-cutters. Recent interest concerns the properties of these materials on the nano-scale for high-definition display materials and immunoassays. This presentation will review the optical studies of RE^{3+} doped into insulating nanomaterials (REDIN) since there are many recent publications and some of these have found conflicting results. There are two previous reviews [1,2].

Various methods have been utilized for the preparation of REDIN and the latter may have different crystal structures from (bulk) micron-size materials. The methods include sol-gel synthesis in aqueous or non-aqueous media (with lyophilization), spray-pyrolysis and rapid firing techniques, precipitation methods, combustion syntheses, gas-phase condensation and ion implantation. The sol-gel REDIN products comprise irregularly-shaped grains. The crystallite sizes inferred from X-ray diffraction patterns or calculated from Raman spectra are much smaller than the large clusters observed by scanning electron microscopy. Sintering produces micron-scale particles, but the use of low temperatures leads to surface defects including the presence of water and impurities such as carbonate. Optical experiments of REDIN, mainly using Er^{3+} and Eu^{3+} in insulators such as RE_2O_3, Y_2O_2S and $Y_3Al_5O_{12}$, have produced interesting and new phenomena some of which will be described in the presentation. Quantum size effects are not as important as in semiconductors because the $4f^N$ electronic wavefunctions are localized. However, the absence of low-frequency acoustic modes and the confinement of vibrational excitations give rise to an anomalous thermalization. Thus hot bands remain at temperatures of a few Kelvins and the population of the relevant excited states (such as $^2H(2)_{11/2}$ of Er^{3+}) may change energy transfer probabilities from the bulk materials. The increase in surface area/volume ratio in REDIN increases nonradiative rates due to the influence of surface defects. Increased radiative rates have also been reported, due to symmetry reduction of the RE^{3+} ion environment. The interaction of the RE^{3+} ions with the surrounding medium also affects the radiative lifetimes and relaxation rates. The different relaxation rate behaviour in REDI versus REDIN leads to different quantum efficiencies, different relative intensities of transitions from different multiplets, and to different upconversion behaviour. Not only is there a shift in the charge-transfer (CT) band in REDIN compared with REDI, but other changes in the CT band and in the intensity of the 4f - 5d transition occur in REDIN under ultraviolet light excitation. On-off blinking of RE^{3+} ions in REDIN occurs on a variable timescale under continuous irradiation. In conclusion, many optical phenomena may be tailored from the design and size of REDIN and this work is in its infancy.

Acknowledgement: This work is supported by the HK UGC Research Grant CityU 102304.

References

[1] B.M. Tissue, Chem. Mater. 10 (**1998**) 2837-2845.
[2] S.P. Feofilov, Phys. Solid State 44 (**2002**) 1407-1414.

Sensitivity of Stabilized a-Se Based X-Ray Photoconductors

S.O. Kasap*, M.Z. Kabir and M. Yunus
[1] *Department of Electrical Engineering, University of Saskatchewan, Saskatoon, S7N 5A9, Canada*

Research in the last ten years has shown that direct conversion stabilized a-Se based x-ray image detectors can provide excellent x-ray images. These detectors are now commercially available. Even though the progress in the technology has enabled the commercialization of these direct conversion x-ray image detectors, there is still much fundamental work to be done in understanding some of the basic principles. Stabilized a-Se based x-ray detectors have shown a decrease in the sensitivity as a result of accumulated x-ray exposure. The reduction in the x-ray sensitivity with exposure means that the sensitivity of the photoconductor has been altered in a way that depends on the previous image, which leads to what is called "ghosting". The latter is essentially a phenomenon in which the image has remnants of a previous image, because the previous exposure has selectively modified the x-ray sensitivity. As yet, we do not have a suitable quantitative model that can account for the observed "ghosting", though it has been attributed to the deep trapping of electrons in the bulk of the semiconductor. The present paper provides a suitable model for the observed ghosting, reduction in sensitivity, in terms of a number of physical phenomena that occur as the stabilized a-Se photoconductor is exposed to x-rays. (a) Trapping of electrons and the subsequent recombination of drifting holes with trapped electrons. (b) The evolution of bulk space charge with x-ray exposure, due to trapping, that modifies the internal field and hence modifies the electron-hole pair generation across the photoconductor. The ionization energy $W_{\pm}$ is a-Se is strongly field dependent, and any modification of the internal field also alters the x-ray charge photogeneration efficiency. (c) x-ray generation of new deep traps. We have found that all three factors are necessary for a satisfactory explanation of the observed reduction in the x-ray sensitivity. The predictions of the proposed model are compared with reported experimental data. The reduction in the sensitivity due to accumulated x-ray exposure seems to be a fundamental property of stabilized a-Se, though it does not prevent a-Se from being used as an acceptable x-ray photoconductor in recently commercialized flat panel x-ray image detectors.

Session: *Radiation Imaging and Dosimetry*. Chair: Andrew Edgar.

* Contact author: sok533@engr.usask.ca

Performance of Glass-Ceramic X-ray Storage Phosphors

A. Edgar[1,2*] G.V.M. Williams[2,3], S. Schweizer[4], J.-M. Spaeth[4]

[1] *MacDiarmid Institute for Advanced Materials and Nanotechnology*
[2] *School of Chemical and Physical Sciences, Victoria University, Wellington NEW ZEALAND*
[3] *Industrial Research Ltd, Wellington, NEW ZEALAND*
[4] *Experimental Physik, University of Paderborn, GERMANY*

Storage phosphor materials[1] formed into X-ray imaging plates[2] are now widely used in medical and non-destructive testing. They compete in those markets with several other new technologies based on scintillator/CCD or CMOS array combinations, and with direct electrical imaging based on amorphous selenium[3]. We have developed several new glass-ceramic x-ray storage phosphor materials [4,5] which offer several advantages over existing materials, and other technologies. The active component in the glass ceramics are rare-earth doped nano or micro-crystallites, which are embedded in a glass matrix. The specific materials which we have studied so far are primarily fluoride glasses containing binary and ternary halide nanocrystals.

In this paper, we present a comparative review of the performance of these glass ceramic storage phosphors for X- and gamma-ray imaging. The key parameters include conversion and stimulation efficiency, storage time, read-out time, and spatial resolution. These parameters are all related to the glass ceramic microstructure, and to the character of the atomic charge-carrier trapping centers and photo-active rare-earth dopants which underpin the photo-stimulated luminescence effect, which is the basis for the storage phosphor effect. We present in particular new measurements of the spatial resolution, which shows a significant improvement compared to standard crystalline storage phosphor materials. The spatial resolution, or pixel size in digital terms, limits the detail discernible in objects under test, and is of critical importance in applications such as mammography and crack testing in metals. In the case of X-ray storage phosphors, the powdered nature of the phosphor currently used, BaFBr, results in light scattering of the laser beam used in the read-out process. This scattering widens the area of plate stimulated into fluorescence by the laser beam beyond the focal spot, and degrades the resolution, so that for conventional plates the resolution is limited to 100μ, whilst for special dye-tinted plates, the resolution improves to 50μ.

We present here the results of measurements of the spatial resolution of glass ceramic storage phosphors using a commercial confocal Raman spectrometer, a semi-commercial laser scanning system, and a custom-built laboratory system which includes a confocal geometry option. We have measured the spatial resolution, summarised by the Modulation Transfer Function, for various glass ceramic combinations and relate these to the microstructure as determined by electron microscopy. The implications of these results for X-ray and gamma ray imaging are discussed.

References

[1] S. Schweizer, Physica Status Solidi **187,** 335-393 (2001).

[2] J. A. Rowlands, Phys. Med. Biol. **47,** R123-R166 (2002).

[3] S. O. Kasap and J. A. Rowlands, Proceedings of the IEEE **90,** 591-604 (2002).

[4] A. Edgar, G. V. M. Williams, and G. A. Appleby, J. Luminescence **108,** 19-23 (2004).

[5] M. Secu, S. Schweizer, J.-M. Spaeth, A. Edgar, G. V. M. Williams, and U. Rieser, J. Phys. Condensed Matter **15,** 1097-1108 (2003).

* Contact author: Andy.Edgar@vuw.ac.nz

SESSION Th E1
MATERIALS MODELLING

Thursday 10 February 2005 1030–1210

Copthorne III

Session Chair **Shaun Hendy, Industrial Research Ltd., NZ**

10:30 **Atomic scale models for defect structure and transport predictions**
Th E1.1 R. W. Grimes[1], J. Ball[1], M. Levy[1], S. R. Phillpot[2], B. Uberuga[3] and K. Sickafus[3] (Invited Talk)
[1]*Imperial College, London, UK*
[2]*University of Florida, Gainsville, USA*
[3]*Los Alamos National Laboratory, Los Alamos, USA*

10:55 **3-D model of nanostructure formation from colloidal suspensions during drying**
Th E1.2 Y.Yamaguchi[1], M. Fujita[1] and Y. Yasuda[2]
[1]*University of Tokyo, Tokyo, Japan*
[2]*Mitsubishi Research Institute, Tokyo, Japan*

11:10 **Simulations of growth and optical anisotropy of obliquely deposited thin films**
Th E1.3 M. D. Arnold[1,2], I. J. Hodgkinson[1] and R. J. Ballagh[1]
[1]*University of Otago, Dunedin, NZ*
[2]*University of Canterbury, Christchurch, NZ*

11:25 **Metastability of surface nanostructure arrays studied using the Fokker-Planck equation**
Th E1.4 D. E. Jesson[1], T. P. Munt[2], V. A. Shchukin[3] and D. Bimberg[3]
[1]*Monash University, Victoria, Australia*
[2]*Heriot-Watt University, Edinburgh, UK*
[3]*Technische Universität Berlin, Berlin, Germany*

11:40 **Atomic coordination number imperfection reverses the Hall-Petch relationship in the nanometer regime**
Th E1.5 C. Q. Sun, C. M. Li, S. Li and B. K. Tay
Nanyang Technological University, Singapore

11:55 **A micromechanical study of texture evolution in thermally annealed copper interconnects**
Th E1.6 K. S. Cheong, D. M. Knowles and K.J. Stevens
Industrial Research Limited, Lower Hutt, NZ

Atomic Scale Models for Defect Structure and Transport Predictions

Robin W. Grimes*, Jon Ball*, Mark Levy*,
Simon R. Phillpot**, Blas Uberuga***, Kurt Sickafus***

** Department of Materials, Imperial College London, London SW7 2BP, UK*
*** Dept. of Materials, University of Florida, Gainesville Fl 32611, USA*
****MST-8 Los Alamos National Laboratory, Los Almos, NM 87545, USA*

The properties of both functional and structural materials are usually dictated by the distributions of defects that form as a consequence of equilibrium and non-equilibrium processes. Atomic scale computer simulation can be used to predict the energetics of defect structures and their transport. However, the range of lattice and defect types means that a variety of approaches are necessary. Early models treated defects at low concentration and have traditionally assuming the dilute limit via simple mass action equations. As defects quickly accumulate, they cannot be regarded as isolated and thus it is necessary to consider the formation of defect clusters. In oxides defect cluster formation is dictated by long range coulomb interactions between opposite charged defects. If equilibrium is assumed between the clusters and their isolated components it is a simple matter to derive models for the relative distribution of these species. Of course, for many applications equilibrium is not valid. A key issue is therefore to assess models against experimental data, for example, the variation of lattice parameter with defect concentration. Here results will be presented that suggests in oxides clusters may begin to dominate at relatively low concentrations. Furthermore, molecular dynamics simulations show that even minority defect clusters can still be responsible for atomic transport.

Recently it has been demonstrated possible to predict the binding energy of a large cluster by evaluating the sum of the component defect pair interactions. By using a Monte Carlo algorithm to construct trail distributions of defects, this pair approximation will allow us to generate distributions of defects within very large lattice structures. Nevertheless, eventually concentrations of defects become sufficiently high that it is necessary to simulate them using large unit cell repeat units. The energy of a large unit that incorporates specific defects can be evaluated using energy minimization to optimize all the atom positions within the cell. Statistical distributions of those defective cells are predicted by employing the Metropolis algorithm. This is an example of a hybrid approach. Similarly by using a combination of conventional and temperature accelerated dynamics approaches it is possible to bridge time scales. Examples of both types of approach will be presented.

3-D Model of Nanostructure Formation from Colloidal Suspensions During Drying

Y.Yamaguchi[1,*] M. Fujita[1], and Y. Yasuda[2]
[1] *Department of Chemical System Engineering, University of Tokyo, Japan*
[2] *Mitsubishi Research Institute, Ohtemachi, Tokyo, Japan*

A set of numerical models for three-dimensional self-organization of nanoparticles in a liquid film on a substrate is developed and numerical simulations[1] are carried out to investigate relationship between process conditions and structures of self-organized nanoparticles as shown in Fig.1. The three-dimensional Langevin equation is employed to track particles on a substrate with time. Each nanoparticle is subject to multiscale surface forces such as capillary force, contact force, electrostatic force, van der Waals force and friction drag as well as Brownian force and fluid drag. The modeling shows that no surface force can be neglected in the self-organization process because magnitude of the surface forces strongly depends on interparticle distances and a thickness of liquid film. Three principles of two-dimensional selforganization are proposed based on unsteady behavior of nanoparticles. Isotropic ordering factor and non-dimensional boundary length are introduced to quantify structures of self-organized nanoparticles. Every structure of nanoparticles obtained here can be classified according to sets of these criteria.

It was found that all surface forces considered here could become primary components in a coating-drying process, because a proportion of magnitude of each force remarkably changed during an evaporation of solvent due to change of interparticle distance and contact height of interface. Therefore, the multiscale and multiphysics modeling proposed here that contains a variety of surface forces is indispensable to simulate colloidal nanoparticles during drying. As a result of simulations, three principles of three-dimensional self-organization of nanoparticles in a liquid film could be derived as follows: 1) Self-organization by long-distance attractive force, such as capillary force, 2) Selforganization by random force and short-distance attractive force, such as Brownian force and van der Waals force, 3) Self-organization by repulsive force, such as electrostatic force. The three principles form unique three-dimensional structures, isotropic crystallization, non-isotropic aggregation and isotropic arrangement, respectively. These structures were quantified by two structure criteria, IOF (Isotropic Ordering Factor) and NBL (Non-dimensional Boundary Length) proposed in the present study. The classification of structure of nanoparticles by these structure criteria agreed well with human intuition. In addition, it was emphasized that each result of simulation could be mapped in a quantitative structure space, which could contain a huge variety of structures of self-organized nanoparticles as structure points whose coordinates were structure variables, IOF or NBL. It can be concluded that the present study clarified a part of relationships between principles of three-dimensional self-organization and structure variables, which were indispensable for efficient structure designs.

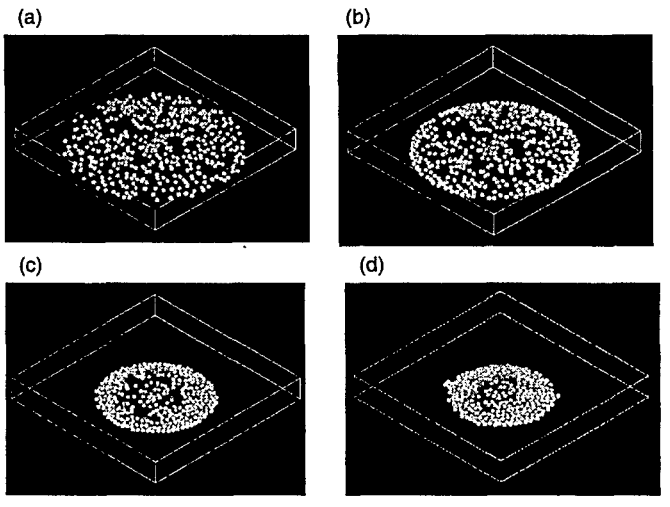

Fig.1 *3-D dynamic simulation of nanoparticles of 50 nm on a substrate during drying. (a),(b),(c),and (d) show time evolutions.*

References

[1] M. Fujita, H. Nishikawa, T. Okubo, Y. Yamaguchi, J. J. of Applied Physics, 43, 7A, 4434-4442, 2004

* Contact author: yukiyama@chemsys.t.u-tokyo.ac.jp.

Simulations of Growth and Optical Anisotropy of Obliquely Deposited Thin Films

M. D. Arnold[a, b,*] I. J. Hodgkinson[a], R. J. Ballagh[a]
[a] *Department of Physics, University of Otago, Dunedin, NEW ZEALAND*
[b] *Department of Electrical and Computer Engineering, University of Canterbury, Christchurch, NEW ZEALAND*

Materials grown by oblique physical vapour deposition (OPVD) exhibit structural and consequently optical anisotropy[1]. The optical anisotropy is a particularly useful property and enables the production of thin film polarizing elements[2]. Here we seek to better understand the sometimes subtle relationship between structural and optical anisotropy via direct simulation, and present some initial investigations on the effect of texturing of the substrate.

As a first step in the process, the structure of the film is simulated. A range of simulation techniques have been reported, all with a trade-off between accuracy and speed. Here we require large scale 3D modelling, which effectively precludes full molecular dynamics (MD) on the basis of prohibitive computational requirements. Further, reasonably representative behaviour is possible using simpler approaches, such as ballistic deposition with coordination-dependent diffusion. Hence, we attempt to code a simulator based on some such suitable schemes in the literature[3, 4]. After necessary empirical calibration, we simulate some growth regimes appropriate to particular experimental equipment. In particular, we demonstrate the effect of serial bi-deposition (SBD) on both biaxial and chiral films.

The structure can be linked to empirical models[5] of optical anisotropy via correlation analysis[6], but it is well known that the models are sometimes inaccurate, so we seek a more direct path to the solution. We are most interested in the long-wavelength regime where wave effects like scatter and diffraction are minimized, and hence quasi-static approximations can be applied. Many methods that directly solve Maxwell's equations appear to scale poorly with the increased complexity inherent in the statistical structure used here. We adopt a Green's function method (discrete dipole approximation) [6, 7], which we find has superior numerical convergence particularly under bi-conjugate gradient iteration. The formulation can even be competitively converged using fixed-step steepest descent which we use to maximize storage-efficiency. The optical anisotropy of a number of growth regimes is simulated, and in particular we can clearly show the vertical inhomogeneity of chiral films. Finally, we demonstrate possible enhancement of optical anisotropy of coatings deposited onto grating structures.

References

1. Messier, R. and A. Lakhtakia, *Sculptured thin films - II. Experiments and applications.* Materials Research Innovations, 1999. **2**(4): p. 217-222.

2. Hodgkinson, I.J. and Q.h. Wu, *Birefringent Thin Films and Polarizing Elements.* 1997: World Scientific Publishing Co. Pte. Ltd.

3. Smy, T., et al., *Three-dimensional simulation of film microstructure produced by glancing angle deposition.* Journal of Vacuum Science & Technology a-Vacuum Surfaces and Films, 2000. **18**(5): p. 2507-2512.

4. Suzuki, M. and Y. Taga, *Numerical study of the effective surface area of obliquely deposited thin films.* Journal of Applied Physics, 2001. **90**(11): p. 5599-5605.

5. Bragg, W.L. and A.B. Pippard, *The Form Birefringence of Macromolecules.* Acta Crystallographica, 1953. **6**: p. 865-867.

6. Sen, A.K. and S. Torquato, *Effective Conductivity of Anisotropic 2-Phase Composite Media.* Physical Review B, 1989. **39**(7): p. 4504-4515.

7. Hodgkinson, I.J. and J.R. Gee. *Computer modeling of optical thin film deposition.* in *Optical Interference Coatings.* 1994. Grenoble, France: SPIE.

* Contact author: m.arnold@elec.canterbury.ac.nz

Metastability of Surface Nanostructure Arrays Studied using the Fokker-Planck Equation

D. E. Jesson,[1,*] T. P. Munt [2], V. A. Shchukin [3] and D. Bimberg [3]
[1] *School of Physics and Materials Engineering, Monash University, Victoria 3800, AUSTRALIA*
[2] *Department of Physics, School of Engineering and Physical Sciences, Heriot-Watt University, Edinburgh EH14 4AS, UNITED KINGDOM*
[3] *Institut für Festkörperphysik, Technische Universität Berlin, D-10623 Berlin, GERMANY*

Surface nanostructures which possess a minimum in formation energy per atom as a function of island size (MA systems) are particularly attractive candidates for device applications because they are associated with a thermodynamically favoured size. By simply annealing such structures, one might anticipate the creation of arrays with good size uniformity. Although it is not possible to identify MA systems a-priori, theoretical studies have shown that coherently strained two-dimensional (2D) islands,[1,2] three-dimensional (3D) islands with surface stress discontinuities at their edges[3,4] or 3D islands with strain renormalized surface energy[4] are potential candidates for MA systems. It is therefore important to understand how the minimum in formation energy per atom as a function of island size influences the coarsening behaviour of MA systems in order to best exploit this characteristic to obtain good size uniformity.

Here, we focus on an array of 2D strained islands which is the simplest system in which a thermodynamically favoured size is expected to exist.[3,4] To describe the evolution of the 2D strained island array we use the Fokker-Planck equation, consisting of drift and diffusion terms, which is derived as an approximation of the kinetic Becker-Döring model for the aggregation of particles.[5] A surprising feature arising from our simulations of MA system coarsening is the phenomenon of metastable island arrays which are associated with regions of positive chemical potential gradient.[6] Islands undergo inverse ripening associated with the drift term; small islands with a chemical potential below the mean field chemical potential grow and large islands, with a chemical potential above the mean-field, shrink. Therefore, the distribution narrows about the mean island size but is opposed by the diffusion term which increases in magnitude as the distribution sharpens. When the drift and diffusion terms are very nearly equal in magnitude but opposite in sign, a long-lived transient state is created. We find such states to be a universal feature of MA system coarsening.

Metastable states should play a significant role in the coarsening of all surface nanostructures provided that positive gradients in chemical potential exist. Therefore, if material is deposited such that the mean-field chemical potential is only slightly enhanced by the deposition flux, the island size distribution will be dominated by the metastable state at that particular coverage. In regions of positive gradients in chemical potential, the size distribution can then be tuned to a desired size by depositing material for the required time.[6] This offers the prospect of narrow size distributions which do not broaden with increasing coverage, as would be expected during conventional coarsening. This unusual coarsening behaviour has recently been experimentally observed for metallic islands[7] which are thought to possess a minimum in chemical potential (i.e. regions of positive gradient).[3] As discussed above, this is a necessary condition for the existence of metastable states. Given the likely occurrence of MA systems across a wide range of material systems and island geometries,[1-4] it might be hoped that chemical potential induced metastability will see significant applications in the fabrication of nanostructure arrays.[8]

References

[1] V. I. Marchenko, JETP Lett. **33**, 381 (1981).
[2] D. Vanderbilt, Surf. Sci. **268** (1992) L300; K. Ng and D. Vanderbilt, Phys. Rev. B. **52**, 2177 (1995).
[3] F. Liu, Phys. Rev. Lett. **89**, 246105 (2002).
[4] V. A. Shchukin, N. N. Ledentsov, P. S. Kop'ev and D. Bimberg, Phys. Rev. Lett. **75**, 2968 (1995).
[5] J. J. L. Velázquez, J. Statistical Phys. **92**, 195 (1998).
[6] D. E. Jesson, T. P. Munt, V. A. Shchukin and D. Bimberg, Phys. Rev. Lett. **92**, 115503 (2004).
[7] Z. Gai, B. Wu, J. P. Pierce, G. A. Farnan, D. Shu, M. Wang, Z. Zhang, and J. Shen, Phys. Rev. Lett. **89**, 235502 (2002).
[8] T. P. Munt, D. E. Jesson, V. A. Shchukin and D. Bimberg, Appl. Phys. Lett. **85**, 1784 (2004).

* Contact author: david.jesson@spme.monash.edu.au

Atomic coordination number imperfection reverses the Hall-Petch relationship in the nanometer regime

Chang Q Sun,* C. M. Li, S. Li, and B. K. Tay
School of Electrical and Electronic Engineering, Nanyang Technological University, Singapore 639798, SINGAPORE

An atomistic model for the size-and-temperature dependence of the mechanical strength and compressibility of a nanosolid has been derived based on the recent bond order-length-strength (BOLS) correlation mechanism [1,2]. It is proposed that the bond strengthening due to atomic coordination-number (CN) imperfection at grain boundaries contributes directly to the mechanical strength of the solid at temperature below the melting point (T_m), while the lowered atomic cohesive energy (E_C, a production of the single bond energy and the atomic CN) lowers the barrier for atomic dislocation. In the nanometer regime, the atomic E_C and the T_m decrease, and therefore, the mechanical strength drops as the solid size is reduced. Matching predictions to measurements, as shown in Figure 1, reveals that the critical size, in the range of 7 ~ 30 nm, at which the slope of the inverse Hall-Petch relation transits depends uniquely on the T/T_m ratio where T is the temperature at which measurement is conducted.

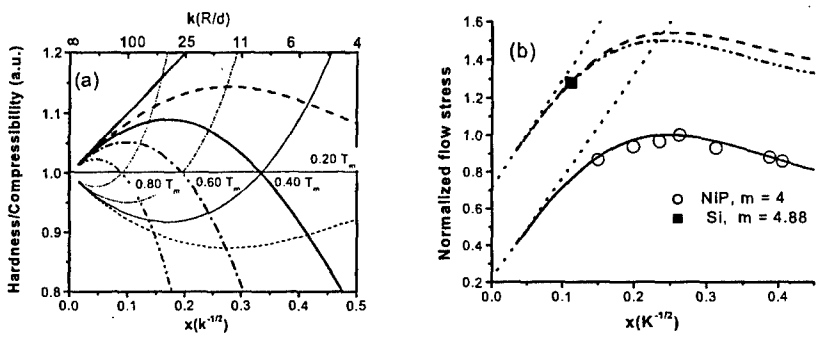

Figure 1 (a) Theoretical prediction of temperature dependence of the mechanical stress and its inverse-compressibility. (b) Comparison of the calculated (solid line) with the measured IHPR (scattered data) of NiP and Si (offset). The dashed lines are calculation considering only the activation energy. The dotted lines are the traditional HPR and its intercept at the y-axis corresponds to the normalized hardness of the bulk counterparts. One measured data should be sufficient to calibrate the IHPR such as the case of Si. K = R/d is the number of atoms lined along the radius of a spherical dot.

References

• E-mail: ecqsun@ntu.edu.sg; Fax: 65 6792 0415; http://www.ntu.edu.sg/home/ecqsun/

[1] C. Q. Sun, C. M. Li, S. Li, B. K. Tay, Breaking limit of atomic distance in an impurity-free monatomic chain, *Phys. Rev.* B69, 245402 (2004)
[2] C. Q. Sun, Nanosolid Physics: bond order-length-strength correlation for the significance of atomic CN imperfection, *Physics Reports*, in press.

AMN2 '05

A MICROMECHANICAL STUDY OF TEXTURE EVOLUTION IN THERMALLY ANNEALED COPPER INTERCONNECTS

K. S. Cheong*, D. M. Knowles, K.J. Stevens
Materials Performance Technologies, Industrial Research Limited, Gracefield, New Zealand
k.cheong@matperf.com, d.knowles@matperf.com;k.stevens@matperf.com*

With the continuous scaling of integrated circuits below sub-micron levels, the grain structure of interconnect lines is controlled by the relation between line width and grain size. In addition, the associated decrease in thickness leads to interconnect lines with columnar grain structures. Since a strong (111) texture is known to significantly improve interconnect reliability [1], it is desirable to optimize post-patterning annealing conditions in interconnect fabrication. Texture evolution is governed by the simultaneous minimization of the grain boundary, strain and surface—interface energy contributions. The texture favoured is therefore dependent on the relative magnitudes of these driving energies. Due to their anisotropic elastic properties, differently textured grains will have differing strain energies resulting in preferential grain growth [2].

In this work, a micromechanical model is developed to examine the influence of annealing temperatures on texture evolution in interconnect lines. The grain structure of these lines is assumed to be quasi two-dimensional, consisting of columnar grains. Thermo-elastic and plastic behaviour due to the mismatch in thermal expansion coefficients between the interconnect metal (eg. Cu, Al), passivating dielectric (SiO_2) and wafer material (Si) are assumed to be governed by crystal plasticity. For isothermal plastic behaviour, the constitutive response of each grain is modeled at the single crystal level using a dislocation-mechanics based crystallographic theory [3], while the dielectric and wafer materials are modeled to be isotropic and linear-elastic. For simplicity, the interconnect-dielectric-wafer interfaces are assumed to be perfectly bonded and the system is initially stress-free at ambient temperature. The figure below shows schematic drawings of the interconnect system to be modeled, with each interconnect metal grain explicitly described using crystal plasticity through the multiplicative decomposition of the deformation gradient **F** into elastic, plastic and thermal parts.

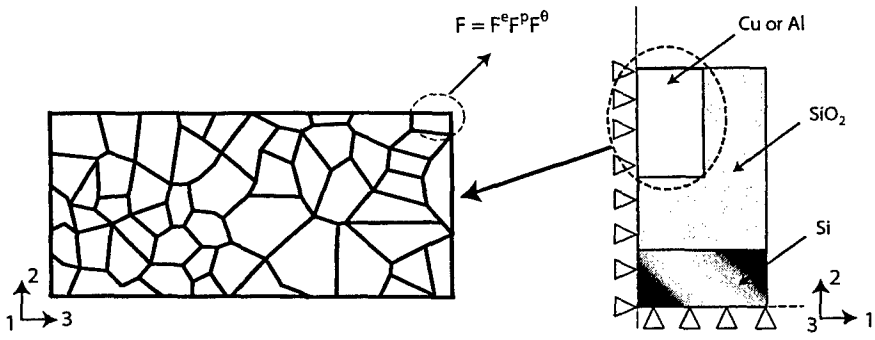

Figure – Schematic drawings of the micromechanical model showing the (a) interconnect grain structure, and (b) cross-section of the interconnect system.

Based on the concept of energy minimization, parametric studies are carried out using the finite-element method to investigate the effects of temperature and geometry on the evolving texture in such systems.

References

[1] K. T. Lee, J. A. Szpunar, A. Morawiee, D. B. Knorr and K. P. Rodbell, *Can. Metall. Quart.* **V(34)**, 287 (1995).
[2] S. P. Riege and C. V. Thompson, *Scripta Mat.* **V(41)**, 403 (1999).
[3] K. S. Cheong and E. P. Busso, *Acta. Mat.*, in press. (2004).

Thursday 10 February
Oral Session Two

SESSION Th A2
SEMICONDUCTOR GROWTH AND CHARACTERISATION II

Thursday 10 February 2005 1320–1500

Galaxy I

Session Chair **Steven Durbin, University of Canterbury, NZ**

13.20 **Ultrafast spectroscopy of carrier dynamics in III-N epilayers and heterostructures**
Th A2.1 A.N. Cartwright
(Invited Talk)
State University of New York, Buffalo, USA

13.45 **Optical and electrical properties of GaN nanowires synthesized with N_2-quenched pulsed laser ablation**
Th A2.2 D.K.T. Ng[1], L.S. Tan[1], and M.H. Hong[1,2]
[1] *National University of Singapore, Singapore*
[2] *Data Storage Institute, DSI Building, Singapore*

14.00 **Optoelectronics of highly disordered gallium nitride**
Th A2.3 A. Koo[1] F. Budde[1], B.J. Ruck[1], H.J. Trodahl[1] and A. Bittar[2]
[1] *Victoria University of Wellington, Wellington, NZ*
[2] *Industrial Research Ltd., Lower Hutt, NZ*

14.15 **TEM characterisation of GdN thin films**
Th A2.4 W.R. McKenzie[1], P.R. Munroe[1], F. Budde[2], B.J. Ruck[2], S. Granville[2] and H.J. Trodahl[2]
[1] *University of New South Wales, Sydney, Australia*
[2] *Victoria University of Wellington, Wellington, NZ*

14.30 **Persistent photo-effects in nitride-based electronic devices**
Th A2.5 O.Katz[1], D. Mistele[1] G. Bahir[1] J. Salzman[1] and S. Prawer[2]
[1] *Technion, Israel Institute of Technology, Haifa, Israel.*
[2] *University of Melbourne, Parkville, Australia.*

14.45 **Silicon vacancy annealing and the D_I luminescence in 6H-SiC**
Th A2.6 M. V. B. Pinheiro[1,2], E. Rauls[1], U. Gerstman[1], S. Greulich-Weber[1] and J. M. Spaeth[1]
[1] *Universität Paderborn, Paderborn, Germany*
[2] *Universidade Federal de Minas Gerais, Belo Horizonte, Brasil*

Ultrafast Spectroscopy of Carrier Dynamics in III-N Epilayers and Heterostructures

A. N. Cartwright*
Department of Electrical Engineering and Institute for Lasers, Photonics and Biophotonics, University at Buffalo, State University of New York, Buffalo, NY, 14260 USA

III-N materials remain as an active field of materials research because of their continued potential for developing UV and visible LED and laser sources. There have been a number of technological breakthroughs resulting in successful commercialization of light emitters from these materials [1]. However, deep UV laser sources and additional tunability in the visible wavelengths remain as major challenges for nitride materials. Moreover, the recent unexpected discovery [2] of a narrow band gap energy of InN (~0.7 eV) opens a whole new opportunity for the application of InGaN ternary alloy, such as multijunction solar cells and infrared emitters. The fundamental physics underlying the material properties and operation of these devices must be understood to further optimize device performance, find new applications, and solve remaining problems.

In this talk, temperature and intensity dependent femtosecond optical studies (pump/probe spectroscopy and time-resolved photoluminescence) as well as CW spectroscopy of InGaN/GaN heterostructures, AlN/GaN heterostructures, InN epilayers and highly doped AlGaN epilayers will be presented. The optical mechanisms that complicate the complete understanding of these materials will be discussed. Specifically, piezoelectricity, spontaneous polarization, and localization effects and their relative contributions will be presented. Femtosecond time-resolved and CW spectroscopy will be demonstrated as an effective method for studying recombination mechanisms in these structures. Specifically, we will present measurements of (i) perpendicular transport using ultrafast differential transmission (Figure 1) and localization using time-resolved photoluminescence in InGaN/GaN heterostructures [3,4], (ii) infrared studies of hot carrier relaxation in InN epilayers using two-color femtosecond pump/probe spectroscopy (Figure 2) [5] The relevance of these measurements to device design will be addressed.

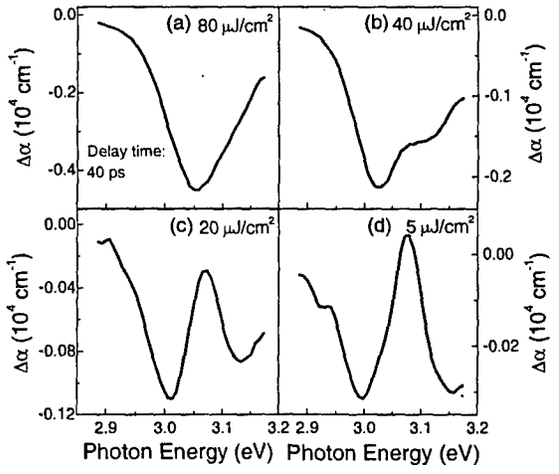

Figure 1. Differential absorption spectra for an InGaN/GaN MQW structure at a time delay of 40 ps as a function of pump fluence demonstrates the transition from excitonic bleaching (a) to screening (d).

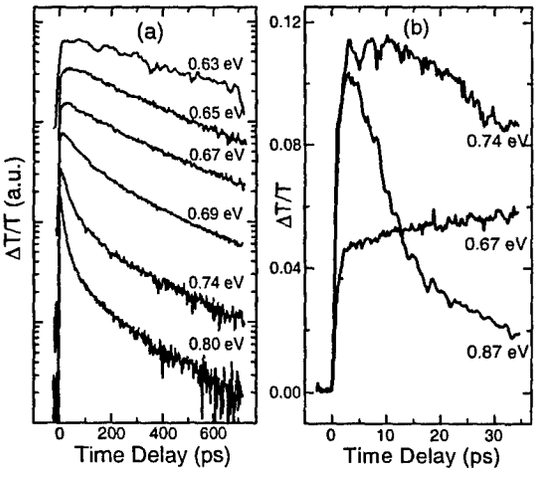

Figure 2. (a) Strength of the differential transmission signal vs. time delay for different photon energies on an InN epilayer. (b) Differential transmission signals at short times as a function of time delay.

References

1. S. Nakamura and G. Fasol, *The Blue Laser Diode* (Springer, Berlin, 1997).
2. J. Wu *et al.*, Appl. Phys. Lett. 80, 3967 (2002).
3. Fei Chen and A. N. Cartwright, Phys. Rev. B 68, 233304 (2003).
4. Fei Chen, M. C. Cheung, P. M. Sweeney, W. D. Kirkey, M. Furis, and A. N. Cartwright, J. Appl. Phys. 93, 4933 (2003).
5. Fei Chen, A. N. Cartwright, Hai Lu, and W. J. Schaff, Appl. Phys. Lett. 83, 4984 (2003).

* Electronic mail: anc@buffalo.edu

Optical and Electrical Properties of GaN Nanowires synthesized with N_2-quenched Pulsed Laser Ablation

D. K. T. Ng[1], L. S. Tan[1,*] and M. H. Hong[1,2]
[1] *Department of Electrical & Computer Engineering, National University of Singapore, SINGAPORE*
[2] *Data Storage Institute, DSI Building, SINGAPORE*

GaN nanowires were successfully grown on gold-coated sapphire substrates by pulsed laser ablation of a composite target of GaN powder in low-pressure nitrogen gas. The laser ablation induced Ga and N vapor directly towards the substrate to initialize Vapor-Liquid-Solid (VLS) mechanism [1]. Physical properties of the GaN nanowires were studied using Scanning Electron Microscopy (SEM), X-Ray Diffraction (XRD) and X-Ray Photoelectron Spectroscopy (XPS). The nanowires formed (Figure 1) were from 300 nm to 500 nm in length with diameters from as small as 16 nm to around 50 nm. XRD spectrum showed that the nanowires were of hexagonal wurtzite structure of GaN and that each peak showed single crystalline structural nature at its respective Miller indices. XPS studies were further carried out and it was discovered that the binding energy of the nanowires was at around 1117 eV which confirmed the formation of GaN nanowires. Specifically, we did a detailed study of the optical and electrical properties of the GaN nanowires using Photoluminescence (PL) and I-V curve analyzer respectively. For the PL spectra, a blue-shift was observed for the GaN nanowires compared to the bulk GaN powder. The presence of a Schottky barrier was observed when the I-V curve was plotted. The trend of the I-V curve is characteristic of the presence of a Schottky barrier between 2 metallic electrodes and semiconducting wires [2]. Furthermore, Fowler-Nordheim (F-N) plot was also obtained to further examine the field emission behavior. The enhancement factor and the turn-on field were calculated as these were believed to be the key for the high emission current of the GaN nanowires due to its high aspect ratio.

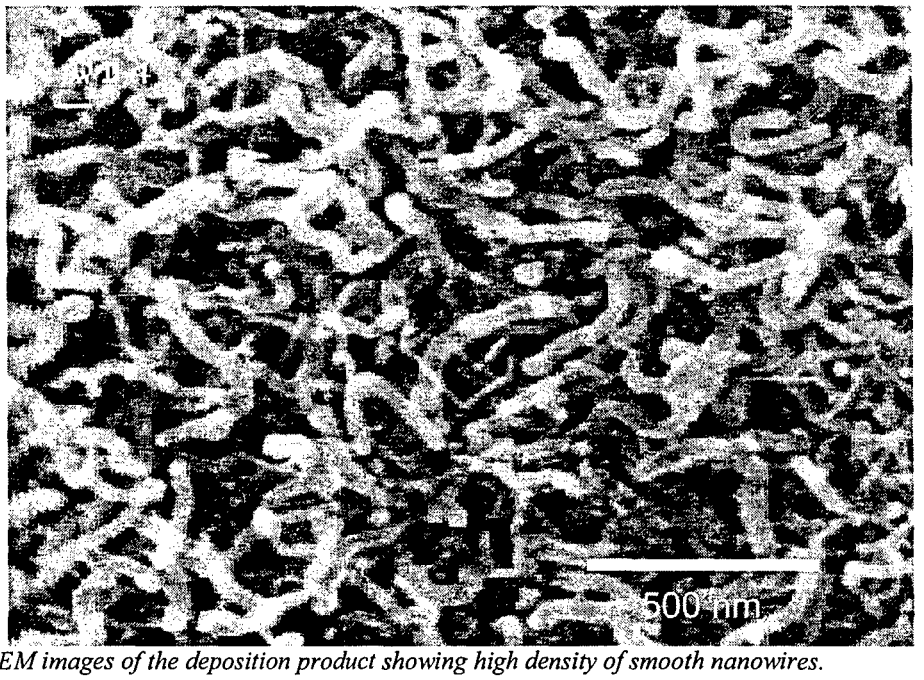

Figure 1: SEM images of the deposition product showing high density of smooth nanowires.

References

[1] X. Duan and C. M. Lieber, J. Am. Chem. Soc. **122,** 188 (2000)
[2] J. R. Kim, B.-K. Kim, I. J. Lee, J.-J. Kim, J. Kim, S.C. Lyu, and C. J. Lee, Physical Review B **69,** 233303 (2004)

* Contact author: eletanls@nus.edu.sg

Optoelectronics of highly disordered Gallium Nitride

A. Koo[1,*] F. Budde[1], B.J. Ruck[1], H. J. Trodahl[1] and A. Bittar[2]
[1] *School of Chemical and Physical Sciences, Victoria University of Wellington, Wellington, NEW ZEALAND*
[2] *Industrial Research Ltd., Lower Hutt, NEW ZEALAND*

Crystalline GaN has in recent years become widely used in optoelectronic devices operating in the blue-UV part of the spectrum despite a large density of defects. This study examines the potential of highly defective GaN in the form of nanocrystalline GaN (nx-GaN) and amorphous GaON grown by ion assisted deposition (IAD) [1] to contribute to this field of applications, specifically as a visible-blind UV detector.

We have investigated the effect of the disorder, both structural and via the introduction of oxygen, on the optoelectronic properties by the temperature dependence of the dark conductivity as well as a range of photoconductive experiments. We find that the disordered GaN films are highly resistive: $>10^9$ Ωcm at room temperature for all films and have large thermal activation energies of between 0.8 and 1.1 eV. Optically, while IAD grown nx-GaN has an optical absorption edge at 3.4 eV (the band gap of crystalline GaN), the incorporation of oxygen moves the absorption edge to higher energies. This trend is followed by the photoconductive response. The more amorphous material also exhibits a much higher photoconductive response: 10^{-1} A/W at a 9 V bias rather than 10^{-8} in nx-GaN. We have also observed that in the amorphous GaON, persistent photoconductivity after the light is turned off can last for up to days and this is attributed to the effects of long-lived deep traps that are populated during illumination.

We have also found that heating of the amorphous films subsequent to cessation of illumination shows evidence of emptying of these traps: the conductivity increases as electrons are thermally liberated into the conduction band and are able to recombine. The positions and intensities of the maxima in the conductivity during heating depend critically on the history of the material so yield information regarding the position and nature of trap states in the films. An example of a set of curves obtained by illuminating an amorphous film to load the traps to differing degrees and subsequently heating the film is shown in figure 1.

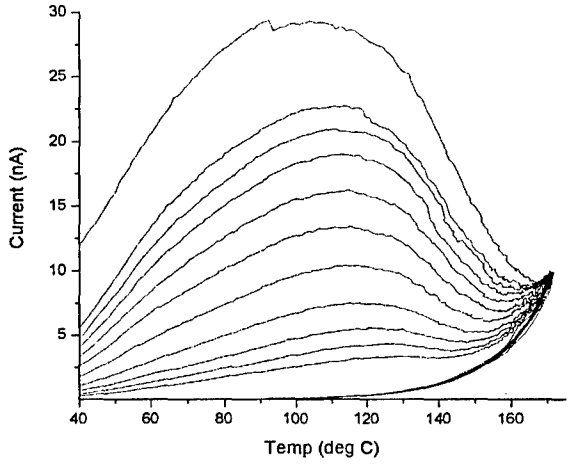

Figure 1: Thermal depletion of traps by heating after different loading of deep traps at room temperature

A significant fast component to the photoconductivity can also be isolated by chopping the incident light. The wavelength dependence of this fast component has been determined and the potential for commercial application of these materials as UV detectors will be discussed.

References

[1] F. Budde, B. J. Ruck, A. Koo, S. Granville, H. J. Trodahl, A. Bittar, G. V. M. Williams, M. J. Ariza, B. Bonnet, D. J. Jones, J. B. Metson, S. Rubanov and P. Munroe, arXiv:cond-mat/0407659 (2004).

* Contact author: a.koo@irl.cri.nz

TEM characterisation of GdN thin films

W. R. McKenzie[1,*], P. R. Munroe[1], F. Budde[2], B. J. Ruck[2], S. Granville[2], H.J. Trodahl[2]
[1]*School of Materials Science and Engineering, UNSW, Sydney, New South Wales, AUSTRALIA*
[2]*MacDiarmid Institute for Advanced Materials and Nanotechnology, School of Chemical and Physical Sciences, Victoria University of Wellington, Wellington, NEW ZEALAND*

Rare earth metal nitrides have been predicted to show a wide range of electronic structures, ranging from ferromagnetic to half-metallic to semiconducting [1]. However, these materials have been paid relatively little attention in the literature, in part due to difficulties that are encountered in their production. Most notably, the rare-earth nitrides react quickly upon exposure to air, although the details of this reaction have not been fully explored. In this study the structural properties and the effects of atmospheric exposure on thin films of one such nitride, GdN, are investigated. This work represents part of a larger study into the properties of GdN in light of the possibility that it may possess novel opto-electronic and magnetic properties.

GdN thin films were grown at room temperature onto silicon substrates by thermally evaporating the Gd metal under a pressure of around 10^{-4} mbar of ultra-pure nitrogen. The vacuum system used for the deposition was pumped to below 10^{-8} mbar prior to deposition. Attempts have been made to protect some of the films from oxidation by capping them with various layers such as aluminium, magnesium fluoride, or gold, while others have been left bare. Detailed structural characterization of these films was carried out using a variety of techniques such as X-ray Diffraction (XRD), Transmission Electron Microscopy (TEM), and Rutherford Backscattering Spectroscopy (RBS).

High resolution TEM analysis indicates the uncapped films are nanocrystalline, with crystallite sizes ranging from as small as 5 nm to close to the total film thickness of 100 nm. Electron diffraction studies found GdN was still abundant despite the films oxidation. RBS measurements also indicate that the films exposed to air still contain significant levels of nitrogen, as well as oxygen, implying that the films are not converted to a simple gadolinium oxide.

TEM image of the GdN thin film grown on a silicon substrate.

References

[1] C. M. Aerts, P. Strange, M. Horne, W. M. Temmerman, Z. Szotek, and A. Svane, Phys. Rev. B **69**, 045115 (2004).

* Warren@Materials.unsw.edu.au

Persistent photo-effects in Nitride-based electronic devices.

O. Katz[1], D. Mistele[1], G. Bahir[1], J. Salzman[1,*] and S. Prawer[2].
[1] *Department of Electrical Engineering and Microelectronics Research Center, Technion, Israel Institute of Technology, Haifa 32000, Israel.*
[2] *School of Physics, University of Melbourne, Parkville, Victoria 3010, Australia*

GaN based devices, such as photoconductors, Schottky diode photodetectors, and transistors, subject to UV illumination exhibit persistent photo-effects. The persistent effects can be described as a dielectric relaxation signal which deviates from the typical Maxwell-Debye exponential decay. For high speed devices such as Heterostructure Field Effect Transistors (HFET's), persistent effects are undesirable, may change the DC bias point stability, and cause an overall degradation in the device performance.

Several physical mechanisms were proposed in order to explain the PPC phenomenon [1]. The most common mathematical description for the time evolution of PPC uses the stretched-exponential, also called KWW decay function [2]. Although it is commonly accepted that PPC is related to defect states or traps, no accurate physical model has been proposed to interpret the KWW functional time behavior in crystalline semiconductors, and a better description of PPC is required.

Here, we report measurements of persistent photo-effects in GaN-based UV detectors and transistors. The GaN detectors and AlGaN/GaN based HFETs were implemented using layers grown by low-pressure metal organic vapor phase deposition (LP-MOVPE) [3, 4]. The Schottky barrier detectors consist of an Ohmic contact and a Semi-transparent Schottky contact on top of the unintentionally doped n$^-$GaN layer. The transistor fabrication consist of source and drain ohmic contacts evaporation followed by ion bombardment for isolation [3]. Finally, 2μm and 0.4μm Schottky gate contacts were evaporated. The device exhibits maximum drain current of 930 mA/mm and cutoff frequency of 4 GHz and 20 GHz for the 2μm and 0.4μm gates, respectively. Photoresponse decay was measured for the Schottky detector, the transistor drain and gate currents, finding that all currents exhibit non-exponential power law decay for several thousands of seconds.

We developed a model describing the temporal evolution of the drain and gate currents, and predict a time invariant power law current decay. The model describes the dynamics of the device surface charging after illumination, and its effect on the Schottky barrier recovery and channel charge. Excellent agreement, over several decades, is found between the measured temporal evolution of the currents and the prediction of our model. We extract the physical parameters of the material and the device, such as trap density and their carrier capture coefficient. We have also conducted a comparison of the present physical model for the temporal response with the phenomenological "stretched-exponential". We show that the two functions show similar temporal behavior on a limited time range. This might indicate that in many reported cases of PPC, the observed phenomena could be explained by our proposed barrier recovery model..

References

[1] X.Z. Dang, C.D. Wang, E.T. Yu, K.S. Boutors, and J.M. Redwing, Appl. Phys. Lett. 72, 2745 (1998).
[2] W. Williams, and D.G. Watts, Trans. Faraday Sor. 60, 80 (1970).
[3] O. Katz, A. Horn, G. Bahir, J. Salzman, IEEE Trans. Elec. Dev. 50, 2002 (2003).
[4] O. Katz, G. Bahir, and J. Salzman, Appl. Phys. Lett. 84 (20), p.4092 (2004)

* Contact author: salzman@ee.technion.ac.il

Silicon vacancy-annealing and the D_I-luminescence in 6H-SiC

M. V. B. Pinheiro,[1,2] E. Rauls,[3] U. Gerstmann,[3] S. Greulich-Weber,[1] and J.-M. Spaeth[1*]
[1] *Experimentalphysik, Universität Paderborn, D-33098, Germany*
[2] *Departemento de Física, ICEX, Universidade Federal de Minas Gerais, CP702, 30.123-970 Belo Horizonte, MG, Brasil*
[3] *Theoretische Physik, Universität Paderborn, D-33098 Paderborn, Germany*

Silicon carbide (SiC) is suitable for many high power, high frequency, and high temperature electronic applications due to its unique electronic and thermal properties. As most dopants diffuse prohibitively slow into SiC, ion implantation is the preferred doping method in device fabrication, but the implantation processs inevitably creates radiation-induced defects. Although sometimes helpful as recombination centres in high frequency devices, radiation-induced defects usually are unwanted by-products of the implantation process compensating the implanted dopants which leads to an inferior device quality. An understanding of the electronic properties of radiation-induced defects and of successive defects created by annealing is, therefore, crucial for an improvement of the material.

In a previous paper it was shown using electron paramagnetic resonance (EPR), magnetic dichroism of the optical absorption (MCDA) and MCDA-detected EPR (MCDA-EPR) that the isolated Si-vacancy (V_{Si}) , a basic radiation defect in SiC which anneals out at 750°C, transforms into a carbon vacancy-carbon antisite (V_CC_{Si}) pair at 750°C in a first annealing stage [1,2]. The experimental findings were interpreted with the help of total energy and spin density data obtained from standard local-spin density approximation of the density-functional theory, using relaxed defect geometries obtained from the self-consistent charge density-functional theory based tight binding scheme [2]. However, since the V_CC_{Si} pair defect is still electrically and optically active, at least a second annealing step is required to remove the electrical activity of silicon-vacancy related defects [2]. Another common characteristic in practically all irradiated 6H-SiC material is the so-called D_I photoluminescence (PL), which is well known to appear at 800°C and to survive high temperature annealing above 1700°C. For its explanation an excitonic pseudo-donor model was widely accepted [3], but it remained unclear from which atomistic configuration the excitonic transition occurs.

Combining EPR measurements with *ab-initio* calculations, we identify the $V_CC_{Si}+Si_CC_{Si}$ complex as a second annealing product of the silicon vacancy via an analysis of resolved carbon hyperfine interactions and of the zero-field splitting parameter of its excited triplet state. At high temperatures the carbon vacancy can dissociate from this complex leaving behind a diamagnetic $Si_C(C_{Si})_2$ complex, which is proposed to be an excellent candidate to cause the D_I PL-spectrum: the calculated local vibrational modes fit very well with the characteristic phonon-assisted structure of the PL-spectra. Furthermore our model provides a detailed explanation for the excitonic electron-hole recombination responsible for the D_I-luminescence.

References

[1] E. Rauls, T. Lingner, Z. Hajnal, S. Greulich-Weber, T. Fraunheim, and J.-M. Spaeth, phys.stat.sol (b) **217/2,** p.R1, (2000)
[2] Th. Lingner,.U. Gerstmann, E. Rauls, S. Greulich-Weber, J.-M. Spaeth, H. Overhof, and Th. Fraunheim, Phys. Rev.B **64,** 245323 (2001)
[3] E. Janzén, I. G. Ivanov, N. T. Son, B. Magnusson, Z. Zolnai, A. Henry, J. P. Bergman, L. Storasta, and F. Carlsson, Physica B **340-342**, 15 (2003)[1]

[1] *Contact author: martin@family-spaeth.de

SESSION Th B2
NANOSCALE OPTICS

Thursday 10 February 2005 1320–1500

Meeting Room V

Session Chair **Richard Blaikie, University of Canterbury, NZ**

13.20 **Plasmonic nanophotonics**
Th B2.1 V.M. Shalaev
(Invited Talk)
Purdue University, West Lafayette, USA

13.45 **Plasmon resonances of silver colloids aggregates studied by surface enhanced raman spectroscopy**
Th B2.2 E.C. Le Ru and PG. Etchegoin
Victoria University of Wellington, Wellington, NZ

14.00 **Towards nonlinear left-handed metamaterials**
Th B2.3 I.V. Shadrivov[1], N.A. Zharova[1,2], A.A. Zharov[1,2], and Yu.S. Kivshar[1]
[1] *Australian National University, Canberra, Australia*
[2] *Russian Academy of Sciences, Nizhny Novgorod, Russia*

14.15 **A comparison of near-field lithography and planar lens lithography through simulation and experiment.**
Th B2.4 D.O.S. Melville, M.M. Alkaisi and R.J. Blaikie
University of Canterbury, Christchurch, NZ

14.30 **Bending light with photonic crystals**
Th B2.5 S.J. McNab[1], N. Moll [2] and Yu. Vlasov[1]
[1] *IBM T.J. Watson Research Center, Yorktown Heights, USA*
[2] *IBM Zurich Research Laboratory, Rüschlikon, Zurich, Switzerland*

14.45 **Sculpturing thin films for DUV wavelengths**
Th B2.6 L. De Silva, I. Hodgkinson and Q.H. Wu
University of Otago, Dunedin, NZ

Plasmonic Nanophotonics

Vladimir M. Shalaev
School of Electrical and Computer Engineering, Purdue University
West Lafayette, IN 47907, USA; email: shalaev@purdue.edu

There is ample evidence that photonic devices can be reduced to the nanoscale using optical phenomena in the near field, but there is also an incompatibility between light wavelength at the *microscale* and devices and processes at the *nanoscale* which must first be addressed. Plasmonic nanostructures can act as nanoantennae and thus serve as optical couplers across the nano–micro interface. Recent advances in this rapidly developing area now enable us to mount a systematic approach toward the goal of full systems-level integration of photonics with nanotechnology using nanoscale plasmonics. Plasmonic nanophotonics also promises to create entirely new prospects for guiding light on the nanoscale, some of which may have revolutionary impact on present-day optical technologies. In this talk I outline some of our recent studies on manipulating light and sensing molecules with plasmonic nanostructures.

Plasmon resonances of silver colloids aggregates studied by Surface Enhanced Raman Spectroscopy

E. C. Le Ru* and P. G. Etchegoin
The MacDiarmid Institute for Advanced Materials and Nanotechnology
School of Chemical and Physical Sciences
Victoria University of Wellington
PO Box 600 Wellington, NEW ZEALAND

Surface Enhanced Raman Scattering (SERS) [1] has the potential to become an important analytical tool with many fields of applications. Although the effect has been discovered a few decades ago, it has been the subject of a renewed interest recently for several reasons. First, it has been shown that the sensitivity of SERS was strong enough to observe the signal from single molecules [2], with important applications, for example in biological tags detection. Also, the progresses in nanotechnology, such as electron microscopy and confocal Raman systems, make it easier to study and use this technique. Despite this, the mechanisms responsible for this effect are still not fully understood.

The large enhancements of the Raman signal observed under SERS conditions are believed to be mainly due to single or collective plasmon resonances producing large amplifications of the laser field in a localized region of the metal surface, thus boosting the intensity of the otherwise weak Raman scattering process. The plasmon resonances of SERS active substrates are usually characterized by measuring the optical extinction of the sample as a function of wavelength. This technique, applied to colloidal silver for example, shows a clear peak corresponding to the plasmon resonance of a single colloid, and a wider resonance at longer wavelength associated to coupled plasmon resonances. However, due in part to interference with scattering, it is very difficult to extract from these measurements in the far field a connection with the field enhancements of the local field.

We use here SERS as a probe of plasmon resonances, since the SERS signal is also an indirect measurement of the resonance profile. Two types of resonant effects occur, when the plasmon is resonant with either the laser wavelength or the Raman scattered photons. In a typical SERS experiment, a large Raman background is observed in addition to the Raman peaks from the analyte. We show evidence that both the intensity of these backgrounds and of the peaks at different Stokes and Antistokes shifts are connected the dispersion of the plasmon resonance. Similarly, using lasers at different wavelengths, we can probe different parts of the resonance spectrum. This underlying resonance explains simply why anomalous (higher or lower) Antistokes to Stokes ratio have been observed in SERS experiments. Moreover, by studying the fluctuations of the SERS signal as a function of time, we are able to characterize the distribution of plasmon resonances in a colloidal silver solution containing different types of aggregates and, therefore, different plasmon resonances. We believe this method not only helps to characterize the plasmon resonances, but it is also useful for the understanding of the mechanisms of SERS enhancements.

References

[1] M. Moskovits, Rev. Mod. Phys. **57**, 783 (1985).
[2] S. Nie and S. R. Emory, Science **275**, 1102 (1997).

* Contact author: Eric.LeRu@vuw.ac.nz

Towards nonlinear left-handed metamaterials

I. V. Shadrivov[1], N.A. Zharova[1,2], A. A. Zharov[1,3], and Yu. S. Kivshar[1]
[1]*Nonlinear Physics Centre, Research School of Physical Sciences and Engineering, Australian National University, Canberra ACT 0200, Australia*
[2] *Institute of Applied Physics, Russian Academy of Sciences, Nizhny Novgorod 603600, Russia*
[3] *Institute for Physics of Microstructures, Russian Academy of Sciences, Nizhny Novgorod 603950, Russia*

Left-handed materials, also known as metamaterials or materials with negative refraction, were first described theoretically by Veselago in 1960-s as materials with both negative dielectric permittivity and negative magnetic permeability. Such materials possess a number of peculiar properties such as negative refraction at the interface between a left-handed material and normal dielectrics, inverse Vavilov-Cherenkov and inverse Doppler effects. Recently fabricated metamaterials are composed of arrays of wires and a lattice of split-ring resonators. Metamaterials possess left-handed properties only in some finite frequency range, which is determined by the structure geometry. A possibility to control the effective parameters of the metamaterial using nonlinearity has recently been suggested in Refs. 1,2. Here we present the results of our study of nonlinear effects introduced either (i) by inserting nonlinear dielectric inside the metallic composite, or (ii) by including a diode in the split-ring resonators. In the former case, the effective magnetic permeability of the metamaterial becomes a nonlinear function of the external magnetic field, and it can be controlled effectively by the intensity of the electromagnetic wave (see Fig. 1). Importantly, one can switch between the left- and right-handed regimes (negative and positive [1]) changing the magnetic field intensity. In Fig. 1, we summarize nonlinear magnetic properties of the left-handed composite for different types of nonlinear infilling dielectric, and for different electromagnetic wave frequency ω with respect to the SRR eigenfrequency ω_0.

Including a diode into the split-ring-resonator circuit, one can introduce the $\chi^{(2)}$ nonlinearity achieving a quadratic nonlinear response of the metamaterial. Such properties are important in the case of the composite structures, since they have strong frequency dispersion. As an example, we consider a source of electromagnetic waves with the frequency ω, at which the material is opaque. Electromagnetic waves emitted by the source are reflected from a slab of such a composite material (see Fig. 2), and only an exponential tail of the field penetrates into the slab. Due to the nonlinear properties of the material, the second harmonic of the field is generated. At a proper choice of the material parameters at the frequency 2 ω, both permittivity and permeability of the material become negative, and the second-harmonic field can propagate through the slab.

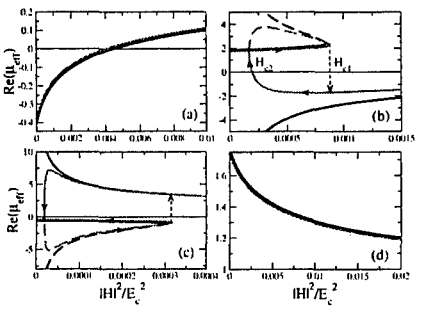

Fig. 1
Real part of the effective magnetic permeability vs intensity of the magnetic field: (a) $\omega > \omega_0$, self-focussing dielectric; (b) $\omega < \omega_0$, self-focussing dielectric, (c) $\omega > \omega_0$, self-defocusing dielectric; and (d) $\omega < \omega_0$, self-defocusing dielectric. Black — the lossless case, grey — the lossy case. Dashed curves show unstable branches.

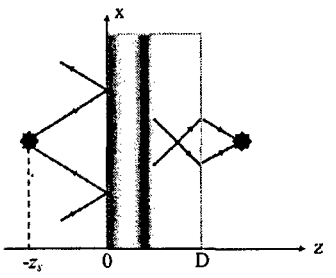

Fig. 2
Schematic of the imaging with a nonlinear lens. The electromagnetic waves from the source reflected from the slab. However, the second harmonic field generated in the nonlinear left-handed slab, propagates through the slab and forms the image of the source.

References

[1] A.A. Zharov, I.V. Shadrivov, and Yu.S. Kivshar, Phys. Rev. Lett. **91**, 037401 (2003).
[2] M. Lapine, M. Gorkunov, and K. H. Ringhofer, Phys. Rev. E **67**, 065601 (2003).

A Comparison of Near-Field Lithography and Planar Lens Lithography through Simulation and Experiment.

D. O. S. Melville*, M. M. Alkaisi, and R. J. Blaikie
MacDiarmid Institute for Advanced Materials and Nanotechnology,
Department of Electrical and Computer Engineering, University of Canterbury,
Christchurch, NEW ZEALAND

Near-field optical lithography using a planar silver lens has been proposed and in a recent publication the planar silver lens's ability to image the near-field of a UV light source was demonstrated.[1] This type of lithography has been called Planar Lens Lithography (PLL). The quality of this imaging when compared to hard-contact lithography is the focus of this presentation.

Silver's plasmonic resonance in the UV produces a wavelength at which the relative permittivity equals –1 plus a loss term. In a controversial paper by Pendry[2], it was predicted that this property could produce sub-diffraction-limited images through a planar slab of silver (a super-lens). Currently, sub-wavelength images have been achieved by PLL, with dense 175 nm features produced. This will be compared with the current sub-diffraction-limited hard-contact lithography resolution that has achieved 85 nm dense lines. All results were achieved using a broadband mercury lamp with optimised exposure and develop times. The reasons for the differences in the maximum resolution achievable with each technique will be discussed by analysing experimental and simulation results.

Figure 1 shows an Atomic Force Microscope (AFM) scan of 200-nm period features in photoresist that has been exposed by hard-contact lithography and then developed. Figure 2 shows an AFM scan of 500-nm period features in photoresist that has been exposed with PLL. Although simulation predicts it, PLL has yet to achieve the resolution shown in Fig. 1 experimentally.

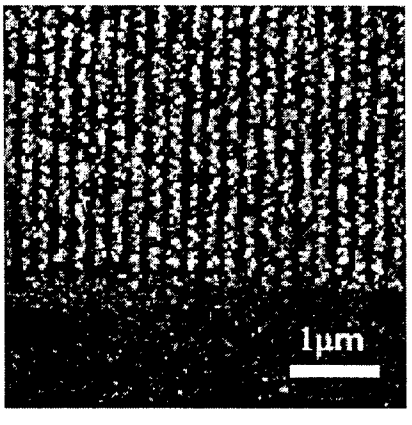

Figure 1: Atomic force microscope scan image of 85 nm features at a 200 nm period in photoresist, which were produced with near-field lithography techniques.

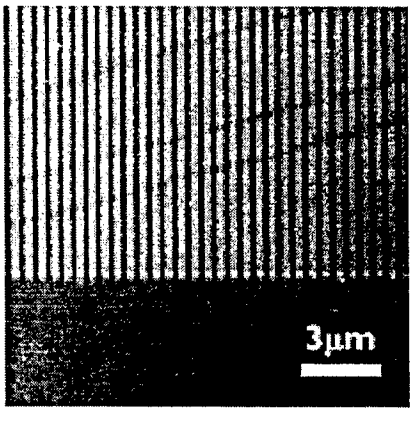

Figure 2: Atomic force microscope scan image of 200 nm features at a 500 nm period in photoresist, which were produced with planar lens lithography.

References

[1] D. O. S. Melville, R. J. Blaikie, and C. R. Wolf, *Appl. Phys. Lett.* **84**, 4403 (2004).
[2] J. B. Pendry, *Phys. Rev. Lett.* **85**, 3966 (2000).

* Contact author: dom15@student.canterbury.ac.nz

Bending light with photonic crystals

S. J. McNab[1,*], N. Moll [2] and Yu. Vlasov [1]
[1] *IBM T. J. Watson Research Center, Yorktown Heights, NY 10598, USA*
[2] *IBM Zurich Research Laboratory, Rüschlikon, Zurich, SWITZERLAND*

One of the often touted properties of photonic crystals is the possibility to guide and control light at a scale comparable to the wavelength. The ability to transmit light around sharp bends with a bending radius of only one period of the lattice has made photonic crystals a subject of intense interest owing to the impact they could have in enabling dense integration of optical devices[1].

We have investigated the bending properties of single row missing waveguides in a 2D slab type photonic crystal in silicon on insulator (SOI). Bending losses of 0.21dB/turn +/- 0.03 are reported with small uncertainty owing to measurements of devices with large numbers of bends. While this bending loss figure suggests losses are approaching an acceptable level, significant band narrowing was observed notably at frequencies near the band edge that coincides with the "slow light" regime. This introduces unwanted losses at that region of the spectra where photonic crystals exhibit their most interesting properties. An approach to improve the bandwidth by modification of the holes in the vicinity of the bend will be described and a performance comparison made to conventional total internal reflection waveguides also made in SOI [2].

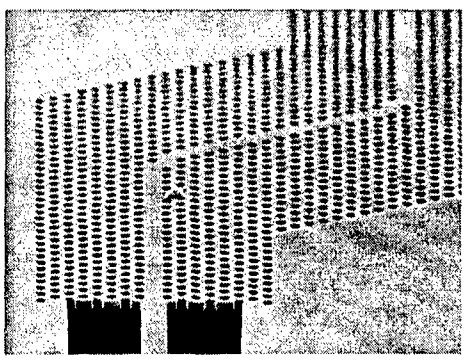

Fig 1. SEM image of W1 waveguide showing two 60° bends. The waveguide is coupled to a strip waveguide.

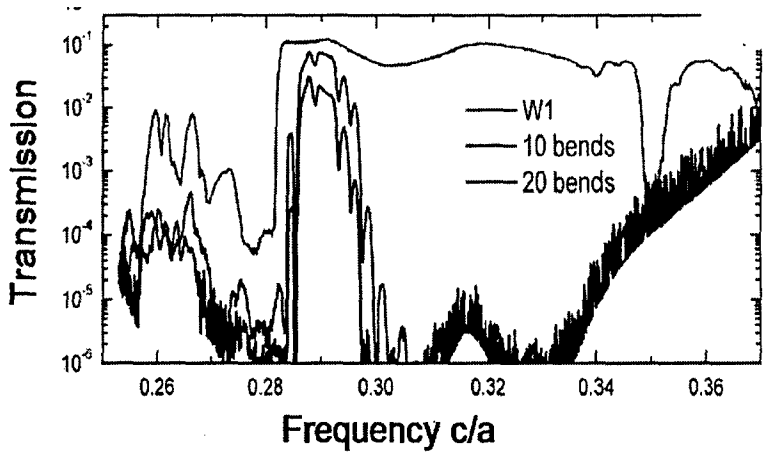

Fig 2. Transmission through zero, ten and twenty 60° degree bends. Band narrowing is observed at band edge ~ 0.285 c/a.

References

[1] S. J. McNab, N. Moll and Yu. A. Vlasov, "Ultra-low loss photonic integrated circuit with membrane-type photonic crystal waveguides", Optics Express, **11**, 2927 (2003).
[2] Yu. A. Vlasov, and S. J. McNab "Losses in single-mode silicon-on-insulator strip waveguides and bends", Optics Express, **12**, 1622 (2004).

* Contact author: shareem@us.ibm.com

Sculpturing Thin Films for DUV Wavelengths

Lakshman De Silva, Ian Hodgkinson[1] and Qi hong Wu
Department of Physics, University of Otago, PO Box 56, Dunedin, New Zealand

The unrelenting quest for smaller and smaller electronic components-on-a-chip has ushered photolithography into an awkward area. Optics is difficult at deep ultraviolet (DUV) and vacuum ultraviolet (VUV) wavelengths due to the inferiour properties of available substrate and thin film materials. The close proximity of absorption bands causes intolerable losses in many materials that are transparent and behave in a satisfactory manner at visible wavelengths. As well scatter from surfaces and from thin film microstructure tends to increase as the wavelength of incident light is reduced.

Recent reports indicate that DUV losses in isotropic thin films can be minimized through choice of deposition method, deposition parameters, and by post-deposition treatment. Thus Yoshida *et al* have used ion beam sputtering to fabricated fluoride coatings for DUV/VUV optics [1], Liu *et al* have shown that losses in MgF_2 and GdF_3 evaporated from a resistively heated boat can be minimized by choosing a substrate temperature of about 300°C, and Taki *et al* have improved the optical performance of fluoride films by post-deposition replenishment of fluorine [3].

In this study we focus on the feasibility of fabricating sculptured thin films (STFs) for the DUV. In an STF the basic columnar structure that develops due to oblique deposition is *modified*, for example from the tilted-columnar biaxial form to the normal-columnar biaxial form, or *modulated* to introduce a second spatial scale, usually via changes to the angle of incidence of the vapour on the substrate as deposition proceeds. Apart from the issue of transparency, the diameter of the microstructural columns is of concern at small wavelengths.

Our experiments on LaF_3, NdF_3, and SmF_3 show that the *structural modification* process of serial bideposition (SBD) [4] can be translated for use at DUV wavelengths. In general we have found that it is possible to grow normal-columnar biaxial films with substantial in-plane birefringence, $\Delta n = n_3 - n_2 \approx 0.1$ for light that is incident normally. In our notation the subscript-2 refers to the direction that is parallel to both the surface of the substrate and the deposition plane and is the fast axis when the film is viewed as a wave plate. Similarly the subscript-3 refers to the direction normal to the deposition plane and is the slow axis. Our results show that both the real and imaginary parts of the principal refractive indices are anisotropic, but with opposite sign. Typically k_2 was found to exceed k_3 by about 20%. A preliminary result indicates higher transmittance for deposition at elevated substrate temperature, a few percent for 700-nm LaF_3 films deposited at 300°C rather than at 250°C.

In summary our results show that the transparency of SBD (structurally modified) anisotropic films can be improved by depositing at elevated temperatures. Currently we are proceeding with experiments that combine structural modification and structural modulation of films for use in the DUV, in an attempt to fabricate chiral materials and circular Bragg resonators such as those that we have reported for wavelengths as low as 400 nm [4]. Our work is supported financially by the New Zealand New Economy Research Fund contract UOCX0212, and by the MacDiarmid Institute for Advanced Materials and Nanotechnology.

References

[1] T. Yoshida, K. Nishimoto, K. Sekine and K. Etoh, in Optical Interference Coatings on CD ROM (The Optical Society of America, Washington, DC, 2004), WF5.

[2] M-C. Liu, C-C. Lee, M. Kaneko, K. Nakahira and Y. Takano, in Optical Interference Coatings on CD ROM (The Optical Society of America, Washington, DC, 2004), WF3.

[3] Y. Taki, S. Watanabe and A. Tanaka, in Optical Interference Coatings on CD ROM (The Optical Society of America, Washington, DC, 2004), WF7.

[4] I.J. Hodgkinson and Q.H. Wu, Inorganic Chiral Optical Materials, Advanced Materials **13**, 889-897 (2001).

[1]Contact author: ijh@physics.otago.ac.nz

SESSION Th C2
NANOTUBES

Thursday 10 February 2005 1320–1500

Copthorne I

Session Chair **Yung Woo Park, Seoul National University, South Korea**

13.20 **Phase behaviour of carbon nanotube dispersions: percolation and nematic states**

Th C2.1 S. Badaire[1], C. Zakri[1], B. Vigolo[1], C. Coulon[1], M. Maugey[1], P. Poulin[1], N. Barisci[2] and G. Wallace[2]
(Extended Oral Talk)
[1] *Centre de Recherche Paul Pascal – CNRS, Pessac, France.*
[2] *University of Wollongong, Wollongong, Australia.*

13.45 **Peculiarities in the synthesis of carbon nanotubes from Müller clusters**

Th C2.2 K. Edgar and J.L. Spencer
Victoria University of Wellington, Wellington, NZ

14.00 **Field emission from carbon nanotubes produced on a substrate treated by arc-discharge**

Th C2.3 R. Shastry and J. Abrahamson
University of Canterbury, Christchurch, NZ

14.15 **Manipulation and purification of multiwalled carbon nanotubes by dielectrophoresis within a large array**

Th C2.4 X. Liu[1], J.L. Spencer[1], A. B. Kaiser[1] and W. M. Arnold[2]
[1] *Victoria University of Wellington, Wellington, NZ*
[2] *Industrial Research Ltd, Lower Hutt, NZ*

14.30 **CNTs for field emission applications: use of nanoimprint lithography and PE CVD techniques**

Th C2.5 S.M.C. Vieira[1], K.B.K Teo[1], E. Minoux[2], L. Gangloff[2], P. Legagneux[2], P. Andrew[3], G.A.J. Amaratunga[1] and W.I. Milne[1]
[1] *University of Cambridge, Cambridge, UK*
[2] *Thales Laboratoire Central de Recherches, Orsay Cedex, France*
[3] *Nanoscience Centre, Cambridge, UK*

14.45 **Synthesis of nano-magnets and nano-tubes using high magnetic fields**

Th C2.6 H. Garmestani, H. Dahmen, M. Fathi
Georgia Institute of Technology, Atlanta, USA

Phase behavior of carbon nanotube dispersions: percolation and nematic states

S. Badaire[1], C. Zakri[1], B. Vigolo[1], C. Coulon[1], M. Maugey[1], P. Poulin[1]
N. Barisci[2], G. Wallace[2]
[1] *Centre de Recherche Paul Pascal – CNRS, Avenue Schweitzer, 33600 Pessac, France*
[2] *ARC Centre for Nanostructured Electromaterials*
Intelligent Polymer Research Institute, University of Wollongong,
Northfields Avenue, Wollongong, NSW 2522, Australia

We present recent results on the phase behavior of carbon nanotube dispersions. We show how interactions between carbon nanotubes can be controlled by using molecular or polymeric dispersants. Tuning the nature and the strength of the interactions between nanotubes can dramatically affect the structure formed by the systems and their further processing. Attractive interactions, induced by entropic depletion of surfactant micelles, allow the percolation threshold of carbon nanotube dispersions to be significantly lowered, when compared with non-interacting nanotubes. This result can be of major interest in applications targeting electrically conducting networks out of dilute nanofibres. Oppositely, repulsive interactions, induced for example by adsorbing and amphiphilic polymers such as denaturated DNA, allow nanotube dispersions to be highly concentrated without any clustering. Homogeneous suspensions, up to 8%w/w in water, could be achieved. More importantly, at high concentration, nanotube dispersions are not any longer isotropic but instead form nematic phases with long range rotational order. These systems are potential useful as basis for multifunctional materials comprised of oriented nanotubes, such as fibers. Some examples will be shown. We discuss the phase diagrams, the onset of percolation and the isotropic-nematic transitions in view of the dimensions of the carbon nanotubes, as experimentally measured for the first time by depolarised dynamic light scattering, a technique that allows a significantly higher statistics than any imaging microscopy technique (electron, AFM, STM).

Peculiarities in the Synthesis of Carbon Nanotubes from Müller Clusters

K. Edgar[1,*] and J. L. Spencer[1]
[1] *MacDiarmid Institute for Advanced Materials and Nanotechnology, Victoria University of Wellington Wellington, NEW ZEALAND*

The synthesis of single walled carbon nanotubes from Müller clusters was first reported in 2002 by Liu *et al*, using a cluster that can be simplified to $[Mo_{84}Fe_{30}]$ [1]. It was argued in this paper that the size of the bare metallic cluster was closely related to the diameter of the resultant single walled nanotubes. In order to test this hypothesis work has been undertaken using seven different clusters on a variety of support materials, both mesoporous and monolithic, for the chemical vapour deposition of carbon. The results have shown that pure molybdenum clusters are poorer catalysts than iron-molybdenum bimetallic clusters but that the activity and reaction products of both types of cluster depend dramatically on the support material used. Peculiarities in the experimental observations of the reaction products of the various catalysts (as illustrated in Figures 1 and 2) will be discussed with relation to the nature of the support, the support-cluster interactions, and the stoichiometry and size of the cluster itself.

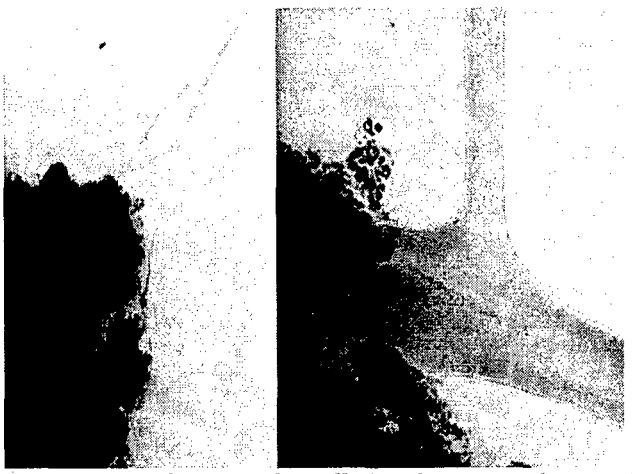

Fig. 1. $[Mo_{84}Fe_{30}]$ produces single-walled carbon nanotubes on alumina.

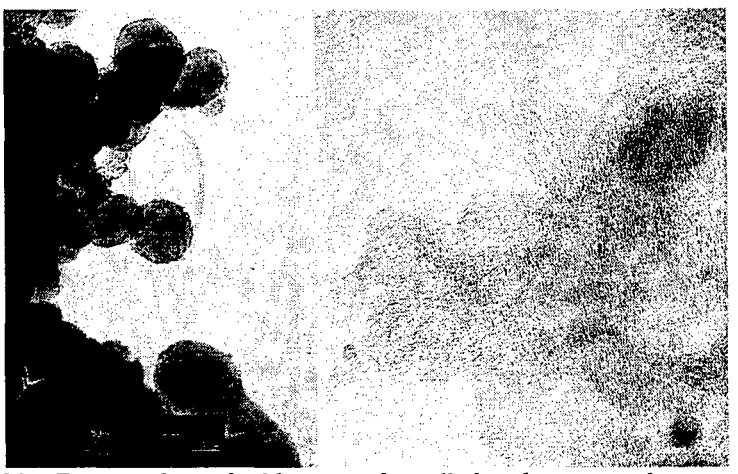

Fig. 2. $[Mo_{84}Fe_{30}]$ produces double- or triple-walled carbon nanotubes on magnesia

References

[1] L. An *et al.*, J. Am. Chem. Soc. **124**, 13688 (2002)

* Contact author: kirstenedgar@fastmail.fm

Field emission from carbon nanotubes produced on a substrate treated by arc-discharge.

Rahul Shastry and John. Abrahamson*.
Department of Chemical and Process engineering, University of Canterbury, New Zealand

One of the main challenges of modern vacuum microelectronics is the fabrication of highly efficient, low-voltage electron emitters. Cold cathode emission offers an invaluable alternative to thermionic emission for many applications as the former mechanism can be controlled by the applied external field. The key factors in advancing vacuum microelectronics relate to fabrication of field emitter arrays [1]. The recognition that field emission occurs most easily from fine surface structures has led to the use of field emission cathodes based on films and coating of various forms of carbon such as nanoclusters, diamond like films, nanofibres and nanotubes.

Carbon nanotubes are at the forefront of these materials because of their unique physical properties such as their aspect ratio and low work function with exceptional mechanical and chemical stability. They also exhibit high current densities at low applied electric field with very low turn-on voltages. These properties with their relative ease of production through various methods make them the most desirable materials for cold field emission cathodes.

A general overview of field emission from nanotubes are discussed. The field emission characteristics of different types of nanotubes produced from different methods are compared. The effect of their arrangement and their geometry on field emission characteristics arre considered. A brief overview of the mechanisms governing field emission from nanotubes are discussed.

A novel method of continuously producing nanotubes on a substrate employing arc discharge is described. The field emission characteristics of nanotubes obtained from this method is compared with reported results from other methods. The development of a luminescent tube and a gas sensor using these nanotubes is discussed.

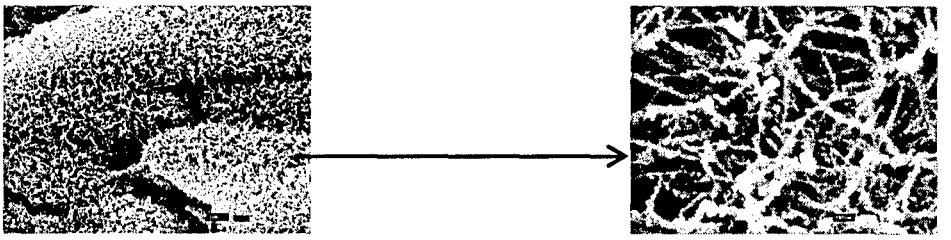

Nanotubes on a substrate, Scale 2μm

Higher magnification, Scale 300nm

References:

[1] Takao Utsumi , in *IEEE Transactions on Electron Devices,* Vol.38, 10(1991).

* Contact author: john.abrahamson@canterbury.ac.nz

Manipulation and Purification of Multiwalled Carbon Nanotubes by Dielectrophoresis within a Large Array

Xianming Liu[1], John L. Spencer[1], Alan B. Kaiser[1] and W. Mike Arnold[2*]
[1]*MacDiarmid Institute for Advanced Materials and Nanotechnology, School of Chemical and Physical Sciences (SCPS), Victoria University of Wellington, P O Box 600, New Zealand*
[2] *Industrial Research Limited, PO Box 31-310, Lower Hutt, New Zealand*

We have demonstrated previously that carbon nanotubes (CNTs) can be collected from suspensions by high-frequency dielectrophoresis (DEP) [1, 2]. This is thought to occur because CNTs are much more conductive and therefore polarizable than the suspending medium or the remainder of the as-grown samples. We now present a scaled-up DEP electrode array, which facilitates the application of dielectrophoretic force to larger volumes of a recirculating CNT-suspension. Comparison of data from SEM and Raman microprobe between untreated and after-treatment samples shows that purification can be achieved by this prototype device.

The alignment of CNTs has long been pursued as a desirable step in the formation of CNTs/polymer composites [3] because it lowers the electrical percolation threshold of the composites. That is, it can reduce the loading of CNTs required to achieve conductivity or more complex electronic functionality in composites for the automotive and aerospace industries. A method which yields aligned multiwalled carbon nanotubes within a poly vinyl alcohol matrix is being developed.

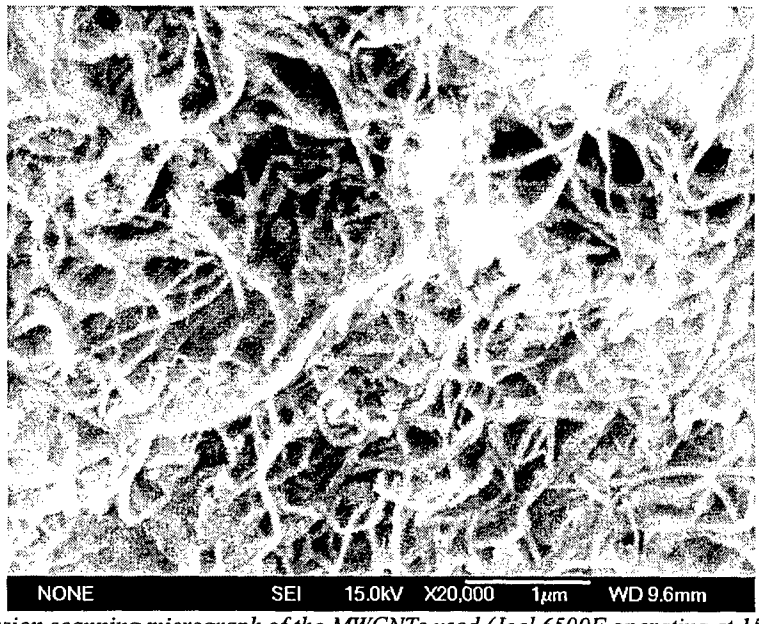

Field emission scanning micrograph of the MWCNTs used (Joel 6500F operating at 15.0kV).

References

[1] Xianming Liu, John L. Spencer, Alan B. Kaiser and W. Mike Arnold, *Electric-Field-Induced Accumulation and Alignment of Carbon Nanotubes.* Annual Report Conference on Electrical Insulation and Dielectric Phenomena, IEEE, 2002: p. 31-34.

[2] Xianming Liu, John L. Spencer, Alan B. Kaiser and W. Mike Arnold, *Electric-field oriented carbon nanotubes in different dielectric solvents,* Current Applied Physics, 2004. 4(2): p. 125-128.

[3] J. K.W. Sandler, J. E. Kirk, I. A. Kinloch, M.S. P. Shaffer, A. H. Windle, *Ultra-low electrical percolation threshold in carbon-nanotube-epoxy composites.* Polymer, 2003. 44: p. 5893-5899.

* Contact author: m.arnold@irl.cri.nz

CNTs for Field Emission Applications: use of Nanoimprint Lithography and PE CVD Techniques

S.M.C. Vieira[1,*], K.B.K Teo[1], E. Minoux[2], L. Gangloff[2], P. Legagneux[2], P. Andrew[3], G.A.J. Amaratunga[1] and W.I. Milne[1]

[1]*Department of Engineering, University of Cambridge, Trumpington Street, Cambridge CB2 1PZ, UK*
[2]*Thales Laboratoire Central de Recherches, Domaine de Corbeville. 91404, Orsay Cedex, France*
[3]*Nanoscience Centre, Nanoscience Building, Cambridge CB3 0FF, UK*

There is considerable interest in the use of carbon nanotubes as field emission electron sources because of their whisker-like shape, high aspect ratio, high conductivity, thermal stability and resistance to electromigration. In particular, the fabrication of individual vertically aligned CNTs by dc-plasma enhanced CVD is a good candidate for field emission applications because it is possible to synthesize straight, vertically aligned nanotubes which are extremely uniform (4% deviation in diameter, 6% deviation in height) and localised.

We have previously used electron-beam lithography to obtain selective growth of CNTs by patterning Si substrates with 100 nm diameter Ni catalysts. The resulting CNTs obtained had lengths of up to 5 μm and 50 nm tip diameter. These arrays exhibit high emission current densities (1A/cm^2 in dc mode). However, electron beam lithography is a slow serial process and hence inherently not suitable for scaling.

In this work, we investigate nanoimprint lithography as a potential route to produce wafer scale arrays of CNTs simultaneously. Nanoimprint lithography for our application is advantageous over other self-assembled lithographies (eg. nanosphere lithography) because it can produce a suitable mark/space ratio (1/100) to obtain high aspect ratio CNTs which are spaced appropriately apart to avoid electrostatic field shielding. The nanoimprint process uses a silicon mould which is fabricated by deep reactive ion etching and then perfluorinated. This mould is pressed against a silicon substrate coated with PMMA to transfer the pattern. The PMMA is then ashed and the pattern used as a lift off mask for the Ni catalyst. The nanotube growth is then performed using plasma enhanced chemical vapour deposition of NH_3:C_2H_2 (200 : 54 sccm). We investigate the uniformity of the structures by scanning electron microscopy and also their field emission properties.

*Contact author: Dr Sara Vieira
Department of Engineering
University of Cambridge
Trumpington Street
Cambridge CB2 1PZ
United Kingdom
Phone number: +44 1223 7 65587
Fax number: +44 1223 3 32662
Email Address: smc81@cam.ac.uk.

Synthesis of Nano-Magnets and Nano-Tubes Using High Magnetic Fields

H. Garmestani, H. Dahmen, M. Fathi
Georgia Institute of Technology
Materials Science and Engineering
771 Ferst Drive, N.W.
Atlanta, GA 30332-0245

Processing of materials under the influence high magnetic fields has been reported to cause significant changes in the microstructure and enhancements in useful properties of many materials. The mechanisms of influence of magnetic field on texture development, grain growth, and recrystallization need to be understood in order to optimize the processes and to develop commercial applications of in-field heat treatment processes. We have processed materials at field up to 32 Tesla and temperatures up to 1600 C. This paper describes the effect of high field and temperatures in producing a new range of nano-tubes and nano-magnets using high magnetic fields. We will also describe a new methodology for in-field processing of nano-tube composite materials.

SESSION Th D2
MATERIALS CHARACTERISATION TECHNIQUES

Thursday 10 February 2005 1320–1500

Copthorne II

Session Chair **Mark Waterland, Massey University, NZ**

13.20 **Anisotropy in the optical response of metal surfaces and interfaces**
Th D2.1 O. Hunderi
(Extended Oral Talk)
Norwegian University of Science and Technology, Trondheim, Norway

13.45 **Stretching single polysaccharide molecules using AFM**
Th D2.2 M.A.K. Williams[1,2], R. Haverkamp[2] and J.E. Scott[3]
[1] *Massey University, Palmerston North, NZ*
[2] *MacDiarmid Institute for Advanced Materials and Nanotechnology, NZ*
[3] *Manchester University Medical School, Manchester, UK*

14.00 **TEM investigation of hydrogen-implanted and annealed single-crystal $SrTiO_3$**
Th D2.3 G.K.H. Pang[1], Y. Wang[1], W.L. Liu[2], Z.T. Song[2], S.L. Feng[2], H.L.W. Chan[1] and C.L. Choy[1]
[1] *The Hong Kong Polytechnic University, Kowloon, Hong Kong*
[2] *Chinese Academy of Science, Shanghai, China*

14.15 **Predicting non-linear optical properties in push-pull molecules using vibrational spectroscopy and density functional theory**
Th D2.4 C. McGoverin[1], K.C. Gordon[1], A.J. Kay[2] and A.D. Woolhouse[2]
[1] *University of Otago, Dunedin, NZ*
[2] *Industrial Research Limited, Lower Hutt, NZ*

14.30 **Neutron irradiation effect of poly-$Si_{1-x}Mn_x$ semiconductors grown by MBE**
Th D2.5 D. Kwon[1], Y.E. Ihm[1], S.W. Lee[1], D. Kim[1], H. Kim[1], J.M. Sohn[2], Y.H. Kang[2], C.S. Kim[3], H. Ryu[3] and S.J. Oh[4]
[1] *Chungnam National University, Daejeon, Korea*
[2] *Korea Atomic Energy Research Institute, Daejeon, Korea*
[3] *Korea Research Institute of Standards and Science, Daejeon, Korea*
[4] *Korea Basic Science Institute, Daejeon, Korea*

14.45 **Atomic force microscopy on adsorbed organics**
Th D2.6 S. O'Shea, R. Lim, J. Yan, N.N. Gosvami, L. Lim and A. Lau
Institute of Materials Research and Engineering (IMRE), Singapore

Anisotropy in the optical response of the metal surfaces and interfaces

Ola Hunderi,

Department of Physics,
Norwegian University of Science and Technology,
N-7034 Trondheim, Norway

Reflection anisotropy spectroscopy (RAS) is a non-destructive optical probe capable of operating in a wide range of environments. The technique was originally developed to study semiconductor growth but has recently been used to probe the optical properties of metal surfaces. The technique is a highly sensitive method for detecting small anisotropies at the surface of materials with cubic symmetry.The break-down in translational symmetry at surfaces causes Neumann's principle as applied to a bulk crystal to lose its validity. At (110) oriented surfaces the reflection coefficient may therefore depend on whether the [-110] chains are parallel with or normal to the polarization vector. We have measured the complex normalized reflection difference $\Delta r/r = 2(r_{\cdot 110} - r_{001})/(r_{\cdot 110} + r_{001})$ for clean and oxygen reconstructed Cu(110) and Ag(110) between 1.5 and 6.0 eV by means of reflection anisotropy spectroscopy. Using expressions for the screened dipole-dipole interaction we have found that both the surface local-field effect and polarisation dependent transitions between surface states at the $\overline{Y}$ point of the surface Brillouin zone are responsible for the main features in the spectra. The change in the signal upon formation of ordered oxygen overlayers will be discussed. The Ag(110) surface was also studied at various stages of annealing and ion bombardment cycles by means of RAS combined with scanning tunneling microscopy (STM).

Reconstructed surfaces may also give rise to anisotropy in the optical properties. We have used RAS combined with STM to study this effect in connection with reactions at metal surfaces. In the report we will concentrate on the optical anisotropy of the Pt and Au(100) reconstructed phases. These cubic materials are known to reconstruct with a hexagonal outer layer which results in a wavy surface due to the «incommensurability» of the hexagonal outer layer and the cubic bulk. The transition from the Pt hex-R0.7° to the Pt(1x1) structure was also studied. We found that the spectrum of Pt(100)-hex-R0.7° was dominated by a surface polariton like absorption due to the wavy nature of the first layer superstructure, but an additional absorption was also observed in the reconstructed layer. After exposure to CO the surface transformed to Pt(1x1) covered with Pt islands. The growth of the (1x1) phase was highly anisotropic, i.e. the growth being much faster along the $[0\bar{1}1]$ direction than along [011]. The islands were elongated in the fast-growth direction and we observed an optical anisotropy from the island-covered surface which was comparable to that of the Pt(100)-hex-R0.7° surface.

Reflectance anisotropy spectroscopy so far has been mostly used for surface studies. In the work reported here we briefly discuss that RAS can also be used to study the anisotropy of hidden interfaces (IDA).

Stretching Single Polysaccharide Molecules using AFM

M. A. K. Williams[1,2*], R. Haverkamp[2,3] and J.E.Scott[4]
[1] *Institute of Fundamental Sciences, Massey University, NZ*
[2] *MacDiarmid Institute for Nanotechnology and Advanced Materials, NZ*
[3] *Institute of Technology and Engineering, Massey University, NZ*
[4] *Department of Chemical Morphology, Manchester University Medical School, UK*

AFM has emerged as the technique of choice for conducting single molecule force spectroscopy, owing largely to the limited range of forces that can be applied by competing methodologies such as the use of optical tweezers or magnetic beads [1]. Although examples of single polynucleotides, proteins, polysaccharides and synthetic polymers have all now been stretched using AFM [1-6], there remain relatively few studies on polysaccharide molecules. At first site polysaccharides may appear not to offer the same exciting opportunities as nucleotides, whose duplexes can be mechanically separated, or proteins, that may be mechanically denatured. They do, however, exhibit their own richness of behaviour including, uniquely among the biopolymers, the possibility of force-induced conformational transitions of the pyranose rings [5, 6]. Furthermore, the fact that polysaccharides are key elements of many biomaterials, including plant cell walls, has fuelled increasing speculation about the potential physiological significance of such force-induced transitions in-vivo.

Here we discuss a methodology we have been developing using AFM to investigate the nanomechanical properties of polysaccharide chains, describe the results of some theoretical modelling, and discuss the possible implications of single chain behaviour for the mechanical properties of materials comprised of such polymers.

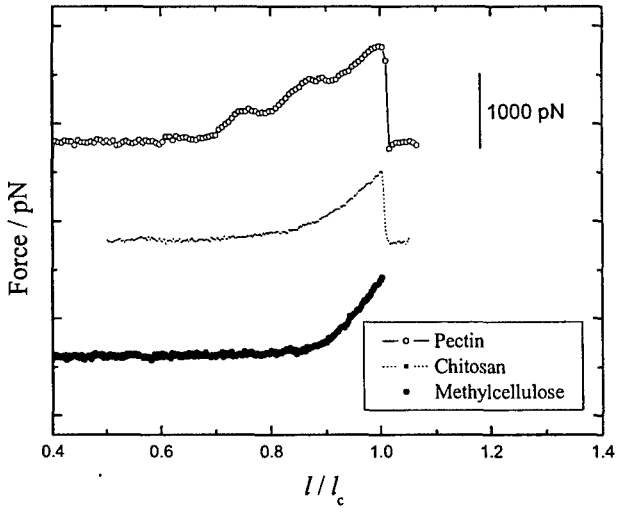

FIG 1: *Force extension curves for single polysaccharide molecules measured using AFM. Pectin shows distinct plateaus corresponding to conformational transitions of the sugar ring. In contrast, the molecular structures of chitosan and methylcellulose do not afford such possibilities.*

References

[1] T.R. Strick et al, Rep.Prog.Phys. **66**, 1, (2003).
[2] S.A. Harris, Contemporary Physics **45**, 11, (2004).
[3] J.M. Fernandez et al, Nature **393**, 181, (1998).
[4] C. Ortiz and G. Hadziioannou, Macromolecules **32**, 780, (1999).
[5] J.M. Fernandez et al, Nature **396**, 661, (1998).
[6] P.E. Marszalek, PNAS **96**, 7894, (1999).

* Contact author: m.williams@massey.ac.nz

TEM investigation of hydrogen-implanted and annealed single-crystal $SrTiO_3$

G.K.H. Pang[1*], Y. Wang[1], W.L. Liu[2], Z.T. Song[2], S.L. Feng[2], H.L.W. Chan[1] and C.L. Choy[1]
[1]*Department of Applied Physics, The Hong Kong Polytechnic University, Hung Hom, Kowloon, HONG KONG*
[2]*Institute of microsystem and information technology, Chinese Academy of Science, Shanghai, CHINA*

Single-crystals $SrTiO_3$ implanted with H^+ have been investigated by transmission electron microscopy (TEM).

It has been reported that high quality single-crystal thin films of perovskite $BaTiO_3$, $LiNbO_3$, $LiTaO_3$ and $SrTiO_3$ were obtained by the crystal ion slicing (CIS) method [1-5]. The process involved ion-implantation into a single crystal bulk material and a subsequent treatment of thermal annealing. Thin layer of material is obtained due to the internal stress state causing by the extended defects merging at a depth below the sample surface after annealing. The structural characterization of the defective layer formed after annealing is important for the understanding the damage evolution process and the aim of the present study is to investigate the influence of annealing on the H^+ implanted single crystal $SrTiO_3$.

Single crystals $SrTiO_3$ were implanted with H^+ at energy 25 keV with a dose of 5.5×10^{16} cm^2 using semiconductor implanter (IM-200M). TEM dark field image (Fig. 1) shows that the 100 nm thick defective layer of the as implanted $SrTiO_3$ is highly disordered due to the point defects introduced by H^+. Fig. 2 shows the TEM bright field image of the sample after annealing at 600 °C for 5 minutes. Extended defects having {110} and {100} habit planes were observed at a depth of 100 nm below the surface. High resolution TEM reveals the extended defects are highly distorted crystallites of typical dimension of 5 nm. It is believed that the stressed extended defects eventually lead to $SrTiO_3$ cracking similar with the process suggested in the silicon/H^+ system [6].

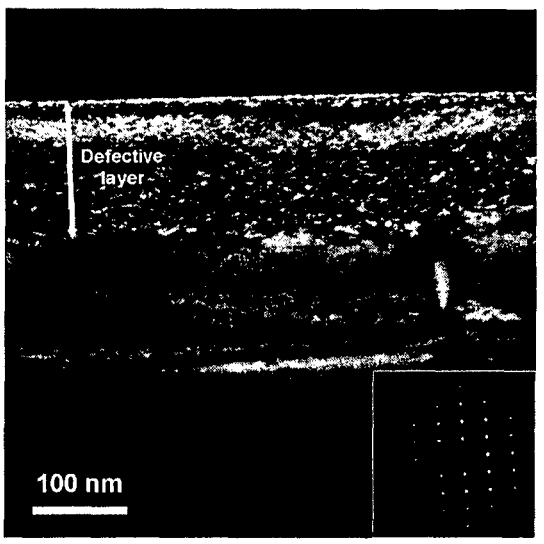

FIG. 1. TEM dark field image of the as implanted sample showing a highly disordered defective layer of 100 nm thick.

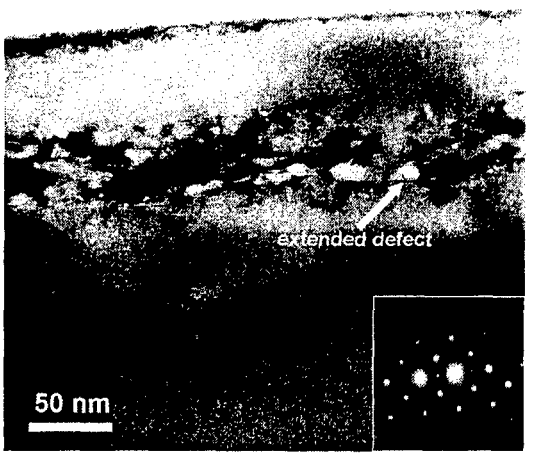

FIG. 2. TEM bright field image of the annealed sample showing the extended defects at a depth of 100 nm below the surface.

References

[1] T. Izuhara *et al.*, Appl. Phys. Lett. **82**, 616 (2003).
[2] M. Levy *et al.*, Appl. Phys. Lett. **71**, 2617 (1997).
[3] M. Levy *et al.*, Appl. Phys. Lett. **73**, 2293 (1998).
[4] M. Levy *et al.*, Appl. Phys. Lett. **77**, 2124 (2000).
[5] F. J. Kub *et al.*, Electron. Lett. **35**, 477 (1999).
[6] S. Frabboni, Phys. Rev. B **65**, 165436 (2002)

* Contact author: apgpang@polyu.edu.hk

Predicting non-linear optical properties in push-pull molecules using vibrational spectroscopy and density functional theory

Cushla McGoverin[1*], Keith C. Gordon[1], Andrew J. Kay[2], Anthony D. Woolhouse[2]
[1] *MacDiarmid Institute for Advanced Materials and Nanotechnology, University of Otago, Department of Chemistry, Union Place, Dunedin, NEW ZEALAND*
[2] *Opto-Organics Group, Industrial Research Limited, P.O. Box 31 310, Lower Hutt, NEW ZEALAND*

The intense interest in NLO materials arises from application possibilities, such as in electro-optic switches and modulators,[1] frequency doublers[2] and optical storage devices[3]. With the quest for methods of storing greater amounts of information in smaller physical devices, the field of nonlinear optics is providing some promising possibilities.[2]

Currently the process by which new NLO molecules are developed is a time consuming and expensive one. While design strategies have been used for decades in relation to the maximisation of the NLO response, e.g. using electronic push-pull molecules containing an electron donor (D), conducting chain (π) and electron acceptor (A), D-π-A, there is a desire to reduce further the empirical approach currently taken in the design of new NLO molecules. Screening of compounds computationally before synthetic energy is expended will reduce the expense involved in the development of NLO devices.

We have used density functional theory (DFT) to study a series of novel push-pull compounds specifically designed to have significant NLO response,[4] as shown in Figure 1. We find that there are a number of interesting challenges in modelling such compounds, these include: torsional flexibility of the π-chain; rotational isomers due to the acceptor ring system; solvent effects. We have systematically modelled each of these phenomena using the correlation between experimental and calculated vibrational spectra as a guide to modelling success.

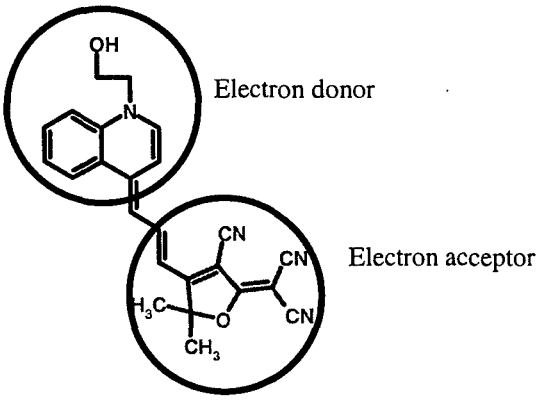

Figure 1. Example of electron donor-π-chain-electron acceptor push-pull molecule

References

[1] F. Ghebremichael, M. G. Kuzyk, and H. S. Lackritz, Prog. Polym. Sci. **22**, 1147 (1997).
[2] R. F. Shi and A. F. Garito, in *Characterization techniques and tabulations for organic nonlinear optical materials*, edited by M. G. Kuyzk and C. W. Dirk (Marcel Dekker, New York, 1998), Vol. 60, p. 1.
[3] L. R. Dalton, W. H. Steier, B. H. Robinson, et al., J. Mater. Chem. **9**, 1905 (1999).
[4] A. J. Kay, A. D. Woolhouse, Y. Zhao, et al., J. Mater. Chem. **14**, 1321 (2004).

* cmcgoverin@alkali.otago.ac.nz

Neutron irradiation effect of poly-$Si_{1-x}Mn_x$ semiconductors grown by MBE

Dhang Kwon[1], Young Eon Ihm[1,*], Seoung Won Lee[1], Dojin Kim[1], Hyojin Kim[1],
Jae Min Sohn[2], Young Hwan Kang[2], Chang Soo Kim[3], Hyun Ryu[3] and Sang Jun Oh[4]
[1] *School of Materials Engineering, Chungnam National University, Daejeon, 305-764, Korea*
[2] *Korea Atomic Energy Research Institute, Daejeon, 305-353, Korea*
[3] *Korea Research Institute of Standards and Science, Daejeon, 305-600, Korea*
[4] *Korea Basic Science Institute, Daejeon, 305-333, Korea*

Recently magnetic semiconductors have attracted a lot of interests due to the potential applications of spin-polarized injection such as magnetic sensors, magnetic storage media and magnetic random access memories [1,2]. In this work, the neutron irradiation effect of polycrystalline $Si_{1-x}Mn_x$ semiconductor thin films has been studied. The $Si_{1-x}Mn_x$ semiconductor thin films were grown on SiO_2/(100)Si substrate at 400°C by using a MBE. The electrical resistivities of as-grown $Si_{1-x}Mn_x$ semiconductor thin films are $1.8x10^{-4}$~$4.3x10^{-4}$ ohm.cm. The as-grown $Si_{1-x}Mn_x$ semiconductor thin films have p-type carriers whose concentration and mobility are around $2.6x10^{21}/cm^3$ and $10.5cm^2/V.sec$, respectively. The XRD and TEM analysis demonstrate that the as-grown $Si_{1-x}Mn_x$ semiconductor thin films are polycrystalline and contain the magnetic phases such as MnSi, Mn_5Si_3 and Mn_4Si_7. The saturation magnetizations of the as-grown $Si_{1-x}Mn_x$ semiconductor thin films measured by using a MPMS are 113emu/cc at 5K and 13emu/cc at room temperature. The as-grown specimens are irradiated by the fast neutrons of 0.82MeV in a neutron research reactor at the Korea Atomic Energy Research Institute located in Daejeon, Korea. The irradiation rate is $3.45x10^{10}$ neutrons/cm^2sec and the irradiation amounts are $2.4x10^{14}$, 10^{15} and 10^{16} neutrons/cm^2, respectively. After neutron irradiation the electrical and magnetic properties were analyzed in the same ways, which have been done on the as-grown specimens. The electrical resistivities of neutron-irradiated specimens increase with the irradiation amount, while the saturation magnetizations decrease (Fig. 1). Hall analysis reveals that the mobility of neutron-irradiated specimen decreases remarkably. The XRD and TEM analysis show that phase change is not occurred by the neutron irradiation (Fig. 2). From the results, it may be concluded that the formation of defects induced by the neutron irradiation causes the change of electrical and magnetic properties of the polycrystalline $Si_{1-x}Mn_x$ semiconductor thin films. *This work was supported by the Research Center for Advanced Magnetic Materials (Chungnam National University) and BK21 Program (the Ministry of Education & Human Resource Development in Korea).*

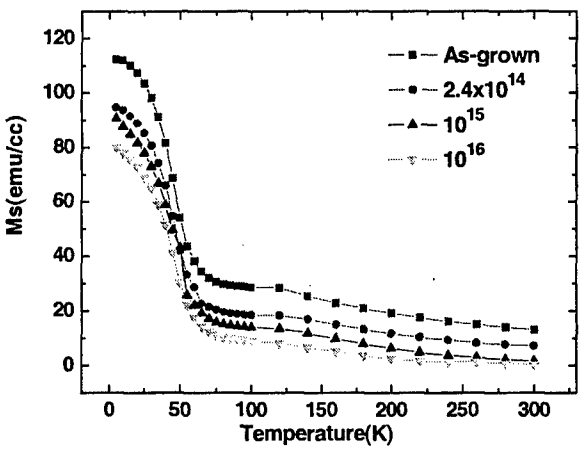

Fig. 1. Variation of the saturation magnetization as a function of the temperature for as-grown and neutron irradiated specimens. (Applied field: 2T)

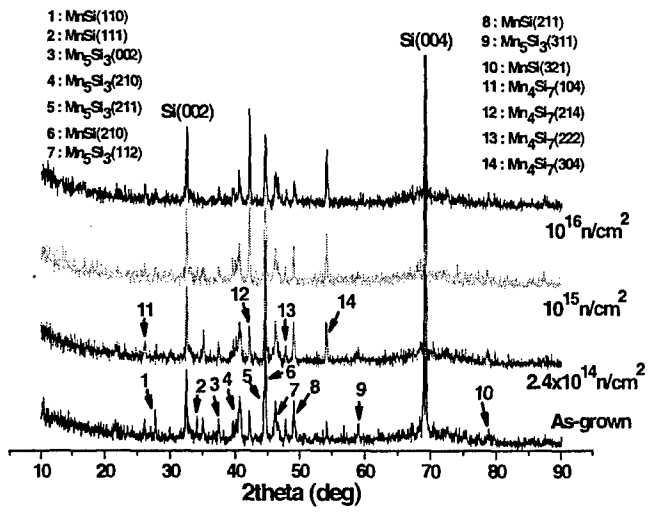

Fig. 2. XRD patterns of as-grown and neutron irradiated specimens.

References

[1] J. K. Furdyna, J. Vac. Sci. Technol., A4(4), (1986), 2002.
[2] J. K. Furdyna et al, J. Appl. Phys., 61(8), 15, (1987), 3526.

* Contact author: yeihm@cnu.ac.kr

Atomic Force Microscopy on Adsorbed Organics

Sean O'Shea, Roderick Lim, Jiang Yan, Nitya Nand Gosvami, Leonard Lim and Aaron Lau
Institute of Materials Research and Engineering (IMRE), 3 Research Link, Singapore.

We will discuss the use of Atomic Force Microscopy (AFM) in liquid environments to image and measure the physical properties of simple organic molecules adsorbed on solid surfaces. True atomic resolution imaging has not been achieved in liquids, despite the importance of such a breakthrough for biological and chemical applications. Some general issues on this problem and current methodologies being pursued will be outlined. We will illustrate with data taken for two systems, namely simple liquids adsorbed on graphite (a model system for the study of confined liquids) and mixed self assembled monolayers (SAM) on gold (a useful system for molecular electronics studies).

AFM imaging of organic molecules adsorbed on graphite (HOPG) in liquids is an interesting system as several simple organics, such as linear alkanes and alkanols, have molecular structures commensurate with the underlying graphite lattice structure and are preferentially adsorbed. The molecules may self-assemble into domains of lamellae whose structure and orientation is defined by the graphite lattice. These systems are well known from previous STM work and therefore provide a good model for understanding the limitations of AFM imaging in liquids.

Further, by measuring force curves i.e. the force acting on the tip as a function of tip-surface separation, one can greatly elucidate the imaging mechanisms and nature of adsorbed molecules on a surface. We are particularly interested in the observation of oscillatory solvation forces, which arise when liquid molecules are squeezed between two surfaces. One finds that even for nanoscale confinement volumes, as experienced in AFM experiments, the liquid may order near the surface into discrete "solid-like' layers. The confined molecules closest to the substrate surface are tightly bound but that does not imply such molecules can be imaged. As a generalisation no AFM images of molecules were observed unless there was strong *lateral* ordering of the molecules. This also appeared to be the situation even when confinement of the liquid molecules between the tip and the substrate induced strong molecular ordering (i.e. solvation forces) *normal* to the substrate surface.

The mixed SAM we study consist of organic molecular wires (either thiol or dithiol terminated) inserted into an insulating alkanethiol matrix SAM formed on gold (111). We have monitored the insertion process in-situ by liquid AFM. Not surprisingly the inserted molecules appear as holes or protrusions depending on the length of the alkanethiol matrix. By choosing the matrix alkanethiol appropriately one can form reasonably flat mixed SAM surfaces allowing for the AFM measurement of friction and conduction without gross mechanical deformation of the inserted molecules.

SESSION Th E2
CATALYSIS, CORROSION AND CAPILLARITY

Thursday 10 February 2005 1320–1500

Copthorne III

Session Chair **Nick Laycock, Industrial Research Ltd, NZ**

13.20 **Electrochemistry in nanometer-scale domains**
Th E2.1 B. Zhang, E. Ervin, R.J. White, J.J. Watkins, Y. Zhang and H.S. White
(Extended Oral Talk)
University of Utah, Salt Lake City, USA

13.45 **Chemistry in really hot water**
Th E2.2 D. D. MacDonald
Pennsylvania State University, USA

14.00 **Towards electrocatalysis of fuel oxidation using non-noble materials**
Th E2.3 G.T. Burstein, D.R. McIntyre and A. Vossen
University of Cambridge, Cambridge, UK

14.15 **Control of microfluidic flows using surfaces with switchable wettability**
Th E2.4 J. Burnell[1], T. Cooper[2] and S.C. Hendy[1]
[1] *Industrial Research Limited, Lower Hutt, NZ*
[2] *MacDiarmid Institute for Advanced Materials and Nanotechnology, Victoria University of Wellington, Wellington, NZ*

14.30 **Multiscale computer simulation of pit propagation in stainless steels**
Th E2.5 S.P. White, N.J. Laycock and D.P. Krouse
Industrial Research Limited, Lower Hutt, NZ

14.45 **Boundary slip in Newtonian fluids: impliations for microfluidics**
Th E2.6 V.S.J. Craig
Australian National University, Canberra, Australia

Electrochemistry in Nanometer-Scale Domains

Bo Zhang, Eric Ervin, Ryan J. White, John J. Watkins, Yanhui Zhang, Henry S. White*
Department of Chemistry, University of Utah, Salt Lake City, Utah, USA

Advances in the fabrication of nanometer-scale electrodes during the past decade have created exciting opportunities in both physical chemistry and analytical measurements. Disk- and conical-shape metal electrodes of radius as small as 2 nm can now be synthesized and the faradaic currents at these electrodes are readily measured using standard electrochemical instrumentation. A relatively unexplored issue is whether the principles employed to describe the behavior of macroscopic electrodes require modification as the electrode size is reduced to nanometer dimensions.

This presentation will describe how Pt electrodes of nanometer dimensions are synthesized and characterized, and presents a few examples of their applications in fundamental studies of electron-transfer mechanisms and in analytical chemistry. The concept of comparing the electrode size to the length scales of other chemical structures (e.g., the electrical double layer) that define electrochemical reactions is emphasized. Examples include investigations of the dependence of electron-transfer kinetics and molecular diffusion on interfacial electric fields [1], and electrochemical detection of very small quantities of a redox-active species (zeptomole detection) [2].

The electrochemical behavior of a new device, the "nanopore electrode" [3], will also be presented. The glass nanopore electrode is a Pt microdisk electrode embedded at the bottom of a conical pore in glass, the circular orifice of the pore having nanometer dimensions. The Pt microdisk acts as an electrochemical or conductivity sensor, while the SiO_x surface of the nanometer scale pore is chemically modified to impart separation capability to the device. We view the pore orifice as a nanoscale chromatography column. While such a short column would be inefficient for separation of conventional samples, the nanometer-scale dimensions are ideal for separation of small numbers of molecules encountered in ultralow trace detection.

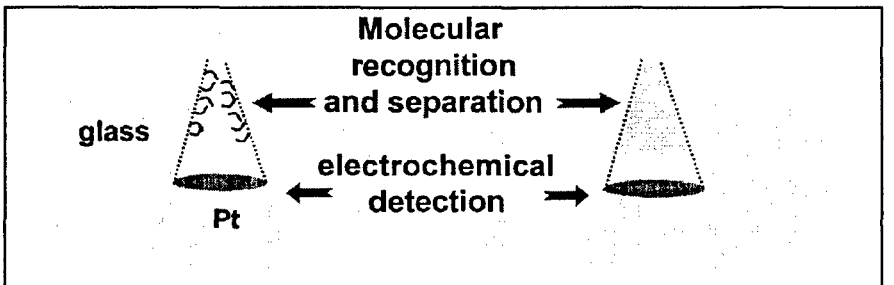

Figure 1. *The nanopore electrode. Molecular selectivity results from surface modification of the pore walls (left) or from a volume filling gel (right).*

References

[1] J. J. Watkins, J. Chen, H. S. White, E. Maisonhaute and C. Amatore, Anal. Chem. **75**, 3962 (2003).
[2] J. J. Watkins and H. S. White, Langmuir **20**, 5474 (2004).
[3] B. Zhang, Y. Zhang, and H. S. White, Anal. Chem., in press.

* Contact author: white@chem.utah.edu

Chemistry in Really Hot Water

Digby D. Macdonald
Center for Electrochemical Science and Technology
Department of Materials Science and Technology
Pennsylvania State University
University Park, PA 16802, USA

Super Critical Water (SCW) is now being actively explored as a reaction medium of unusual properties for the synthesis of novel materials, including nano particles, and as a means of destroying resilient organic waste [Super Critical Water Oxidation (SCWO)]. These systems employ water at T > 374.15 °C, but more typically at temperatures in excess of 500 °C. In the case of SCWO, a high fugacity of oxygen is maintained in the system, in order to oxidize and destroy the organic component of the waste, thereby reducing the volume for subsequent disposal. SCWO offers considerable advantages over other volume reduction technologies, such as incineration and pyrolysis, in that it is carried out in a closed cycle with zero emissions, and it is capable of achieving conversion efficiencies close to 100 %. For that reason, SCWO has become the technology of choice for destroying the World's arsenals of chemical weapons (VX, Sarin, etc). However, because of the high oxygen fugacity, corrosion of the structural materials is the principal operating problem, which to date has prevented SCWO from achieving its full potential. A significant difficulty in controlling corrosion is the lack of effective sensors for monitoring the chemical and electrochemical properties of the supercritical aqueous environment. A second difficulty is that the properties of super critical aqueous solutions are so different from their sub critical counterparts that it is uncertain whether corrosion mechanisms and corrosion control technologies developed for sub critical systems are applicable or effective at super critical temperatures.

This talk outlines our work on developing novel chemical and electrochemical sensors for monitoring important process parameters in SCW, on identifying and characterizing corrosion mechanisms, and on developing novel corrosion control technologies. The sensors are based on extensive research that has been carried out in the author's laboratory over the past decade in measuring chemical (e.g. pH, $[H_2]$, $[O_2]$) and electrochemical (corrosion potential and redox potential) parameters in aqueous solutions at temperatures as high as 528 °C. In particular, rugged pH, oxygen, hydrogen, and redox potential combination sensors, based on YSZ membranes, will be described, and the sensing mechanisms will be discussed in terms of the defect structures of the materials. The development of electrochemical emission spectroscopy (EES) as a means of monitoring corrosion rate *in-situ* in SCWO systems will also be discussed. This work has demonstrated the efficacy of three-electrode EES for *in-situ* corrosion monitoring at temperatures up to 390°C; that is, at low supercritical temperatures, but we have also used two-electrode techniques successfully at temperatures above 500 °C. A primary objective of our current work is to extend the operating temperature to above 600 °C and to develop an electrochemically "quiet" reference electrode, which will provide a reference potential that is stable to within ±0.1 mV.

Finally, the solvent properties of SCW span those from a dense liquid at very high pressures to those of a low pressure gas at low pressures, because the density is an independent variable. Thus, at high pressures (high densities), corrosion processes are postulated to be dominated by electrochemical mechanisms, because the environment is sufficiently ionizing to support charge transfer reactions at the interface, whereas at low pressures, gas-phase oxidation is expected to prevail. These mechanisms may be delineated using EES, and it is found that the electrochemical mechanism prevails in the corrosion of carbon steel at densities higher than about 0.06 g/cm^3. This is a surprising result, because aqueous fluids of this density are essentially "dense gases" with low dielectric constants and hence possess low ionizing powers.

Towards Electrocatalysis of Fuel Oxidation Using Non-Noble Materials

G.T. Burstein, D.R. McIntyre and A. Vossen
Department of Materials Science and Metallurgy
University of Cambridge
Pembroke Street
Cambridge CB2 3QZ
United Kingdom

One of the major impediments to the full-scale development and exploitation of fuel cells for transport power is the very high costs in relation to conventional power sources. A significant part of this cost is the platinum required for the electrodes over which the fuel and the oxidant (air) are passed. If the fuel-cell powered vehicle is to become commercially viable, these costs must be reduced. One method of attempting to achieve this is the quest for electrodes made from non-platinum materials which allow sufficient electrocatalysis of the fuel for the anode reaction, and of oxygen for the cathode reaction. This paper addresses the problems involved in the search for suitable electrocatalysts made from base materials, and shows new insight into how such materials might be developed. Some of them show unique features in electrocatalysis [1,2], not encountered in noble-metal catalysis, and this requires new mechanistic understanding to determine the modes by which they operate.

The present research concerns fuel cell systems designed to operate at low temperature, typically up to 100°C, and in acidic electrolytes. Unlike the alkaline electrolytes, acidic electrolytes allow a carbon dioxide tolerance without degradation in performance. The primary requirements of a non-platinum-based electrocatalyst for use in acidic electrolytes can be defined clearly. The material must be a good electron conductor. It must of course be electrocatalytic towards the reactant. It must also be very passive towards corrosion in acidic electrolytes. We have synthesised a range of metal carbides for this purpose. The basis for these is the passivation against corrosion. These are designed from metals which show a high degree of passivity in sulphuric acid. Several synthetic routes have been used, including wet synthesis or mechanical alloying, followed by high-temperature carburisation, also through a number of routes. Sputtering of reactive plasma provides a useful means of screening potentially applicable materials.

A material made by carburising mechanically alloyed tantalum and nickel has been synthesised. The surface of this carbide can be selectively passivated against acid-corrosion by a metal-rich oxide layer or by a carbon-rich layer. The electrocatalytic activity of the material towards anodic oxidation of hydrogen and of methanol shows that the different surface treatments imposed also imparts a selectivity. When the surface is metal-rich, the material is catalytic towards hydrogen oxidation, but completely inactive towards methanol oxidation. When the same material is made carbon-rich, it becomes catalytically active towards the methanol oxidation reaction, but inactive towards hydrogen. Observation of this selectivity is new, and has not been found with any other electrocatalyst, including those based on platinum. A tentative mechanism for this behaviour involving functionalisation of the carbon is proposed. The present experiments also show that some base electrocatalysts can be made which show activity towards anodic oxidation of hydrogen, but the catalytic activity is almost unaffected by the presence of carbon monoxide contamination. This is also unique in electrocatalysis; electrocatalysts based on platinum are inevitably poisoned by the presence of small concentrations of CO in the fuel stream. Such poisoning of platinum-based electrocatalysts is one of the banes of hydrogen fuel-cell technology, since the fuel must be purified rigorously to prevent degradation in performance; even Pt/Ru is poisoned this way. The small amount of poisoning that does occur over these base electrocatalysts is also rapidly reversible when the CO source is removed.

Finally, we show that there are some systems which show some small degree of electrocatalytic activity towards methanol oxidation at low overpotentials. This too is unique. Discussion of how these electrocatalysts function is presented. The work shows how new electrocatalysts may be developed, and what characteristics might be expected from them.

References

[1] G T Burstein, D R McIntyre and A Vossen. Electrochem. Solid State Letters, 5, A80 (2002)
[2] D R McIntyre, A Vossen, and G T Burstein. J. Power Sources, 107, 67 (2002)

Control of microfluidic flows using surfaces with switchable wettability

J. Burnell[1], T. Cooper[2] and S. C. Hendy[1,2,*]
[1] *Industrial Research Ltd, PO Box 31-310, Lower Hutt, NEW ZEALAND*
[2] *MacDiarmid Institute for Advanced Materials and Nanotechnology, Victoria University of Wellington, Wellington, NEW ZEALAND*

A surface with wettability that is controlled by electrical potential has recently been demonstrated [1]. This *switchable surface* exploits reversible conformational changes in a self-assembled layer of alkanethiolates on gold that are controlled by the gold surface potential. There are many potential applications of this technology including the possibility of controlling microfluidic and nanofluidic flows. We perform a theoretical study of the use of such switchable surfaces in microfluidic devices.

At the molecular scale we have studied the response of alkanethiolates to an electric field with chain lengths from 10 to 16 carbon atoms using molecular dynamics and density functional theory. We find that the conformational change associated with the change in wettability is controlled by an activation energy. Thus the switching can be thought of as a structural phase transition which can be studied as function of temperature and electric potential.

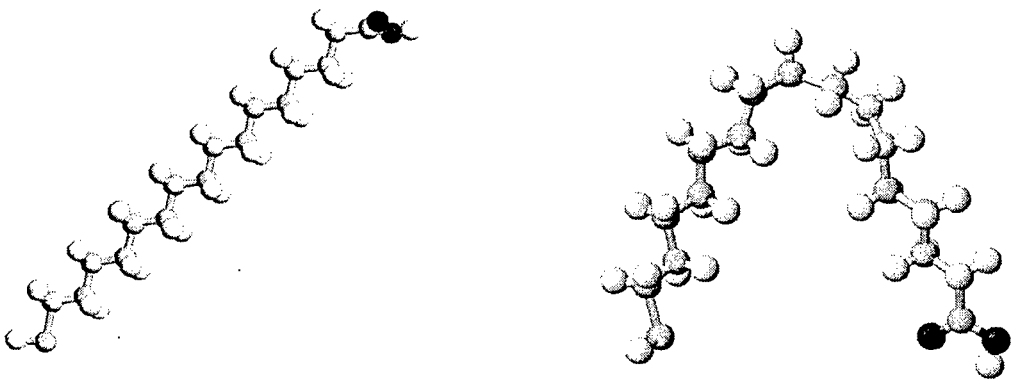

As noted above, wettability can be used to alter microfluidic flows. From a macroscopic perspective, fluid flowing across a non-wetting surface can slip, violating the usual 'no-slip' boundary condition. The slip can be characterized by a slip length, δ, which is the distance at which the fluid velocity vanishes if it is extrapolated beyond the surface. Indeed large-scale molecular dynamics simulations have shown that a non-wetting surface can induce slip lengths of several tens of molecular diameters in the fluid flow past the surface [2].

In principle, by controlling the wettability of surface, one can induce a slip-length at the surface. Thus, a switchable surface would allow spatial and temporal control of the slip length and hence control of a microfluidic or nanofluidic flow. To model such situations we consider viscous flows in a channel with a slip length $\delta=\delta(x,t)$ operating at the channel walls. We show that with an appropriate choice of $\delta(x,t)$, pumping or valving of the flow can be induced.

References

[1] J. Lahann et al., "A reversibly switching surface", Science **299**, 371 (2003).
[2] J.-L. Barrat and L. Bocquet, "Large Slip Effect at a Non-Wetting Fluid-Solid Interface", Phys. Rev. Lett. **82**, 4671-74 (1999).

* Corresponding author: s.hendy@irl.cri.nz

MULTISCALE COMPUTER SIMULATION OF PIT PROPAGATION IN STAINLESS STEELS

S.P. White[1], N.J. Laycock[2] and D.P Krouse[1]

[1]*Applied Mathematics*
[2]*Materials Performance Technologies*
Industrial Research Ltd, Gracefield Research Centre
PO Box 31-310, Lower Hutt, New Zealand

Artificial pit electrodes of 904L stainless steel have been used to measure the variation of the anodic current density as a function of the local chemistry within a propagating pit. Measurements have been made both above and below the Critical Pitting Temperature (CPT) for this alloy. The data have been used to estimate input parameters for a model of pitting corrosion, thereby enabling numerical simulation of pitting experiments at different temperatures. These simulations qualitatively reproduce many experimentally observed features of pitting corrosion, including a very sharply defined CPT.

The model is based on the requirement of a near-saturated local chemistry in the pit and uses an equation previously formulated for the anodic dissolution kinetics in this environment. Salt film precipitation, electrolytic migration and transport outside the pit are each considered explicitly. Numerical simulations of pit growth have reproduced the experimentally observed characteristics of pitting, including development of a pit cover, spontaneous repassivation of metastable pits, increased stability at higher applied potentials, and a tendency for pits to become dish-shaped rather than hemispherical.

This micron-scale deterministic model of single pit growth is combined with a purely stochastic model of pit nucleation. Monte Carlo simulations are used to compare the predictions of this combined model with potentiodynamic experimental measurements of the pitting potential at the centimeter scale and to simulate free corrosion of a centimeter-scale stainless steel surface.

[1] Contact Author: S.White@irl.cri.nz

Boundary Slip in Newtonian Fluids: Implications for microfluidics.

V. S. J. Craig
Department of Applied Mathematics, Research School of Physical Sciences, Australian National University, Canberra ACT 0200 AUSTRALIA

The hydrodynamic drainage force on a silica sphere approaching a flat wall perpendicularly in a viscous liquid, was measured using an Atomic Force Microscope in two modes - including a novel nanorheological approach. The experimental results are compared to existing theoretical models. These measurements show clear evidence of boundary slip in a Newtonian liquid with slip lengths of up to 100nm. The degree of boundary slip is found to be a function of the liquid viscosity and the shear rate [1]. The influence of surface roughness on the boundary condition has been investigated using completely wetting surfaces [2]. The degree of slip is found to increase with surface roughness. The influence of surface wettability has been studied by comparing measurements in pure water and in solutions of a cationic surfactant (cetyltrimethylammonium bromide, CTAB) [3]. The previously reported dependence of slip on the local shear rate is suppressed if surfactant molecules are adsorbed on the solid surfaces. Furthermore, when the surfaces are partially covered by surfactant molecules, slip ceases to depend directly on surface wettability, and a similar degree of slippage is measured on hydrophilic and hydrophobic surfaces.

This leads to the conclusion that in most practical situations boundary slip takes place, leading to a reduction of the hydrodynamic drainage force and greater ease of flow in highly confined liquids. Surface roughness would appear to be a significant factor in the degree of slip. This will be explored.

These findings have implications for confined biological systems, the permeability of micro-porous media and for the lubrication of nano-machines and will be important in the micro-control of liquid flow.

References

[1] V. S. J. Craig, C. Neto and D. R. M Williams, Phys. Rev. Lett. **87**, 054504 (2001)
[2] E. Bonaccurso, H.-J. Butt and V. S. J. Craig, Phys. Rev. Lett. **90**, 144501 (2003)
[3] C.L. Henry *et al.*, Physica A **339**, 101-105 (2004)

Thursday 10 February
Oral Session Three

SESSION Th A3
SEMICONDUCTOR GROWTH AND CHARACTERISATION III

Thursday 10 February 2005 1530–1645

Galaxy I

Session Chair **John Kennedy, Institute of Geological and Nuclear Sciences, NZ**

15.30 **A novel HgCdTe material growth process for infrared detector applications**
Th A3.1 C.A. Musca[1], G. Heim[2] and L. Faraone[1]
[1] *University of Western Australia, Perth, Australia*
[2] *Spitfire Semiconductors Ltd, Auckland, NZ*

15.45 **Room temperature fabrication of large mobility (> 10 $cm^2(Vs)^{-1}$) amorphous oxide semiconductor and application to thin film transistor**
Th A3.2 K. Nomura, T.Kamiya, H.I. Ohta, A. Takagi, H. Yanagi, M. Hirano and H. Hosono
Tokyo Institute of Technology, Yokohama, Japan

16.00 **Nanosensors based on ultra thin wall bell-shaped shells.**
Th A3.3 A.V. Kopylov, A.V. Prinz and V.Ya. Prinz
Institute of Semiconductor Physics, Novosibirsk, Russia

16.15 **On ZnO p-n junctions, characterisations and gas sensor applications**
Th A3.4 S. Basu and S.K. Hazra
Indian Institute of Technology, Kharagpur, India

16.30 **Synchrotron-based measurements of the electronic structure of transition metal phthalocyanines**
Th A3.5 J.E. Downes[1], H.J. Trodahl[1], Y. Zhang[2] and K.E. Smith[2]
[1] *Victoria University of Wellington, Wellington, NZ*
[2] *Boston University, Boston, USA*

A novel HgCdTe material growth process for infrared detector applications

C. A. Musca [1,*], G. Heim [2], L. Faraone [1]
[1] *School of Electrical, Electronic & Computer Engineering, The University of Western Australia, Perth, Australia*
[2] *Spitfire Semiconductors Ltd, Auckland, New Zealand*

Infrared (IR) detector and imaging technology is important for a large number of applications, including resource exploration, mine site rehabilitation monitoring, surveillance, bush fire detection, environmental monitoring, and pollution identification, as well as being a requirement for more traditional scientific, aerospace and defence needs. A number of infrared detection devices exist, with the highest performance IR detectors based on direct detection of infrared photons incident on the detector. The highest performance detectors in the strategically important short-wave infrared (SWIR; 1.5 - 3μm), mid-wave infrared (MWIR; 3 – 5 μm) and the long-wave infrared (LWIR; 8 – 14 μm) atmospheric windows is achieved in devices using the semiconductor mercury cadmium telluride ($Hg_{1-x}Cd_xTe$). HgCdTe has a number of qualities that make it an ideal detector material for IR including; The band structure of HgCdTe provides it with high quantum efficiency, high carrier mobility and long minority carrier lifetime. The ability to change the wavelength to which the material is sensitive over a range from less than 1 μm, to greater than 25 μm by changing the mole fraction, x, of $Hg_{1-x}Cd_xTe$. This allows the cutoff wavelength of the detector to be tailored to anywhere within the IR region of the spectrum. State-of-the-art HgCdTe devices are currently manufactured using epilayers grown by liquid phase epitaxy (LPE) or molecular beam epitaxy (MBE). Both of these methods allow for good control of the semiconductor properties, but suffer from the fact that they need to be grown on near lattice matched substrates, limiting the maximum wafer size and increasing the cost of layers.

As an alternative to the costly growth processes, in this work we investigate the use of a bulk growth process for HgCdTe and the subsequent type conversion and thinning of the layers. The as-grown bulk HgCdTe is normally p-type, with a thickness of approximately 500 μm. Conversion to n-type is carried out at high temperatures under a Hg atmosphere, which converts the material to n-type for a certain thickness from the top and bottom of the wafer. The wafers (n-type or p-type) are thinned using a mechanical/chemical approach to 20 to 30 μm, and adhered to quartz substrates. Thin layers are required for detector fabrication to limit the amount of thermally generated noise in the fabricated detectors.

Two types of IR photodetectors will be fabricated from the HgCdTe to investigate the quality of the material; Photoconductors (PC) and photodiodes (PD). PCs are fabricated on n-type material and the device is essentially a radiation sensitive resistor. An applied constant current bias is applied and the variation in voltage is measured as the material conductance varies with varying amounts of impinging IR. The PDs fabricated are n-on-p junctions where the junction is formed in p-type starting layer using a plasma process technique [1]. Hall measurements were performed on bulk grown, thinned n-type, x = 0.2 HgCdTe (LWIR), giving very good electron mobility in the order of 1×10^5 cm^2/Vs. PC devices were fabricated on the material and gave good response in the LWIR region, with extracted minority carrier lifetime of 0.5 μs.

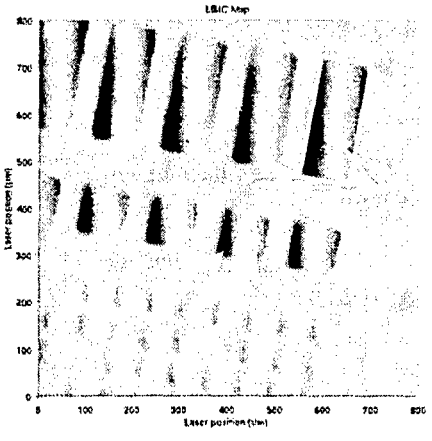

Fig. 1. False colour image of 2D LBIC map of variable area test array. Note that wafer orientation is slightly rotated with respect to laser scan.

Initial studies of PD devices were carried out by testing if type conversion occurred after plasma processing. An MWIR bulk layer was processed and the quality of the square or rectangular junctions was assessed using laser beam induced current (LBIC). LBIC allows the analysis of n-p junctions prior to complete device fabrication [2]. Figure 1 shows a false colour image of an LBIC scan, with the light and dark colours (current levels) indicative of an n-p junction. The strength of the LBIC signal indicates a high quality junction.

The initial investigation of this novel approach to HgCdTe material shows promise and further results will be presented showing the resulting high quality IR detectors.

[1]M.H. Rais, *et al.*, Microelectronics J., 31, 7, pp. 545-551 (2000)
[2]K.A. Fynn, *et al.*, IEEE Trans. Electron Devices 42, 1775 (1995).

* Contact author: charlie@ee.uwa.edu.au

Room Temperature Fabrication of Large Mobility (> 10 $cm^2(Vs)^{-1}$) Amorphous Oxide Semiconductor and Application to Thin Film Transistor.

Kenji Nomura[1], Toshio Kamiya[1,2], Hiromichi Ohta[1], Akihiro Takagi[2], Hiroshi Yanagi[2], Masahiro Hirano[1] and Hideo Hosono[1,3]

[1]*ERATO-SORST, JST, in Frontier Collaborative Research Center, Tokyo Institute of Technology, 4259 Nagatsuta, Midori-ku, Yokohama 226-8503, JAPAN*
[2]*Materials and Structures Laboratory, Tokyo Institute of Technology, 4259 Nagatsuta, Midori-ku, Yokohama 226-8503, JAPAN*
[3]*Frontier Collaborative Research Center, Tokyo Institute of Technology, 4259, Nagatsuta, Midori-ku, Yokohama 226-8503, JAPAN*

Amorphous oxide semiconductors (AOSs) are highly favorable for developing novel and practical electronic devices because of their advantageous properties such as high optical transparency in visible region and low temperature film formation [1]. Further, they have unique carrier transport properties such as large electron mobility > 10 cm^2 $(Vs)^{-1}$ and absence of Hall voltage sign double anomaly. These futures originate from the conduction band composed of spherical metal *ns*-orbital, which is insensitive to bond angle distortions. [2]. Amorphous In_2O_3-Ga_2O_3-$(ZnO)_m$ system, a-IGZO, is one type of n-type AOS and exhibits Hall mobilities > 15 cm^2 $(Vs)^{-1}$ [3]. However, detailed carrier transport properties have not been investigated yet. In this study, we have investigated carrier transport properties of a-IGZO in detail. Electronic structure and transport mechanisms are discussed from temperature dependence of Hall effect measurements. We demonstrated room temperature fabrication and operation of transparent thin film transistors (TTFTs) using the a-IGZO films for an n-channel.

We employed a pulsed laser ablation technique using crystalline $InGaZnO_4$ sintered target. Thin films were deposited on SiO_2 glass substrates without substrate heating. Carrier concentration of the films was varied from $<10^{15}$ - 10^{20} cm^{-3} by controlling oxygen pressure during the deposition. Hall-effect measurements were carried out using the van der Pauw configuration in the temperature range from room temperature to 30 K. Au electrodes were used as ohmic contacts. We fabricated top gate type TTFTs using a-IGZO as n-channel. Source and drain electrodes were fabricated using indium-tin oxide (ITO) with high conductivity and high transparency. Y_2O_3 was used as gate insulator with dielectric constant ~ 16. Device characterization was performed at room temperature and in air.

The Hall mobility (μ_{Hall}) was stepwise increased from ~ 3 to >13 cm^2 $(Vs)^{-1}$ as carrier concentration increased. The temperature dependence of carrier concentration changed from thermally-activated behavior to degenerated behavior at 1.0×10^{17} cm^{-3}, while that of μ_{Hal} shows thermally activated behavior even when carrier concentrations were 3×10^{18} cm^{-3} and degenerated. These results suggested that Fermi levels exist in band-tail states originating from structural randomness when *Ne* is < 3×10^{18} cm^{-3}. As definite Hall voltages were observed, we conclude that the tail states are not localized and the carriers run over distribution of potential barriers formed in the vicinity of the conduction band bottom. This carrier transport mechanism is obviously different from those in covalent amorphous semiconductors such in a-Si:H.

The TTFTs fabricated at room temperature exhibited good performances with an on /off current ratio ~10^3 and field effect mobility ~ 8 cm^2 $(Vs)^{-1}$, which is much larger than those in amorphous base TFTs.

References

[1]S. Narushima al. *Adv. Mater.* 15, 1409 (2003).
[2]H. Hosono et al. *J. Non-Cryst. Sol.* **203,** 334 (1996)
[3]M. Orita et al., *Phil. Mag. B*, 81, 501 (2000).

Nanosensors based on ultra thin wall bell-shaped shells.

A.V. Kopylov* A.V. Prinz and V.Ya. Prinz
Institute of Semiconductor Physics, 13, Academician Lavrentyev Avenue, Novosibirsk 630090, Russia

In [1], it was shown possible to detach an ultra-thin (to 2ML) film from the substrate on which this film was preliminarily grown by molecular-beam epitaxy (MBE). On local detachment from substrates, under the action of the internal stress, such a film, depending on particular boundary conditions, either rolls in a tube or undergo buckling [2].

One of the main properties of such nanoobjects is their good precision, resulting from the fact that the thickness and the internal stress in the film can be precisely predefined at the MBE stage. These nanoobjects, self-formed from ultimately thin films of a molecular thickness, present very promising buildings blocks for supersensitive nanosensors. In the present study, nanoshells of the most promising (in our opinion) shape, namely, bell-shapes shells, are considered. It is shown that a bell-shaped shell rigidly fixed over its perimeter to the substrate presents a unique elastic- and quantum-mechanical object. First of all, the mechanical stress in the shell varies from a compression one around the contour to a tensile one at the bell apex.

In this work, within the framework of continuous elasticity theory a model for the self-formation of bell-shaped shells was proposed. Based on the constructed solution, both the shape of the self-formed nanoshell and the distribution of mechanical stresses and deformations in it were predicted. Next, the quantum theory of solid was invokes to predict, with allowance for the obtained distribution of mechanical stresses, quantum-confinement effects in this structure. In the present study, of our primary concern was the case of InAs/GaAs structures in which the bilayered film was detached from the substrate over a small local region of 50x50 nm for two thickness of the film 1.1 nm (4ML) and 3.9 nm. Such shells can also be obtained on a wide spectrum of other semiconductor materials.
Based on performed calculations, the possibility of using such bell-shaped shells in nanosensors is shown. Nanosensors analogous to already available microsensors [3,4], and also fundamentally new nanosensors based on quantum confinement of charge carriers in the shells, are considered.

With the example of InAs/GaAs systems, the possibility of preparation of such bell-shaped shells is experimentally shown. Estimates of the natural oscillation frequencies of the shells and the sensitivity to external forces and electric and magnetic fields are given.

Reference

[1] V.Ya. Prinz, V.A. Seleznev, A.K Gutakovsky, A.V. Chehovsky, V.V. Preobrazhensky, M.A. Putyato, and T.A. Gavrilova, Physica E, **6** 828 (2000).
[2] V.Ya. Prinz., Microelectronic Engineering 69 (2003) 466-475.
[3] Sensors, vol.7 (1994), Edited by W. Gopel, J. Hesse, J.N. Zemel., VCH Publishers Inc., New York, NY (USA).
[4] Sensors, vol.8 (1995), Edited by W. Gopel, J. Hesse, J.N. Zemel., VCH Publishers Inc., New York, NY (USA).

* Contact author: black-hawk@rambler.ru

On ZnO p-n junctions, characterizations and gas sensor applications

S. Basu*, S. K. Hazra
Materials Science Centre, Indian Institute of Technology, Kharagpur – 721302, India

It is known that compared to the conventional semiconductors like Si or GaAs the oxide semiconductor systems have strikingly complex surfaces and interfaces because the oxide surface structures are mostly irregular with cation or anion vacancies and other defects that distinguish the interface from the bulk. In spite of this the oxide thin films have recently attracted attention of the researchers for producing electronic and other devices for various important technological applications.

In this study we report on deposition of p-type ZnO thin films using an innovative CVD method on n-type ZnO films produced by conventional D. C Sputtering on glass substrates. The formation of ZnO p-n homojunctions has been studied by current-voltage characteristics [Xiong (Ref 1)]. The barrier height and the ideality factor for forward bias have been measured as a function of temperature. The barrier height at 300 °C and 400 °C are 1.38 (V) and 1.63 (V) respectively. The ideality factor was found to decrease with increasing temperature thereby showing an improvement of the junction property at higher temperature possibly due to reduction in defects. However, relatively higher ideality factor can be attributed to the defective oxide interfaces common with these types of materials.

The hydrogen sensor studies with these p-n junctions were conducted at 300 °C & 400 °C with 500 ppm & 1000 ppm H_2. Almost constant sensor signal was obtained for number of cycles of measurements in each case. The corresponding response times for two different hydrogen concentrations and two different temperatures are shown in the following table I.

Our separate studies with catalytic metal (Pd) contact showed further appreciable reduction in the response time. The response time has been reduced by using the catalytic metal contact due to quick splitting of the hydrogen molecule and the formation of hydrogen atoms, which readily diffuse towards the junction. It is also observed from the table that the response time is reduced considerably by increasing the temperature of measurements from 300 °C to 400 °C.

In conclusion, this is the first report on the gas sensor study with novel ZnO p-n homojunctions and the results are encouraging for further investigations.

Table: I

Temperature (°C)	Response time (seconds)			
	500 ppm H_2		1000 ppm H_2	
	p-ZnO/n-ZnO	Pd/(n-ZnO)/(p-ZnO)	p-ZnO/n-ZnO	Pd/(n-ZnO)/(p-ZnO)
300	296	150	238	150
400	139	70	150	50

References

[1] Gang Xiong, John Wilkinson, Brian Mischuck, S. Tuzemen, K. B. Ucer and R. T. Williams, Appl. Phys. Lett, **80(7)** 1195 (2002)

* Corresponding author: Email: sb@matsc.iitkgp.ernet.in (S. Basu)
sukumar_basu@yahoo.co.uk (S. Basu)

Synchrotron-Based Measurements of the Electronic Structure of Transition Metal Phthalocyanines

J. E. Downes[1,*], H. J. Trodahl[1], Y. Zhang[2], and K. E. Smith[2]
[1] *MacDiarmid Institute, Victoria University of Wellington, Wellington, NEW ZEALAND*
[2] *Department of Physics, Boston University, Boston, MA 02215, USA*

Organic semiconductors are the subject of intense study due to the challenge they pose to our understanding of the physical properties of complex solids and due to technological interest in developing carbon-based electronic devices[1]. Copper phthalocyanine (CuPc) is regarded as a prototypical organic semiconductor but, in fact, many other transition metal ions also form semiconducting phthalocyanine compounds. The phthalocyanine ligand has a complex electronic structure which is further complicated by the introduction of a transition metal ion into the system, such as Ni^{2+}. The overlap of the metal *3d* electronic states with ligand *2p* states within the molecule produces a combination of both localized and delocalized states near the Fermi level (E_F). Accurate determination of this electronic structure near E_F is of general importance in understanding the properties of organic semiconductors. Many photoemission studies have been undertaken to measure the electronic structure of phthalocyanine compounds, but it is important to appreciate that photoemission spectroscopy measures the electronic structure of an ionized system.

We report here a synchrotron radiation-excited resonant soft x-ray emission (SXE) spectroscopy study of the electronic structure near E_F of vacuum-deposited thin films of several transition-metal phthalocyanines. Where published calculations exist, our results are in excellent agreement with theory, but differ significantly from published x-ray emission and photoemission results. The organic films were discovered to be highly susceptible to synchrotron radiation beam damage. We successfully circumvented this effect by continuous translation of the films during measurement. Resonant SXE spectra from undamaged samples typically show spectral features near E_F that are not observed from damaged samples. For CuPc these states are predicted to exist, but have not previously been observed by either photoemission spectroscopy or soft x-ray emission spectroscopy[2]. Since it is the properties of the highest occupied molecular orbital (HOMO) states that are of most interest, the ability of resonant SXE to accurately measure these states is significant, as is our discovery that previously published SXE studies of organic semiconductors are dominated by beam damage effects. This application of resonant SXE has important consequences for the determination of band gap energies in organic molecular crystal systems, since it allows determination of the non-ionized electronic structure.

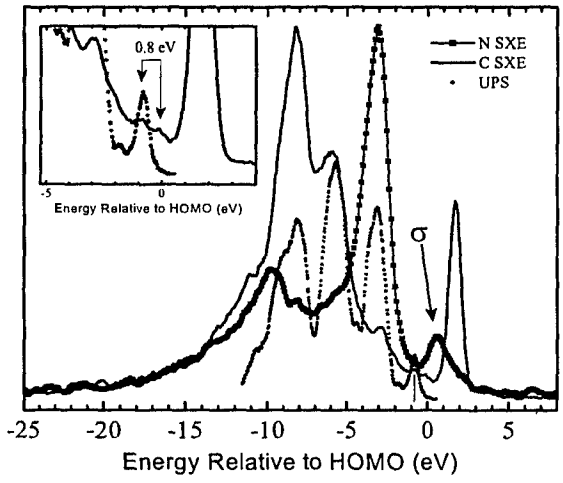

Figure 1 *Combined C and N x-ray emission, and ultra-violet photoemission spectroscopy results from CuPc thin films. The apparent shift of the HOMO state observed in the UPS spectrum is due to strong final state effects.*

References

[1] S. R. Forrest, J. Quant. Electron. **6**, 1072, (2000).
[2] J. E. Downes, C. McGuinness, P.-A. Glans, T. Learmonth, D. Fu, P. Sheridan, K. E. Smith, Chem. Phys. Lett. **390**, 203, (2004) .

* Contact author: james.downes@vuw.ac.nz

SESSION Th B3
MICRO- AND NANO-FABRICATION

Thursday 10 February 2005 1530–1645

Meeting Room V

Session Chair **Henry Smith, Massachusetts Institute of Technology, USA**

15.30 **Thermal lithography technique for nano scale structure fabrication**
Th B3.1 M. Kuwahara[1], J. Kim[2] and J. Tominaga[1]
[1] *National Institute of Advanced Industrial Science and Technology (AIST), Tsukuba, Japan*
[2] *Samsung Electronics Co. Ltd, Suwon City, Korea*

15.45 **Light-induced bending of photo-beams**
Th B3.2 D. Corbett and M.Warner
University of Cambridge, Cambridge, UK

16.00 **Controlled folding of nanopatterned membranes using the nanostructured origami™ 3D fabrication and assembly process**
Th B3.3 H.J. In, W. Arora, H.I. Smith, G. Barbastathis
Massachusetts Institute of Technology, Cambridge, USA

16.15 **Rubber stamp making process utilizing self-organized ordered meso-porous structure and its use for contact charge nanoparticle arrangements**
Th B3.4 T. Nagasawa, Y. Nakamura, H. Sasakura and I. Matsui
University of Tokyo, Tokyo, Japan

16.30 **Zone plate array optimization for maskless lithography**
Th B3.5 G. Barbastathis, R. Menon, and H. I. Smith
Massachusetts Institute of Technology, Cambridge, USA

Thermal Lithography Technique for Nano Scale Structure Fabrication

M. Kuwahara[1,*], J. Kim[2] and J. Tominaga[1]
[1] *Center for Applied Near-Field Optics Research (CAN-FOR), National Institute of Advanced Industrial Science and Technology (AIST), Tsukuba, Japan*
[2] *Digital Media R&D Center, Samsung Electronics Co., LTD, Suwon City, Korea*

We have proposed a new lithography technique for applying to optical disk mastering process. The technique, called as Thermal Lithography , allowed us to fabricate nano scale dots and isolated line [1-3]. The intensity of a focused laser beam spot has a Gaussian shape, accordingly, a temperature inside the spot is not uniform but has a distribution, in which the highest temperature area appears near the center of the spot. Using the area within more than a threshold temperature enables to generate a much smaller spot, which is adjusted by the laser power and the mobile speed of the spot. Figure 1 schematically shows this principle. Therefore, it becomes possible to confine physical or chemical thermal reaction just within the tiny area. We have attempted to produce dot and line by the combination of this technique and thermally cross-linked reaction of a photoresist film. Figure 2 shows the atomic force microscope (AFM) images of fabricated small dots (a) and isolated line (b) on lands of a polycarbonate optical disk substrate. Minute structures in approximately 100-nm dimension are clearly seen. In this experiment, the wavelength (λ) of the laser light and numerical aperture (NA) of an objective lens were 635 nm and 0.6, respectively. The diffraction limit estimated from the optics was $\lambda/2NA$ = 530 nm. We succeeded in fabricating further minute structures with one-fifth of the limit. We also tried other materials for producing a smaller structure and improving the reproducibility. We found that a sample consists of TbFeCo and ZnS-SiO_2 layers can induce mutual diffusion when they are heated up at more than a threshold. As a result, the volume increased [4]and a convex portion was generated on the sample surface. Figure 3 shows the top view AFM images of fabricated smallest dots (a) and our institute acronym by arranging dots (b) on SiO_2 flat disk substrate. A blue laser beam (λ=405 nm) and an objective lens with NA= 0.65 were used in this experiment. Smallest dot diameter reached approximately 50 nm, which was one-sixth of the diffraction limit, and letters within 1 μm square was successfully drawn. Furthermore, in this conference, we present further improvement of the dot fabrication performance using another sample structure, and the detailed images by cross-sectional transmitted electron microscope (TEM).

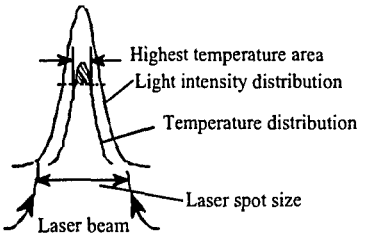

Figure 1 Distribution of light intensity and temperature inside a focused laser spot.

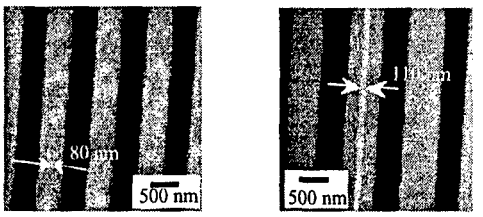

(a) (b)

Figure 2 Top view AFM images of dots (a) and an isolated line (b) in a photoresist.

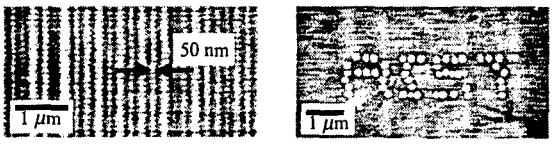

(a) (b)

Figure 3 AFM images of dots with 50 nm diameter (a) and drawn letter by arranging dots (b) in TbFeCo and ZnS-SiO_2 materials

References

[1] M. Kuwahara *et al.*, Jpn. J. Appl. Phys., **41**, L1022 (2002).
[2] M. Kuwahara *et al.*, Jpn. J. Appl. Phys., **43**, L1045 (2004).
[3] M. Kuwahara *et al.*, Microelectron. Eng., **73-74**, 69 (2004).
[4] J. Kim *et al.*, Appl. Phys. Lett., **80**, 2764 (2002).

* Contact author: kuwaco-kuwahara@aist.go.jp

Light-induced bending of photo-beams

D. Corbett* and M. Warner

Cavendish Laboratory, Madingley Road, Cambridge CB3 0HE, UK

New photo-responsive solids can reversibly change length by up to ~400% on illumination by visible or UV light over timescales ranging between milli-seconds to minutes. Device applications depend on understanding the problems we raise below.

Recently Ikeda *et al.* [1] demonstrated a directed bending of an elastomer film due to irradiation with plane polarised light. The film was a poly-domain, nematic liquid-crystalline network that crucially contained an azobenzene chromophore. Absorption of a photon at the correct wavelength (366nm) stimulates a *trans*→*cis* isomerisation which leads to a local length contraction along the nematic director where this happens to be along the light's electric vector. Attenuation of the light as it passes through the film sets up a differential length contraction through the thickness of the film, which results in bending. Figure 1 (Ikeda) shows: (a) the undeformed polymer film, (b) curling after illumination with plane polarised light of wavelength 366nm and (c) curling when the plane of polarisation is rotated by -45^0. White arrows show the direction of polarisation.

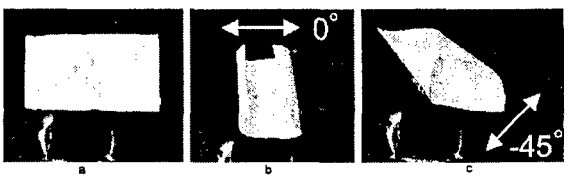

Fig. 1: (a) unilluminated film, (b)&(c) film illuminated with light polarised along the direction indicated.

The local curvature of such films has been calculated [2], a model we extend to the steady-state profiles adopted by a *finite* beam of such a material. Of crucial importance is the *trans* number density (n_{tr}) as a function of depth (z). We propose a dynamics for n_{tr} with depletion proportional to the intensity $I(z,t)$, itself a function of $n_{tr}(z,t)$ – hence non-linearities arise. Relaxation is characterised by a time scale τ, thus:-

$$\dot{n}_{tr}(z,t) = -\eta I(z,t) n_{tr}(z,t) + (n_0 - n_{tr}(z,t))/\tau.$$

Light falls obliquely on a curling beam and hence the effective $I(z,t)$ depends also on $\theta(s)$, the angle of a beam a distance s along its length. The local strain in the beam is related to the *cis* number density ($n_c = 1 - n_{tr}$). For very long times we reach a steady-state where the *trans* population remains fixed. The beam profile can be calculated analytically see figure 2(a). The beam never quite manages to reach 90^0 to the horizontal. In contrast (b) corresponds to $t/\tau << 1$, the back reaction has not yet set in and curvature is accumulated from light absorbed at earlier times and obliquity of the beam. The beam manages to pass 90^0 and shading of the lower beam by the upper section becomes important.

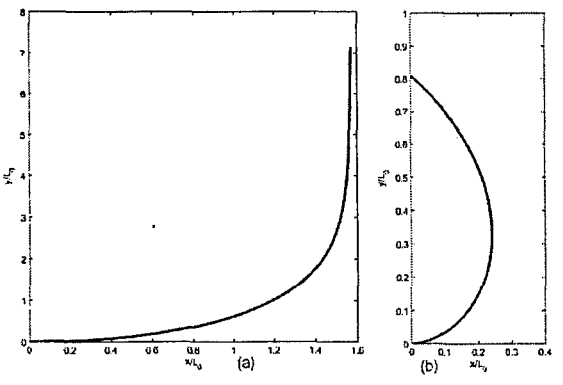

Fig. 2: The beam profile within two time regimes: (a) for $t/\tau >> 1$, in this case L_0 is simply a characteristic length, (b) for $t/\tau << 1$, in this case L_0 can be identified with the initial length of the beam.

References

[1] T. Ikeda et al., *Nature* **425**, 125 (2003).
[2] M. Warner and L. Mahadevan, *PRL* **92(13)**, 134302 (2004).

*Contact author: dc243@cam.ac.uk

Controlled Folding of Nanopatterned Membranes Using the Nanostructured Origami™ 3D Fabrication and Assembly Process

Hyun Jin In[1,*] Will Arora,[2] Henry I. Smith,[2] George Barbastathis[1]
[1] *Department of Mechanical Engineering*
[2] *Department of Electrical Engineering and Computer Science, Massachusetts Institute of Technology, Cambridge, MA 02139, USA*

The Nanostructured Origami™ 3D Fabrication and Assembly Process is a technique for fabricating and assembling three-dimensional (3D) nanosystems. In a process that depends solely on conventional fabrication tools, a two-dimensional (2D) membrane is first patterned with various micro- and nanoscale features and then folded into the desired 3D shape [1].

Nanopatterned membranes made of both silicon [1] and SU-8 [2] have been fabricated and folded successfully (Fig. 1). To eliminate the need for manual assembly, Lorentz force and stressed metal actuation methods are used. In the Lorentz force method, gold wires patterned on the 2D membranes act as current carrying loops, and in the presence of an external magnetic field provide an upward force. The stressed metal method relies on bi-layer hinges that curl with a controllable radius of curvature (Fig. 2). Folding of more complex 3D shapes, such as multi-layer stacking devices and corner cubes, is demonstrated using a new fabrication process. In addition, rigid membranes are patterned to demonstrate functionality and folded into over ten different origami shapes.

Alignment precision among the folded layers is crucial in applications such as 3D photonic crystal fabrication. In this case, nanometer-scale precision must be achieved in both layer-to-layer spacing and lateral alignment of the folded layers. Pyramidal alignment features fabricated via anisotropic etching have demonstrated sub-micron spacing and alignment precision [2]. To push the resolvable level of precision beyond the resolution of the optical microscope, moiré and vernier patterns are incorporated into the device for improved alignment characterization. Proposed diffraction-based techniques will provide even greater levels of precision.

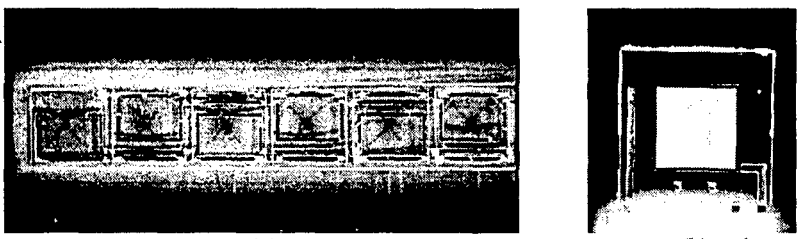

(a) (b)

Figure 1 *Top views of (a) 6-layer, Lorentz force actuated SU-8 device before folding and (b) 3-layer SU-8 device after folding.*

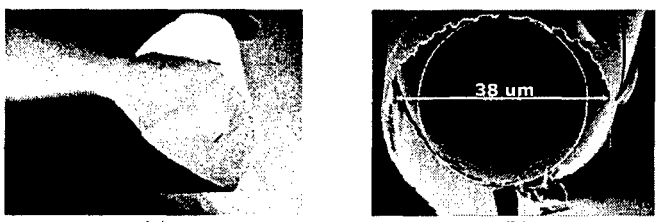

(a) (b)

Figure 2 *Strain induced curling of chromium / silicon nitride bilayer: (a) Timed underetch resulting in 180 degree fold; (b) Full curl radius of 19μm matches well with theory.*

References

[1] S. M. Jurga *et al.*, in *Proceedings of the 3rd IEEE Conference on Nanotechnology, 2003*, p. 220.
[2] H. J. In *et al.*, in Proceedings of the 4th IEEE Conference on Nanotechnology, 2004 (to be published).

* Contact author: hji@mit.edu

Rubber stamp making process utilizing self-organized ordered meso-porous structure and its use for contact charge nanoparticle arrangements

Tazumi Nagasawa*, Yoshiaki Nakamura, Hideshi Sasakura & Isao Matsui
Japan Chemical Innovation Institute,
Department of chemical system engineering, University of Tokyo, Hongo7-3-1, Bunkyo-ku, Tokyo, Japan

Nanoparticle arrangements in the micrometer or sub-micrometer range on a substrate enable the fabrication of photonic or quantum electronic devices. Many approaches to create nanoparticle arrangements on a substrate have been performed. Rubber stamp contact methods have been widely studied and are known as soft lithography process. In almost all cases, the stamp was molded out of silicone rubber, where the silicone rubber was put into lithography patterned silicon substrate. Essentially the rubber stamp would not go beyond the lithography resolutions. We previously reported the nanoparticle arrangement from the gas phase by use of the rubber stamp contact charge dry process [1], where we used lithography patterned silicone rubber as a stamp material to obtain both large contact charge density and parallel line arrangements over an entire substrate at one time. Here we show a non-lithography method for making less than 300 nm resolution rubber stamps and nanoparticle patterning results from the newly developed rubber stamp.

We utilised the self-organized ordered mesoporous structure in place of lithography. The process for the rubber stamp making is as follows;

1. nanoparticle solution, which contains several nanometer size silica particles, 500 nanometer size polystyrene particles and TEOS(tetra ethoxy silane), was spin-coated on the substrate,
2. self-organization of nanoparticle arrangements occurred and hexagonal packed polystyrene particle array imbedded in silica particles was obtained,
3. after drying, polystyrene particles were incinerated and ordered mesoporous structure was established on the substrate,
4. silicone rubber material was put onto the substrate,
5. the substrate was annealed and the rubber stamps were peeled away from the substrate.

By utilizing 500 nanometer size polystyrene, we succeeded in making the ordered less than 300 nanometer size hemispherical silicone dot array with about 500 nanometer pitch as shown in Fig..

The above developed rubber stamp was used for electric charge patterning on the acrylic resin substrate. The substrate surface was entirely negatively-charged by a conventional corona discharger, where the surface potential obtained was set by the applied voltage to the corona discharger. And then the rubber stamp was pressed onto the substrate for contact charging. The stamp contact areas on the substrate were positively charged. The charge intensity was determined by contact pressure. Negatively charged 50 nm size polystyrene particles from the gas phase were fed onto the acrylic resin substrate. Array of particle islands, consisting of a few to several particles, with 500 nanometer pitch was arranged on the substrate, where the apparent stamping pressure was set at about 50 kPa and the surface potential of negatively pre-charged area was set at about several 100 negative volts. The stamping pressure and the intensity of negative pre-charge were shown to have crucial effects on the resolution of the nanoparticle arrangements.

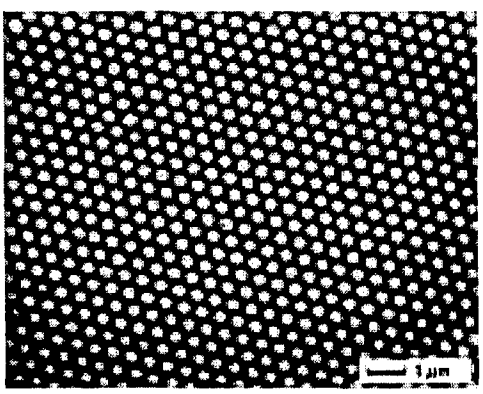

Fig. Newly developed rubber stamp

(This research is financially supported by New Energy and Industrial Technology Development Organization.)

References

[1] Hiraoka etal., MRS 2003 fall meeting M5.3.

* contact author: tazumi@chemsys.t.u-tokyo.ac.jp

Zone plate array optimization for maskless lithography

George Barbastathis[1,*] Rajesh Menon,[2] and Henry. I. Smith[2]
[1] *Department of Mechanical Engineering*
[2] *Department of Electrical Engineering and Computer Science*
Massachusetts Institute of Technology, Cambridge, MA 02139, U.S.A.

Zone plate array lithography (ZPAL) [1] eliminates the need for costly and time-consuming to manufacture masks, while simplifying the optics and improving lithographic quality. ZPAL functions in dot-matrix printer fashion as follows: An array of zone plates is placed one focal distance away from the substrate. Each zone plate is individually addressed by a spatial light modulator. Thus, arbitrary dot-illumination matrices are generated. With a precise scanning stage, the die surface is patterned in its entirety. The Fresnel zone plates are transmission binary diffractive optical elements fabricated with numerical apertures as high as 0.85 using e-beam lithography. An additional benefit of the dot-matrix approach is that the image is formed incoherently; therefore, diffraction artefacts such as ringing are absent. ZPAL has been used experimentally to demonstrate features smaller than 200nm using 400nm wavelength illumination. Quantitative comparison has shown that ZPAL performs better than an equivalent projection lithographic tool with resolution factor of k_1=0.32 [2].

Here we report on the optimization of zone plates for lithographic performance. We present two approaches, (1) virtual phase-shift masking (VPSM) and (2) phase apodization (PA). VPSM is inspired by the phase-shift mask technique which is commonly used in microscopy and optical projection lithography to control the size and phase profile of the point-spread function (PSF). Usually, one optimizes the lateral shape of the PSF in terms of narrowness or depressed side-lobes. To apply this method to ZPAL, we place a phase-shift ring in the common path of the optical beams leading to the zone-plate array, such that the ring is imaged onto the arrays with a slight defocus. The defocused field produced by the ring interferes with the field diffracted by the zone plate, and the PSF narrows as result. An example of the ring's effect is shown in simulation in Figure 1. Instead of using a real ring, the effective field produced by the ring can be modulated on the zone plate itself – hence the name "virtual" PSM. The PA method also modulates the zone plate, i.e. the phase delay introduced by successive zones is not fixed to π, but it is determined by the apodization function. Traditional choices are Gaussian, sinusoidal, etc. Figure 2 shows typical simulation results obtained with Gaussian PA. Non-traditional phase profiles, e.g. cubic-phase modulation may be used to control the longitudinal features of the PSF, such as depth of focus. The ease of manipulating the PSF via modulation of the diffractive element is compelling for using ZPAL in advanced mask-less lithography systems.

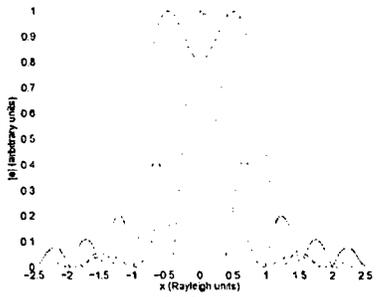

Figure 1 *Virtual phase-shift masking (solid line: unmasked; dashed: ring image; dot-dashed: VPSM aerial image).*

References

[1] H. I. Smith, J. Vac. Sci. Technol. B **14**, 4318 (1996).
[2] D. Gil, R. Menon, and H. I. Smith, J. Vac. Sci. Technol. B **21**, 2810 (2003).

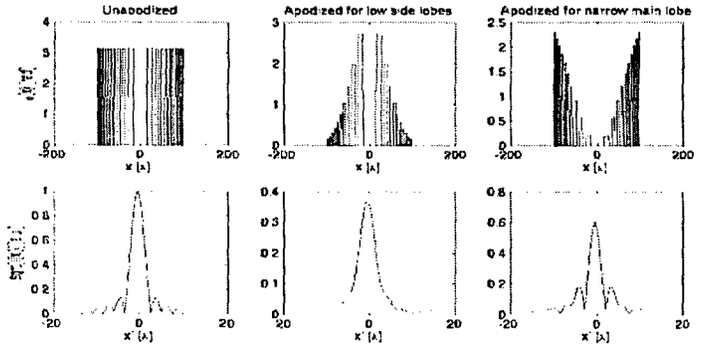

Figure 2 ***Phase apodization (top row: phase profile of the zone plate, bottom: cross-section of the radially symmetric PSF; left column: unapodized, center: apodized for small side lobes, right: apodized for narrow main lobe.)***

* Contact author: gbarb@mit.edu

SESSION Th C3
ORGANIC ELECTRONICS AND PHOTOVOLTAICS

Thursday 10 February 2005 1530–1645

Copthorne I

Session Chair **Keith Gordon, University of Otago, NZ**

15.30 **Improving photovoltaic performance of P3OT:fullerene bulk heterojunction solar cells with Na doped BCP/Al electrode**

Th C3.1 C. Lee [1], I. Yoo [2], J.Y. Kim[3], D.W. Kim [3] and D.H. Hwang[4]
[1] *Seoul National University, Seoul, Korea.*
[2] *Inha University, Incheon, Korea.*
[3] *Samsung SDI, Kongseri, Yongin, Kyungki, Korea.*
[4] *Kumoh National Institute of Technology, Kumi, Korea.*

15.45 **Excited state structures in terthiophene oligomers: a spectroscopic and computational study.**

Th C3.2 K.C. Gordon[1], S. MacArthur[1], T.M. Clarke[1], D.L. Officer[2] and P. Wagner[2]
[1] *University of Otago, Dunedin, NZ*
[2] *Massey University, Palmerston North, NZ*

16.00 **New p- and n-type conjugated materials for organic solar cells**

Th C3.3 J. Li, F. Dierschke, J. Jacob, M. Kastler, A.C. Grimsdale and K. Müllen
Max-Planck-Institute for Polymer Research, Ackermannweg, Germany

16.15 **Synthesis and electrochemical behaviour of styryl-substituted oligothienylenvinylens as materials for electrooptic purpose**

Th C3.4 P. Wagner, W. M. Campbell, A. M. Ballantyne and D. L. Officer
Massey University, Palmerston North, NZ

16.30 **Three dimensional molecular circuits from photosynthetic complexes**

Th C3.5 M.A. Baldo and M. Segal
Massachusetts Institute of Technology, Cambridge, USA.

Improving photovoltaic performance of P3OT:fullerene bulk heterojunction solar cells with Na doped BCP/Al electrode

Changhee Lee [1*], Insun Yoo [2], Ji-Young Kim [3], Dae-Won Kim [3], Do-Hoon Hwang [4]
[1] *School of Electrical Engineering and Computer Science and Nano Systems Institute National Core Research Center, Seoul National University, Seoul 151-744, Korea*
[2] *Department of Physics, Inha University, Incheon 402-751, Korea*
[3] *Samsung SDI, Kongseri, Yongin, Kyungki, 449-902, Korea*
[4] *Department of Applied Chemistry, Kumoh National Institute of Technology, Kumi 730-701, Korea*

Organic solar cells with active layers consisted of donor-acceptor (D-A) bulk heterojunctions have been a recent research focus due to their potential advantages of low cost fabrication, flexibility, and large area. Very efficient photoinduced electron transfer in a conjugated polymer and fullerene blend system results in enhanced charge-carrier generation [1]. Another essential factor for the enhancement of solar energy conversion is the carrier extraction efficiency at the electrode interfaces [2]. It has been demonstrated that the insertion of LiF between organic layers and Al electrode enhances the open-circuit voltage (V_{oc}) and short-circuit current density (J_{sc}) [3].

In this work, we study the effect of the n-type doping at the organic/Al electrode interface on the photovoltaic properties of solar cells with poly(3-octylthiophene) (P3OT):fullerene (C_{60}) blends. P3OT is the electron donor and C_{60} is the electron acceptor. The n-type doping layer is prepared by doping Na metal into bathocuproine (BCP) layer. The cell with the Na-doped BCP layer, ITO/PEDOT:PSS/P3OT:C_{60}/BCP:Na/Al, exhibits larger V_{oc} and J_{sc} compared with the cell without the doping layer, ITO/PEDOT:PSS/P3OT:C_{60}/BCP/LiF/Al. The solar cell performance is V_{oc}~0.42 V, J_{sc}~28 A/m^2 and the power conversion efficiency of η~2.1 % under monochromatic photoexcitation of about 2 mW/cm^2 at 490 nm. The increased solar cell performance can be attributed to lowering the series resistance of the cell by the insertion of Na-doped BCP layer at the organic/Al interface, which thereby increases the solar energy conversion efficiency.

Acknowledgments
We gratefully acknowledge the funding from the Korean Ministry of Science and Technology (M1-0213-27-0002-03-B15-27-002-12) in republic of Korea.

References

[1] C. H. Lee, G. Yu, D. Moses, K. Pakbaz, C. Zhang, N. S. Sariciftci, A. J. Heeger, and F. Wudl, Phys. Rev. B **48**, 15425 (1993).
[2] V. D. Mihailetchi, L. J. A. Koster, and P. W. M. Blom, Appl. Phys. Lett. **85**, 970 (2004).
[3] C. J. Brabec, S. E. Shaheen, C. Winder, N. S. Sariciftci, and P. Denk, Appl. Phys. Lett. **80**, 1288 (2002).

* Contact author: chlee7@snu.ac.kr

Excited state structures in terthiophene oligomers: a spectroscopic and computational study.

Keith C. Gordon[1*], Sam MacArthur[1], Tracey M. Clarke[1], David L. Officer[2] and Pawel Wagner[2]
[1] *MacDiarmid Institute for Advanced Materials and Nanotechnology, University of Otago, Department of Chemistry, Union Place, Dunedin, NEW ZEALAND*
[2] *MacDiarmid Institute for Advanced Materials and Nanotechnology, Nanomaterials Research Centre, IFS - Chemistry, Massey University, Palmerston North, NEW ZEALAND*

Electroluminescent materials using conducting polymers have been widely studied for over a decade. The utility of these materials is based on their ease of processing and the ability to tune properties such as emission colour. We have studied a series of terthiophene-based compounds in which the terthiophene units are covalently attached to distyrylbenzene species. These are highly emissive materials and as well as characterising these emissive properties, we have used computational chemistry, namely density functional theory, to gain insight into the charge-transport properties of these compounds. Substituents on the distyrylbenzene units have a profound affect on the nature and extent of the molecular orbitals. The nature of these molecular orbitals controls the charge-transport and emissive properties of the bulk material.

Terthiophene species are a versatile class of conducting polymers because they can be readily functionalised, have good p-type semiconductor properties, and have relatively good stability in air for both the neutral and oxidised states.[1,2]

We are interested in understanding the properties of substituted thiophene species in terms of their optical, electro-optical and electronic structure properties. These may be investigated using spectroscopic methods and computational chemistry. The compounds we report in this study are based on thiophenes and the highly emissive distyryl-benzene unit and are shown in Scheme 1.

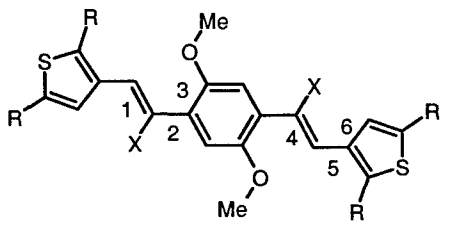

Figure 1. ThioDSB, R=X=H; ThioCNDSB, R=H, X=CN; TerthDSB, R=thiophene, X=H; TerthCNDSB, R=thiophene, X=CN. The numbers 1-6 label adjacent bonds in the structure representing the critical dihedral angles.

In order to determine the predictive usefulness of the computational chemistry we compared the vibrational spectra of the materials of interest to the calculated spectra. As the compounds are conformationally flexible it was necessary to establish the favoured conformers using conformer search methods. It was also instructive to examine the thio-DSB and thio-CN-DSB materials as these are conformationally less complex and the vibrational spectra are simpler to interpret. The terth-DSB and therth-CN-DSB compounds were also used as a component in the fabrication of electroluminescent panels.

References

[1] G. Daminelli, J. Widany, A. Di Carlo and P. Lugli, J. Chem. Phys. **115,** 4919 (2001).
[2] J. Roncali, Chem. Rev. **92,** 711 (1992).

* Contact author: kgordon@alkali.otago.ac.nz

New P- and N-Type Conjugated Materials for Organic Solar Cells

Jiaoli Li, Frank Dierschke, Josemon Jacob, Marcel Kastler, Andrew C. Grimsdale,* and Klaus Müllen
Max-Planck-Institute for Polymer Research, Ackermannweg 10, 55128 Mainz, Germany. Tel.: +49 6131 379317, Fax: +49 6131 379100. E-mail: grimsdal@mpip-mainz.mpg.de

New p- and n-type materials have been prepared and tested in organic solar cells. Two new types of electron donors are reported. New hexa-substituted hexa-*peri*-hexabenzocoronene (HBC) derivatives **1** have been made with substituents which lower their isotropisation temperature and thus maximise their processability from solution. New ladder-type carbazoles **2** and **3** have been synthesised[1] in which the nitrogen atoms significantly enhance the electron-donating properties as confirmed by CV measurements. As novel electron acceptors we have prepared materials based on a new pentaphenylene diketone **4** [2] which is shown by CV to have good electron-accepting properties. We report the results from solar cells using these materials in comparison with existing n- and p- type materials. Devices with external quantum efficiencies above 15% and power efficiencies of over 0.5% have been constructed. The performance of solar cells using blends of these materials of various compositions are reported and the results correlated with the morphology of thin films of the blends as seen by AFM.

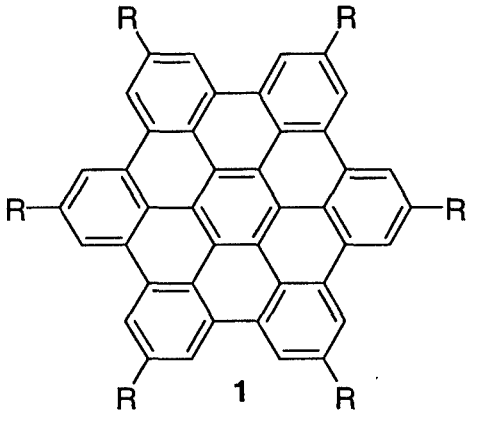

1

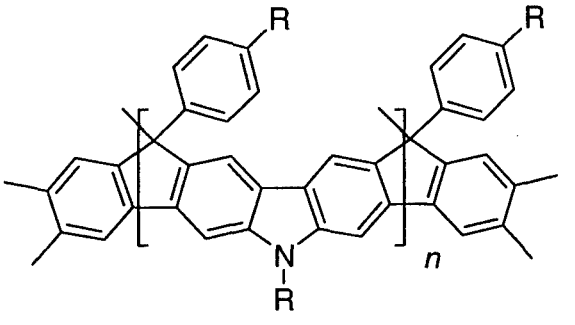

2

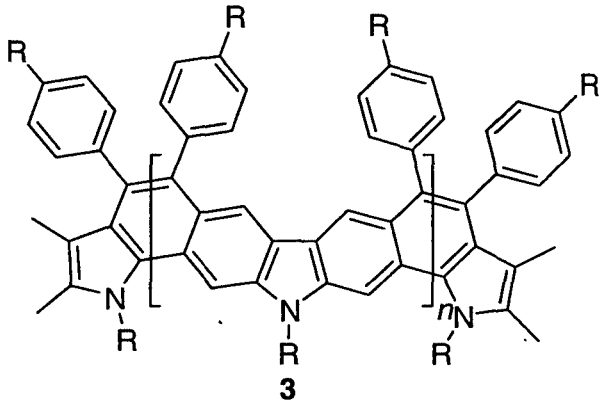

3

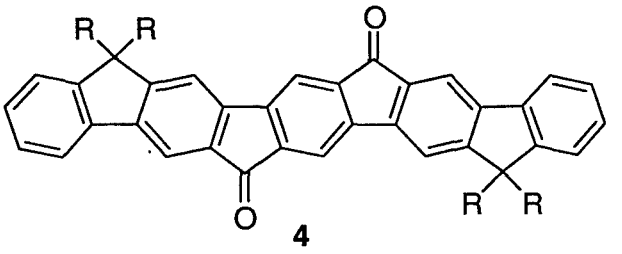

4

References

[1] F. Dierschke, A. C. Grimsdale, K. Müllen, Macromol. Chem. Pnys. 205 (2004) 1147.
[2] J. Jacob, S. Sax, T. Piok, E. J. W. List, A. C. Grimsadle, K. Müllen, J. Am. Chem. Soc. 126 (2004) 6987.

Synthesis and Electrochemical Behaviour of Styryl-substituted Oligothienylenvinylens as Materials for Electrooptic Purpose

Pawel Wagner, Wayne M. Campbell Amy M. Ballantyne and David L. Officer

Nanomaterials Research Centre, Institute of Fundamental Sciences,Massey University, Private Bag 11 222 Palmerston North, New Zealand

Linear π-conjugated molecules or oligomeric and polymeric material based on thiophenevinylene unit (PTV) are the focus of extensive research interest for their potential application in the field of optoelectronic devices such as diodes, non-linear optics or nanowires.[1] Oligomers based on the thienylenevinylene unit, due to the lower aromaticity of the system have better electronic properties compared to the conventional polythiophene materials.

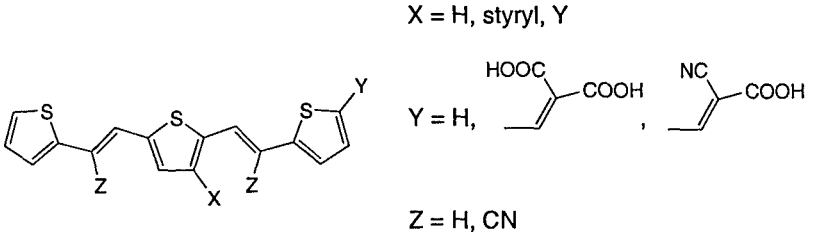

Scheme 1

In order to investigate a variety of functionalized thienylenevinylene oligomers, a convenient method of synthesis of a wide range of 3 and 5'-substituted and 2,5-bis(2-thienylvinyl)thiophenes has been developed (Scheme 1). The functionality at the 3-position of the thiophene moiety can play two different roles namely it can be involved as a binding bridge to adsorb the molecule onto surfaces such as TiO_2 or used to attach chromophore, changing or the improving absorption characteristic of the resulting system. The potential applications of these oligomers will be discussed.

References

[1] . Roncali, *Chem. Rev.* **1997** (*97*), 173-205.

Three Dimensional Molecular Circuits From Photosynthetic Complexes

M.A. Baldo
MIT, Dept. of Electrical Engineering and Computer Science, Cambridge, MA 02138, USA

Perhaps the only existing examples of functional molecular circuits are self-assembled by organisms in three dimensional complexes of molecules and protein scaffolding. Evolved over millions of years in plants and bacteria, these biological protein-molecular complexes rely on a unique architecture that allows the positioning of molecules in three dimensions with sub-nanometer control. In biology these circuits participate in photosynthesis, guiding optically excited molecular states, generating charge, and then guiding current flow.

We describe the engineering of such archetype molecular circuits for electronic applications and also their integration with solid-state semiconductors and contacts, a crucial first step in the more general use of this fabrication scheme. In the figure below, we demonstrate the solid-state integration of reaction center complexes from *R. sphaeroides* by matching their absorption spectrum with the photocurrent spectrum of an integrated device.

We will also report on the characterization of reaction center complexes in three terminal field effect transistors.

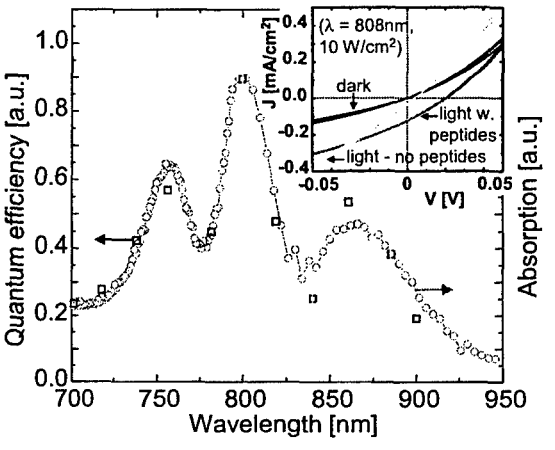

The photocurrent spectrum of solid-state photovoltaic devices employing bacterial reaction centers (RCs). A comparison between the photocurrent spectrum of solid-state (■) and wet electrochemical cell devices (□), and the solution absorption spectrum of the bacterial reaction centers (–o–), demonstrates that the observed photocurrent originates in the reaction centers. ***Inset****: stabilization of reaction center complexes with A_6K/V_6D peptides improves the internal quantum efficiency of the devices to 12% under short circuit conditions.*

SESSION Th D3
NANOSTRUCTURED METALS AND METAL ALLOYS

Thursday 10 February 2005 1530–1645

Copthorne II

Session Chair **Jim Metson, University of Auckland, NZ**

15.30 **Morphology and electrochemical properties of self-organizing low density mesoporous WO_3 films prepared by electrodeposition**

Th D3.1 B. Yang, H. Li, M. Blackford and V. Luca
Australian Nuclear Sciences & Technology Organization, Lucas Heights, Australia

15.45 **Nanoscale coatings of $AuAl_x$ and $PtAl_x$ and their mesoporous elemental derivatives**

Th D3.2 M. B. Cortie[1], A. Maaroof[1], G. B. Smith[1], P. Ngoepe[2].
[1] *University of Technology, Sydney, Australia*
[2] *University of the North, Sovenga, South Africa*

16.00 **Microstructure development and mechanical properties of alumina-titanium aluminide interpenetrating composites**

Th D3.3 C.Z. Han[1,2], I.W.M. Brown[1], D.L. Zhang[2]
[1] *Industrial Research Ltd, Lower Hutt, NZ*
[2] *University of Waikato, Hamilton, NZ*

16.15 **Nanoscale surface properties of metals treated by electrochemical and physico-chemical methods**

Th D3.4 H. Nanjo[1], M. Fujimura[2], M. Nishioka[1], N.J. Laycock[3] and J. Onagawa[2]
[1] *National Institute of Advanced Industrial Science & Technology, Sendai, Japan*
[2] *Tohoku Gakuin University Chuo, Tagajo, Japan*
[3] *Industrial Research Ltd., Lower Hutt, NZ*

16.30 **Atomistic strain studies on a silver nanorod**

Th D3.5 S.W. Hla[1], H.J.P. van Midden[2], A. Prodan[2]
[1] *Ohio University, Athens, USA*
[2] *Jožef Stefan Institute, Ljubljana, Slovenia*

Morphology and Electrochemical Properties Self-organizing Low Density Mesoporous WO_3 Films Prepared by Electrodeposition

Bin Yang*, Huijun Li, Mark Blackford and Vittorio Luca
Australian Nuclear Sciences & Technology Organization
New Illawarra Road, Lucas Heights
NSW 2234, Australia

Lower density mesoporous tungsten trioxide (WO_3) films were deposited on ITO-glass and Ti foil cathodic substrates by electrodepostion. Electrolytes consisted of 50 mM of peroxy-tungstic acid, in 50:50 water;2-propanol with some sulfuric acid. The morphology of the films can be controlled by varying the sulfuric acid concentration of the electrolyte. Comparison of films deposited from electrolytes with different pH values (between 0.50 and 1.95) (Figure 1), it was possible to obtained the optimum condition of the deposition to achieve high quality mesoporous films with remarkable electrochemical and photochemical activity. The films were characterized by X-ray diffraction, SEM, TEM and cyclic voltammetry. We are presently investigating the performance of these films in a range of applications including, in the photoelectrolysis of water to produce hydrogen, as Li-ion battery electrodes and for the fabrication of solar cells. It is anticipated that the mesoporous structure created by nanoscopic particles will have enhanced functionality.

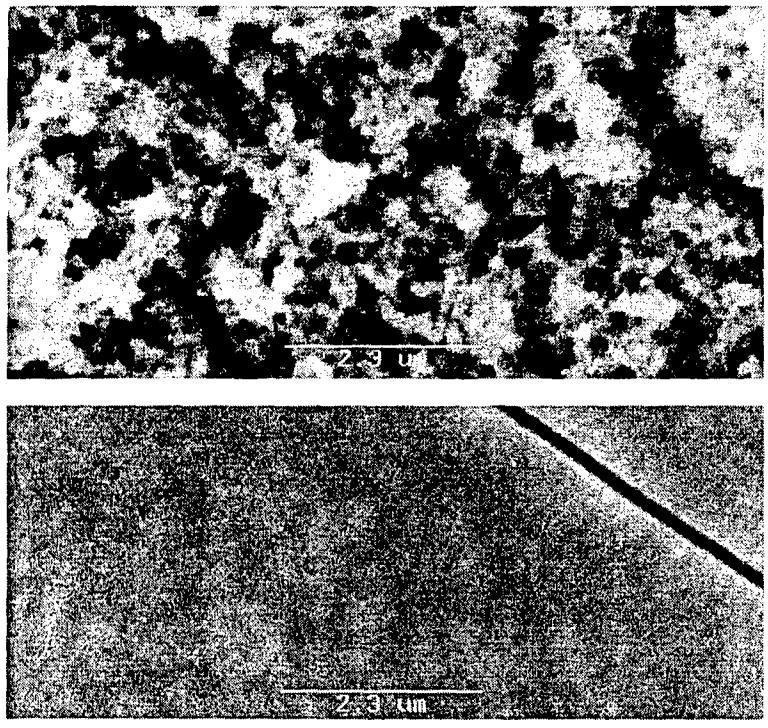

Figure 1. The SEM imagines of the films prepared cathodically from the electrolytes with (top) and without (bottom) adding sulfuric acid.

References.

(1) S.H. Baeck, T. Jaramillo, G.D. Stucky and E. W. McFarland; Nano letters 2(8):831 (2002)
(2) E. A. Meulenkamp; J. Electrochem. 144(5) 1664 (1997)

* Contact author: byz@ansto.gov.au

Nanoscale Coatings of $AuAl_x$ and $PtAl_x$ and their Mesoporous Elemental Derivatives

M.B. Cortie[1,*], A. Maaroof[1], G.B. Smith[1], P. Ngoepe[2]
[1] *Institute for Nanoscale Technology, University of Technology Sydney, AUSTRALIA*
[2] *Materials Modelling Center, University of the North, P/Bag X 1106, Sovenga, 0727, SOUTH AFRICA*

The compounds $AuAl_2$ and $PtAl_2$ have the cF_{12} (CaF_2) structure and, like most other intermetallic compounds with this lattice, are highly coloured. $AuAl_2$ is bright purple whereas $PtAl_2$ is yellow. Both substances have been previously investigated for application in jewellery on account of their content of precious metals [1,2], and as precursors for catalysts analogous in preparation to Raney nickel [3]. However, due to the high value of Au and Pt, nanoscale coatings of these compounds may have better possibilities for technological development. We have prepared such coatings using vacuum co-deposition of the elements, using a process that leads directly to formation of the intermetallic compound without the necessity for subsequent heat treatment. The colours of the coatings are similar to those of the bulk phases, suggesting that they may have decorative applications too. However, the coatings may also be de-alloyed in acid or base to produce mesoporous films of gold or platinum with other possible uses. Such films are catalytically active, have interesting optical properties, are resistant to oxidation, and exhibit high electrochemical capacitance. The transmission of light through glass coated with a sponge derived from $AuAl_2$ is examined, and it is found that it has an unusual dispersion relation, with the performance in the infra-red in particular being non-metallic in nature. Models for the transmission (mesoporous Au) and reflection ($AuAl_2$) spectra were developed, which will facilitate future work on these materials. The electrochemical capacitance obtainable from mesoporous coatings of Au was found to be of the order of $2x10^{-3}$ F/cm^2 which is about 50 times greater than that obtainable from bulk gold. However, the electrochemical behaviour of the gold surfaces is complex, and the active surface area of the coatings may be increased or decreased by appropriate cyclic variations in applied voltage (Fig.1).

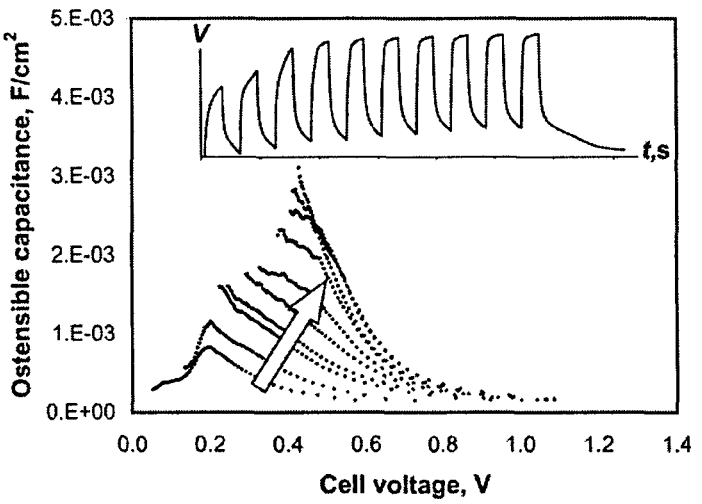

Figure 1. Effect of voltage cycling on the ostensible capacitance of a prototype electrochemical capacitor based on mesoporous Au coatings

References

[1] C. Cretu and E. van der Lingen , Gold Bulletin, **32**(4), 115 (1999).
[2] J. Hurly and P.T. Wedepohl, J. of Materials Science, **28**(20), 5648 (1993).
[3] M.B. Cortie, E. van der Lingen and G. Pattrick, in Proc. Asia Pacific Nanotechnology Forum, Cairns, 19-21st November 2003, World Scientific, Singapore, pp.79-82 (2004).

* Contact author: michael.cortie@uts.edu.au

Microstructure development and mechanical properties of Alumina-Titanium Aluminide interpenetrating composites

Ching Zen Han[1,2], Ian W. M. Brown[1], D. L. Zhang[2]
[1]*Industrial Research Limited, Lower Hutt, New Zealand*
[2]*Department of Materials and Process Engineering, The University of Waikato, Private Bag 3105, Hamilton, New Zealand*

Interpenetrating phase Al_2O_3-Ti_3Al composites have been fabricated by reaction sintering of discus milled composite powder containing Al and TiO_2 using carefully controlled heat-treatment in non-oxidizing atmospheres. Pressureless sintering and hot pressing of the powders has been carried out under vacuum and argon at temperatures between 1278°C and 1500°C and a heating rate of 5°C/min. Densification of the composites was investigated as a function of temperature. It was shown that higher bulk density and lower apparent porosity were obtained by hot pressing compared to pressureless sintering.

The microstructure development and mechanical properties of dense Al_2O_3-Ti_3Al composites fabricated by hot pressing of Al-TiO_2 powder blends were examined. Fully dense microstructures could only be achieved by pressureless sintering at 1480°C under argon, whereas hot pressing experiments showed that dense composites were produced at 1380°C under vacuum. Fig. 1 shows the microstructure of a fully densified composite in which the Al_2O_3 grains are embedded in the Ti_3Al matrix. The phases are continuous and hence exhibit an interpenetrating network, which is expected to enhance the mechanical properties. The increase of Vickers hardness was observed with the increase of temperature, which can be attributed to the increase of density and the decrease of the level of porosity of the composites. Both the biaxial strength and the elastic modulus increase with increasing temperature.

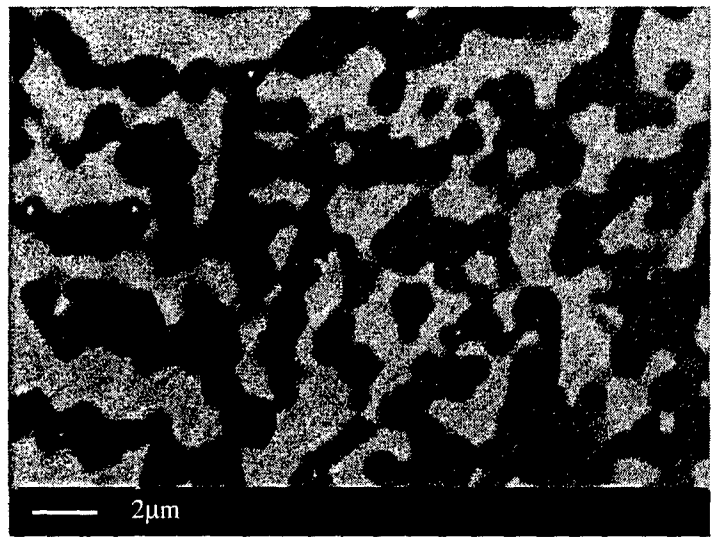

Fig. 1. Microstructure of fully densified Al_2O_3-Ti_3Al composite

References

1 C. Z. Han, I. W. M. Brown, D. L. Zhang, "Consolidation and properties of a Ti_3Al/Al_2O_3 advanced composite material", Proceedings of the 8th Engineering and Technology Postgraduate Conference, Hamilton, New Zealand, p17-22 (2001)
2 C. Z. Han, I. W. M. Brown, D. L. Zhang, "Effect of powder characteristics on microstructural development in bodies produced by pressureless sintering of Al/TiO_2 composite powder", Materials Science Forum, Vols. 437-438., p173–176 (2003)
3 C. Z. Han, I. W. M. Brown, D. L. Zhang, "Effect of powder characteristics on the solid state reactions and sintering of Al/TiO_2 composite powder", Proceedings of Joint SCENZ/FEANZ/SMNZI Conference, Hamilton, New Zealand, p44-48 (2004)

[1] c.zenhan@irl.cri.nz

Nanoscale Surface Properties of Metals Treated by Electrochemical and Physico-Chemical Methods

H. Nanjo[1,*], M. Fujimura[2], M. Nishioka[1], N. J. Laycock[3] and J. Onagawa[2]
[1] *Laboratory for Membrane Chemistry, National Institute of Advanced Industrial Science and Technology (AIST), 4-2-1, Nigatake, Miyagino-ku, Sendai 983-8551, JAPAN*
[2] *Tohoku Gakuin University 1-13-1, Chuo, Tagajo 985-8537, JAPAN*
[3] *Industrial Research Ltd., PO Box 31-310, Lower Hutt, NEW ZEALAND*

After passivating electrochemical treatments, the nanoscale structure of metallic surfaces gradually becomes stable, on a time scale of about one minute [1]. It is suggested that the electrochemical treatment causes rapid anodic processes such that the initial surface structure just after the treatment is amorphous and includes water or oxide-terminated hydroxyl groups, and that the surface structure then gradually relaxes from an amorphous to crystalline state. However, complete surface crystallization is sterically hindered and so only partially crystalline surfaces are observed in experimentally feasible timescales. Previous attempts to produce atomically flat crystalline surfaces through anodic passivation after cathodic reduction of the air formed surface oxide film have been unsuccessful [2]. However, it is known that UV irradiation of some metals can increase the breakdown potential for pitting corrosion [3], which may be at least partly due to a reduction in the number density of surface defects in the protective passive film. Consequently, we have recently begun to investigate the influence of UV irradiation on the surface structure of electrochemically passivated metals.

In this presentation we describe experiments in which a sample of pure iron is electrochemically treated at cathodic potentials and then passivated at 800 mV vs. Ag/AgCl in a mildly alkaline borate buffer solution. After this passivation, the sample is irradiated in air by UV light with a wavelength of 254 nm and an intensity of 3 mW/cm^2. Following this treatment, the sample surface is observed with scanning tunnelling microscopy and spectroscopic ellipsometry, and the protective properties of the passive film are evaluated with electrochemical methods such as open circuit potential decay and cyclic voltammography.

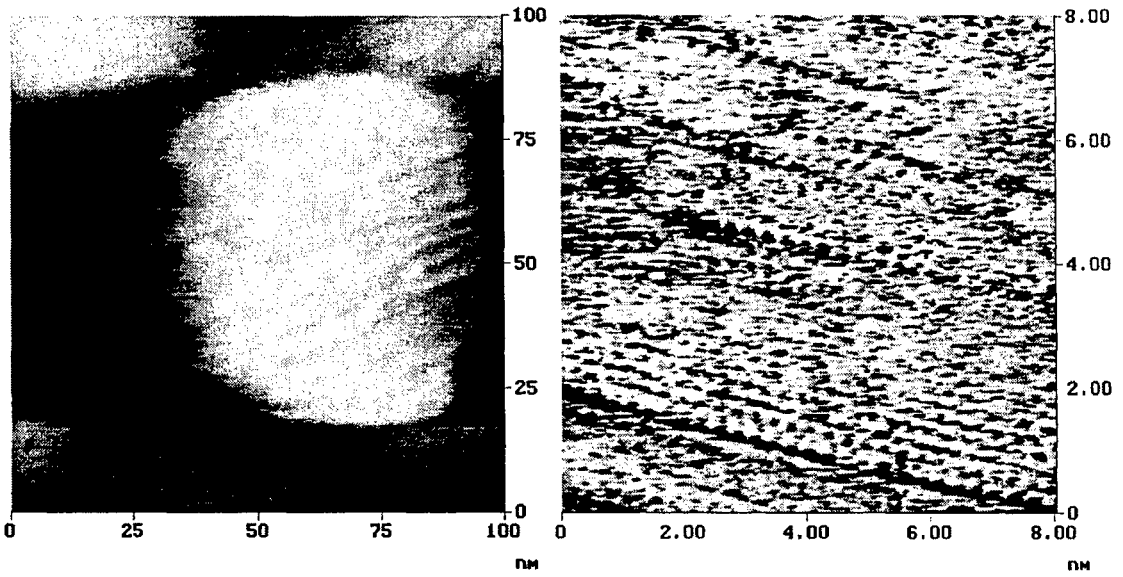

Figure 1: The surface of an entire surface oxide grain, showing a step-terrace structure at the atomic scale (left) and an atomic-resolution image of isolated monatomic steps on the oxide surface (right) of pure iron treated by UV irradiation for two hours. The atomic terrace width is about 3.3 nm.

References

[1] H. H. Deng, I. Ishikawa, M. Yoneya, H. Nanjo, J. Phys. Chem. B **108**, 9138 (2004).
[2] H. Nanjo, N. J. Laycock, H. H. Deng, I. Ishikawa, N. Sanada, Current Applied Physics, **4**, 156 (2004).
[3] P. Schmuki, H. Böhni, Electrochim. Acta **40**, 775 (1995).

* Contact author: hi-nanjo@aist.go.jp

Atomistic Strain Studies on a Silver Nanorod

S.-W. Hla[1], H. J. P. van Midden[2], A. Prodan[2*]
[1]*Nanoscale & Quantum Phenomena Institute, Physics & Astronomy Department, Ohio University, Athens, USA*
[2]*Jožef Stefan Institute, Ljubljana, Slovenia*

Surface processes like nucleation, growth and diffusion are of great importance for the emerging nanotechnologies. Important details on an atomic scale can be studied on model systems like noble metals on transition-metal dichalcogenides (MX_2) [1]. It is shown that small deviations from the bulk atomic positions, taking place during heteroepitaxial growth of silver on β-$MoTe_2$, can be measured by scanning tunneling microscopy (STM).

β-$MoTe_2$ single crystals were grown by chemical transport reactions with iodine as the transport agent and silver was deposited either from a tungsten boat or from a Knudsen source. Constant current (CCM) and constant height (CHM) mode STM measurements were performed at room temperature under ultra-high vacuum conditions (10^{-9}-10^{-10} hPa).

Thermally deposited silver on β-$MoTe_2$ first tends to form elongated tapes along the substrate [010] direction [2], followed by a growth of nanorods, similar in their appearance to those formed by gold [3]. As determined by electron diffraction [4], the growth is epitaxial at deposition temperatures below 470K. The mutual relationship, (112)[1-10]Ag ‖ (001)[010]β-$MoTe_2$), requires accommodation of a rather large misfit between the two planes in contact. The d_{111} (3 x 0.2359 nm) and the perpendicular d_{011} (0.2889 nm) periodicities of silver are locked-in with the d_{100} (0.6330 nm) and d_{010} (0.3469 nm) periodicities of β-$MoTe_2$. The interfaces between the nanorods and the substrate are locked-in by adjusting the parameters in the deposit to those in the substrate. This results in a tensile stress along the [0-11] direction and a compressive stress along the perpendicular [1-1-1] direction of the nanorods [5].

The nanorods are regularly only a few atomic layers high and often show incomplete topmost adlayers. STM images with atomic resolution, recorded across the edges of the nanorods (e.g. Fig.1) reveal relatively large deviations in surface interatomic distances, particularly in case of very narrow adlayers. These tend to be bent by a tensile strain. Contrary, the first subsurface layers experience a compressive strain, often accompanied by a reconstructed region close to the adlayers. These observations are in qualitative agreement with recent calculations [6], where a relatively large stress variation was predicted in the two topmost layers of a reconstructed (111) gold surface.

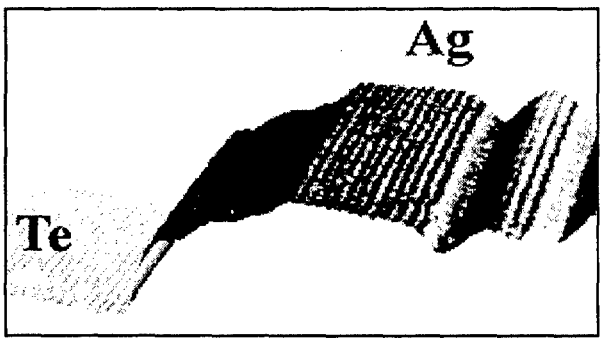

Fig.1: Three-dimensional STM image of a part of a silver nanorod on β-$MoTe_2$ [about 50 x 30 nm^2, , CCM, U_g = 0.1 V, I_t = 1 nA, t = 600 μs, W tip].

References

[1] F. Hulliger, F. Lévy (Ed.), *Structural Chemistry of Layered-Type Phases, in PhysicsanChemistry of Layered Structures* 5, D. Reidel Publ., Dordrecht, Holland, 1976.
[2] S. W. Hla, V. Marinković and A. Prodan. Surf. Sci. 377-379 (1997) 979.
[3] S. W. Hla, V. Marinković and A. Prodan, Thin Sol. Films 317 (1998) 14.
[4] S. W. Hla, V. Marinković and A. Prodan, Surf. Sci. 356 (1996) 130.
[5] S. W. Hla, A. Prodan, H. J. P. Van Midden, Nano Letters 4(2004) 1221.
[6] U. Tartaglino, E. Tosatti, D. Passerone, F. Ercolessi, Phys. Rev. B 65 (2002) 241406(R).

* Contact author: albert.prodan@ijs.si

SESSION Th E3
SEMICONDUCTOR QUANTUM DOTS AND METAL-OXIDE NANOPARTICLES

Thursday 10 February 2005 1530–1645

Copthorne III

Session Chair **Richard Tilley, Victoria University of Wellington, NZ**

15.30 **Solution-phase synthesis of one-dimensional (1-D) transparent conducting oxide (TCO) nanostructures with controllable aspect ratios**
Th E3.1 E.T. Samulski and B. Cheng
University of North Carolina at Chapel Hill, Chapel Hill, USA

15.45 **Hierarchical design of advanced 1-D metal oxide nanostructures**
Th E3.2 L. Vayssieres
National Insititute for Materials Science, Tsukuba, Japan and Lawrence Berkeley National Laboratory, Berkeley, USA

16.00 **Novel surface processing with sulfonic acid for quantum dot and its characters**
Th E3.3 A. Shiohara, N. Manabe, A. Hoshino and K. Yamamoto.
International Medical Centre of Japan, Tokyo, Japan

16.15 **Characterization of photoluminescent CdTe/CdSe composite nanoparticles synthesized by the precipitation method**
Th E3.4 H. Y. Chang, P. J. Chiang and H. I. Chen
National Cheng Kung University, Tainan, Taiwan

16.30 **Nonuniform carrier trapping among quantum dots**
Th E3.5 Y.S. Su and C.F. Lin
National Taiwan University, Taipei, Taiwan

Solution-phase Synthesis of One -dimensional (1-D) Transparent Conducting Oxide (TCO) Nanostructures with Controllable Aspect ratios

Edward T. Samulski and Bin Cheng
Department of Chemistry, University of North Carolina at Chapel Hill
Chapel Hill, NC 27599-3290 USA

One-dimensional (1-D), transparent conducting oxide (e.g. SnO_2, ZnO) nanostructures were prepared in solution under novel low-temperature conditions.[1,2] The aspect ratios of the 1-D nanostructures are tunable by delicately-selected experimental conditions, allowing for generation of structures ranging in size from nanorods to nanowires. The structures of the as-synthesized nanorods and nanowires were characterized by XRD, TEM, SAED and HRTEM, the surface and optical properties of these novel nanostructures are reported.

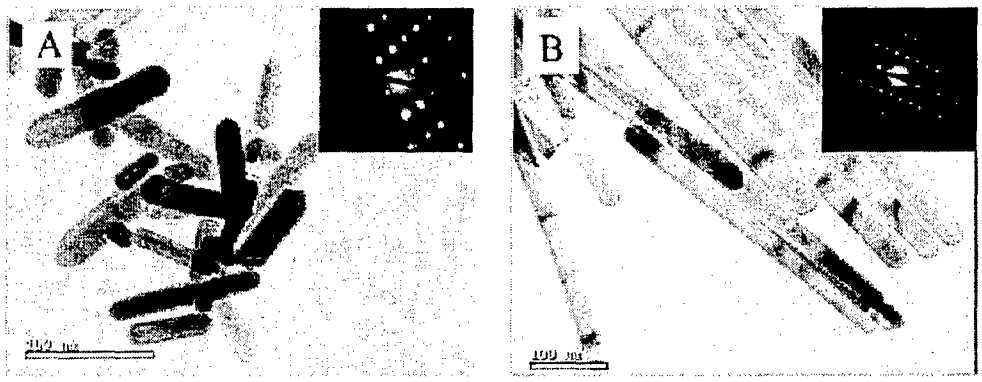

Figure 1 TEM images of ZnO nanorods with different aspect ratios, (a)4:1; (b)10:1.

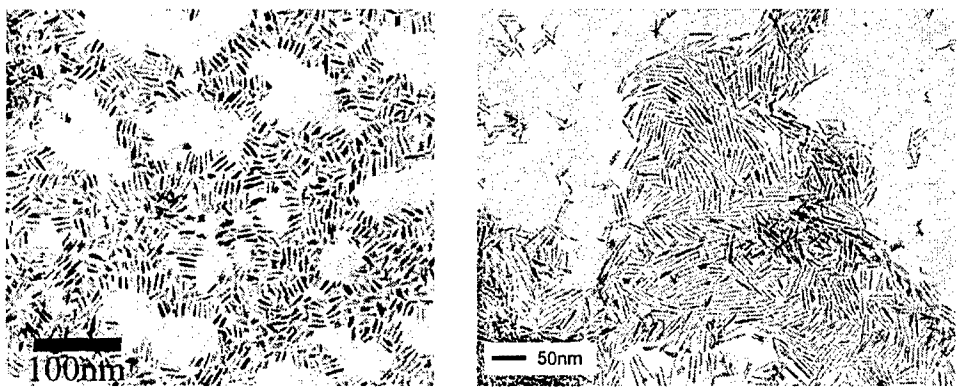

Figure 2 TEM images of SnO_2 nanorods with different aspect ratios, (a)5:1; (b)10:1.

References

[1] B. Cheng, E. T. Samulski, Chem. Commun.,986 (2004);
[2] B. Cheng, J. M. Russell, W. S. Shi, L. Zhang, E. T. Samulski, J. Am. Chem. Soc **126**, 5972 (2004).

Hierarchical Design of Advanced 1-D Metal Oxide Nanostructures

L. Vayssieres*
International Center for Young Scientists, National Institute for Materials Science, Tsukuba, JAPAN
Chemical Sciences Division, Lawrence Berkeley National Laboratory, Berkeley, CA USA

The hierarchical design of well-defined and highly oriented two- and three-dimensional arrays of conventional semiconductor nanomaterials and their large scale manufacturing at low cost remain a crucial challenge to unfold the very promising future of nanodevices. In addition to economical manufacturing of nanostructured semiconductors, better fundamental knowledge of their electronic structure, physical, interfacial and structural properties and stability, is required to fully exploit their fascinating photoelectrochemical potentials. To combine such essential requirements, the creation of structurally well-defined and well-ordered functional and multi-functional materials is essential.

As an attempt to achieve such ambitious goals, a novel strategy to nanostructured semiconductor fabrication has been investigated. A thermodynamic growth control concept based on the chemical and electrostatic lowering of surface energy and thin film direct growth techniques have been developed. Such approach allows the generation, at large scale and at low cost, of novel materials. Advanced metal oxide structures consisting of oriented multidimensional arrays featuring building blocks of controlled morphologies, sizes, aspect ratios and orientations at nano-, meso-, and micro-scale are genuinely fabricated without template, surfactant, undercoating nor applied field directly onto various substrates of large physical areas (figure 1) from the hydrolysis-condensation of aqueous metal salts and their heteronucleation at mild temperatures, ca. below 100° C [1].

Recent innovative advances in the fabrication of highly oriented and functional semiconductor nanostructure arrays along with the in-depth investigations of their structural characteristics as well as their electronic structure performed at synchrotron radiation facilities by soft x-ray spectroscopies [2], including polarization dependence [3] and resonant inelastic x-ray scattering. Such studies revealed important insight of direct relevance for photovoltaics, optoelectronic, and sensing nanodevices, which will be illustrated and demonstrated.

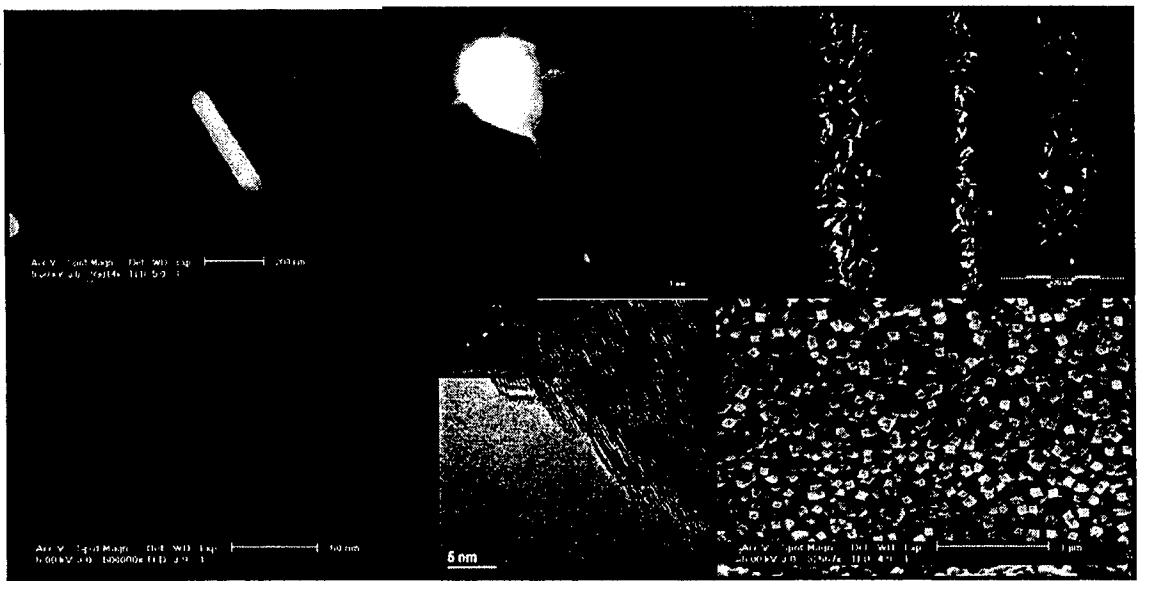

Figure 1 Electron microscopy images of c-elongated ZnO (top) and SnO_2 (bottom) 1-D nanostructures fabricated by aqueous chemical growth at 90°C onto silicon wafers and transparent conducting substrates.

References

[1] L. Vayssieres, *Int. J. Nanotechnology* **1**, 1 (2004); *Angew. Chem. Int. Ed.* **43**, 3666 (2004); *Adv. Mater.* **15**, 464 (2003); *NanoLett.* **2**, 1393 (2002); *Chem. Mater.* **13**, 4395 (2001); *Pure Appl. Chem.* **72**, 47 (2000)
[2] C. L. Dong et al, *Phys. Rev. B* **70**, (2004) in press
[3] J. Guo et al, *J. Phys. Condens. Matter* **14**, 6969 (2002)

* Vayssieres.lionel@nims.go.jp

Novel surface processing with sulfonic acid for quantum dot and its characters

Amane Shiohara, Noriyoshi Manabe, Akiyoshi Hoshino, Kenji Yamamoto*

Department of Medical Ecology and Informatics, Research Institute, International Medical Center of Japan, 1-21-1 Toyama, Shinjyuku, Tokyo 162-8655, Japan

Quantum dots (QDs) such as CdSe QDs have been introduced as new fluorophores. The functions of QDs vary widely, depending on their surface processing. Recently, QDs covered with polymer such as PEG coat (1) are popular because of their stability in water, however, such QDs sometimes cause uneven staining in immunostainig because of their large sizes. We synthesized the smaller sized QDs which are covered with sodium 2-mercaptoethanesulfonate having $SO3^-$; Mesna-QD, and compared its stability in acid, buffer solution, cellular toxicity, and fluorescent intensity with that of QDs covered with mercaptoundecanoic acid. The fluorescent intensity, of MUA-QD was about three times larger than that of Mesna-QD. However for stability in acid, MUA-QD was unstable in pH 3.7 while Mesna-QD was stable in the same pH. For stability in base, MUA-QD was unstable in 0.5M tris HCl while Mesna-QD was stable in same solution. Moreover, for stability in buffer solution, Mesna-QD showed high stability in NaCl solutions with different concentrations, MEM, PBS, and 0.5M tris-HCl. On the contrary, MUA-QD cohered in all the buffer solution described above. Similarly in the evaluation of cell damage, Mesna-QD was better than MUA-QD because Mesna-QD caused no damage to cells in the range of 0.05mg/mL～0.4mg/mL (2), while MUA-QD did some damage in the same range. The synthesis of this Mesna-QD suggests a great advantage in the application of QDs for biological and medical field.

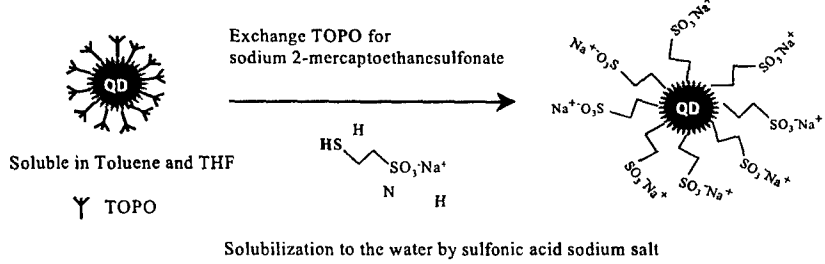

Synthesis of QD covered with sodium 2-mercaptoethanesulfonate

References

[1] Xiaohu Gao, Yuanyuan Cui, Richard M Levenson, Leland W K Chung, Shuming Nie., Nature biotechonology. **22**, 969-976 (2004).

[2] Amane Shioahara, Akiyoshi Hoshino, Ken-ichi Hanaki, Kazuo Suzuki, Kenji Yamamoto., Microbiology and Immunology. **48**(9), 669-675 (2004)

*Contact author: backen@ri.imcj.go.jp

Characterization of Photoluminescent CdTe/CdSe Composite Nanoparticles Synthesized by the Precipitation Method

H. Y. Chang, P. J. Chiang and H. I. Chen*
Department of Chemical Engineering, National Cheng Kung University, Tainan, 70101, TAIWAN

In this study, photoluminescent CdSe/CdTe composite nanoparticles were synthesized by the precipitation of $CdSO_4$ with NaHTe/NaHSe in aqueous alkaline solutions [1]. An appropriate amount of 3-mercaptopropionic acid (MPA) was added as the stabilizer [2]. The effects of $Cd^{2+}/Se^{2-}/Te^{2-}$ ratio, stabilizer concentration, and reaction time on the particle size, shape, crystalline structure, and optical and photoluminescent properties were investigated. The adding sequence of reactants during particle formation was also studied. Experimental results showed that, in the presence of MPA, pure fcc structured CdSe/CdTe nanoparticles, sizing from 5 to 13 nm, could be obtained without the impurities of $Cd(OH)_2$. For the CdSe/CdTe particles derived from coprecipitation route, the PL intensity increased rapidly with increasing the reaction time and shifted toward longer wavelengths (red shift) (Fig 1). This was inferred that the more crystalline nanoparticles were obtained as the reaction time is prolonged. In addition, the growth of particles resulted in the red shift in PL spectra. However, for the CdSe/CdTe particles obtained from the sequential route (CdTe as the nucleating agent), the characteristic peaks in PL spectra shifted toward shorter wavelengths (blue shift). Also, the PL intensity was increased with increasing reaction time (Fig 2). Since the bandgap energy for bulk CdSe (1.70 eV) was larger than bulk CdTe (1.56 eV), the products were inferred to be the core-shell structured CdTe(core)/CdSe(shell) nanoparticles.

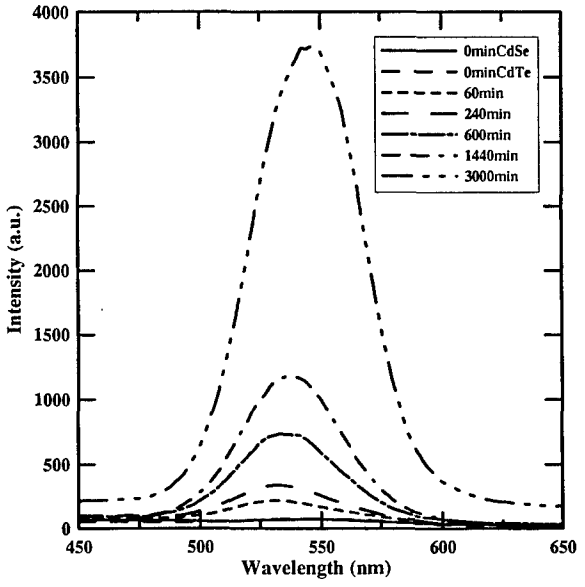

Fig 1 Photoluminescence spectra of the Sample prepared from CdSe + CdTe system. (Cd^{2+}:Te^{2-}:Se^{2-}=2:1:1)

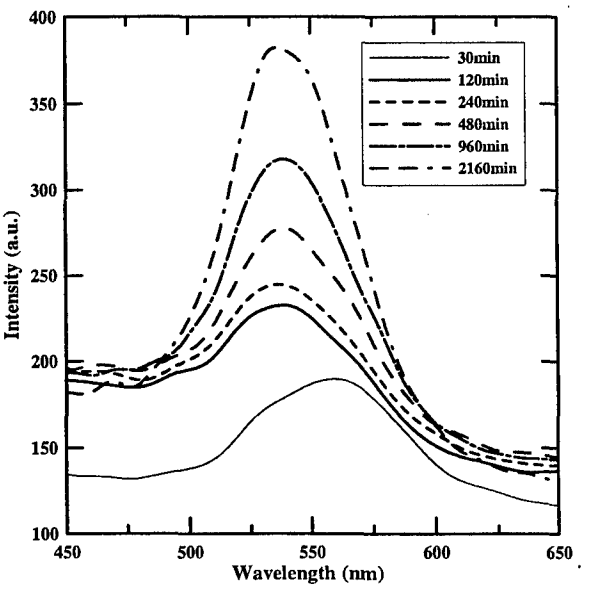

Fig 2 Photoluminescence spectra of the Sample prepared from CdTe + HSe^- system. (Cd^{2+}:Te^{2-}:Se^{2-}=2:1:1)

References

[1] H. Zhang, B. Yang, *Thin Solid Films*, 418(2), 169-174 (2002).
[2] M. A. Vairavamurthy, W. S. Goldenberg, *Marine Chemistry*, 70, 181-189 (2000).
[3] S. M. Sze, *Physics of Semiconductor Device*, New York, Wiley, pp.848-849 (1981).

* Contact author: hueying@mail.ncku.edu.tw

Nonuniform Carrier Trapping among Quantum Dots

Yi-Shin Su and Ching-Fuh Lin[1*]
Graduate Institute of Electro-Optical Engineering
[1] *also with Department of Electrical Engineering and Graduate Institute of Electronics Engineering*
National Taiwan University Taipei 106, Taiwan ROC

Quantum dot (QD) devices have the advantage of high differential gain, low threshold current and improved efficiency [1], because they have the unique delta function like density of states. However, growing single-size QDs is difficult. On the other hand, some researchers take advantage of the size fluctuation of QDs and demonstrate tunable lasers with more than 200nm tuning range [2]. When the QDs do not have a single size, their corresponding emission wavelengths are different, leading to different characteristics for carriers trapped in different QDs. Here we discover that the injected carriers are not trapped among those QDs uniformly. At the low current level, the carriers tend to be trapped in large QDs. When the current level is increased, small QDs gradually trap carriers with increasing number.

Devices are fabricated on a wafer with the active region containing several layers of QDs. The QDs are intentionally grown to have a large size fluctuation. Whether the carriers are trapped in QDs uniformly or nonuniformly can be clarified from the spectrum measurement of the devices. In order to avoid the influence of Fabry-Perot resonance on the spectrum, the waveguide for light guiding is tilted at an angle from the cleaved facets. In addition, each device has two separated electrodes. Only one electrode is injected with current to make the other portion absorb light. Thus, we will always measure light output without resonance effect.

There are two emission peaks in the EL spectrum measured. They are attributed to the emission of the first and the second quantized states. Because of bandgap shrinkage caused by the thermal effect, the peak wavelength corresponding to the first quantized states increases for 10 nm as the current increases from 10 mA to 80 mA. The emission wavelength of the second quantized states should increases for the same reason. However, the observed peak emission wavelength of the second quantized states decreases by 4.7nm for the same increasing range of current. This is attributed to different carrier trapping effect among the QDs when the injection current is different. At the low current level, carriers are trapped mostly among large QDs that have small energy separation between the first and the second quantized states. As the current level increases, more carriers are trapped in QDs of small sizes. Then more emissions are contributed from the small QDs, so the emission peaks have increasing spectral separation. Our investigation shows that carrier trapping amo ng QDs is not uniform and depends on the level of current injection. The details will be explained.

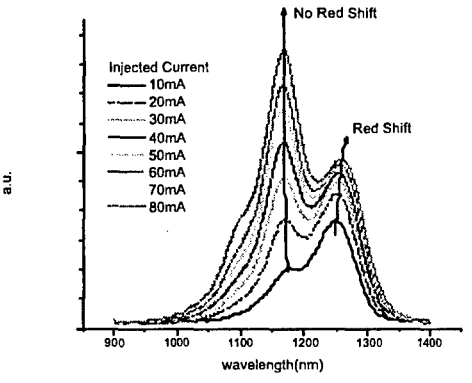

Figure 1. EL Spectrum of the QD sample

References

[1] Q. Xie, P. Chen, A. Kalburge, T. R. Ramachandran, A. Nayfonov, A. Konkar, and A. Madhukar, "Realization of optically active strained InAs island quantum boxes on GaAs (100) via molecular beam epitaxy and the role of island induced strain fields," *J. Cryst. Growth*, vol. 150, p. 357, 1995.
[2] P. M. Varangis, H. Li, G. T. Liu, T. C. Newell, A. Stintz, B. Fuchs, K. J. Malloy, and L. F. Lester, "Low-threshold quantum dot lasers with 201 nm tuning range," *Electron. Lett.*, vol. 36, pp. 529–530, 2000.

* Contact author : cflin@cc.ee.ntu.edu.tw

Friday 11 February
Poster Session Two

POSTER SESSION 2

Friday 11 February 2005 0800–1000

Galaxy Ballrooms II and III

POSTER GROUP 9 METALS AND METAL ALLOYS

PG9.1 **Structure and microhardness of quasicrystalline Al-Cu-Fe alloys and coatings**
S.I. Sidorenko, L.D. Demchenko, Y.N. Makogon and S.M. Zakharov

PG9.2 **Electron microscopy of electromigration damage in metallic nanowires**
K.J. Stevens, K.S. Cheong, D.M. Knowles, N.J. Laycock, S.A. Brown and S.C. Hendy

PG9.3 **Optical spectroscopies of potentially half metallic Heusler alloys**
A. Bittar, C.E.A. Grigorescu, N. Strickland, E.Valerio and H.J. Trodahl

PG9.4 **Interface diffusion in pulsed laser deposition of NiMnSb on silicon**
C.E.A. Gigorescu, E. Valerio, J. Kennedy, P. Caminat, R. Notonier, O. Monnereau, M. Autric, H.J. Trodahl and A. Markwitz

POSTER GROUP 10 SURFACE AND INTERFACE PHENOMENA

PG10.1 **Visualization of a cell membrane surface and dynamics using atomic force microscopy**
P. Savigny and K.M. McGrath

PG10.2 **Electrochemical grafting of multilayer amine films onto thin-film carbon substrates**
E.S.Q. Tan and A.J. Downard

PG10.3 **Fabrication and surface modification of composite carbon and silicon hybrid materials**
S.S.C. Yu, A.J. Downard, P.A. Brooksby, E.S.Q. Tan and R.J. Blaikie

PG10.4 **Effect of UV irradiation on the structure of passive oxide films**
H. Nanjo, M. Fujimura, M. Nishioka, I. Ishikawa and J. Onagawa

PG10.5 **Electrochemistry of room temperature ionic liquids**
A. Gestos, W.E. Price and G.G. Wallace

PG10.6 **Origin of the optical anisotropy oscillations of Si(001) surfaces during oxidation**
W. G. Schmidt, F. Fuchs and F. Bechstedt

PG10.7 **Nitrophenyl and nitroazobenzene thin films on carbon surfaces**
P.A. Brooksby and A.J. Downard

PG10.8 **Isothermal microcalorimetry as a technique for material characterization**
V.E. Ostrovskii

POSTER GROUP 11 CONDUCTING POLYMERS

PG11.1 **Spectroscopic studies of interactions of polyaniline with some Cu(II) compounds**
M. Gizdavic-Nikolaidis, J. Travas-Sejdic, R.P Cooney and G.A. Bowmaker

PG11.2 **Soluble alkoxy-substituted poly(terthiophenes): polymerisation, characterisation and device fabrication**
A.M. Ballantyne, D.L. Officer, S.B. Hall, G.G. Wallace, C. Wang, Y.Wu, V.J. Misoska and G.Tsekouras

PG11.3 **Biocidal and electronic properties of intrinsically conducting polymer-based composites**
M.J. Richardson, J.H. Johnston and T. Borrmann

PG11.4 **Semiconducting polyaniline-vanadium oxide nanocomposites**
I. Karatchevtseva, V. Luca, M. Blackford and Z. Zhang

PG11.5 **Soluble poly-3-alkylpyrrole polymers on films and fabrics**
R. Foitzik, A. Kaynak, J. Beckmann and R. Russell

POSTER GROUP 12 MAGNETIC AND SUPERCONDUCTING MATERIALS AND DEVICES

PG12.1 **Effect of milling on the perovskite phase formation of $Pb(Mg_{1/3}Nb_{2/3})O_3$ using the starting precursors PbO and $MgNb_2O_6$**
A. Chaipanich and T. Tunkasiri

PG12.2 **Ferromagnetism and magnetoresistance in chromium-doped indium tin oxide**
H.S. Kim, S.H. Ji, B.S. Lee, H. Kim, S.-K. Hong, D. Kim, Y.E. Ihm and W.K. Choo

PG12.3 **The effect of uniaxial stress to spin reorientation transition and hysteresis in magnetic thin-films : Monte Carlo investigation**
Y. Laosiritaworn, R. Yimnirun and J. Poulter

PG12.4 **Magnetic behaviour of nanocomposites containing self-assembled magnetite particles dispersed in a paraffin wax matrix**
C.-R. Lin, T.-W. Sung and R.-K. Chiang

PG12.5 **Dielectric Charaterization of $Ba_xSr_{1-x}TiO_3$ by Solid Solution of $BaTiO_3$ and $SrTiO_3$**
S. Kongtaweelert, D.C. Sinclair and S. Phanichaphant

PG12.6 **Synthesis of magnetic nanomaterials using spinning disc reactor technology**
N. Hill, C. L. Raston, M. Saunders, and R. Woodward

PG12.7 **Magnetic and electrical properties of MBE-grown $(Ge_{1-x}Si_x)_{1-y}Mn_y$ thin films**
S.S. Yu, Y.M. Cho, Y.E. Ihm, D. Kim, H. Kim, S. Oh and C.S. Kim

PG12.8 **Neutron irradiation effect on polycrystalline $Ge_{1-x}Mn_x$ thin films grown by MBE**
Y.M. Cho, S.S. Yu, Y.E. Ihm, S.W. Lee, D. Kim, H. Kim, J.M. Sohn, B.G. Kim, S. Oh, C.S. Kim and H.J. Lee

POSTER GROUP 13 SOFT MATTER AND COMPLEX FLUIDS

PG13.1 **Aging and rejuvenation of soft glassy materials**
S.A. Rogers and P. T. Callaghan

PG13.2 **Symmetry considerations in the NMR of complex fluids**
B.S. Douglass and P. T. Callaghan

PG13.3 **Rheological and mechanical property studies on ultra-high molecular weight polyethylene / carbon nanotubes**
L. Linli,W. Xinpeng, W. Yanping and W. Yimin

PG13.4 **Mass transport in porous media: the non-local dispersion tensor and nuclear magnetic resonance**
M.W. Hunter, A.N. Jackson and P.T. Callaghan

POSTER GROUP 14 MICRO- AND NANO-FABRICATION

PG14.1 **Starting out in microfluidics**
W. Collier, J. Carson and A. Hart

PG14.2 **Fabrication of GaN based photonic crystal by using electron beam lithography**
A. Motogaito, T. Yamada, F. Matsuoka and K. Hiramatsu

PG14.3 **Fabrication of 3D nanoimprint lithography molds**
M. Konijn, M.M. Alkaisi and R.J. Blaikie

PG14.4 **Enhanced mixing of microfluidic flows using variable surface potentials**
J. Burnell and G.J. Weir

PG14.5 **Resist deformation at low temperatures in nano-imprint lithography (NIL)**
K. Mohamed, M.M. Alkaisi and J. Smaill

PG14.6 **Lithographic patterning of obliquely deposited polarizing elements**
M.D. Arnold, I. J. Hodgkinson, Q.h. Wu and R.J. Blaikie

PG14.7 **Sub-wavelength texturing for solar cells using interferometric lithography**
W.L. Chiu , M.M. Alkaisi, R.J. Blaikie, R.J. Reeves and S.J. Drake

PG14.8 **Distortion in evanescent near field optical lithography conformable masks**
A.J. Wright, R.J. Blaikie and G. Turner

PG14.9 **Silicon etch process options for micro- and nanotechnology using inductively coupled plasmas**
C.C. Welch, A.L. Goodyear, G. Ditmer and G. Tan

PG14.10 **Fabrication of nanoscale SiC-based ceramic patterns with near-zero residual layers using imprinting techniques**
K.-H. Park and D.-P. Kim

PG14.11 **Highly anisotropic reactive ion etch for fabrication of silicon nanostructure**
E.-Z. Liang, C.-J. Huang and C.-F. Lin

PG14.12 **Microfabrication of interfacial force microscope sensor components**
C.M. McCague and P.R. Norton

PG14.13 **Photoresist as an anti-reflection coating for interference lithography**
S.J. Drake, N. Kohn, R.J. Blaikie, R.J. Reeves and M.M. Alkaisi

PG14.14 **Microfluidic circuit integration using multilayer soft lithography methods and PDMS**
E.S. Berthier, F. l'Hostis, M.M. Alkaisi, A. Downard and R.J. Blaikie

PG14.15 **Low pressure nanoimprinting process for SiC-based ceramic pattern using viscous photocurable preceramic polymers**
A.T. Pham and D.-P. Kim

PG14.16 **Nanostructuration of conjugated polymer thin films**
K. Matczyszyn, L. Rocha, C. Fiorini, S. Bartkiewicz and F. Kajzar

POSTER GROUP 15 SEMICONDUCTOR DEVICES

PG15.1 **The effect of surface area increase due to plasma texturing on the carrier lifetime of silicon solar cell substrates**
G. Kumaravelu, M.M. Alkaisi and D. Macdonald

PG15.2 **Fabrication of metallic nanotransistors**
H.H. Cheng, M.M. Alkaisi and J.K. Siaw

PG15.3 **HSQ as a surface protection layer for the preparation of TEM samples by focused ion beam milling**
E. Boyd, W. Smith, S. McFadzean, A. Craven and I.G. Thayne

PG15.4 **Electrical properties of three quantum well play a leading part of quantum cascade laser by C-V and deep-level transient spectroscopy**
J.S. Kim, E.K. Kim, J.D. Song and I.K. Han

PG15.5 **Symmetry of non-linear electric conduction in semiconductor nano-devices**
C.A. Marlow, A. Löfgren, I. Shorubalko, R.P. Taylor and H. Linke

POSTER GROUP 16 SEMICONDUCTOR GROWTH AND CHARACTERISATION

PG16.1 **Pulsed chemical vapor deposition technology**
S.I. Baluti and S.P. Krumdieck

PG16.2 **Design and function of a pulsed laser deposition facility for growth of novel thin film materials in HV, UHV and plasma environments**
I.L. Farrell, R.J. Reeves and S.M. Durbin

PG16.3 **Photoluminescence and photoconductivity exhibited by PAMBE grown InN**
L. Williams, P.A. Anderson, S.M. Durbin and R.J. Reeves

PG16.4 **Development of Si/SiO_2 super-lattices deposited by RF reactive sputtering**
E. Boyd and R.J. Blaikie

PG16.5 **Physical and electronic structure of disordered gallium nitride**
B.J. Ruck, F. Budde, A. Koo, S. Granville, H.J. Trodahl, G.V.M. Williams, A. Bittar, and J.B. Metson

PG16.6 **Synthesis and characterization of indium nitride micro- and nanostructures**
H. Timmers, V. Edge, J. Anderson, G. Lawes, S.K. Shrestha, R. Dogra and A.P. Byrne

PG16.7 **Optimising the growth conditions of oxidised zinc films for photoluminescence properties**
P. Miller, Z. Li, W. Gao and R.J. Reeves

PG16.8 **Comparison of DC and RF sputtered ZnO thin films**
L.P. Schuler, M.M. Alkaisi, P. Miller, R.J. Reeves, S. Brown and A. Markwitz

PG16.9 **Nanostructuring of silicon by electron beam annealing**
S.P. Lansley, P.-Y. Kuo, C.-T. Lu, S. Johnson, A. Markwitz and R.J. Blaikie

PG16.10 **The annealing behaviour of nc-GaN and a-GaN:O films; dot formation, SEM, luminescence and Raman spectroscopy**
C.E.A. Grigorescu, H.J. Trodahl, B.J. Ruck, F. Budde, A. Tonetto, R. Notonier and O. Monnereau

PG16.11 **Modification of electrical conductivity in RF magnetron sputtered ZnO films and ZnO crystals by low-energy hydrogen ion implantation**
J. Kennedy, A. Markwitz, Z. Li, W. Gao, S.M. Durbin and R. Reeves

PG16.12 **Diffusion coefficients of proton in $CsHSeO_4$**
Y. Yoshida, Y. Matsuo and S. Ikehata

PG16.13 **Synthesis of nano-sized ZnO powders by thermal decomposition of zinc acetate from pulp (*Broussonetia papyrifera* (L.) Vent.) precursor**
Liewhiran C. and Phanichphant S.

Structure and Microhardness of Quasicrystalline Al-Cu-Fe Alloys and Coatings

S. I. Sidorenko[1], L. D. Demchenko[1*], Yu. N. Makogon[1], S. M. Zakharov[2]
[1] *National Technical University of Ukraine "KPI",37 Peremogy prospect, Kiev 03056, UKRAINE*
[2] *Institute for Metal Physics of NAS of Ukraine, 36 Vernadsky Avenue, Kiev 03680, UKRAINE*

Nowadays the creating of wear resistance hard coatings with high fracture toughness on aluminium alloys is one of the main problems of searching of scientists of many countries, the solution of which would allow to increase the details lifetime of the aircraft and automobile machines. The great attention is paid to the creation of the alloys with *nano-* and *quasicrystalline* structures under the particular conditions and that could be used for the strengthening of wear resistive coatings for the details of mechanical engineering. One of the methods is the obtaining of the quasicrystalline coatings from the aluminides.

The *purpose* of this work is to investigate the structure and mechanical properties of quasicrystalline Al-Cu-Fe alloys of various compositions and coatings on their basis prepared using ion-plasma deposition, to estimate percentage of phases with different microhardness and to find the optimal compositions of Al-Cu-Fe alloys for such coatings.

The Al-Cu-Fe alloys of various chemical compositions with different amount of quasicrystalline phase (tab. 1) were melted and the coatings on their basis were deposited on Al- and Al-based alloys substrates using ion-plasma technology. The alloys were investigated by means of X-ray diffractometry (XRD), optical metallography and Vickers microhardness (HV) tests by microindentation to compare their structure and properties.

Table 1 The chemical and phase composition of Al-Cu-Fe alloys and the percentage of phases with different microhardness

Alloys	Chemical composition, at.%			Phase composition (literature data)	Percentage of phases with different microhardness, vol.%					Average HV of alloys, GPa
	Al	Cu	Fe		Highest HV 10.1-19.0, GPa	High HV 8.1-10.0, GPa	Medium HV 6.1-8.0, GPa	Low HV 4.0-6.0, GPa	Lowest HV 0.5—3.9, GPa	
$Al_{38}Cu_{32}Fe_{10}$	38	32	10	i-φ	5	5	80	10	-	7.0
$Al_{56}Cu_{32}Fe_{12}$	56	32	12	β-φ-i	-	20	80	-	-	7.5
$Al_{60}Cu_{26.5}Fe_{13.9}$	60	26.5	13.9	1/2β-1/2i	-	5	45	25	25	5.4
$Al_{60}Cu_{32}Fe_{8}$	60	32	8	θ-φ-i	-	-	40	50	10	5.4
$Al_{61}Cu_{26}Fe_{13}$	61	26	13	i-β	5	15	80	-	-	8.1
$Al_{63}Cu_{27}Fe_{10}$	63	27	10	i-θ	-	15	80	5	-	7.5
$Al_{64}Cu_{21}Fe_{15}$	64	21	15	i-λ	-	10	90	-	-	7.7
$Al_{64}Cu_{24}Fe_{12}$	64	24	12	i→λ	-	10	90	-	-	7.4
$Al_{65}Cu_{20}Fe_{15}$	65	20	15	i	-	10	85	5	-	7.2
$Al_{65.5}Cu_{23}Fe_{11.5}$	65.5	23	11.5	i-ω	5	-	40	35	20	5.6
$Al_{66}Cu_{26}Fe_{8}$	66	26	8	ω-θ-i	-	-	30	60	10	5.4
$Al_{67}Cu_{22}Fe_{11}$	67	22	11	1/2ω-1/2i	-	35	25	40	-	6.9
$Al_{68}Cu_{18}Fe_{14}$	68	18	14	ω-λ-i	-	40	10	50	-	6.8
$Al_{91}Cu_{5}Fe_{4}$	91	5	4	Al-λ-ω	-	-	-	20	80	1.9
$Al_{58}Cu_{26}Fe_{14}Ti_{4}$	58	26	14	i-β-α-ω	-	-	20	55	25	4.9

The X-ray diffractometry investigations showed that the maximum (80-90 wt.%) of *i*-phase formed in $Al_{64}Cu_{21}Fe_{15}$, $Al_{64}Cu_{24}Fe_{12}$, $Al_{65}Cu_{20}Fe_{15}$ alloys, the composition of which approached to *i*-phase stochiometric one. The other Al-Cu-Fe alloys of various chemical compositions contain different amount of intermetalic phases (tab. 1). In $Al_{91}Cu_{5}Fe_{4}$ the *i*-phase is not revealed, the alloy is mainly presented by fcc-solid solution of Cu and Fe in Al (70 wt.%).

The average HV of Al-Cu-Fe alloys of different compositions is in the range 5.4-8.1 GPa. The 85-90vol.% of phases with medium microhardness is observed in $Al_{64}Cu_{21}Fe_{15}$, $Al_{64}Cu_{24}Fe_{12}$, $Al_{65}Cu_{20}Fe_{15}$ alloys containing the maximum of *i*-phase. The microhardness of *i*-phase measured by microindentation approximates 7–8 GPa. With the decrease of *i*-phase quantity in alloy the microhardness falls. The high content of intemetallic compounds in these alloys does not always result in the microhardness increase.

The researches were supported by Science and Technology Centre in Ukraine (Project No 2469).

* Contact author: demles@yahoo.com

Electron Microscopy of Electromigration Damage in Metallic Nanowires

K.J. Stevens[1,2,*], K.S. Cheong[1], D.M. Knowles[1,2], N.J. Laycock[1,2], S.A. Brown[2,3] and S.C. Hendy[1,2]
[1] *Industrial Research Ltd*
PO Box 31-310, Lower Hutt, NEW ZEALAND
[2]*The MacDiarmid Institute for Advanced Materials and Nanotechnology,*
P.O. Box 600, Wellington, NEW ZEALAND
[3]*Nanostructure Engineering Science and Technology Group, Department of Physics and Astronomy, University of Canterbury, Private Bag 4800, Christchurch, NEW ZEALAND*

One of the principal failure mechanisms in nanowires is current assisted mass transport or electromigration [1-3]. Electromigration is growing in importance with the increasing trend to miniaturisation to achieve faster speed in microelectronics and for nanotechnology applications. This project is using multiscale modelling techniques such as Finite Element Mathematics (FEM) coded using ABAQUS and ANSYS commercial software packages to understand the electromigration phenomenon and to aid in future design work. An important aspect of this work is validation of the models using electron microscopy to characterise the evolution of the electromigration damage. The electromigration is modelled by applying a potential to the wire geometry, and solving for the current distribution and temperature changes due to Joule heating. The current is coupled to diffusion mass transport, with different diffusion constants for the bulk, grain boundaries, interfaces and surfaces. Mass transport creates voids, hillocks and a stress distribution. An iterative process is required in which, for example, void and hillock formation changes the localised current distribution and therefore the mass diffusion and rate of growth of defects. Deformation and dislocation activity is coupled in using crystal plasticity FEM techniques [4].

Electron Backscattered Diffraction (EBSD) on a FEG SEM [5] is being used to characterise the fcc grain structure of the nanowires (50 nm to 10 μm) fabricated using vapour deposition and optical and electron beam lithography. The wires can be 1 grain wide (the so called bamboo structure) or polycrystalline. EBSD measures the orientation of the grains relative to one another and the long axis of the wires, and the tilt and twist nature of the grain boundaries ($\Sigma 3$, $\Sigma 5$, Σ 9 etc, in Coincident Site Lattice models). FEG SEM is used to observe the surface breaking voids and hillocks. The dislocation structure and internal voids are observed using TEM samples.

With decreasing line dimensions, the microelectronics industry is moving from aluminium to the higher conductivity copper wires. The copper wires are fabricated by a damascene process. In this project experimental work has concentrated on gold wires than can be fabricated in New Zealand using the optical lithography system at IRL for pad deposition and the Raith electron beam lithography system in the NEST group at Canterbury for interconnecting wires. Overseas collaborations are being used to source aluminium and gold wires. Nanowires can be constructed using nanocluster deposition techniques [6]. In this project, nanoclusters are being characterised using high resolution TEM. Accelerated electromigration testing is carried out in accordance with international standards [7,8] to measure the mean time to failure of the wires. The use of synchrotron techniques is being investigated for stress measurement [9]. A 1-3 micron diameter beam is required to achieve the spatial resolution sufficient to measure stress within grains.

References

[1] C.S. Hau-Riege, Microelectronics Reliability 44 (2004) p195-205.
[2] J.R. Black, IEEE Trans. On Electron Devices, Vol. ED-16, No. 4, (April 1969), p338-347.
[3] C. Durkan and M.E. Welland, Ultramicroscopy 82 (2000) p125-133.
[4] K.S. Cheong, *Dislocation-mechanics based Modelling of Deformation in multiphase FCC single crystals and polycrystalline aggregates*, Ph.D. Thesis, (2003).
[5] A. Buerke, H. Wendrock and K. Wetzig, Cryst. Res. Technol., 35 (2000) p721-730.
[6] J. G. Partridge, S. A. Brown, C. Siegert, A. D. F. Dunbar, R. Nielson, M. Kaufmann, and R. Blaikie, Microelectronic Engineering 73-74 (2004), p583-587.
[7] ASTM Electromigration Test Standards 1259, 1260 and 1261, 1996.
[8] JEDEC Electromigration Test Standards JESD33B, JESD61, JESD87, JEP119A and JEP139, 1998-2004, http://www.jedec.org/ .
[9] G.S. Cargill, Solid-State Electronics 46 (2002) p1139-1143.

Acknowledgements: This project was funded by NZ FRST NERF contract CO8X0409-Multiscale Modelling. NEST group at Canterbury University for electron beam lithography and nanocluster samples. VUW SCPS and the MacDiarmid Institute for access to electron microscopes.

*Contact author: k.stevens@matperf.com

OPTICAL SPECTROSCOPIES OF POTENTIALLY HALF METALLIC HEUSLER ALLOYS.

A Bittar[1,2], C.E.A. Grigorescu[3], N. Strickland[1], E.Valerio[5] and H.J. Trodahl[2,4]

[1] Industrial Research Ltd., Lower Hutt, New Zealand
[2] MacDiarmid Institute of Advanced Materials and Nanotechnology
[3] National Institute R&D Optoelectronics INOE 2000-Bucharest, Romania
[4] Victoria University, Wellington, New Zealand
[5] Université de Provence, Marseille, France

Cobalt-Manganese based Heusler alloys are predicted to be half metals and therefore to show complete electronic spin polarisation[1]. We have prepared the series of alloys Co_2MnGe, Co_2MnSi and Co_2MnSb films using low temperature Pulsed Laser Deposition (PLD) on a number of substrates. In an attempt to characterise the electronic states in these materials, we have measured their reflectance in the whole wavelength range from UV to far infrared (0.01eV to 5.0eV) and used Kramers-Kronig relations to obtain dielectric constants and conductivities fro the three alloys. The results indicate a free electron like component in the infrared spectral range as well as onsets in the visible-ultraviolet wavelength regions above 1.0eV. The latter are indicative of the predicted "semiconductor like" minority spin gap onset and interband transitions[1] while the former are attributable to majority spin free electron conduction at the fermi level expected of metallic materials. The trends in these features across the Ge, Si and Sn alloy series is highlighted.
By comparing the reflectivity data with spectral ellipsometric measurements in the visible UV wavelength range we have confirmed these results and also obtained information on the morphology of the surfaces and the quality of the films produced by this low temperature PLD technique.

References:
1- Picozzi et al, PRB 66, 094421

Contact author: a.bittar@irl.cri.nz

Interface Diffusion in Pulsed Laser Deposition of NiMnSb on Silicon

C.E.A. Gigorescu[1], E. Valerio[2], J. Kennedy[3*], P. Caminat[2], R. Notonier[4], O. Monnereau[5] and M. Autric[2], H.J. Trodahl[6] and A. Markwitz[3]

[1]*INOE 2000, Bucharest, ROMANIA*

[2]*IRPHE, Univ. de la Mediterranee, Marseille, FRANCE*

[3] *Institute of Geological and Nuclear Sciences, P.O. Box 31-312, 30 Gracefield Road, Lower Hutt, New Zealand*

[4]SCM- Univ. Provence, Marseille, FRANCE

[5]*MADIREL, Univ. Provence, Marseille, FRANCE*

[6]*MacDiarmid Institute of Advanced Materials and Nanotechnology, Victoria University, Wellington, New Zealand*

The ferromagnetic half-Heusler alloy NiMnSb is predicted to display 100% spin polarisation at the Fermi level (half-metallic behaviour), so that it has been investigated in both its bulk and thin film forms with a view to spintronic applications. Within this application it is important to determine the properties of films deposited on various substrates. Recent research has been directed toward film deposition techniques enabling a satisfactory reproducibility of the structural properties and stoichiometry of the bulk material seeking to preserve the half-metallic behaviour in the thin films required for exploitation in devices. Pulsed laser deposition has been shown to be very promising from this point of view. PLD films have been prepared by several groups, using UV pulsed lasers (λ=248nm, τ=30ns), polycrystalline targets and substrates ranging from Si to narrow-gap III-V semiconductors.

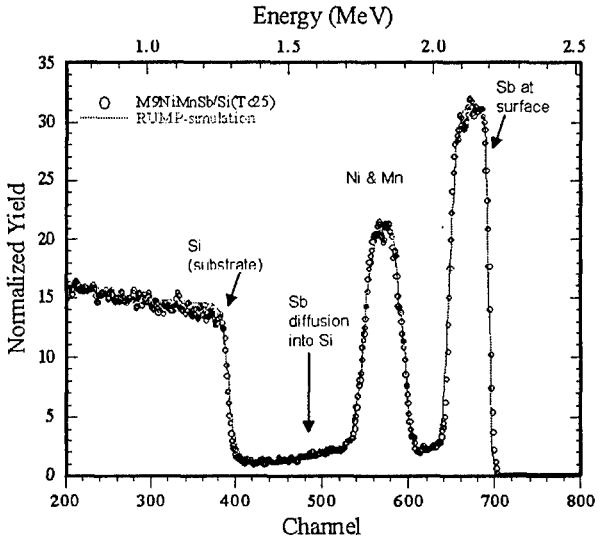

In this work we refer to NiMnSb films deposited on silicon, which have been investigated for stoichiometry, structure and optical conductivity. The ablation/deposition runs were carried out in vacuum (10^{-6} – 10^{-8} mbar) at substrate temperatures ranging from 300K to 500K. Characterisation of the samples has been performed by SEM, EDS and RBS – for morphology and composition, while IR reflectivity and ellipsometry measurements were carried out to determine their optical properties [1]. A special attention has been devoted to the NiMnSb/Si interface, which has been primarily analysed by RBS. The results show Sb diffusion into the Si substrate, which amounts at different levels according to the thickness of the films and hence to the number of laser shots performed, while the substrate temperature seems to influence less than expected.

References

[1] C.E.A. Grigorescu, H.J. Trodahl, N.M. Strickland, A. Bittar, S.A. Manea, J. Giapintzakis, O. Monnereau, R. Notonier and V.J. Kennedy, J. Appl. Phys., in press.

* Corresponding author: j.kennedy@gns.cri.nz

Visualization of a cell membrane surface and dynamics using Atomic Force Microscopy

P. Savigny* and K. M. McGrath
School of Chemical and Physical Sciences, Victoria University of Wellington, PO Box 600, Wellington, New Zealand

Exocytosis is a key biological process, which controls the neurotransmission and release of hormones from cells. Cells are in gross several microns in diameter, but the release of hormones from the intra to the extracellular medium through a cell membrane pore (called a fusion pore or porosome) occurs on the length scale of a few hundred nanometres. The imaging of living cells is now quite widely used, but only in the last two years has pore fusion been successfully captured, using Transmission Electron Microscopy and Atomic Force Microscopy (AFM). This has been reported for three types of cells: pancreatic acinar [1,2], chromaffin [3] and growth hormone- secreting cells [4].

This project deals with Luteinizing Hormone (LH), which is one of several hormones released by the pituitary gland, and whose surge is responsible for ovulation in females. It is known that this surge is controlled by two different peptides: gonadotrophin-releasing hormone (GnRH) and oxytocin, both being synthesized in the hypothalamus. However, the detailed cellular response of gonadotrophs to the exposure of GnRH and oxytocin remains scantily understood [5,6]. And the dynamics of the membrane during the LH exocytosis, by cells called gonadotrophs, remain completely unknown. A better understanding of these processes would allow improved contraception methods and the ability to solve the sterility problem.

The need to image soft surfaces, such as cell membranes, under fluid, in real time and at a nanometre resolution, makes AFM a very powerful and attractive tool. The AFM technique is based on the measurement of the interaction force between a probe tip (attached to a cantilever) and the sample. The tip scans the surface, oscillating at its resonant frequency over it and touching it briefly and intermittently. This operation mode is called tapping mode or intermittent mode, and is the most appropriate mode for imaging soft samples since the force applied to the surface is lower than when using contact mode. In tapping mode, by maintaining a constant oscillation amplitude of the cantilever, a 3D image of the surface can be obtained. Despite the reduced applied force in tapping mode, high-resolution imaging of living cells requires:
1/ determination of the best method to image living cells with AFM (choice of cantilever, spring constant, imaging mode, resonance frequency, scan rate...);
2/ maintenance of cell viability prior and during scanning by using appropriate cell culture procedures, and imaging under physiological medium at 37°C and,
3/ cell immobilization on the substrates achieved by using poly-l-lysine or Cell-Tak as coating agents or specifically fabricated "biochip" platforms.

Living gonadotroph plasma membrane images have been achieved pre and post stimulation with potassium under physiological conditions (temperature and medium) using tapping mode AFM. Initial stimulation with GnRH has been performed but the GnRH and oxytocin influence on the membrane topography remain to be investigated.

References

[1] A. Jeremic, M. Kelly, S.-J. Cjo, M. H. Stromer and B. P. Jena, Biophysical Journal **85**, 2035 (2003).
[2] B. P. Jena, S.-J. Cho, A. Jeremic, M. H. Stromer and R. Abu-Hamdah, Biophysical Journal **84**, 1337 (2003).
[3] S.-J. Cho, A. Wakade, G.D. Pappas, B.P. Jena, Annals of the New York Academy of Sciences **971**, 25 (2002).
[4] S.-J. Cho, K. Jeftinija, A. Glavaski, S. Jeftinija, B.P. Jena, L.L. Anderson, Endocrinology **143**, 1144 (2002).
[5] J.J. Evans, A.H. Youssef, M.M. Abbas, J. Schwartz, Journal of Endocrinology **163**, 345 (1999).
[6] J.J. Evans, S. Janmohamed, M.L. Forsling, Brain Research Bulletin **48**, 93 (1999).

*Pascale.Savigny@vuw.ac.nz

Electrochemical Grafting of Multilayer Amine Films onto Thin-film Carbon Substrates

Emelyn S. Q. Tan* and Alison J. Downard
Department of Chemistry, University of Canterbury, Christchurch, New Zealand.
The MacDiarmid Institute for Advanced Materials and Nanotechnology, New Zealand.

Electrochemical grafting of primary amines onto carbon surfaces can provide useful materials with applications in biosensing and immunodiagnostics [1,2]. However, the modification process has not been widely studied. Modification occurs by electrochemical oxidation via a radical coupling mechanism, resulting in covalent coupling of the amine to the carbon surface, as shown in Figure 1 [3].

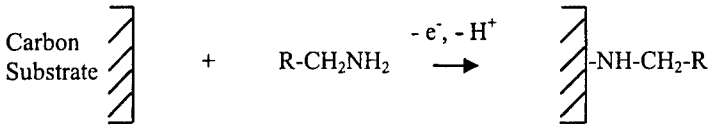

Figure 1. Mechanism for the electrochemical oxidation of primary amines to carbon substrates.

In this work, three primary amines: 1,12-diaminododecane, *n*-tridecylamine, 4-nitrophenylethylene amine, were covalently coupled to the carbon surface using electrochemical oxidation. These specific amines were selected in order to compare film thickness and surface coverage for a monoamine, diamine and aromatic amine film.

Varied electrolysis times were applied to yield multilayer films of different thickness for all three amines. Atomic force microscopy (AFM) scratching was used to monitor the thickness of these multilayer amine films and surface coverage was monitored using X-ray photoelectron spectroscopy (XPS) and electrochemistry. The reduction of the nitro- (NO_2) groups of the aromatic amine was used to measure its surface coverage.

Very smooth carbon films (pyrolysed photoresist film (PPF)) were the substrates used. PPF was prepared by spin-coating photoresist onto silicon wafers and pyrolysing at 1050 °C. The resulting films are 1.5 μm thick with physical and electrical properties similar to glassy carbon but with typical RMS surface roughness of 0.2-0.5 nm.

References

[1] H. Tanaka, A. Aramata, J. Electroanal. Chem. **437** (1997)
[2] X. Han, L. Wang, B. Qi, X. Yang, E. Wang, Anal. Chem. **75**, 23 (2003)
[3] B. Barbier, J. Pinson, G. Desarmot, M. Sanchez, J. Electrochem. Soc. **137**, 6 (1990)

* Contact author: sqt10@student.canterbury.ac.nz

Fabrication and surface modification of composite carbon and silicon hybrid materials

Samuel S.C Yu [1]*; Alison J Downard [1]; Paula A Brooksby [1]; Emelyn S.Q Tan [1]; Richard J Blaikie [2]
[1] *Department of Chemistry, University of Canterbury, Christchurch, New Zealand*
[2] *Department of Electrical Engineering, University of Canterbury, Christchurch, New Zealand*
The MacDiarmid Institute of Advanced Materials and Nanotechnology

Patterning surfaces with chemical functionalities is an important objective for preparing functional materials with potential applications in areas of nanotechnology such as molecular electronics, sensors and biochips. Developing the capability to controllably graft simple molecules onto surfaces in patterns and to assemble functional species (e.g: nanoparticles and/or recognition molecules) on these patterned arrays to form larger structural aggregates is of fundamental importance in the bottom-up fabrication of molecular architectures and novel materials (Figure 1).

We sought to develop the substrate materials and methods to form novel composite materials that incorporate both silicon and carbon in the same substrate, which can then be modified to give areas that exhibit different chemical properties. Composite hybrid structures were fabricated by the pyrolysis of photoresist materials in combination with utilising photolithography technology. The photoresist material carbonises during pyrolysis and deposit as a thin film that behaves similarly to commercially available glassy carbon but has a surface RMS roughness between 0.4 – 0.6 nm.

By manipulating the diverse physical and chemical properties of the two materials that make up the composite, different attachment chemistry were utilised. Modification of the silicon material via silane chemistry and the layer-by-layer (LbL) deposition of polyelectrolyte were investigated. Pyrolysed carbon and glassy carbon substrate materials were modified via electrochemically induced radical coupling methods (i.e: reduction of diazoniums, oxidation of aryl carboxylates and amines).

Assemblies of gold and latex nanoparticles were constructed to aid in visualisation of the underlying patterned surface. These assemblies also have wider applications as sensing layers and in catalysis.

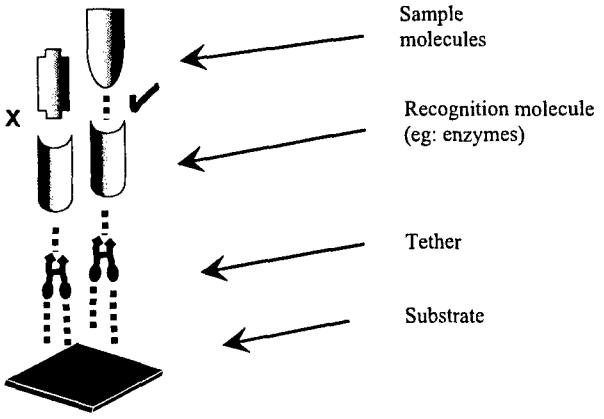

Figure 1: Functional materials can be made when recognition molecules are attached to the tethers patterned on the substrate surface. These molecules are able to selectively recognize target molecules via specific chemical interactions, thus any molecules of interest can be detected. This is the basis of many sensor device designs.

* Presenting author: ssy14@student.canterbury.ac.nz

Effect of UV Irradiation on the Structure of Passive Oxide Films

H. Nanjo[1,*], M. Fujimura[2], M. Nishioka[1] I. Ishikawa[1] and J. Onagawa[2]
[1] *Laboratory for Membrane Chemistry, National Institute of Advanced Industrial Science and Technology (AIST), 4-2-1, Nigatake, Miyagino-ku, Sendai 983-8551, JAPAN*
[2] *Tohoku Gakuin University 1-13-1, Chuo, Tagajo 985-8537, JAPAN*

Ultra-Violet (UV) irradiation of some passive metals has been found to increase the pitting potential (which is measured in aggressive, chloride-containing, aqueous environments), thereby inhibiting pitting corrosion of that metal. Although surface-emergent non-metallic inclusions or other impurity particles are usually identified as the microscopic sites of pit initiation, it remains unclear as to what nanoscopic surface sites are involved in the true nucleation of a corrosion pit. One possibility is that such sites are simply defects of one sort or another in the structure of the passive oxide film, and that UV irradiation can reduce the number density of such defects and thereby decrease the probability of pit nucleation.

Here we describe experiments to investigate the effect of UV irradiation on the surface structure of pure iron, anodically passivated in mildly alkaline borate buffer solution. As in previous work, in which the crystalline surface structure of passivated stainless steel was clearly observed [1,2], atomic-resolution scanning tunnelling microscopy (STM) has been used. In addition, spectroscopic ellipsometry has been used together with standard electrochemical methods such as open circuit potential decay and cyclic voltammography.

We have shown previously that passivated iron surfaces display a stable structure in given conditions, but remain able to show structural changes in response to environmental stimuli, for up to about 140 minutes exposure to air after passivation [3]. Hence, in this work, samples were always irradiated within 140 min of the electrochemical passivation treatment being completed. The UV irradiation itself was carried out for two hours, using light of wavelength 254 nm and an intensity of 3 mW/cm^2. Preliminary results, see Figure 1, indicate that the surface structure, as imaged by STM, tends to become increasingly crystalline as a result of the UV treatment.

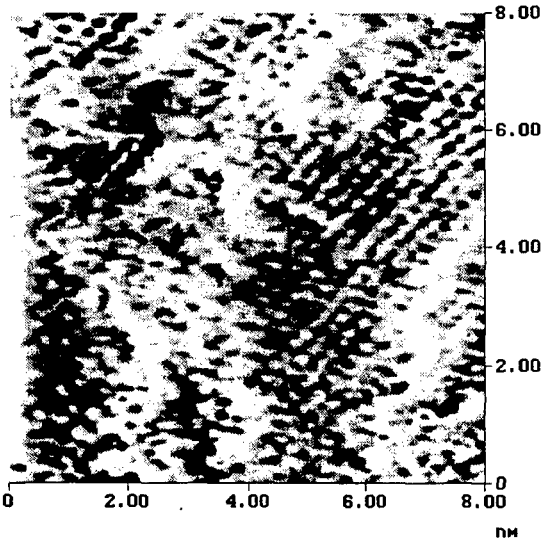

Figure 1: Atomic-scale image of passive iron surface treated with UV irradiation with 254 nm and 3 mW/cm^2 for two hours.

References

[1] H. Nanjo, H. H. Deng, I. Ishikawa, Y. Kurata, and N. Sanada, Research Trends, **9**, 21-218 (2003).
[2] H. Nanjo, N. J. Laycock, H. H. Deng, I. Ishikawa, N. Sanada, Current Applied Physics, **4**, 156 (2004).
[3] H. H. Deng, I. Ishikawa, M. Yoneya, H. Nanjo, J. Phys. Chem. B **108**, 9138 (2004).

* Contact author: hi-nanjo@aist.go.jp

Electrochemistry of room temperature ionic liquids

Adrian Gestos, William E. Price[1] and Gordon G. Wallace.
Intelligent Polymer Research Institute and Department of Chemistry, University of Wollongong, Wollongong, NSW 2522 Australia.

Room temperature ionic liquids (IL) are increasingly finding applications as electrolytes in a range of devices and composites with conducting polymers and other advanced materials. [1] In order to fully exploit these IL it is necessary to fully understand their properties. One particular area of interest is their electrochemical properties. Here this study focuses on redox chemistry in a common IL, 1-butyl –3-methylimidazoium tetrafluoroborate

The potential window for butyl methyl imidazolium (BMI)-BF_4 with a glassy carbon electrode was found to be 4.15 V (-2.15 to +2 V) Cathodic and anodic peaks appeared at -0.75 and -0.67 V respectively. The peaks were not affected by differing potential limits applied to the CV. When 0.02 M Cu (II) as $Cu(NO_3)_2$ was added to BMI-BF_4 and CVs were carried out at a glassy carbon working electrode, the resultant voltammogram showed clear redox peaks which were not present in the blank ionic liquid. Therefore these peaks may be attributed to the oxidation and reduction of copper (Cu^{2+}/Cu).

The Voltammogram of Cu (II) in BMI-BF_4 with glassy carbon working electrode is shown in Fig. 1. Clear redox chemistry of Cu (II) was observed with highly reproducible results. The first cathodic peak at +0.23 V was not present in the CV conducted during the preliminary tests, so it is probably due to a contaminant that is presently unknown. The next two cathodic peaks at +0.05 and -0.22 V are due to the reduction of Cu (II) with the two separate peaks most likely due to its two separate oxidation states. Two anodic peaks seen at +0.37 and +0.54 are due the oxidation of the reduced copper and tentatively assigned to its two separate oxidation states. The presence of two separate peaks relating to the two oxidation states of copper has also been seen in other studies in both di-alkylimidazolium [2] and in chloroaluminate based ionic liquids. [3] In aqueous solutions, due to the low stability of Cu (I) the two separate peaks are not observed due to the rapid reduction to copper or oxidation to Cu (II).

ASV experiments carried out at a glassy carbon working electrode show that with increasing deposition times, the size of the resultant oxidation peaks would increase (Fig. 2). The peaks seen in these ASVs are all attributable to the oxidation of copper and so the increase in deposition time results in increased amounts of copper being deposited. The presence of two separate peaks in each of the ASVs carried out is attributed to the oxidation of copper to two oxidation states,

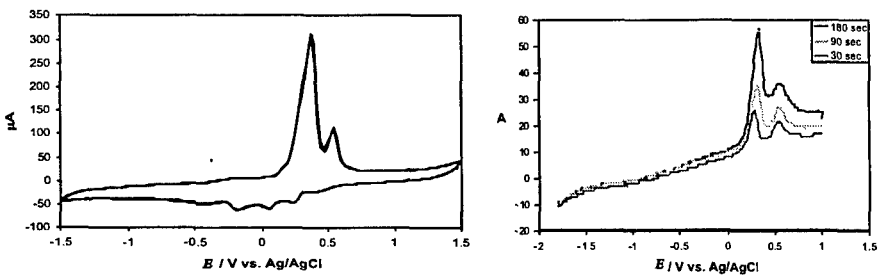

Fig. 1 & 2. CV and ASVs of Cu (II) 0.02 M in BMI-BF_4 with glassy carbon electrode, scan rate 100 mV/S at -1.8 V for 180, 90 and 30 seconds.

The size of the oxidation peak increased with increasing deposition times indicated that the amount of copper deposited at the electrode increased with increasing deposition time. Further experiments showed that decreasing the negative potential used during deposition resulted in a decrease in the size of the oxidation peaks with around –1.2V being the minimum needed to deposit reduce copper (0).

References

[1]. W . Lu et al., Science, 297, (2002) 983-987.
[2]. P-Y. Chen and I.W. Sun,Electrochimica Acta, 45, 1999, 441-450.
[3]. C.L. Hussey, L.A. King, and R.A. Carpio, J. Electrochemical Society, 126, 1979, 1029-1034.

[1] William Price. Email: wprice@uow.edu.au

Origin of the optical anisotropy oscillations of Si(001) surfaces during oxidation

W. G. Schmidt*, F. Fuchs, and F. Bechstedt
Institut für Festkörpertheorie und -optik,
Friedrich-Schiller-Universität, Max-Wien-Platz 1, 07743 Jena, Germany

The oxidation of Si(001) is of high scientific interest and of extreme technological relevance, due to importance of thin insultating SiO_2 layers and SiO_2/Si interfaces for the operation of many electronic devices. The finding by Yasuda *et al.* [1] that the oxidation of silicon gives rise to distinct optical fingerprints that repeatedly change their polarity during the oxidation has a large potential for the in-situ monitoring and control of the oxidation process as well as for highly accurate thickness measurements of silicon oxid films. In order to realize that potential, however, one needs to understand the physics behind the oscillations of the optical signal and to determine the precise relation between the micoscopic structure of the SiO_2/Si interfaces and its optical response.

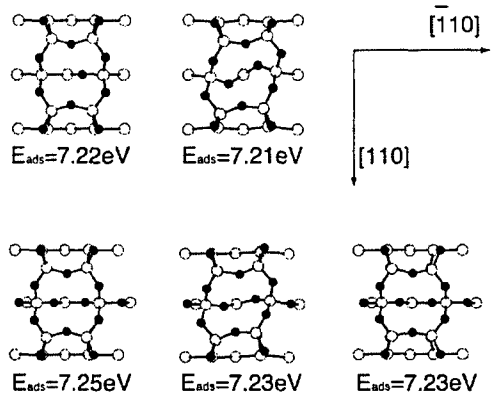

Figure: Examples for models used to describe oxidation of the first and second Si(001) layers. Dark and grey symbols indicate O and Si atoms, respectively.

We calculated the optical response of a large number of oxidized surface [2] and bulk structures as well as differently strained silicon lattices from first principles. The calculations are performed within the gradient-corrected density functional theory (DFT-GGA) in conjunction with the projector-augmented wave (PAW) method [3] as implemented in the VASP package [4]. The optical anisotropy spectra are calculated in the independent-quasiparticle approximation using all-electron wave functions obtained from the PAW method.

Comparison of the simulated spectra with measured data confirms that the oxidation proceeds layer-by-layer and shows that changes of the interface optical response are directly related to the alternating oxidation of Si-Si bonds in the (-110) and (110) plane. The local strain around the inserted oxygen atoms is identified as cause of the measured optical anisotropies. Our results lead to a better understanding of the Si oxidation process and suggest optical spectroscopy for monitoring microscopic details of the oxidation process.

* Email: W.G.Schmidt@ifto.physik.uni-jena.de

References

[1] T. Yasuda *et al.*, Phys. Rev. Lett. **87**, 037403 (2001).
[2] T. Yamasaki, K. Kato, and T. Uda, Phys. Rev. Lett. **91**, 146102 (2003).
[3] G. Kresse and D. Joubert, Phys. Rev. B **59**, 1758 (1998).
[4] G. Kresse and J. Furthmüller, Comp. Mat. Sci. **6**, 15 (1996).

Nitrophenyl and Nitroazobenzene Thin Films on Carbon Surfaces.

Paula A. Brooksby *and Alison J. Downard
Department of Chemistry, University of Canterbury, Christchurch, NEW ZEALAND

The chemical modification of carbon surfaces during the electrochemical reduction of aryl diazonium salts is one way of functionalizing the carbon interface, and in recent years this method has been successfully applied to metallic substrates. Unlike gold-SAM surfaces that exhibit relatively well-ordered monolayers, the diazonium route to surface modification produces thin films that are comparatively disordered and mulitlayered, and little is known about their bulk structure. This study investigated the thin films that are formed on flat carbon surfaces during the non-aqueous reduction of dilute solutions of nitrophenyl (NP) and nitroazobenzene (NAB) diazonium salts for selected electrolysis times[1].

The surface confined nitro group introduces a versatile functionality to the interface. It can be used as an in-situ electrochemical probe providing information about film coverage, or it can be easily converted to the amine group required for many additional chemical-coupling mechanisms. The current response in aqueous acidic solutions, from the complete reduction of $-NO_2$ to $-NH_2$, was determined using cyclic voltammetry (Fig.1 left) and the apparent number NP or NAB groups calculated from the area of the current peak[1]. Additionally, the film heights were profiled with an AFM tip that was used to mechanically remove a section of the film from the surface[1]. These surface trenches are easily re-examined between experiments; hence each films thickness could be monitored after particular experimental steps (Fig.1 right).

The film height data indicate NP and NAB films grow rapidly in the first minute during electrolysis and thereafter only small changes occur. Although the electrochemical data show similar trends, the time required to attain limiting conditions is marginally longer, and the peak potentials do not remain constant (Fig.1 left). This last feature is associated with changing electron-transfer dynamics within the film as it grows. Further, there is an apparent loss of the nitro group electroactivity in NAB films that can arise from either the loss of nitro groups during the coupling of each new film layer to an existing one, or due to the imbedding of the nitro group at locations where diffusion of solutions species are hindered. Both NP and NAB film heights were determined to be sensitive to ion-solvent interactions. Film swelling and shrinking was monitored after potential cycling in aqueous and non-aqueous solutions. The results show the free volume in the NAB films is near 50 %, whereas for NP it is 20 %.

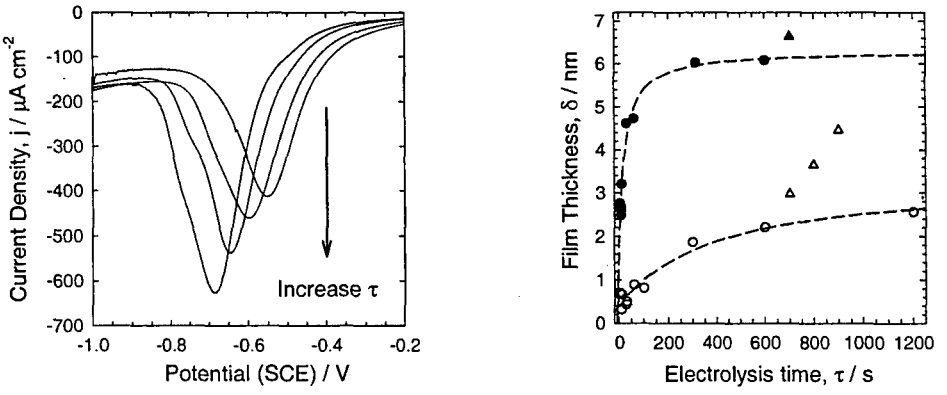

Figure. 1 (left) Cyclic voltammograms of selected NAB surfaces illustrating peak behavior as electrolysis time (τ) increases for τ = 60, 100, 300 and 600 s. (right) Plot of NAB film thickness (δ) against electrolysis time before and after electrochemical reduction in 0.1 M H_2SO_4.

Reference

(1) Brooksby, P. A.; Downard, A. J. *Langmuir* **2004**, *20*, 5038.

* Contact address: paula.brooksby@canterbury.ac.nz

Isothermal Microcalorimetry as a Technique for Material Characterization

Victor E. Ostrovskii
Karpov Institute of Physical Chemistry, Voronrsovo Pole Str. 10, 105064 Moscow, Russia, e-mail: vostrov@cc.nifhi.ac.ru

Microcalorimetry as such and in combination with several analytical physico-chemical techniques, for example, mass-spectrometry or chromatography or physical techniques, for example, conductivity-metry represents the unique non-destructive method allowing for characterizing quantitatively (1) the surface and body chemical states of different materials; (2) the degree of their stability and reactivity in different gaseous media at different temperatures; and (3) their thermo-physical properties. Calorimetric sensors of chemical effects have several important features, for example, they: (1) are capable of quantitative measuring not only the direct chemical actions but also the post-effects and of distinguishing the exothermic processes from the endothermic ones; (2) allow differentiating the surface effects from the body effects; (3) allow integrating the effects from a number of objects of any system; therewith, the current and time-integrated signals are proportional to the reaction rate and product amount, respectively; and (4) allow continuous controlling the material states or reaction rates for many-month periods and under different well-defined temperature regimes.

The instruments, techniques, and procedures, including their possibilities and main "pitfalls" that should be turned aside by experimenters, will be considered on the basis of our recent reviews [1, 2].

The illustrative examples from [1-7] demonstrating a number of applications of calorimetric methods for characterizing the surfaces and bodies of different metal, oxide, and polymer materials and for clarification of the chemical processes proceeding in these solids under different conditions will be presented and considered.

References:

[1]. V.E. Ostrovskii, "Differential microcalorimeter for isothermal measurements of heat effects in two-phase systems and examples of its application", Rev. Sci. Instr., 73 (2002) 1304-1312.
[2]. V.E. Ostrovskii, "Some problems in adsorption and calorimetric studies of the steps of catalytic processes", J. Natural Gas Chem., 13(3) (2004) 15-40.
[3]. V.E. Ostrovskii, ""Paradox of heterogeneous catalysis": paradox or regularity", Ind. Eng. Chem. Res., 43 (2004) 3113-3126.
[4]. V.E. Ostrovskii, "Mechanisms of methanol synthesis from hydrogen and carbon oxides at Cu-Zn-containing catalysts in the context of some fundamental problems of heterogeneous catalysis", Catal. Today, 77 (2002) 141-160.
[5]. V.E. Ostrovskii, B.V. Tsurkova, E.A. Kadyshevich, and B.V. Gostev, "Comparison study of the acrylamide-water and polyacrylamide-water systems: differential heat effects, kinetics, and mechanisms of drying and vapor-phase wetting", J. Phys. Chem. B, 105 (2001) 12680-12687.
[6]. V.E. Ostrovskii, "Metal-oxygen-hydrogen solid system of controlled composition: differential heat effects, kinetics, and mechanism of the $CuO \rightarrow Cu_4 \cdot OH_2$ grading", Intern. J. Modern Phys. B, 16 (1-2) (2002) 42-49.
[7]. V.E. Ostrovskii, "Combined use of calorimetric and kinetic methods for the study of the mechanisms of catalytic processes", J. Therm. Anal., 14 (1978) 27-43.

Spectroscopic studies of interactions of polyaniline with some Cu(II) compounds

M. Gizdavic-Nikolaidis[1],* J. Travas-Sejdic[1], R. P Cooney[1] and
G. A. Bowmaker[1]
[1]*Polymer Electronics Research Center, Department of Chemistry,*
The University of Auckland, Private Bag 92019, Auckland, NEW ZEALAND

The interaction of polyaniline (PANI) with metal atoms is important in relation to the increasing use of this polymer in organic electronics [1], electroluminescent devices [2], as protective coating against corrosion of metal surfaces [3, 4], etc. In this work, anion exchange of emeraldine salt-polyaniline (ES-PANI = HCl-doped emeraldine base-polyaniline, EB-PANI) with Cu(II) complex anions $[Cu(II)PcTs]^{4-}$ and $[Cu(II)Cat]^{2-}$ (PcTs = phthalocyaninetetrasulfonate; Cat = catecholate), and reactions of EB-PANI following different levels of reduction or HCl doping with 0.1 M $CuCl_2$ aq. solution are investigated by EPR and FTIR spectroscopy. The conductivities of the resulting samples also have been measured.

The EPR spectra of PANI show a decrease in the intensity of the EPR signals from polarons following ion-exchange doping by Cu(II) complexes. This probably results from the formation of more bipolarons as the Cu(II) anion concentration increases, suggesting that Cu(II) dopants cause a shift in the polaron/bipolaron equilibrium such that the bipolaron state is favored due to the 2- or 4- charges on the dopants. Similar observations have been made previously for Cu(II) complex-doped PITN powders (PITN = polyisothianaphthene) [5]. The influence of the solvent on the ion-exchange between ES-PANI and $[Cu(II)PcTs]^{4-}$ anions has been investigated by FTIR and EPR spectroscopy. The highest conductivity of 0.3438 S/cm was observed for $[Cu(II)Cat]^{2-}$ doped PANI. The measured conductivity of $[Cu(II)PcTs]^{4-}$ doped PANI sample was 0.05282 S/cm which is similar to the value observed for $[Cu(II)PcTs]^{4-}$-doped polypyrrole studied by Saunders et al. [6], where doping with $[Cu(II)PcTs]^{4-}$ was reported to have little influence on the conductivity.

We also investigated the reaction of R-PANI (EB-PANI reduced with hydrazine [7]), EB-PANI and ES-PANI with 0.1 M $CuCl_2$ (aq.) solution. The polaron peak in the EPR spectra of EB-PANI and R-PANI samples increases after doping with 0.1 M $CuCl_2$, while in ES-PANI the polaron peak decreases (similar to the case of PANI doped with Cu(II) complex anions). The FTIR spectrum of R-PANI shows an increase in the intensity of the quinoid peak and a shift to lower frequency of the peaks 1593.4 and 1164.5 cm^{-1} (to 1581.1 and 1139.8 cm^{-1} respectively), as in the case of EB-PANI (1159.7 to 1142.2 cm^{-1}) upon reaction with $CuCl_2$. The EPR and FTIR results indicate that the polymer has undergone oxidation by reaction with $CuCl_2$. In the case of R-PANI, the polymer becomes oxidized and protonated at the same time. This interpretation differs from that presented in a previously published study of similar EB-PANI-metal complex salts systems, where the interaction between metal cations and the polymer was described as coordination of the metal cations to nitrogen atoms of both benezenoid and quinoid groups in adjacent chains of EB-PANI [8-10].

References:

[1] J. Paloheimo, K. Laakso and H. Isotalo, Synth. Met. **68**, 257 (1995).
[2] S. N. Cheng, K. R. Chuang, C. I. Chao and H. T. Lee, Synth. Met. **82**, 207 (1996).
[3] A. J. Epstein, A. O. Smallfield, H. Guan and M. Fahlman, Synth. Met. **102**, 1374 (1999).
[4] J. Posdorfer and B. Wessling, Synth. Met. **119**, 363 (2001).
[5] W. T. Chen, G. A. Bowmaker and R. P. Cooney, Phys. Chem. **4**, 4218 (2002).
[6] B. R. Saunders, K. S. Murray and R. J. Fleming, Synth. Met. **47**, 167 (1992).
[7] X. R. Zeng and T. M. Ko, Polymer **39**, 1187 (1997).
[8] O. P. Dimitriev, Polymer Bulletin **50**, 83 (2003).
[9] O. P. Dimitriev, Synth. Met. **142**, 299 (2004).
[10] O. P. Dimitriev, Macromolecules **37**, 3388 (2004).

* Contact author: m.gizdavic@auckland.ac.nz

Soluble Alkoxy-substituted Poly(terthiophenes): Polymerisation, Characterisation and Device Fabrication

A. M. Ballantyne,[1,*] D. L. Officer,[1] S. B. Hall,[1] G. G. Wallace,[2] C. Wang,[2] Y.Wu,[2] V. J. Misoska[2] and G.Tsekouras[2]

[1] *Nanomaterials Research Centre and McDiarmid Institute for Advanced Materials and Nanotechnology Massey University, Palmerston North, NEW ZEALAND*

[2] *Intelligent Polymer Research Institute, University of Wollongong, Wollongong, AUSTRALIA*

Conducting polymers display properties such as high conductivity, light weight, processability and redox activity giving them great potential for use in many applications.[2] Polythiophenes[34] have proved to be particularly useful because they have good chemical stability and are easily functionalised.

Solubility in organic solvents is desired for processing by techniques such as electrospinning, spin-coating and casting to prepare materials for use in devices and can be achieved simply by attaching alkyl or alkoxy substituents to the polymer backbone. While much work has been focused on attaching alkyl substituents to increase solubility, these polymers are often found to have low stability in the oxidised state. Although less studied due to their lower solubility, alkoxy-substituted polythiophenes display a higher stability in the conducting state due to the electron-donating influence of the oxygen causing smaller bandgaps and lower oxidation potentials.[115]

We have produced a 4,4"-di(decyloxy)-3'-styrylterthiophene polymer (Figure) on gram-scale by chemical polymerisation with iron chloride. Fractions of different oligomers have been separated by subjecting the crude polymer to soxhlet extractions in different solvents, and these have been studied using MALDI-MS and UV-VIS-NIR. Oligomer lengths of up to 90 thiophene units have been detected, and the compact, bronze coloured films produced display conductivities exceeding 1 S cm^{-1}. The results of preliminary investigations into the use of these materials in actuators and other devices will be presented and discussed.

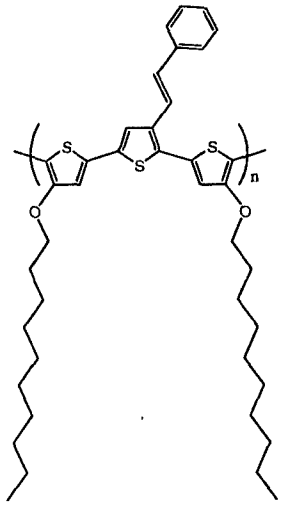

Poly(4,4"-di(decyloxy)-3'-styrylterthiophene)

References

[1] A. G. MacDiarmid, Synthetic Metals. **125**, 1, (2001).
[2] J. Roncali, Chemical Reviews. **92**, 4, (1992).
[3] G. Zotti, M. C. Gallazzi, G. Zerbi, and S.V. Meille, Synthetic Metals. **73**, 3, (1995).

* Contact author: a.m.ballantyne@massey.ac.nz

Biocidal and Electronic Properties of Intrinsically Conducting Polymer-Based Composites

M. J. Richardson,* J. H. Johnston and T. Borrmann[1]
[1] *MacDiarmid Institute for Advanced Materials and Nanotechnology, and the School of Chemical and Physical Sciences, Victoria University, Wellington, NEW ZEALAND*

Intrinsically conducting polymers (ICP's), first reported by MacDiarmid, Heeger and Shirakawa [1], are based on a backbone of oxidised or reduced monomers comprising conjugated double bond systems. Generally formed as intractable and insoluble powders or films, mechanical processing of the polymers can be problematic. While much work has been undertaken on the polymers alone, little is known regarding their properties when formed as composites with other organic materials.

Initial studies have shown that i*n-situ* polymerisation of pyrrole, aniline and derivatives with cellulosic substrates can provide composite materials with potentially useful properties. Conductivity relative to the untreated substrate is increased, and an inverse relationship of conductivity to dielectric, and hence capacitance is observed. When the substrate comprises *Pinus radiata*, *Ochroma pyramidale* or conventional filter paper, the conductivity is enhanced by the conducting polymer to a level where a metallic layer such as copper may be deposited electrochemically onto the composite surface (Figure 1). The metal surface may be oxidised to form either the green carbonate patina commonly seen on bronze statues, or a deep red oxide layer. When the polymer used is polypyrrole, metallic silver may be reduced onto the surface from a solution of silver ions following reduction of the polymer *via* hydrazine or sodium borohydride. The ICP-cellulose composites and their metallic derivatives have been characterised *via* scanning electron microscopy, infrared spectroscopy, impedance analysis and conductivity measurements [2].

Wood-polypyrrole composites are resistant to fungal and microbial degradation, offering a potential replacement for the problematic copper, chrome and arsenic-based technologies currently used for timber preservation.

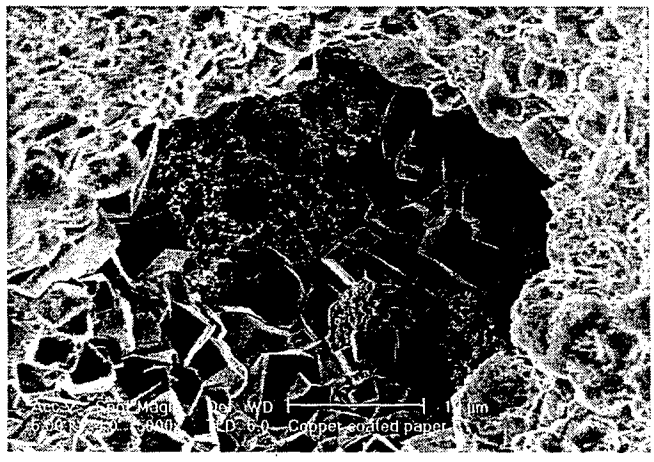

FIG1. *Scanning electron image of copper-coated paper.*

References

[1] Chiang, C. K.; Fincher, C. R., Jr.; Park, Y. W.; Heeger, A. J.; Shirakawa, H.; Louis, E. J.; Gau, S. C.; MacDiarmid, A. G. Electrical conductivity in doped polyacetylene. Phy. Rev. Lett., **39**, 17, 1098 (1977).

[2] Richardson, M. J. and Johnston, J. H., Wood-polymer composites, NZ Provisional Patent 533816, June 2004.

* Contact author: michael.richardson@vuw.ac.nz

Semiconducting Polyaniline-Vanadium Oxide Nanocomposites

Inna Karatchevtseva, Vittorio Luca, Mark Blackford, and Zhaoming Zhang
Materials and Engineering Science, Australian Nuclear Science & Technology Organisation, Sydney, Australia

Application of conducting polymers in electronic devices often requires nanosized components with diverse periodicities, orientation and morphologies which can lead to enhanced conductivity and other properties compared with bulk materials [1,2]. Recently, much interest has been shown in enhancing the order and consequent conductivity of polyaniline by using either a template- [3,4] or template-free based approach. The latter approach can utilize, for example, β–naphthalene sulfonic acid [5] (NSA) or camphor sulfonic acid [6] (CSA) as dopants. Recently a number of attempts [7,8] have been made to produce nanocomposites comprising V_2O_5 and polyaniline. One of the most common methods to prepare PANI-V_2O_5 nanocomposites is the *in-situ* oxidative polymerization/intercalation of aniline in V_2O_5 xerogel. However, this method has been reported to yield V_2O_4 [9], which decreases the cell capacity and alters the optical absorption properties of the composite.

It has been reported that the semi-conducting metal oxides, such as vanadium pentoxide (V_2O_5), for example, which is often employed in secondary lithium batteries to improve the capacity, reversibility and stability, can be used to alter PANI properties and therefore V_2O_5 (E_g = 2.8 eV) is used as the semiconducting component.

In this study electrochemical methods are explored for the preparation of novel interpenetrating network morphologies involving conducting polymers and semiconducting oxides components with novel properties. This method involves the electrochemically stimulated manipulation of novel materials at the molecular level. PANI-V_2O_5 nanocomposites have been prepared by electrochemical means using titanium metal plates as working electrodes. Electrochemical deposition has the potential advantages of short fabrication times, ease of preparation, and the ability to control the film thickness and morphology. Structure and composition of these nanohybrids were investigated by SEM, TEM, FTIR, XRD, and XPS. Morphology of electrochemically prepared polyaniline films is fibrillar in nature and very porous as shown in Figure 1 a. It has also been shown that the morphology of PANI-V_2O_5 nanohybrids depends strongly on the experimental conditions: the nature and surface preparation of electrodes, current density (Figure 1 b and c) and deposition time.

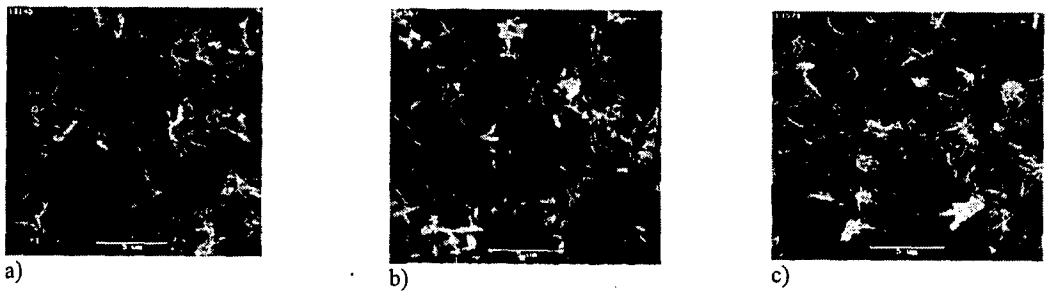

a) b) c)

Figure 1. SEM images of (a) PANI film, and PANI-V_2O_5 nanocomposites deposited for 30 min at (b) 2mA/cm^2 and (c) 6mA/cm^2

Reference:

[1] T.Bein, P.Enzel, Angew. Chem. Int. Engl., **28** (1989)
[2] V.P.Menon, J.Lei, and C.R.Martin, Chem. Mater., **8** (1996)
[3] P.N.Bartlett *et al.*, J.Mater.Chem., **11** (2001)
[4] M.Delvaux *et al.*, Synthetic Metals, **113** (2000)
[5] Z.Zhang, and M.Wan, Synthetic Metals, **132** (2003)
[6] Y.Long et al., Appl.Phys.Lett., **83**, 9 (2003)
[7] M.G.Kanatzidis *et al.*, J.Am. Chem. Soc., **111** (1989)
[8] F.Huguenin, R.M.Torresi, and D.A.Buttry, J. Electrochem.Soc., **149**, 5 (2002)
[9] F.Leurox *et al.*, J.Electrochem.Soc., **144** (1997)

Contact author : ikm@ansto.gov.au

Soluble Poly-3-alkylpyrrole polymers on Films and Fabrics.

Richard Foitzik, Akif Kaynak, Jens Beckmann, Richard Russell

Deakin University, School of Engineering & Technology, Geelong, Victoria 3217 Australia

Soluble conductive polymers have been intensely studied over the last 15 years, due to their versatility and functionality interest on them has grown rapidly. Poly(3-alkylpyrroles) are soluble in limited organic solvents. Conductive textiles are a relatively new field with boundless applications. By chemical polymerisation of 3-alkylpyrroles with Iron (III) Chloride in the presence of textiles, conductive textiles with specific properties can be produced. The addition of dopants and wetting agents has also been investigated with an optimum procedure being created. The morphologies of these coatings are altered from the traditional conductive coatings, having a more intense coating. Comparison under a SEM show's substantial differences.

Effect of milling on the perovskite phase formation of $Pb(Mg_{1/3}Nb_{2/3})O_3$ using the starting precursors PbO and $MgNb_2O_6$.

A. Chaipanich* and T. Tunkasiri
Department of Physics, Faculty of Science, Chiang Mai University, Chiang Mai, Thailand 50200

SMART $Pb(Mg_{1/3}Nb_{2/3})O_3$ (PMN) ferroelectric relaxor have found used in many applications such as capacitors, actuators and ultrasonic transducers [1-3]. The perovskite structure PMN possesses high dielectric properties but is plagued by the occurrence of pyrochlore phase which caused the reduction of the dielectric constant [4-6]. Many current processes are concerned with chemical routes as well as solid-state reaction using mixed oxide methods in producing pyrochlore free PMN [7-10]. These works often relates to the calcination condition in terms of temperature required in obtaining the perovskite phase at a particular milling time. It is believed that finer particles can improve the reaction and consequently reduced the calcination temperature [11]. In this work, a columbite method pioneered by Swartz and Shrout [6] was investigated further in terms of the effect of milling. Columbite, $MgNb_2O_6$, were ball milled with PbO for 24, 48, 72 and 96 hours before calcining at 650-750°C for 2 hours. An average particle size was found to reduce from 4.26μm (at 24 hours) to 1.05μm after milling for 96 hours. At a given calcination temperature, more perovskite phase and less impurities were detected by X-ray diffraction (Fig. 1) for samples those were milled longer compare to the conventional 24 hours milling. The results agree with the differential analysis curve results (Fig. 2) where less exothermic heat were given in longer milled samples, suggesting the heat energy required for PMN reaction would be less in these samples compared to sample that was milled only for 24 hours. Furthermore, by milling the particles of the precursors finer, it was found that calcination temperature required to obtain similar percentages of perovskite phase were reduced.

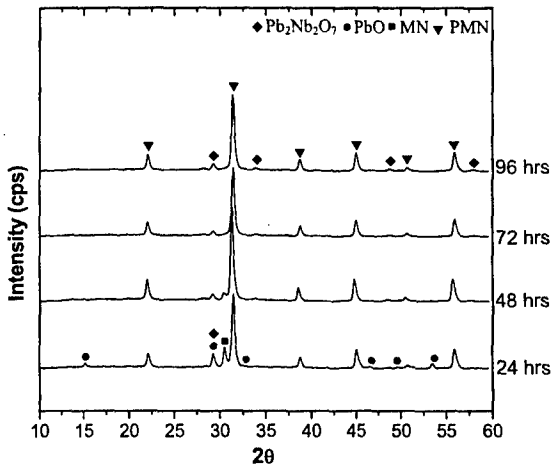

Figure 1 XRD patterns of calcined PMN powders at 750°C for 2 hours

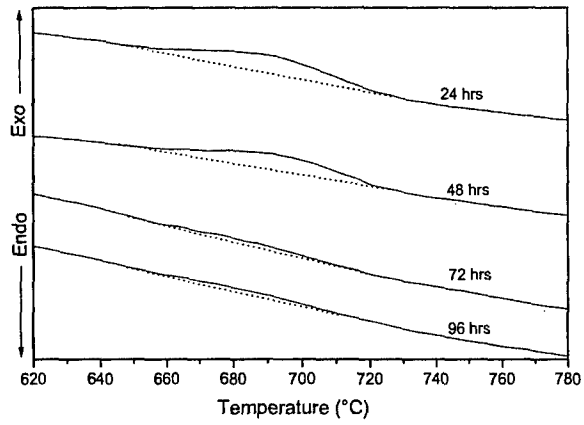

Figure2 DTA results at different milling time

References

[1] R.E. Newnham, A. Amin, Chem.Tech. 29, 38 (1999).
[2] K. Uchino, Piezoelectrics and Ultrasonic Applications, Kluwer, Deventer, (1998).
[3] S. Trolier-McKinsty, R.E. Newnham, Mater. Res. Bull. 18, 27 (1993).
[4] A.J. Moulson, J.M. Herbert, Electroceramics, 2nd Ed., Wiley, (2003).
[5] T.R. Shrout, S.L. Swartz, Mater. Res. Bull. 18, 663 (1983).
[6] S.L. Swartz, T.R. Shrout, Mater. Res. Bull. 17, 1245 (1982).
[7] S. Ananta, N.W. Thomas, J. Euro. Ceram. Soc. 19, 155 (1999).
[8] C.H. Lu, H.S.Yang, Mat. Sci. B - Solid B84, 159 (2001).
[9] N.K. Kim, Mater. Lett, 32, 127 (1997).
[10] E.R. Camargo, M. Kahihana, E. Longo, E.R.J. Leite, J. Alloy. Compd. 314, 140 (2001).
[11] B.D. Stojanovic, J. Mater. Process. Tech. 143, 78 (2003).

* contact author: arnon@chiangmai.ac.th

Ferromagnetism and Magnetoresistance in Chromium-doped Indium Tin Oxide

Hyoun Soo Kim[1], Sung Hwa Ji[2], Byoung Seon Lee[2], Hyojin Kim[2,*], Soon-Ku Hong[2], Dojin Kim[2], Young Eon Ihm[2] and Woong Kil Choo[1]

[1]*Department of Materials Science and Engineering, Korea Advanced Institute of Science and Technology, 373-1 Gusong-dong, Yousong-gu, Daejeon 305-701, Korea*

[2]*Department of Materials Science and Engineering, Chungnam National University, Daeduk Science Town, Daejon 305-764, Korea*

Recently wide bandgap semiconductors have attracted much attention as promising candidates for room temperature ferromagnetic semiconductors in the form of diluted magnetic semiconductors, which is referred to as semiconductor alloys in which some atoms are randomly substituted for by magnetic atoms.[1] Among them, transition-metal-doped ZnO and GaN have been investigated most extensively and intensively to yield controversial results yet to be elucidated. Indium oxide (In_2O_3) has a cubic bixbyite structure with a direct bandgap as wide as 3.75 eV. Indium tin oxide (ITO) is a widely used transparent conducting oxide with high electron concentration due to the doping effect of Sn. Here we report the observation of room temperature ferromagnetism in Cr-doped ITO (henceforth referred to as ITO:Cr).

Pure $(In_{0.95}Sn_{0.05})_2O_3$ [ITO] and 5 mol% Cr-doped $(In_{0.90}Cr_{0.05}Sn_{0.05})_2O_3$ [ITO:Cr05] films are grown on SiO_2/Si substrates by pulsed laser deposition at substrate temperature of 400℃ in an oxygen pressure of 100 mtorr, using sintered targets synthesized by standard solid-state reaction method. They are carefully examined by x-ray diffraction, and optical, magnetic and transport measurements. Structural analysis indicates that the all (100)-oriented films of bixbyite structure are grown without any detectable formation of secondary phases. The magnetic measurements for ITO:Cr05 clearly establish the presence of a ferromagnetic ordering with a Curie temperature above room temperature and a saturation magnetization of ~0.7 emu/cm^3 at 300K, while the pure ITO film shows diamagnetism. The ITO:Cr05 film exhibits *n*-type semiconducting character with an electron concentration of 1.22×10^{20} cm^{-3} and a resistivity of 1.45×10^{-2} Ω cm at 300 K. The Cr doping leads to a reduction of the optical band gap energy from 3.50 eV for ITO to 3.45 eV for ITO:Cr05 and an increase of resistivity with a slight decrease in electron concentration. The magnetoresistance behavior observed in ITO:Cr05 can be explained in terms of weak localization, s-d exchange coupling between the conducting carrier and localized spins of Cr ions, and spin-disorder scattering.

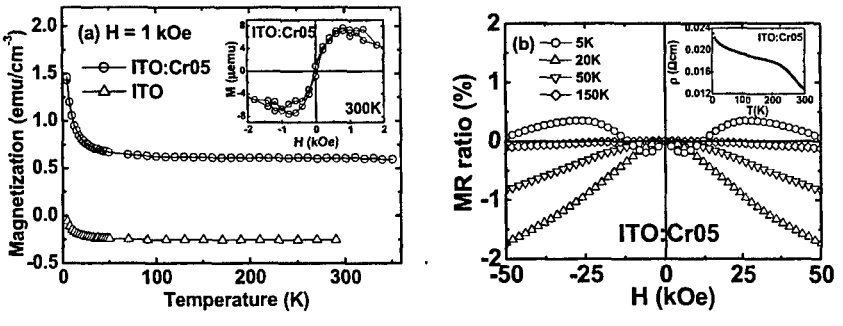

Figure 1. *(a) Magnetization vs. temperature measured in a field of 1 kOe for ITO and ITO:Cr05 films. The insert shows a magnetization vs. magnetic field measured at 300 K for a ITO:Cr05 film. (b) Magnetoresistance for a ITO:Cr05 film. The insert displays resistivity vs. temperature for a ITO:Cr05 film.*

References

[1] S. J. Pearton, C. R. Abernathy, M. E. Overberg, G. T. Thaler, D. P. Norton, N. Theodoropoulou, A. F. Hebard, Y. D. Park, C. Ren, J. Kim, and L. A. Boatner, J. Appl. Phys. **93**, 1 (2003).

* Contact author: hyojkim@cnu.ac.kr

The Effect of Uniaxial Stress to Spin Reorientation Transition and Hysteresis in Magnetic Thin-Films : Monte Carlo Investigation

Y. Laosiritaworn and R. Yimnirun*
Department of Physics, Faculty of Science, Chiang Mai University, Chiang Mai, Thailand.

J. Poulter
Department of Mathematics, Faculty of Science, Mahidol University, Bangkok, Thailand.

The growth of magnetic multi-layers on non-magnetic substrates has nowadays gained its interest as a result of both technological and fundamental importance [1]. Of particular interest is the technological applicability such as high-storage magnetic recording media. Due to the demanding on high areal densities of the recording media, the transition from longitudinal to perpendicular recording is required, in the context of the 'superparamagnetic limit', since the perpendicular recording provides a higher coercivity, smaller magnetic grains and a higher signal-to-noise ratio [2]. As a result, the knowledge about spin reorientation from in-plane to out-of-plane of the magnetic multi-layers is therefore very crucial.

Particularly, the reorientation of the magnetic spins in multi-layer films is due to the competition between the dipolar interaction and the out-of-plane magneto-crystalline anisotropy. The crystalline anisotropy is often contributed from mechanical stress. Even in an unstrained lattice, it can be regarded as the strained crystal due to some slightly different atomic position, e.g. the lattice mismatch at the interfaces between the magnetic layers and the substrates. Therefore, it is the objective of this study to model such a situation. Monte Carlo simulations [3] are performed using the Heisenberg Hamiltonian to investigate how the magnetic properties, including their layer resolutions, depend on temperature, thickness and the mechanical uniaxial stress being supplied on the surface layers of the magnetic films. In addition, under the influence from external sinusoidal magnetic field, the hysteresis loop is measured as a function of mechanical stress. From our preliminary results, it is found that the mechanical stress shifts the spin reorientation transition to a higher temperature. For the hysteresis loops, the stress suppresses the saturated magnetization and hence the remanence while coercivity is not significantly changed. Furthermore, the area inside the loop decreases with increasing stress which specifies the decrease of the energy dissipation.

References

[1] M.T. Johnson, P.J.H. Bloemen, F.J.A. den Broeder, and J.J. de Vries, Rep. Prog. Phys. **59**, 1409 (1996).
[2] J.H. Judy, J. Magn. Magn. Mater. **235**, 235 (2001),
[3] D.P. Landau and K. Binder, *A Guide to Monte Carlo Simulations in Statistical Physics* , (CUP,Cambridge, 2000)

* Contact author: RattikornYimnirun@yahoo.com

Magnetic Behaviour of Nanocomposites Containing Self-Assembled Magnetite Particles Dispersed in a Paraffin Wax Matrix

Chun-Rong Lin [1,*] Ti-Wen Sung[1] and Ray-Kuang Chiang [2]
[1]*Department of Mechanical Engineering, Southern Taiwan University of Technology, Tainan Hsien 710, Taiwan, Republic of China*
[2] *Department of Chemical Engineering, Far East College, Tainan 744, Taiwan, Republic of China*

Nanocomposites have attracted much attentation in recent years because of useful and unusual properties exhibited by them. In this study we report the preparation and magnetic properties of magnetite-paraffin wax nanocomposites. The monodisperse magnetite (Fe_3O_4) nanoparticles were prepared by following Sun's method [1] using the high-temperature solution phase reaction of iron (III) acetylacetonate with 1, 2-hexadecanediol in the presence of oleic acid and oleylamine. The particle size was estimated by the X-ray diffraction method as well as from the micrograph taken by a transmission electron microscope. To study particle size effect on the magnetic behaviour, three different particle sizes of magnetite (particle diameter $d \sim$ 4nm, 6nm, and 8 nm) were dispersed in paraffin wax. The weight ratio of Fe_3O_4 nanoparticles and paraffin wax was 1: 2.

Magnetic measurements show that all samples are superparamagnetic in the temperature range 77-300 K. From the Belov-Arrott plots (Fig. 1) we found that samples with 6 nm and 8 nm Fe_3O_4 nanoparticles have the magnetic ordering temperatures (T_m) above 300 K. Furthermore, the T_m for sample containing 4 nm Fe_3O_4 nanoparticles is approximately 150 K (inset of Fig. 1). The fit of the temperature-dependent magnetization to the Bloch law [2], $\sigma(T) = \sigma(0)(1 - BT^b)$, we found that the Bloch exponent differ from b =1.5 for the bulk phase (Fig. 2).

The permeability μ of magnetite-paraffin wax nanocomposites had been measured by the reflection/transmission coaxial line method in the range from 300 kHz to 8.5 GHz. The influence of size and chemical composition of particles upon dynamic permeability were studied.

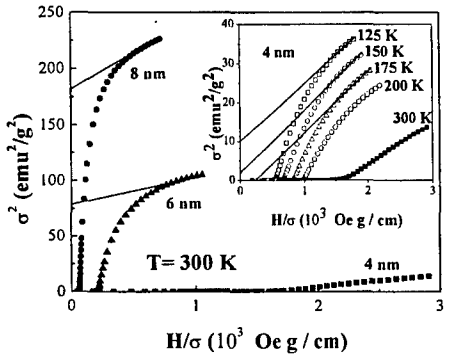

Fig. 1 Belov-Arrott plots for the magnetite-paraffin wax nanocomposites measured at 300 K. Inset: Belov-Arrott plots for nanocomposite containing 4 nm magnetite particles at various temperatures.

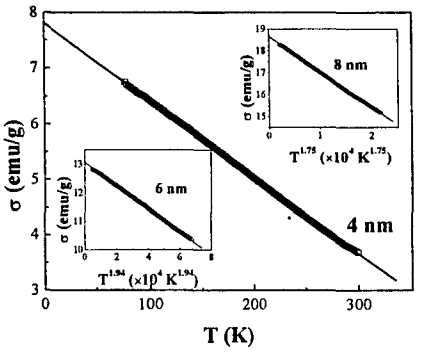

Fig. 2 Magnetization versus temperature for nanocomposite containing 4 nm magnetite particles. The solid line is the fit using the Bloch law. Inset: graph σ (T) vs T^b of nanocomposites containing 6 nm and 8nm magnetite particles to show the linear relation up to 300 K.

References

[1] S. Sun and H. Zeng, J. Am. Chem. Soc. 124 (2002) 8204.
[2] B. D. Cullity, in *Introduction to Magnetic Materials* (Addison-Wesley, New York, 1972).

* Contact author: crlin@mail.stut.edu.tw

Dielectric Charaterization of $Ba_xSr_{1-x}TiO_3$ by Solid Solution of $BaTiO_3$ and $SrTiO_3$

S. Kongtaweelert[1], D.C. Sinclair[2] and S. Phanichaphant[3]
[1]Department of Chemistry, Faculty of science King Mongkut Institute of Technology Ladkrabung, Thailand 50202
[2]Department of Engineering Materials, Mappin St, University of Sheffield, S1 3JD,UK [3]Department of Chemistry, Faculty of science Chiang Mai University, Thailand 50202

Email: samart75@hotmail.com

Ferroelectrics have become increasingly important as materials for electronic devices. The most widely used ferroelectrics occur in the perovskite family with the general formula ABO_3 such as Barium Titanate ($BaTiO_3$), Strontium Titanate($SrTiO_3$) and Barium Strontium Titanate ($Ba_XSr_{1-X}TiO_3$).

This study aims to investigate the effects of the calcination and sintering conditions on the relative permittivity and sintering behaviours of $Ba_XSr_{1-X}TiO_3$ system (x= 0.6, 0.7 and 0.8) prepared by a solid solution method. The phase transition of calcined $Ba_XSr_{1-X}TiO_3$ powders are characterized by X-ray diffraction. Analyses of the phase transition will be used to support relative permittivity and sintering behaviour data of $Ba_XSr_{1-X}TiO_3$ ceramics.

The perovskite phase of $Ba_XSr_{1-X}TiO_3$ system can be obtained by calcining at 1300 and 1400 ^{0}C. The particle size was slightly increasing at higher calcining temperature and x ratio.The Curie temperatures was increased with increasing x ratio. The frequency dependence of ε_r was slightly decreased with increasing frequency accepted at the 1 MHz as shown in Fig 1.

REFFERENCES

1. K.Kinoshita and AYamaji, J. Appl. Phys., **47**,(1976),371.
2. T. Noh, S. Kim and C. Lee, J. Am. Ceram. Soc., **79**, (1996), 255.
3. M.H. Frey and D.A. Payne, Phy. Rev.B., **54**,(1996), 3158.
4. N. Setter and R. Waser, Acta. Mater., **48**,(2000), 151.

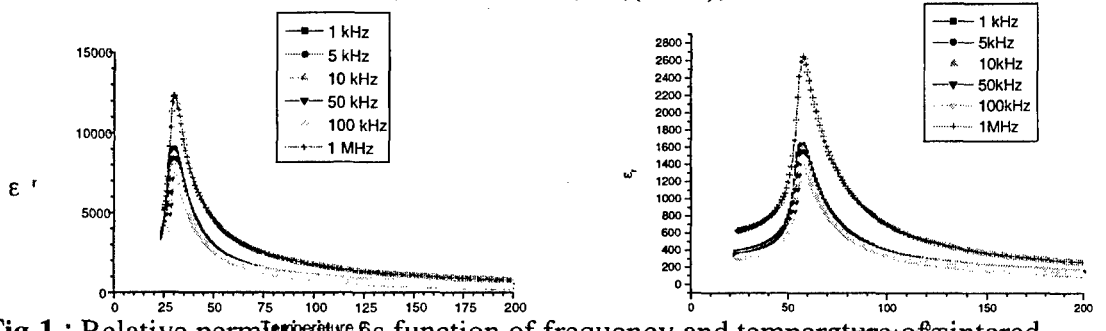

Fig.1 : Relative permittivity as function of frequency and temperature of sintered a) $Ba_{0.8}Sr_{0.2}TiO_3$ ceramics b) $Ba_{0.9}Sr_{0.1}TiO_3$ ceramics at 1400 ^{0}C for 2 hrs

Synthesis of Magnetic Nanomaterials Using Spinning Disc Reactor Technology

N. Hill,[1] C. L. Raston,[2,*] M. Saunders,[1] and R. Woodward[3]
[1]*Centre for Microscopy and Microanalysis, University of Western Australia, Crawley, 6009.*
[2]*School of Chemistry & Biomedical Sciences, University of Western Australia, Crawley, 6009.*
[3]*School of Physics, University of Western Australia, Crawley, 6009.*

Traditional fluid based synthesis techniques for the production of nanomaterials have demonstrated limitations in particle morphology and composition selectivity.[1] In particular, these limitations are relevant for the production of samples and sample-series with continuous variations in these characteristics. In conjunction with these limitations, the particle size distributions achievable are insufficiently narrow for a deterministic investigation into the factors affecting magnetic behaviour arising within nanomaterials produced on the sub-10 nm scale.

Refinements in conventional solution synthesis techniques have sought to influence particle size and distribution characteristics through particle growth control. This has been achieved with the use of surfactants, concentration control and self limiting formation and growth processes.[2] When combined with conditions promoting nucleation and the rapid extinction of reactants, the resultant techniques achieve very small particle sizes often at the cost of throughput and/or increased size spread.

As a novel technique for the synthesis of these materials, Spinning Disk Reactor (SDR) processing (Figure 1) has displayed potential for overcoming these limitations[3,4] SDR processing generates very thin (1 to 200μm) fluid films on a rapidly rotating surface (10 to 3000 rpm), within which particle formation occurs. Viscus drag induces a high degree of turbulent mixing within these centrifugally motivated films (Figure 2), leading to rapid interleaving and diffusion of reactant solutions. The resulting super-saturations and large surface areas at the interface of mixing lead to high nucleation rates and rapid particle growth. Reactant extinction rapidly follows and the nanoparticles generated have demonstrably narrower size distributions.

In addition, SDR synthesis has the potential for the production of new and novel materials as a result of the tuneable mixing characteristics upon the surface of the disk. Multi-feed or multi-pass processing will enable the production of multi-layered materials[5] which promise to be exciting subjects for microscopic and magnetic analysis. Finally, tuneable particle geometries and morphology, combined with narrow size distributions observed from SDR based production will provide great potential for studies into self assembly on the nanometre scale.

This presentation will explore traditional fluid based techniques for nanoparticle synthesis and contrast them with SDR processing. Areas covered will include an introduction into SDR processing, particle nucleation and growth control mechanisms, size effects in magnetic materials, applications for these nanomaterials, novel materials potentially producible using SDR synthesis and the relative strengths of different characterisation techniques appropriate for this class of materials, particularly TEM.

References

[1] T. Hyeon, "Chemical Synthesis of Magnetic Nanoparticles". *ChemComm*, 927 (2002)
[2] R. Massart, "Magnetic fluids and process for obtaining them", USP: 4329241 (1982)
[3] L. M. Cafeiro, *et al.*, "Process Intensification: Precipitation of Barium Sulphate Using a Spinning Disk Reactor", *Ind. Eng. Chem. Res.*, 41, 5240 (2002)
[4] P. Oxley, *et. al.*, "Evaluation of Spinning Disk Reactor Technology for the Manufacture of Pharmaceuticals", *Ind. Eng. Chem. Res.*, 39, 2175 (2000)
[5] C. J. O'Connor, *et. al.*,"Fabrication and properties of magnetic particles with nanometer dimensions", *Synthetic Metals*, 122, 547 (2001)

* Contact author: clraston@chem.uwa.edu.au

Magnetic and Electrical properties of MBE-Grown $(Ge_{1-x}Si_x)_{1-y}Mn_y$ thin films

Sang Soo Yu[1], Young Mi Cho[1], Young Eon Ihm[1*], Dojin Kim[1], Hyojin Kim[1],
Sangjun Oh[2], Chang Soo Kim[3]

[1]*Chungnam National University, Daejeon, 305-764, Korea*

[2]*Korea Basic Science Institute, Daejeon, 305-333, Korea*

[3]*Korea Research Institute of Standards and Science, Daejeon, 305-600, Korea*

The $(Si_{1-x}Ge_x)_{1-y}Mn_y$ thin films have been grown by using MBE and investigated of magnetic properties. The thin films were grown in high vacuum approximate 10^{-7}torr and have thickness around 5000□. Composition of thin films firstly fixed Si and Ge component like x= 1, 0.9, 0.7, 0.5, 0.3, 0 and then Mn concentration that was changed by controlling the temperature effusion cell, was added in the fixed the $Si_{1-x}Ge_x$. Simultaneously, Mn compositions have value from 5at% to 50at%. %. The each of the atomic concentration of Si, Ge and Mn was examined by RBS. Structural, magnetic and electrical properties of $(Si_{1-x}Ge_x)_{1-y}Mn_y$ thin films were investigated by XRD, 4-point probe, Hall measurement, temperature dependent resistivity measurement (R-T), VSM and SQUID. Ferromagnetic phase like Ge_3Mn_5 and SiMn are mainly formed when Ge is rich, and $(Si_{1-x}Ge_x)_3Mn_5$, SiMn are mainly formed when Si rich. These formations of specific phases are provable from structure analysis by XRD and magnetic properties by MPMS. At low Ge composition, Saturation magnetization values and Curie temperature generally increase with Ge composition. Hall measurement shows $(Si_{1-x}Ge_x)_{1-y}Mn_y$ thin films have p-type carriers and the carrier concentration is in the range of 10^{17}-10^{21}/cm^3 at room temperature. Carrier concentration increases with Mn concentration, while the electrical resistivity decreases with Mn concentration.

Reference

[1] H. Ohno, Science, **281**, 951 (1998)

[2] T.Dietl, H.Ohno, Science, **287,** 1019 (2000)

[3] Y. D. Park et al., Science, **295,** 651 (2002)

1

*Contact Author: yeihm@cnu.ac.kr

Neutron irradiation effect on polycrystalline $Ge_{1-x}Mn_x$ thin films grown by MBE

Young Mi Cho[1], Sang Soo Yu[1], Young Eon Ihm[1*], Seoung Won Lee[1], Dojin Kim[1], Hyojin Kim[1], Jae Min Sohn[2], Bong Goo Kim[2], Sangjun Oh[3], Chang Soo Kim[4], Hwack Joo Lee[4]

[1]*School of Materials Engineering, Chungnam National University, Daejeon, 305-764, Korea*

[2]*Korea Atomic Energy Research Institute, Daejeon, 305-353, Korea*

[3]*Korea Basic Science Institute, Daejeon, 305-333, Korea*

[4]*Korea Research Institute of Standards and Science, Daejeon, 305-600, Korea*

Polycrystalline $Ge_{1-x}Mn_x$ thin films were irradiated by neutrons and their electrical and magnetic properties have been investigated. The polycrystalline $Ge_{1-x}Mn_x$ thin films were grown on SiO_2/ (100) Si substrate using a MBE. Average growth rate was ~100Å/min and film thickness was 3,000Å~5,000Å. As-grown specimens have p-type carriers and electrical resistivities are in the range of $1.3x10^{-4}$~$5.2x10^{-4}$ ohm·cm at room temperature. The magnetization characteristics measured by using a SQUID show that the as-grown $Ge_{1-x}Mn_x$ thin films are ferromagnetic and Curie temperature is ~310K. The as-grown specimens were irradiated by the fast neutrons of 0.82MeV in a high-flux advanced neutron application reactor at the Korea Atomic Energy Research Institute located in Daejeon, Korea. The irradiation rate was $3.45x10^{10}$neutrons/cm^2sec, and the irradiation amounts were $2.4x10^{14}$, 10^{15} and 10^{16}neutrons/cm^3, respectively. After the irradiation of neutrons the carrier type is not changed, but the electrical resistivities increase with the irradiation amount dramatically. In addition, the variation of electrical resistivities with respect to temperature shows that at low temperature some of neutron-irradiated $Ge_{1-x}Mn_x$ thin films transform from the semiconductor characteristics into the metallic characteristics. The saturation magnetizations of neutron-irradiated $Ge_{1-x}Mn_x$ thin films decrease with the irradiation amounts, but the Curie temperature is not changed appreciably. The XRD and TEM analysis show that phase transformation is not taken place by the neutron irradiation. It considered that the defects generated by the neutron-irradiation are responsible for the change of electrical and magnetic properties of neutron-irradiated $Ge_{1-x}Mn_x$ thin films.

References

[1] H. Ohno et al, Appl. Phys. Lett. 69, 363(1996)

[2] Y. D. Park et al, Science, 25, (2002), 651

* Contact author: yeihm@cnu.ac.kr

Aging and rejuvenation of soft glassy materials

S. A. Rogers[1,*] and P. T. Callaghan[1]
[1] *MacDiarmid Institute for Advanced Materials and Nanotechnology, School of Chemical and Physical Sciences, Victoria University of Wellington, NEW ZEALAND*

We each deal with soft glassy materials (SGM) every day. From the toothpaste we clean our teeth with to the mayonnaise we eat with our foods to the glass of our windows, examples of SGM are all around us. Traditional definitions of solids and liquids mean that SGM can be classified as both, depending on the time-scale over which they are examined. SGM show interesting rheological properties including shear thickening (an increase in viscosity with increased shear rate), shear thinning (a decrease in viscosity with increased shear rate) and shear banding (where bands of different viscosity form within a sheared sample).

Development of high-precision rheometers has meant SGM have become a hot topic of study over the last few years both in terms of theories predicting their behaviour and the development of experiments that probe their properties. Many types of SGM have been studied using various techniques ranging from optical to rheological.

Presented here are velocimetry measurements on core-shell latex spheres [1] of average diameter 370 nm. The particles are comprised of an NMR-sensitive oil core and a solid latex shell. Attached to the shell are hairs of polyvinyl alcohol, which act to soften the hard-sphere interactions.

Typical velocimetry experiments measuring flow-induced displacements down to a few hundreds of nanometres in a concentric cylinder Couette cell [2] take on the order of 20 minutes. We have performed experiments, using a newly developed NMR pulse-sequence, lasting on the order of 1 second, while achieving a similar velocity sensitivity. These experiments give only an average velocity across the sample, but the time-scale at which they can be carried out allows us to follow aging and rejuvenation phenomena. We report here velocimetry measurements showing the time evolution of a solid-to-liquid transition.

References

[1] A. Loxley, B. Vincent, Preparation of Core-Shell Latex Particles, J. Colloid Interface Sci. 208 (1998) 49

[2] H. Wassenius, P. T. Callaghan, Nanoscale NMR velocimetry by means of slowly diffusing tracer particles, J. Magn. Reson. 169 (2004) 250-256

* Contact author: rogerssi@vuw.ac.nz

Symmetry considerations in the NMR of complex fluids

B.S. Douglass* and P.T. Callaghan
MacDiarmid Institute for Advanced Materials and Nanotechnology, VUW, Wellington, NEW ZEALAND

We look at the fascinating interplay between deformation and relaxation in several interesting entangled polymeric materials by exploring their response to being squished and squashed through various novel geometries.

Thanks to the inherent ability of nuclear magnetic resonance to take a closer look at both molecular orientation and movement or flow, we present some investigations undertaken on polymers in solution primarily through the use of deuterium spectroscopy. While the quadrupolar nature of the deuteron is beneficial for orientational investigations, sensitivity difficulties that come with these techniques throw up new experimental challenges that are overcome here through symmetry considerations and the use of the Hankel integral transform - the cousin of the Fourier transform using the Bessel functions as the kernel. We incorporate this technique into an experiment yielding 2-dimensional results from a 1-dimensional experiment called radial spectroscopic imaging (RSI) [1].

$$\mathcal{H}[f(x)] = \int_0^\infty dx\, f(x) J_0(2\pi x r)\, x$$

Prototypically we have used polyethylene oxide (PEO) in solution (0.5 - 2.0 wt%) as the basis for our work, attempting to use D_2O as the solvent and the probe of orientation, as well as moving on to other untagged solvents containing deuterated probe molecules with greater affinity for PEO. By pumping such fluids through geometries such as the extensional flow cell inside the NMR magnet, responses in molecular orientation can be found for various driving deformations, in addition to the extraction of values of important material properties such as extensional viscosity [2].

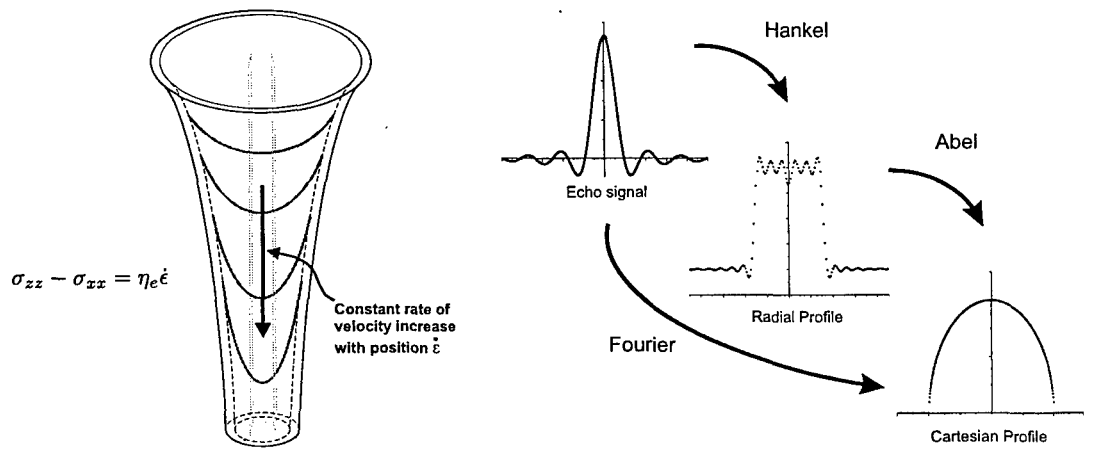

The results of such investigations are widely relevant in dynamic macromolecular deformation processes, from the fascinating ability of the body to retain its shape despite the daily stresses it endures, to the rigorous buffeting that is given to materials at various stages of synthetic polymer processing.

References

[1] M. Meininger et al., *J. Magn. Reson.* **125**, 325-331 (1997).
[2] P.D. Majors and A. Caprihan, *J. Magn. Reson.* **94**, 225 (1991).

*Contact author: douglabrad@student.vuw.ac.nz

Rheological and Mechanical Property Studies on Ultra-high Molecular Weight Polyethylene / Carbon Nanotubes

Liang Linli*,Wang Xinpeng, Wang Yanping and Wang Yimin

College of Material Science and Engineering, Donghua University, Shanghai, China

Abstract Carbon nanotubes have been attracted a considerable attention because of their exceptional properties. These properties observed at the nanoscale have motivated researchers to utilize carbon nanotubes as reinforcement in composite materials. In this study, the ultra-high molecular weight polyethylene (UHMWPE)/carbon nanotubes (CNTs) composite fibers were prepared by gel spinning and ultra drawing. The rheological behavior of UHMWPE / CNTs gels with 1 to 5 wt% carbon nanotubes were investigated using oscillatory rheometer. TEM and SEM were used to characterize the CNTs, its dispersion in the matrix and the interaction between the CNTs and the matrix. Fiber mechanical properties were measured and the results showed that fiber tensile strength and modulus could be improved by 5 to 10%, respectively.

Fig.1 TEM of purified CNTs (50000 magnitude)

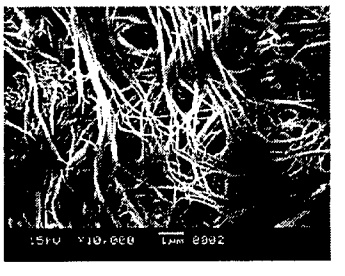

Fig.2 SEM of UHMWPE/CNTs composite fiber

References

[1] Petra Potschke, T.D. Fornes and D.R.Paul., Polymer, B43, 3247 (2002).

[2] Zhi Wang, Zhiyong Liang, Ben Wang and Chuck Zhang, Composites, Part A, B35, 1225 (2004).

[3] C.L. Barrie, P.C. Griffiths, R.J. Abbott, I.Grillo, E. Kudryashov, and C. Smyth, Journal of Colloid and Interface Science, B272, 210 (2004)

[4] Qian-ming Gong, Zhi Li, Dan Li, Xiao-dong Bai and Ji Liang, Solid State Communications, B131, 399 (2004)

*Contact author: 111@mail.dhu.edu.cn

Mass Transport in Porous Media: The Non-Local Dispersion Tensor and Nuclear Magnetic Resonance

M. W. Hunter*, A. N. Jackson+ and P. T. Callaghan
MacDiarmid Institute for Advanced Materials and Nanotechnology,
Victoria University of Wellington, P O Box 600, NEW ZEALAND

The importance of mass transport in porous media in a wide range of applications is well documented, and covers systems such as oil and water in rock, contaminants in groundwater and reagents in packed-bed chemical reactors. Dispersion describes the phenomenon whereby particles on the same streamline separate during flow. The physics of dispersion is governed by stochastic processes arising from the interplay between advective velocity gradients, molecular diffusion and boundary layer effects [1].

The measurement of dispersion conventionally involves the use of a set of "tracer" particles to monitor the spreading. Nuclear Magnetic Resonance (NMR) provides a useful tool for non-invasively labelling the molecules uniformly over the sample. To model a porous medium, a cylinder of monodisperse latex or glass spheres is commonly used [2].

The dispersion tensor, $\mathbf{D}^*$, is a local measurement in the sense that it does not depend on positional relationships and is measured as time asymptotes. For situations where the length- and time-scales on which transport occurs are not much larger than the scale of the fluctuations in the velocity field, a non-local description is required [3].

Pulsed Gradient Spin Echo (PGSE)-NMR provides a wealth of information about the velocity correlations in porous media. Presented here is a set of NMR pulse sequences and a superposition designed to extract the velocity correlations necessary to calculate the dispersion as a function of displacement and hence the non-local dispersion. Comparisons to computational results will be made to verify the experimental design.

The Lattice-Boltzmann algorithm has been shown to successfully predict the flow field in porous media [4], and has been used to model the flow field through our model porous medium. This flow field is used to simulate a large ensemble of virtual tracer particles, from which numerical estimates for both the local and non-local dispersion can be determined. Our implementation of this approach is presented here along with a comparison between the experimental and computational results.

References

[1] A. A. Khrapitchev and P. T. Callaghan, Phys. Fluids, **15**, 9 (2003)
[2] J. D. Seymour and P. T. Callaghan, AIChE J. **43**, 8 (1997).
[3] D. L. Koch and J. F. Brady, J. Fluid Mech. **180** (1987)
[4] B. Manz *et al.*, AIChE J. **45**, 9 (1999).

* Contact author: mark.hunter@vuw.ac.nz, +anj@anjackson.net

Starting Out in Microfluidics

Wendy Collier[1], James Carson[2] and Alan Hart[1,*]
[1]*AgResearch Ltd, Palmerston North, NEW ZEALAND*
[2]*AgResearch Ltd, Hamilton, NEW ZEALAND*

A description will be given of initial work in microfluidics. Simple devices, H-filters, were fabricated using photomasks and UV light to polymerise monomers in a mould. Connectors were made to couple the devices to the outside world. Liquid flow was pressure-driven, using syringe pumps. A mathematical model to describe diffusion of material between donor and acceptor streams was developed. We have demonstrated a colorimetric assay, the reaction between iron and phenanthroline. Detection of the Fe(phen) complex was *in situ* (over the range 0-10 mM), using a digital camera, or by spectrophotometric assessment of the output stream (over the range 0-5 mM). Differences in diffusion coefficients, which become important at microfluidic dimensions, were exploited to achieve the quantitative detection of glucose and lactate in a complex matrix, milk, without any prior sample treatment. Reagents for detection, enzymes and chromophores, were in the acceptor stream. The analytes were detected in a few minutes, glucose over the range 0-8 mM, and lactate over the range 0-4 mM. In the various reactions, the ratios of acceptor/ donor concentrations were not as high as predicted by the model. With further refinements, particularly in fabrication, fluid control and detection, microfluidics will allow development of small-scale, point-of-need analytical devices.

*alan.hart@agresearch.co.nz

Fabrication of GaN based photonic crystal by using electron beam lithography

A. Motogaito*, T. Yamada, F. Matsuoka and K. Hiramatsu
Department of Electrical and Electronic Engineering, Mie University,
1515 Kamihama, Tsu Mie 514-8507, Japan

Ultraviolet (UV) detectors are one of the most attractive devices in the group III-nitride semiconductors. The responsivity spectra of GaN based Schottky UV detectors have already reported [1]. AlGaN alloys have direct bandgap materials between 3.4 eV (365 nm, GaN) and 6.2 eV (AlN, 200 nm) and they have strong chemical bonding compared with Si. Thus, the solar blind operation and realizing radiation proof are possible by using AlGaN. However, it is problem for GaN based UV detectors that the responsivity is decreasing rapidly less than 300 nm [1].

On the other hand, there are a few reports on GaN based blue LEDs using photonic crystals [2]. In these references, they are described the extraction efficiency is improved by using nano-meter order photonic crystals in the InGaN MQWs. From these results, the responsivity of UV detectors will be able to be improved by using nano-meter order photonic crystal between the transparent Schottky electrode and the absorbing layer, because more UV lights can be absorbed at the photonic crystal like antenna compared with flat Schottky electrode. Furthermore, the transmittance of GaN in visible region is about 70% [3]. Therefore, GaN has possibilities to control the propagation of near UV and visible light using by photonic crystals. In this paper, to make study on the process of fabricating nano-meter order photonic crystal on the structure of UV detectors, we fabricate nano-meter order photonic crystal with triangular lattice of circle air hole on the surface of GaN substrate by using electron beam lithography and characterize optical properties.

The process of photonic crystal is as follows. First, the surface of GaN is spin-coated by positive resists (ZEP-520) and then, the pre-baking is done. After that, the electron beam lithography is carried out (CRESTEC CABL-8000). After development and post-baking, the RIE (reactive ion etching) is carried out using by Cl_2.

Prior to fabricating photonic crystals, the condition of electron beam lithography is examined. Figure 1 shows the plane view SEM image of the pattern of the triangular lattice of circle air hole. The beam current is 100 pA and the dose time is 140 μsec for each circle. The diameter of one circle is 100 nm. The lattice period between each circle is 200 nm. The thickness of resist is 130 nm by cross sectional SEM images. The resist is passed through to the surface of GaN by the above mentioned amount of doze. We also fabricate the pattern with different thickness of positive resist and then RIE is carried out. In case of the 70-nm thickness resist, the both GaN and resist layer are etched by Cl_2 thus photonic crystal can't be fabricated. Therefore, the thick resist layers (ticker than 70 nm) are needed for RIE using Cl_2.

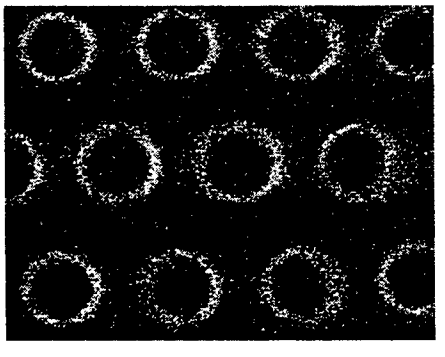

Figure 1 The plan view SEM image of the pattern of the triangular lattice of circle air hole on GaN surface by using electron beam lithography.

Acknowledgements
The authors would like to thank Dr. H. Miyake (Mie Univ.) for reactive ion etching and Mr. H. Okagawa and Mr. Y. Ohuchi (Mitsubishi Cable Co. Ltd.) for supplying GaN substrate. This work is partly supported by Industrial Technology Research Grant Program from New Energy and Industrial Technology Development Organization (NEDO) of Japan (02A23018b), Grant-in-Aid for Scientific Research from the Ministry of Education, Science, Sports and Culture (15360008) and the Joint Studies Program of the Institute for Molecular Science (16-543).

References

[1] A.Motogaito, et al.: phys. stat. sol. (a), **188** 337 (2001).
[2] T.N.Oder, et al.: Appl. phys. Lett., **83** 1231 (2003).
[3] H. Yoshida et al.: Jpn J. Appl. Phys., **41** L1134 (2002)

* Contact author: motogaito@elec.mie-u.ac.jp

Fabrication of 3D Nanoimprint Lithography Molds

M. Konijn[1], M.M. Alkaisi, R.J. Blaikie
MacDiarmid Institute for Advanced Materials and Nanotechnology, Department of Electrical and Computer Engineering, University of Canterbury, Private Bag 4800, Christchurch, NEW ZEALAND

Three dimensional structures have a number of uses in nanotechnology applications. These include on-chip optics, NEMS and MEMS devices, biochip applications and T-gate transistors[1]. The ability to pattern these in a single step process will allow for vastly simplified fabrication. Nanoimprint lithography (NIL) is ideally suited for use in this area as 3D processing will remain very similar to the conventional 2D techniques. NIL is also a very high resolution lithography method, periods as small as 14 nm have been reported [2], capable of wafer scale patterning [3], and the molds can be self cleaning [4].

However creating 3D molds is still a challenging process. What we present here is a simple process for creating 3D molds. Firstly a silicon nitride (SiN) coated silicon sample is spin-coated with a negative tone DUV and e-beam sensitive resist (ma-N2403). Then the desired pattern was written by a Raith 150 electron beam lithography (EBL) tool. By varying the electron dosage, the height of the resist remaining after development can be controlled. This 3D pattern is then transferred into the SiN by a single reactive ion etch (RIE) process. The molds are now ready for use and have been successfully imprinted into poly(methyl-methacrylate) (PMMA).

To demonstrate the process, a small relief map of the New Zealand landscape was created, as shown in Fig. 1. To create the pattern, ma-N2403 resist was patterned by controlling the electron dosage, between 5 $\mu C/cm^2$ for the low areas and 20 $\mu C/cm^2$ for the higher. This was then dry etched for 120 seconds using the following conditions: 25 sccm CHF3, 5 sccm O2, pressure of 20 mTorr, temperature of 273 K and 200W RF power. This etch had a selectivity of 1:1, so the etched SiN had the same height profile as the resist. Other patterns developed and tested resulted in the construction of 3D structures with lateral dimensions smaller than 100 nm.

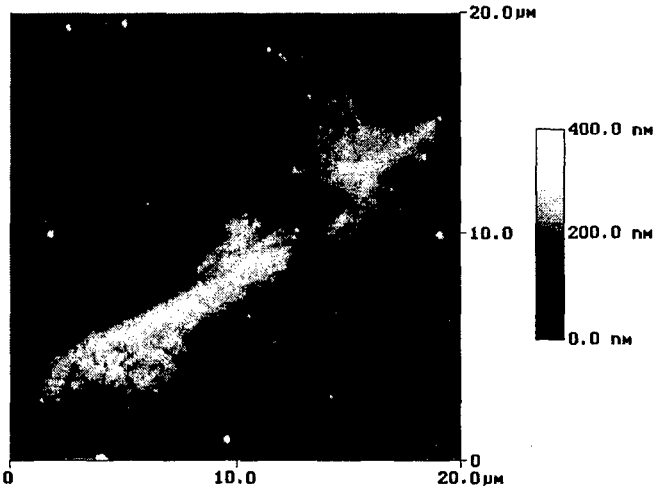

Figure 1. AFM image of a 3D nanoimprint mold showing a detailed topographical map of the New Zealand landscape.

References

[1] Y. Chen, D.S. Macintyre, E. Boyd, D. Moran, I.G. Thayne, S. Thoms, Microelectron. Eng., 67-68, (2003) 189.
[2] M.D. Austin, H. Ge, W. Wu, M. Li, Z. Yu, D. Wasserman, S.A. Lyon, S.Y. Chou, Appl. Phys. Lett., 84 (26), (2004) 5299.
[3] M. Li, L. Chen, W. Zhang, S.Y. Chou, Nanotechnology, 14(1), (2003) 33.
[4] T. Bailey et al., J. Vac. Sci. Technol. B, 19(6), (2001) 2806.

[1]mkonijn@elec.canterbury.ac.nz

Enhanced mixing of microfluidic flows using variable surface potentials

J. Burnell[1] and G. J. Weir[1*]
[1] *Industrial Research Ltd, PO Box 31-310, Lower Hutt, NEW ZEALAND*

Microfluidic cells are micron-scale liquid-state flow-reactors. They are fabricated using conventional silicon-chip-like microfabrication techniques such as lithography and chemical plasma etching. Microfluidic reactors are finding increasing application in biotechnologies, including DNA sequencing [1], protein separation [2], immunoassays [3] and biotoxin detection. They benefit from high surface to volume ratios and lend themselves to parallel processing in arrays but are currently restricted by their limited range of basic functions and their need for external pumps.

Our aim is to embed responsive nano-structure on the surfaces of microfluidic cells, so that their range of basic functions can be greatly enhanced and internal pumps with no moving parts can be implanted. We envisage responsive nano-surfaces that alter their molecular conformation under external stimulus such as voltage [4]. Such nanostructures may be in the form of self-assembled monolayers or conducting polymer films, which can induce surface functionality through altering their hydrophilicity or by exposing catalysts in microchannels. These developments could lead to programmable microreactors, for example.

Small length scales in microfluidic cells induce low Reynolds number laminar flow, which hinders mixing and effective micro-synthesis. Finn and Cox [5] have reviewed methods for quantifying mixing in such systems, including use of potential theory, topological stretching theory and numerical methods.

To increase mixing rates [6], flow stimulation of polar or magnetic fluids using electric or magnetic fields [7] will be explored using mathematical modeling. The effect of variable surface potentials will be lmodeled to calculate the resulting flow paths in a microfluidic channel and to estimate the corresponding enhanced mixing. The effect of surface and body forces is quantified, and the role of the non-symmetric stress tensor is investigated.

References

[1] B.M. Paegal, R.G. Blazej and R.D. Mathies, Current Opion in Biotechnology 14, 42, 2003.
[2] R.A. Fuller et al., Analytical Biochemistry 313, 331, 2003.
[3] K. Sato, A. Hibara, M. Tokeshi, H. Hisamoto and T. Kiamori, Advanced Drug Delivery Reviews, 55, 379, 2003.
[4] J. Lahann et al., A reversible switching surface, Science, 299, 371, 2003.
[5] M.D. Finn and S.M. Cox, J. Fluid Mechanics, 2003.
[6] J.M. Ottino and S. Wiggins, Designing Optimal Micromixers, Science, 23 July, 2004.
[7] R.E. Rosensweig, Ferrohydrodynamics, Dover, 1997.

* Corresponding author: g.weir@irl.cri.nz

Resist Deformation at Low Temperature in Nano-Imprint Lithography(NIL)

K. Mohamed[1,*], M. M. Alkaisi[1] and J. Smaill[2]
[1] *Department of Electrical and Computer Engineering, University of Canterbury, Christchurch, NEW ZEALAND*
[2] *Department of Mechanical Engineering, University of Canterbury, Christchurch, NEW ZEALAND*

Low temperature process is essential for a number of applications especially for organic devices and material that don't tolerate high temperatures. Nanoimprint Lithographgy (NIL) is a promising candidate for future device technology as it has demonstrated that increasing resolution is possible with no additional manufacturing cost. However, there is still a need to explore the low temperature low pressure process capability of this technique.
In this work, the squeeze flow of thin Polymethyl methacrylate (PMMA) film into microcavities has been investigated in order to understand and optimise the imprint process conditions. This work was focused primarily on the PMMA flow behaviour at temperature below the glass transition temperature T_g(<105 °C). The cavity and structure patterns were fabricated on Silicon Nitride molds. PMMA thin films were spun on Silicon substrates at various thicknesses.

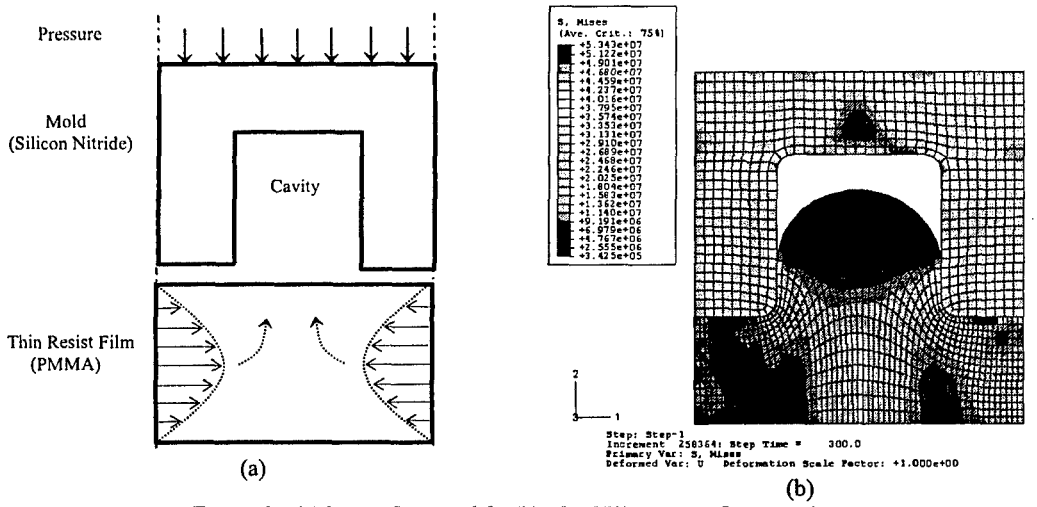

Figure 1 : (a) Resist flow model (b) ABAQUS squeeze flow simulation

The experimental works have been carried out by examining the final resist profiles under various imprint conditions such as pressure, temperature, imprint time, resist thickness, cavity size, and resist molecular weight.

An ABAQUS/ÇAE finite element software package has been employed to simulate the squeeze flow and predicting the final resist shape. Figure 1(a) shows the model of the resist flow while Figure 1(b) shows the simulation results based on the model inputs. This model allows us to study additional effects such as frictions between mold and substrate and resist elastic and plastic behaviour.
We will present the simulation results and a comparison between the experimental finding and the reflow predicted by the model under different imprint conditions.

* Contact author: kmo39@student.canterbury.ac.nz

Lithographic Patterning of Obliquely Deposited Polarizing Elements

M. D. Arnold[a, b,*] I. J. Hodgkinson[a], Q. h. Wu[a], and R. J. Blaikie[b]
[a] *Department of Physics, University of Otago, Dunedin, NEW ZEALAND*
[b] *Department of Electrical and Computer Engineering, University of Canterbury, Christchurch, NEW ZEALAND*

Obliquely deposited coatings have structurally-induced anisotropy of a number of useful properties, and in particular significant optical anisotropy lends itself to the production of polarizing elements such as retarders[1], linear- and circular- polarizers. In general, lithographic patterning of materials brings a range of associated application benefits such as miniaturization and integration with other useful technologies. Specifically, patterning of optical polarization elements finds application in optical lithography, display technology, and particularly polarization imaging. A range of competing technologies are evident in the literature[2-4], all with specific advantages and disadvantages which give justification for alternatives such as obliquely deposited films. Here we systematically investigate the patterning of obliquely deposited birefringent materials, progressing through conventional techniques such as reactive ion etching (RIE) and lift-off patterning, as well as developing a novel masking technique.

Conventional RF-excited RIE of polarizing elements was investigated, for materials appropriate to various wavelength ranges. We find that silicon (near infrared) is a most amenable material in this particular equipment, but metal oxides (visible) likely require high-density RIE sources, and fluorides (ultraviolet) are unsuitable for this technique. Continuing with studies of silicon, different polarizing elements including retarders, linear polarizers and chiral films were all etched successfully. Relatively thick films could be etched using hard masks, provided that the porous films were first capped with a dense layer to prevent moisture transport during wet processing. Increased film roughness during partial etching and deceleration of etching close to the substrate were observed, consistent with a recent study on aged electrochemical porous silicon[5]. Further, systematic parametric studies of the etching of obliquely deposited silicon illustrate one clear trend: that the porous silicon etches more slowly than the solid equivalent, nearly independent of expected porosity. This is believed to be due to the oxide passivation that arises from natural aging and possibly from lithographic processing steps, and is partially consistent with a comparable study[5].

Moving now to additive techniques, lift-off patterning is applicable to a wider range of material. However, a significantly undercut sacrificial profile is required to prevent conformal coating. The profile was generated using a tri-layer process with high-pressure oxygen undercut of the PMMA base layer. Further, deposition temperature had to be reduced to ensure integrity of the polymer profile. The method was successfully applied under demanding deposition angles to some different materials, including silicon and titanium dioxide. Observations of the optical properties that result in partially shadowed regions has lead to the development of a novel masking process, which has some advantages including simpler process requirements. The masking process was used to generate different retarders on the same substrate, a requirement of many applications.

References

1. Motohiro, T. and Y. Taga, *Thin-Film Retardation Plate by Oblique Deposition.* Applied Optics, 1989. **28**(13): p. 2466-2482.

2. Guo, J.P. and D.J. Brady, *Fabrication of high-resolution micropolarizer arrays.* Optical Engineering, 1997. **36**(8): p. 2268-2271.

3. Guo, J.P. and D. Brady, *Fabrication of thin-film micropolarizer arrays for visible imaging polarimetry.* Applied Optics, 2000. **39**(10): p. 1486-1492.

4. Hamamoto, T., H. Toyota, and H. Kikuta, *Micro-retarder array for imaging polarimetry in the visible wavelength region.* Proceedings of the SPIE, 2001. **4440**: p. 293-300.

5. Tserepi, A., et al., *Dry etching of porous silicon in high density plasmas.* Physica Status Solidi a-Applied Research, 2003. **197**(1): p. 163-167.

* Contact author: m.arnold@elec.canterbury.ac.nz

Sub-wavelength texturing for solar cells using Interferometric Lithography

W.L. Chiu[1,*], M.M. Alkaisi[1,3], R.J. Blaikie[1,3], R.J. Reeves[2,3], S.J. Drake[1,3]
[1]*Department of Electrical and Computer Engineering,*
[2]*Department of Physics and Astronomy,*
University of Canterbury, Christchurch, NEW ZEALAND
[3] *MacDiarmid Institute for Advanced Materials and Nanotechnology, Wellington, NEW ZEALAND*

In this paper we investigate the reflectivity of sub-wavelength surface textured silicon. Surface texturing is employed to suppress reflectance at solar cells surfaces and enhance light trapping efficiency.. Previous work done by G.Kumaravelu, et al [1] demonstrated that reflectance as low as 0.4% can be achieved using Reactive Ion Etching (RIE) process. However, the solar cells' performance as measured from the minority carrier lifetime was degraded due to surface damage caused by the RIE process.

In the present work, most of the plasma induced damage is avoided by fabricating sub-wavelength textured structures. The feature size of these structures is less than 400 nm, hence it requires a much shorter RIE process. The patterns for these structures were defined using interferometric lithography (IL). IL is a maskless lithography technology which is often used to define periodic structures. Both gratings and dot patterns can be defined by this technique as shown in **Figure1a** and **b**.

The theoretical limit of the feature size for the interferometric lithography is half of the wavelength of the light source used for exposure. Hence, it is ideal for patterning sub-wavelength textured structures in the visible light range required for solar cells. Interferometric lithography is also well suited for large area parallel process with potential for low cost high throughput technology. The development of IL for sub-wavelength texturing will be presented and reflections and damage induced by this technique will be compared with other plasma texturing methods.

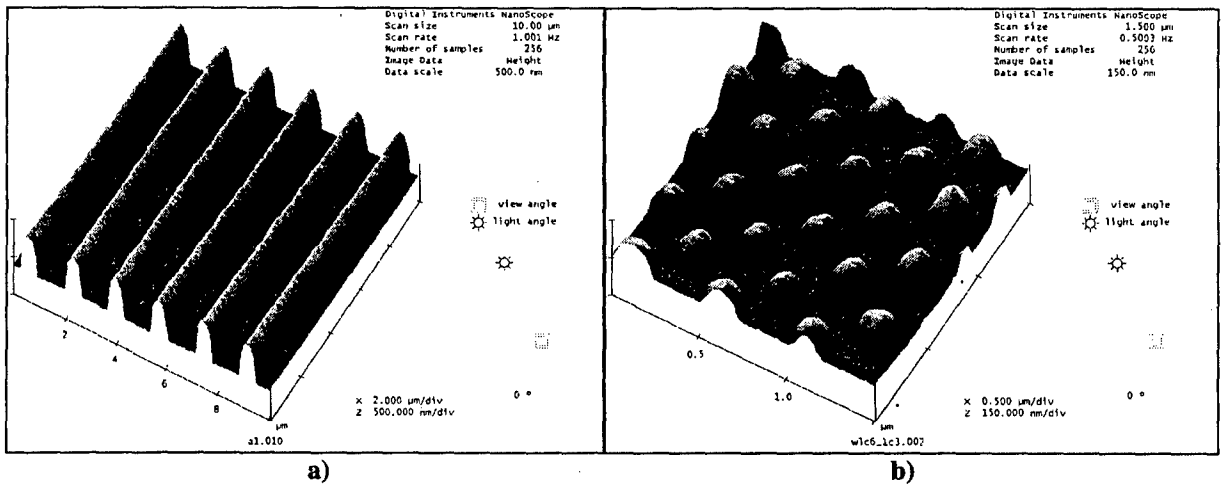

a) **b)**

Figure1. Atomic Force Microscope (AFM) image of a) a grating pattern and b) a dot pattern defined in photoresist using IL.

References

[1] G.Kumaravelu, M.M.Alkaisi, and A.Bittar, "Surface texturing for silicon solar cells using reactive ion etching technique," *29th IEEE Photovoltaic specialists conference*, New Orleans, Louisiana, USA, 2002.

* Contact author: wlc18@student.canterbury.ac.nz

Distortion in evanescent near field optical lithography conformable masks

A. J. Wright*, R. J. Blaikie and G. Turner
Department of Electrical and Computer Engineering, University of Canterbury, NEW ZEALAND

Optical lithography is rapidly approaching its limit on resolution. Current lithography equipment is governed by the diffraction limit, which places a restraint on the smallest features possible to that of half the exposing wavelength. However, it has been shown that the diffraction limit can be overcome through use of the evanescent near field, which was first implemented in a lithography process in [1]. Without the use of optical interference resolution of 140nm periods from broadband 365-600nm light have been obtained[2], and simulations [3] predict resolutions of $\lambda/20$ possible. Evanescent near field optical lithography (ENFOL) requires the use of conformable masks due to its use of evanescently decaying components of light. Without the use of a conformable mask, areas in which the mask and substrate are not in intimate contact do not get exposed. However, use of a conformable mask means that features can be distorted as the mask conforms to the substrate. It is this in-plane pattern distortion that has been characterised.

Distortion has been characterised by performing ENFOL exposures and comparing the placement of features on masks and substrates through measuring using a Raith 150 electron beam lithography machine with a laser interferometer controlled stage. The conformable masks consist of a 150μm thick glass cover slip with 30nm thick sputtered tungsten as an absorber. Markers were then patterned and their postions then measured in the Raith 150. Following this the mask was glued onto a glass holder and was used to expose samples. The samples then had the marker patterns transferred through cryogenic reactive ion etching. These markers were then measured using the Raith 150. Measurements took place over an area of 15x13mm and all measuring scans had repeated measurements of one mark to facilitate compensation for beam drift. The resultant data points were then corrected for beam drift, followed by scan shift and rotation correction using least squares. Comparison of mask and sample data revealed a mean distortion of 695nm and a three sigma result of 1.97μm absolute distortion. The resultant distortion map is shown in Fig 1 and the displacement histogram is shown in Fig 2. In order to develop ENFOL as a method for integrated circuit manufacturing distortion needs to be less than ten percent of the highest resolution achievable. With ENFOL's potential for $\lambda/20$ resolution in-plane distortion would have to be only a few nm. In-plane distortions of average 58nm have been reported in [4] using 150μm thick embedded absorber conformable masks. Therefore much improvement in distortion is required toward the realisation of viable manufacturing process using ENFOL.

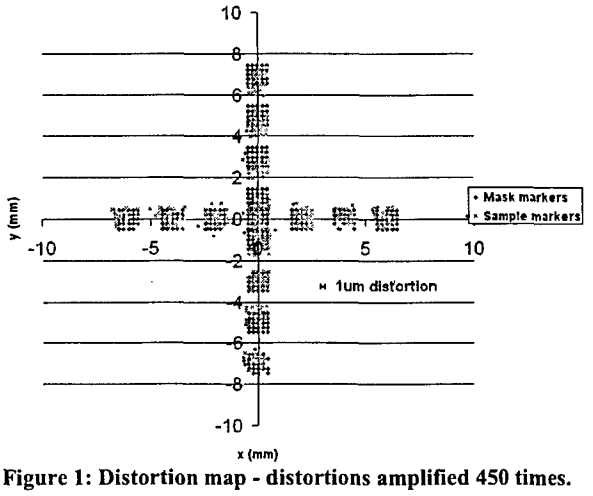

Figure 1: Distortion map - distortions amplified 450 times.

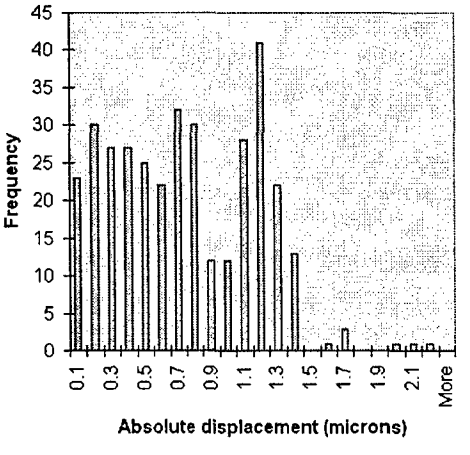

Figure 2: Absolute displacement histogram

References

[1] R. J. Blaikie, M. M. Alkaisi, S. J. McNab, D. R. S. Cumming, R. Cheung, and D. G. Hasko, "Nanolithography using optical contact exposure in the evanescent near field," *Microelectronic Engineering*, vol. 46, pp. 85-88, 1999.

[2] M. M. Alkaisi, R. J. Blaikie, and S. J. McNab, "70 nm features on 140 nm period using Evanescent Near Field Optical Lithography," *Microelectronic Engineering*, vol. 53, pp. 237-240, 2000.

[3] S. J. McNab and R. J. Blaikie, "Contrast in the evanescent near field of lambda/20 period gratings for photolithography," *Applied Optics*, vol. 39, pp. 20-25, 2000.

[4] J. G. Goodberlet and B. L. Dunn, "Deep-ultraviolet contact photolithography," *Microelectronic Engineering*, vol. 53, pp. 95-99, 2000.

* Contact author: ajw113@student.canterbury.ac.nz

Silicon Etch Process Options for Micro- and Nanotechnology using Inductively Coupled Plasmas

C.C. Welch[1*], A.L.Goodyear, G.Ditmer, G.Tan
[1] *Oxford Instruments Plasma Technology, North End, Yatton, Bristol BS49 4AP, England*

Silicon is suitable material for an ever-expanding range of micro- and nanoscale opto-and microelectronic devices such as 2d-photonic crystals, micro-silicon waveguides, nano-SOI MOSFETS and grating structures. However until recently exploitation of such technology has been restricted by the difficulty of fabricating the continually decreasing smaller features and higher aspect ratios demanded. In this work several solutions are presented for the micro- and nanoscale etching of silicon for devices using inductively coupled plasmas (ICP).

Silicon etch process development has been carried out in the Oxford Instruments Plasma Technology System 100 ICP380 (or ICP 180) tool (see Figure 1). The following three process strategies provide excellent solutions to the various different challenges that arise in the micro- and nanoscale etching of silicon.

Hydrogen Bromide (HBr) based silicon on insulator (SOI) process (Figure 2)
This process is useful when very high selectivity over a silicon dioxide (SiO_2) insulator is required, such as for nanoscale MOSFETS. Etch depths are in the range 0.05μm to 1μm. Generally an SiO_2 mask is preferred as this yields very high selectivity (>200:1 achievable), but a vertical resist mask is also acceptable. The processing temperature is in the range 20°C to 70°C.

Room temperature fluorinated chemistry silicon etch process (Figure 3)
This choice has the benefit of using non-corrosive plasma chemistry around room temperature and is suitable for depths 0.05μm to 10μm. It also has generally higher selectivity over resist masks (c.5:1) but lower selectivities over SiO_2 (c.10:1)than the HBr process.

Cryogenic silicon etch process (Figure 4)
The cryogenic silicon etch offers the best performance of all the choices by using sub-minus 100°C processing temperatures in conjunction with a non-corrosive chemistry: sulphur hexafluoride (SF_6)-oxygen (O_2). At these temperatures the etch product (a silicon oxy-fluoride) is marginally volatile and provides sidewall passivation for good profile control. Very high selectivities over resist (>75:1) and SiO_2 (>150:1) are possible and very high aspect ratios (>30:1) have been observed over depths between 0.2μm to >100μm.

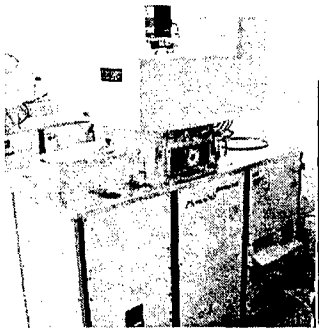

Figure 1
System 100 ICP 380

Processing of sample pieces up to 200mm wafers

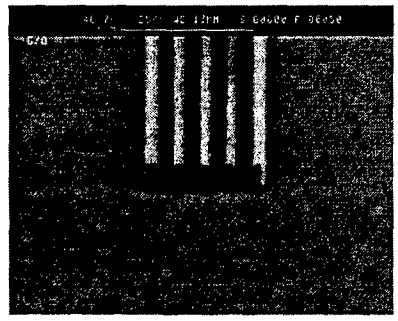

Figure 2
HBr based etch of 0.1μm wide polysilicon lines and spaces stopping on 3nm gate SiO_2. HSQ masked.

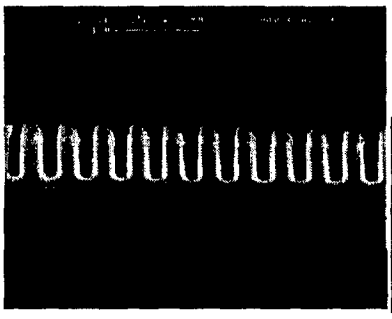

Figure 3
Room temperature F-based Si etch. 0.2μm wide holes x 0.4μm deep

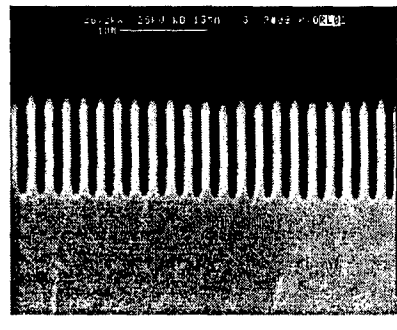

Figure 4
Cryogenic Si etch. 0.1μm gaps etched 1μm deep. Aspect ratio 10:1

* Contact author: colin.welch@oxinst.co.uk

Fabrication of Nanoscale SiC-based Ceramic Patterns with Near-zero Residual Layers Using Imprinting Techniques

Kyoung-Hoon Park and Dong-Pyo Kim

Dept. of Fine Chemical Engineering and Chemistry, Chungnam National University,

Daejon, Korea 305-764

Microelectromechanical systems (MEMS) is a rapidly growing technology with a broad range of commercial applications and a diverse collection of evolving MEMS sensors and actuators. However, silicon and organic polymers, the most commonly used materials for MEMS today, can not be utilized as the structural materials in harsh conditions [1, 2]. Therefore, it has been concerned to develop new fabrication techniques for triboligical non-oxide ceramic MEMS which is able to use at high temperatures and corrosive circumstances. And it came to our concern that the capillary force lithography (CFL), as a modified imprinting technique with soft PDMS mold is a secure, promising method to achieve large area patterns using polydimethylsiloxane (PDMS) mold [3]. In this study, nano-scale siliconcarbide-based ceramic patterns on Si substrates were fabricated by CFL technique for the first time using a liquid ceramic precursor (KiON VL20, www.kioncorp.com) and CD-R and DVD as economic nano-scale masters. The ceramic patterns were prepared by low temperature (70~90°C) thermal curing with thermal initiators, such as peroxide compounds, followed by high pyrolytic temperature (800°C) in a nitrogen gas atmosphere. And, in order to control the thickness of residual layers which is considerably one of main problems in the imprinting processes, we investigated on the effect of processing parameters such as the concentration of the ceramic precursor and the spinning speed to obtain the optimum film thickness for near-zero residual layers of patterning. Moreover, the etching kinetics of the various polymeric and ceramic patterns is comparatively studied to remove effectively the residual layer by Ar ion etching as shown in Fig. 1. High temperature stabilities, and the morphologies of SiC-based ceramic patterns were characterized by AFM (Atomic Force Microscopy), SEM (Scanning Electron Microscope) and TGA (Thermal Gravimetric Analysis).

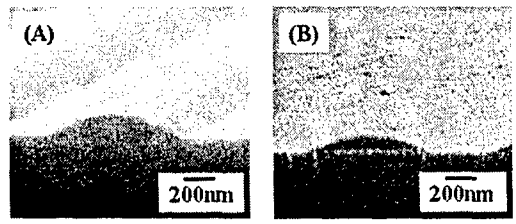

Figure 1. SEM images of the cured polymeric patterns prepared by CFL technique under different conditions; (A) 30% polymer concentration and 2500rpm spinning rate, and (B) after Ar ion etching process on the cured polymeric pattern.

References

1. H. Yang, P. Deschatelets, S. T. Brittain and G. M. Whitesides, *Adv. Mat.*, 2001,13, 54.

2. S. Roy, C. A. Zorman, M. Mehregany and R. DeAnna, *ANASYS Solutions*, 1999, 1(2), 22.

3. K. Y. Suh, Y. S. Kim, and H. H. Lee, *Adv. Mater.*, 2001, 13, 1386.

Highly Anisotropic Reactive Ion Etch for Fabrication of Silicon Nanostructure

Eih-Zhe Liang[1], Chao-Jei Huang[1], and Ching-Fuh Lin[1,2]*
[1]*Graduate Institute of Electro-optical Engineering,*
[2]*Also with Department of Electrical Engineering and Graduate Institute of Electronics Engineering*
National Taiwan University, Taipei, Taiwan, Republic of China

Dry etch is an important tool to fabricate decananometer nanostructures. Concerning single electron transistor or coupled quantum devices, reactive ion etch (RIE) must provide both high anisotropy and no undercut. We demonstrate SF_6/O_2 system can create steep sidewall with 90% anisotropy and no observable undercut. To prove its applicability for nanostructure, silicon nanorods with high density of $2x10^{11}cm^2$ and diameter of 20nm are fabricated on single crystalline silicon. Spin-coated monolayer of silicon dioxide nanoparticle is used as the etch mask.

Plasmalab 80Plus (Oxford Instrument) is used for RIE. The lower electrode is graphite plate of diameter 240mm. SF_6 and O_2 is used to etch silicon with silicon dioxide as etch mask. Etching parameters such as gas mixture ratio, r.f. power, and gas ambient pressure are optimized for anisotropy. Anisotropy is defined as $1-V_L/V_H$, where V_L is the laterally etched width and V_H is the vertically etched depth. The principal etching mechanism is formation of gaseous SiF_x to remove silicon. This etching is isotropic and silicon-oxygen complex is formed at sidewall for protection. With lower SF_6 percentage and higher content of oxygen, anisotropy is better and less undercut. The best case is 90% anisotropy using 5sccm SF_6, 25sccm O_2, 10mtorr pressure, and 120mW r.f. power. As shown in Fig 1a) there is no observable undercut beneath the mask if the etch depth is less than 300nm.

To test the etching recipe in creating nanostructure, we fabricate silicon nanorods on single-crystalline silicon surface by reactive ion etch. Silicon dioxide nanoparticle is dispersed on surface by spin-coating to form monolayer for etching mask. The SiO_2 particles have a sphere shape with 20~30nm diameter and dispersed in isopropanol with 1% in weight. The criterion of monolayer formation depends on temperature, solvent, concentration of solution. It is empirical that solvent with higher viscosity, raisied temperature and adequate concentration will lead to uniform monolayer within an area up to $5x5cm^2$. After RIE is performed over monolayer of SiO_2 nanoparticle, it is treated with buffered-oxide-etchant to remove the oxide mask, shown in Fig 1b) and Fig 1c). The silicon nanorods has diameter 15~25nm and height 20nm. The nanorods have trapezoidal shape and the top is slightly rounded due to pattern transfer from spherical mask.

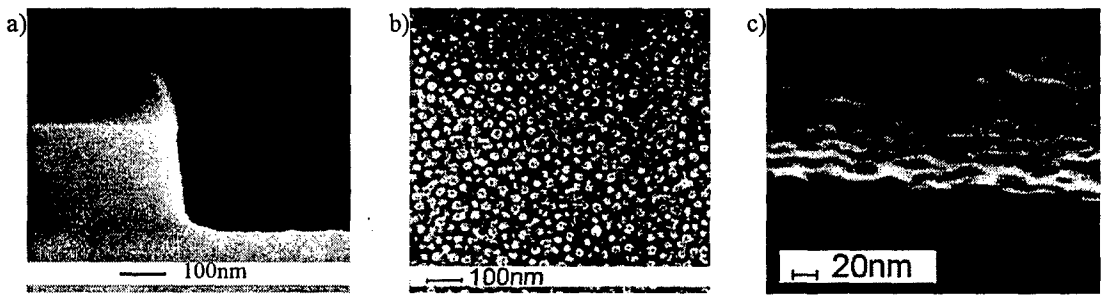

Fig. 1a) Side view of etched profile (SF_6:O_2=5sccm:25sccm P10mtorr/120W). 1b) Top view of silicon nanorods. 1c) Side view of silicon nanorods.

For decananometer structure, surface to volume ratio becomes ten times larger than in hundred nanometer scale. This means surface states have ten times greater influence. Reactive ion etch case is known to produce polymeric surface contamination and lattice damage. Lattice damage depends on impact ion species and external r.f. power. We use microwave-reflectance photoconductance decay (MWPCD) to monitor the etch damage. The surface quality, i.e. surface traps or surface recombination velocity, can be derived from measured minority carrier life time. By a removal and probe scheme (by KOH), surface recombination velocity versus removed thickness can be obtained. It shows that highly damaged silicon is about 30~40nm and lightly damaged silicon extends into more than 100nm.

*Contact author: cflin@cc.ee.ntu.edu.tw

Microfabrication of Interfacial Force Microscope Sensor Components

C. M. McCague[1,2*] and P.R. Norton[1,2]
[1] *Interface Science Western, Department of Chemistry, University of Western Ontario, Ontario, CANADA*
[2] *Ontario Photonics Consortium, University of Western Ontario, Ontario, CANADA*

The interfacial force microscope (IFM) is a novel scanning probe instrument combining high resolution imaging and quantitative nanomechanical properties testing capabilities [1]. The IFM has a capacitance-based force sensor-actuator which is stable under both attractive and repulsive loads and allows for the measurement of nanonewton forces during indentation experiments with penetration depths of a only a few nanometers. The IFM can be used to map the nanomechanical properties of materials that are heterogeneous on a nanometer-micrometer length scale in relation to variations in surface topography [2-3].

IFM sensor components are fabricated from glass and silicon wafers. The glass substrates have recessed Au/Cr capacitor pads, electrical leads and bonding pads for electrical connections. The common plate features a teeter-totter structure defined by cuts etched through 100 μm thick Si (001) wafer. One fabrication challenge is providing sufficient support to the fragile 100 μm Si wafers to avoid losses during processing. A thicker "handle wafer" is used to provide support. The simple approach of using photoresist as an adhesive for wafer bonding, has had mixed results. We are presently testing other adhesives and wafer bonding methods, as well as redesigning our common plate pattern to connect individual common plates to a supportive framework..

While the use of new materials, fabrication techniques and assembly methods has yielded sensors with more consistent properties, sensor preparation remains labour intensive and a barrier to the commercialization of IFM. With the addition of an e-beam nanolithography and focused ion beam milling systems to the microfabrication facilities at the University of Western Ontario, our work has expanded from batch fabrication of needed components to the development and testing of new component designs. We seek to develop simple, efficient methods for sensor component fabrication and assembly to support our IFM operations and to explore further advances in sensor design.

References

[1] J.E. Houston and S.A. Joyce, *Rev. Sci. Instrum.* **62**, 710 (1991)
[2] J.F. Graham, C. McCague and P.R. Norton, *Tribol. Lett.* **6**, 149 (1999)
[3] J.F. Graham *et al.*, *J. Mater. Res.* **13**, 1 (1998)

* Contact author: cmmccagu@uwo.ca

Photoresist as an Anti-Reflection Coating for Interference Lithography

S. J. Drake[1,*], N. Kohn[1], R. J. Blaikie[1], R. J. Reeves[2] and M. M. Alkaisi[1]
[1] *Department of Electrical and Computer Engineering, MacDiarmid Institute for Advanced Materials and Nanotechnology, University of Canterbury, Christchurch, NEW ZEALAND*
[2] *Department of Physics and Astronomy, MacDiarmid Institute for Advanced Materials and Nanotechnology, University of Canterbury, Christchurch, NEW ZEALAND*

Anti-reflection coatings (ARCs) are often recommended for optical lithography when light reflected from the substrate leads to an optical standing wave that can hinder the transfer of the intended pattern. ARCs are particularly useful for lithography with coherent illumination, such as interference lithography (IL) which typically requires laser light to form an interference pattern. Commercial ARCs are available with excellent performance, but their high cost and short shelf lives means that it may be impractical to procure low volumes of such ARCs for intermittent use in a university research laboratory.

A trilayer resist process using photoresist as both the imaging layer and the ARC has been developed to facilitate IL experiments. Resists from the Shipley S1800 family have been used, although the process should be applicable to other products. Since photoresist does not absorb light as effectively as a purpose-designed ARC, a thicker layer is required to sufficiently suppress reflected light. In this case, S1813 resist with a thickness of 1.3 μm provides adequate suppression of substrate reflections. This is hard baked for one hour at 185 °C to prevent deformation during subsequent process steps [1], prior to deposition of an evaporated silicon dioxide intermediate hard mask layer. Finally, S1805 resist with a thickness of 500 nm is spin cast as the final imaging layer of the trilayer stack.

After exposing and developing the imaging layer, reactive-ion etching (RIE) with CHF_3 is used to transfer the pattern into the intermediate layer. Subsequent O_2 RIE is used to etch the ARC. Etch conditions have been tuned [1, 2] to reduce the lateral etch rate. Figure 1 shows scanning electron microscope (SEM) images of arrays of 200 nm dots on a 1 μm period formed by double-exposure IL and transferred into the bottom resist using this process. The patterns are well defined, with no evidence of surface standing wave effects, demonstrating the suitability of the bottom resist layer to act as an ARC. The resulting resist pillars have aspect ratios of approximately 10:1, which indicates that the bottom layer is mechanically robust and that the RIE pattern transfer process has excellent anisotropy.

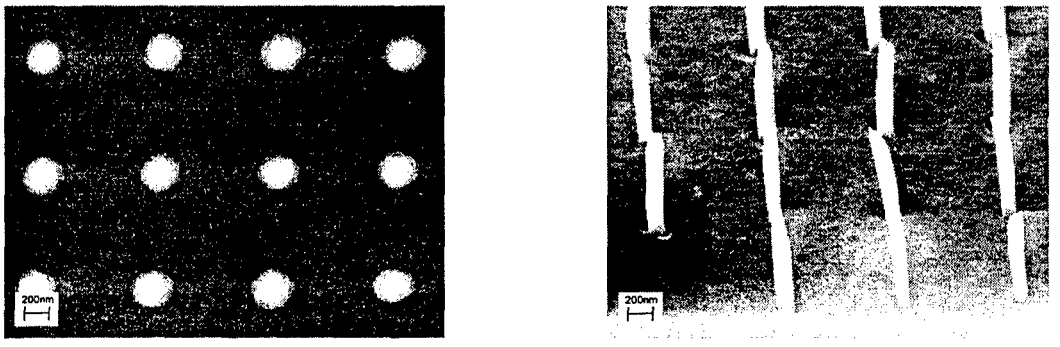

(a) *(b)*

Figure 1: SEM images of trilayer resist stack (a) after exposure and development and (b) after RIE etching to transfer pattern to bottom layer.

References

[1] H. Namatsu, Y. Ozaki, and K. Hirata, J. Vac. Sci. Technol. **21**(2), 672 (1982)
[2] M. L. Schattenburg, R. J. Aucoin, and R. C. Fleming, J. Vac. Sci. Technol. B **13**(6), 3007 (1995)

* Contact author: sjd57@student.canterbury.ac.nz

Microfluidic circuit integration using multilayer soft lithography methods and PDMS.

E. S. Berthier[1,*], F. l'Hostis[1] , M.M. Alkaisie[1], A. Downard[2], and R. J. Blaikie[1]
[1] *MacDiarmid Institute for Advanced Material and Nanotechnology. Department of Electrical and Computer Engineering, University of Canterbury, Christchurch, NEW ZEALAND*
[1] *MacDiarmid Institute for Advanced Material and Nanotechnology. Department of Chemistry, University of Canterbury, Christchurch, NEW ZEALAND*

The microfluidics field has undergone a great expansion since the generalization of the usage of PolyDiMethylSiloxane (PDMS) as a microchannel substrate[1,2,3]. PDMS offers a great number of interesting chemical and mechanical properties, among which are a very high biocompatibility, a good ease of use and a real versatility. A single person can now create in less than a day a complete microfluidic device using this polymer.

The Department of Electrical and Computer engineering of the University of Canterbury decided implement a number of the microfluidic projects and has set up a project to start PDMS experiments. The Department already had a good knowledge of photoresist polymers; therefore the creation of SU-8 molds based on silicon wafers was a natural starting point for theses experiments[1]. The ultimate aim of this project is to couple it with the work of others to create an autonomous integrated fluidic circuit for biomedical usage.

So far a good progress has been made in the creation of microfluidic channels. Binding of PDMS on to a flat glass substrate has been achieved as well as multilayer PDMS binding. Fluid flow in simple 200 micron channels has been attained also and reasonably characterized (Figure 1). The next step in this project is to go towards further integration of fluid channels[4,7], which means a higher complexity in the channel scheme, and also the creation of microfluidic devices such as microvalves and micropumps[5,6,7].

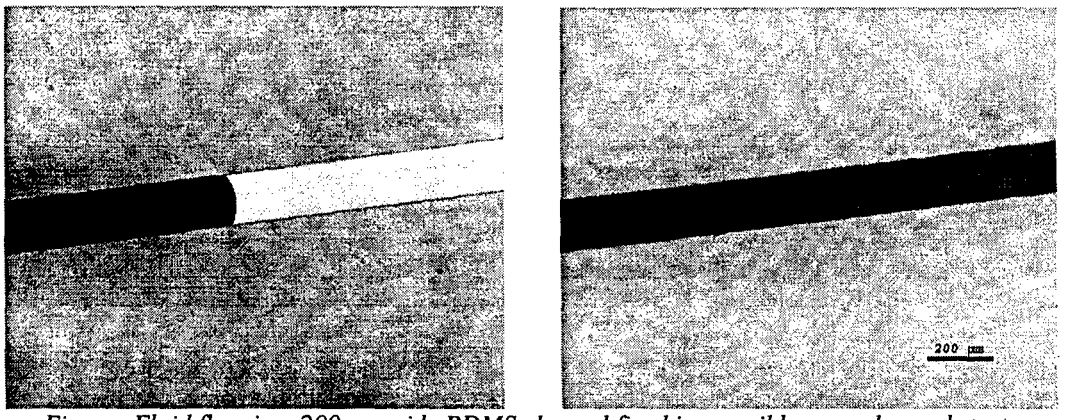

Figure: Fluid flow in a 200 µm wide PDMS channel fixed irreversibly on a glass substrate

References

[1] G. M. Whitesides, Y. X. a. G. M. (1998). "Soft Lithography." Angew. Chem. Int. Ed.(37): 550-575.
[2] J. Cooper Mcdonald, G. M. Whotesides (2001). "Poly(dimethylsiloxane) as a Material for Fabricating Microfluidic Devices." ACCOUNTS OF CHEMICAL RESEARCH.
[3] K.A. Rose, P. Krulevitch, J. Hamilton (2001). Microfluidic Applications of Soft Lithography. Materials Research Society Spring Meeting, San Francisco, Lawrence Livermore National Laboratory.
[4] Todd Thorsen, S. J. Maerkl, Stephen R. Quake (2002). "Microfluidic Large-Scale Integration." SCIENCE **298**: 580 - 584.
[5] Marc A. Unger, H.-P. C., Todd Thorsen, Axel Scherer, and S. R. Quake (2000). "Monolithic Microfabricated Valves and Pumps by Multilayer Soft Lithography." SCIENCE **288**(APRIL 2000): 113 - 116.
[6] M. J. Felton (2003). "The new generation of microvalves." ANALYTICAL CHEMISTRY **october 2003**: 429 - 432.
[7] W. H. Grover, et al. (2002). "Monolithic membrane valves and diaphragm pump for practical large-scale integration into glass microfluidic devices." Sensors and Actuators **B 89**: 315-323.

* Contact author: erwin.berthier@wanadoo.fr

Low Pressure Nanoimprinting Process for SiC-based Ceramic Pattern using Viscous Photocurable Preceramic Polymers

Anh Tuan Pham, Dong-Pyo Kim*

Dept. of Fine Chemical Engineering and Chemistry, Chungnam National University, Daejeon, Korea 305-764. E-mail: dpkim@cnu.ac.kr

Ultraviolet-nanoimprinting lithography (UV-NIL) is a promising method for the fabrication of cost-effectively defining nano-scale structures with high-resolution, high-throughput at room temperature and low pressure. UV-NIL has been developed in efforts to reduce feature size below 100nm via photo-induced solidification of liquid precursors [1, 2]. It is advantageous to use low pressure patterning process while stiction at the interface between the solidified polymer and the mold is problematic. It is demonstrated that the elastomeric polydimethylsiloxane (PDMS) mold, which is low reactivity, low surface energy, recycle and inexpensive, improved the demolding ability after curing without damage of the patterned features. In this study, 100~500nm scale of SiC-based ceramic patterns were fabricated by UV-NIL with low pressure of soft PDMS mold which was prepared from a master via EBL (electron beam lithography). The technique is based on UV polymerization of photocurable preceramic polymers as SiC-based ceramic precursors that was patterned by application of a nano-scale PDMS mold, followed by post-thermal curing and pyrolysis at 800°C under nitrogen gas atmosphere. The UV-curable polymers were synthesized by chemical modification of polyvinylsilazane (KiON) with methacrylate and vinyl containing compounds via hydrosilylation or coupling reaction routes [3]. The chemical structure and photosensitivity of the synthesized polymers were characterized by using various analytical instruments.

The several processing parameters including differential pressures process and the swelling of mold materials by the polymer was comparatively studied to improve the fidelity of PDMS mold. The morphology of the PDMS mold and SiC-based ceramic patterns were characterized by scanning electron microscope (SEM) as shown in Fig 1.

As the photocurable preceramic polymers are feasible for low pressure NIL with reduction of sub-100 patterns size, it is very promissing to fabricate the components of MEMS devices such as for free-standing gears using a rapid prototype stereolithography.

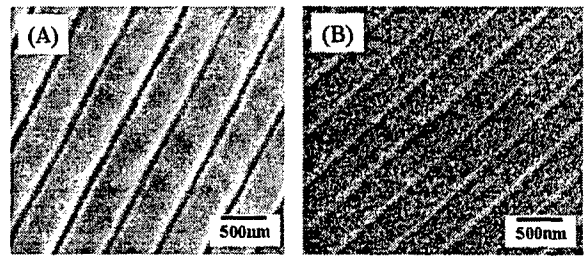

Fig. 1 SEM images of (A) PDMS mold and (B) SiC patterns imprinted with mold (A), pyrolyzed at 800℃ under N_2 atmosphere.

References

[1] B. Vratzov et al., J. Vac. Sci. Technol. **B21(6)**, 2760-2764 (2003)

[2] A. Lebib et al., Microelectronic Engineering **61-62**, 371-377 (2002)

[3] Ya-Li Li et al., Appl. Organometal. Chem. **15**, 820-832 (2001)

Nanostructuration of conjugated polymer thin films

Katarzyna Matczyszyn[1,2*], Licinio Rocha[2], Celine Fiorini[2], Stanislaw Bartkiewicz[1], Francois Kajzar[2]
[1]*Institute of Physical and Theoretical Chemistry, Wroclaw University of Technology, Wyb. Wyspianskiego 27, 50-370 Wroclaw, Poland*
[2]*CEA SACLAY, DRT/LITEN/DSEN/GENEC/L2C, Bât 451 91191 Gif sur Yvette Cedex, France*

Recently a large interest in study of the nanoscale behavior of different photoactive materials with the use in devices for photonic applications has been put. It is well known that an illumination with a coherent monochromatic light source of an organic polymer functionalized with photoisomerising azo dyes leads to the surface relief grating formation: the molecules escape from the areas of the high intensity optical field towards the low intensity areas. It is best seen in two beam coupling experiments where the interference of two coherent laser beams, with wavelength exciting the photoisomerization process creates well defined surface relief grating with period depending on the angle between the two interfering laser beams and the wavelength of the used light. The grating period can be varied continuously from ca. 300 nm (illuminating with UV light) to a few microns (VIS light). This light induced nanostructuration of thin films offers wide opportunities of practical applications such as f.i. aligning of other materials.

The series of experiments with two wave mixing technique and with a Lloyd mirror with a continues and nanopulse lasers of different wavelength were performed. The materials under study consist of thin films of polymers such as PPV, polyanilinine and poly(3-alkyl thiophenes) and polymers doped with azo-dyes. The structures obtained were scanned with the AFM and proved to be very interesting. The films were not only structured on the simple relief grating but showed also interesting, regular "hole" structure.

The influence of parameters such as the laser intensity, the irradiation time, the thickness of the polymer film but also the irradiation wavelength is studied towards a better understanding of the process. Practical applications of those structures will be also discussed.

*Contact author: katarzyna.matczyszyn@pwr.wroc.pl

The effect of surface area increase due to plasma texturing on the carrier lifetime of silicon solar cell substrates

G.Kumaravelu[1], M.M.Alkaisi[1*], D. Macdonald[2],
[1]*Department of Electrical and Computer Engineering, University of Canterbury, Private Bag 4800, Christchurch, New Zealand.*
[2]*Dept. of Engineering, FEIT, ANU, Australia.*

Plasma texturing is applied to reduce reflections from silicon solar cell wafers. Texturing induced damage has been monitored through minority carrier lifetime measurements. We report here on the effects of the increase of surface area due to texturing on the measured minority carrier lifetime and associated implied open circuit voltage(V_{oc}). The influence of increasing cell surface area due to the formation of plasma textured structures has not been fully investigated. The origin and nature of defects induced in the bulk and at the surface due to texturing could be better understood by measuring the minority carrier lifetime and implied open circuit voltage for cells having different surface areas.
Minority carrier lifetimes of various wafers were measured using the Quasi Steady State Photo Conductance technique and the corresponding implied V_{oc} were calculated. The starting silicon wafers were 50mm in diameter, double side polished, <100> oriented, p-type, FZ-Silicon of 5Ω cm resistivity. Three different patterns were photolithographically defined and the photoresist was used as an etch mask for reactive ion etching (RIE). Atomic Force Microscopy (AFM) data and SURFER8 software were used to calculate the textured surface areas.

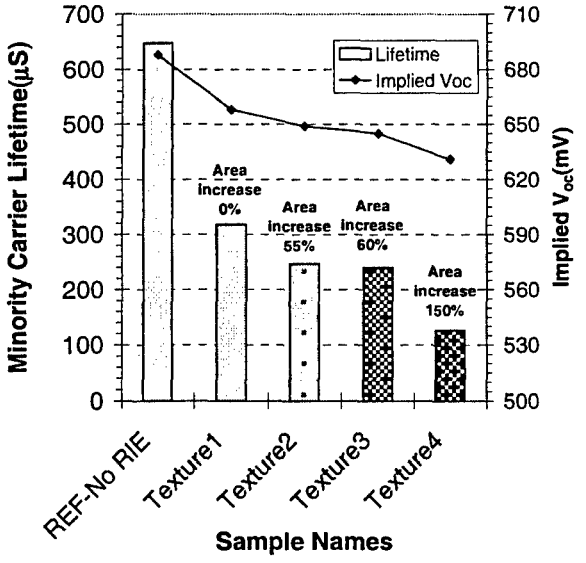

Fig 1. Minority carrier lifetime and implied V_{oc} of RIE textured FZ-Si for wafers with different surface areas.

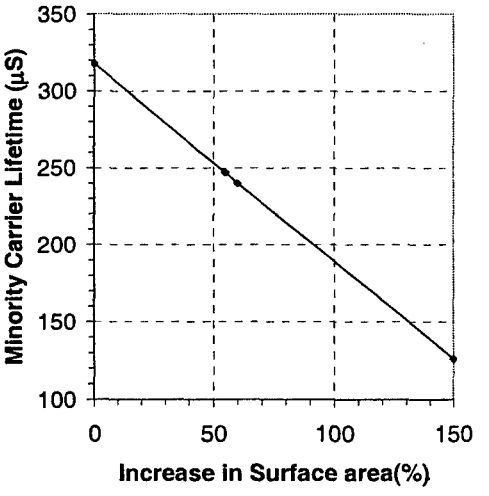

Fig.2. The minority carrier lifetime of RIE textured wafers as a function of increase in surface area.

Fig.1 shows a comparison of the effective minority carrier lifetime measured on a reference and SF6 plasma etched wafers. Texture1 has a smooth polished surface after a maskless etch process while the other wafers have various textured structures. By using same etching parameters for all wafers, but forming structures with different surface areas, it was possible to study the influence of surface area on minority carriers lifetimes and open circuit voltage
The textured surface area increases up to 150% compared to untextured wafers. All wafers were subjected to a defect removal etching (DRE) in HF:HNO_3 (1:50) solution in order to remove a layer of about 250nm prior to Si_xN_y passivation. Fig.2. shows a linear decrease in minority carrier lifetime as the textured area increases. Therefore, the drop in minority carrier lifetime is not only due to plasma induced damage, but partly due to an increase in surface recombination due to an increase in the surface area.

*Contact author: maan.alkaisi@elec.canterbury.ac.nz

Fabrication of Metallic Nanotransistors

H.H. Cheng*, M.M. Alkaisi, J.K. Siaw.
The MacDiarmid Institute of Advanced Materials and Nanotechnology
Department of Electrical and Computer Engineering
School of Engineering, University of Canterbury
Private Bag 4800, Christchurch, New Zealand.

In order to fabricate ultra small devices beyond the edge of optical lithography for the next decade, new types of electronic devices have been researched and explored. Metallic nanotransistors are transistor structures made from a single layer of metal with dimensions in the ~20 nanometre scale. The one-dimension structure of metallic transistors allows the use of nanoimprint technology in terms of rapid and economical fabrications. This kind of transistor operates by governing the flow of electrons through a narrow channel.

In this work, an electron beam lithography (EBL) process has been developed to fabricate structures at 20nm scale using the RAITH-150 EBL machine at University of Canterbury. Various structures of nanotransistors have been fabricated including the field-effect and the Y-shaped models. The field-effect model (*Fig. 1*) provides the transistor with a JFET like structure. The drain-and-source regions were formed using either metallic or semiconducting nanowires, where the current is controlled with gates separated by ~20nm gaps. The Y-shaped model was designed to split the current between two branches depending on the applied gate voltage. Both of these nanoscale transistors were fabricated on insulating materials such as SiN-coated Si substrate.

The single pass exposure technique in Electron beam lithography process has been employed to deliver patterns of lines and dots around 20nm in size. The surface charging effects during EBL have also been greatly minimised by pre-depositing a layer of metal on the insulating substrates. Metallisation was performed using lift-off procedure with various types of metals including gold, silver, and aluminum. The fabrication and characterisations of nanoscale metallic transistors will be presented and several EBL issues such as the charging effect of the insulating materials, the proximity effects, and the single pass exposures will be discussed.

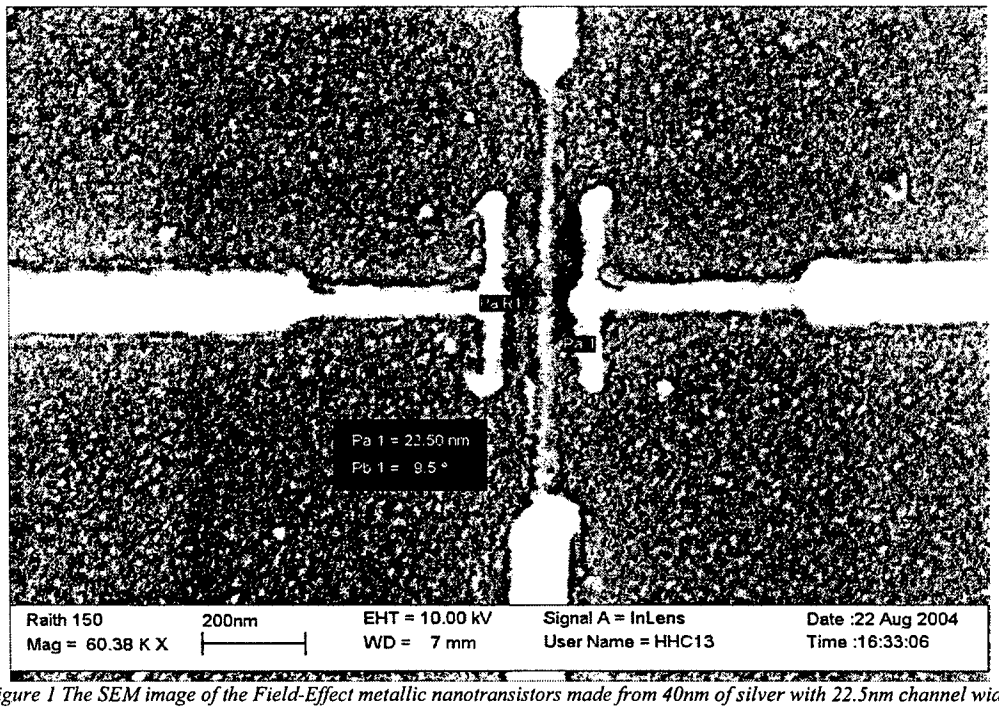

Figure 1 The SEM image of the Field-Effect metallic nanotransistors made from 40nm of silver with 22.5nm channel width

* Contact author: hhc13@student.canterbury.ac.nz

HSQ as a surface protection layer for the preparation of TEM samples by Focused Ion Beam Milling.

E. Boyd[a†*], W. Smith[b], S. McFadzean[b], A. Craven[b], I.G. Thayne[a]

[a] *Department of Electronic and Electrical Engineering, University of Glasgow, Scotland, G12 8LT.*
[b] *Department of Physics, University of Glasgow, Glasgow, Scotland, G12 8SQ*
[†] *Now at MacDiarmid Institute, Department of Electrical and Computer Engineering, University of Canterbury, Christchurch New Zealand.*

The use of HSQ as a surface protection layer for the preparation of high-resolution TEM samples by focused Ion Beam (FIB) Milling is described. Preparation of cross sectional sample using FIB Milling allows sample to be prepared with great positional accuracy with minimal damage to surrounding devices. The use of a flowable oxide as opposed to the PECVD oxide allows regions under the T shaped gate to be protected during milling. Using this method samples were prepared of HEMTs with a T shaped gate with a length of 50nm.

High Electron Mobility Transistors (HEMTs) have demonstrated the highest cut-off frequency of any transistor. This performance has been achieved by reducing the length of the gate. As the size of the gate is reduced the accurate determination of the critical dimensions such as the gate length becomes increasingly important. Using cross-sectional TEM is it possible to measure the smallest features with a high degree of accuracy. However the sample preparation of TEM samples is far from straight forward, particularly for fragile structures such as HEMTs. This paper discusses the development of a low damage process for the preparation of TEM sample of HEMT samples using Focused Ion Beam Milling.

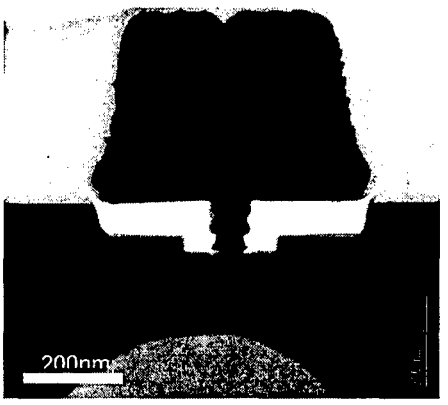

Figure 1 TEM image of T-gate protected by SiO_2 layer.

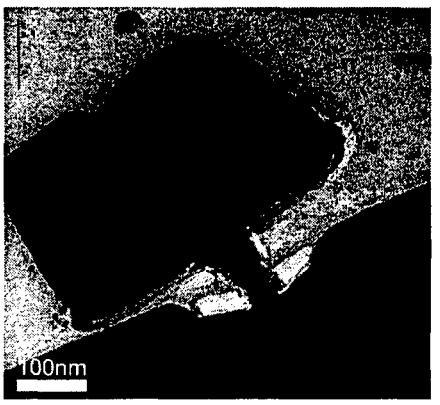

Figure 2 TEM image of T-gate protected by HSO layer.

The FIB tool used in this work was the FEI FIB200TEM. The cross sections were prepared using the lift-out method in order to minimise the pre-milling preparation and reduce the damage to the surrounding devices. A thin slice (<100nm) of the device is milled and then lifted out from the sample onto a TEM grid. A cross section of a 50nm HEMT was prepared and inspected using a FEI TECNAI F20 TEM. It was seen that the T shaped gate had been lifted up and deposited some distance from its original position. The direction that the gates were shifted corresponded to the direction of the platinum deposition used to protect the sample surface. Some protection was therefore required to prevent damage to the T-gate from the platinum deposition. It was decided to encase the gate in a thick layer of PECVD SiO_2 prior to platinum deposition. Figure 1 shows a TEM image of a device prepared in this way, it is seen that the SiO_2 layer has protected the fragile gate. There has been some damage to the semiconductor surface, thought to be due to the air gap under the metal T-gate. A dielectric had to be found that would be able to fill this region. This could be achieved by using a flowable dielectric such as hydrogen silsesquioxane (HSQ). This is originally a liquid but turns into its oxide state upon exposure to electrons. A sample was prepared using this method and the image is shown in Figure 2. It can be seen that the HSQ has flowed under the head of the gate and filled the air gap, protecting the surface of the sample. This method will allow extremely high resolution imaging of HEMT sample with minimum damage from the milling process.

* Corresponding Author: e.boyd@elec.canterbury.ac.nz

Electrical Properties of Three Quantum Well Play an Leading Part of Quantum Cascade Laser by C-V and Deep-Level Transient Spectroscopy

Jin Soak Kim[1], Eun Kyu Kim[1,*], Jin Dong Song[2] and Il Ki Han[2]
[1]*Department of Physics and Quantum Photonic SRC, Hanyang University, Seoul 133-791, KOREA*
[2]*Nano-Device Research Center, Korea Institute of Science and Technology, Seoul 130-650, KOREA*

Quantum cascade laser (QCL) is a kinds of mid-infrared laser that consist of numerous number of semiconductor quantum well (QW) such as InGaAs/GaAs, AlGaAs/InAlAs, etc. The QCL is applicable to gas sensor communication device used in inter atmosphere communication. Superiorities of the QCL are very powerful output power and an easy controlling of wavelength. It is possible to control wavelength due to the changing of thickness of quantum well (5~20 μm). Recently, the QCL structures divide into several classes such as mini-band transient structure, quantum well structure, vertical transient structure, etc., but, all kinds of the structures have two kinds of region which are injection and active [1].

In this study, we investigated electrical properties of three QW active region structure by C-V and deep-level transient spectroscopy (DLTS) methods. Because the QCL is a kind of optical devices, optical properties that measure by optical methods such as photoluminescence and Fourier transform infra-red spectroscopy are very important. However, it is necessary that tunnelling and transient processes of carrier in the active region in order to make lasing in the QCL devices, electrical properties such as offset of energy level and existence of defect are also important from the reasons. In order to this work, we make 3QW consist of AlGaAs/GaAs on n^+-GaAs substrate except for other region. Originally, the 3QW QCL structure is made up of 26^{th}~40^{th} period of injection/active region, but the structure is too complicated to analyze electrical properties. Thus, we used simple structure in this study. And then, in order to measure C-V, we made Au-gate on the structure and indium ohmic below the backside.

Figure 1(a) is result of C-V measurement and 1(b) is DLTS spectra of 3QW sample. We expect the 0 V pulse and -1.5 V measure bias ranges contains QW region and -2 V pulse and -3 V measure bias contains buffer region. Two spectra shown in figure 1(b) are different from each other. The 0 V ~ -1.5 V spectra have very complicate signal but, the -2 V ~ -3 V spectra is flat, as same words buffer layer have not any defect or carrier capture structure but 3QW region have carrier capture and emission processes in it. However, we don't know origin of the signal yet. We think it may be thermal emission from confined energy level of the QW, carrier tunnelling from the QW or the GaAs deep-trap related to the AlGaAs. In order to find origin of the signal, more exact measurement is required and the result and analysis will be presented.

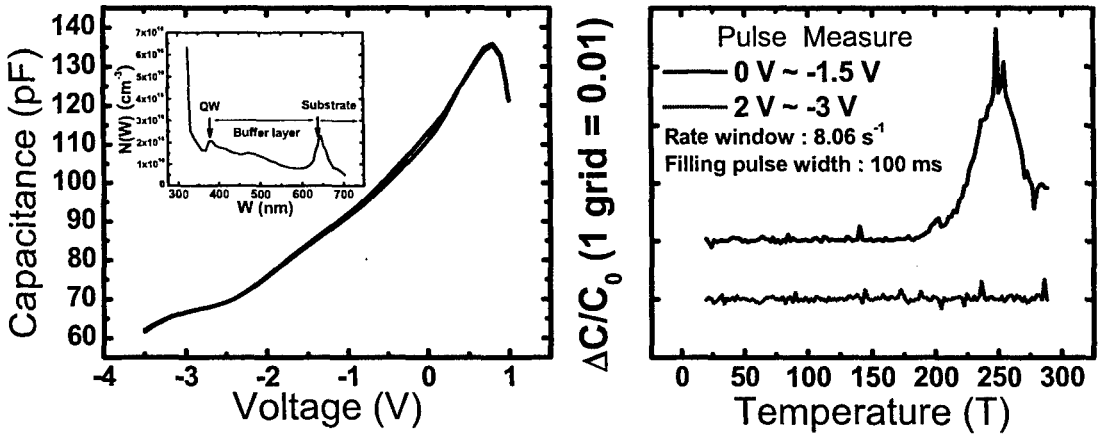

(a) (b)

Figure 1. (a)C-V measurement of 3QW structure and inset of the graph is depth profile from C-V (b)DLTS spectra of 3QW structure.

References

[1] F.Capasso, A.Y. Cho, J. Faist, A.L. Huthchinson, S. Luryi, C. Sirtori, and D.L. Siveo, U.S. Patent 5 457 709, (1995)

* Contact author: ek-kim@hanyang.ac.kr

Symmetry of non-linear electric conduction in semiconductor nano-devices

C.A. Marlow[a], A. Löfgren[b], I. Shorubalko[b], R.P. Taylor[a], T. P. Martin[a] and H. Linke[a]
[a] *Physics Department, University of Oregon, Eugene OR 97403-1274, USA*
[b] *Solid State Physics, Lund University, Box 118, S – 22100 Lund, Sweden*

In linear response, the reciprocity relation [1] describes the electric conductance of mesoscopic, two-terminal devices to be symmetric with respect to the direction of an external magnetic field and the sign of the voltage. The conductance symmetry breaks down however, in the non-linear regime of transport for the general case, where the device has no geometrical symmetry. While the breakdown of the reciprocity relation in the non-linear transport regime is well known [2-4], the possibility of surviving symmetries of the non-linear conductance has received much less attention [5]. Here, we consider the case of symmetric mesoscopic, phase-coherent devices. Using basic symmetry arguments, we predict and experimentally confirm a set of symmetry relations with respect to bias voltage and magnetic field for the electric conductance in the non-linear regime.

Experimentally we use ballistic GaInAs/InP semiconductor devices purposely designed both with and without symmetry axes parallel and perpendicular to the current direction to investigate symmetries. We refer to a device as left-right (LR) symmetric when it possesses a symmetry axis perpendicular to the current direction, and up-down (UD) symmetric when it possesses a symmetry axis parallel to the current direction. The conductance through the billiards for a particular bias voltage $|V|$ is measured as a function of perpendicular magnetic field under reversal of voltage, magnetic field, and lead orientation. The observed conductance fluctuations serve as a "magnetofingerprint" of the electrostatic potential experienced by the electrons, which allows the details of the different traces to be compared to ascertain symmetries present in the device. For example, in the presence of perfect UD symmetry conductance fluctuations, CF, should be unaltered with a reversal in the direction of the magnetic field. We observe this experimentally by comparing structure of the CF traces for an UD symmetric device taken for $\pm B$. For the LR-symmetric device the conductance is symmetric in B when $V = 0$ (linear regime), while at finite V (non-linear regime) we observe the data traces taken not to be symmetric in B, due to a lack of UD symmetry. We do observe however that $g(V, B) \approx g(-V, -B)$.

In summary, using a sensitive experimental test, we have confirmed a set of novel symmetry relations for the electrical conductance of mesoscopic, phase-coherent devices in the non-linear regime and in the presence of a magnetic field [6].

[1] M. Büttiker, IBM J. Res. Developm. **32**, 317 (1988).
[2] M. Büttiker, J. Phys.: Condens. Matter **5**, 9361 (1993); T. Christen and M. Büttiker, Europhys. Lett. **35**, 523 (1996).
[3] S. B. Kaplan, Surf. Sci. **196**, 93 (1988); P. G. N. de Vegvar, et al., Phys. Rev. B **38**, 4326 (1988); R. A. Webb, S. Washburn, and C. P. Umbach, Phys. Rev. B **37**, 8455 (1988); P. A. M. Holweg, et al., Phys. Rev. Lett. **67**, 2549(1991); D. C. Ralph, K. S. Ralls, and R. A. Buhrman, Phys. Rev. Lett. **70**, 986 (1993).
[4] H. Linke, et al., Europhys. Lett. **44**, 341 (1998).
[5] H. Linke, et al., Phys. Rev. B **61**, 15914 (2000).
[6] A. Löfgren, et al., Phys. Rev. Lett. **92**, 046803 (2004)

Pulsed Chemical Vapor Deposition Technology

Silviu I. Baluti and Susan P. Krumdieck
Advanced Energy and Material Systems Laboratory, Department of Mechanical Engineering
Private Bag 4800, University of Canterbury, Christchurch, NEW ZEALAND

Chemical Vapour Deposition (CVD) is a widely used process for deposition of thin film materials in high technology industrial applications. A range of processing variations such as Low Pressure CVD, Atmospheric Pressure CVD, and assisted methods have been developed and studied over the past thirty years. Pulsed-CVD represents an innovation in the technology used to accomplish and control the deposition process. This paper introduces the operating conditions unique to Pulsed-CVD and presents the results of a study to characterize the flow field conditions as a function of the design and operating parameters.

The Pulsed CVD reactor conditions are unique to the CVD technology. In conventional CVD systems the reactants are passed through the reactor in a steady flow of carrier gas. The diffusion controlled deposition of this method results in low conversion efficiencies and often poor film uniformity and microstructure control. In the new Pulsed CVD technique metered reactant quantities are injected at equal time intervals in a continuously evacuated reactor, as seen in the figure. Previous research has demonstrated high conversion efficiencies and growth rates, as well as good film uniformity and microstructure control in deposition of titania and zirconia.

The reactor pressure cycle encompasses three pressure flow regimes, from viscous, to transition and finally to molecular flow. This study concentrates on characterizing this new flow field, and measuring the flow uniformity inside the Pulsed CVD reactor. For the reactor flow uniformity determination the naphthalene sublimation technique, usually employed in viscous flow for the indirect determination of the convective heat transfer coefficient, is used. The method is presented together with the experimental results of the reactants pulsed flow uniformities in comparison to their uniformities in equivalent steady flow regimes.

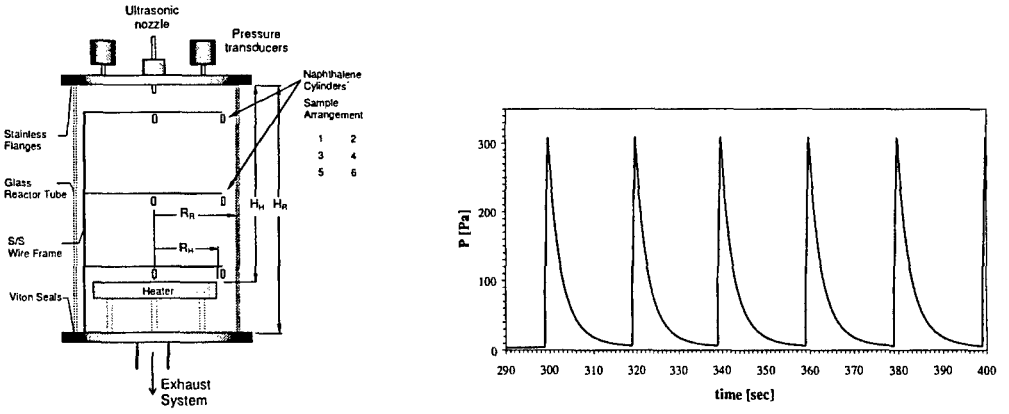

Pulsed CVD flow dynamics experimental set-up with naphthalene measurement technique and the reactor pressure profile displayed.

References

[1] S.P. Krumdieck *et al.*, Unique Precursor Delivery and Control Afforded by Low-Pressure Pulsed-CVD Process with Ultrasonic Atomization, *Journal de Phisique IV*, **11** (PR3) 1161-1168 (2001)

[2] S.P. Krumdieck, R. Raj, Conversion Efficiency of Alkoxide Precursor to Oxide Films Grown by an Ultrasonic-Assisted, Pulsed Liquid Injection, Metalorganic Chemical Vapor Deposition (Pulsed-CVD) Process, *Journal of the American Ceramic Society*, **82** (6) 1605-1607 (1999)

[3] S.P. Krumedieck *et al.*, YSZ layers by Pulsed-MOCVD on solid oxide fuel cell electrodes, *Surface and Coatings Technology*, **167** 226-223 (2003)

[4] A. Roth, *Vacuum Technology* (North-Holland, Amsterdam, 1990)

Design and function of a Pulsed Laser Deposition facility for growth of novel thin film materials in HV, UHV and plasma environments.

Ian L. Farrell[1,*], Roger J. Reeves[1] and Steven M. Durbin[2]

[1]*Dept of Physics and Astronomy, MacDiarmid Institute for Advanced Materials and Nanotechnology, University of Canterbury, Christchurch, New Zealand*
[2]*Dept of Electrical and Computer Engineering, MacDiarmid Institute for Advanced Materials and Nanotechnology, University of Canterbury, Christchurch, New Zealand*

A Pulsed Laser Deposition facility has been developed at the MacDiarmid Institute for the purposes of growth and study of a range of novel thin film materials. A Lambda Physik Compex 205 KrF excimer laser is being used as the ablating source. Two custom designed vacuum chambers have been used for materials growth. The ultra-high vacuum (UHV) chamber has RHEED and RGA in-situ monitoring capabilities in addition to four effusion cells for MBE growth. Film composition can be varied using the in-chamber 6-target carousel and they are mounted facing upwards, allowing liquid targets to be used. A load lock transfer mechanism enables substrate and sample removal without loss of vacuum in the UHV chamber. The high vacuum (HV) chamber is simpler in design and has been constructed to include oxides in the range of materials grown. Both chambers are equipped with a plasma source. The present research interests include nitride, oxide, spintronic and half-metal materials and initial film growth results are presented here. The materials grown have been analysed using the optical, electronic and x-ray facilities available on-site at the University of Canterbury.

* Contact author: ian.farrell@canterbury.ac.nz

Photoluminescence and Photoconductivity exhibited by PAMBE grown InN

L. Williams[1,*], P. A. Anderson[2], S. M. Durbin[2], R. J. Reeves[1]
[1] *Department of Physics and Astronomy, University of Canterbury, Christchurch, NEW ZEALAND*
[2] *Department of Electronic and Computer Engineering, Canterbury, Christchurch, NEW ZEALAND*

InN has been the subject of great debate over the last few years. Early research using optical absorption of sputter deposited films suggested that the band gap was around 1.9 eV. [1] Subsequent improvement of growth techniques has suggested that in that research InN:O was possibly studied due to growth in an high vacuum chamber. More recent work suggests that the true band gap of crystalline InN grown under UHV is around 0.7 eV. [2] However, this is still controversial as the low energy optical features have been attributed to stress, non-stoichiometry, defect states and even Mie resonances caused by indium metal within the film [3].

We report on the photoluminescence (PL) and photoconductivity (PC) properties of InN grown by plasma-assisted molecular beam epitaxy (PAMBE) on sapphire and YSZ substrates. Hall measurements on selected samples have shown electron carrier concentrations at room temperature to be in the order of 10^{18} cm^{-3} to 10^{20} cm^{-3}. All PL measurements at 4 K have revealed strong emission peaks ranging from 0.64 eV to 0.8 eV with no signals detected in the visible region to within five orders of magnitude.

Figure 1 shows photoconductivity measurements that clearly demonstrates an increase in conduction at 0.71 eV. This indicates a band gap at around 0.7 eV as PC is unlikely to be attributed to Mie resonances from In clusters, donor or defect states given the extent of the increase in conduction.

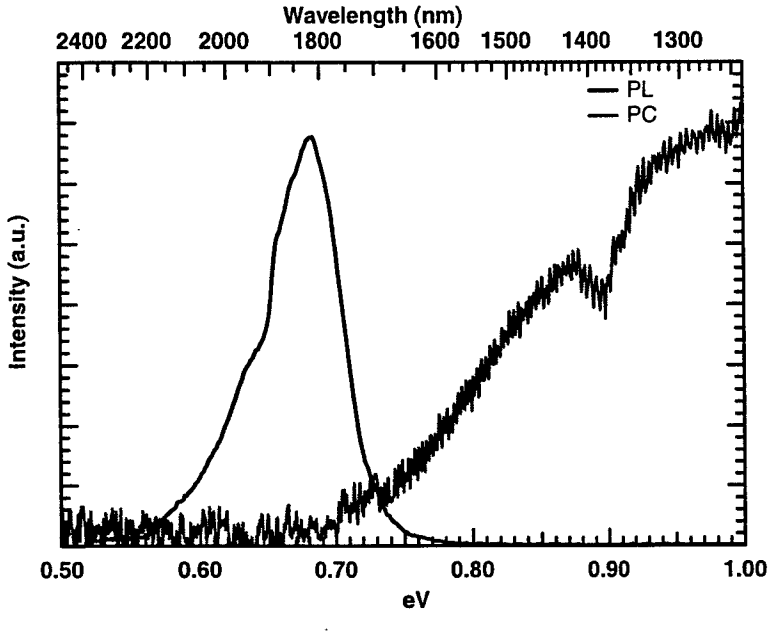

Figure 1 Low temperature (4K) photoluminescence and photoconductivity signals from InN

References

[1] T. L. Tansley and C. P. Foley, J. Appl. Phys. **59**, 3241 (1986).
[2] M. Yoshimoto, H. Yamamoto, W. Huang, H. Harima, J. Saraie, A. Chayahara, and Y. Horino, Appl. Phys. Lett. **83**, 3480 (2003).
[3] T. V. Shubina, S. V. Ivanov, V. N. Jmerik *et al.*, Phys. Rev. Lett. **92**, 117407 (2004).

* E-mail address: lwi21@student.canterbury.ac.nz

Development of Si/SiO_2 super-lattices deposited by RF reactive sputtering

E. Boyd* and R.J. Blaikie

MacDiarmid Institute, Dept Electrical and Computer Engineering, University of Canterbury, Christchurch, New Zealand

Wide-Field of View, narrow band spectral filters based on a proposal by Nakagawa [1] operating in the millimetre regime have been demonstrated previously [2]. These devices used a silicon-air two-dimensional photonic crystal operated at 84GHz and demonstrated only a 0.4GHz shift over a 120 degree field of view. We are now concentrating on scaling of the device to operating within the telecommunication wavelengths (1.3-1.5μm). This requires the ability to deposit alternating layers of silicon and silicon dioxide with a thickness of 150nm and 300nm respectively with high uniformity. It is desirable to be able to deposit these layers in the same vacuum system, and for this purpose RF reactive sputtering has been employed.

The super-lattice is deposited using an Edwards Auto 500 sputter tool. This tool is capable of RF and DC sputtering in addition to electron beam evaporation. In this work only the RF source is used; this allows flexibility for further process development including the addition of a third dielectric material. A silicon target is used to deposit both materials. The silicon layers are deposited in an argon atmosphere with an argon flow rate of 10sccm. The power used is 150W, which is a relatively low power and prevents the sample heating during deposition. The rate of deposition is approximately 2nm/min and allows the thickness to be carefully controlled. The silicon dioxide is deposited using the silicon target by admitting a small amount of oxygen into the chamber in addition to the argon. The oxygen reacts with the silicon ions to form silicon dioxide. The fraction of oxygen that was necessary to oxidise the silicon and form silicon dioxide was found to be low. Increasing the oxygen fraction from 3% to 8% caused the optical transmission to improve and ellipsometry has confirmed the refractive index to be close to that of silicon dioxide. Above this value increasing the flow rate had little effect on the quality of the film and slightly reduced the deposition rate. This agrees with the work of Valletta et al. [3]

The advantage of using a single source for both layers is that multi-layer dielectrics with two or more dielectric materials can be deposited without the need to bring the chamber to air and replace the targets. This is both time consuming and can introduce contaminants into the super-lattice. In order to ensure that there is good contrast between the alternating layers the chamber is pumped down between layers to remove any remaining process gases.

Super-lattices have been produced using this method with up to seven alternating layers of Si and SiO_2. These layers have been studied using a variety of analytical techniques including cross-sectional SEM to determine the layer thickness (Figure 1) and IR spectroscopy to investigate the transmission properties of the layers.

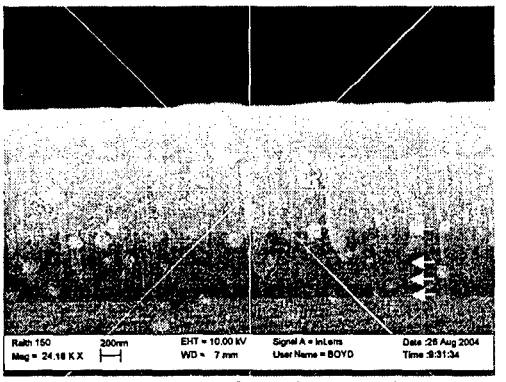

Figure 1 SEM image of multilayer stack. Arrows show interface of layers

References

[1] W. Nakagawa et al., Opt Lett. **27**, 2002, p191
[2] R.J. Blaikie et al., Microelectronic Engineering **73-74**, 2004, p357
[3] Valletta et al., Electrochemical Technology **4**, 1966, p402

*Corresponding Author: e.boyd@elec.canterbury.ac.nz

Physical and electronic structure of disordered gallium nitride

B. J. Ruck[1], F. Budde[1], A. Koo[1], S. Granville[1], H. J. Trodahl[1], G. V. M. Williams[2], A. Bittar[2], and J. B. Metson[3]
[1] *School of Chemical and Physical Sciences, Victoria University of Wellington, Wellington, NEW ZEALAND*
[2] *Industrial Research Ltd, Lower Hutt, NEW ZEALAND*
[3] *Department of Chemistry, Auckland University, Auckland, NEW ZEALAND*

Determining the atomic scale structure and the resulting electronic properties of complex material systems is an ongoing challenge in physics research. An especially interesting material with a complex structure is disordered gallium nitride (GaN). It has been predicted that fully amorphous GaN has a well-defined band gap relatively free of in-gap states, and may provide a useful alternative to its crystalline counterpart [1]. However, the amorphous state is not in itself unique, and the optical and electronic properties depend sensitively on the details of the atomic-scale configuration. In light of this we have investigated the atomic and electronic structure of a series of GaN films that range from nanocrystalline to fully amorphous. We find that amorphous GaN can only be formed in the presence of impurities such as oxygen or excess gallium, and thus the predicted useful properties of an amorphous network of stoichiometric GaN are unlikely to be realized. On the other hand we have found that amorphous GaN films stabilized by oxygen impurities have a relatively strong photoconductive response [2], so understanding the properties of this material is also of interest.

The disordered GaN films were grown by ion-assisted deposition, where Ga atoms are deposited onto a substrate in the presence of an energetic beam of nitrogen ions. In some cases oxygen was intentionally incorporated into the films by introducing water vapour during the growth. The structure and composition of the samples were determined by Rutherford backscattering spectroscopy, x-ray diffraction, extended x-ray absorption fine structure, secondary ion mass spectroscopy (SIMS), and transmission electron microscopy (TEM). The TEM image in Figure 1 shows the change in structure of the films from amorphous to nanocrystalline as the oxygen content is reduced. We believe that the oxygen relaxes the bonding constraints that prevent formation of an amorphous network.

The unfilled electronic states of the films have been probed by x-ray absorption spectroscopy (XAS), while the corresponding filled states have been studied using x-ray emission spectroscopy (XES). The spectra from amorphous, oxygen-containing samples exhibit less structure than those from nanocrystalline films, although both show features that can be identified with peaks in the spectra from single crystal GaN. This correspondence results from the similar short-ranged bonding order in all three types of samples. The presence of oxygen impurities also shifts the valence band maximum to lower energy, thus contributing to an overall larger band gap in this material than in oxygen-free GaN.

In addition to the contribution from the GaN matrix we see a clear signal in the XAS and XES associated with molecular nitrogen embedded within the films, and this is found to account for anything from a few percent to as much as twenty percent of the total nitrogen content. Understanding the presence of these nitrogen molecules is essential for interpreting measurements of the films' atomic composition.

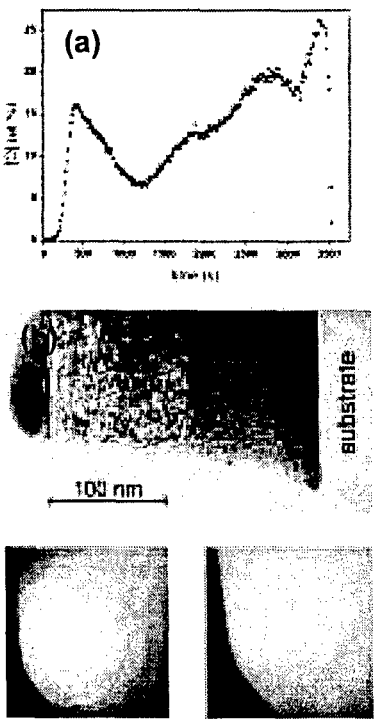

Figure 1: (a) SIMS profile showing graded oxygen content through a film. (b) Corresponding TEM and electron diffraction images showing an abrupt change from amorphous to nanocrystalline structure.

References

[1] P. Stumm and D. A. Drabold, Phys. Rev. Lett. **79**, 677 (1997).
[2] A. Koo *et al.*, submitted to Appl. Phys. Lett. (2004).

Synthesis and characterization of indium nitride micro- and nanostructures

Heiko Timmers[1)], Vernon Edge[1)], James Anderson[1)], Geoff Lawes[1)], Santosh K. Shrestha[1)], Rakesh Dogra[2,3)], Aidan P. Byrne[3,4)]

[1)]*School of Physical, Environmental and Mathematical Sciences, University of New South Wales at the Australian Defence Force Academy, Canberra, ACT 2600, Australia*
[2)]*Department of Electronic Materials Engineering, Research School of Physical Sciences and Engineering, Canberra, ACT 0200, Australia*
[3)]*Department of Nuclear Physics, Research School of Physical Sciences and Engineering, Canberra, ACT 0200, Australia*
[4)]*Department of Physics, The Faculties, Australian National University, Canberra, ACT 0200, Australia*

Indium nitride is predicted to have better electron transport properties than gallium nitride. This makes it a promising material for future transistors. While the electronic band-gap of indium nitride is still contested, suggested values of as low as 0.7 eV, and indium-gallium-nitride alloying, would give complete coverage of the visible spectrum, so that the material is also highly thought after in the context of novel photovoltaic cells. In stark contrast to gallium nitride, the reliable growth of crystalline indium nitride films of a quality necessary for device engineering has, however, not been achieved. This is largely due to the low dissociation temperature of the compound, which also explains why little information is available on the synthesis and properties of indium nitride crystal grains of nanometer dimensions. The exploitation of quantum effects in possible future devices based on the indium nitride semiconductor will require such knowledge.

In this work indium nitride grains have been synthesized from indium oxide and ammonia at different growth temperatures. The successful synthesis of indium nitride grains has been confirmed by x-ray diffraction spectroscopy which has also indicated that the grain size is small. The grains have been imaged with optical transmission and scanning electron microscopy. A diverse spectrum of grain morphologies has been found including curled strands with lengths of tens of micrometers and diameters of only a few hundred nanometers.

The highly-structured material has been studied further by diffusing the radioisotope tracer indium-111 into the grains. Using perturbed angular correlation spectroscopy, γ-photons from the radioactive decay of the tracer nuclei have been detected. While this technique generally probes the lattice on a local scale, in this case the conversion of indium nitride to indium oxide has been identified. It is reasoned that this indium oxide formation occurred as a consequence of the radiotracer diffusion at a temperature of 550° C at the grain surfaces. In addition to the indium oxide signal an unknown perturbation frequency has been discovered, however, which may correspond to the incorporation of the radioactive indium tracer into the indium nitride lattice. If confirmed this frequency may be used to study the indium nitride lattice at the nanometer scale.

Optimising the growth conditions of oxidised zinc films for photoluminescence properties.

Paul Miller[1,*], Zhengwei Li[2], Wei Gao[2], Roger J. Reeves[1]

[1]*Dept of Physics and Astronomy, MacDiarmid Institute for Advanced Materials and Nanotechnology, University of Canterbury, Christchurch, New Zealand*
[2]*Dept of Chemical and Materials Engineering, The University of Auckland, Private Bag 92019, Auckland, New Zealand*

Zinc Oxide is a wide bandgap semiconductor with many interesting properties. It has a bandgap near 3.3eV and a strong exciton binding energy of 60meV making it an ideal candidate for optical systems in the UV. It is also highly transparent to the optical part of the solar spectrum, has a bandgap tunable by alloying, is non toxic and can be grown as a low resistivity semiconductor, which makes it particularly useful for manufacturing cheap efficient solar cells. In this report, zinc was deposited on a glass substrate by DC sputtering and later oxidised over a select range of temperatures and pressures as well as for different periods of time. This has the effect of altering the photoluminescent properties of the films. We report on an investigation into optimising the conditions of zinc film oxidation for photoluminescence (PL) properties. Room temperature PL studies between 350 and 620 nm show a strong band edge emission centred at 3.335eV and a deep level emission centred at 2.43eV. The band gap is shown to be independent of oxidation temperature and an optimum oxidation temperature of 540 C has been identified. Results for optimal oxidation time and pressure have also been obtained.

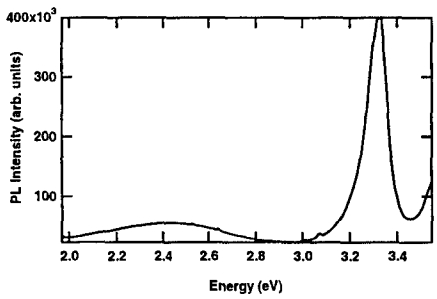

fig. 1) Room temp PL spectra for zinc oxidised at a temperature of 550 C

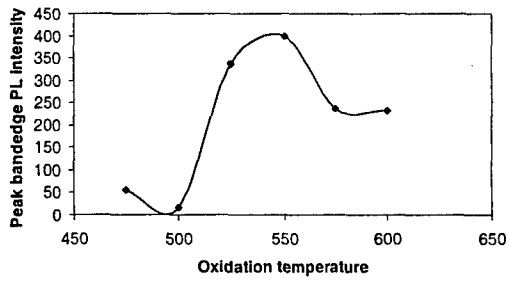

fig.2) Measured 3.335eV PL peak intensity as function of oxidation temperature

* Contact author: pmi18@student.canterbury.ac.nz

Comparison of DC and RF sputtered ZnO thin films

Leo P. Schuler[1,*], M. M. Alkaisi[1], P. Miller[2], R. J. Reeves[2], S. Brown[3], A. Markwitz[4]
[1,2,4]*MacDiarmid Institute for Advanced Materials & Nanotechnology*
[1]*Department of Electrical and Computer Engineering, University of Canterbury, Christchurch, New Zealand*
[2]*Department of Physics and Astronomy, University of Canterbury, Christchurch, New Zealand*
[3]*Deparment of Geological Sciences, University of Canterbury, Christchurch, New Zealand*
[4]*Institute of Geological & Nuclear Sciences, Lower Hutt, New Zealand*

In recent years, there has been increased interest in Zinc Oxide (ZnO) in terms of potential applications as piezoelectric coatings for Surface Acoustic Wave devices, for IR and visible light emitting devices and UV sensing. ZnO has a unique combination of high values of band gap energy, cohesion and exciton stability. The very high exciton binding energy (60meV) gives it a very high potential for room temperature light emission.

Zinc Oxide Films (ZnO) have been deposited using both DC and RF sputtering. ZnO was deposited using reactive DC sputtering with a Zn target in O_2 / Ar atmosphere. The power was 250 W and the pressure typically in the Pa range, which resulted in a deposition rate of up to 10 nm/min. RF sputtering with a ZnO target in Ar atmosphere was also used, with a forward power of 150 W, the pressure typically in the Pa range, which resulted in a deposition rate of up to 35 nm/min.

In this work we compare the grain size, crystal structure, and roughness of ZnO films deposited on glass using DC and RF sputtering (Figure 1). Generally, DC sputtered films have a grain size of around 200 to 300 nm with corresponding higher surface roughness and are piezoelectric, and X-Ray diffraction shows a high peak which corresponds to polycristalline ZnO growth normal to the surface. RF sputtered films have generally smaller grain size of around 50 nm and smoother surface; X-Ray diffraction shows a smaller peak which corresponds to polycristalline ZnO growth.

The photoluminescence response (PL) and Rutherford Backscattering (RBS) of the various films were determined and will be discussed.

Dry etching of the films was also compared (Figure 1). Reactive Dry Etching (RIE) was performed using CHF_3 and Methane/H_2. Generally, the etch rate was slow using CHF_3 (< 5 nm/min), the etching smoothened the surface and introduced voids, which are visible using SEM imaging. Results of RIE etching and the influence on the film quality will be presented.

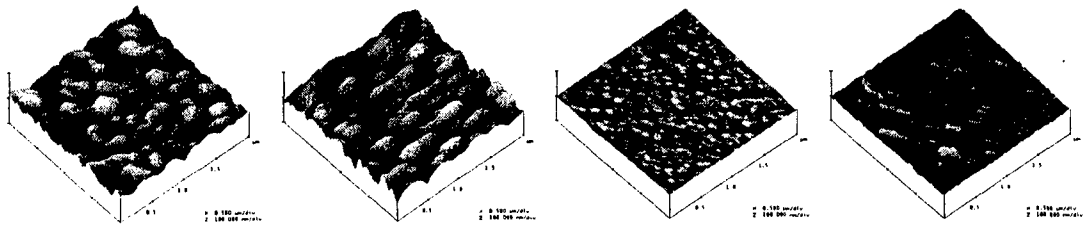

DC sputtered ZnO (Not etched) | *DC sputtered ZnO (etched using CHF_3)* | *RF sputtered ZnO (Not etched)* | *RF sputtered ZnO (etched using CHF_3)*

Figure 1: AFM micrographs of sputtered ZnO

* Contact author: Leo.Schuler@elec.canterbury.ac.nz

Nanostructuring of Silicon by Electron Beam Annealing

S.P. Lansley[1,*], P.-Y. Kuo[1], C.-T. Lu[1], S. Johnson[2], A. Markwitz[2,3] and R.J. Blaikie[1,3]
[1] *Department of Electrical & Computer Engineering, University of Canterbury, Private Bag 4800, Christchurch, NEW ZEALAND*
[2] *Institute of Geological and Nuclear Sciences, PO-Box 31-312, 30 Gracefield Road, Lower Hutt, NEW ZEALAND*
[3] *The MacDiarmid Institute for Advanced Materials and Nanotechnology*

Silicon nanostructures form when untreated silicon substrates are subjected to electron beam annealing (EBA) using appropriate conditions. Nanostructuring occurs as a result of kinetic amplification of the surface disorder induced by thermal decomposition of the native oxide layer and occurs in the temperature range 800 °C to 1200 °C [1]. Following annealing of a Si (100) substrate at 1100 °C for 15 s using a raster-scanned 20 keV electron beam, nanostructures are observed which are distributed randomly over the entire substrate surface with an average density of 11 μm^{-1} and an average height of 8 nm TEM images indicate that the features are crystalline and square-based pyramidal structures

Similar square-based pyramidal structures have also been found to form on Si (110) substrates. However, on Si (111) substrates, the growth of silicon nanostructures occurs preferentially along step-edges formed on the vicinal surfaces and significant differences in the shapes of nanostructures formed along the step-edges and on the terraces are observed, see Figure 1.

High-resolution AFM tips have been employed to obtain high resolution images of silicon nanostructures on Si (100), (110) and (111) surfaces. Large-area current-voltage characteristics of substrates covered in these nanostructures and current-voltage characteristics of individual silicon nanostructures (using Ti/Au coated AFM tips) are currently being investigated and will be presented along with the AFM imaging results.

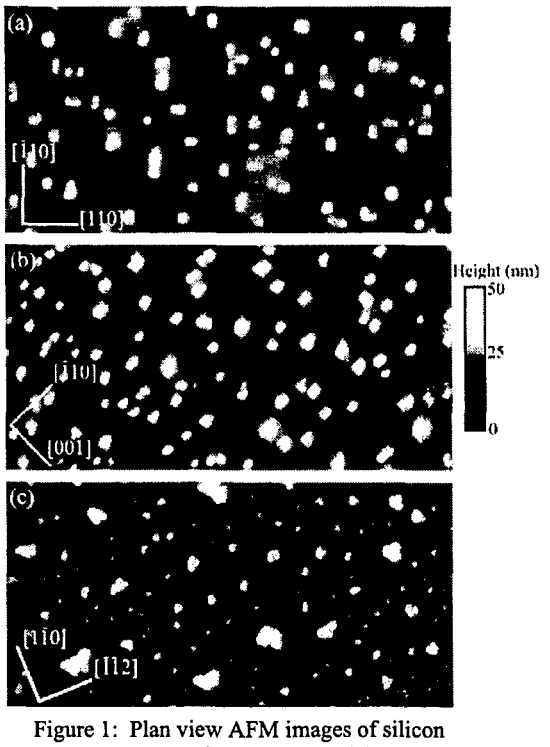

Figure 1: Plan view AFM images of silicon nanostructures formed on (a) Si (100), (b) Si (110) and (c) Si (111) surfaces.

References

[1] S. Johnson, A. Markwitz, M. Rudolphi, and H. Baumann, J. Appl. Phys. **96**, 605 (2004).

* Contact author: s.lansley@elec.canterbury.ac.nz

The Annealing Behaviour of nc-GaN and a-GaN:O Films; Dot Formation, SEM, Luminescence and Raman Spectroscopy

C.E.A. Grigorescu[1*], H.J. Trodahl[2], B.J. Ruck[2], F. Budde[2], A. Tonetto[3], R. Notonier[3] and O. Monnereau[4]
[1] *National Institute for Optoelectronics, Bucharest, Romania*
[2] *School of Chemical and Physical Sciences, Victoria University of Wellington, NEW ZEALAND*
[3] *Service Microscopie Electronique, Université de Provence, Marseille, France*
[4] *Madirel, Université de Provence, Marseille, FRANCE*

The wide band gap semiconductor GaN is currently the material of choice for optoeletronic devices in the UV-blue region of the spectrum, especially as regards light emitting diodes and diode lasers. The commercial fabrication route for the material is epitaxial growth, normally on sapphire. There remains an interest on seeking alternative growth routes, and in exploring the behaviour of the material that results from them. Our group in Wellington has investigated an ion assisted deposition (IAD) technique [1-3] which leads to disordered nanocrystalline or even amorphous material. Here we discuss annealing of the GaN and Ga oxynitride films.

Both GaN consisting of random-stacked nanocrystals and amorphous GaN:O films have been annealed *in situ* in a scanning electron microscope (SEM) to observe the medium-scale changes associated with reconstruction. The films have been subjected to study by Raman spectroscopy both before and after annealing to study changes in their atomic configuration. Luminescence spectroscopy was also monitored.

Stoichiometric GaN films show no remarkable behaviour during annealing; there is evidence only of a general reduction of the disorder associated with the random stacked nanocrystalline state. In contrast the oxynitride films display a weak but easily observed photoluminescence, and develop an island structure during annealing, with dots of 1-5 micron diameter on the films surface. They remain amorphous, but with a reduced level of bond angle disorder being inferred from Raman spectra. The dots appear to be approximated by flattened hemispheres, their separation is not very different from visible wavelengths so that they are potentially optical bandgap systems, but their diameters are much larger than those that might show quantum confinement behaviour.

This poster will present Raman and XRD results on as-prepared and annealed films, and SEM images of the development of the films' structure during the annealing process.

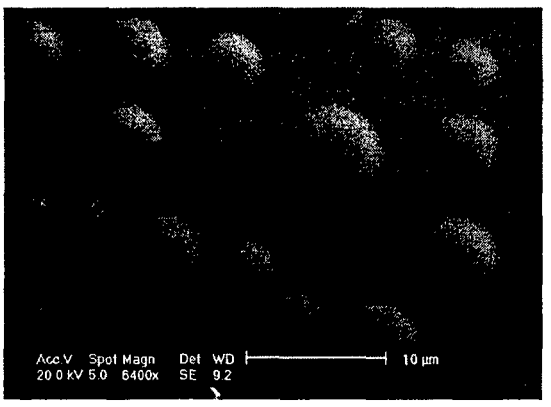

Figure 1. Scanning electron microscope image of the surface of a gallium oxynitride film (approximate Ga:N:O composition 40:40:20) after annealing at a temperature of 600 °C. The features are raised islands with the same composition as the remaining flat film, and they are filled rather than hollow. The entire film, including the islands, developed a more ordered structure after annealing, but it was still an amorphous network in contrast with the crystalline form of annealed stoichiometric GaN films. This film was on a Si substrate.

References

[1] A.Bittar, H.J. Trodahl, N.T. Kemp and A. Markwitz, Appl. Phys. Lett. **78**, 619 (2001).
[2] U.D. Lanke, A. Koo, B.J. Ruck, H.K. Lee, A. Markwitz, V.J. Kennedy, A.J. Ariza, D.J. Jones, J. Rozière. A. Bittar and H.J. Trodahl, J. Mater. Res. Soc. Symp Proc. **693**, 347 (2002).
[3] A. Koo, B.J. Ruck, U.D. Lanke, H.J. Trodahl, A. Bittar, J.B. Metson, M.J. Ariza, D.J. Jones and J. Rozière, Proc. 16th Conference on the Physics of Semiconductors, Ed.s A.R. Long and J. H. Davies, Institute of Physics Publishing, Bristol (UK) and Philadelphia (USA), (ISBN: 0-7503-0924-5), (2003).

*Corresponding author: cgrigor@inoe.inoe.ro

Modification of electrical conductivity in RF magnetron sputtered ZnO films and ZnO crystals by low-energy hydrogen ion implantation

J. Kennedy[1,2*], A. Markwitz[1,2], Z. Li[3], W. Gao[3], S.M. Durbin[4] and R. Reeves[4],
[1] Rafter Research Centre, Institute of Geological and Nuclear Sciences, P.O. Box 31-312, 30 Gracefield Road, Lower Hutt, New Zealand
[2] The MacDiarmid Institute for Advanced Materials and Nanotechnology, Victoria University of Wellington, New Zealand
[3] Department of Chemical and Materials Engineering, University of Auckland, Auckland, New Zealand
[4] MacDiarmid Institute for Advanced Materials and Nanotechnology, University of Canterbury, Christchurch, New Zealand

Zinc oxide (ZnO) shows great potential for broad device applications from photonics, electronics and several emerging areas such as nanostructures and spintronics [1,2]. Many fundamental questions regarding the basic properties of ZnO and the fabrication of optoelectronic devices based on ZnO remain elusive. In general, ZnO exhibits strong n-type conductivity which is attributed to native defects. However, recent first principle calculations revealed that none of the native defects can provide a high concentration of shallow donors and that hydrogen impurities might be responsible for n-type conductivity [3]. Our current research is focused on understanding the influence of hydrogen doping of ZnO in order to particularly reduce the n-type conductivity and thus preparing the material for subsequent ion implantation processes that aim to achieve p-type doping, which is essential for future optoelectronic device applications.

In the present study, ZnO films prepared on various substrates such as silicon, glass and quartz by RF magnetron sputtering were doped with hydrogen using the low energy ion implanter at the Institute of Geological & Nuclear Sciences (GNS). Hydrogen ions were implanted at 25 keV into the various ZnO films with high doses ranging from $5x10^{16}$ to $1.5x10^{17}$ ions cm^{-2}. The implantation depth is about 200 nm. The thickness and stoichiometry of the films were determined at GNS with Rutherford backscattering spectrometry (RBS) and nuclear reaction analysis (NRA). For comparison reasons, ZnO crystals were doped with hydrogen using similar implantation protocols. High resolution quantitative hydrogen depth profiles of the un-doped and doped samples were measured non-destructively with elastic recoil detection analysis (ERDA) using a finely focussed 2.5 MeV $^4He^+$ ion beam impinging onto the samples under 20° [4]. Structural, optical and electrical measurements were carried out on the films and crystals by SEM, XRD, PL and Hall probe techniques to explore the effects of hydrogen doping. It was observed that the electrical conductivity is decreased by as much as an order of magnitude after hydrogen implantation in contrast to other reports in literature [2,5]. Detailed results regarding the ion implantation process and the results obtained from the various characterisation techniques will be discussed.

References

[1]. D.C. Look, Mater.Sci.Eng B 80,383 (2001)
[2]. S.J. Pearton, D.P. Norton, J.Ip, Y.W.Heo and T. Steiner, J. Vac.Sc.Technol B 22, 932,(2004)
[3] C.G. Van de Walle, Phys.Rev.Lett 85,1012, (2000)
[4]. J.P. Stoquert and T. SZorenyi, Phy.Rev.B 66, 144108 (2002).
[5]. S. Kohiki, M. Nishitani, T. Wada and T. Hirao, Appl.Phys.Lett 64, 2876 (1994)

*Contact author: j.kennedy@gns.cri.nz

Diffusion coefficients of proton in $CsHSeO_4$

Yukihiko Yoshida*, Yasumitsu Matsuo and Seiichiro Ikehata

Department of Applied Physics, Faculty of Science, Tokyo University of Science, 1-3 Kagurazaka, Shinjuku-ku, Tokyo, 162-8601, Japan

It is known that $CsHSeO_4$ undergoes structural phase transition at T_c = 401 K. Particularly, electrical conductivity drastically changes from the insulator to the semiconductor by the phase transition with increasing temperature [1]. Moreover it is assumed that the high-electrical conductivity results from the increase in conducting path caused by the breaking of hydrogen bonds accompanied by a reorientational motion of SeO_4 tetrahedrons [2]. In addition to these properties, $CsHSeO_4$ shows the interesting feature that proton transport is related to the high-electrical conductivity [2]. Recently it is noted that material with proton transport is used for the electrolyte of proton exchange membrane fuel cells (PEMFC). Furthermore PEMFC shows the high-energy efficiency, low pollution level and needs only a very small space [3]. Moreover it is also expected that the fuel cell based on $CsHSeO_4$ has the advantage of unnecessity of humidity condition required in the fuel cell of the hydrated perfluorosulfonic acid (Nafion) membranes [4-6]. Therefore it is significant to investigate proton dynamics in $CsHSeO_4$ from the viewpoint of investigating diffusion coefficients of proton. In order to understand the mechanism of the semiconductivity in $CsHSeO_4$, we have investigated diffusion coefficients of proton by the ^{1}H-NMR measurement

Figure 1 shows temperature dependence of diffusion coefficients D in $CsHSeO_4$. As shown in Fig. 1, D increases with increasing temperature and is approximately 10^{-10}~10^{-12} cm^2s^{-1} in temperature range below T_c. This result indicates that proton also moves in the insulator phase below T_c. Moreover the diffusion coefficients below T_c are very small compared with those observed in semiconductor phase of $RbHSeO_4$ and NH_4HSeO_4 typically 10^{-7} cm^2s^{-1} [7]. From these results, we deduced that proton moves in a local region even below T_c.

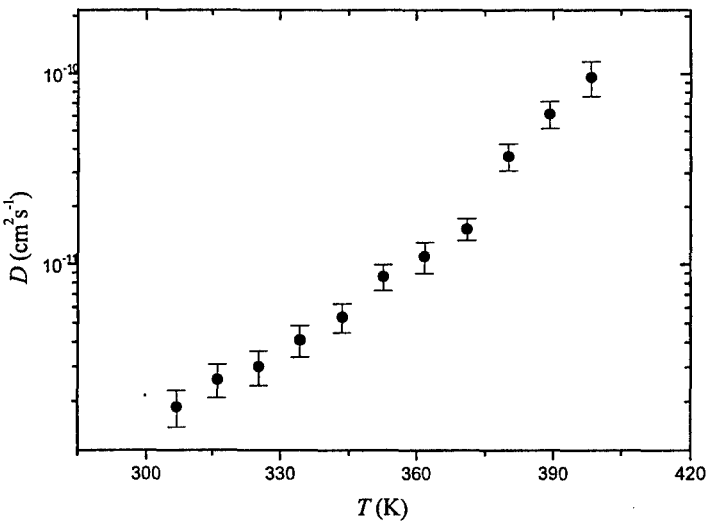

Figure1 Temperature dependence of diffusion coefficients D in CsHSeO4.

References

[1] A. I. Baranov, L. A. Shuvalov and N. M. Shchagina : JETP Lett. (1982) **36**, 459
[2] M. Komukae, M. Tanaka, T. Osaka, Y. Makita, K. Kozawa and T. Uchida : *J. Phys. Soc. Jpn.* (1990) **59**, 197.
[3] S.M. Haile, D.A. Boysen, C.R.I. Chisholm and R.B. Merle : Nature (2001) **410**, 910.
[4] N. Wagner, W. Schnumberger, B. Muller and M. Lang, Electrochimi : Acta (1998) **43**, 3785.
[5] D. Singh, D.M. Lu and N. Djilali : Int. J. Engng Sci. (1999) **37**, 431.
[6] S. Srinivasan, O.A. Velev, A. Parthasarathy, D.J. Mankoa and A.J. Appleby : J. Power Sources (1991) **36**, 299.
[7] Yu. N. Moskvich, A. A. Sukhovskii and O. V. Rozanov : Sov. Phys. Solid State (1984) **26**, 21

Synthesis of nano-sized ZnO powders by thermal decomposition of zinc acetate from pulp (*Broussonetia papyrifera* (L.) Vent.) precursor

Liewhiran C. and Phanichphant S.

Department of Chemistry, Faculty of Science, Chiang Mai University, Thailand 50200.

Nano-sized ZnO powders were synthesized by thermal decomposition of zinc acetate and pulp (*Broussonetia papyrifera* (L.) Vent.). Zinc acetate solution was prepared and the pulp was soaked in this solution for 24h. The impregnated mixture was dried at 70°C for 48h. The mixture was calcined between 600-900°C with 100 degree increment. The reaction mechanism was followed by Fourier transform infrared spectroscopy (FT-IR) technique for the calcined powders at different temperatures. The calcined powders were characterized by X-ray diffraction (XRD) and scanning electron microscopy (SEM). The particle size of the calcined powders at 600-900°C were found to be in the range of 20-80 nm.

REFERENCES

1. Y. Yang *et. al.*, *J. Crystal Growth*, **12,** 2003, p.10.
2. T. Masaki *et. al.*, *J. Ceram. Proc. Res.*, **4**(3), 2003, p.135.
3. J. Wang and L. Gao, Synthesis and characterization of ZnO nanoparticles assembled in one-dimensional order, *Inorg. Chem. Comm.*, **6**, 2003, p.877.
Y. J. Kwon *et. al.*, *J. Ceram. Proc. Res.*, **3**(3), 2002, p.146.

Friday 11 February
Oral Session One

Galaxy I **1045-1200**
Session Fr A1 **Nanostructured Semiconductors.....317**

Meeting Room V **1045-1200**
Session Fr B1 **Superconducting and Ferroelectric Ceramics 323**

Copthorne I **1045-1200**
Session Fr C1 **Surface and Interface Phenomena.....329**

Copthorne II **1045-1200**
Session Fr D1 **NMR Studies and Techniques 335**
Session sponsored by Biolab Ltd

Copthorne III **1045-1215**
Session Fr E1 **Quantum-Effect Electronic Devices.....341**

SESSION Fr A1
NANOSTRUCTURED SEMICONDUCTORS

Friday 11 February 2005 **1045–1200**

Galaxy I

Session Chair **Andreas Markwitz, Institute for Geological and Nuclear Sciences, NZ**

10.45 **Dielectric transition of nano-diamond and nano-silicon**
Fr A1.1 C.Q. Sun, L.K. Pan and C.M. Li
Nanyang Technological University, Singapore

11.00 **Field emission properties of self-assembled silicon nanostructures formed by electron beam annealing**
Fr A1.2 S. Johnson[1], A. Markwitz[1,2], M. Rudolphi[3], H. Baumann[3], S.P. Oei[4], K.B.K. Teo[4] and W.I. Milne[4]
[1] *Institute of Geological and Nuclear Sciences, Lower Hutt, NZ*
[2] *The MacDiarmid Institute for Advanced Materials and Nanotechnology, NZ*
[3] *J.W. Geothe-University, Frankfurt, Germany*
[4] *University of Cambridge, Cambridge, UK*

11.15 **InGaN nanostructures: a combined AFM and TEM study**
Fr A1.3 N.K. van der Laak, R.A. Oliver, M.J. Kappers and C.J. Humphreys
University of Cambridge, Cambridge, UK

11.30 **Investigating the fabrication of SiC nanoboulders *on* Si (100) surface by ^{12}C implantation and electron beam annealing**
Fr A1.4 A. Markwitz[1,2], S. Johnson[1], J. Kennedy[1,2], M. Rudolphi[3], H. Baumann[3], P.-Y. Kuo[4] and R. Blaikie[2,4]
[1] *Institute of Geological and Nuclear Sciences, Lower Hutt, NZ*
[2] *The MacDiarmid Institute for Advanced Materials and Nanotechnology, NZ*
[3] *J. W. Goethe-University, Frankfurt, Germany*
[4] *University of Canterbury, Christchurch, NZ*

11.45 **Field-effect transistor and field emission display devices using nanoporous inorganic semiconductor C12A7:e-**
Fr A1.5 T. Kamiya, Y. Toda, S. Aiba, M. Miyakawa, K. Nomura, K. Hayashi, M. Hirano and H. Hosono
Tokyo Institute of Technology, Yokohama, Japan

Dielectric transition of nano-diamond and nano-silicon

Chang Q. Sun,* L. K. Pan and C. M. Li
School of Electrical and Electronic Engineering, Nanyang Technological University, Singapore 639798, SINGAPORE

Impedance measurement with respect to frequency and temperature change allows one to inspect the detailed transport processes inside materials through their electrical analogues [1]. In conjunction with structural characterization, impedance analysis yields a complete physical picture of various phenomena occurring in the specimen under different conditions. The most important advantage of impedance measurements is that they can distinguish individual contributions to electrical conduction or to electron polarization arising from different sources like bulk, grain boundaries, intergranular contact regions, and electrode/sample interface regions where defect states are generated due to chemical reaction [2] or coordination number imperfection [3]. This forms also advantages for biosensors with high resolution of signals [4].

The dielectric behavior of nano-silicon and nano-diamond films with given dimensions have been examined by using impedance analyzer up to 798 K within the frequency range of 50 ~ 1.0 MHz. Multiple semicircles in a Cole-Cole plot has been observed when the temperature is raised. It is found for that the conductivity contributed from both bulk grain interior and grain boundary increases with increasing temperature, an opposite trend exhibits when the size is reduced. At temperatures above 673 K and 523 K, the impurities at the nano-Si and nanodiamond grain boundaries are thermally activated, respectively; and thus contribute to the dielectric relaxation of the specimens. The temperature dependent conductivity follows an Arrhenius law. For the nanodiamond, the thermal transition happens at 573 K with activation E_A transition from 0.13 to 0.67 eV. Similar E_A at the same temperature is found for the Arrhenius plot of relaxation frequencies from 0.14 to 0.73 eV. For a nano-Si, the thermal E_A transition from 0.07 to 0.79 eV happens at 565 K. The dielectric transition is explained as the change of crystal field caused by the thermal expansion or by surface bond contraction of the nanosolid [3]. The E_A transition in conductivity indicates band tail hopping mechanism that occurs around the Fermi edge. At a critical temperature, a high degree of dispersion in the real and imaginary parts of the permittivity also occurs at low frequencies. This dispersion behavior is interpreted as a combination of electron-phonon (lattice) polarization associated to the band tail hopping and the crystal field weakening due to thermal expansion.

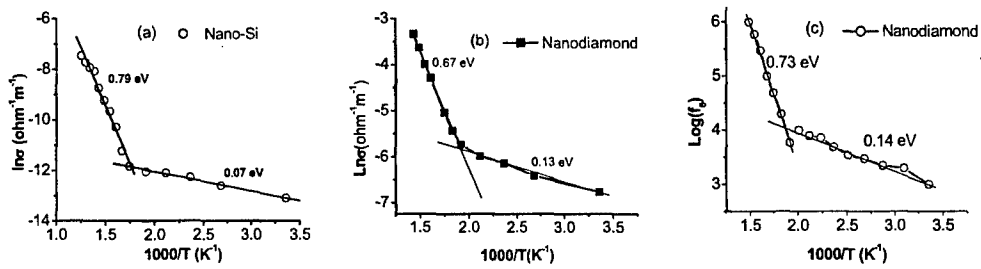

Figure 1 Arrhenius plots of conductivity activation energy E_A transition of (a) nano-Si from 0.07 to 0.79 eV at about 565 K, and (b) the nanodiamond films from 0.13 to 0.67 eV at about 523 K, and (c) relaxation frequency transition from 0.14 to 0.73 eV of nanodiamond at 561 K.

References

• E-mail: ecqsun@ntu.edu.sg; Fax: 65 6792 0415; http://www.ntu.edu.sg/home/ecqsun/

[1] N. Hirose and A. R. West, J. Am. Ceram. Soc. 76, 1633 (1996).
[2] C. Q. Sun, Oxidation electronics: bond-band-barrier correlation and its applications, Prog. Mater. Sci. 48, 521-685 (200).
[3] C. Q. Sun, Nanosolid Physics: bond order-length-strength correlation for the significance of atomic CN imperfection, Physics Reports, in press.
[4] C. M. Li, C. Q. Sun, S. Song, V.E. Choong, G. Maracus, X.J. Zhang, Impedance Labelless detection-based polyrrole DNA biosensor, Front. Biosci. In press.

Field Emission Properties of Self-Assembled Silicon nanostructures Formed by Electron Beam Annealing

S. Johnson[1,*], A. Markwitz[1,2], M. Rudolphi[3], H. Baumann[3], S. P. Oei[4], K.B. K. Teo[4] and W. I. Milne[4]
[1] *Institute of Geological and Nuclear Sciences, PO-BOX 31-312, 30 Gracefiled Road, Lower Hutt, NZ*
[2] *The MacDiarmid Institute for Advanced Materials and Nanotechnology*
[3] *Institute for Nuclear Physics, J. W. Geothe-University, August-Euler-Str. 6, 60486 Frankfurt, Germany*
[4] *Department of Engineering, University of Cambridge, Trumpington Street, Cambridge, CB2 1PZ, U. K*

For several years there has been much interest in vacuum microelectronic devices, primarily due to their unique properties: ballistic electron transport, high current densities, and operating characteristics effectively independent of radiation and temperature. These result in a wide range of potential applications including high frequency devices, sensors, and high brightness electron sources for electron-beam applications. In the new area of vacuum nanoelectronics, devices that operate at voltages approaching those of solid-state transistors may be realised[1]. Further, emission from nanometre scale cathodes show characteristics associated with their atomic size[2]: narrow energy spread, very high brightness and coherence[3].

The key technological challenge facing vacuum nanoelectronic devices is the identification of suitable fabrication techniques. In a previous study we demonstrated the self-assembly of silicon nanostructures by exploiting preferential nucleation of islands on a silicon (100) surface disordered by the thermal decomposition of the native oxide layer[4]. The nanofabrication method employs electron beam annealing (EBA) of untreated Si(100) substrates in the temperature range 800 °C to 1200 °C. The small apex radius of the resulting nanostructures and the ease of fabrication make these ideal structures for the study of field emission phenomena from nano-scale cathodes.

The field emission characteristics of nanowhiskers formed on n-type (Sb-doped, 0.07-0.09 Ωcm) and p-type (B-doped, 1-10 Ωcm silicon (100) substrates was performed in a parallel plate diode configuration. Electrical isolation and cathode-anode separation was achieved using a 100μm thick PTFE film, and measurements were performed under vacuum of 1×10^{-6} mbar. Samples were prepared by EBA at 1100 °C for 15s and with electron beam energy of 20keV. The resulting nanowhiskers exhibit an average height of 8 nm and a surface density of 11 μm^{-2}, independent of conductivity type.

Following conditioning, the Si nanostructure field emission characteristics become stable and reproducible with Fowler-Nordheim tunnelling occurring for fields as low as 2 $V\mu m^{-1}$ for nanostructures formed on p-type Si substrates. A significant difference in the threshold field for electron emission from nanostructures on n- and p-type substrates was consistently observed, with n-type substrates requiring an additional field of 3 $V\mu m^{-1}$ for emission to occur. This has been attributed to the formation of a potential barrier in the n-type cathodes due to the existence of negatively charged surface states. In the high electric field region, current saturation effects are observed to occur concurrently for the n- and p-type substrates. These studies suggest that the mechanism influencing current saturation at high fields acts largely independently of substrate conduction type and is related to space charge limited conduction.

References

[1] A.A.G Driskill-Smith, D.G. Hasko, and H. Ahmed, J. Vac. Sci. Technol. B **18**, 3481-3487 (2000).
[2] V. T. Binh, N. Garcia, and S. T. Purcell, *Advances in Electron Imaging and Electron Physics, Vol 95* (P. W. Hawkes, Ed.), Academic Press. p. 63 (1996).
[3] H. –W. Fink, W. Stocker, and H. Schmid, Phys. Rev. Lett. **65**, 1204 (1990).
[4] S. Johnson, A. Markwitz, M. Rudolphi, and H. Baumann, J. Appl. Phys. **96**, 605 (2004).

* Contact author: s.johnson@gns.cri.nz

InGaN Nanostructures: A Combined AFM and TEM Study

N.K. van der Laak, R.A. Oliver, M.J. Kappers and C.J. Humphreys
Department of Materials, University of Cambridge, Pembroke Street, Cambridge CB2 3QZ, UK

Group-III nitride semiconductors are direct bandgap materials that are have attracted much interest due to their applications in optoelectronic devices such as blue and green light-emitting diodes (LEDs) and blue laser diodes (LDs) [1]. InGaN/GaN quantum well (QW) structures have been successfully used as the active layer of LEDs and LDs [2]. Devices with quantum dots (QDs) embedded in the active layer are expected to have lower threshold currents and narrower emission spectra due to the three-dimensional confinement in the QD structures [3]. InGaN nano-islands grown by metalorganic vapour phase epitaxy (MOVPE) can be realised through self-assembled growth. Growth typically follows a Stranski-Krastanow (SK) growth mode, in which nano-islands form on top of a two-dimensional wetting layer to relieve strain induced by the lattice mismatch between the substrate and epilayer material [4].

Self-assembled InGaN/GaN nano-islands have been grown by MOVPE and the variation in island distribution with epilayer thickness has been investigated. Following the wetting layer growth, the island density initially increases very steeply, and then plateaus at a maximum island density of approximately 2 x 10^9 cm^{-2}. This change of island density with deposition time is fairly typical of SK growth in arsenide and other group-III nitride systems [5]. Surprisingly, once the dot density has saturated the average nano-island height also tends to stabilise. Using AFM and cross-sectional TEM measurements, we have been able to relate these observations to changes in the morphology of the 2D wetting layer. We propose that the 2D layer grows thicker via the nucleation and growth of flat platelets, but the 3D island distribution remains unchanged on top of the growing layer.

The island shape has also been investigated using both AFM and cross-sectional TEM. Standard AFM analysis does not provide sufficient resolution due to the convolution between the tip and sample. Therefore, we have used ultra-sharp tips in conjunction with TEM cross-section analysis. Initial results suggest that the islands are truncated with flat tops ((0001) facets). This is in general agreement with previous studies in molecular beam epitaxy (MBE) growth of nitrides nano-islands [6].

The understanding of island growth mechanisms and the relationships between structure and physical properties for self-assembled systems is essential if we are to reproducibly grow well-controlled arrays of uniformly sized islands for implementation in electronic or optical devices. These results are a stepping stone to acquiring the information needed for realising such devices with superior properties realised in the future.

References

[1] S. Nakamura, Science, **281**, 956 (1998).
[2] S. Nakamura, M. Senoh, S. Nagahama, N. Iwasa, T. Matsushita and T. Mukai, Appl. Phys. Lett. **76**, 22 (2002).
[3] C. Adelmann, J. Simon, G. Feuillet, N.T. Pelekanos, B. Daudin and G. Fishman, Appl.Phys.Lett **76**, 1570 (2002)
[4] K. Tachibana, T. Someya, and Y. Arakawa, Appl. Phys. Lett, **74**, 3, (1999).
[5] C. Adelmann, B. Daudin, R.A. Oliver, G.A.D. Briggs and R.E. Rudd, Phys. Rev. B (to be published).
[6] F. Widmann, B. Daudin, G. Feuillet, Y. Samson, M. Arlery and J.L. Rouviere, MRS Internet Journal of Nitride Semiconductor Research, **2**, 18-20, art.no.20 (1997).

*Contact author: nkv21@cam.ac.uk

Investigating the fabrication of SiC nanoboulders *on* Si (100) surface by ^{12}C implantation and electron beam annealing

A. Markwitz[1,2], S. Johnson[1], J. Kennedy[1,2], M. Rudolphi[3], H. Baumann[3], Ping-Yu Kuo[4] and R. Blaikie[2,4]

[1] Rafter Research Centre, Institute of Geological and Nuclear Sciences, P.O. Box 31-312, 30 Gracefield Road, Lower Hutt, New Zealand
[2] The MacDiarmid Institute for Advanced Materials and Nanotechnology, Victoria University of Wellington, New Zealand
[3] Institute for Nuclear Physics, J. W. Goethe-University, August-Eulerstr. 6, D-60486 Frankfurt, Germany
[4] MacDiarmid Institute for Advanced Materials and Nanotechnology, Department of Electrical and Computer Engineering, University of Canterbury, Christchurch, New Zealand

High dose ion implantation of elements combined with an annealing process is a promising method for producing precipitates or complete layers of compounds which reside below the surface of the implanted material. One prominent example of such ion beam synthesis (IBS) is the fabrication of buried insulator layers, typically SiO_2 in silicon for application in SOI devices. Less established is the use of IBS for the fabrication of silicon carbide (SiC), a wide band gap semiconductor which is receiving pronounced interest due to its potential in high power electronics and sensors. SiC layers formed by IBS involve implantation of C ions into Si, followed by an annealing process above 900 °C to crystallise the amorphous SiC layer. Varying the fluence and energy of the implanted C ions provides precise control over the C/Si-ratio, mean projected range and the distribution of the C ions. For example, implanting C ions in the energy range from 1.5 MeV - 20 keV and post-annealing at 1250°C in Ar- or N_2-atmosphere, results in a buried crystalline β-SiC layer whose depth below the surface reduces with implantation energy. However, even at low implantation energies, the SiC layer tends to lie below the substrate surface which, for many technological applications, necessitates a preliminary etching step to expose the buried SiC layer.

In a previous study we demonstrated the growth of 200 – 300 nm diameter SiC nanocrystals on silicon by 10 keV $^{13}C^+$ implantation into (100) Si followed by electron beam annealing (EBA) [1,2] (fig. 1). Under appropriate implantation conditions the nanocrystals, called nanoboulders, exhibit a surface coverage of up to 10 %. Such surface based features are of great interest for the microelectronics industry, enabling direct contact to the SiC features without the necessity for a preliminary etching step.

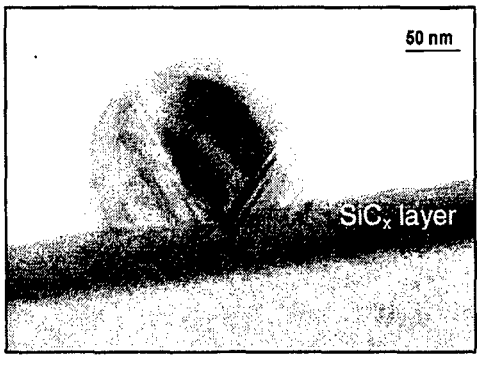

Figure 1: TEM image of a SiCx nanoboulder grown on silicon after 10 keV ^{13}C implantation with 7.6 x 10^{16} cm^{-2} and EBA at 1000 °C for 15 s. [2]

Comprehensive characterisation of nanoboulders has been performed using a number of analytical techniques, notably AFM, high resolution TEM and nuclear reaction analysis (NRA). In particular, non-resonant and resonant NRA has been critical in identifying and evaluating the nanoboulder ^{13}C content [1]. This information and the nanoboulder geometry and spatial distribution suggest a growth mechanism based on: precipitation of implanted ^{13}C, predominately at the surface [3] where nucleation sites are kinetically more favourable; and crystal growth by diffusion of C and Si adatoms across the surface, made possible by annealing under high vacuum conditions. Adatoms maintaining this growth are supplied either from diffusive species provided from the bulk material or from smaller islands which act as feed stock for the larger islands [4]. In order to refine and clarify the growth mechanism, 10 keV $^{12}C^+$ implantations and subsequent EBA into Si have been performed using similar implantation and annealing protocols. AFM and IBA studies to investigate the role of the $^{12}C^+$ implantation on the nanoboulder formation are discussed.

[1] A. Markwitz, V. J. Kennedy, S. Johnson, W. J. Trompetter, M. Rudolphi and H. Baumann, Nuclear Instruments and Methods in Physics Research **B217**, 583 (2004)
[2] A. Markwitz, S. Johnson, M. Rudolphi, H. Baumann and A. Mücklich, submitted Applied Physics Letters
[3] S. Chevacharoenkul, J. R. Ilzhoefer, D. Feijoo, and U. Gosele, Appl. Phys. Lett. **58**, 1434 (1991)
[4] P. W. Voorhees, Ann. Rev. Mater. Sci. **22**, 197 (1992)

Field-effect transistor and field emission display devices using nanoporous inorganic semiconductor C12A7:e^-

T. Kamiya[1,2,3], Y. Toda[1,2], S. Aiba[1], M. Miyakawa[2], K. Nomura[3], K. Hayashi[2], M. Hirano[1,2,3] and H. Hosono[1,2,3]
[1] *Materials and Structures Laboratory, Tokyo Institute of Technology, 4259 Nagatsuta, Midori-ku, Yokohama 226-8503, JAPAN*
[2] *Frontier Collaborative Research Center, Tokyo Institute of Technology, 4259 Nagatsuta, Midori-ku, Yokohama 226-8503, JAPAN*
[3] *ERATO-SORST, JST, in Frontier Collaborative Research Center, Tokyo Institute of Technology, 4259 Nagatsuta, Midori-ku, Yokohama 226-8503, JAPAN*

$12CaO{\cdot}7Al_2O_3$ (C12A7) crystal has a unique crystal structure composed of subnanometer-sized (~0.4 nm in innersize) cages and clathrated free oxygen ions (O^{2-}). The free oxygen ions may be replaced with other active anions such as O^- and H^-, leading to appearance of novel functions such as strong oxidation power and UV-induced persistent insulator-conductor conversion [1,2]. The free oxygen ions may be replaced also with electrons, forming an inorganic electride C12A7:e^-, in which electrons act as anions [3]. Conventional organic electrides known to date are unstable in ambient atmosphere and at room temperature; therefore there have been no report on device application although unique properties and functions are expected for its exotic electronic structure. In contrast, C12A7:e^- is the first room-temperature and air-stable electride. In this paper, we have investigated device applications of the inorganic electride C12A7:e^- to probe the fundamental carrier dynamics and electronic structure of this material and to examine the potential as an electronic device material.

For the measurements of electron field emitter, C12A7:e^- single crystal was prepared by a Ca-treatment method [3]. Field emission was measured at ~6×10^{-5} Pa using a mirror-polished surface to examine the fundamental material properties. The distance between the emitter surface and an extraction electrode was adjusted precisely to be 0.05 mm using a 0.05-mm-thick mica plate. It was observed that electron emission is controlled by thermionic emission at low extraction voltages < 1500 V, while the emission mechanism was changed to Fowler-Nordheim (FN) field-emission at higher voltages and the current density reached 22 $\mu A/cm^2$ at ~1600 V The work function was estimated from the thermionic and FN emission models, both of which provided a value of ~ 0.6 eV. The electronic structure was also investigated by ultraviolet photoelectron spectroscopy, which gives a larger work function value of ~ 3.7 eV. We tentatively consider that the discrepancy in the work function values arises from surface band-bending. Field emission display devices were fabricated using sodium salicylate or ZnO:Zn for phosphor, which displayed bright light emission clearly visible in typical ambient light.

For field-effect transistors (FETs), electrons were doped to C12A7 single crystal by extracting some portion of the free oxygen ions. Top-gate type FET structures were fabricated using standard photolithography and lift-off techniques. It was observed that source-to-drain current (I_{ds}) was modulated by applying gate voltage, and field-effect mobility of ~0.08 $cm^2(Vs)^{-1}$ was obtained. This value is somewhat lower than the drift mobility of C12A7:e^- (~0.1 $cm^2(Vs)^{-1}$). I_{ds}-V_{ds} characteristics showed non-linear behaviour around V_{ds} ~ 0 V, which is due to non-ohmic source and drain contacts originating from small electron affinity of C12A7:e^-.

References

[1] Q. X. Li et al. Appl. Phys. Lett. **80**, 4259 (2002)
[2] K. Hayashi et al., Nature 419, 462 (2002)
[3] S. Matsuishi et al., Science 301, 626 (2003)

SESSION Fr B1
SUPERCONDUCTING AND FERROELECTRIC CERAMICS

Friday 11 February 2005 **1045–1200**

Meeting Room V

Session Chair **Jeff Tallon, Industrial Research Limited, NZ**

10.45 **Oxygen loading in second-generation high-temperature superconductor tapes**

Fr B1.1 N.M. Strickland[1], A. Semwal[1,2] G.V.M. Williams[1,2], W. Zhang[3] and D.T. Verebelyi[3]

[1] *Industrial Research Ltd., Lower Hutt, NZ*

[2] *Victoria University of Wellington, Wellington, NZ*

[3] *American Superconductor Corporation, Westborough, USA*

11.00 **The effect of substituents on magnetic order and superconductivity in $RuSr_2R_{2-x}Ce_xCu_2O_{10-a}$ (R=Gd,Eu)**

Fr B1.2 S.K. Goh[1,2], G.V.M. Williams[2] and J.L. Tallon[1,2]

[1] *Victoria University of Wellington, Wellington, NZ*

[2] *MacDiarmid Institute for Advanced Materials and Nanotechnology, Industrial Research Ltd., Lower Hutt, NZ*

11.15 **Scattering effects in single crystal cuprate superconductors**

Fr B1.3 T.M. Benseman

University of Cambridge, Cambridge, U.K.

11.30 **Epitaxial growth of the ferroelectric $Pb(Zr_{0.2}Ti_{0.8})O3$ thin films grown on $SrRuO_3/SrTiO_3$ for nano-data storage application**

Fr B1.4 W.S. Lee, K.J. Choi and S.G. Yoon

Chungnam National University, Daejon, Korea

11.45 **Effects of uniaxial stress on dielectric properties of ferroelectric ceramics**

Fr B1.5 R. Yimnirun, S. Wongsaenmai, A. Ngamjarurojana, and S. Ananta

Chiang Mai University, Thailand

Oxygen loading in second-generation high-temperature superconductor tapes

N.M. Strickland[1], A. Semwal[1,2], G.V.M. Williams[1,2], W. Zhang[3], and D.T. Verebelyi[3]
[1]*Industrial Research Ltd, Lower Hutt, New Zealand*
[2]*The MacDiarmid Institute for Advanced Materials and Nanotechnology, Victoria University of Wellington, Wellington, New Zealand*
[3]*American Superconductor Corporation, Westborough, MA 01581, USA*

Overcoming the weak inter-granular links has been the overiding problem facing the production of long-length wires based on the $YBa_2Cu_3O_{7-\delta}$ high-temperature superconductor material. However, with the thin film technology of second-generation "coated conductor" wires, the transport critical current density now approaches that of the intraganular current density. It then becomes important to consider other factors affecting the fundamental superconducting properties. In particular, the hole-doping state in the CuO_2 layers can be varied widely by changing the annealing conditions. It was noted early on that the superconducting transition temperature, T_c, follows a universal curve as a function of doping state for all the cuprate superconductors with a maximum near p=0.16 holes per Cu [1]. However, the dependence of the critical current density, J_c, on this doping state is poorly understood, mainly due to difficulties in measuring true current densities in sintered ceramic samples. Previous results have suggested that J_c is maximised on the overdoped side, near p=0.19, rather than at the state of maximum T_c [2,3]. We report variations in T_c, J_c, c-axis length, and irreversibility as functions of doping state supporting the view that overdoping is desirable to optimize J_c in $YBa_2Cu_3O_{7-\delta}$ coated conductors.

References

[1] M.R. Presland, J.L. Tallon, R.G. Buckley, R.S. Liu and N.E. Flower, Physica C **176**, 95 (1991).
[2] J.G. Ossandon, J.R. Thompson, D.K. Christen, B.C. Sales, H.R. Kerchner, J.O. Thomson, Y.R. Sun, K.W. Lay, and J.E. Tkaczyk, Phys. Rev. B **45**, 12534 (1992); J.R. Thompson, J.G. Ossandon, D.K. Christen, Y.R. Sun, B.C. Sales, H.R. Kerchner, J.E. Tkaczyk, and K.W. Lay, Cryogenics **32**, 982 (1992).
[3] G.V.M. Williams, J.L. Tallon, and J.W. Loram, Phys. Rev. B **58**, 15053 (1998); J.L. Tallon, J.W. Loram, G.V.M. Williams, J.R. Cooper, I.R. Fisher, J.D. Johnson, M.P. Staines, and C. Bernhard Phys. Stat. Sol. (b) **215**, 531 (1999).

The Effect of Substituents on Magnetic Order and Superconductivity in $RuSr_2R_{2-x}Ce_xCu_2O_{10-\delta}$ (R=Gd,Eu)

S. K. Goh[1,2,*] G. V. M. Williams[2] and J. L. Tallon[1,2]
[1] *School of Chemical and Physical Sciences,*
Victoria University of Wellington, P.O. Box 600, Wellington, NEW ZEALAND
[2] *The MacDiarmid Institute for Advanced Materials and Nanotechnology,*
Industrial Research, P.O. Box 31310, Lower Hutt, NEW ZEALAND

We report the results of a resistivity and magnetization study on the ruthenocuprate $RuSr_2R_{2-x}Ce_xCu_2O_{10-\delta}$ (R=Gd,Eu) that displays magnetic order and superconductivity. This compound contains CuO_2 and RuO_2 planes that are separated by insulating layers. The superconducting and magnetic states were probed by the partial substitution of Ru by Sn and Nb in the RuO_2 planes while the CuO_2 planes were studied by partially substituting Zn for Cu. We found that Zn substitution leads to a rapid suppression of the superconducting critical temperature but there was no significant effect on the magnetic ordering temperature.

Nb and Sn substitutions for Ru do not significantly affect the superconducting critical temperature but the magnetic ordering temperature was suppressed. In the case of $RuSr_2Gd_{1.4}Ce_{0.6}Cu_2O_{10-\delta}$, only 5 % Sn substitution for Ru was required to completely destroy the magnetic order as can be seen in the figure below. There was an associated large increase in the temperature where the bulk Meissner phase commences, which provides direct support for the spontaneous vortex phase model that has been applied to $RuSr_2R_{2-x}Ce_xCu_2O_{10-\delta}$ to account for coexisting magnetic and superconducting order.

The experimental results are consistent with decoupled CuO_2 and RuO_2 planes where superconductivity arises in the CuO_2 planes and the magnetic order is due to ordering of the Ru moments in the RuO_2 planes.

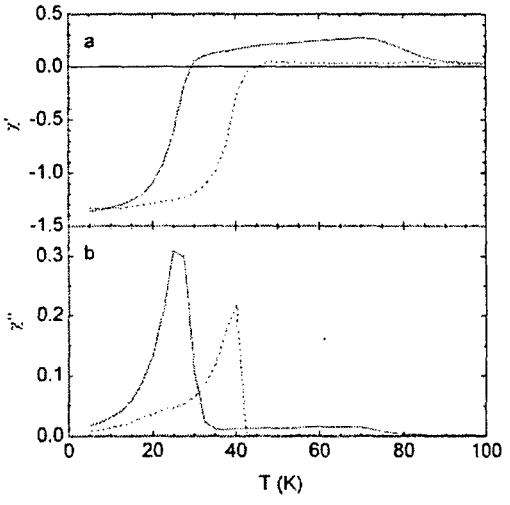

Plot of the real (a) and imaginary (b) parts of the ac susceptibility against temperature for $Ru_{1-x}Sn_xSr_2Gd_{1.4}Ce_{0.6}Cu_2O_{10-\delta}$ with x=0 (solid curve) and x=0.05 (dashed curve). The data have not been corrected for demagnetization effects. The measurements were made using a SQUID magnetometer with an ac field of 5×10^{-6} T and at a frequency of 333 Hz.

* Contact author: gohswee@student.vuw.ac.nz

Scattering effects in single crystal cuprate superconductors

T. M. Benseman[1,*]
[1] *Cavendish Laboratory, University of Cambridge, UNITED KINGDOM*

All the high temperature superconducting cuprates contain CuO_2 planes, in which partially filled Cu(3d) and O(2p) orbitals give rise to mobile charge carriers. Consequently, an atom of another metal on a Cu site strongly perturbs the surrounding electronic environment. Impurity substitution in the high-temperature superconducting (HTS) cuprates is thus a powerful microscopic probe of both the normal and superconducting states of these materials.

We have used the travelling floating zone method to grow large, high-quality single crystals of the HTS cuprate $Bi_2Sr_2CaCu_2O_8$ (Bi-2212). This has been done for the pure compound, and also for single crystals in which 2% of the Cu atoms have been replaced by Co. Growth of impurity-substituted single crystals poses particular problems, especially where crystals with a known, homogeneous level of impurity substitution are required.

Here we present our studies to date of the magnetic susceptibility of these crystals.

In highly anisotropic HTS compounds such as Bi-2212, it has been established that pairs of adjacent CuO_2 planes act as so-called *intrinsic Josephson junctions* [1]. The electronic density of states can thus be probed directly via the study of tunnelling through 'mesa' structures, consisting of a few such junctions in series. Mesas a few microns square by a few nm high can be microfabricated on the surface of a single crystal. By doing this for a cobalt-substituted crystal, we intend to investigate the scattering resonances in the density of states generated by impurities.

Impurity substituted single crystals will also provide an ideal opportunity to investigate the universal relation between T_c and residual resistivity expected for a d-wave superconductor [2].

Having successfully grown crystals of cobalt-substituted Bi-2212, we now plan to apply the same technique for crystals substituted with Fe and Mn, to permit comparison between results for different magnetic impurities, as well as substituting with a non-magnetic impurity such as Li or Al.

The work described here was performed in conjunction with Dr John Cooper of the University of Cambridge, and Dr Geetha Balakrishnan of the University of Warwick.

References

[1] V. M. Krasnov *et al.*, Phys. Rev B **59**, 8463 (1999).
[2] H. Alloul *et al.*, European Physics Letters **50**, 81 (2000).

* Contact author: tb312@cam.ac.uk

Epitaxial growth of the ferroelectric $Pb(Zr_{0.2}Ti_{0.8})O_3$ thin films grown on $SrRuO_3/SrTiO_3$ for nano-data storage application

Woo-Sung Lee, Kyu-Jeong Choi, and Soon-Gil Yoon*

Department of Materials Science and Engineering, Chungnam National University, Daeduk Science Town, 305-764, Daejon, Korea

ABSTRACT

At present there is considerable interest in ferroelectric thin films as a medium for non-volatile data storage.[1] In particular much attention is focused on investigating high density giga-bit data storage using scanning probe techniques.[2] It is known that the thickness of a 180° domain wall in ferroelectric thin film is 1-2 nm.[3] This fact indicates that ferroelectric thin films have potential to be a medium for scanning probe microscopy (SPM)-based ultrahigh density (100 G bit/cm^2 class) data storage. It has been proposed that employing ferroelectric films as recording media inherently has several advantages; 1) the recorded data are non-volatile, 2) the recording density can be ultra high because of narrow domain wall thickness, 3) the ferroelectric domains can have fast switching speed, 4) information bits can be written and read electrically.

Among the various perovskite oxide materials, $PbZr_{1-x}Ti_xO_3$ (PZT) seems to be suitable to such a storage medium, since it is stable and its remanent polarizations are high. In this application, the decrease of thickness in PZT thin films produces the decrease of domain size, resulting in ultrahigh density regimes due to the decrease of bit size. The decrease of remanent polarization attributing to the decrease of film thickness was solved a little by the heteroepitaxial growth of PZT films. The $SrRuO_3$ (SRO) is a conductive oxide (a room temperature resistivity of 280 μΩ·cm for single crystals), pseudo-cubic perovskite with a lattice constant of 0.39 nm, which has a modest lattice mismatch with $PbZr_{1-x}Ti_xO_3$ (PZT) (~ 2.7 %) and a low mismatch with $SrTiO_3$ (STO) (~ 0.6 %) allowing the growth of high quality epitaxial PZT thin films.[4] In this study, highly tetragonal $Pb(Zr_{0.2}Ti_{0.8})O_3$ films were grown on $SrRuO_3$ oxide electrodes epitaxially grown on TiO_2-terminated STO (100) single crystal substrates by pulsed laser deposition. The influences of surface flatness of STO substrate on the surface morphology and ferroelectric properties of epitaxial PZT thin films grown on SRO/STO will be investigated.

References

1. J.F. Scott, Ferroelectric memories, Vol. 3 of the Springer series on "Advanced Microelectronics", (Springer, Heidelberg, April 2000).
2. T. Hidaka, T. Mayurama, M. Saitoh, N. Mikoshiba, M. Shimizu, T. Shiosaki, L.A. Wills, R. Hiskes, S.A. Dicarolis, and J. Amano, Appl. Phys. Lett. **68**, 2358 (1996).
3. M.E. Lines and A.M. Glass, Principles and Applications of Ferroelectrics and Related Materials (Oxford University Press, Oxford, England, 1977), p. 525.
4. S. Geller, J. Chem. Phys. **24**, 1236 (1956).

Effects of Uniaxial Stress on Dielectric Properties of Ferroelectric Ceramics

R. Yimnirun*, S. Wongsaenmai, A. Ngamjarurojana, and S. Ananta
Department of Physics, Faculty of Science, Chiang Mai University 50200 THAILAND

Lead magnesium niobate ($Pb(Mg_{1/3}Nb_{2/3})O_3$ or PMN) and lead zirconate titanate ($Pb(Zr_{1-x}Ti_x)O_3$ or PZT) ceramics are widely used in devices like piezoelectric actuators and electromechanical transducers. With the complementary features of PMN and PZT, a solid-solution of PMN-PZT ceramics is expected to possess more desirable features than single-phase PMN and PZT. In practice, these ceramics are often subjected to external mechanical loading when used in specific applications, such as in actuators and transducers. A prior knowledge of how the material properties change under different load conditions is crucial for proper design of a device and for suitable selection of materials for a specific application. In this study, effects of uniaxial stress on the dielectric properties of ceramics in PMN-PZT system are investigated. The ceramics with the formula $(1-x)Pb(Mg_{1/3}Nb_{2/3})O_3$ - $(x)Pb(Zr_{0.52}Ti_{0.48})O_3$ when x=0.0, 0.1, 0.3, 0.5, 0.7, 0.9 and 1.0 are prepared by a conventional mixed-oxides method. The physical properties, phase formation behavior, and microstructure studies indicate that the ceramics obtained are perovskite materials. Their physical properties and microstructures are proportionally dependent of the PMN and PZT contents in the composite. The dielectric properties under the uniaxial stress of the PMN-PZT ceramics are observed at stress levels up to 5 MPa. It is found that with increasing applied stress the dielectric constant of the PZT-rich compositions increases slightly, while that of the PMN-rich compositions decreases. On the other hand, changes in the dielectric loss tangent with stress are found to be compositional independent. This study clearly shows the influences of the domain wall motion, degradation and depoling mechanisms on the variation of the dielectric properties of PMN-PZT ceramics under the uniaxial stress.

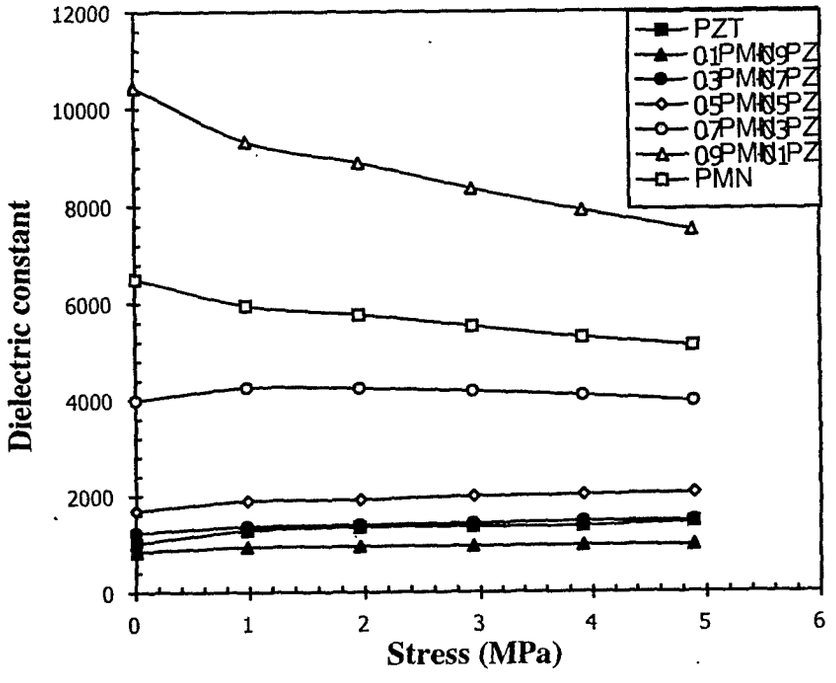

Uniaxial stress dependence of dielectric constant of PMN-PZT ceramics

References

[1] R. Yimnirun, S. Ananta, E. Meechoowas, and S. Wongsaenmai, J. Phys. D: Appl. Phys. **36**, 1615 (2003).
[2] R. Yimnirun, S. Ananta, and P. Laoratanakul, Mater. Sci. Eng. B **112**, 79 (2004).

* Contact author: rattikornyimnirun@yahoo.com

SESSION Fr C1
SURFACE AND INTERFACE PHENOMENA

Friday 11 February 2005 **1045–1200**

Copthorne I

Session Chair **Alison Downard, University of Canterbury, NZ**

10.45 **Changing the pattern of surface chemistry**
Fr C1.1 A.N. Parbhu[1], J.D. Franklin[1], S. Sharma[1], A.P. Quist[2] and R. Lal[2]
[1] *Industrial Research Limited, Auckland, NZ*
[2] *University of California, Santa Barbara, USA*

11.00 **Semiconductor surface optical response upon organic functionalization: first-principles study of a π-conjugated molecular monolayer on Si(001)**
Fr C1.2 W.G. Schmidt, A. Hermann and F. Bechstedt
Friedrich-Schiller-Universtät, Jena, Germany

11.15 **Delving into the nanostructure of self assembled porphyrin monolayers**
Fr C1.3 A.F. Le Blanc and D.L. Officer
Massey University, Palmerston North, NZ

11.30 **STM on self-organised supramolecular assembly**
Fr C1.4 R. Goh, E.R. Waclawik and J.M. Bell
Queensland University of Technology, Brisbane, Australia

11.45 **Effects of metal-molecule interface conformations on the electronic conductance of single molecules**
Fr C1.5 P. Bai[1], E.P. Li[1] and Z.K. Chen[2]
[1] *The Capricorn, Singapore*
[2] *Institute of Materials Research and Engineering, Singapore*

Changing the pattern of surface chemistry

A. N. Parbhu[1*], J. D. Franklin[1], S. Sharma[1], A. P. Quist[2] and R. Lal[2]
[1]*Industrial Research Limited, Auckland, New Zealand.*
[2]*Neuroscience Research Institute, University of California Santa Barbara, Santa Barbara, CA 93106, USA*

Recent research[1,2] has shown the formation of low-density self-assembled monolayers (LD-SAM) of alkanethiols can produce surfaces with interfacial properties that can be reversibly switched with external stimuli. We have synthesised a capped alkanethiolate that can undergo post SAM formation hydrolysis to produce a low-density, surface confined, single layer of molecules or LD-SAM. Under the influence of applied potential the molecules can reversibly switch their conformation, resulting in a dynamic change in interfacial properties. To demonstrate the switchability of surface properties in response to external stimulus we have employed μ–contact printing (μCP). We have patterned a LD-SAM on a gold substrate using a poly(dimethylsiloxane) stamp, backfilled with a conventional SAM, following established techniques[3]. The magnitude of the influence of molecular conformational changes on the functionality of the surface has been monitored by lateral force microscopy and colloidal force microscopy using chemically modified scanning probe microscope (SPM) probes. Gold coated SPM probes were chemically modified with an alkanethiolate SAM to increase the difference in the interaction potential between the probe and the two regions of the chemically patterned surface, thus increasing the contrast in the lateral force images[4]. This presentation will show the usefulness of this technique to monitor the reversible switching of the surface confined molecules.

Later force mode (friction-mode) image obtained from patterned SAMs after μCP, 5μm square pattern can be readily distinguished.

References

[1] Lahann, J., Mitragotri, S., Tran, T. N., Kaido, H., Sundaram, J., Choi, I.S., Hoffer, S., Somorjai, G.A. and Langer, R., Science, 2003, 299, 371.
[2] Liu, Y., Mu, L., Liu, B., Zhang, S., Yang, P. and Kong, J. Chem. Commun., 2004, 1194.
[3] Whitesides, G. M., Ostuni, E., Takayama, S., Jiang, X. and Ingber, D. E., Annu. Rev. Biomed. Eng., 2001, 3, 335.
[4] Noy, A., Frisbie, C. D., Roznyai, L. F., Wrighton, M. S. and Lieber, C. M., J. Am. Chem. Soc. 1995, 117, 7943.

* Contact author: a.parbhu@irl.cri.nz

Semiconductor surface optical response upon organic functionalization: First-principles study of a π-conjugated molecular monolayer on Si(001)

W. G. Schmidt*, A. Hermann, and F. Bechstedt
Institut für Festkörpertheorie und -optik,
Friedrich-Schiller-Universität, Max-Wien-Platz 1, 07743 Jena, Germany

The functionalization of semiconductor surfaces with organic molecules is a fascinating new object of surface physics with many applications such as organic and molecular electronics or biological sensors. Since optical, electronic and structural properties are intimately connected, optical methods should be very helpful in characterizing the structure and properties of organic layers. However, while optical spectroscopies are widely used in research and industry to explore semiconductor surfaces and to control growth and adsorption processes, the optical response of organic thin films adsorbed on semiconductors is not really understood.

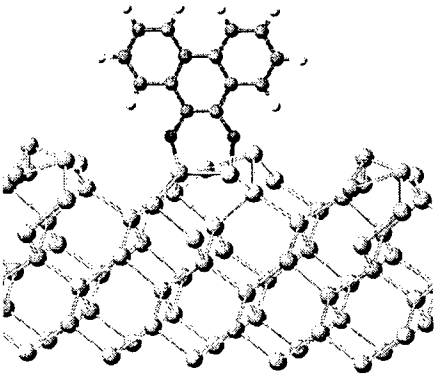

Figure: Energetically favored bonding configuration of PQ adsorbed on Si(001).

In order to clarify the respective roles of intramolecular transitions and substrate signals we perform detailed first-principles calculations on the structural, electronic and optical properties of 9,10-phenanthrenequinone (PQ) adsorbed on Si(001). This is a prototypical example for a π-conjugated molecular monolayer on the Si(001) surface and it is one of the few cases where experimental data are available[1]. The calculations are performed within the gradient-corrected density functional theory (DFT-GGA) in conjunction with the projector-augmented wave (PAW) method [2] as implemented in the VASP package [3]. The optical anisotropy spectra are calculated in the independent-quasiparticle approximation using all-electron wave functions obtained from the PAW method. It is shown that the optical anisotropy of the substrate is significantly altered. The calculations are in good agreement with experiment. The detailed analysis of the spectrum shows that a simplified interpretation of the spectra in terms of anisotropic molecular transitions fails: The molecule-substrate bonding leads to strong modifications of the intramolecular transitions, even for molecules where bonding and functional groups are seemingly decoupled. Specific π-π* transitions were identified as main source of the organic layer anisotropy signals. However, the total spectrum is dominated by contributions from adsorption-modified Si bulk states.

* Email: W.G.Schmidt@ifto.physik.uni-jena.de

References

[1] C.A. Hacker and R. J. Hamers, J. Phys. Chem. B **107**, 7689 (2003).
[2] G. Kresse and D. Joubert, Phys. Rev. B **59**, 1758 (1998).
[3] G. Kresse and J. Furthmüller, Comp. Mat. Sci. **6**, 15 (1996).

Delving into the Nanostructure of Self Assembled Porphyrin Monolayers

A .F. Le Blanc[1,*] and D. L. Officer[1]
[1] *MacDiarmid Institute for Advanced Materials and Nanotechnology and Nanomaterials Research Centre, Massey University, Palmerston North, NEW ZEALAND*

Interest in renewable forms of energy is increasing, not only as a result of the need for more sustainable energy supply but also because of the increase in costs of traditional energy sources. In this regard, the development of cheap and efficient photovoltaic devices is a major research challenge. This could be achieved by developing non-silicon solar cells based on organic dyes. Nature utilises porphyrins (chlorophyll) for the purpose of energy conversion and demonstrates the power of this type of molecule for light absorption and electron transfer. Since porphyrin derivatives are easy to synthesise, they are of increasing interest in research on new photovoltaic devices.

We have recently demonstrated the best efficiencies for porphyrin-sensitised titanium dioxide-based solar cells (≈ 4% efficient) [1]. Nevertheless a lot of work has still to be done to achieve the same stability and efficiency as for silicon based solar cells (≈15% efficient). One of the keys to improve the efficiency of dye-sensitised devices is to exert influence on the assembly process on the surfaces the dyes are immobilised on.

To better understand the assembly of porphyrins on surfaces, we have employed a variety of spectroscopic and microscopy techniques such as AFM, STM, TEM, NMR and surface enhanced Raman spectroscopy. Other techniques such as angular resolved, polarised UV-Vis absorption and fluorescence spectroscopy have also been utilised after simple modifications in standard spectrometers. Self assembled monolayers (SAMs) of porphyrins of the type shown in figure 1 were prepared on metal and metal oxide surfaces (e.g. ultra flat gold [2] and ITO). As illustrated in figure 2, the porphyrin SAM was analysed in comparison to spectra obtained from solution and nanostructured aggregates of these compounds [3]. The structure of the self assembled porphyrin monolayers will be discussed in light of these results and a variety of other data.

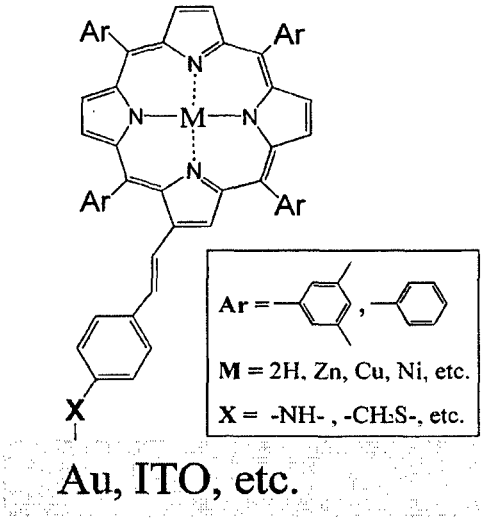

figure 1

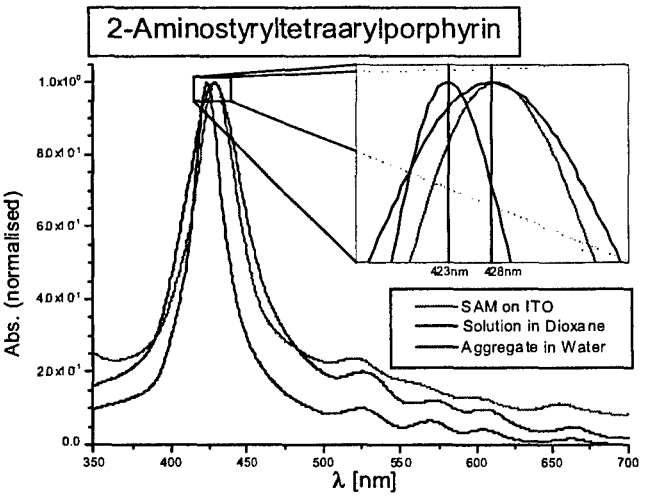

figure 2

References

[1] Md. K. Nazeeruddin, R. Humphry-Baker, David L. Officer, Wayne M. Campbell, Anthony K. Burrell, and M. Grätzel, Langmuir 2004, 20, 6514-6517
[2] Peter Wagner, Martin Hegner, Hans-Joachim Güntherodt and Giorgio Semenza, Langmuir 1995, 11, 3867-3875
[3] Johannes M. Kroon, Robert B. M. Koehorst, Marinus van Dijk, Georgine M. Sandersa and Ernst J. R. Sudhölter, J. Mater. Chem., 1997, 7(4), 615–624

* Contact author: A.LeBlanc@massey.ac.nz

STM on self-organised supramolecular assembly

R. Goh[1,*], E. R. Waclawik[2], J. M. Bell[1]
[1] *Centre for Built Environment and Engineering Research, Queensland University of Technology, Brisbane, AUSTRALIA*
[2] *Inorganic Materials Research Program, School of Physical and Chemical Sciences, Queensland University of Technology, Brisbane, AUSTRALIA*

Supramolecular approaches to self assembled systems have huge potential in nanotechnology and organic electronics. The scanning tunnelling microscope (STM) is a powerful tool for directly visualising the details of supra-molecular absorption and organisation on surfaces. In this contribution, we will report on our recent progress in the study of the self-organisation of various conjugated molecules using STM, including for the first time, rare-earth *bis* and *tris* - phthalocyanines at liquid/HOPG interface (D. Arnold, A. Fuchs, R. Goh, T. Takami, K. Sugiura, in preparation) and the conjugated polymer poly-(3hexylthiophene) (P3HT) on single walled carbon nanotubes (SWNT) (R. Goh, E. Waclawik, N. Motta, J. Bell, in preparation).

STM reveals the dynamic conformation and self-organisation of planar phthalocyanine (Pc) molecules in liquid, for example, as seen in *Figure 1* for ZnPcOC8, one of the "simpler" molecules in our study, the interface between the mobile precursor phases and the final absorbed phase is clearly seen. This and our latest STM studies on the sandwiched Pc complexes will be addressed.

Polymer organisation onto carbon nanotubes will open the way for a variety of application including solar cells, optoelectronic memory, and for purification of nanotubes. For these applications a highly interpenetrating network is desirable. We will report on our latest work on STM imaging of a highly interpenetrating network of SWNT and P3HT drop-casted from solution onto HOPG. As seen in *Figure 2*, the polymer is assembled intimately on the SWNT in a highly organised manner as corroborated by TEM and photoluminescence (PL) studies. Notably, topographic profiles along polymer-wrapped tubes show a chain-to-chain distance (d_{cc}) of *ca.* 1.45nm, which is in close agreement with d_{cc} values reported by Grévin *et al.* [1] for self-organised P3HT on HOPG. Here, we will address in detail the conformation of polymer wrapping on SWNT.

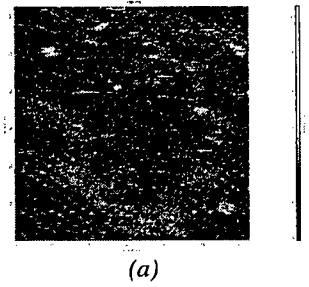

(a)

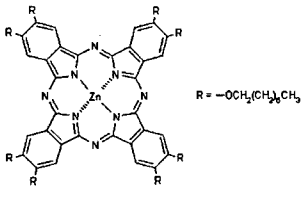

(b)

Figure 1. Boundary region showing transition from mobile phases to final absorbed state (a). Molecular structure of zinc 2,3,9,10,16,17,23,24-octakis(octyloxy)-29H,31H-phthalocyanine (ZnPcOC8) (b)

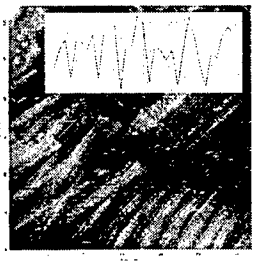

Figure 2. Polymer wrapped nanotubes; a high degree of organisation of polymer on SWNT is observed from a typical line profile along a single polymer wrapped SWNT backbone (inset); image is taken at an area of polymer/SWNT composite film where bundles are observed to protrude from the film

References

[1] B. Grévin, P. Rannou, R. Payerne, A. Pron, and J.P. Travers, Adv. Mater., **15**, 881 (2003)

* Contact author: r.goh@qut.edu.au

Effects of Metal-Molecule Interface Conformations on the Electronic Conductance of Single Molecules

P. Bai[1,*] E. P. Li[1] and Z. K. Chen[2]
[1] *Institute of High Performance Computing, Science Park road, #01-01 The Capricorn, Singapore 117528*
[2] *Institute of Materials Research and Engineering, 3 Research Link, Singapore 117602*

Molecular electronics has got great attention recently and big progress has been achieved. Metal-molecule-metal (MMM) junction is the fundamental structure to construct molecular devices. Small devices tend to be dominated by effects at the contacts and often deliver low on-currents. It has been demonstrated that the nature of the electrode-molecule coupling (physisorbed and chemisorbed molecules) strongly change the electronic properties of the molecule [1]. In either the break junction or the scanning tunneling microscope setup, the geometry of the molecule-electrode interface is poorly understood. It is not clear where the terminal atom sits on the electrode surface, e.g. at the hollow site or on the top of a surface atom.

We use *ab initio* modelling method [2] to investigate the nature of metal-molecule interface by studying the electron transport of MMM junction. The junction is an infinite system and approximated with a finite structure confined in the device region and the effects from semi-infinite electrodes on the device region are considered through self-energy by nonequilibrium Green's function (NEGF) approach. Density functional theory (DFT) within the local density approximation (LDA) is used to describe the electronic structure self-consistently and the self-consistent calculations are conducted only within the device region.

In our study, Au is chosen as electrodes and thiolated benzene as core molecule to construct the MMM junctions. We first optimize the geometries of core molecule and 3-D atomic gold electrodes separately. Then the optimized molecule is sandwiched between gold (111) electrodes. The distance between two electrodes is decided according to atomic radii and single-point energy calculations. The molecule is contacted to the surface at different locations on the Au (111) surface, on the top of surface atom, at the hollow site and on the bridge as in Fig. 1. Then the sandwiched structure is optimized again with gold atoms fixed.

The transmission function (TF), density of states (DOS), and current-voltage (I-V) characteristics of the MMM junctions are calculated to study the interface conformation effects. Fig. 2 shows the TF of MMM junctions with different interface conformations under zero biases. The transmission is dominated by the highest occupied molecular orbital (HOMO) which is nearer to the Fermi level E_f. Hollow contact has similar TF as bridge contact. On-atom contact has a HOMO closer to E_f that may leads to good conductance at lower bias. However its TF at the valley between HOMO and Lowest unoccupied molecular orbital (LUMO) is much smaller than those with other two cases. This will have negative effects on the electron conductance. Fig. 3 shows the ccurrent-voltage (I-V) characteristics of three cases. Again hollow contact and bridge contact have similar I-V characteristics. On-atom contact has larger conductance when external bias is less than 1.4eV due to HOMO near to the E_f. With bias increase hollow and bridge contacts show better coupling. Our simulation results show that the metal-molecule contact conformation has great effects on the electron conductance of the molecule. These may explain why the experiment results have poor repeatability.

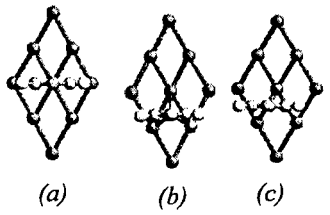

Fig 1. Metal-molecule interface conformations (a) on-atom contact (b) hollow contact (c) bridge contact

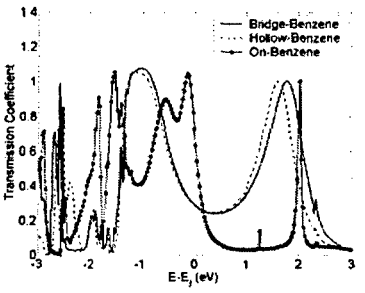

Fig 2. Transmission functions

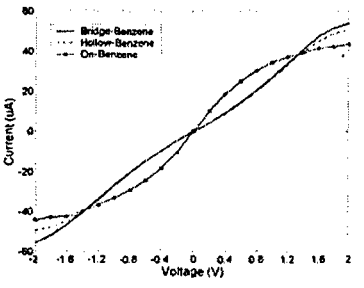

Fig 3. Current-voltage curves

References

[1] X. D. Cui, A. Primak, X. Zarate, J. Tomfohr, O. F. Sankey, A. L. Moore, T. A. Moore, D. Gust, G. Harris and S. M. Lindsay, *Science* **294**, 571 (2001).
[2] Brandbyge, M., et al., *Phys. Rev. B* **65**, 165401 (2002).

* Contact author: baiping@ihpc.a-star.edu.sg

SESSION Fr D1
NMR STUDIES AND TECHNIQUES

Session Sponsor: Biolab Ltd

Friday 11 February 2005 **1045–1200**

Copthorne II

Session Chair **Paul Callaghan, Victoria University of Wellington, NZ**

10.45 **NMR studies on ion diffusion in the lithium salt doped room temperature ionic liquids**

Fr D1.1 K. Hayamizu

National Institute of Advanced Industrial Science and Technology, AIST, Tsukuba, Japan

11.00 **Boomerang: The path to sensitive magnetic resonance on small samples**

Fr D1.2 L.A. Madsen[1], G.M. Leskowitz[1], T. George[2], P.J. Carson[1], and D.P. Weitekamp[1]

[1]*California Institute of Technology, Pasadena, USA*

[2]*NASA-JPL, Pasadena, California, USA*

11.15 **A study of water diffusion in lyotropic liquid crystals using a novel two-dimensional NMR technique**

Fr D1.3 P.L. Hubbard, K.M. McGrath and P.T. Callaghan

Victoria University of Wellington, Wellington, NZ

11.30 **Diffusion measurement in a Couette flow using multi-double PGSE NMR sequences**

Fr D1.4 A. Lutti. and P.T. Callaghan

Victoria University of Wellington, Wellington, NZ

11.45 **Characterisation of the rheology of worm-like micelles using diffusing wave spectroscopy**

A. Raudsepp[1], P.T. Callaghan[1] and Y. Hemar[2]

Fr D1.5 [1]*School Of Chemical And Physical Sciences, Victoria University, Wellington, NZ*

[2]*Fonterra Research Centre, Palmerston North, NZ*

NMR Studies on Ion Diffusion in the Lithium salt doped Room Temperature Ionic Liquids

Kikuko Hayamizu

National Institute of Advanced Industrial Science and Technology, AIST Tsukuba Center 5, Tsukuba 305-8565, Japan

The room temperature ionic liquids (RTIL) are composed of an organic anion and a large-sized anion and stable liquid at and below the room temperature. Most of the RTILs are chemically and electrochemically stable, non-flammable, with negligible vapor pressure and high ionic conductivity. They are recognized as a new solvent and their potential usage is wide for clean solvents, electrolytes for solar cells, fuel cells, double-layer capacitors, and batteries. In this study, the individual ion diffusion behaviors are studied by NMR method with doping the lithium salt. The cations are following.

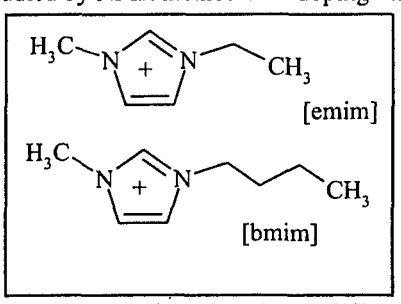

The anions are BF_4, PF_6, $N(SO_2CF_3)_2$ (TFSI) and $N(SO_2C_2F_5)_2$ (BETI). The samples were prepared by adding 1M lithium salt with the corresponding anions. The diffusion measurements were made by the PGSE method by ^7Li, ^{19}F and ^1H NMR for the lithium ion, anion and organic cation, respectively.

We have reported physicochemical properties of neat RTILs [1] Where the organic cation always diffuses faster than the anion. Also the effects of doping $LiBF_4$ in [emim][BF4] have been studied [2] and the organic cation diffuses much faster than other species and the lithium ion diffuses the slowest. These features are similar to polymer gel and solution electrolytes where the lithium ion always diffuses the slowest. The temperature dependences of the diffusion coefficients were well fit on the VTF equation and each ion has the different fitting parameters. The behaviors of the component ions vary depending on the species included. For example, the doping of $LiBF_4$ in the [emim][BF_4] brought the decrease of the diffusion coefficients for all the ions in the [Li][emim][BF_4] system, while in the [Li][bmim][PF_6] system, the diffusion coefficients of the [bmim] and [PF_6] were almost unchanged. Just after the sample preparation, the lithium diffusion plots were not straight lines at the lower temperatures and had the similarity to the lithium ion behaviors in the polymer electrolytes [3], and the structure relaxation brought the free diffusion after a long time. The salt-doped RTILs have some microstructures which change in structure gradually during long time. The interactions between the organic cation, lithium ion and anion will be discussed.

Reference

[1] Tokuda, H.; Hayamizu, K.; Ishii, K.; Susan, M.A.B.H.; Watanabe, M., *J. Phys. Chem.* B, in press.

[2] Hayamizu, K.; Aihara, Y.; Nakagawa, H.; Nukuda, T.; Price, W. S., *J. Phys. Chem.* B, contributed.

[1] Hayamizu, K.; Bando, T.; Aihara, Y; Price, W. S., *Macromolecules* **36**, (2003) 2785-2792.

* hayamizu.k@aist.go.jp

BOOMERANG: The Path to Sensitive Magnetic Resonance on Small Samples

L.A. Madsen[1]*, G.M. Leskowitz[1], T. George[2], P. J. Carson[1], and D.P. Weitekamp[1]
1) Arthur Amos Noyes Laboratory of Chemical Physics, California Institute of Technology Pasadena, California, USA
2) Microdevices Laboratory, NASA-JPL, Pasadena, California, USA

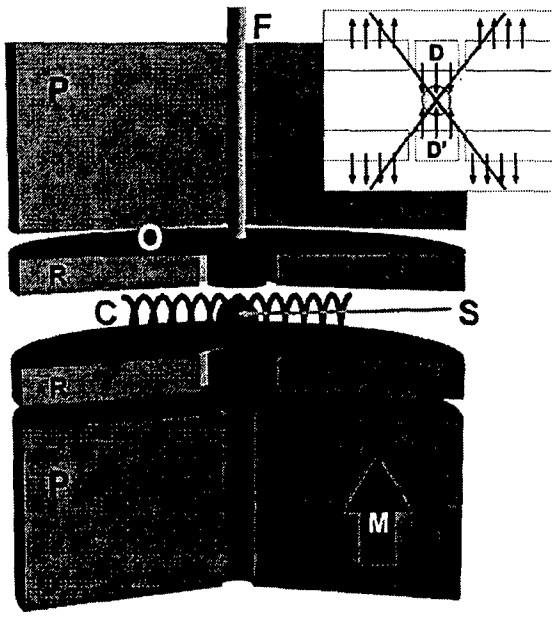

Fig. 1. Cutaway view of prototype BOOMERANG spectrometer. Inset shows forces on magnetic components.

The design appears scalable to micron-scale samples where it should have sensitivity advantages over inductive detection with microcoils and where it holds great promise for application of magnetic resonance in biology, chemistry, physics, and materials science. We will discuss extensions of the BOOMERANG method to the micron and nanometer scales. This will include our efforts toward microfabrication of NMR instruments for use in massively parallel NMR analysis on sample libraries and portable in-situ spectroscopy, and include our solutions to the problem of quantum-statistical noise in the sample when detecting small numbers of spins.

Nuclear magnetic resonance (NMR) provides exquisitely detailed information when applied to spectroscopy and spatial imaging of materials, but traditional NMR suffers from low inherent sensitivity. We will present a method of NMR that relies on detecting mechanical displacements of a small ferromagnet pushed by the spin magnetism of a nearby sample. In this method of "force-detected" NMR, termed BOOMERANG (*b*etter *o*bservation *o*f *m*agnetization, *e*nhanced *r*esolution, *a*nd *n*o *g*radient), the sample experiences a *homogeneous magnetic field* as in traditional NMR, allowing application of modern NMR imaging and spectroscopy techniques.

The prototype millimeter-scale NMR spectrometer shows signal and noise levels in agreement with the design principles [1]. We will present ^{1}H and ^{19}F NMR in solid and liquid samples, including time-domain Fourier-transform NMR spectroscopy, multiple-pulse echoes, and heteronuclear *J*-spectroscopy [2]. By measuring a ^{1}H-^{19}F *J*-coupling, this last experiment represents chemically specific spectroscopy using force-detected NMR.

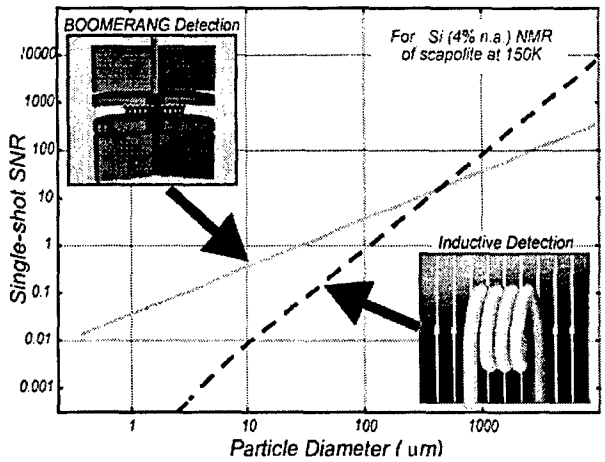

Fig. 2. Sensitivity comparison between traditional inductive NMR and BOOMERANG.

References

[1] G. M. Leskowitz, L.A. Madsen, and D.P. Weitekamp, *Sol. St. Nucl. Magn. Reson.* **11**, 73 (1998)
[2] L.A. Madsen, G. M. Leskowitz, and D.P. Weitekamp, *Proc. Natl. Acad. Sci.* **101**, 12804 (2004)

* Contact author: lmadsen@email.unc.edu

A study of water diffusion in lyotropic liquid crystals using a novel two-dimensional NMR technique

P. L. Hubbard[1,*] K. M. McGrath and P. T. Callaghan
[1] *MacDiarmid Institute for Advanced Materials and Nanotechnology, Victoria University of Wellington, Wellington, NEW ZEALAND*

Lyotropic liquid crystals possess long-range orientational order of surfactant molecules within a fluid medium, which is often aqueous. Nuclear Magnetic Resonance (NMR) allows us to trace the translational motion of the water molecules by encoding the spins using a Pulsed Gradient Spin Echo (PGSE) experiment. The self-aggregation of the surfactant molecules represents a barrier to the free movement of the water molecules, and as such we expect a local reduction in the self-diffusion coefficient

In the case where signals decay exponentially, the inverse Laplace transform is the natural transformation and ideally leads to a sum of well-resolved delta functions, i.e. a diffusion (D) spectrum [1]. A two-dimensional inverse Laplace transformation [2] was performed on the q-vector domain data in order to separate any multi-exponential behaviour that results from local anisotropy within globally isotropic solutions. Double PGSE experiments with contiguous gradient pulse pairs, both collinear and orthogonal, have been performed on a range of samples and clearly show the presence of local anisotropic diffusion [3], the experiment is known as diffusion-diffusion correlation spectroscopy (DDCOSY). Figure 1 shows the appearance of off-diagonal features in the correlation map with the application of orthogonal gradient pulse pairs, as expected.

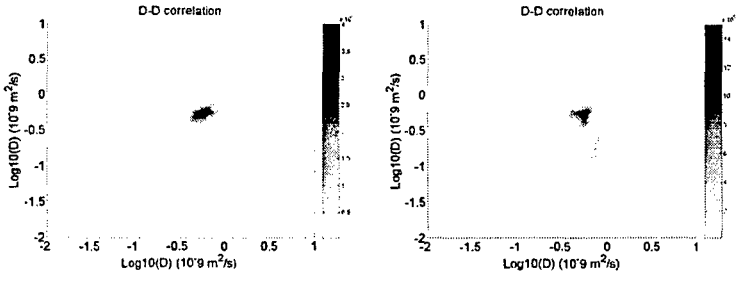

Figure 1 *DDCOSY spectra for ternary system containing AOT, water and decanol in the lamellar mesophase, with gradients applied collinearly (xx) and orthogonally (xy).*

Information about the domain sizes may be obtained by the insertion of a variable mixing time in between the successive gradient pulse pairs. The DEXSY (diffusion-diffusion exchange spectroscopy) experiment also reveals information about mesophase defects, a characteristic of particular importance in the study of systems such as AOT that have been shown to be defect-rich below 30% surfactant concentration [4]. Studies of another lyotropic liquid crystal system containing the non-ionic surfactant $C_{12}E_5$ have also revealed a preferred orientation of the lamellae after several months of equilibration [5].

This work highlights the value of this new NMR correlation method in the study of liquid crystalline structures and the potential for the study of systems of biological importance, such as drug delivery systems and biomembranes [6].

References

[1] S. W. Provencher, Computational Physics Communications **27**, 229 (1982).
[2] Y.-Q.-. Song, L. Venkataramanan, M. D. Hurlimann, et al., Journal of Magnetic Resonance **154**, 261 (2002).
[3] P. T. Callaghan, S. Godefrey, and B. N. Ryland, Magnetic Resonance Imaging **21**, 243 (2003).
[4] L. Coppola, C. La Mesa, G. A. Ranieri, and M. Terenzi, Journal of Chemical Physics **98**, 5087 (1993).
[5] P. L. Hubbard, K. M. McGrath, and P. T. Callaghan, (in preparation).
[6] M. Malmsten, *Surfactants and polymers in drug delivery* (Marcel Dekker, New York, 2002).

* Contact author: penny.hubbard@vuw.ac.nz

Diffusion measurement in a Couette flow using multi-Double PGSE NMR sequences

A. Lutti* and P.T.Callaghan
MacDiarmid Institute for Advanced Materials and Nanotechnology, VUW, NEW ZEALAND

Diffusive behavior of small molecules can be used to probe the shape and orientation of surrounding barriers in lyotropic liquid crystals [1]. Pulsed Gradient Spin Echo (PGSE) NMR has proved to be a well-adapted method for measuring self-diffusion of probe molecules within complex structures for time scales between 8ms and 500ms corresponding to a distance scale of 1 to 50 μm.

In this work, we are interested in measuring anisotropic diffusion within complex fluids under shear. A Couette cell is used as it requires a fairly small amount of sample and produces a very homogeneous shearing field. However, this configuration requires a rapid compensation of the rotating flow, implemented applying two encoding gradient pairs of inverse polarization (double PGSE). The formalism developed by Stepisnik[2] helps us correlate the results of this spin echo experiment to its gradient modulation spectrum and the frequency dependent diffusion coefficient within the system under study.

$$E(t) = e^{1/2\pi^2\gamma^2 \int D_{\alpha\beta}(\omega)^* |g(\omega,t)|^2 / \omega^2 d\omega} \qquad \text{with} \qquad g(\omega,t) = \int_0^t g^*(t')e^{-i\omega t'}dt'$$

This clearly shows that the diffusion spectrum is sampled with a function characteristic of the gradient spectrum. To obtain an accurate picture of the former, we therefore need a gradient spectrum consisting mainly of a narrow peak. This is achieved by using a repetitive train of alternating sign gradient pulses. The train keeps the compensation effect needed to avoid the effect of shear. The location of the peak in the spectrum is changed setting *T*.

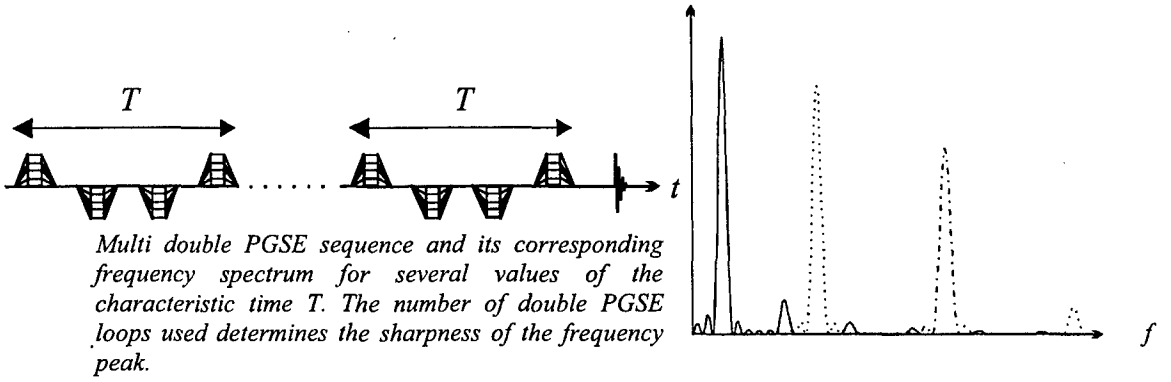

Multi double PGSE sequence and its corresponding frequency spectrum for several values of the characteristic time T. The number of double PGSE loops used determines the sharpness of the frequency peak.

References

[1] P.T.Callaghan, "Principles of NMR Microscopy", Oxford: Clarendon Press, 1991.
[2] P.T.Callaghan, J.Stepisnik, Advances in magnetic and optical resonance, **19**, 325 (1996).

* Contact author: luttianto@scs.vuw.ac.nz

Characterisation of the Rheology of Worm-Like Micelles using Diffusing Wave Spectroscopy

A. Raudsepp[1,*], P. Callaghan[1] and Y. Hemar[2]
[1] *School of Chemical and Physical Sciences, Victoria University, Wellington, NEW ZEALAND*
[2] *Fonterra Research Center, Palmerston North, NEW ZEALAND*

Diffusing wave spectroscopy is a relatively new optical technique that can be used to study the dynamic behavior of scattering centres in high concentration. Recently DWS has been combined with rheometry in order to probe the rheology of complex fluids. Parallel studies of this kind are required in order to resolve the rheological behavior of complex fluids as it can deviate significantly from that of classical "simple" fluids.

In solution, surfactant molecules may self-assemble into a variety of structures including work-like micelles, forming a complex fluid. The rheological behavior of work-like micelles has been studied using a number of techniques including nuclear magnetic resonance [1], optical birefringence [2] and photon correlation spectroscopy [3].

To date, no attempt has been made to characterise the rheology of worm-like micelles using rheo-DWS. In this study, we report rheo-DWS measurements made on the Rehange-Hoffmann worm-like micelles system, cetyl pyridinium chloride/sodium salicylate (100mM/60mM) in water, and compare these results to those of previous workers.

References

[1] M.M. Britton and P. Callaghan, Eur. Phys. J. B **7**, 237-249 (1999)
[2] P. Deeruppe *et al.*, Colloid. Polymer Sci. **273**, 346-351 (1995)
[3] J. Salmon, A. Colin and S. Manneville, Phys. Rev. Lett., **90**, 228303, (2003)

* Contact author: raudsealla@student.vuw.ac.nz

SESSION Fr E1
QUANTUM-EFFECT ELECTRONIC DEVICES

Friday 11 February 2005 **1045–1215**

Copthorne III

Session Chair **Simon Brown, University of Canterbury, NZ**

10.45 **Observation of interdot coupling phenomena in nanocrystalline silicon point-contact structures**

Fr E1.1 M. Khalafalla[1,3], H. Mizuta[2,3], Z.A.K. Durrani[1,3], H. Ahmed[1,3] and S. Oda[2,3]

[1] *University of Cambridge, Cambridge, UK*

[2] *Tokyo Institute of Technology, Tokyo, Japan*

[3] *CREST, JST (Japan Science and Technology)*

11.00 **The role of confinement on fractal interference phenomena in nanoscale ballistic devices**

Fr E1.2 T.P. Martin[1], C.A. Marlow[1], R.P. Taylor[1], H. Linke[1], G.D.R. Hall[1], I. Shorubalko[2], I. Maximov[2], W. Seifert[2], L. Samuelson[2], and T.M. Fromhold[3]

[1] *University of Oregon, Eugene, USA*

[2] *Lund University, Lund, Sweden*

[3] *University of Nottingham, Nottingham, UK*

11.15 **Semiconductor structures for quantum information processing.**

Fr E1.3 D.A. Williams[1], E. Emiroglu[2], X. Xu[2], D.G. Hasko[2] and J.R.A. Cleaver[2]

[1] *Hitachi Cambridge Laboratory, Cambridge, UK*

[2] *University of Cambridge, Cambridge, UK*

11.30 **InAlN/GaN HFET layer characterization and transistor performance**

Fr E1.4 O. Katz, D. Mistele, B. Meyler, G. Bahir and J. Salzman.

Israel Institute of Technology, Haifa, Israel

11.45 **Thin-film field-effect transistor of layered tungsten oxide system**

Fr E1.5 S.V. Chong,[1] Y. Yuan,[1] B. Ingham,[2] and J.L. Tallon[1,2]

[1] *Industrial Research Limited, Lower Hutt, NZ*

[2] *Victoria University of Wellington, Wellington, NZ*

12.00 **Selective reduction of intersubband relaxation in doped multi-quantum wells due to a magnetic field applied perpendicularly to the wells layers**

Fr E1.6 G.S. Vieira[1], P.S.S. Guimarães[2], S.J. Allen[3], K.L. Campman[3] and A.C. Gossard[3]

[1] *Instituto de Estudos Avançados, Centro Técnico Aeroespacial, Brazil*

[2] *Universidade Federal de Minas Gerais, Brazil*

[3] *University of California, Santa Barbara, USA*

Observation of Interdot Coupling Phenomena in Nanocrystalline Silicon Point-Contact Structures

M. Khalafalla[1,3], H. Mizuta[2,3,*], Z. A.K. Durrani[1,3], H. Ahmed[1,3] and S. Oda[2,3]
[1] *Microelectronics Research Centre, University of Cambridge, Cambridge, UK*
[2] *Department of Physical Electronics, Tokyo Institute of Technology, Tokyo, Japan*
[3] *CREST, JST (Japan Science and Technology)*

Nanocrystalline silicon (nc-Si) devices are potential candidates for the development of single-electron transistors (SETs) and quantum information devices compatible with large-scale integration processes. These devices use thin nc-Si films where nanometre-scale crystalline silicon grains 'naturally' form large numbers of silicon quantum dots (QDs), isolated by tunnel barriers formed at thin amorphous silicon or silicon oxide grain boundaries (GBs). The small grain size leads to large electron-confinement and single-electron charging energies, raising the possibility of room-temperature operation of QDs and SETs. The densely-packed nature of the QDs is of also of interest for quantum information processing in silicon.

In this work we study electrostatic 'Coulomb' interactions and coherent electron wave function coupling effects between two adjacent nc-Si grains by using point-contact single-electron transistors (PC-SETs: Fig.1 (left)). The PC-SETs with a very small channel with 30 nm × 30 nm in lateral dimensions were formed on a 40 nm thick nc-Si film with lateral grain size of 20 – 25 nm. The electrostatic potential on the grains are controlled via the bias applied to two side gates. After patterning the PC-SETs, oxidation at 750°C for 60 minutes and annealing at 1000°C were applied, which convert the GBs into a solid tunnel barrier. We observed the switching of the Coulomb oscillation current peaks at 4.2K as we swept the two side gate voltages V_{g1} and V_{g2} (Fig. 1 (right)) [1]. We found that the switching phenomenon is caused by the electrostatic coupling effects between two adjacent parallel nc-Si grains formed in the PC channel, and the gap between the two peak lines in the switching region is determined by the coupling capacitance between the grains.

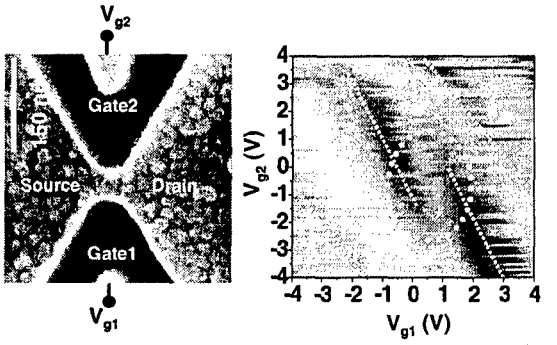

Fig. 1 SEM micrograph of a nc-Si PC-SET (left) and gray scale image of current as a function of two side gate bias voltages V_{g1} and V_{g2}.(right)

Next we adopted oxidation at 750°C for 30 minutes without the following annealing in order for making the GB tunnel barrier more transparent so that the adjacent grains couple each other more strongly. The PC-SETs then exhibited delocalisation of the electron wavefunctions over the coupled grains. Two peak lines in the plot of the device conductance at 4.2K (Fig. 2(left): white dotted lines) show intersecting and splitting (a broken circle with an arrow) caused by electrostatic interactions when the energy levels in the two grains are in resonance [2]. In this strong coupling region, we observed that the characteristics are decomposed into four Lorentzian peaks (Fig. 2(left)) – two main peaks (arrows with '*B*') with two small peaks (arrows with '*A*'). This is attributed to the tunnel coupling across two adjacent grains, resulting in bonding- and anti-bonding-like resonance peaks. These molecular states may be used to realize a Si-based charge qubit.

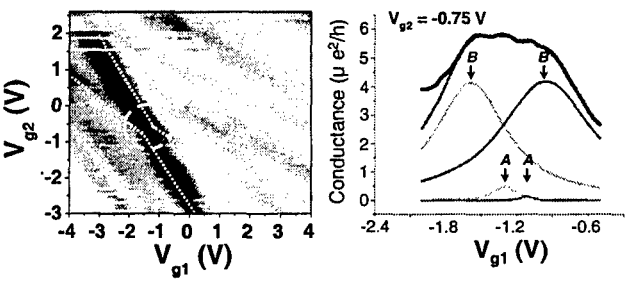

Fig. 2 Two conductance peak lines intersect and split (left) and conductance-V_{g1} curve fitted using four Lorentzian peaks.(right)

References

[1] M. Khalafalla, H. Mizuta and Z.A.K. Durrani, IEEE Trans. Nanotechnol. **2**, No.4 (2003).
[2] M. Khalafalla, Z.A.K. Durrani and H. Mizuta, Appl. Phys. Lett. **85**, in press, Sept. 2004.

Contact author: mizuta@pe.titech.ac.jp

The Role of Confinement on Fractal Interference Phenomena in Nanoscale Ballistic Devices

R. P. Taylor[1], T. P. Martin[1], C. A. Marlow[1], H. Linke[1], G. D. R. Hall[1], I. Shorubalko[2], I. Maximov[2], W. Seifert[2], L. Samuelson[2], and T. M. Fromhold[3]

1. Department of Physics, University of Oregon, Eugene, OR 97403-1274, U.S.A.
2. Division of Solid State Physics, Lund University, BOX 118, S-221 00 Lund, Sweden.
3. School of Physics and Astronomy, University of Nottingham, NG7 2RD, U.K.

Ballistic transport through nano-scale semiconductor devices is generally expected to be highly dependent on the wall profile that confines electrons to the device geometry. We present a study of interference effects in etched $Ga_{0.25}In_{0.75}As$/InP devices and compare our results to the more traditional GaAs/AlGaAs system.

In both types of devices electrons are confined to a plane by a two-dimensional electron gas (2DEG) established through their respective heterostructures. However, while GaAs/AlGaAs devices give rise to 'soft' walls with parabolic potential profiles,[1,2] the etched walls of the GaInAs/InP devices studied are expected to have harder profile gradients. In order to determine the extent of the profile's hardness, we experimentally measure the potential profile of our etched GaInAs/InP devices and show that they are in close agreement to simulation.[3] Compared to the soft walled profile of a GaAs/AlGaAs device, we find that the GaInAs/InP profiles have energy gradients that are steeper by a factor of 10.

Ballistic transport through soft walled devices has been predicted[2] and demonstrated[4-6] to exhibit fractal conductance fluctuations (FCF) arising from quantum interference effects within the device. Although the FCF are expected to be critically sensitive to the precise profile of the device walls, the statistical properties of the FCF have been shown to depend solely on an empirical parameter Q that quantifies the resolution of the energy levels in the device and is independent of this energy profile.[5] We experimentally demonstrate that the FCF in our etched, GaInAs/InP devices follows the same behavior as the softer walled GaAs/AlGaAs devices, despite the difference in profile gradient, and also show that this behavior is robust to changes in device geometry.[7] Thus we establish a remarkable insensitivity of quantum interference effects to wall profile. We also consider the potential consequence that fractal fluctuations will form a fundamental limitation for the room temperature performance of future nano-scale devices.

1 T. M. Fromhold et al., *Physica B* **249-251**, 334 (1998).
2 R. Ketzmerick, *Phys. Rev. B* **54**, 10841 (1996).
3 T. P. Martin et al., *Superlatt. Microstruc.* **34**, 179 (2004).
4 A. S. Sachrajda et al., *Phys. Rev. Lett.* **80**, 1948 (1998).
5 A. P. Micolich et al., *Phys. Rev. Lett.* **87**, 036802 (2001).
6 A. P. Micolich et al., *Appl. Phys. Lett.* **80**, 4381 (2002).
7 C. A. Marlow et al., 'Sensitivity of Quantum Interference Effects to the Wall Profile of GaInAs/InP Billiards', *submitted to Phys. Rev. Lett.*

Semiconductor Structures for Quantum Information Processing.

D.A. Williams,[1,*] E. Emiroglu,[2] X. Xu,[2] D.G. Hasko[2] and J.R.A. Cleaver[2]
[1] *Hitachi Cambridge Laboratorye, Hitachi Europe Ltd, Cambridge, CB3 0HE U.K.*
[2] *Microelectronics Research Centre., Cavendish Laboratory, University of Cambridge, Madingley Road, Cambridge, CB3 0HE, U.K.*

A number of new ways of manipulating information, generically known as quantum information processing, have been postulated in the last 15-20 years. Several have been demonstrated experimentally, but there remains a large gap between principle and practice, particularly in quantum computation. The success of solid-state electronics and optoelectronics in classical information processing leads many to the conclusion that condensed matter systems will provide the best way of bridging this gap.

We will describe some of our approaches to making solid-state structures for quantum information processing, presenting recent experimental results, and will discuss the various mechanisms which help and hinder the development of this field. There has been substantial progress in the last year, and we will give our view of the best ways to make usable structures for quantum computation and cryptography, particularly emphasising the many areas where an improved theoretical understanding would greatly assist progress.

Semiconductor quantum dots are promising for optically driven quantum computing and as interface devices for quantum communication. To enable these applications, single- and entangled-photon sources are needed. A challenging goal is to realize electrically pumped photon sources, which means that photon emission can be controlled with an electrical pulse or ideally with single-electron injection. In this talk recent experiment realizations of single-photon sources from single quantum dots in a lateral p-i-n junction will be reported. The devices can be driven optically and electrically at high repetition rates.

Also, we will report measurements of charge oscillations within a silicon qubit using a capacitively-coupled asymmetric single-electron transistor. Our qubit is embodied in the pseudo-molecular eigenstates of an isolated double-quantum-dot, made from a silicon-on-insulator wafer.

* Contact author: williams@phy.cam.ac.uk

InAlN/GaN HFET layer characterization and transistor performance

O. Katz, D. Mistele, B. Meyler, G. Bahir, and J. Salzman.
Department of Electrical Engineering and Microelectronics Research Center, Technion, Israel Institute of Technology, Haifa 32000, Israel.

Group-III Nitride are wide band gap semiconductors used for heterostructure field effect transistors (HFET) and have achieved record breaking currents and output power levels at high frequencies. However the conventional AlGaN/GaN structure suffers from surface-trap related phenomena such as current collapse, persistent photo current and RF compression. The undesired high concentration of surface states seem to be intrinsically related to the polarization fields.

Here, we study the alternative way in which the *AlGaN* layer is replaced by an $Al_xIn_{1-x}N$ barrier for HFET implementation. The $In_xAl_{1-x}N$ layer composition can be adjusted to be lattice matched *(x=0.17)* or polarization matched to *GaN (x=0.32),* or, alternatively, centro-symmetric polarization-free *(x=0.43).* Therefore, by applying polarization engineering it is possible to overcome the above mentioned limitations to the HFET performance. Only few reports have been published on InAlN epitaxial layers, and to our knowledge, InAlN/GaN based HFET were previously proposed [1] without any experimental work. We have recently demonstrated the implementation of epitaxially grown InAlN/GaN heterostructures and HFET fabrication [2, 3].

Here, we show the implementation of an improved HFET based on this material system. The InAlN/GaN heterostructures were grown by low-pressure metal-organic vapor phase epitaxy (MOVPE). The layer's composition and crystal quality were characterized by X-ray photoemission spectroscopy (XPS) and high-resolution x-ray diffraction (XRD) (See Fig.1) measurements, and the resulting In content is 4% to 15% with high crystal quality.

Temperature dependent Hall effect measurements exhibit a two-dimensional electron gas (2DEG) typical dependence (See Fig.2). The low-temperature high conductivity value of the InAlN/GaN heterostructures is more than 2 orders of magnitude higher that of our GaN template. The InAlN/GaN structure shows high values of 2DEG concentration, up to $4x10^{13}cm^{-2}$. Carrier concentration profiles of the InAlN/GaN heterostructures, determined using capacitance-voltage (CV) profiling, are also indicative of 2DEG formation, with peak concentration values similar to the Hall data. Both DC and RF characteristics of the InAlN/GaN HFETs were measured, showing values approaching the performance of state of the art AlGaN/GaN transistors.

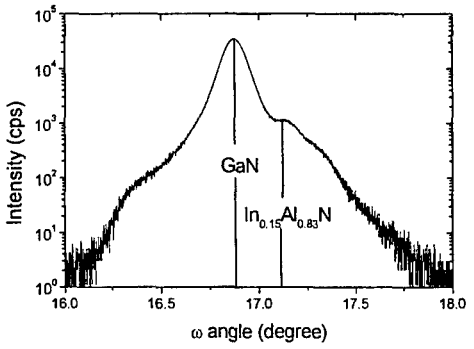

Figure 1. (0002) x-ray diffraction rocking curves of $In_{0.15}Al_{0.83}N$ on GaN.

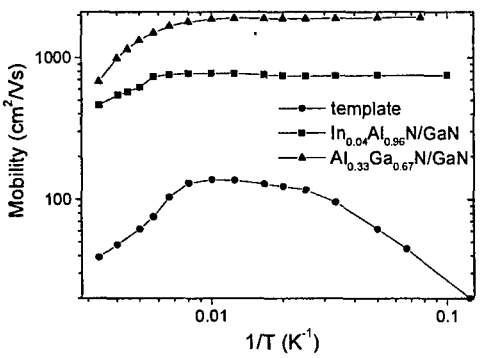

Figure 2. Temperature dependent electron mobility for $In_{0.04}Al_{0.96}N/GaN$, $Al_{0.33}Ga_{0.67}N/GaN$ heterostructures, and for bulk GaN.

References

[1] Kuzmik, J., Semicond. Sci. Technol. 2002, **17**, pp.540-544

[2] O. Katz, D. Mistele, B. Meyler, G. Bahir, and J. Salzman, "Characteristics of $In_xAl_{1-x}N$/GaN High Electron Mobility Field-Effect Transistor ", to be published in IEEE Trans Elec. Dev. (2004)

[3] O. Katz, D. Mistele, B. Meyler, G. Bahir, and J. Salzman, "InAlN/GaN Heterostructure Field-Effect Transistor DC and Small Signal Characteristics", to be published in Electronics Letters (2004).

Thin-Film Field-Effect Transistor of Layered Tungsten Oxide System

S. V. Chong,[1,*] Y. Yuan,[1] B. Ingham,[2] and J. L. Tallon[1,2]
[1] *Industrial Research Limited, Lower Hutt, NEW ZEALAND*
[2] *School of Chemical and Physical Sciences, Victoria University of Wellington, Wellington, NEW ZEALAND*

The importance of tungsten oxide as a functional material in various devices has driven the ongoing investigation of this transition metal oxide. It is not only that this oxide possesses excellent electrochromic properties, which has sparked various studies at first, but its catalytic and gas-sensing ability has also been harnessed in other applications. An important "supporting-act" to all of these is owed to the fact that tungsten oxide is one of the few metal oxides that can be deposited as thin films using low-cost techniques such as spin- or dip-coating and even via self-assembled monolayer procedure. The former technique is usually coupled with sol-gel chemistry where films in the micron-range thickness can be fabricated, while the latter technique is more powerful as "film" thicknesses of a monolayer (a few angstroms) can be self-assembled on a suitable substrate. The use of sol-gel chemistry in WO_3 film preparations usually proceeds through the tungstic acid phases [1-2], which is the starting material for a series of layered organic-tungsten oxide hybrid materials our group has investigated [3]. These compounds, consist of alternating layers of tungsten oxide and organic spacer molecules, provide an excellent opportunity to study the effect that the organic spacers have on the electronic properties of the metal oxide layers. One such property is the field-effect-transistor (FET) behaviour of this system. Herein we report the first attempt to measure the field-effect mobility of tungstic acid hydrate ($H_2WO_4 \cdot H_2O$; two dimensional layers of $WO_3 \cdot H_2O$ with H_2O occupying the space in between layers) using the conventional metal oxide semiconductor field-effect-transistor (MOSFET) principles, with a subsequent aim to extend this to the organic-inorganic hybrids.

The thin-film-transistor device consists of a spin-coated tungstic acid hydrate semiconducting channel with a heavily n-doped silicon wafer acting as the gate electrode. The gate dielectric layer is a 1500Å thick thermally grown oxide (SiO_2) patterned on top with e-beam deposited Au source and drain electrodes (channel length of 30 or 60μm, and width of 1000μm). The current-voltage curve below shows a typical p-channel transistor behaviour with a "linear region" at low drain voltage (I_D increases linearly with V_D) and a "saturation region" occurring at higher V_D upon the application of negative bias voltages V_G. The field-dependent mobility (on V_G) is depicted in the adjacent figure which shows a maximum mobility of ~2.3cm^2/V-sec is reached at an applied bias voltage of -5.0 ± 0.5V.

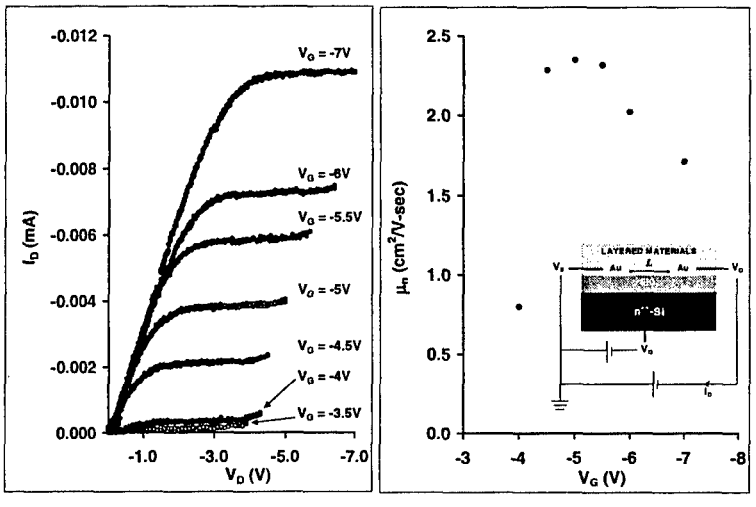

FIG. 1. Left: Drain current (I_D) versus drain voltage (V_D) at various of gate voltages (V_G) for a $H_2WO_4 \cdot H_2O$ spin-coated film with channel length (L) and width (W) of 30μm and 1000μm, respectively. Right: The relationship between the mobility (μ_n) at saturation and V_G; $\mu_{n,sat.}$ is calculated based on a basic MOSFET behaviour in the saturation region: $I_{D,sat.} \approx mW\mu_n C_i(V_G - V_{th})^2/L$ [4], where m is a doping concentration factor taken here as 0.5, C_i is the capacitance of the insulating gate oxide and V_{th} is the threshold voltage which is obtained from plotting $(I_{D,sat.})^{1/2}$ versus V_G.

References

[1] P. Judeinstein, R. Morineau, and J. Livage, Solid State Ionics **51**, 239 (1992).
[2] A. Chemseddien, R. Morineau, and J. Livage, Solid State Ionics **9-10**, 357 (1983).
[3] B. Ingham, S.V. Chong, and J.L. Tallon, MRS Symposium Proceedings **775**, 165 (2003).
[4] S.M. Sze, *Physics of Semiconductor Devices* (John Wiley & Sons, 1981), Chap. 8, p. 442.

* Contact author: s.chong@irl.cri.nz

Selective Reduction of Intersubband Relaxation in Doped Multi-Quantum Wells Due to a Magnetic Field Applied Perpendicularly to the Wells Layers

G. S. Vieira[1], P. S. S. Guimarães[2], S. J. Allen[3], K. L. Campman[4] and A. C. Gossard[4]
[1]*Instituto de Estudos Avançados, Centro Técnico Aeroespacial, 12228-840 São José dos Campos, SP, Brazil*
[2]*Departamento de Física, Universidade Federal de Minas Gerais, 30123-970, Belo Horizonte, MG, Brazil*
[3]*Center for Terahertz Science and Technology, University of California at Santa Barbara, CA 93106, USA*
[4]*Materials Department, University of California at Santa Barbara, CA 93106, USA*

Intersubband relaxation in multi-quantum wells has been the object of much study due to its importance in the performance of devices based on intersubband transitions, like quantum cascade lasers and quantum well infrared detectors. It is well known that the longitudinal optical phonon plays a major role in such relaxations and it is well established that the relaxation time increases considerably [1] as the intersubband transition energy becomes smaller than the longitudinal optical phonon energy. Kastalsky and Efros [2] found theoretically that a magnetic field applied perpendicular to the quantum wells layers should quench the acoustic phonon scattering, thus enhancing dramatically the relaxation time between two subbands separated by an energy smaller than the longitudinal optical phonon energy. Yang Ji et al. [3] observed the suppression of both acoustic and longitudinal optical phonons in an undoped three-barrier structure, when a sufficiently large magnetic field was applied perpendicular to the wells layers. In this work, we found that in a doped GaAs/AlGaAs multi-quantum well structure a magnetic field applied perpendicularly to the wells layers will generate a significant reduction of the relaxation rate between subbands separated by an energy gap smaller than the longitudinal optical phonon energy, while affecting just slightly the relaxation rate between subbands with gap larger than the longitudinal optical phonon energy, even if the gap does not match a multiple of the longitudinal optical phonon energy. Those results are in disagreement with Yang Ji's results since they found a magnetically induced suppression of the interssubband relaxation with an intersubband gap larger the longitudinal optical phonon energy. This disagreement may be caused by the fact that that the well of their device was not dopped while the wells of our devices are dopped.

References

[1] D. Y. Obeli, D. R. Wake, M. V. Kein, J. Klem, T. Henderson, and H. Morkoc, Phys. Rev. Lett. **59**, 696 (1987).
[2] A. Kastalsky and A. L. Efros, J. Appl. Phys. **69**, 841 (1991).
[3} Yang Ji, Yuanzhen Chen, Kejian Luo, Houzhi Zheng, Yuexia Li, Chengfang Li, Wenchao Cheng, and Fuhua Yang, Appl. Phys. Lett. **72**, 3309 (1998).

Friday 11 February
Oral Session Two

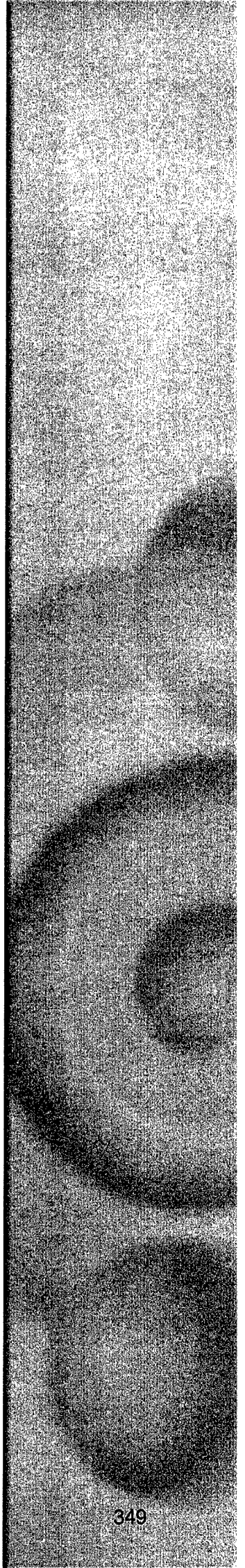

SESSION Fr A2
SPIN DEPENDENT TRANSPORT

Friday 11 February 2005 **1320–1500**

Galaxy I

Session Chair **Ulrich Zuelicke, Massey University, New Zealand.**

13.20 **Spintronics meets nanophysics: spin-dependent transport through quantum dots**

Fr A2.1 J. Konig[1], M. Braun[1] and J. Martinek[2,3]
[1] *Institut fur Theoretische Physik III, Ruhr-Universitat Bochum, Germany*
[2] *Institut fur Theoretische Festkorperphysik, Universitat Karlsruhe, Germany*
[3] *Polish Academy of Science, Poznan, Poland*

13.45 **Scattering and interaction of one-dimensional electrons with spin-orbit interaction and magnetic field**

Fr A2.2 Y. Tokura
NTT Basic Research Laboratories, Kanagawa, Japan.

14.00 **Chemo-elastic modification of interfaces in nanostructures for spintronics**

Fr A2.3 S.D. Conradson[1], A.G. Adeva[1], R. Howell[1], D.R. Conradson[1] and S.S.P. Parkin[2]
[1] *Los Alamos National Laboratory, USA*
[2] *IBM Almaden Research Centre, USA*

14.15 **Magnetotransport properties of amorphous $Ge_{1-x}Mn_x$ films**

Fr A2.4 S.S.Yu[1], T. T. Lan Anh[1], Y.Eon Ihm[1],D. Kim[1], H. Kim[1], S. Oh[2], C.S. Kim[3], H.J. Lee[3] and B.C. Woo[3]
[1] *Chungnam National University, Daejeon, Korea*
[2] *Korea Basic Science Institute, Daejeon, , Korea*
[3] *Korea Research Institute of Standards and Science, Daejeon, Korea*

14.30 **Magnetic periodic structures – magneto-photonic and magnonic crystals**

Fr A2.5 S.A.Nikitov and Yu.V. Gulyaev
Russian Academy of Sciences, Moscow, Russia.

14.45 **Positive magnetisation in carbon nanoclusters**

Fr A2.6 A.V. Rode, N.R. Madsen, E.G. Gamaly, B. Luther-Davies, S.T. Hyde and A.G. Christy
Australian National University, Canberra, Australia.

Spintronics meets Nanophysics: Spin-Dependent Transport through Quantum Dots

Jürgen König[1,*], Matthias Braun[1], and Jan Martinek[2,3]
[1] *Institut für Theoretische Physik III, Ruhr-Universität Bochum, 44803 Bochum, GERMANY*
[2] *Institut für Theoretische Festkörperphysik, Universität Karlsruhe, 76128 Karlsruhe, GERMANY*
[3] *Institute of Molecular Physics, Polish Academy of Science, 60-179 Poznan, POLAND*

Spintronics devices rely on spin-dependent transport behavior evoked by the presence of spin-polarized electrons. Transport through nanostructures, on the other hand, is dominated by strong Coulomb interaction. We study a model system in which both concepts are combined, namely a single-level quantum dot attached to ferromagnetic leads, doubbed "quantum-dot spin valve". The interplay of spin-polarization in the leads and strong Coulomb interaction in the quantum dot gives rise to qualitatively new phenomena that are absent for either non-interacting or unpolarized electrons. In particular, we predict the existence of an effective exchange field experienced by the electrons in the quantum dot [1].

We discuss two different transport regimes in detail. First, weak dot-lead tunnel coupling is considered. We develop a systematic diagrammatic transport theory [2,3] that covers both the linear and nonlinear transport regime and allows for noncollinear magnetization of the leads. The transmission through the dot depends on the dot's occupation and accumulated spin, for which we derive generalized rate equations. We find that the effective exchange field yields a precession of the accumulated spin. As a consequence, a nontrivial dependence of the conductance on the angle between the lead magnetizations [2,3] and a negative differential conductance is predicted [3]. Furthermore, we discuss transport in the presence of an external magnetic field and predict [4] signatures of spin precession analogous to the Hanle effect.

Second, we consider strong dot-lead coupling and analyze how the spin polarization of the leads affects the Kondo effect. In this case, the exchange field is visible in transport via an induced level splitting [1]. Based on a scaling approach we predict [5] a splitting of the zero-bias Kondo anomaly. With an additional magnetic field, this splitting can be compensated, and the strong-coupling limit of the Kondo effect is recovered. These results are backed up by rigorous numerical-renormalization-group calculations [6,7].

References

[1] J. König, J. Martinek, J. Barnas, and G. Schön, cond-mat/0404509, to be published in Lecture Notes on Physics.

[2] J. König and J. Martinek, Phys. Rev. Lett. **90**, 166602 (2003).

[3] M. Braun, J. König, and J. Martinek, cond-mat/0404455, accepted for publication in Phys. Rev. B.

[4] M. Braun, J. König, and J. Martinek, unpublished.

[5] J. Martinek, Y. Utsumi, H. Imamura, J. Barnas, S. Maekawa, J. König, and G. Schön, Phys. Rev. Lett. **91**, 127203 (2003).

[6] J. Martinek, M. Sindel, L. Borda, J. Barnas, J. König, G. Schön, and J. v. Delft, Phys. Rev. Lett. **91**, 247202 (2003).

[7] J. Martinek, M. Sindel, L. Borda, J. Barnas, R. Bulla, J. König, G. Schön, S. Maekawa, and J. v. Delft, cond-mat/0406323.

* Contact author: koenig@tp3.ruhr-uni-bochum.de

Scattering and interaction of one-dimensional electrons with spin-orbit interaction and magnetic field

Yasuhiro Tokura[1]
NTT Basic Research Laboratories 3-1 Wakamiya, Morinosato, Atsugi 243-0198, Japan

Introduction. The importance of the spin-orbit (SO) effect in low dimensional system is now well recognized. In two-dimension, the well-known Rashba and Dresselhaus terms had been studied and intriguing phenomena have been predicted including spin Hall effect. In zero-dimension (quantum dots), SO effect is critical since it determines the statistics of the energy levels and is the most important channel to determine the life-time of spin. However, its role in one-dimension has not been fully explored yet, although strong motivation of the research in this field resides in the proposal by Datta and Das[1], which is effectively one-dimensional system. In this report, we study the electron quantum transport problem in a quantum wire with relatively strong SO coupling. Special attention is paid to peculiar spin *chiral* states, which are realized by applying an in-plane magnetic field B.

Resonance. The system Hamiltonian is $H = \frac{\vec{p}^2}{2m^*} + V(x,z) - i\alpha_R(\vec{\sigma}\times\vec{\nabla})\cdot\hat{y} - \frac{1}{2}g^*\mu_B\vec{B}\cdot\vec{\sigma}$, where α_R is Rashba parameter, m^* and g^* are effective mass and effective g-factor, respectively. We neglected Dresselhaus term and the electrons are strongly confined in $x-z$ plane and further confined in z direction. When the magnetic field is applied in the x direction, the electron dispersion opens a pseudo-gap.(Fig.1a)[2] When the Fermi energy is in this pseudo-gap, the system is effectively made up of a right-going mode and a left-going mode, which have non-collinear spin states. We solved a scattering problem by single repulsive potential without dent. Amazingly, we found that at some energy the electron is reflected resonantly $\mathcal{T} = 0$.(Fig.1b) This could be understood as a *Fano resonance*, where the propagating mode are hybridized with the distinctive quasi-bound state.

Interaction and dynamics. This bare scattering amplitude is renormalized by electron-electron interaction in the one-dimensional reservoirs. We estimated the temperature dependence of the conductance by Poor man's scaling.[3] Since the spin states at two Fermi points, $\pm k_F$, are non-collinear, the $2k_F$ backscattering process is suppressed.[4] Consequently, the conductance power-exponent on the temperature decreases with B, where spin states approach the collinear configuration. Finally, by dynamically controlling the external parameters, *i.e.*, potential strength, α_R, and magnetic field, we can show that the electron/spin pumping is possible in this system.

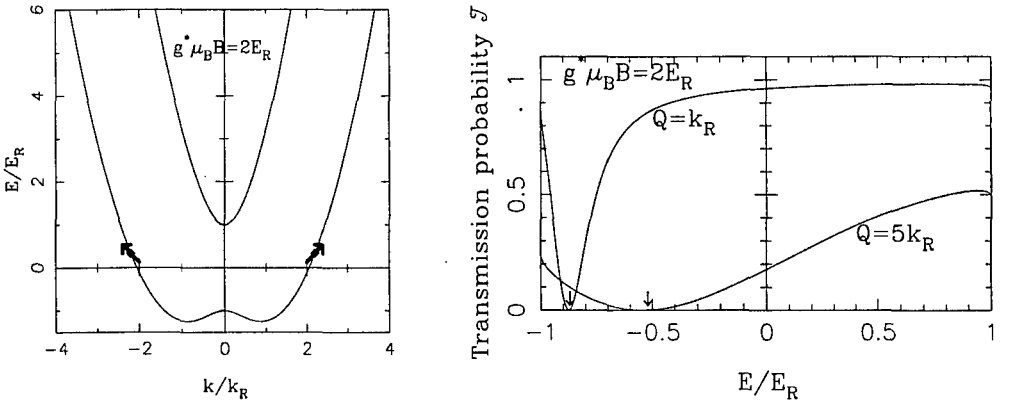

Figure 1: *(a) Dispersion of a wire with SO and B. (b) Energy dependence of transmission probability $\mathcal{T}$ in the pseudo-gap through a potential $V(x) = \frac{\hbar^2}{2m^*}Q\delta(x)$ $(Q>0)$. $k_R = \frac{m^*\alpha_R}{\hbar^2}$, $E_R = \frac{\hbar^2 k_R^2}{2m^*}$.*

References

[1] S. Datta and B. Das, Appl. Phys. Lett. **56** (1990) 665.
[2] M. Cahay and S. Bandyopadhyay, Phys. Rev. **B 68** (2003) 115316.
[3] K. Matveev, D. Yue, and L. I. Glazman, Phys. Rev. Lett. **71** (1993) 3351.
[4] M. Governale and U. Zülicke, Phys. Rev. **B 66** (2002) 073311.

[1]Contact author: tokura@nttbrl.jp

Chemo-Elastic Modification of Interfaces in Nanostructures for Spintronics

Steven D. Conradson, Angel Garcia-Adeva, Rafael Howell, Dylan R. Conradson
Materials Science and Technology Division, Los Alamos National Laboratory

Stuart S. P. Parkin
IBM Almaden Research Center

In addition to the GMR read heads that have made possible the current generation of inexpensive, ultrahigh density magnetic storage devices, a variety of other technologies based on spin-sensitive nanostructures are under development, e.g., magnetic tunnel junctions for non-volatile memory. In addition to the scientific challenge of the fundamental physics, understanding the mechanism of spin discrimination is critical in optimizing these devices for specific applications and fabrication methods. A primary, unresolved issue in the mechanism is the importance of the interfaces between the components of the device vis-à-vis the intrinsic properties of the components themselves. One aspect of the interface that is often overlooked is the role of elastic strain in modifying the structure and properties relative to bulk materials. The elastic relaxation length is often comparable to the thickness of a component material, so that epitaxial mismatch may modify the structure of all of the atoms in a nanoscale film. Alternatively, elastic-electronic feedback may result in extremely high electron-phonon coupling focused at the atoms at the interface so that the novel properties derive from narrowly confined structures involving only the interface atoms. We have probed interfacial structures by performing X-ray Absorption Fine Structure (XAFS) spectroscopy measurements on both metal and metal-metal oxide samples. In these the thickness of the material under investigation is varied from one–two through several atom layers so that interface-dependent distortions can be identified and characterized at the 0.1–0.2 Å resolution limit of the method. These have been supplemented by MD simulations in which the potentials are varied to fit the local structure data as a means of refining the structures. Subsequent electronic structure calculations on these refined structures are used to investigate the underlying structure:function relationships in these systems in which DFT-based energy calculations are invalid because the cooperative effects increase the numbers of atoms beyond those calculable with DFT. Using this combined approach we have found some systems, e.g., antiferromagnetisim in NiMn, in which bulk properties appear to originate in locally ordered, nanoscale domains embedded in a matrix with minimal long range order, and other, e.g., Cu-Fe interfaces, in which the interface itself shows large distortions for bond lengths in particular directions that modify the local electronic structure. Similar effects are also observed in selected metal-metal oxide systems, which are also subject to charge transfer at the interface because of the oxygen. Chemo-elastic coupling to the local ordering and discontinuities between the ordering on multiple length scales are therefore a fundamental aspect of the unusual properties of nanoscaled materials and devices.

Magnetotransport properties of amorphous $Ge_{1-x}Mn_x$ films

Sang Soo Yu[1], Tran Thi Lan Anh[1], Young Eon Ihm[1*],Dojin Kim[1], Hyojin Kim[1],

Sangjun Oh[2], Chang Soo Kim[3], Hwack Joo Lee[3], Byung Chill Woo[3]

[1]*Chungnam National University, Daejeon, 305-764, Korea*
[2]*Korea Basic Science Institute, Daejeon, 305-333, Korea*
[3]*Korea Research Institute of Standards and Science, Daejeon, 305-600, Korea*

Recently diluted magnetic semiconductors have attracted a lot of interests because of the potential applications of spin injection devices. However, some of the critical factors of the diluted magnetic semiconductors, such as the Curie temperature (T_C) and the saturation magnetization, are not good enough for practical applications. One of the attempts to improve the critical factors is growing the amorphous magnetic semiconductors, since in general the solubility of amorphous phase is much higher than those of crystalline phases. In this work, amorphous $Ge_{1-x}Mn_x$ thin films were grown successfully in order to expand the solubility limit of Mn. The amorphous $Ge_{1-x}Mn_x$ thin films were grown on (100)Si substrate at 373K by using a thermal evaporator. Growth rate was ~350Å/min and average film thickness was around 5,000Å. The structural analysis was carried out by using XRD and TEM, and shows that the Mn in amorphous $Ge_{1-x}Mn_x$ thin films reaches up to 15at%. The magnetization characteristics measured by using SQUID show that the amorphous $Ge_{1-x}Mn_x$ thin films are ferromagnetic and the T_C is ~150K. The largest saturation magnetization of amorphous $Ge_{1-x}Mn_x$ thin films is ~100emu/cc for x=0.118 at 5K. The variation of electrical resistivity with respect to temperature reveals that the $Ge_{1-x}Mn_x$ thin films have semiconductor characteristics. The in-field electrical resistivity of amorphous $Ge_{1-x}Mn_x$ thin films is lower than the zero-field electrical resistivity when $T<T_C$, but the reverse is true when $T>T_C$. However, the in-field electrical resistivity of amorphous $Ge_{1-x}Mn_x$ thin films is always higher than the zero-field electrical resistivity when Mn concentration is larger than ~12at%. In Addition, magnetotransport characteristics of amorphous $Ge_{1-x}Mn_x$ thin films show anomalous Hall phenomenon and negative magnetoresistance when $T<T_C$. The results suggest that the Mn atoms in amorphous $Ge_{1-x}Mn_x$ thin films be related to spin dependent scattering depending on magnetization.

Reference

[1] H. Ohno, Science, **281**, 951 (1998)

[2] T.Dietl, H.Ohno, Science, **287,** 1019 (2000)

[3] Y. D. Park et al., Science, **295,** 651 (2002)

1

*Contact author : yeihm@cnu.ac.kr

Magnetic Periodic Structures – Magneto-Photonic and Magnonic Crystals

S.A.Nikitov[1*], Yu.V. Gulyaev[1]
1Institute of Radioengineering & Electronics, Russian Academy of Sciences, 101999, 11, Mokhovaya St., Moscow, Russia

In a current work a new class of magnetic materials is described and analyzed. Drawing an analogy with photonic crystals possessing a photonic band, namely the frequency range where the wave propagation if completely forbidden, such magnetic media can be named **magnonic (magneto-phononic)** crystals. Such crystals represent the magnetic medium in which the magnetic properties are varied periodically. The simplest type of the one-dimensional magnonic crystals is a multilayered periodic structure composed from the magnetic layers with the different magnetization. Spin waves and magneto-elastic waves propagation through this structure is prohibited within the restricted bands. It is shown that a localized spin wave mode (magneto-elastic wave mode) can exist in a forbidden zone if the periodicity of the system is broken in a particular place. Such magnonic crystals in a microwave frequency range can be a challenge for photonic crystals operating at the visual light frequency band. The analysis of such systems is provided along with theoretical and numerical calculations of forbidden zones and spin wave modes. The dispersion characteristics of spin waves (magneto-elastic waves) in such magnonic crystals are considered along with reflection and transmission of spin waves through such a structure. In particular, the one-dimensional periodic magnetic structure is considered containing magnetic layers with the same thickness but different magnetization. The wave spectrum contains forbidden zones and the transmission coefficient from such a structure almost equal to 0, thus the wave totally reflected. Numerical calculations are provided for real multilayered structures. It is further shown that three-dimensional periodic magnetic systems can possess a full magnonic band where spin-wave propagation in a particular frequency band is prohibited in all directions. On the contrary to the photonic crystal bands the magnonic band can be tuned by the variation of the external magnetic field. The propagation of optical radiation in a magnetic waveguides with the periodic domain structures (magneto-photonic crystals) is further investigated. Two types of periodic structures are studied – one- and two-dimensional. Optical modes conversion is possessed by both the first- and the second-order magneto-optic effects and scattering by the domains. In the two-dimensional periodic structures conversion becomes anisotropic and strongly depends on the parameters of the structure. The parameters of the domain structures depend on the external magnetic field, therefore the conversion efficiency can be modulated by the variation of this field. A numerical analysis is provided of the dispersion of the interacting modes as well as of the dependence of the intensity of the converted radiation on the parameters of the domain structures. The new class of two-dimensional magnonic and magneto-photonic crystals is proposed on a base of α- and γ-phases of Fe_2O_3 spinel films and the magnetic films with bubble domains.

* Contact author: *: nikitov@cplire.ru*

Positive magnetisation in carbon nanoclusters

A. V. Rode,[a,b*] N. R. Madsen[a], E. G. Gamaly[a,b], B. Luther-Davies[a,b], S. T. Hyde[c], A. G. Christy[d]

[a]*Laser Physics Centre, Research School of Physical Sciences and Engineering,*
[b]*ARC Centre for Ultra-high Bandwidth Devices for Optical Systems (CUDOS)*
[c]*Department of Applied Mathematics, Research School of Physical Sciences and Engineering,*
[b]*Department of Earth and Marine Science,*
Australian National University, Canberra, ACT 0200, Australia

We report the production of a hierarchically nanostructured magnetic carbon foam by a high-repetition-rate laser ablation of glassy carbon in Ar. The clusters contain both sp^2 and sp^3 bonded carbon atoms. The material contains graphite-like sheets with hyperbolic curvature, as proposed for "schwarzite". In addition to other unusual properties, the all-carbon nanofoam exhibits para- and maybe ferromagnetic behavior up to 90 K, showing a narrow hysteresis curve with a coercive force H_c = 420 Oe and remnant magnetisation of 5×10^{-3} emu/g at low temperatures, susceptibility of the order of 10^{-5} emu/g-Oe and a high saturation magnetization (up to 0.8 emu/g at 1.8 K).

We postulate that localized unpaired spins occur because of topological and bonding defects associated with the sheet curvature, and that these spins are stabilized for > 1 year due to the steric protection offered by the convoluted sheets [1,2].

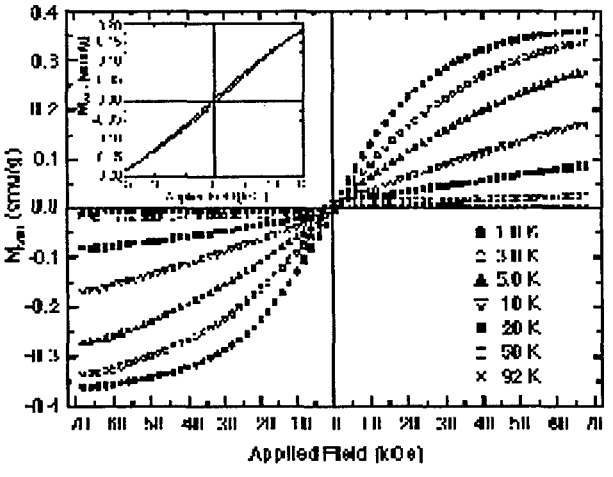

Fig.1: *Mass magnetization as a function of the applied magnetic field atT =1.8 - 92 K. Inset: M(H) hysteresis loop at T = 1.8 K exhibiting a coercive force H_c =420 Oe.*

References

1. A. V. Rode, E. G. Gamaly, A. G. Christy, J. D. Fitz Gerald, S. T. Hyde, R. G. Elliman, B. Luther-Davies, A. I. Veinger, J. Androulakis, J. Giapintzakis, Phys. Rev. B, **70**, 054407 (2004).
2. A. V. Rode, R. G. Elliman, E. G. Gamaly, A. I. Veinger, A. G. Christy, S. T. Hyde, B. Luther-Davies, Appl. Surf. Science **197-198**, 644-649 (2002).

e-mail: avr111@rsphysse.anu.edu.au

SESSION Fr B2
HYBRID AND NANOCOMPOSITE MATERIALS

Friday 11 February 2005 **1320–1500**

Meeting Room V

Session Chair **Ken MacKenzie, Victoria University of Wellington, NZ**
Ian Brown, Industrial Research Ltd, Lower Hutt, NZ

13.20 **Down scaling in piezoelectrics and polar materials: microdevices, nanofabrication, small features and size effects**
Fr B2.1 N. Setter
(Extended Oral Talk)
Swiss Federal Institute of Technology EPFL, Lausanne, Switzerland

13.45 **Layered tungsten oxide-based hybrid materials incorporating transition metal ions**
Fr B2.2 B. Ingham[1], S.V. Chong[2] and J.L. Tallon[1,2]
[1] *Victoria University of Wellington, Wellington, NZ*
[2] *Industrial Research Ltd., Lower Hutt, NZ*

14.00 **Structural and thermal characterisation of nanostructured alumina templates**
Fr B2.3 I.W.M. Brown, M.E. Bowden, T. Kemmitt and K.J.D. MacKenzie
Industrial Research Ltd., Lower Hutt, NZ

14.15 **Advances in understanding the synthesis mechanism and properties of geopolymeric materials**
Fr B2.4 K. MacKenzie[1,2], D. Brew [2], C. Nicholson[2], R. Fletcher[2] and M. Schmücker[3]
[1] *Victoria University of Wellington, Wellington, NZ*
[2] *NZ Institute for Industrial Research and Development, Lower Hutt, NZ*
[3] *German Aerospace Centre, Cologne, Germany*

14.30 **Nanoporous materials chemistry: membranes for clean hydrogen**
Fr B2.5 S.A. Bagshaw, C.F. Hosie, M.E. Bowden.
Industrial Research Ltd., Lower Hutt, NZ

14.45 **Superhard nanocomposite thin films: experiment and simulation**
Fr B2.6 Y.G. Shen
City University of Hong Kong, Kowloon, Hong Kong

Down Scaling in Piezoelectrics and Polar Materials: Microdevices, Nanofabrication, Small Features and Size Effects

N. Setter

Ceramics Laboratory, Swiss Federal Institute of Technology EPFL, Lausanne, Switzerland

Nava.setter@epfl.ch

Piezoelectric materials in the form of thin and thick films are finding new applications in diverse fast growing fields such as wireless communications and environment monitoring[1]. The number of applications that will benefit from availability and implementation of these films is likely to grow.

Size reduction of ferroelectric-based micro-components, both in thickness and in lateral dimensions is required for various applications. This can be achieved by a reductive approach of etching of the sintered continuous layers, or by an additive approach in which a treatment of the substrate results in the creation of patterned structures prior to the annealing step. Recent local characterisation techniques, e.g. piezoelectric force microscopy, allow the analysis of properties in such small components and to manipulate them (fig. 1)[2].

Various microdevices produced at our laboratory are described and issues in fabrication technology (in particular in relation with piezoelectric MEMS[3] and with tunable rf-MEMS[4]) are discussed. Data and interpretation of local measurements are reviewed. Size effects in ferroelectrics and their significance in emerging applications are discussed[5].

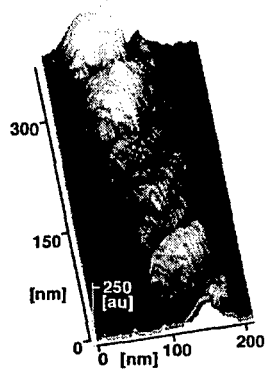

Fig. 1: 3D picture of the piezoelectric activity of part of a nano-rod of $K(Ta,Nb)O_3$

References:

[1] Electroceramic MEMS – Special double issue in the Journal of Electroceramics, Guest editor: N. Setter, 12 (5-144) 2004 and references herein.

[2] G. Suyal, E. Colla, R. Gysel, M. Cantoni, N. Setter, *Piezoelectric response and polarization switching in small anisotropic perovskite particles*, Nano Letters 4 (2004) 1339-1342.

[3] N. Ledermann, P. Muralt, J. Baborowski, S. Gentil, K. Mukati, M. Cantoni, A. Seifert, N. Setter, *{100}-texture, piezoelectric $Pb(Zr_x, Ti_{1-x})O_3$ thin films for MEMS: integration, deposition and properties*, Sensors & Actuators A105/2 (2003) 162-170.

[4] A.K. Tagantsev, V.O. Sherman, K.F. Astafiev, J. Venkatesh, N. Setter, *Ferroelectric materials for microwave tunable applications*, Journal of Electroceramics 11 (2003) 5-66.

[5] I. Stolichnov, E. Colla, A. Tagantsev, S. Hong, N. Setter, *Direct nanoscale observation of size effect on polarization instability in $Pb(Zr,Ti)O_3$ film capacitors*, Mat. Res. Soc. Symp. Proc., Vol. 688 (2002) C7.16.1-C7.16.6.

Layered Tungsten Oxide-Based Hybrid Materials Incorporating Transition Metal Ions

B. Ingham,[1*] S. V. Chong[2] and J. L. Tallon[1,2]
[1] *School of Chemical and Physical Sciences, Victoria University of Wellington, Wellington, NEW ZEALAND*
[2] *Industrial Research Limited, Lower Hutt, NEW ZEALAND*

One example of a simple system with great potential for nanotechnological applications is that of the tungsten oxide-based hybrid materials, consisting of tungsten oxide-based layers separated by organic amine/ammonium molecules. The organic molecules can be chosen to have a specific desired functionality that is then integrated with the more rigid and thermally stable oxide layers. The oxide layers can also be altered in both thickness and composition, rendering the general system quite diverse in possible functions and stoichiometries. By selecting appropriate organic and inorganic components one can obtain and even tune the electronic properties of the resulting hybrid.

Recent work by our group has concentrated primarily on the relatively simple compound, WO_4-$H_3N(CH_2)_nNH_3$, in which the organic molecule is a saturated diammonium alkane with chain lengths from n = 2 to n = 12 [1-3]. In this case the organic amines act primarily as 'spacer' molecules to vary the separation of the inorganic layers. WO_6-octahedra are corner-shared in two directions to form layers. This is structurally quite similar to tungsten trioxide (WO_3) in which the WO_6-octahedra are shared in all three directions.

Following this, one might expect that other tungstate systems might be suitable candidates as starting materials for similar hybrid materials. A number of transition metal tungstates, $M^{2+}WO_4$, are known to exist; many of which can be found as pure or mixed tungstate ores (e.g. wolframite, ferberite, stolzite). The $M^{2+}WO_4$ species primarily exist in either the wolframite or scheelite structure, depending on the size of the M^{2+} ion [4]. A hybrid material based on metal tungstates allows us to study the effects of the incorporation of transition metal ions in the tungsten oxide hybrid materials, through either substitution of tungsten or the formation of different inorganic structures.

We have explored the addition of the transition metal ions Mn, Fe, Co, Ni and Cu in the tungsten oxide–diaminoalkane hybrid system. The materials were produced by various solution-based methods as appropriate and characterised by powder X-ray diffraction (XRD), scanning electron microscopy (SEM), energy dispersive x-ray (EDX) analysis, infrared and Raman spectroscopy, and magnetisation measurements.

XRD and SEM of these new hybrids strongly indicate the presence of layered structures, some of which are structurally similar to either that of the 'plain' tungsten oxide-based compounds or each other, according to the infrared and Raman vibrational spectra. Preliminary magnetisation results of the transition metal-incorporated tungsten oxide-diaminoalkane hybrids show that these systems have interesting properties. All of these materials, with the exception of those incorporating nickel ions, have negative Curie-Weiss temperatures. The parent tungstate materials also exhibit this behaviour [5]. The manganese-incorporated species demonstrate an antiferromagnetic transition at low temperatures. The transition temperature decreases with increasing alkyl chain length, which corresponds to the inorganic interlayer spacing. This indicates that the interlayer magnetic coupling is frustrated as the distance between the layers increases.

References

[1] S.V. Chong, B. Ingham, J.L. Tallon, Curr. Appl. Phys. 4 (2004) 197.
[2] B. Ingham, S.V. Chong, J.L. Tallon, MRS Symposium Proceedings 775 (2003) 165.
[3] B. Ingham, S.V. Chong, J.L. Tallon, Phys. Rev. B (submitted, cond-mat/0405241).
[4] A.W. Sleight, Acta Cryst. B 28 (1972) 2899.
[5] L.G. van Uitert, R.C. Sherwood, H.J. Williams, J.J. Rubin, W.A. Bonner, J. Phys. Chem. Solids 25 (1964) 1447.

* Contact author: b.ingham@irl.cri.nz

Structural and Thermal Characterisation of Nanostructured Alumina Templates

I.W.M. Brown[1*], M.E. Bowden[1], T. Kemmitt[1] and K.J.D. MacKenzie[1],
[1]*MacDiarmid Institute for Advanced Materials and Nanotechnology, Industrial Research, PO Box 31-310, Lower Hutt, NEW ZEALAND*

Nanostructured anodic aluminium oxide contains a two dimensional array of high aspect ratio aligned pores of 10-250 nm diameter (figure 1). The nanoporous morphology (pore diameter, wall thickness, channel length) can be controlled by selection of the acid electrolyte and the anodisation voltage [1]. These regular arrays can be used as templates for producing new nanomaterials whose functionality may be controlled through the design and manipulation of coatings applied to the alumina substrate, through infilling the nanopores to form nanorods or wires, or through chemical or thermal modification of the substrate itself. An example of templating to obtain specific functionality is the growth of TiO_2 (anatase) nanocrystallites on the internal alumina pore surfaces to achieve photocatalytic activity [2].

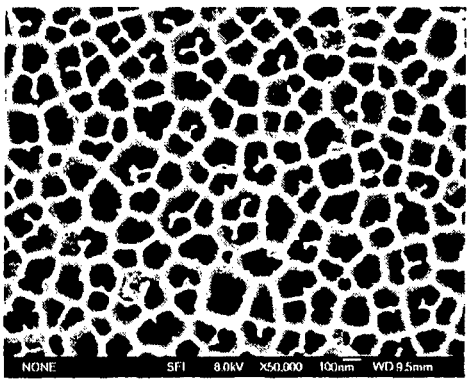

Figure 1.
Electron micrograph of 200nm channels in anodic alumina

This paper examines the structural and thermal characteristics of nanostructured anodic aluminium oxides. While some thermal and structural features have previously been elaborated [3], there remains a need for a thorough and detailed knowledge and understanding of these features as a pre-requisite to achieve chemical and physical control of nanopore surfaces and their functionality.

Commercially prepared alumina membranes 13 mm dia. x 60 μm thick were characterised using XRD, SEM, solid state NMR and thermal analysis (TG/DSC) techniques. The materials are X-ray amorphous and develop crystalline structure only very slowly on extended heating at elevated temperature. The absence of long range order makes these materials ideal candidates for study using ^{27}Al MAS NMR techniques, which is reported here as a function of thermal treatment. Specimens heated in flowing air at 10 °C/min show negligible weight loss (1-2 wt%) on heating to 1260 °C. Nevertheless, thermal analysis shows two discrete exothermic events, at 850 °C and 1020 °C. These events are irreversible on thermal cycling and represent permanent structural changes within the alumina ceramic substrate. Neither exothermic event gives rise to any significant development of long range order in the structures, as assessed by XRD. However, ^{27}Al MAS NMR gives valuable insights into the development of local ordering. XRD of anodic alumina heated to 1200 °C shows poorly crystallized θ-Al_2O_3 and δ-Al_2O_3 while material heated to 1260 °C displays improved crystallinity in the θ-Al_2O_3 phase and the beginnings of α-Al_2O_3 (corundum) formation.

References

[1] O. Jessensky, F Müller and U Gösele, Appl Phys Letts., **72**, 1173 (1998).
[2] T. Kemmitt, M.E. Bowden and I.W.M. Brown, to be presented at AMN-2, see abstract.
[3] R. Ozao, H. Yoshida, Y.Ichimura, T. Inada and M. Ochiai, J. Therm. Anal. Cal. **64**, 915 (2001).

* Contact author: i.brown@irl.cri.nz

Advances in understanding the synthesis mechanism and properties of geopolymeric materials

Kenneth MacKenzie[1,2], Dan Brew [2], Catherine Nicholson[2], Ross Fletcher[2], Martin Schmücker[3]
[1]*MacDiarmid Institute for Advanced Materials and Nanotechnology, Victoria University of Wellington, P.O. Box 600 Wellington*
[2]*NZ Institute for Industrial Research and Development, Lower Hutt*
[3]*German Aerospace Centre, Cologne, Germany*

Geopolymers are inorganic materials with the high-temperature properties of ceramics but which, unlike ceramics, are prepared at ambient temperatures (<100°C) by cross-linking aluminate and silicate units under highly alkaline conditions into a three-dimensional tetrahedral framework structure. The resulting materials are fireproof and can be used as the matrix material for composites with both organic and inorganic fibres and granular fillers. This leads to potential applications as structural materials, fire-resistant vehicle body components and matrices for encapsulation and immobilization of hazardous waste such as mine tailings, heavy metal sludges and radioactive waste.

Conventionally, these materials are prepared from aluminosilicate clay minerals and sodium silicate, and were thought to exist in a restricted range of Si/Al compositions, but recent work presented here indicates that neither of these conditions is strictly true. Viable silica-rich geopolymers have been prepared with Si/Al ratios up to 300, with the higher-silica members showing unexpected plastic deformation properties. Aluminosilicate geopolymers have also been produced without the use of layer-lattice aluminosilicate templates, and the incorporation of tetrahedral borate and phosphate units into the framework structure has also been accomplished. These results shed fresh light on fundamental questions concerning the mechanism of the geopolymerisation reaction and have implications for the definition of geopolymers themselves.

[1]kenneth.macenzie@vuw.ac.nz

Nanoporous Materials Chemistry: Membranes for Clean Hydrogen

Stephen A. Bagshaw*, Camilla. F. Hosie, Mark E. Bowden.
R&D Operations, Industrial Research Ltd., PO Box 31310, Lower Hutt, NEW ZEALAND

Nanoporous silicate and ceramic materials have played major roles in the development of the fossil fuel economy.[1] The application of zeolites in particular, as molecular sieves and catalysts made possible the chemical manufacture of high grade petrochemicals and gasoline.[2] As we transition into the 21st century however, we are increasingly looking towards replacements for the petroleum-based energy economy. In this context, New Zealand is now beginning to invest in the concept of the Hydrogen economy. At Industrial Research we are developing new science that will draw nanoporous zeolite membrane technologies into this new energy economy.

A joint research and technology development programme has CRL Energy and Industrial Research investigating routes to the clean and efficient conversion of coal to hydrogen and thereon to distributed energy.[3] Such a process is viewed as an important intermediate step in the creation of a viable hydrogen economy. A vital aspect of this energy conversion system, especially in cases where the hydrogen is to be used in fuel cells, is the clean-up of the synthesis gas that is formed by gasification and reforming of the coal. We are investigating the synthesis and application of hierarchical porous membrane technologies to separate the hydrogen from the other components of the gas mixture. Macroporous alumina/nanoporous zeolite composite membranes appear to possess the characteristics necessary to perform this task [4].

In this contribution we will briefly describe our hypotheses, our synthesis approaches and some preliminary results of the progress of the programme to date. Our work has focussed on the preparation of both known zeolite membrane types, such as silicalite (MFI) and zeolite A (LTA), and the application of zeolites not previously used in membrane applications such as zeolite W (LTW) [5]. The porous alumina ceramic membrane used is also new and is prepared by starch-consolidation techniques [6]. We have found that preferred surface nucleation events induce preferential growth along the long axis of the MFI crystals both inside the pore volumes of the alumina support and also at the internal surfaces of those pores. Judicious modifications of known synthesis routes has allowed us to create hierarchical pore systems in the interior of the alumina supports. This contrasts with much of the current thinking which has tended towards concepts of producing supported films on the outer surfaces of the porous substrates.[3]

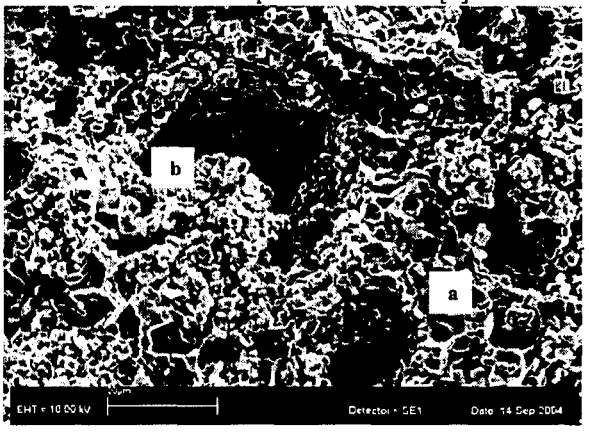

Fig. 1 SEM micrograph of Alumina/silicalite membrane. a = alumina framework, b = zeolite crystals in and on surface of pores.

References

[1] Roskill reports, The Economics of Zeolites, April 2003. (http://www.roskill.com/reports/zeolites)
[2] A. Corma, Chem. Rev. **97**, 2373 (1997).
[3] Foundation for Research Science and Technology contract CO8X0204.
[4] A. Tavolaro and E. Drioli, Adv. Mater. **11**, 975 (1999).
[5] *Atlas of zeolite framework types* 5th edition, edited by Ch. Baerlocher, W. M Meier and D. H. Olsen, 5th ed, (Elsevier, Amsterdam, 2001).
[6] M. E. Bowden and M. S. Rippey, Key Engineering Materials, **206-213**, 1957 (2002).

* Contact author: s.bagshaw@irl.cri.nz

Superhard nanocomposite thin films: experiment and simulation

Y.G. Shen

Department of Manufacturing Engineering & Engineering Management, City University of Hong Kong,Tat Chee Avenue, Kowloon, Hong Kong

Superhard nanocomposite nc-TiN/a-SiN_x thin films were deposited onto Si(100) substrates by reactive unbalanced close-field magnetron sputtering in an Ar-N_2 gas mixture. Film bonding states and microstructure were investigated by x-ray photoelectron spectroscopy (XPS), x-ray diffraction (XRD), and transmission electron microscopy (TEM). Surface morphology was measured by atomic force microscopy (AFM) and quantitatively analyzed using height-height correlation function. The mechanical properties were evaluated from nanoindentation measurements. The films consisted of nanometer-sized TiN crystallites embedded in an amorphous SiN_x matrix. A maximum hardness of ~50 GPa was observed in a film with silicon content of 8.6 at.%. The improved mechanical properties of nc-TiN/a-SiN_x with the addition of Si into TiN were attributed to their densified microstructure with development of fine grain size and reduced surface roughness. The results have been interpreted with the help of a Monte Carlo Potts model simulation. The simulation results show that nanocomposite films with microstructures comprising nanocrystalline TiN grains in an amorphous SiN_x matrix is driven by the energy difference between the TiN grain boundary energy and TiN/SiN_x interfacial energy. The SiN_x matrix formed can constrain TiN grain growth and thus causes a remarkable reduction in TiN grain size. These simulation results are in reasonable agreement with experimental observations.

*Corresponding author: E-mail: meshen@cityu.edu.hk

SESSION Fr C2
CONDUCTING POLYMERS I

Friday 11 February 2005 **1320–1500**

Copthorne I

Session Chair **David Officer, Massey University, NZ**

13.20 **Nanoparticles and conducting polymers: novel routes toward DNA sensing**
Fr C2.1 J. Travas-Sejdic, H. Peng, M.B. Cannell, R.P. Cooney, G.A. Bowmaker and C. Soeller
(Extended Oral Talk)
University of Auckland, Auckland, NZ

13.45 **Inherently conducting polymer nanostructures by templating techniques**
Fr C2.2 V. Misoska, W.E. Price, S.F. Ralph and G.G. Wallace
University of Wollongong, Wollongong, Australia

14.00 **Spectroscopic studies of doping reactions in polypyrrole actuators**
Fr C2.3 P.A. Kilmartin, K.-C. Li, N.A. Vigar, G.A. Bowmaker, R.P. Cooney, C. Soeller, M.B. Cannell, R. Archer, M. Biglari-Abhari, A. Bigdelli and J. Travas-Sejdic
University of Auckland, Auckland, N.Z.

14.15 **Towards amine-functionalised polymer surfaces**
Fr C2.4 S. Gambhir, K. Wagner and D.L. Officer
Massey University, Palmerston North, NZ

14.30 **Macromolecular asymmetric induction: a novel route to optically active polyanilines from achiral reagents using a chiral emeraldine salt initiator**
Fr C2.5 L.A.P. Kane-Maguire, Y. Pornputtkul, P.C. Innis and G.G. Wallace
University of Wollongong, Wollongong, Australia

14.45 **Synthesis of conducting polymers in ionic liquids**
Fr C2.6 J.M. Pringle, D.R. MacFarlane and M. Forsyth
Monash University, Melbourne, Australia

Nanoparticles and Conducting Polymers: Novel Routes Toward DNA Sensing

J. Travas-Sejdic*, H. Peng, M. B. Cannell, R.P. Cooney, G.A. Bowmaker and C. Soeller
Polymer Electronics Research Centre
The University of Auckland, PO Box 9019, Auckland, New Zealand

Major developments in human genetics have resulted in a need for rapid, sensitive and specific detection of DNA. The specific base-pair complex formation (hybridization) between complementary sequences is a well-established method used in DNA sensors. Transduction and signal amplification of this recognition event has proven to be more challenging, and several different approaches have been suggested [1,2]. Electronic transducers have been of particular interest due to their direct electric readout capability and methods using cyclic voltammerty and electrochemical impedance have been demonstrated [3,4]. In such approaches, metal electrodes or other conducting or semiconducting thin films are modified with the probe sequence and the change in the electrical and electrochemical properties of the sensor film are monitored. We have previously demonstrated an electrochemical DNA sensor based on functionalized polypyrrole where oligonucleotide (ODN) probe molecules were covalently bonded to the polymer [4].

Here we present a novel route toward gene sensors based on conducting polymers where the electrochemical sensor response is amplified by the presence of CdS nanocrystals. In such a sensor the ODN sample is entrapped in a polypyrrole film and then hybridized with the complementary ODN tagged with CdS nanocrystal particles. We found that the formation of the ODN duplex altered the electrode interfacial properties, as observed by cyclic voltammetry and electrochemical impedance spectroscopy (EIS), and that the effect was significantly enhanced when the ODNs are tagged with CdS. This presentation will discuss the mechanism of signal amplification by CdS nanoparticles and present results of modelling of the impedance spectra. Figure 1 shows representative EIS spectra of an Au/PPy/ODN film before and after hybridisation with CdS-ODN (points) and corresponding model data (curves). The Figure presents the equivalent circuit used for fitting, together with the total impedance (|Z|), phase angle (theta) and the complex admittance plot (Y'' vs. Y') for the film.

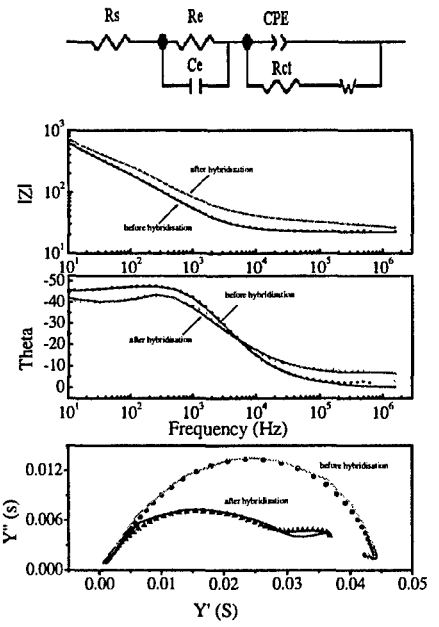

Figure 1. See text for explanation.

References:

[1] K. Doré et al., J.Am.Chem. Soc., 126 (2004) 4240
[2] J. Wang, Analytica Chimica Acta, 500 (2003) 247
[3] Y. Xu et al., 16 (2004) 150
[4] H. Peng et al., *Biosensors & Bioelectronics,* in press

Acknowledgement:
The authors would like to thank the University of Auckland VC Development and Staff Research Funds for financial support.

*Contact author: j.travas-sejdic@auckland.ac.nz

Inherently Conducting Polymer Nanostructures by templating techniques

Violeta Misoska, William E. Price[1], Stephen F. Ralph and Gordon G. Wallace
Intelligent Polymer Research Institute & Department of Chemistry
University of Wollongong
NSW 2522
Australia

The nanoparticle domain (less than 100 nm) has been until recently dominated by a focus on inorganic materials such as metals and semiconductors, because they are well characterized materials and have been utilized for electronic and photovoltaic devices. An expanding trend has been to fabricate nanomaterials as composite structures and devices. This has been driven by a desire to enhance the properties of the nanomaterials. One of the consequences of the above trends has been a number of groups studying the synthesis and characterization of inherently conducting polymer (ICP) nanocomponents in recent years. [1] This paper looks at two recent studies from our laboratory where templating techniques have been used to produce nanoscale ICP composite materials using polypyrrole.

In the first study, [2] using a technique first applied by Burford and others, controlled pore conventional membranes were used as substrates. In this instance, the conducting polymer was grown electrochemically through the platinised PVDF membrane electrode substrate with a nominal pore size of 45 micron. The substrate was then dissolved away using a base leaving free standing hollow nanotubes of conducting polypyrrole. The major role the counterion dopant in the polymer plays a major role in the physical and electrochemical properties of the final nanostructure is discussed. The resultant structure is shown in the electron micrographs in Figure 1.

Figure 1: Electron Micrograph of nanostructured ICP fibrillar membranes obtained through using conventional porous membranes as templates for growth

In the second study [3], conducting polypyrrole chloride was electrochemically prepared between the open void spaces in a polystyrene synthetic opal crystal. The synthetic opal was formed by the sedimentation of colloidal polystyrene (ca. 315 nm) to produce self-assembled face centered cubic (fcc) films exhibiting opalescence. The voids between the colloids were filled by polypyrrole grown through opal deposited onto Indium-Tin-Oxide (ITO) glass slide or platinum coated PVDF filter. The template was then removed to produce an inverse nanostructure. Electrochemical studies as well as UV-visible spectroscopic studies on the films are discussed.

References:

1. G.G. Wallace and P. Innis, J. Nanosci and NanoTech. **2**, 441, (2002).
2. V. Misoska, PhD Thesis, U. Wollongong (2002).
3. V. Misoska et al, Synth. Met, **121**, 1501, (2001).

[1] William Price. Email: wprice@uow.edu.au

Spectroscopic Studies of Doping Reactions in Polypyrrole Actuators

P. A. Kilmartin[1,2,*], K.-C. Li[1,2], N. A. Vigar[1,2], G. A. Bowmaker[1,2], R. P. Cooney[1,2], C. Soeller[1,3], M. B. Cannell[1,3], R. Archer[1,4], M. Biglari-Abhari[1,5], A. Bigdelli[1,5], J. Travas-Sejdic[1,2]
[1] *Polymer Electronics Research Centre,* [2] *Chemistry Department,* [3] *Physiology Department,* [4] *Department of Engineering Science,* [5] *Department of Electrical and Electronic Engineering, University of Auckland, Private Bag 92019, Auckland, NEW ZEALAND*

The performance of the conducting polymer polypyrrole as an electromechanical actuator is being actively investigated [1-3]. The volume change which occurs during doping and dedoping provides a low voltage actuation which can reach strains of 26% for cm-sized strips of polypyrrole with suitably large counter ions [3] and 35% perpendicular to the plane for films around 1 μm in thickness [2]. The rate and extent of doping are key aspects of polypyrrole actuation which need to be examined in more detail particularly as different dopant ions, solvents and operating conditions are considered.

The use of in situ Raman spectroscopy provides a means of determining and monitoring the extent of conducting polymer oxidation and doping [4]. The technique has been applied to composite actuators to separate regions containing polypyrrole and polythiophene [5]. In the present report, in situ Raman spectroscopy has been used to following oxidative doping for polypyrrole prepared in various solutions and with various dopant anions. For one film formed on a Pt electrode by 6 cycles to 0.76 V (SCE) at 50 mV s^{-1} in 0.1 M pyrrole and 0.1 M NaCl , several Raman bands typical of polypyrrole were readily identified in situ (Figure 1), using the Ar^{+} 514.5 nm laser line at a Jobin-Yvon U100 spectrometer.

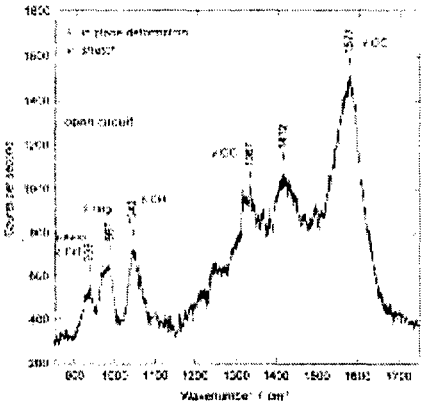

Figure 1. Raman spectra of a polypyrrole film tested in 0.1 M NaCl at open circuit potential.

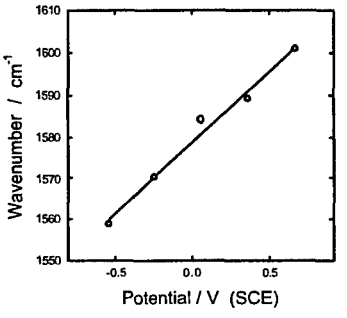

Figure 2. Shift in CC stretching mode position with increasing electrode potential and polypyrrole oxidation state.

Of particular interest is the band at 1559 to 1601 cm^{-1} ascribed to a CC stretching mode, which shifts from lower wavenumbers for the fully reduced film at lower potentials to higher wavenumbers as oxidised forms appear at higher electrode potentials (Figure 2). Using the facilities of the Renishaw Raman spectrophotometer, the kinetics of polypyrrole actuation and the extent of doping are being monitored in situ, allowing both spatial and temporal mapping of actuator performance.

References

[1] G. M. Spinks, L. Liu, G. G. Wallace and D. Zhou, Adv. Funct. Mat. **12**, 437 (2002).
[2] E. Smela and N. Gadegaard, Adv. Mat. **11**, 953 (1999).
[3] S. Hara, T. Zama, W. Takashima and K. Kaneto, J. Mater. Chem. **14**, 1516 (2004).
[4] C. J. Zhong, Z. Q. Tian and Z. W. Tian, J. Phys. Chem. **94**, 2171 (1990).
[5] G. Han and G. Shi, Sens. Act. B **99**, 525 (2004).

* Contact author: p.kilmartin@auckland.ac.nz

Towards Amine- Functionalized Polymer Surfaces

Sanjeev Gambhir*, Klaudia Wagner and David L. Officer
Nanomaterials Research Centre and the MacDiarmid Institute for Advanced Materials and Nanotechnology, Massey University, Private Bag 11-222, Palmerston North, New Zealand

Functionalized conducting polymers present the opportunity to create micro- and nano- scale electrodes as active components of chemical and biosensors [1,2]. This is a result of the ease with which conducting polymer monomers can be selectively electrochemically oxidized to give stable redox- active films [3]. If appropriate functionality can be built into the polymer, the film surface can be modified with a wide variety of bioactive species [4-6].

In this regard we have been investigating the synthesis of amino-functionalized polythiophenes. As part of our building block approach to polythiophenes, we have chosen 3′-aminoterthiophene for the purpose. 3-aminothiophene itself is unstable and oligomerises on standing [7,8]. We anticipated that 3′-aminoterthiophene would be less reactive and be more suitable for fictionalization with bulky biomolecules. The resulting surfaces could then be utilized in sensor development utilized for activating cell growth or for the development of biocompatible conducting polymer structures.

3′-aminoterthiophene was synthesized for the first time and its chemical and electrochemical polymerization was studied. Chemical polymerization using $FeCl_3$ resulted in black sticky polymer with no indication of electroactivity, whereas electrochemical polymerization of 3′-aminoterthiophene gave two different polymer growth processes. In order to probe these processes, we have investigated the polymerization of protected 3′-aminoterthiophene (II) and aminoterthiophene activated with alkoxy substituents (III and IV).

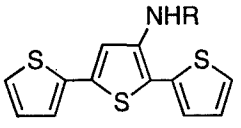

I R= H
II R= Ac

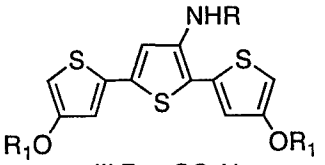

III $R_1 = OC_6H_{13}$
IV $R_1 = OC_{10}H_{21}$

We will discuss the electrochemical polymerization and characterization of the resulting polymers from I- IV, and describe our attempts to produce functionalized polymer surfaces.

References

[1] K. S. Ryder; D. G. Morris; J. M. Cooper, Journal of the Chemical Society, Chemical Communications, 1471-1473 (1995).
[2] P. Baeuerle; G. Goetz; M. Hiller; S. Scheib; T. Fischer; U. Segelbacher; M. Bennati; A. Grupp; M. Mehring; et al., Synthetic Metals 61, 71-79 (1993).
[3] J. Labuda, Selective Electrode Reviews 14, 33-86 (1992).
[4] G. Li; G. Kossmehl; W. Kautek; W. Plieth; H. Zhu; H. S. O. Chan; S. C. Ng, Macromolecular Chemistry and Physics 201, 21-30 (2000).
[5] J. Liu; R. D. McCullough, Macromolecules 35, 9882-9889 (2002).
[6] J. A. Stafford; S. D. Rothstein; D. E. Tallman; S. C. Rasmussen, Polymer Preprints (American Chemical Society, Division of Polymer Chemistry) 45, 181-182 (2004).
[7] J. M. Barker; P. R. Huddleston; M. L. Wood, Synthetic Communications 25, 3729-3734 (1995).
[8] C. Paulmier, Sulfur Reports 19, 215-284 (1996).

* Contact author: S.Gambhir@massey.ac.nz

Macromolecular Asymmetric Induction: A Novel Route to Optically Active Polyanilines from Achiral Reagents Using a Chiral Emeraldine Salt Initiator

L.A.P. Kane-Maguire*, Y. Pornputtkul, P.C. Innis and G.G. Wallace
Intelligent Polymer Research Institute, ARC Centre for Nanostructured Electromaterials, University of Wollongong, Wollongong, NSW 2522, AUSTRALIA

There has been considerable recent interest in chiral, electrically conducting polyanilines (PAn's) because of their potential applications in areas such as chiral sensors, chiral separations and electrochemical asymmetric synthesis. A useful route to optically active PAn.HA emeraldine salts has been the incorporation of chiral dopant anions (A^-) during oxidative polymerisation of aqueous aniline in the presence of a chiral acid HA [1]. Using electrochemical polymerisation route, we have reported the preparation of chiral PAn.(+)-HCSA and PAn.(-)-HCSA (HCSA = 10-camphorsulfonic acid) films whose circular dichroism (CD) spectra exhibited strong, mirror-imaged bands. The observed optical activity was attributed [1] to the polyaniline chains preferentially adopting a one-handed helical screw (depending on the hand the incorporated chiral dopant CSA^- anion).

We wish now to report a novel and potentially widely applicable route to optically polyanilines generated via polymerisation from achiral reagents, using a chiral emeraldine salt as initiator. This unprecedented discovery arose during a wider program exploring the factors controlling the electrochemical synthesis of chiral polyanilines, in which we speculated whether an initially deposited thin film of optically active PAn.(+)-HCSA may exert asymmetric induction during the subsequent electrochemical polymerisation of aniline in the presence of racemic (±)-HCSA. This was indeed found to be the case. A thin film of PAn.(+)-HCSA was electrochemically deposited at room temperature onto an ITO-glass electrode from aqueous aniline (0.20 M) in 1.0 M (+)-HCSA, using an applied potential of 0.9 V (*vs* Ag/AgCl) and passing 25 mC/cm^2 charge. After washing with methanol to remove unreacted reagents, its CD spectrum (Figure 1b) exhibited weak bands at ca. 430 and 700 nm associated with absorption bands seen in this region (Figure 1a). The film was then placed in fresh aqueous aniline in the presence of racemic (±)-HCSA (1.0 M) and the electropolymerisation continued while passing a further 100 mC/cm^2 charge. The emeraldine salt film grew considerably thicker, as shown by the increase in intensity of the absorption bands in Figure 1a. Remarkably, the CD bands for the film were also observed to increase strongly in intensity (Figure 1b), despite the fact that the dopant acid present during the second aniline polymerisation was racemic HCSA.

Related studies were subsequently carried out in which the second electropolymerisation was performed in a range of achiral acids such as HCl or *p*-toluenesulfonic acid. Similar marked induction of optical activity was observed in each case for the PAn.HA (HA = achiral acid) salt films deposited on top of the initial thin, chiral PAn.(+)-HCSA layer. This initial chiral polyaniline therefore appears to behave as a macromolecular asymmetric initiator, inducing new polyaniline chains growing from it to preferentially adopt the same helical hand as itself, irrespective of the nature of the dopant anion (A^-) being incorporated. The paper will discuss the molecular basis of this fascinating asymmetric induction and its potential applications in chiral synthesis.

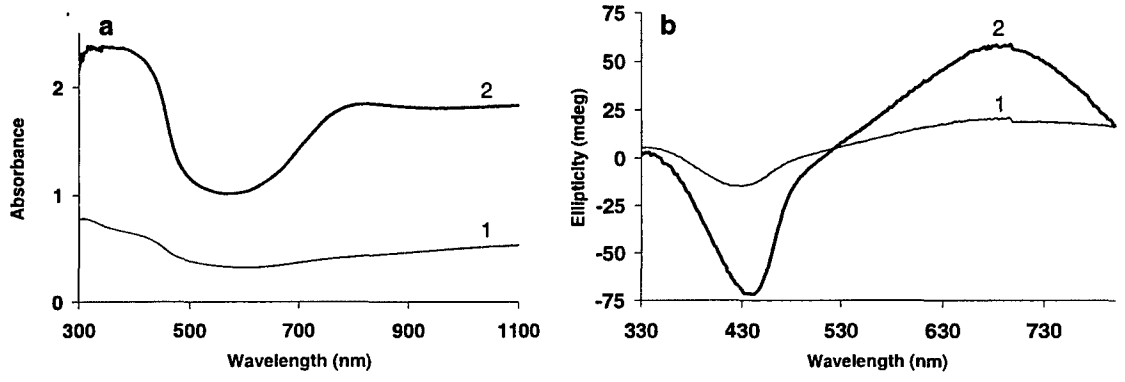

Figure 1. UV-vis and CD spectra of: (1) a PAn.(+)HCSA film deposited on ITO-glass at 0.9 V (25 mC/cm^2 passed), and (2) after depositing a further PAn.(±)-HCSA film (another 100 mC/cm^2 passed).

References

[1] G.G.Wallace, G.M. Spinks, L.A.P. Kane-Maguire, P.R. Teasdale, *Conductive Electroactive Polymers, Intelligent Materials Systems, 2nd Ed* (CRC Press, Boca Raton, 2003), Chapter 5.

Synthesis of conducting polymers in ionic liquids

J. M. Pringle[1,*] D. R. MacFarlane[2] and M. Forsyth [1]
[1] *School of Physics and Materials Engineering, Monash University, Wellington Road, VIC 3800, AUSTRALIA*
[2] *School of Chemistry, Monash University, Wellington Road, VIC 3800 AUSTRALIA*

Use of traditional molecular solvent/electrolyte systems for the electrochemical polymerisation and cycling of conducting polymers commonly results in anion incorporation into the polymer to effect charge balance. However, recent work has suggested that when conducting polymer films are oxidized and reduced in an ionic liquid, the intercalation/de-intercalation of cations rather than anions can occur.[1, 2] Use of ionic liquids in combination with conducting polymers has attracted increasing attention in recent years following some promising initial results - films prepared in conventional solvents but cycled in an ionic liquid show improved actuator performance and significantly increased lifetimes, to up to one million cycles.[3] Here we report the use of ionic liquids as the growth medium for the electrosynthesis of polypyrrole, as well as their use as the supporting electrolyte for the electrochemical cycling of the films.

Ionic liquids are a new class of solvent composed entirely of ions - typically a large organic cation and a smaller inorganic anion - which have a number of advantages over conventional solvents. They have a wide liquid range and negligible vapour pressure, which can overcome the problem of solvent evaporation in electrochemical applications. Of particular importance, ionic liquids possess good electrochemical stability, with electrochemical windows typically over 4V wide. The ionic liquids investigated here include those based on the imidazolium, pyrrolidinium and phosphonium cations, in combination with the TFSA anion:

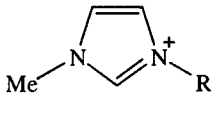

imidazolium
R = Et, But

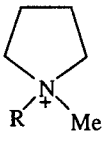

pyrrolidinium,
R = propyl, butyl etc.

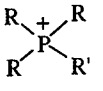

phosphonium
R, R' = alkyl

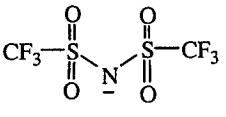

bis(trifluoromethane sulfonyl)amide (TFSA)

We have investigated the influence that the nature of the ionic liquid has on the growth and physical properties of the polypyrrole films. Solid state NMR analysis have been used to study cation and anion intercalation/de-intercalation from the ionic liquids into the polypyrrole films, both during growth and cycling, and to assess how this varies with different ionic liquids. Use of an ionic liquid composed of a phosphonium cation and a fluorinated anion allows the separate detection of the cation and anion within the polypyrrole film by phosphorous and fluorine solid state NMR. Initial results show incorporation of both the cation and anion during film growth and indicate that, despite its large size, the cation can be fully expelled from the film by oxidation.

References

[1] J. Ding, D. Zhou, G. Spinks, G. Wallace, S. Forsyth, M. Forsyth, D. MacFarlane. Chemistry of Materials **15** 2392 (2003)
[2] F. Vidal, C. Plesse, D. Teyssié, C Chevrot. Synth. Met. **142** 287 (2004)
[3] W. Lu et al. Science **297** 983 (2002)

* Contact author: Jenny.Pringle@spme.monash.edu.au

SESSION Fr D2
SOFT MATTER AND COMPLEX FLUIDS

Friday 11 February 2005 **1320–1500**

Copthorne II

Session Chair **Kate McGrath, Victoria University of Wellington, NZ**

13.20 **Electrical and mechanical properties of poly(ethylene oxide)-based ionomers as single ion conductors**
Fr D2.1 S. Dou, S. Zhang, J.P. Runt and R.H. Colby
(Invited talk)
Pennsylvania State University,USA

13.45 **Nano-pattern formation by grafted polymers in poor solvent**
Fr D2.2 S.K. Pattanayek[1], T.T. Pham[1] and G.G. Pereira[2]
[1] *University of Sydney, Sydney, Australia*
[2] *Victoria University of Wellington, Wellington, NZ*

14.00 **Thermotropic biaxial nematic liquid crystals**
Fr D2.3 L.A. Madsen, T.J Dingemans, M. Nakata and E.T. Samulski
University of North Carolina, Chapel Hill, USA

14.15 **Spatio-temporal oscillations and rheochaos in a simple model of shear banding**
Fr D2.4 S.M. Fielding and P.D. Olmsted
University of Leeds, Leeds, UK

14.30 **Spatially periodic orientational instability in nematic cell with finite director anchoring**
Fr D2.5 M.F. Lednei[1] and I.P. Pinkevich[2]
[1] *Kyiv National Taras Shevchenko University, Kyiv, Ukraine*
[2] *University of New South Wales, Sydney, Australia*

14.45 **Influence of oil-surfactant interactions on the stability of oil-in-water emulsion systems**
Fr D2.6 H. Egger[1], E-H Liu[2] and K. M. McGrath[1]
[1] *Victoria University of Wellington, Wellington, NZ*
[2] *University of Otago, Dunedin, NZ*

Electrical and Mechanical Properties of Poly(ethylene oxide)-based Ionomers as Single Ion Conductors

Shichen Dou, Shihai Zhang, James P. Runt and Ralph H. Colby
Materials Science and Engineering Department and Materials Research Institute, Pennsylvania State University, University Park, PA 16802, USA

Polyethers, such as poly(ethylene oxide) (PEO) are of interest for development of advanced lithium batteries because Li^+ ions have facile transport in this media. We make ionomers based on PEO by reacting poly(ethylene glycol) (PEG) oligomers with the sodium salt of dimethyl 5-sulfoisophthalate. The cation can be easily exchanged for another (such as Li^+ or Cs^+) by dialysis in the presence of the appropriate salt. Since the sulfonate group is covalently bonded to the chain, it is essentially immobile and hence these materials are single-ion conductors, with a lithium transference number of 1. The charge spacing on the chain can be directly controlled by the molar mass of the PEG oligomers (we use M = 400, 600 and 900). We can change the amount of Li^+ in the sample and the glass transition temperature, T_g, of the material by adding lithium salts (such as lithium perchlorate) and plasticizers (such as PEG). Conductivity depends strongly on temperature, with nearly identical conductivities in all of our samples at the same $T - T_g$. This observation , coupled with the Vogel termperature dependence of conductivity, strongly suggests that Li^+ ion transport is controlled by segmental motion of the PEO. Despite a dielectric constant of order 5, PEO-based materials have surprisingly facile lithium ion transport that suggests a specific interaction between PEO and Li^+, that likely involves the ether oxygens on PEO.

The figure below shows the frequency dependence of dielectric loss and conductivity, for the lithium ionomer prepared from M = 600 PEG, at three temperatures (80, 50 and 25 °C). The conductivity σ_0 is determined from the plateau level of the frequency-dependent conductivity. Measurement of conductivity is precluded by electrode polarization effects at low frequencies. Conductivity increases with temperature, showing a Vogel temperature dependence that is coupled with the segmental motion of PEO. For this reason, room temperature conductivity increases as the PEG precursor chains are lengthened, despite the reduction in lithium ion content. We surmise that only a small fraction of the Li^+ ions are free in PEO. Our current research is focused on quantifying the fraction of free Li^+, Na^+ and Cs^+ ions in these materials and identifying their surroundings using NMR spectroscopy (with Karl Mueller, PSU Chemistry) and oxygen-edge EXAFS (with Dan Fischer, NIST).

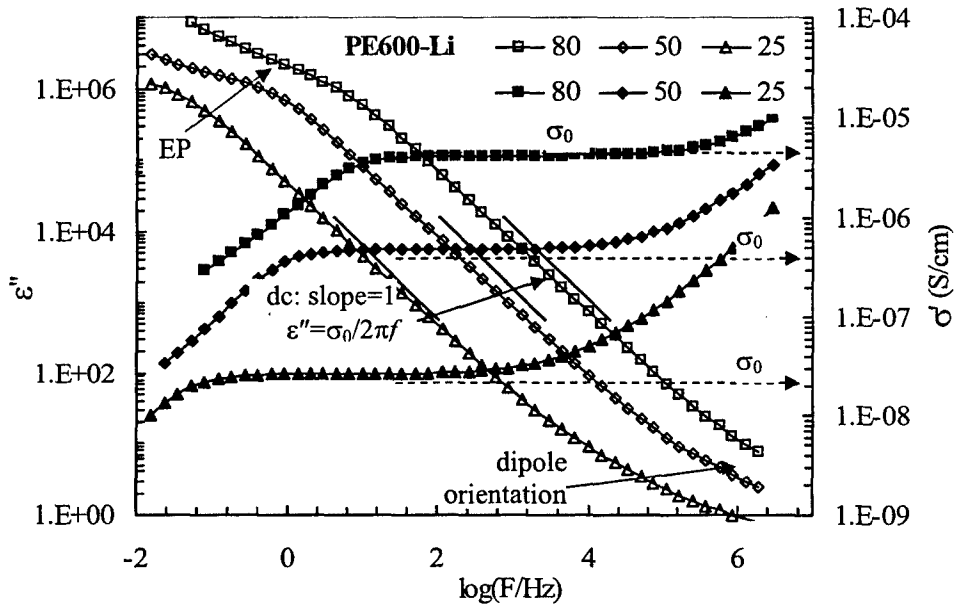

Nano-pattern formation by grafted polymers in poor solvent

S.K. Pattanayek [1], T.T. Pham [1] and G.G. Pereira [2,*]

[1] *Department of Mechanical Engineering, University of Sydney, NSW, 2006, AUSTRALIA*

[2] *School of Chemical & Physical Sciences, Victoria University of Wellington, PO Box 600 NEW ZEALAND*

Diblock copolymers naturally self-assemble into nano-scale patterns. Because of the potential application of these nano-patterns, as well as their inherent scientific interest, these block copolymers have received significant amounts of attention in the past few decades. The structures that form are a result of the (chemical) incompatibility between the different blocks as well as the fact that the different blocks are tethered together at their ends. In this case, the individual polymer chains are still free to move in the polymer melt. However, another interesting polymeric system is that of grafted polymers. Here one end of the chain is grafted (fixed) to a surface. It would be interesting to see if similar "nano-patterns" can be formed with these grafted systems. Earlier work on grafted polymer-solvent systems reveal that in good solvents, polymers are extended in solution due to favorable polymer-solvent interactions. In poor solvents, on the other hand, the polymer structure is of a more condensed form i.e., a globule-like structure, which is a result of the unfavourable polymer-solvent contacts. In poor solvents, when the grafting density is sufficiently high, a continuous polymer layer results. For low grafting density, pinned micelles form. In some theoretical works, "octopus micelles" are also predicted to form. An important question is: are these micelles arranged in certain patterns? From a theoretical point of view, the difficulties in studying this system lie in incorporating the grafted chain ends into our model.

We have used both self-consistent mean field theory (SCFT) for standard Gaussian chains, which has proven to be one of the best theoretical methods for studying macromolecular systems and Monte Carlo simulations to study this system. The polymers, which have N statistical segments, are attached to the xy plane ($z=0$) at one end. The other end is free to move in the solvent. Chains are grafted regularly and uniformly to a two-dimensional flat surface. At comparatively low grafting density, we observe the polymers condensing into micelles which arrange themselves into a regular hexagonal nano-pattern, when the polymers are in a poor solvent. The nano-pattern forms due to unfavorable polymer-solvent interactions as well as stretching of the polymer chains. We discuss how grafting density and polymer chain length affect the nano-pattern structure. At high grafting density we observe the formation of a "holey layer" which, in a sense, is an "inverted micelle". The Figure, below, shows a "holey layer". We continue on to study the behaviour of semi-flexible polymer chains grafted to a surface and find a myriad of novel micro-structures, including tower morphologies, toroidal and archway morphologies.

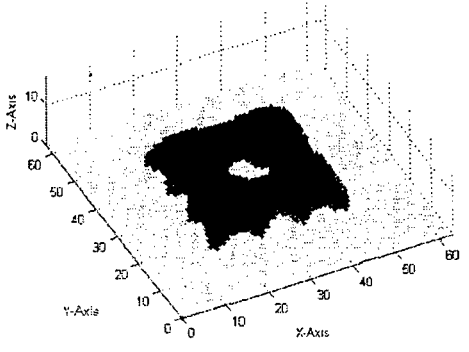

Contact author: Gerald.Pereira@vuw.ac.nz

Thermotropic Biaxial Nematic Liquid Crystals

Louis A. Madsen*, Theo J. Dingemans, Michi Nakata, and Edward T. Samulski

Departments of Chemistry and Materials Science
University of North Carolina, Chapel Hill, NC 27599-3290

Thermotropic nematic liquid crystals (LCs) with a second axis of symmetry, biaxial nematics, were theoretically predicted in 1970 [1]. Such materials may provide avenues for lower power and faster switching LCDs, as well as for a new class of robust LC polymers. Despite vigorous theoretical work, and many experimental efforts to observe them, the existence of these phases has never been confirmed.

We have synthesized LCs based on an oxadiazole biphenyl (ODBP) "boomerang-shaped" core that exhibit atypical calamitic LC phases in the 100-220°C range. Optical polarizing microscopy and conoscopy [2], and X-ray studies [3] have strongly indicated biaxiality in the ODBP nematics.

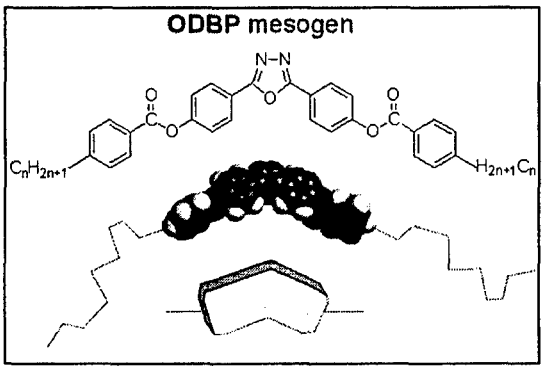

Fig.1. Boomerang-shaped mesogen and its abstraction

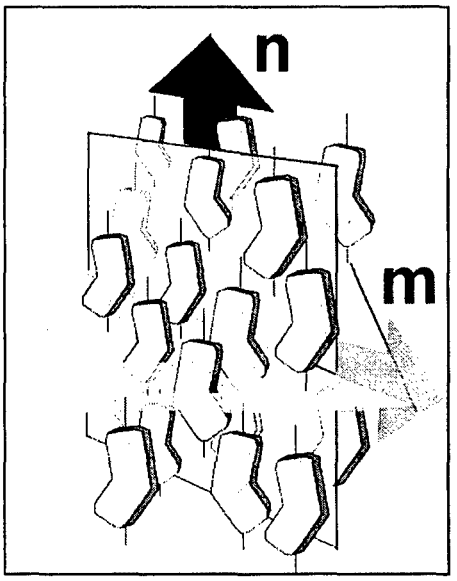

Fig. 2. Schematic illustration of an apolar biaxial nematic phase with major and minor directors **n** and **m**.

We have investigated the biaxiality in these LCs using a homebuilt high-T NMR apparatus to rotate samples about an axis perpendicular to the magnetic field. Rotating the sample creates an isotropic radial 2D distribution of director domains. A fit to the resulting "2D powder" NMR spectrum yields the biaxiality parameter η, which quantifies the biaxial order of the phase. The 2D powder spectra yield η up to 0.11 +/- 0.02 when fit with a detailed and proven theory, thus unambiguously confirming the existence of this phase [2]. We will present rotation NMR experiments on several biaxial nematics in the ODBP family, as well as on the uniaxial nematic TBBA, which has similar LC temperatures as the ODBPs but exhibits $\eta = 0$.

Relative to conventional biaxial-shaped calamitic mesogens, ODBP boomerangs have the added possibility of strong intermolecular associations originating from the large electric dipole moment (~ 4 Debye) of the oxadiazole ring. Such associations may help stabilize the biaxial nematic phase .

References

[1] M. J. Freiser, *Phys. Rev. Lett.* **24**, 1041 (1970).
[2] L. A. Madsen, T. J. Dingemans, M. Nakata, and E. T. Samulski, *Phys. Rev. Lett.* **92**, 145505 (2004).
[3] B. R. Acharya, A. Primak, T. J. Dingemans, *et al.*, *Pramana J. Phys.* **61**, 231 (2003).

* Contact author: lmadsen@email.unc.edu

Spatio-temporal oscillations and rheochaos in a simple model of shear banding

S. M. Fielding* and P. D. Olmsted
Polymer IRC, School of Physics & Astronomy, University of Leeds, Woodhouse Lane, Leeds. LS2 9JT. UK

Complex fluids commonly undergo flow instabilities and flow induced phase transitions that result in spatially heterogeneous "shear banded" states. Classically studied systems include wormlike micellar surfactants [1], lamellar onion phases [2] and polymer solutions [3]. Experimentally, the basic observation is of two coexisting shear bands with differing viscosity and microstructure. Theoretically, this is captured by invoking multiple flow branches in the constitutive relation of shear stress versus shear rate. The system then separates into a steady state comprising two shear bands, each on its own stable flow branch.

However an accumulating body of data shows this basic picture to be oversimplified: Many shear banding systems show oscillations or irregular fluctuations suggesting chaos [4]. In previous work, *tenporal* rheochaos was studied in *homogeneous* models of director dynamics in sheared nematics [5]; and of shear thickening systems with a single-branched flow curve [6]. Here we introduce a model of *spatio*-temporal rheochaos in *heterogeneous* shear banding systems with multi-branched constitutive curves.

Homogeneous flow has long been known to be unstable in any region of negative slope in the underlying constitutive relation. This is easily seen in models that take the stress and strain rate as the relevant dynamical variables. In more realistic models, these "mechanical" variables are coupled to microstructural quantities such as director orientation [7], micellar concentration [8] or micellar length [9]. This coupling can destabilize the rising high shear branch causing, *e.g.*, an instability to nematic wagging or tumbling in the high shear band.

Using this idea, we construct a model with an unstable high shear branch and demonstrate it to have a rich variety of oscillatory and rheo-chaotic shear banded flows. The talk will be structured as follows. After briefly introducing the model's main assumptions and governing equations, we will present our results for:

(i) The linear stability of the homogeneous constitutive curves at fixed stress, demonstrating that coupling of flow to micellar length causes a Hopf bifurcation to instability in the rising high shear branch.
(ii) The model's non linear homogeneous dynamics at fixed stress, demonstrating the existence of a stable limit cycle in which the shear rate and micellar length together oscillate about the unstable high shear branch.
(iii) Heterogeneous shear banded dynamics at fixed average strain rate. By varying the strength of this applied shear rate we will demonstrate several regimes including a) chaotically interacting high shear pulses that ricochet to and fro across the cell, b) oscillating "flip-flop" bands with a defect between them, c) chaotic interactions among multiple wandering defects. In regimes a) and c) we demonstrate a positive Lyapunov exponent.

We note that Chakrabarti et al have recently studied spatio-temporal chaos in a model of sheared director dynamics under imposed uniform strain rate, in which the local model was already chaotic [10] rather than simply oscillatory, as considered here. Study of shear thickening systems was undertaken in Ref. [11].

References

[1] M. M. Britton and P. T. Callaghan, Phys. Rev. Lett. 78 ,4930 (1997). J. F. Berret, G. Porte, and J. P. Decruppe,Phys. Rev. E 55 , 1668 (1997)
[2] O. Diat, D. Roux, and F. Nallet, J. Phys. II (France) 3 ,1427 (1993).
[3] L. Hilliou and D. Vlassopoulos, Ind. Eng. Chem. Res. 41,6246 (2002).
[4] S. M. Fielding and P. D. Olmsted, Phys. Rev. Lett. 92 084502 (2004) and references therein.
[5] M. Grosso, R. Keunings, S. Crescitelli, and P. L. Maffettone, Phys. Rev. Lett. 86 , 3184 (2001); G. Rienacker, A. Kroger, and S. Hess, Phys. Rev. E 66 , 040702 (2002).
[6] M. E. Cates, D. A. Head, and A. Ajdari, Phys. Rev. E 66 , 025202 (2002).
[7] P. D. Olmsted and P. M. Goldbart, Phys. Rev. A41 , 4578 (1990); ibid A46 , 4966 (1992).
[8] S. M. Fielding and P. D. Olmsted, Eur. Phys. J. E 11 , 65 (2003); Phys. Rev. Lett. 90 , 224501 (2003).
[9] M. E. Cates and M. S. Turner, J. Phys. Cond. Matt. 4 ,3719 (1992).
[10] B. Chakrabarti et al. Phys. Rev. Lett. 92, 055501 (2004).
[11] A. A. Aradian and M. E. Cates. Preprint cond-mat/0310660.

* Contact author: s.m.fielding@leeds.ac.uk

Spatially Periodic Orientational Instability in Nematic Cell with Finite Director Anchoring

M. F. Lednei[1] and I. P. Pinkevich[2,*]
[1]*Physics Faculty, Kyiv National Taras Shevchenko University, Kyiv 03022,UKRAINE*
[2]*School of Physics, University of New South Wales, Sydney 2052, AUSTRALIA*

Phenomena of director reorientation in nematic liquid crystals (LC) undergoing electric or magnetic fields are well known. In flexoelectric nematic cell at threshold director reorientation a spatially periodic structure can arise [1,2]. In spite of the orientational transition is a bulk effect, its main characteristics can depend essentially on the strength of director anchoring with the cell surface. We theoretically study the influence of the finite strength of director anchoring with the nematic cell surface on the director reorientation threshold and the spatial period of arising director structure in planeparallel flexoelectric nematic cell with initial planar director orientation. .

To investigate this effect one must include into consideration the surface free energy F_S of the LC cell. We take it in the Rapini-Papoluar model, namely,

$$F_S = -\frac{W_\varphi}{2}\int\cos^2\varphi\, dS - \frac{W_\theta}{2}\int\cos^2\theta\, dS, \quad W_\varphi, W_\theta > 0,$$

where φ,θ are the azimuthal and polar angles of a director with the easy orientation axis on the cell planes, W_φ, W_θ are the azimuthal and polar energies of director anchoring with the cell planes, respectively. After minimization of the full free energy of LC one can get the system of differential equations, which define the director orientation in the cell bulk with corresponding boundary conditions. In general case the only numerical solutions to these equations can be found. On figures below we show the calculated dependence of threshold electric field E_c and wave number Q of director periodic structure, which arise at $E > E_c$ for the case of the azimuthal anchoring parameter $\varepsilon_\varphi = W_\varphi K/L$ is arbitrary, $W_\theta = \infty$. Here K is an elastic constant, L is a nematic cell thickness, and we designated the values of flexoelectric parameter $\nu = \varepsilon_a K/4\pi e^2$ by the numbers as follows, ν=0.2 –1, 0.5 – 2, 0.7 – 3, 0.9 – 4, 1.2 – 5, 1.4 – 6, 1.6 – 7, 1.8 – 8. ε_a is an anisotropy of dielectric susceptibility, e is a difference of flexoelectric coefficients.

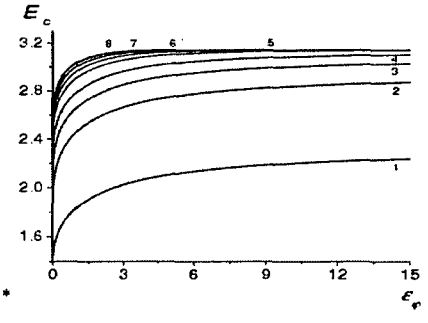

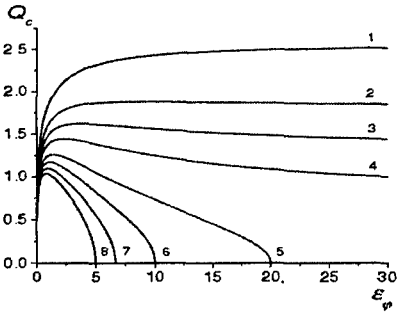

We have shown that to obtain the director periodic structure the flexoelectric parameter ν must satisfy the condition $\nu < 1 + 4/\varepsilon_\varphi$. We studied the case of arbitrary values of the director polar anchoring energy W_θ as well.

Thus the value of director anchoring energy with the cell surface determines not only the threshold electric field value and the director structure period but also the area of values of flexoelectric parameter ν at which the spatially periodic director reorientation takes place. At that in the case of finite values of the azimuthal anchoring energy this area enlarges, and in the case of finite values of the polar anchoring energy it gets narrow in comparison with the case of the infinitely rigid director anchoring

References

[1] Y.P. Bobylev, V.G. Chigrinov , S.A. Pikin, J.de Phys.Coll. **40**, C3-331 (1979).
[2] V.P. Romanov, G.K. Sklyarenko, ZhETF, **116**, 543 (1999).

* Contact author: i_pinkevych@hotmail.com

Influence of oil-surfactant interactions on the stability of oil-in-water emulsion systems

H. Egger[1,*] E.-H. Liu[2], and K. M. McGrath[1]
[1] *School of Chemical and Physical Sciences, Victoria University of Wellington, POBox 600, Wellington, NEW ZEALAND*
[2] *Department of Chemistry, University of Otago, POBox 56, Dunedin, NEW ZEALAND*

Emulsions are dispersions of at least two immiscible components (water and oil) kinetically stabilized by a surfactant working as an emulsifier. Emulsions play a fundamental role in a huge variety of different areas, including e.g. food, cosmetics and paints. The droplet diameter of the dispersed phase is of the order of a few hundred nano to several micrometres depending on the chemicals used as well as the formulation energy. Emulsion stability can vary from a few seconds up to several years. Various mechanisms, like e.g. coalescence or flocculation, can lead to their destabilisation. But despite their technical importance little work was focussed on the basic understanding of these systems from a kinetic perspective [1,2], particularly the interaction of the solvents with the emulsifier. These interactions are crucial for the stability of the amphiphilic film and therefore the kinetics occurring in emulsions are very often unknown or not well understood.

The aim of this work is to understand the different destabilisation mechanisms arising in these systems and to explain the influence of the oil on the properties of the interfacial film. The established opinion on emulsion stability is that it is directly correlated to the rigidity of the emulsifier and the mutual solubility of the solvents. Increasing the rigidity of the emulsifier (e.g. protein emulsifiers in biological systems) and/or decreasing the solubility of the solvents is believed to increase the stability of the emulsion. Even if this simplified picture works for a general classification of different emulsions, it cannot explain the important interactions in detail and therefore it fails quite often if the differences, like e.g. the nature of the oil or the emulsifier, are not very pronounced.

To clarify these destabilisation processes we have chosen systems consisting of just three components, water, triton X-100, a commercial non-ionic surfactant as emulsifier and different hydrocarbons as the oil. Rheology, particle correlation spectroscopy, PGSE-NMR and TEM were used to study the structure of these systems as a function of time. When toluene was used as the oil, for example, different microstructures could be identified depending on the composition of the samples. Unexpectedly, it was shown that two seemingly quite similar droplet phases followed nonequivalent destabilisation processes [3].

In the present study, *n*-octane and *n*-tetradecane were used as the oil. Stable emulsions could be prepared at an oil-to-surfactant-mass-ratio of 5:1 and with 8 to 12 wt-% surfactant at 25°C. Since the two oils differ only in the length of the alkane chain, a very similar behaviour, say kinetics that differ only in their time constant, could be expected in general. But to the contrary our measurements reveal that these two systems behave quite differently. While in the tetradecane system the initially formed oil droplets grow uniformly with time, the octane system shows a much more complex breakdown mechanism due to the different interactions in the interfacial region. After the initial formulation of quite unstable droplets, the octane system seems to follow at least two different destabilisation mechanisms [4]. Moreover, emulsions with different mixing ratios of the two oils mentioned above were investigated to elucidate how this would influence the kinetics of the system.

References

[1] D. E. Tambe, and M. M. Sharma, J. Colloid Interface Sci. **157**, 244 (1993).
[2] A. Kabalnov, and H. Wennerström, Langmuir **12**, 276 (1996).
[3] E.-H. Liu, P. T. Callaghan, and K. M. McGrath, Langmuir **19**, 7249 (2003).
[4] E.-H. Liu, H. Egger, P. T. Callaghan, and K. M. McGrath, in preparation.

* holger.egger@vuw.ac.nz

SESSION Fr E2
CLUSTERS AND NANOPARTICLES

Friday 11 February 2005 **1320–1500**

Copthorne III

Session Chair **Simon Brown, University of Canterbury, NZ**

13.20 **Unusual electronic transport properties in thin polycrystalline bismuth films**
Fr E2.1 R.L. Rosenbaum[1] and J. Galibert[2]
(Extended Oral Talk)
[1] *Tel Aviv University, Ramat Aviv, Israel*
[2] *Magnétiques Pulsés, Toulouse, France*

13.45 **The synthesis of silicon nanoparticles for biomedical applications**
Fr E2.2 R.D. Tilley and J.H. Warner
Victoria University of Wellington, Wellington, NZ

14.00 **Cluster-assembled wires with nano-scale widths**
Fr E2.3 J.G. Partridge[1,2], S.A. Brown[1,2,3], R. Reichel[1,2], M. Kaufmann[1,2], A. Ayesh[1,2] and K.C. Tee[1,3]
[1] *University of Canterbury, Christchurch, NZ*
[2] *The MacDiarmid Institute for Advanced Materials and Nanotechnology, NZ*
[3] *Nanocluster Devices Ltd., University of Canterbury, Christchurch, NZ*

14.15 **Structure and thermal stability of small gold nanoclusters**
Fr E2.4 B. Soulé de Bas, M.J. Ford and M.B. Cortie
University of Technology, Sydney, Australia

14.30 **Self-assembly of nanoscale Bi and Sb surface islands**
Fr E2.5 S.A. Scott[1,2], S.A. Brown[1,2] and M.V. Kral[1]
[1] *University of Canterbury, Christchurch, NZ*
[2] *MacDiarmid Institute for Advanced Materials and Nanotechnology, NZ*

14.45 **Molecular dynamics simulations of soft-landing cluster deposition**
Fr E2.6 A. Awasthi[1], S.C. Hendy[1,2,3], P. Zoontjens[2,3] and S.A. Brown[2,4]
[1] *Industrial Research Ltd., Lower Hutt, NZ*
[2] *MacDiarmid Institute for Advanced Materials and Nanotechnology, NZ*
[3] *Victoria University of Wellington, Wellington, NZ*
[4] *University of Canterbury, Christchurch, NZ*

Unusual Electronic Transport Properties in Thin Polycrystalline Bismuth Films

R. L. Rosenbaum[1,*] and J. Galibert[2]
[1]*School of Physics and Astronomy, Tel Aviv University, Raymond and Beverly Faculty of Exact Sciences, Ramat Aviv, 69978, ISRAEL*
[2]*Laboratoire National des Champs Magnétiques Pulsés – LNCMP, BP 4245, 143 Avenue de Rangueil, Toulouse, Cedex 4, 31432, FRANCE*

Bismuth (Bi), a semimetal, has unusual electronic properties due to its low carrier number concentrations of electrons and holes (about $3*10^{18}$ carriers/cm^3 at 300 K), small carrier effective masses and a highly anisotropic Fermi surface. In single crystals, these characteristics lead to very large magnetoresistance (MR) and quantum oscillations at low temperatures. In contrast, the electronic transport behavior in thin polycrystalline bismuth films differs remarkably from those of bulk samples or epitaxial film samples. For example, the zero field resistivity in a polycrystalline film increases upon cool down to liquid helium by about a factor of four; this increase results from decreases in both the electron and hole carrier densities by a factor of ten upon cool down to liquid helium temperatures. In contrast, the bulk sample or epitaxial film displays a resistivity that decreases by one or two orders of magnitude. In addition, the polycrystalline film exhibits a magnetoresistance (MR) behavior in a *perpendicular* magnetic field that increases only by a factor of four; in contrast the bulk or epitaxial sample displays a *perpendicular* MR that increases by at least several orders of magnitude.

The Hall voltage V_{Hall} and its related Hall coefficient R_{Hall} are anomalous in polycrystalline bismuth films. This work presents experimental data in both the *perpendicular* and *parallel* field orientations over a wide range of temperatures and magnetic fields. In the *perpendicular* orientation, the field is directed perpendicular to the mica substrate of the film (hence parallel to the trigonal axes) and perpendicular to the current flow; in this classical orientation, the measured Hall voltages are large and on the order of a few mV, owing to the very low carrier number concentrations. Hence, these films are candidates for sensitive magnetic field sensors. Surprisingly, the Hall coefficient data, $R_{Hall} = V_{Hall}d/IB$, are field *dependent* and can be described nicely by the *two carrier* expression of Fawcett [1] and Pippard [2]. In the above expression, d is the film thickness, I is the current and B is the magnetic field. The Hall voltage data in the *parallel* field orientation are completely anomalous. In this orientation the field is directed parallel to the current and also parallel to the mica substrate of the film. The Lorentz force should be very small or negligible in this *parallel* orientation, and hence the Hall voltage should be negligible too. But owing to diffused and specular scattering of the carriers at the grain boundaries, the velocities of the carriers are redirected, leading to sizable Lorentz forces on the carriers. The *parallel* Hall voltages are *large* and about five times smaller than the Hall voltages measured in the classical *perpendicular* orientation. The Pippard-Fawcett (P-F) model fits the data well [1,2]. Also the sign of the Hall voltage depends upon the film thickness. For films thinner than about 7000 Å, the sign is *positive*; in thicker films the sign is always *negative*. The Pippard-Fawcett model suggests that the sign of V_{Hall} depends upon the magnitude of the hole mobility relative to magnitude of the electron mobility.

We have also made measurements in the *transverse* field orientation, where the field is directly parallel to the film surface but perpendicular to the current. In this unusual orientation, the Lorentz force directs the carriers either to the top surface (the bismuth – air interface) or to the bottom surface (the bismuth – mica interface). If the film is sufficiently thin, the carriers will undergo partially diffused scattering at the two surfaces. This process is lossy. However upon application of a sufficiently strong *transverse* field, the cyclotron radius of the carrier is shortened sufficiently to prevent the carrier from colliding with the surfaces [3]. Hence this lossy mechanism is eliminated, and the resistance of the sample is reduced. This effect is nicely illustrated in the *transverse* MR data of the thin polycrystalline bismuth films. The data are fitted using the P-F model [1,2] together with the Way-Kao model [3].

A part of this work was performed at the National High Magnetic Field Laboratory (NHMFL), which is supported by the NSF Cooperative Agreement No. DMR 9527035 and by the State of Florida. We greatly thank the Centre National de la Recherche Scientifique and the Université Paul Sabatier et INSA de Toulouse for supporting the pulsed magnetic research phase of this research at Laboratoire National des Champs Magnétiques Pulsés (LNCMP).

References

[1] E. Fawcett, Advances in Phys. **13**, 139 (1964).
[2] A. B. Pippard, *Magnetoresistance in Metals* (Cambridge University Press, Cambridge, 1989) p.29.
[3] Yuan-Shun Way and Yi-Han Kao, Phys. Rev. B **5**, 2039 (1972).

*Contact author: ralphr@post.tau.ac.il or rachel-r@zahav.net.il

The Synthesis of Silicon Nanoparticles for Biomedical Applications

Richard D. Tilley* and Jamie H. Warner

The MacDiarmid Institute of Advanced Materials and Nanotechnology, New Zealand.
School of Chemical and Physical Sciences, Victoria University of Wellington, PO Box 600, Wellington, New Zealand.

Research in the field of semiconductor nanocrystals synthesized in solution has been intense since the formation of cadmium selinide quantum dots by Murray et al 1993 [1]. One of the most promising applications for quantum dots formed in the liquid phase is as biological imaging chromophores. Silicon quantum dots have intense luminescence throughout the visible spectrum due quantum confinement as first reported in porous silicon by Canham [2]. Silicon quantum dots offer the possibility of less toxic replacements to organic dyes in biological imaging when compared to cadmium selinide quantum dots [3].

Silicon nanocrystals have been synthesized in micelles using powerful hydride reducing agents and a number of surfactants. The effect of the surfactant and reducing agent on the size of the silicon nanoparticles and the size distribution will be discussed with a focus on the achievement of uniform sized silicon nanocrystals with sharp emission in the visible region. Particle sizes have been ascertained by transmission electron microscopy, figure 1, and UV-Vis absorption and photoluminescence spectroscopies.

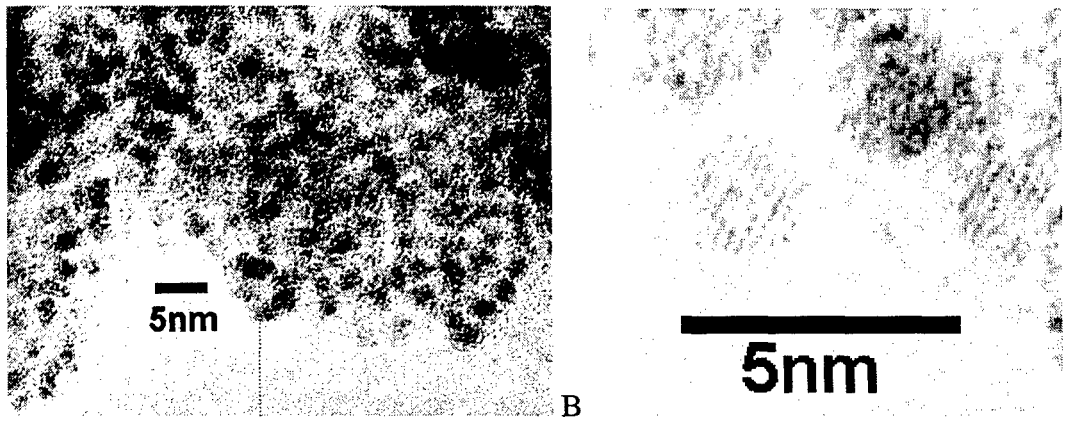

Figure 1: *A) TEM image of 2nm uniform sized 1-heptene capped silicon nanoparticles and B) enlargement*

For biological applications control of the surface character of the nanocrystals is essential. The surface of the silicon particles produced have been modified to produce hydrophobic and hydrophilic particles by reaction with either with 1-heptene or allylamine respectively. FTIR spectra show the surface modification of the particles by 1-heptene or allylamine. The hydrophobic particles have been used in subsequent investigations as bio-imaging agents in cells.

References

[1] C.B.Murray, D.J.Norris and M.G. Bawendi, *J. Am. Chem. Soc.* 1993, *115,* 8706.

[2] L. T. Canham, *Appl. Phys. Lett.* 1990, *57,* 1046.

[3] A. M Derfus, W. C. M. Chan and S. N. Bhatia, *Nano Letters* 2004, *4,* 11.

Cluster-assembled wires with nano-scale widths

J. G. Partridge[1,2], S. A. Brown[1,2,3], R. Reichel[1,2], M. Kaufmann[1,2], A. Ayesh[1,2] and K. C. Tee[1,3]
[1] *Department of Physics and Astronomy, University of Canterbury, Christchurch, NEW ZEALAND*
[2] *The MacDiarmid Institute for Advanced Materials and Nanotechnology, NEW ZEALAND*
[3] *Nanocluster Devices Ltd., University of Canterbury, Christchurch, NEW ZEALAND*

Atomic clusters exhibit a range of useful electronic, chemical and magnetic properties, and show great potential as building blocks for nanoscale electronic and photonic devices. To date, self-assembly of cluster structures has relied on surface diffusion of clusters, or of atoms which aggregate to form clusters.

We report here a templated-assembly method which results in supported self-contacting wires, formed from Bi, Sb or Ag clusters on passivated silicon substrates. These wires have widths down to 100nm and lengths in excess of 100μm. The constituent clusters in these wires are deposited onto the substrates from an inert gas aggregation source. The template in this process is a simple V-groove which is etched into the silicon wafer using KOH solution (40% wt). The momentum of the deposited clusters causes them to bounce or slide to the apex of the V-groove, where they assemble into a wire.

Initially, non-contacted Bi, Sb and Ag wires were produced on arrays of V-grooves and a model was developed to describe the assembly of clusters in V-grooves as a function of the inert gas flow-rate into the source. (Control of the flow-rate of argon gas into the inert gas aggregation source allowed control over the cluster velocity and hence the morphology and width of the wires formed). The validity of the model was tested using various masses of clusters and the source conditions were then optimized to produce compact wires with minimal possibility of conduction occurring outside of the V-grooves.

Subsequently, contacted wires were produced on substrates which were pre-patterned with planar contacts using standard optical lithography. Multiple contacted V-grooves were formed on each 10x10mm passivated silicon substrate. These substrates were then mounted on a cold-finger in a high vacuum deposition chamber. The conduction between the contact pairs on each substrate was monitored throughout the cluster deposition experiment and upon completion of a wire(s), an onset of current flow was observed. Figure 1. shows a pair of contacted Sb cluster-assembled wires (width ~300nm) between two contacts (separation 50μm) and the observed onset of conduction.

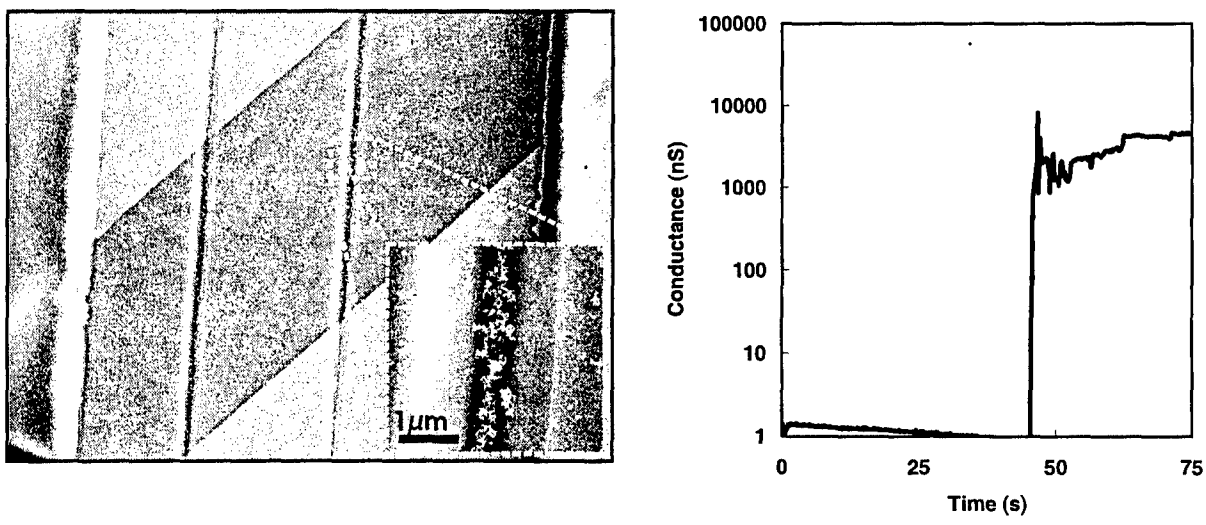

Figure 1. Dual Sb cluster-assembled wires and their associated onset of conduction

Structure and Thermal Stability of Small Gold Nanoclusters

B. Soulé de Bas*, M. J. Ford and M. B. Cortie
Institute for Nanoscale Technology, University of Technology, Sydney, NSW, AUSTRALIA

A structural investigation of small gold clusters was undertaken using a combination of first principle calculations and semi-empirical potential. A Simulated Anneal (SA) with Lennard-Jones and n-body Gupta potentials was used as a first stage optimisation to locate low energy candidates for the *ab initio* structure relaxation. The first principle calculations were carried out using Density Functional Theory (DFT) in the Local Density Approximation as implemented in the SIESTA package [1]. With using this combined scheme of semi-empirical and *ab initio* calculations we investigated the geometry of Au_n, n = 3 to 38 [2].
Here we complement the previous investigation by studying the thermal stability of Au_7, Au_{13} and Au_{20} using isothermal *ab initio* Molecular Dynamics (MD) [1]. For each cluster sizes two different isomers were investigated to compare their relative stabilities. Series of isothermal MD simulations were performed on the global minima for the three sizes reported in [2] and on the Au_7 optimum planar structure [2], the Au_{13} icosahedron and the Au_{20} second lowest energy structure [2]. Discrepancies in the estimated melting temperatures between the three sizes and the isomers were observed. Transition structures as well as a diffusion mechanism were also revealed by the simulations.

References

[1] J M Soler, E Artacho, J D Gale, A Garcia, J Junquera, P Ordejón, D Sánchez-Portal, J. Phys.: Condens. Matter **14**, 2745 (2002).

[2] B Soulé de Bas, M J Ford, M B Cortie, J. Mol. Struct. (Theochem), in press.

* Contact author: benjamin.souledebas@uts.edu.au

Self-Assembly of Nanoscale Bi and Sb Surface Islands

S. A. Scott[1,2], S. A. Brown[1,2*], and M. V. Kral[3]
[1] *Nanostructure Engineering Science and Technology Group (NEST) and The MacDiarmid Institute for Advanced Materials and Nanotechnology , Christchurch, NEW ZEALAND*
[2] *Department of Physics and Astronomy, University of Canterbury, NEW ZEALAND*
[3] *Department of Mechanical Engineering, University of Canterbury, NEW ZEALAND*

The spontaneous formation of patterns in nature has been a source of fascination for many decades. There is a conspicuous similarity between the self-organized patterns observed in snowflake growth, viscous fingering, electro-deposition, bacterial growth, and across many other fields of science [1]. The common thread which links these seemingly different processes is their non-equilibrium growth environment, which results from a diffusion field at the structure's boundary.

A very interesting and potentially technologically important non-equilibrium system is the nucleation and growth of thin films from the vapor phase. Particles deposited on atomically flat and weakly interacting substrates can diffuse over substantial distances. Their migration comes to an end when they collide with another adatom (or defect trap) to nucleate an island. There exists a thermodynamic tendency to minimize the free energy of these surface islands, leading to compact structures. However the continuous diffusion of particles to the island boundaries often leads to dendritic and irregular morphologies, where the kinetics of diffusion is the driving force. An understanding of this delicate interplay between kinetics and thermodynamics can allow the self-assembly of nanoscale surface features with tailored shapes, structures, and properties.

Diffusion and aggregation of Sb_4 and Bi_2 on graphite surfaces have been studied. Deposition was performed under ultra high vacuum conditions at room temperature. The resulting Sb and Bi islands were investigated with scanning electron microscopy (SEM), atomic force microscopy (AFM) and electron backscatter diffraction (EBSD). For Sb_4 we show how altering the growth parameters shifts the balance between kinetics and thermodynamics, resulting in a transition from compact to branched structures (Figure 1).

A new allotropic thin film phase of bismuth has recently been reported on silicon [2], in which layer pairing of {01-12} planes produces very flat rotationally disordered islands on a wetting layer. In the Bi_2/Graphite system we show that the flat islands characteristic of this thin film phase, together with the allotrope's linear atomic chains lead to the formation of some striking examples of spontaneous pattern formation, including nanostars and nanorods (Figure 2). The Bi/Graphite islands grow in the absence of a wetting layer, and with in-plane island rotations matched to the high symmetry directions of the substrate. We have characterized a 6-point star morphology, which grows 2-dimensionally at a fixed height of order 1nm. The morphologies depend on the competition between kinetics and thermodynamics and hence the growth conditions, and can be shifted to more compact hexagonal forms, and also branched morphologies with little evidence of 6-fold symmetry. In the case of the anisotropic diffusion field near the natural step-edges of graphite, the aggregates become rod-like, producing ordered arrays of nanorods on the graphite surface.

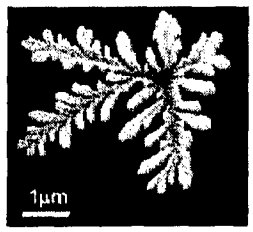

Figure 1: AFM image of an antimony dendrite

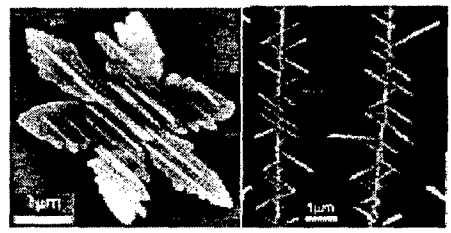

Figure 2: AFM image of a self-assembled bismuth nanostar, and a SEM image of an array of bismuth nanorods

References

[1] E. Ben-Jacob and P. Garik, Nature **8**, 523 (1990).
[2] T. Nagao *et al*, Phys. Rev. Lett. **93**, 105501 (2004).

* Contact author: simon.brown@canterbury.ac.nz

Molecular dynamics simulations of soft-landing cluster deposition

A. Awasthi[1], S. C. Hendy[1,2,3*], P. Zoontjens[2,3], S. A. Brown[2,4]
[1] *Industrial Research Ltd, PO Box 31-310, Lower Hutt, NEW ZEALAND*
[2] *MacDiarmid Institute for Advanced Materials and Nanotechnology*
[3] *Victoria University of Wellington, PO Box 600, Wellington, NEW ZEALAND*
[4] *Department of Physics and Astronomy, University of Canterbury, Christchurch, NEW ZEALAND*

The bouncing of clusters off a surface appears to have played an important role in recent experiments on the templated assembly of cluster-based nanowires [1]. A microscale analogue of cluster bouncing is the bouncing of liquid droplets off surfaces. Whether a microscale liquid droplet bounces off a surface depends on the ratio of droplet kinetic energy to the energy of adhesion to the surface, which is related to wetting angle of the droplet on the surface [2]. The purpose of this study is to improve our understanding of the bouncing process in nanoscale clusters using molecular dynamics simulations.

The molecular dynamics simulations were carried out to study the conditions under which solid clusters impacting on a surface may be reflected from or bounce off a surface. All interatomic interactions were modelled using the Lennard-Jones potential. The cluster-surface interaction energy, the angle of incidence and the impact velocity were all varied for clusters of 1000-2000 atoms. The results were then compared with the predictions of the liquid droplet model [2].

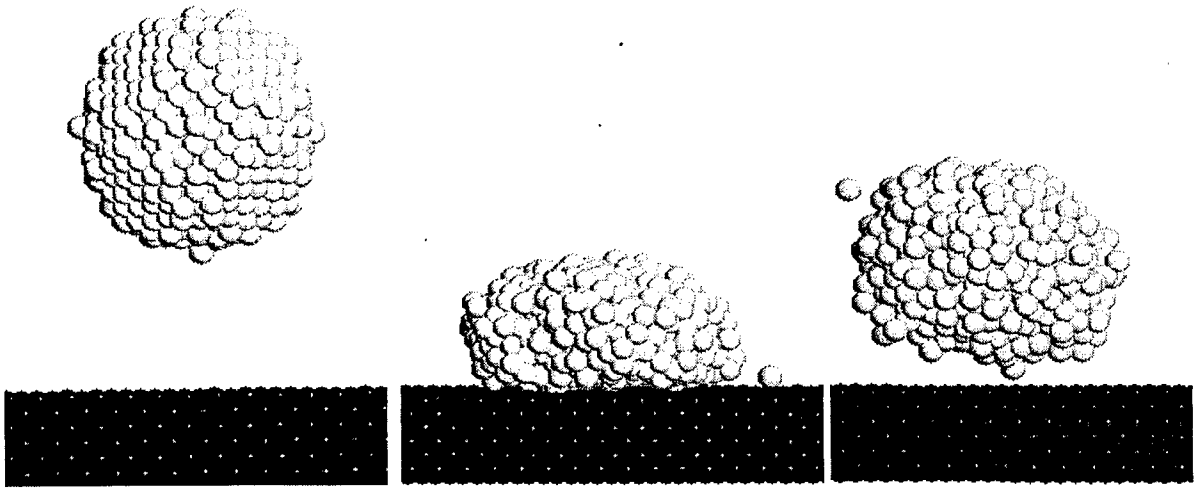

References

[1] J.G. Partridge, S.A. Brown et al, "Template-assembled antimony cluster mesowires and nanowires", IEEE Transactions on Nanotechnology **3**, 61 (2004).

[2] Hartley G S and Brunskill R T 1958 in Danielli J F, Pankhurst K G A and Riddiford A C (Eds.) *Surface Phenomena in Chemistry and Biology* (Pergamon: London) 214.

* Contact author: s.hendy@irl.cri.nz

Friday 11 February
Oral Session Three

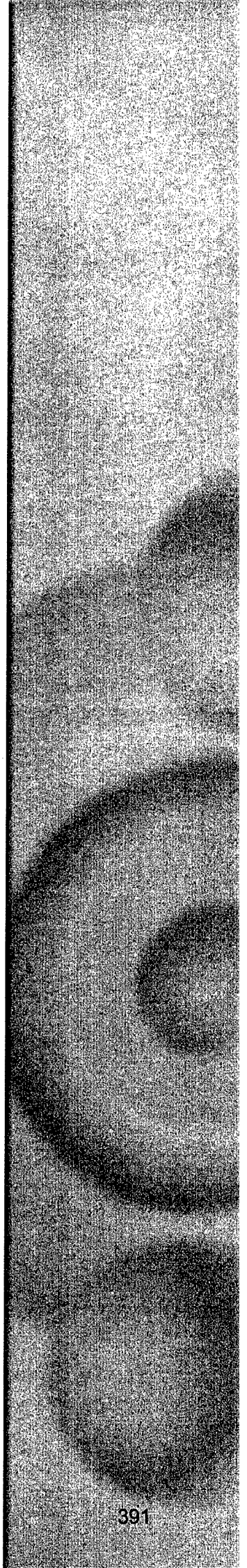

SESSION Fr A3
MATERIALS FOR SPINTRONICS

Friday 11 February 2005 **1530–1710**

Galaxy I

Session Chair **Robert Kinsey, University of Canterbury, NZ**

15.30 **Magnetism in transition-metal-substituted wide bandgap semiconductor systems: towards new materials for spintronics**

Fr A3.1 A.S. Risbud and R. Seshadri
(Extended Oral Talk)
University of California, Santa Barbara, USA

15.55 **Novel magnetic nanostructures: epitaxial cobalt films and wires in transparent fluoride matrix**

Fr A3.2 N. Yakovlev[1], A. Kaveev[2], N. Sokolov[2], B. Krichevtsov[2] and A. Huan[1]
[1] *Institute of Materials Research and Engineering, Singapore*
[2] *Ioffe Physico-Technical Institute, St.Petersburg, Russia*

16.10 **Room temperature ferromagnetism in the $In_{1-x}Cr_xN$ system: a magnetic and optical study**

Fr A3.3 P.A. Anderson[1], R.J. Kinsey[1], C.E. Kendrick[1], L.Williams[1], R.J. Reeves[1], A. Asadov[1], W. Gao[2], V.J. Kennedy[3], A. Markwitz[3] and S.M. Durbin[1]
[1] *University of Canterbury, Christchurch, NZ*
[2] *University of Auckland, Auckland, NZ*
[3] *Institute of Geological and Nuclear Sciences, Lower Hutt, NZ*

16.25 **Growth and characterisation of rare earth nitride thin films**

Fr A3.4 F. Budde[1], B.J. Ruck[1], S. Granville[1], A. Koo[1], H.J. Trodahl[1]and A. Bittar[2]
[1] *Victoria University of Wellington, Wellington, NZ*
[2] *Industrial Research Ltd., Lower Hutt, NZ*

16.40 **Properties of nanocrystalline GaN:Mn thin films**

Fr A3.5 S. Granville[1], F. Budde[1], S. Flewett[1], A. Koo[1], B. Ruck[1], H.J. Trodahl[1], A. Bittar[2], G.V.M. Williams[2], V.J. Kennedy[3], A. Markwitz[3] and J. Cairney[4]
[1] *Victoria University of Wellington, NZ.*
[2] *Industrial Research Ltd., Lower Hutt, NZ*
[3] *Institute of Geological and Nuclear Sciences, Lower Hutt, NZ*
[4] *University of New South Wales, Sydney, Australia.*

16.55 **Hole-induced ferromagnetism in Mn-doped ZnO films grown by reactive sputtering**

Fr A3.6 H.J. Kim[1], J.H. Sim[2], H. Kim[2], S.K. Hong[2], D. Kim[2], Y.E. Ihm[2] and W.K. Choo[1]
[1] *Korea Advanced Institute of Science and Technology, Daejeon, Korea.*
[2] *Chungnam National University, Daejon, Korea.*

Magnetism in Transition-Metal-Substituted Wide Bandgap Semiconductor Systems: Towards New Materials for Spintronics

A.S. Risbud[C] and R. Seshadri
Materials Department, University of California, Santa Barbara, CA 93106, USA

Spintronics, or spin-based electronics, can utilize both the spin and charge of electrons to enhance existing devices or create new ones, such as the Datta-Das spin transistor proposed in 1990 [1].
The search for spintronic devices has led naturally into the need for materials that combine both ferromagnetic and semiconducting properties. Such materials, called dilute magnetic semiconductors (DMSs) include systems such as ZnO:tM, and GaN:tM, where tM is a transition metal such as Fe, Co, or Mn. ZnO has been predicted [2] to be a DMS with five percent transition metal substitution and $10^{20}/cm^3$ hole doping. We have synthesized and studied bulk ZnO:tM materials, namely $Zn_{1-x}Co_xO$ and $Zn_{1-x}Mn_xO$ with $0.00 < x < 0.15$, using an oxalate decomposition technique in order to determine the exact nature of magnetic interactions in the system. Oxalates are suitable precursors as they allow for a random mixing of tM atoms on a crystalline lattice. We find for all well-characterized ZnO:tM systems (characterization includes powder x-ray diffraction and transmission electron microscopy, along with magnetization measurements), the nearest-neighbor coupling is antiferromagnetic. Our experimental and computational results indicate no robust ferromagnetism can be present in ZnO:tM without hole doping [3].

Based on our previous results, it seems that ZnO:tM is not an ideal system for a dilute magnetic semiconductor. Instead, we hope to utilize the inherent anti-alignment of spins in the spinel crystal structure (Figure 1), in order to produce bulk materials that require no conduction electrons for magnetic ordering. An example of such a system is the wide bandgap semiconductor $ZnGa_2O_4$ substituted with the spinel magnetite Fe_3O_4 in order to produce a dilute *ferrimagnetic* semiconductor. Nominal solid solutions $[ZnGa_2O_4]_{1-x}[Fe_3O_4]_x$ were prepared using an oxalate decomposition route similar to that for ZnO:tM, with $0.00 < x < 0.15$. These materials were characterized using x-ray diffraction, UV-Vis reflectance measurements, Mössbauer spectroscopy, and SQUID magnetization measurements. Magnetization as a function of applied field for the $[ZnGa_2O_4]_{1-x}[Fe_3O_4]_x$ samples with $x = 0.05$, 0.10, and 0.15 indicate ferrimagnetic behavior (Figure 2). Along with these results, forthcoming studies on GaN:tM and the novel wurtzite- structured CoO will be presented.

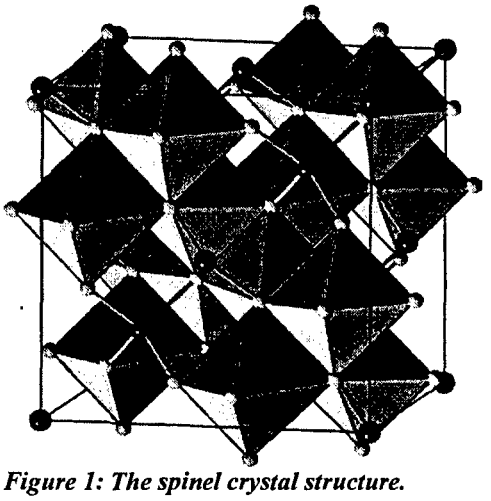

Figure 1: The spinel crystal structure.

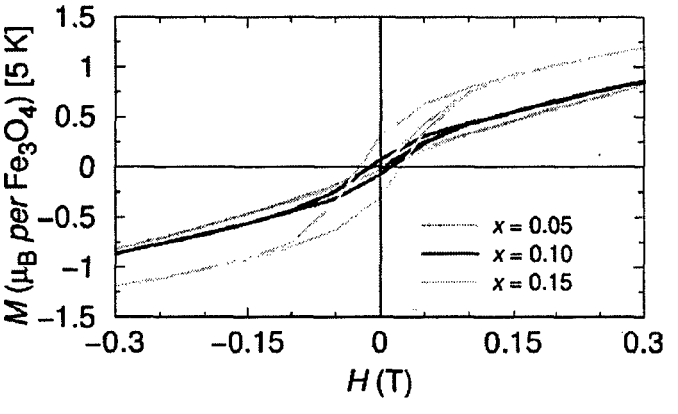

Figure 2: Magnetization as a function of applied field for $[ZnGa_2O_4]_{1-x}[Fe_3O_4]_x$.

References

[1] S. Datta and B. Das. *Appl. Phys. Lett.*, **56** (1990) 665.
[2] T. Dietl, H. Ohno, F. Matsukara, J. Cibert, and D. Ferrand. *Science*, **287** (2000) 1019.
[3] A.S. Risbud, N.A. Spaldin, Z.Q. Chen, S. Stemmer, and R. Seshadri. *Phys. Rev. B*, **68** (2003) 205202.

• [C]ontact author: aditi@engineering.ucsb.edu

Novel Magnetic Nanostructures: Epitaxial Cobalt Films and Wires in Transparent Fluoride Matrix

N. Yakovlev [1,*], A. Kaveev[2], N. Sokolov[2], B. Krichevtsov[2] and A. Huan[1]
[1] *Institute of Materials Research and Engineering, 117602 Singapore.*
[2] *Ioffe Physico-Technical Institute, St.Petersburg 194021 Russia.*

Studies of magnetic materials and nanostructures are stimulated by their broad use in various types of data storage. Optical properties of magnetic structures are of interest in connection with specific applications such as magnetic field detection, control of light using magnetic field, as well as investigation of physics of light interaction with magnetic media. The present work is magneto-optical study of thin epitaxial cobalt layers of different morphology on transparent CaF_2 buffer layers on silicon. Their magnetization was measured by magneto-optical Kerr effect (MOKE), which can be significantly enhanced due to light interference in $CaF_2/Co/CaF_2/Si$ structure.

Single crystal CaF_2 layers were grown by molecular beam epitaxy to have atomically flat (111) surface on Si(111) [1] and goffered (110) surface with {111} facets on Si(100) [2]. It was revealed by reflection high energy electron diffraction that in both cases, Co grows in the face centred cubic lattice at a temperature below 500°C. The axes of Co lattice coincide with those of CaF_2. The factors suppressing hexagonal lattice growth are: templating effect of the fluoride, high lattice mismatch with consequent high strain, kinetics of Co nucleation in the conditions far from thermodynamic equilibrium. On $CaF_2(111)$ surface at sufficiently low temperature, Co grows as a smooth uniform layer, as measured by atomic force microscopy. On the goffered (110) surface, there is nucleation of clusters in the bottom of the grooves; coalescence of the clusters makes a nano-wire. At increasing the temperature, there are more isolated clusters growing with {100} and {111} facets.

Fluoride layers have significant effect on MOKE in these structures. Depending on the thickness of cobalt and fluoride layers, Kerr rotation can have different signs at the same direction of magnetisation of Co layer. In polar geometry, the rotation at saturation field can reach even 1 degree from a modest 3 nm thick cobalt layer, Figure 1. Cobalt nano-wires grown on the goffered CaF_2 surface show in-plane anisotropy with easy axis [110] lying along the goffers, Figure 2. Their coercive field is higher than that of Co grown directly on Si [3]. Remnant magnetisation (M_R/M_S) decreases considerably, when Co layer consists of isolated clusters. Combination of magnetic and transparent materials in one structure allows us to observe a variety of magneto-optical effects and control both magnetic and optical properties.

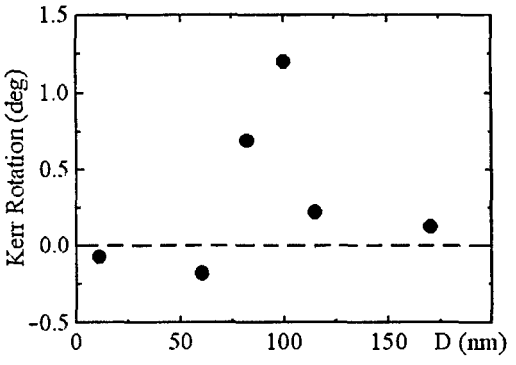

Figure 1. Kerr rotation at saturation in polar MOKE for 3 nm of Co on $CaF_2(111)$ layer of different thickness.

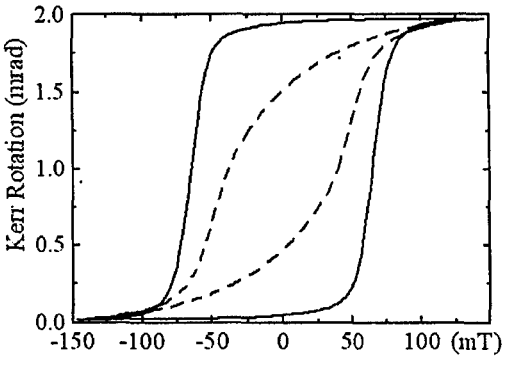

Figure 2. Longitudinal MOKE from Co nano-wires on $CaF_2(110)$; solid line - field along the wires dashed line - field across the wires.

References

[1] J.C.Alvarez, N.S.Sokolov and N.L.Yakovlev, Applied Surface Science **60/61**, 421 (1992).
[2] O. V. Anisimov, A. G. Banshchikov, S. V. Gastev, N. F. Kartenko, N. S. Sokolov, et al. in Proc. 11th International Symp. "Nanostructures: Physics and Technology" (St.Petersburg, Russia, 2003) p. 295.
[3] H.Xu, A.C.H.Huan, A.T.S.Wee, D.M.Tong, Sol.St.Comm. **126**, 659 (2003).

* Contact author: niko-y@imre.a-star.edu.sg

Room temperature ferromagnetism in the $In_{1-x}Cr_xN$ system: A magnetic and optical study

P. A. Anderson[a,*], R. J. Kinsey[a], C. E. Kendrick[a], L. Williams[b], R. J. Reeves[b], A. Asadov[c], W. Gao[c], V.J. Kennedy[d] and A. Markwitz[d] and S. M. Durbin[a]

[a] *Department of Electrical and Computer Engineering, MacDiarmid Institute for Advanced Materials and Nanotechnology, University of Canterbury, Christchurch, NEW ZEALAND*

[b] *Department of Physics and Astronomy, MacDiarmid Institute for Advanced Materials and Nanotechnology, University of Canterbury, Christchurch, NEW ZEALAND*

[c] *Department of Chemical and Materials Engineering, University of Auckland, Auckland, NEW ZEALAND*

[d] *Institute of Geological & Nuclear Sciences, Ltd., 69 Gracefield Rd. Lower Hutt, NEW ZEALAND*

Over the past 15 years the search for a diluted magnetic semiconductor (DMS) exhibiting room temperature ferromagnetism suitable for spintronic based applications has generated great interest. When Munekata *et al.* showed that Mn atoms imbedded in an InAs host order ferromagnetically at low temperatures [1] , the idea of combining conventional electronics with magnetic phenomena became a very attainable prospect. Using both the charge and spin of electrons to control current is not a new concept, but injecting spin polarised electrons from conventional metallic ferromagnets into a semiconductor has so far proven difficult and therefore hampered progress. The use of a semiconducting spin injection layer circumvents such problems.

Much has been achieved with the InMnAs and GaMnAs systems including magnetic field control over the polarisation of electroluminescence, and the switching of magnetic state through the action of a gate electrode. However, cryogenic Curie temperatures (T_c) remains a major limiting factor for these materials. In search of a DMS with above room temperature T_c, many groups have investigated various oxide and nitride thin films doped with a range of transition metals. There have been a number of studies identifying high Curie temperatures in those materials, although the origin of the magnetism remains the subject of debate. Clusters have been shown to cause high T_c in the InMnAs system, and detection of these nanoprecipitates is often beyond the sensitivity of common microstructural techniques, making it difficult to confirm the origin of observed magnetism. Cluster based ferromagnetism typically results in a localization of spin polarised electrons, hence making such materials unsuitable for spin injection layers.

In this study we report on the growth and characterization of $In_{1-x}Cr_xN$ layers with x varying from 0.005 to 0.04. It is found that for low values of x, low Curie temperatures are observed along with weak saturation moments. With $x > 0.01$ a sharp increase in the saturation moment is accompanied with Curie temperatures increasing to above room temperature. Inspection of XRD scans on the films reveals no evidence for clustering but this does not exclude nanoprecipitates. However, cluster based hysteresis is typically of the superparamagnetic type, and temperature dependent magnetisation measurements suggest this is not the case. The optical band structure of the $In_{1-x}Cr_xN$ system was explored via photoluminescence of the $In_{1-x}Cr_xN$ films along with photoluminescence and absorption studies of CrN and InN films. The addition of even low amounts of Cr to the InN matrix was found to quickly quench radiative recombination, consistent with an indirect gap for CrN. The quenched luminescence peak was found to move to higher energy, also suggesting a gamma valley gap > 0.7 eV for CrN.

References

[1] H. Munekata, H. Ohno, S. von Molnar, A. Segmuller, L. L. Chang and L. Esaki, Phys. Rev. Lett. **63**, 1846, (1989).

* *Contact email: paa24@student.canterbury.ac.nz*

Growth and Characterisation of Rare Earth Nitride thin Films

F. Budde[1,*], B. J. Ruck[1], H. Trodahl[1], S. Granville[1], A. Koo[1], H. J. Trodahl[1], A. Bittar[2]
[1] *School of Chemical and Physical Sciences, Victoria University of Wellington, Wellington, NEW ZEALAND*
[2] *Industrial Research Limited, Lower Hutt, NEW ZEALAND*

Rare earth nitrides (ReN) represent a class of materials for which theory predicts a wide range of electronic and magnetic properties. Several of them are promising candidates for spintronic applications due to their magnetic properties. Furthermore, some ReN have recently been predicted to be half-metals [1], i.e. to have a non-zero density of states at the Fermi level for one spin orientation only. This could be used for spin injecting electrodes.

On the experimental side, however, relatively little is known about the electrical and optical properties of ReN. It still remains unclear if ReN have metallic or semiconductor character. Although ReN thin films can easily be grown by thermal evaporation of the Re element in the presence of nitrogen, these films oxidise rapidly in the presence of moisture. Therefore, experimental characterisation requires the growth under clean conditions as well as protection of the films during characterisation.

In this work, various ReN films, with a thickness of ~200 nm, were grown by thermal or electron beam evaporation of the rare earth element with an evaporation rate of 1 Å/s in a high purity nitrogen atmosphere of 10^{-4} mbar. To achieve clean conditions the growth was performed inside an ultra-high vacuum system that was baked out and pumped down to a base pressure $<10^{-8}$ mbar before the growth.

Optical measurements of gadolinium nitride (GdN), neodymium nitride (NdN) and samarium nitride (SmN) films show that these materials have a broad but characteristic bandgap in the visible, similar to disordered semiconductors. On the other hand, published data for ReN [2] show a metal-like increase in resistivity with temperature, which is explained by unintentional doping due to impurities or intrinsic point defects. To exclude the effect of impurities electrical measurements performed under UHV conditions will be presented. Furthermore, the magnetic properties of various ReN films, measured by a SQUID magnetometer, will be discussed (Figure 1).

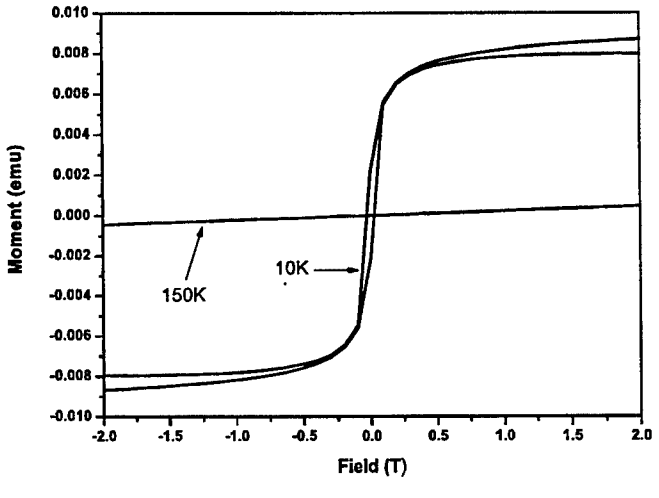

Figure 1: Magnetisation of a GdN film, grown by thermal evaporation of Gd in the presence of nitrogen, above and below the Curie temperature.

References

[1] C. M. Aerts *et al.*, Phys. Rev. B **69**, 045115 (2004).
[2] N. Sclar, J. Appl. Phys. **35**, 1534 (1964).

* Contact author: felix.budde@vuw.ac.nz

Properties of nanocrystalline GaN:Mn thin films

[1*]S. Granville, [1]F. Budde, [1]S. Flewett, [1]A. Koo, [1]B. Ruck, [1]H. J. Trodahl, [2]A. Bittar, [2]G.V. M. Williams, [3]V. J. Kennedy, [3]A. Markwitz, [4]J. Cairney

[1]*MacDiarmid Institute of Advanced Materials and Nanotechnology, Victoria Univ. of Wellington, NEW ZEALAND*

[2]*Industrial Research Limited, Lower Hutt, NEW ZEALAND*

[3]*Institue of Geological and Nuclear Sciences, Lower Hutt, NEW ZEALAND*

[4]*Electron Microscopy Unit, Univ. New South Wales, Sydney, AUSTRALIA*

The wide band-gap semiconductor GaN doped with the transition metal element Mn has been reported to exhibit ferromagnetic ordering with critical temperatures as low as 10K to as high as 940K[1]. The potential suitability of this material as a source for spin-polarised electrons, crucial for the development of spintronic devices, has provoked many groups to extensively investigate this material, focussing almost entirely on single crystal films. The wide range of reported ferromagnetic Curie temperatures in particular demonstrates the strong dependence of the magnetic behaviour of these films on the configuration and distribution of the Mn ions.

In this paper we report on structural, optical, DC resistivity and magnetic characterisation studies of *disordered* GaN films. The films were grown using ion-assisted deposition and incorporate between 4 and 13 at. % Mn. The GaN:Mn films are nanocrystalline with crystallites of ~3-5nm size. Mn is found to be incorporated substitutionally on the Ga lattice site with no evidence found for the formation of metallic precipitates or rogue phases from x-ray diffraction, x-ray absorption or transmission electron microscopy. Optical characterisation shows the films have an absorption edge onset comparable in energy to that of nanocrystalline GaN, but broadened due to the incorporation of Mn. The films have a semiconductor-like temperature dependence of DC resistivity below 300K, in agreement with a variable-range hopping model. Magnetic measurements show no ferromagnetic ordering transitions down to 2K, although spin-glass type magnetisation irreversibility is observed below ~250K. Preliminary annealing studies demonstrate a sharpening of the band-gap corresponding to the removal of gap states, and the potential to enhance both the short-range degree of structural order and magnetic coupling between the Mn ions.

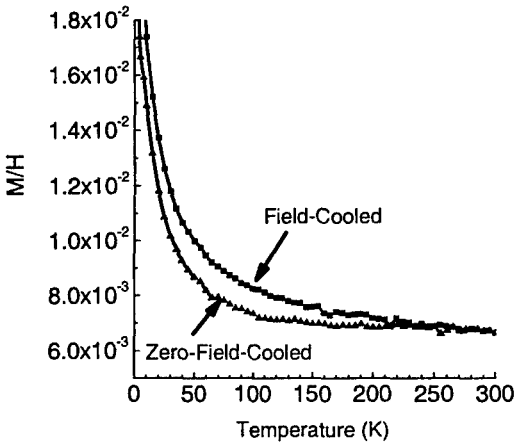

Fig. 1 Magnetisation measurements showing spin-glass type irreversibility below ~250K

References

[1] S. J. Pearton *et al.*, J. Phys.: Condens. Matter **16**, R209 (2004).

* Contact author: granvisimo@student.vuw.ac.nz

Hole-induced Ferromagnetism in Mn-doped ZnO Films Grown by Reactive Sputtering

Hyun Jung Kim[1], Jae Ho Sim[2], Hyojin Kim[2,*], Soon-Ku Hong[2], Dojin Kim[2], Young Eon Ihm[2] and Woong Kil Choo[1]

[1] *Department of Materials Science and Engineering, Korea Advanced Institute of Science and Technology, 373-1 Guseong-dong, Yuseong-gu, Daejeon 305-701, Korea*

[2] *Department of Materials Science and Engineering, Chungnam National University, Daeduk Science Town, Daejon 305-764, Korea*

Mn-doped ZnO (ZnMnO) is one of the most studied diluted magnetic semiconductors (DMSs) for spintronics applications, since the theoretical predictions of Dietl *et al.*[1] and Sato *et al.*[2] have suggested the possibility of room-temperature ferromagnetism in *p*-type ZnMnO. Hitherto, because of the difficulties in fabricating p-type ZnO, most experimental studies on possible magnetic states in ZnMnO have been carried out on *n*-type ZnMnO.

Here we report hole-induced ferromagnetism in $Zn_{1-x}Mn_xO$ (x = 0.01) film grown on SiO_2/Si substrates by reactive magnetron sputtering. The *p*-type conduction with hole concentration over 10^{18} cm^{-3} is achieved by phosphorus doping followed by rapid thermal annealing at 800 °C in a N_2 atmosphere. The magnetic measurements for *p*-type $Zn_{0.99}Mn_{0.01}O$:P clearly reveal ferromagnetic characteristics with a Curie temperature above room temperature, whereas data for *n*-type $Zn_{0.99}Mn_{0.01}O$ shows paramagnetic behavior (Fig. 1). This implies that the ferromagnetic ordering is induced by the holes in Mn-doped ZnO. Nonmetallic transport character and large positive magnetoresistance at low temperatures are observed for *p*-$Zn_{0.99}Mn_{0.01}O$:P. An anomalous Hall effect is also observed at room temperature for *p*-$Zn_{0.99}Mn_{0.01}O$:P, which indicates the presence of an exchange interaction between itinerant holes and localized Mn spins, implying that the charge carriers are possibly spin polarized. Our results manifest an intrinsic hole-induced ferromagnetism in *p*-$Zn_{0.99}Mn_{0.01}O$:P, which we may put to practical use for realization of spintronic devices operable at room temperature.

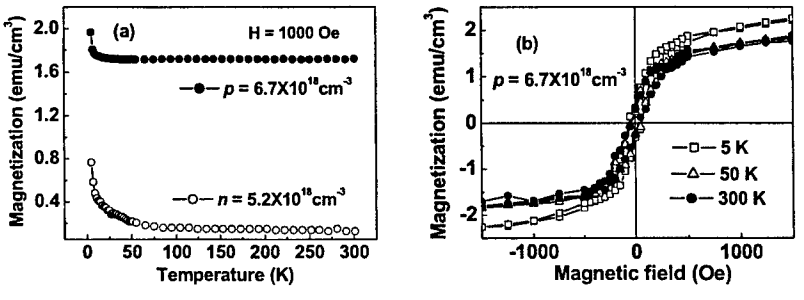

Figure 1. *Magnetic properties of n- and p-type $Zn_{0.99}Mn_{0.01}O$:P films: (a) Temperature dependence of the magnetization measured in a field of 0.1 T, (b) Magnetic field dependence of the magnetization measured at various temperatures.*

References

[1] T. Dietl, H. Ohno, F. Matsukura, J. Cibert, and D. Ferrand, Science **287**, 1019 (2000)

[2] K. Sato and H. Katayama-Yoshida, Jpn. J. Appl. Phys. **40**, 334 (2001)

* Contact author: hyojkim@cnu.ac.kr

SESSION Fr C3
CONDUCTING POLYMERS II

Friday 11 February 2005 **1530–1710**

Copthorne I

Session Chair **Jim Johnston, Victoria University of Wellington, NZ**

15.30 **Synthesis and applications of polyaniline nanofibers**
Fr C3.1 R.B. Kaner[1], J. Huang[1], S. Virji[1,2], C. Baker[1], D. Li[1] and B.H. Weiller[2]
(Invited Talk)
[1] *University of California, Los Angeles, USA*
[2] *Aerospace Corporation, Los Angeles, USA.*

15.55 **Synthesis and properties of organic, electronically conducting fibres : a platform for electronic textiles**
Fr C3.2 G.G. Wallace, V. Mottaghitalab, S.E. Moulton and G.M. Spinks.
University of Wollongong, Wollongong, Australia

16.10 **Polythiophene nanofibres**
Fr C3.3 D.L. Officer[1], A.M. Ballantyne[1], W.J. Belcher[1], S.B. Hall[1], and A.G. MacDiarmid[2]
[1] *Massey University, Palmerston North, NZ*
[2] *University of Pennsylvania, Philadelphia, USA*

16.25 **Nanofibrillar-, microfibrillar- and microplates-reinforced composites – new advanced materials from polymer blends for technical, commodity and medical applications**
Fr C3.4 S. Fakirov and D. Bhattacharyya
University of Auckland, Auckland, NZ

16.40 **Conducting polymer composites with cellulose and protein fibres**
Fr C3.5 J.H. Johnston, J. Moraes, T. Borrmann and F. Kelly
Victoria University of Wellington, Wellington, NZ

16.55 **Large contraction conducting polymer actuators**
Fr C3.6 P.A. Anquetil, H.-h. Yu, T.M. Swager and I.W. Hunter
Massachusetts Institute of Technology, Cambridge, USA

Synthesis and Applications of Polyaniline Nanofibers

Richard B. Kaner[1,*], Jiaxing Huang[1], Shabnam Virji[1,2], Christina Baker[1], Dan Li[1] and Bruce H. Weiller[2]
[1] *Department of Chemistry and Biochemistry and California NanoSystems Institute, University of California, Los Angeles, Los Angeles, CA 90095-1569, USA*
[2] *Materials Processing and Evaluation Department, Space Materials Laboratory, The Aerospace Corporation, P.O. Box 92957/M2-248, Los Angeles, CA, USA*

Conducting polymer nanostructures have attracted a great deal of research interest with the expectation that the combination of organic conducting materials and nanostructures could yield new functional materials or enable new physiochemical properties. By modifying conventional chemical oxidation polymerization processes, we have developed simple approaches to synthesize polyaniline nanofibers with diameters tunable from 30 to 120 nm (Figure 1A).[1,2] We have found that polyaniline nanofibers form naturally during the chemical oxidative polymerization of aniline in water without the need for any template, functional molecule or seed. In conventional polymerization, nanofibers are subject to secondary growth of amorphous particles which leads to irregularly shaped agglomerates. The key to producing pure nanofibers is to suppress secondary growth. This has been achieved with interfacial polymerization where the interface separates nanofiber formation from secondary growth.[1,2] We have also discovered that by rapidly mixing conventional reactions, pure nanofibers can be readily obtained since the initiator molecules are consumed before secondary growth begins.[3] These processes are template-free and readily scalable and can be applied to polyaniline derivatives and some other conjugated polymers.

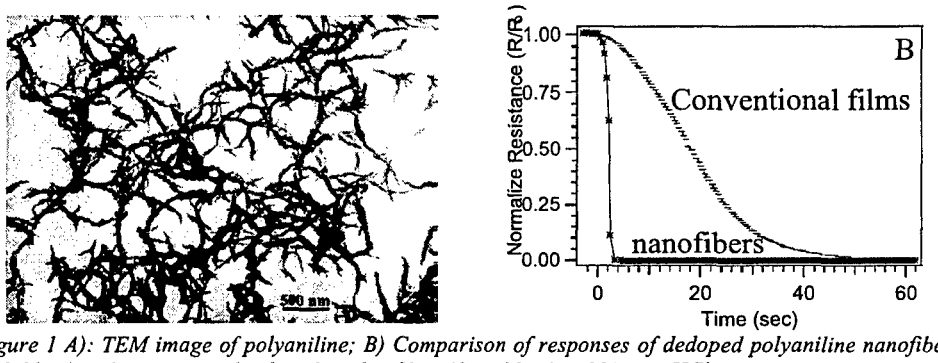

Figure 1 A): TEM image of polyaniline; B) Comparison of responses of dedoped polyaniline nanofiber (solid line) and conventional polyaniline thin films (dotted line) to 100 ppm HCl.

Compared to conventional polyaniline, polyaniline nanofibers exhibit higher surface area and better water dispersibility, which can dramatically enhance many applications such as in chemical sensors. The sensitivity of nanofiber-based sensors can be improved by several orders of magnitude while the response time is significantly shortened (Figure 1B).[4,5] Unlike conventional polyaniline films, nanofiber films show no thickness dependence to their response to vapors.

We have recently discovered that polyaniline nanofibers exhibit an exceptional photothermal effect.[6] The nanofibers can be instantaneously melted and cross-linked upon exposure to a camera flash. By taking advantage of this effect, a novel flash welding technique has been developed that can be used to make asymmetric polymer membranes, form patterned nanofiber films and create polymer based nanocomposites.

References

[1] Huang, J.; Virji, S.; Weiller, B. H.; Kaner, R. B. *J. Am. Chem. Soc.* **2003**, *125*, 314.
[2] Huang, J.; Kaner, R. B. *J. Am. Chem. Soc.* **2004**, *126*, 851.
[3] Huang, J.; Kaner R. B. *Angew. Chem. Inter. Edition* **2004**, in press.
[4] Virji, S.; Huang, J; Kaner R. B.; Weiller B. H. *Nano Lett.* **2004**, 4, 491.
[5] Huang, J.; Virji, S.; Weiller, B. H.; Kaner, R. B. *Chem.-Eur. J.* **2004**. 10, 1314.
[6] Huang, J.; Kaner, R. B. *Nature Mater.* **2004**, in press.

* Contact author: kaner@chem.ucla.edu

Synthesis and Properties of Organic, Electronically Conducting Fibres : A Platform for Electronic Textiles

Wallace, G.G., Mottaghitalab, V., Moulton, S.E., Spinks, G.M.

ARC Centre for Nanostructured Electromaterials,
Intelligent Polymer Research Institute, University of Wollongong,
Northfields Avenue, Wollongong, NSW 2522, Australia.

Putting function into fashion is the catch cry of researchers in the e-textiles area. The seamless integration of sensing and actuating technologies as well as fibre/textile structures capable of generating and storing the energy required to fuel such function is the ultimate goal. To achieve this new electronically conducting fibres are required. Such fibres should possess the mechanical properties required for use in textile structures and preferably be capable of sensing, actuating and/or generating/storing energy.

Fibres based on inherently conducting polymers and/or carbon nanotubes are proving extremely interesting in this regard. In this work we have investigated the use of wet-spinning techniques to produce such fibres. The mechanical and electronic properties of fibres produced to date will be discussed. Their use in applications such as wearable prosthetics and wearable energy storage will also be highlighted.

Polythiophene Nanofibres

D. L. Officer[1,*], A. M. Ballantyne, W. J. Belcher,[1] S. B. Hall,[1] and A. G. MacDiarmid[2]
[1] *Nanomaterials Research Centre and MacDiarmid Institute for Advanced Materials and Nanotechnology, Massey University, Palmerston North, NEW ZEALAND*
[2] *Department of Chemistry, University of Pennsylvania, Philadelphia PA 19104-6323, USA*

There is intense interest in the application of inherently conducting polymers (ICPs) to a wide variety of areas such as photovoltaics, light emitting diodes, actuators and chemical sensing.[1] The key challenge in utilizing ICPs is their ordered integration into devices through control of polymer structure or processing. The difficulties associated with this typically lead to inefficient devices. Thus, better control of polymer structure and morphology at the nanoscale could dramatic improve device performance.

There have been a number of approaches to the formation of ICP nanostructures.[2] Polymer nanoparticles can be formed using steric stabilizers or micellar polymerisation and physical templates used to form nanostructured polymer films. One of the simplest approaches is the use of electrostatic dispersion or electrospinning to produce ICP nanofibres, which have application as high surface area electrode materials for photovoltaics, or in nanoelectronics, actuators and sensor development. Although discovered in the 1930s, electrospinning has only recently been applied to the preparation and processing of conducting polymer nanofibres.[3] Thus polyaniline (PANI)/polyethylene oxide (PEO) nanofibres can be obtained from a PANI/PEO solution subjected to an electric field of 20kV. The method is, however, dependant on the availability of a soluble form of the polymer and the vast majority of conducting polymers are insoluble.

We have been investigating functionalised polythiophenes for a variety of applications such as photovoltaics and batteries. These applications require processable polymers and so we have developed soluble functionalised poly(terthiophenes) and have demonstrated that we can electrospin nanofibres of these soluble polymers. However, it would be greatly advantageous if nanofibres could be prepared from any ICP monomer, without the need to initially prepare soluble polymers. We present here a new modification of the electrospinning process, which allows for the formation of long submicron single fibres of even insoluble polymers such as polypyrrole and poly(ethylenedioxy)thiophene (PEDOT) from solutions of the monomers, containing an oxidant.

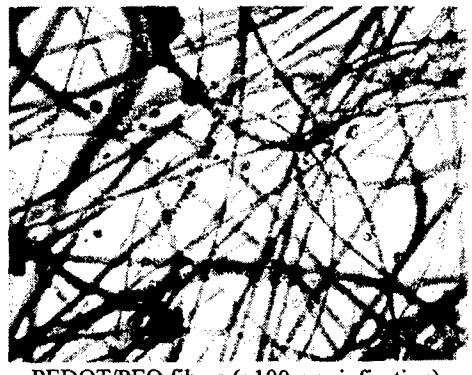

PEDOT/PEO fibers (x100 maginfication).

References

[1] G. G. Wallace, G. M. Spinks, L. A. P. Kane-Maguire, et al., *Conductive Electroactive Polymers: Intelligent Material Systems* (CRC Press, Boca Raton, 2003).
[2] G. G. Wallace and P. C. Innis, Journal of Nanoscience and Nanotechnology **2**, 441 (2002).
[3] A. G. MacDiarmid, W. E. Jones, I. D. Norris, et al., Synthetic Metals **119**, 27 (2001).

* Contact author: DOfficer@massey.ac.nz

Nanofibrillar-, Microfibrillar- and Microplates Reinforced Composites – New Advanced Materials from Polymer Blends for Technical, Commodity and Medical Applications

S. Fakirov[+] and D. Bhattacharyya
Centre for Advanced Composite Materials and Department of Mechanical Engineering, The University of Auckland, Private Bag 92019, Auckland, NEW ZEALAND

Microfibrillar reinforced composites (MFC) are prepared from polymer blends of thermodynamically *immiscible* partners having different melting temperatures, T_m The essential steps of MFC preparation are: (i) melt blending with extrusion, (ii) drawing with good orientation, and (iii) thermal treatment above T_m of the lower-melting component and below T_m of the higher-melting one. During the drawing microfibrils are created (*fibrillization step*); in the subsequent processing – melting of the lower-melting component occurs (*isotropisation step*), with preservation of the microfibrillar structure of the higher-melting component [1].

The mechanical properties of MFC are close to those of commercial short glass fibre-reinforced thermoplastics with the same matrix. When the starting blend comprises two condensation polymers, a *self-compatibilization effect* is also observed due to the interchange chemical reactions resulting in the formation of a copolymer at the phase boundaries. MFC involving polyolefins, such as polypropylene (PP) or polyethylene (PE) as matrices, and poly(ethylene terephthalate) (PET) as reinforcement, show the same morphological and structural characteristics as the better studied MFC types based on condensation polymers involving PET and polyamides. Their mechanical parameters (tensile strength and Young's modulus) are up to five times higher as compared to the neat PP and PE matrices. As compared to short glass fibre (GF)-reinforced composites (30 wt% GF), having the same matrices, the MFC have approximately the same Young's modulus and tensile strength as well as much better (up to 10 times) deformation ability [2]. The manufacturing and processing of MFC is successfully realized on commercial scale equipment. MFC have good application opportunities in the car production since they do not contain mineral reinforcement.

The MFC concept is further applied for manufacturing of microplates reinforced composites (MPC) *via* pressing of the non-drawn extrudate and subsequent processing for manufacturing of films or thin-walled containers. By selecting MPC partners with mutual complementing barrier properties (e.g. PET/PE or PET/PP) it is possible to improve the barrier properties of the conventional packaging materials.

Applying again the MFC approach, nanofibrils, characterised by extremely homogeneous diameters (around 100 nm), were recently obtained and isolated as a single material.

The isolation of nano- and microfibrils *via* selective dissolution of the matrix offers potentials for medical applications as scaffolds for the regenerative medicine or as carriers for controlled drug delivery.

References

[1]. S. Fakirov, M. Evsatiev, K. Friedrich, Nanostructured polymer composites from polyetster blends: structure - properties relationship, in: *Handbook of Thermoplastic Polyesters*, S. Fakirov (Ed.), Wiley-VCH, Weinheim 2002, p. 1093-1129.
[2]. M. Evstatiev, S. Fakirov, B. Krasteva, K. Friedrich, J. Covas and A. Cunha, Recycling of PET as Polymer-Polymer Composites, *Polym. Eng. Sci.* **42** (2002) 826.

[+]) *On leave from University of Sofia, Laboratory on Structure and Properties of Polymers, 1164 Sofia, BULGARIA.*

Conducting Polymer Composites with Cellulose and Protein Fibres

J. H. Johnston*, J. Moraes, T. Borrmann and F. Kelly
School of Chemical and Physical Sciences and the MacDiarmid Institute for Advanced Materials and Nanotechnology, Victoria University of Wellington, Wellington, NEW ZEALAND

The development of conducting polymer composites with cellulose and protein fibres with the polymer fully encapsulating the fibre provides hybrid materials that exhibit the inherent proprieties of both components. These include the electronic and chemical properties of the conducting polymer and the strength, flexibility and relatively high surface areas of the fibres. We have shown that it is possible to coat the cellulose fibres of a paper sheet with polypyrrole and polyaniline. The polymer coating comprises nanosize spheres that are fused together and fully encapsulate the fibres, yet retaining the open matrix of the paper sheet (figure 1). These composite materials possess conductivities of up to 6 S cm^{-1} for paper-polypyrrole composites and of up to $2x10^{-3}$ S cm^{-1} for paper-polypyrrole composites, as well as the redox properties of the conducting polymer [1].

A further suite of composite materials have been prepared where we have coated individual cellulose fibres of bleached *pinus radiata* kraft pulp with polypyrrole using ferric chloride and ammonium persulfate as oxidants. The fibres were dipped into pyrrole solution and then into the oxidant to effect polymerisation. Different concentrations of the pyrrole and oxidant were used. Excess polymer was removed by washing. Electronmicroscopy showed that the polypyrrole similarly comprises nanosize spheres that are fused together and fully encapsulate the individual cellulose fibres. The polymer coating is not removed from the fibre by sonication or acid leaching. This, together with the observed morphology, confirms the integral nature and completeness of the polypyrrole coating which appears to be chemically bound to the hydroxyl groups on the cellulose surface. The masking of the hydroxyl groups by the polymer coating therefore precludes hydrogen bonding between fibres which results in a composite material comprising fully separate and dispersed conducting polymer – cellulose fibres. The fibres are typically 1-2mm long and about 30microns in diameter. Similar composite materials have been prepared by coating wool (protein) fibres with polypyrrole wherein the polymer was observed to similarly fully encapsulate the wool fibre. The wool fibres are much longer than the cellulose fibres, but also remain fully separate. The conductivities, cyclic voltammetry and chemical redox properties of the polypyrrole-cellulose and polypyrrole-wool fibres have been measured, and are comparable.

As these composite fibres are fully separate they can be readily incorporated and dispersed into other common matrices such as plastics and surface coatings to impart strength as well as chemical and electronic functionality to them. In addition, the polypyrrole-wool fibres can be woven into a fabric matrix with such electronic and chemical properties. They therefore provide the basis for the development of new hybrid materials that possess interesting chemical and physical properties.

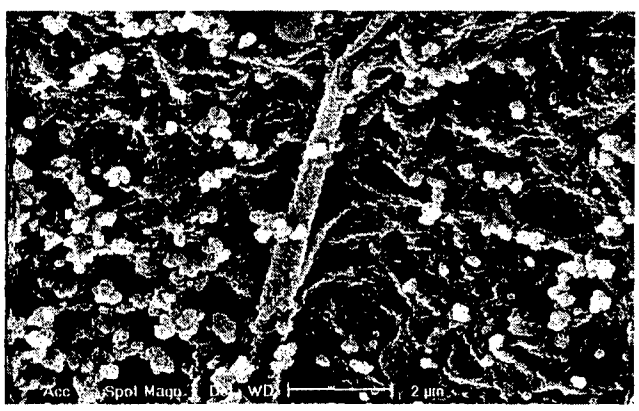

Fig. 1 – Electronmicroscope image of paper coated with polypyrrole using ferric chloride as the oxidant.

References

1. J. H. Johnston, J. Morase, and T. Borrmann. Proceedings of the International Conference on Synthetic Metals, Wollongong, Australia, 2004.

* Contact author: jim.johnston@vuw.ac.nz

Large Contraction Conducting Polymer Actuators

P. A. Anquetil[1,*] H.-h. Yu[2], T. M. Swager[2] and I. W. Hunter[1]
[1] *BioInstrumentation Laboratory, Department of Mechanical Engineering, Massachusetts Institute of Technology, Cambridge, MA 02139, USA*
[2] *Department of Chemistry, Massachusetts Institute of Technology, Cambridge, MA 02139, USA*

Human skeletal muscle exhibits combined performance characteristics of active strain (20 %), active stress (0.35 MPa), active strain rate (100 %/s), power to mass ratio (50 – 100 W/kg) and efficiency (30 – 35 %) which man-made actuator technologies do not match [1]. A lightweight, flexible, muscle-like actuator is highly desirable for applications in life-like robotics, prosthetics, medical devices, propulsion systems or microelectromechanical systems (MEMS). Conducting polymers such as polypyrrole have emerged as a possible artificial muscle technology. These active materials exhibit biomimetic motion characteristics (smooth and silent movement), high active stresses (40 MPa peak), a high power to mass ratio (150 W/kg), and cycle life exceeding the million cycles while being activated at low electrical voltages (~1 – 5 V). However, both the active strain and the speed that current conducting polymers can generate is limited (~ 2 – 7 % at 10 MPa; 3 %/s speed at 0.3 % strain contraction) [2].

This paper presents two strategies to improve the active strain capabilities of conducting polymers. First, the top down approach consists of optimizing current conducting polymer actuators based on polypyrrole via post-synthesis processing and careful choice of the electrolyte environment necessary to activate them electrochemically. Our recent progress shows that polypyrrole actuators activated in room temperature ionic liquids generate large contractions (16.3 % recoverable strain at 2.5 MPa, 24 % max) at slow speeds (0.4 %/s) while showing outstanding electrochemical stability. Benefits and trade offs of utilizing room temperature ionic liquid electrolytes for higher performance in polypyrrole actuation are discussed.

The second, bottom-up strategy, consists of designing the artificial muscle material from the molecular level up. Making use of recent advances in organic chemistry, conducting polymer backbones are designed with shape-changing molecular building blocks that mimic natural mechanisms [3]. These include molecules that distort from bent to planar structures, materials that undergo volume changes due to stacking of red-ox units and molecular scaffolds that behave as "mechanical hinges" enabling to switch the molecule from an extended to a tightly folded molecular conformation (Figure 1). Synthesis (polymerization) and active mechanical properties of these novel contractile materials are presented.

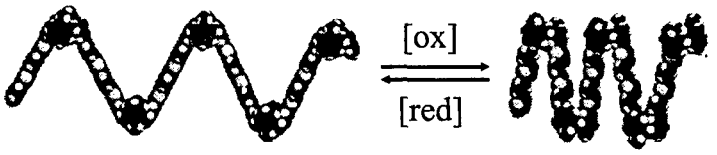

Figure 1: Actuation mechanism of one molecular actuator candidate: poly(Calix[4]arene bis-bithiophene). Both the expanded (left) and contracted (right) states are shown. Switching occurs via electrochemical oxidation or reduction.

References

[1] I. W. Hunter and S. Lafontaine, in *Technical Digest IEEE Solid State Sensors and Actuators Workshop*, 1992, p. 178.
[2] J. D. Madden, P. G. Madden and I. W. Hunter, in *Smart Structures and Materials 2002: Electroactive Polymers Actuators and Devices, edited by Y. Bar-Cohen,*(Proceedings of the SPIE, 2002), Vol. 4695, p. 176.
[3] H. –h. Yu, B. Xu and T. M. Swager, *J. Am. Chem. Soc.*, **125**, 1142, (2002).

* Contact author: patanq@mit.edu

SESSION Fr E3
CLUSTERS AND NANOPARTICLES II

Friday 11 February 2005 **1530–1710**

Copthorne III

Session Chair **Ed Samulski, University of North Carolina, USA**

15.30 **Self-organized surface nanostructures**
Fr E3.1 A.T.S. Wee
(Extended Oral Talk)
National University of Singapore, Singapore

15.55 **Controlled growth, scanning tunneling microscopy and high-resolution spectroscopy for the study of clusters on surfaces**
Fr E3.2 H. Hoevel
University of Dortmund, Dortmund, Germany

16.10 **Iodine doping to self-organized gold nano-particles**
Fr E3.3 S. Saito[1,2], T. Arai[1,2], H. Fukuda[1,2], S. Kimura[2] and T. Onai[1,2]
[1] *Hitachi Ltd, Tokyo, Japan*
[2] *CREST, JST, Japan*

16.25 **Chemically controlled 2D-artificial-lattice composed of metal-nano-particles**
Fr E3.4 T. Arai[1,2], S. Saito[1,2], H. Fukuda[1,2], T. Onai[1,2]
[1] *Central Research Laboratory, Hitachi Ltd, Tokyo, Japan*
[2] *CREST, JST, Japan*

16.40 **A new ultrasonic cavitation approach for the synthesis of zinc ferrite nanocrystals**
Fr E3.5 M. Sivakumar, K. Yasui, A. Towata, T. Tuziuti and Y. Lida
National Institute of Advanced Industrial Science and Technology (AIST), Nagoya, Japan

Self-Organized Surface Nanostructures

A. T. S. Wee
Department of Physics, National University of Singapore,2 Science Drive 3, S117542, SINGAPORE

The spontaneous surface nanostructure formation on several adsorbate-substrate systems, without the use of lithographic techniques, is presented. We have studied the formation of 1D and 2D nanostructures on Cu(210) using STM (scanning tunneling microscopy) [1] and LEED (low energy electron diffraction) [2]. Two-dimensional mesoscopic triangular checkerboard patterns were also observed after the etching of Cu(210) by Br [3]. The multilayer relaxation of Cu(210) has been studied by layer-doubling LEED analysis and pseudopotential density functional theory (DFT) calculations [4]. Multilayer relaxations of such high index fcc transition metal surfaces have also been studied by pseudopotential DFT calculations [5]. A general rule for the multilayer relaxation sequence of open high index metal surfaces is proposed [6].

For the SiC(0001) surface, we have also observed the formation of metastable (6x6)-Si nanoclusters (diameter ~16.5±0.1A) on 6H-SiC(0001)-(3x3) [7],[8]. The occurrence of these regularly-sized "magic" clusters demonstrates the potential of nanostructure formation of Si on SiC. Monodispersed Co nanoclusters of 3 to 5 nm sizes have been grown on the reconstructed 6H-SiC(0001) surface by electron beam evaporation on the C-terminated $6\sqrt{3}x6\sqrt{3}R30°$ template (Fig. 1) at room temperature [9]. *In-situ* STM shows that the average cluster size remains constant for different Co coverage, and the cluster density is linearly dependent on the coverage. The monodispersion of the cluster size is suggested to be due to the physical confinement of the Co clusters by the porous honeycomb structure of the SiC reconstructed surface.

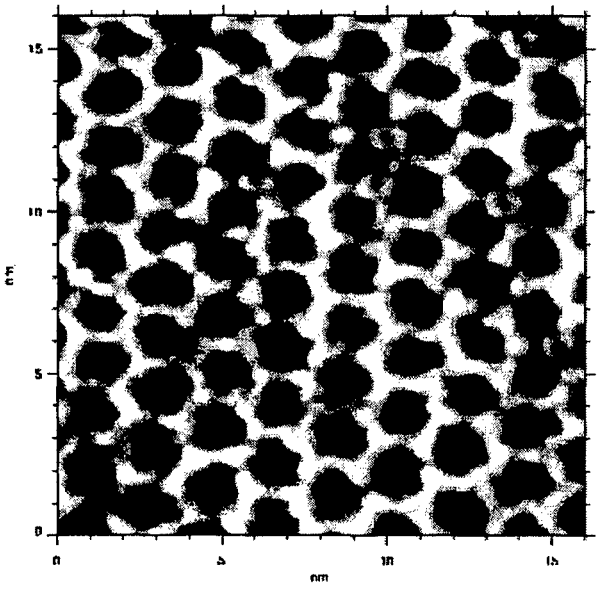

Figure 1: The 6H-SiC(0001)-(6x6) surface reconstruction imaged by STM.

References

[1] A. T. S. Wee, J. S. Foord, R. G. Egdell, J. B. Pethica, *Phys. Rev. B* **58**, R7548 (1998).
[2] Y. P. Guo, K. C. Tan, H.Q. Wang, C. H. A. Huan, A. T. S. Wee, *Phys. Rev. B* **66**, 165410 (2002).
[3] A. T. S. Wee, T. W. Fishlock, R. A. Dixon, J. S. Foord, R. G.Egdell, J. B. Pethica, *Chem. Phys. Lett.* **298**, 146 (1998).
[4] Y. Y. Sun, H. Xu, J. C. Zheng, J. Y. Zhou, Y. P. Feng, A. C. H. Huan, A. T. S. Wee, *Phys. Rev. B* **68**, 115420 (2003).
[5] Y. Y. Sun, H. Xu, Y.P. Feng, A. C. H. Huan, A. T. S. Wee, *Surf. Sci.* **548**, 309 (2004).
[6] Y. Y. Sun, H. Xu, Y.P. Feng, A. C. H. Huan, A. T. S. Wee, *Phys. Rev. Lett.*, in press.
[7] W. J. Ong, E. S. Tok, H. Xu, A. T. S. Wee, *Appl. Phys. Lett.* **80**, 3406 (2002).
[8] E. S. Tok, W. J. Ong, A. T. S. Wee, *Surf. Sci.* **558**, 145 (2004).
[9] W. Chen, K. P. Loh, H. Xu, A. T. S. Wee, *Appl. Phys. Lett.* **84**, 281 (2004).

Controlled Growth, Scanning Tunneling Microscopy and High-Resolution Spectroscopy for the Study of Clusters on Surfaces

Heinz Hövel[1,*]
[1] *Experimentelle Physik I, University of Dortmund, 44221 Dortmund, GERMANY*

Spectroscopy of the electronic properties of clusters on surfaces is still 'work in progress': although quite an amount of data has already been collected, the understanding of the observed effects is much more preliminary than in the case of free clusters. Partly this is due to the increase in complexity which follows from the cluster-surface interaction disturbing the symmetry and isotropic surroundings of the free clusters in vacuum. But there are also experimental reasons. Experiments for the controlled deposition of mass selected clusters without any fragmentation or coalescence are not yet a standard experiment. Even if one is able to deposit mass selected clusters on a surface, small clusters may have different isomers and orientations on the surface, and averaged spectra may not show the full information included in the electronic structure of the single clusters. An alternative approach is the study of individual clusters using scanning probe techniques, in particular scanning tunneling microscopy and spectroscopy.

We followed this route using metal clusters grown on graphite surfaces at preformed nanometer sized pits acting as well defined nucleation centers. Scanning tunneling microscopy was used to characterize the size-dependent cluster morphology [1]. This is an important prerequisite for understanding the electronic cluster-properties, which could be measured for individual clusters using low-temperature scanning tunneling spectroscopy. Since for scanning tunneling spectra of clusters the interpretation is complicated and still a topic of current research, we used ultraviolet photoelectron spectroscopy as a complementary method. It gives information on the occupied electronic states and the cluster-surface interaction. In addition it helps us to study the cluster growth process [2].

For the case of gold clusters on graphite we have investigated a broad range of cluster sizes, from a few ten up to more than 10^4 atoms per cluster. The tunneling spectroscopy data for the large clusters is dominated by a confined Shockley surface state, which can be described quantitatively considering the confinement to the hexagonal (111) facets on top of the clusters [3]. For the small clusters without facets scanning tunneling spectroscopy results of a large number of clusters show remarkably systematic features changing with the cluster size, but here the interpretation is still difficult. It might require not only a detailed analysis of the electron confinement in three dimensions but also an inclusion of special transport phenomena in the tip-cluster-surface system.

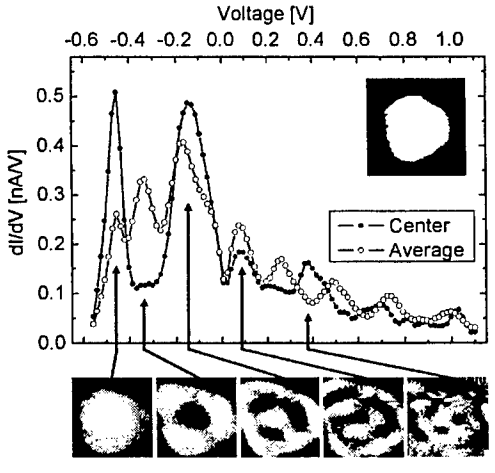

Scanning tunneling spectroscopy measured on the (111) top facet of a gold cluster (facet area 37 nm^2, height of the cluster 3.9 nm, about 1.5x10^4 gold atoms in the cluster).

Top: dI/dV spectra measured in the center of the facet (full dots) and averaged over the total facet area (open dots), respectively. The facet shape is shown in the inset (10x10 nm^2).

Bottom: dI/dV maps (4.5x4.5 nm^2) for 5 different voltages marked with the arrows in the top graph. STS measured at T=5 K with open feedback-loop; setpoint: 1.1 V, 0.1 nA; modulation: 12 mV$_{rms}$.

References

[1] T. Irawan, I. Barke, H. Hövel, Appl. Phys. A, accepted for publication.
[2] H. Hövel, Appl. Phys. A **72**, 295 (2001).
[3] I. Barke, H. Hövel, Phys. Rev. Lett. **90**, 166801 (2003).

* Contact author: hoevel@physik.uni-dortmund.de

Iodine Doping to Self-Organized Gold Nano-Particles

S. Saito[1,2*], T. Arai[1,2], H. Fukuda[1,2], S. Kimura[1], and T. Onai[1,2]
Central Research Laboratory, Hitachi Ltd., Kokubunji, Tokyo 185-8601, Japan
CREST, JST (Japan Science and Technology)

In strongly correlated electron systems, the carrier doping leads to exotic behaviours like the metal-insulator transition, (anti-)ferromagnetism, high temperature superconductivity, colossal magneto-resistance, and so on [1]. Such phenomena are also expected for the *artificial lattice* composed of quantum dots [2]. In order to control the electrical properties of the artificial lattice, it is important to establish the carrier doping method. It is well known that the chemical doping is a powerful method for the conducting polymer [3]. In this work, we examined the impacts of I_2 doping to the artificial lattice of self-organized Au nano-particles on the electronic properties.

We chemically synthesized Au nano-particles covered with butane thiolate ligands [2]. The average diameter of Au core was approximately 3 nm. The charging energy of this nano-particle is estimated to be 0.3 eV, which is much higher than the thermal energy. We prepared the Si substrate with 200 nm thick SiO_2, and the Au electrodes were formed by the lithography and lift off. The length between adjacent electrodes was L=20 μm, and the width was W=200 μm. Then, the monolayer film of the 2-dimentional arrays of these nano-particles was formed by the Langmuir-Blodgett method. We avoided structural defects inside the film, which was necessary to achieve the Ohmic conduction [2]. After that, the sample was exposed to the I_2 gas for the specified time.

The current-voltage (*I-V*) characteristics at room temperature are shown in Fig. 1. Initially, the current increases significantly as increasing the I_2 exposure time. Then, the current decreases for the 10 sec doping, and the current increases again. All these data show the clear Ohmic conduction, which means that the structure of the artificial lattice does not severely affected by the randomness. But, after the doping above 30 sec, the current completely did not flow (less than pA), since the artificial lattice was destroyed by the aggregation of nano-particles. We confirmed this by the Transmission-Electron-Microscope images, and the nano-particles grow up to the size of approximately 100 nm for sample doped for 5 min.

It is difficult to understand the above behaviors simply from the destruction of nano-particles. Instead, the behaviors can be interpreted as the carrier doping to the strongly correlated electron systems made by the artificial lattice. Without the carrier doping, the artificial lattice is considered to be the band insulator, which is confirmed by the increase in the resistivity with decreasing the temperature. The initial decrease in the resistivity upon the doping is simply considered to be the carrier doping to this band insulator. Due to the strong Coulomb repulsion, the resistivity should take a local minimum around the quarter filling, which corresponds to the 5 sec doping. The doping above the quarter filling increases the resistivity, and the Mott insulating state is expected at the half filling (one carrier for each dot) for the 10 sec doping. The doping to the Mott insulator reduces the resistivity again, corresponding to the approximate particle-hole symmetry. Therefore, our results suggest the I_2 doping leads to the metal-insulator transition.

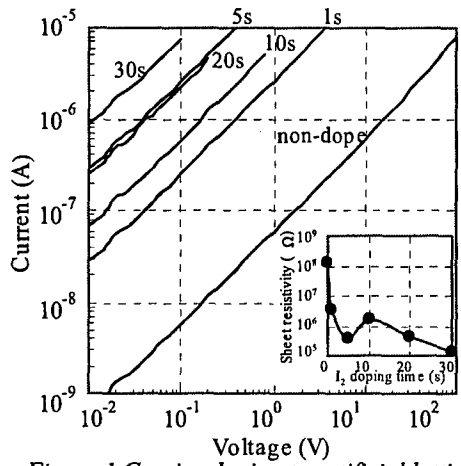

Figure 1 Carrier doping to artificial lattice of nano-particles by the I_2 gas.
Inset: The local maximum of resistivity corresponds to the Mott insulator.

In summary, we fabricated the artificial lattice of self-organized Au nano-particles, and examined the I_2 doping. The measured *I-V* characteristics are consistent with the interpretation that the carriers are successfully doped to the artificial lattice and this system becomes a strongly correlated electron system made by the nano-particles.

References

[1] M. Imada, A. Fujimori, and Y. Tokura, Rev. Mod. Phys. **70**, 1039 (1998).
[2] S. Saito, *et al.*, *Proceedings of Solid State Devices and Materials (SSDM)* (2004).
[3] A. J. Hegger, Rev. Mod. Phys. **73**, 681 (2001); A. G. MacDiarmid, *ibid.*, 701; H. Shirakawa, *ibid.*, 713.

* Contact author: ssaito@crl.hitachi.co.jp

Chemically Controlled 2D-Artificial-Lattice Composed of Metal-Nano-Particles

T. Arai[1,2,*], S. Saito[1,2], H. Fukuda[1,2], and T. Onai[1,2]
[1]*Hitachi, Ltd., Central Research Laboratory, Kokubunji, Tokyo, 185-8601, Japan*
[2]*CREST, Japan Science and Technology*

Nanometer-size metal particles protected by a monolayer of organic compounds such as thiolates have attracted much attention in various fields [1]. Especially, when the size of the nano-particles is smaller than 5-nm, assembled-monolayer films of such particles is regarded as a super-lattice system in which the single electron charging effects can be expected. By changing the lattice-constant of the systems, we can control the transfer of the Hubbard model. This paper discusses the effect of this lattice-constant change from the chemical-approach. The synthesis of the ultra-small nano-particles using thiolate ligands with various chain lengths and electrical characteristics of their monolayer films are shown.

We synthesized Au-nano-particles using the two-phase method (the Brust method) [3]. Pt-nano-particles were synthesized using a one-phase synthesis method developed by Yee et al. [4]. The surfaces of these particles were covered with the alkanethiolate-ligands. The various ligands were prepared such as C4 (butane thiolate), Bz (benzene thiolate), and C12 (dodecane thiolates). The monolayer films of the nano-particles were formed by several methods, such as a droplet method and the Langmuire-Blodgett (LB) method. The uniform films of assembled-monolayer were successfully obtained over a wide area using LB method. Figure 1 shows a typical TEM image for the assembled-monolayer of the synthesized Au-nano-particles capped by C12 ligands, whose diameter is about 3-nm.

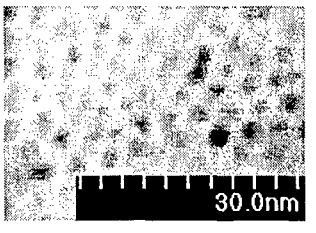

Fig.1 TEM image of Au-C12

The conductance of the assembled-monolayer film was measured for Pt- and Au-nano-particles with various ligands. These monolayer films show the linear I-V characteristics. To achieve this linear behaviour, we believe that it is necessary to reduce structural defects inside the LB film, as suggested by non-linear behaviours in films with defects [5]. The conductance of the films drastically changes with the carbon-chain-length of the alkanethiolate ligands, which reflects distance between nano-particles in the film (Table 1). On the other hand, dependence of the conductance on the metal-core material is small (Table 1). This suggests that the electron transport is limited by electron tunnelling between nano-particles.

Table 1 Sheet Resistances of the monolayer of the nanoparticles

Particles	Au-C12	Au-Bz	Au-C4	Pt-C4
Sheet Resistance (Ω)	$9.8\ 10^{11}$	2.6×10^{9}	4.1×10^{7}	$6.06\ 10^{7}$

In summary, we controlled the conductance of the nano-particle monolayer films over, at least, 4 orders of magnitude by chemical-approach. The conductance mainly depended on the distance between the metal cores (lattice-constant of the system), and hardly depended on the metal core-materials.

References

[1] (a) C. M. Lieber, Solid State Commun., 107 (1998) 607. (b) Y. Wu, and P. Yang, J. Am. Chem. Soc., 123 (2001) 3165. (c) K. Hamond-Schifferli, J. J. Schwrtz, T. A. Santos, S. Zhang, and M. J. Jacobson, Nature 415 (2000) 152. (d) C. P. Collier, R. J. Saykally, J. J. Shiang, S. E. Henrichs, and J. R. Heath, Science, 277 (1997) 1978.
[2] M. Imada, A. Fujimori, and Y. Tokura, Rev. Mod. Phys. 70 (1998) 1039.
[3] M. Brust, M. Walker, D. Bethel, D. J. Schiffrin, and R. J. Whyman, J. Chem. Commun., (1984) 801.
[4] C. Yee, R. Jordan, A. Ulman, H. White, A. King, M. Rafailovich, and J. Sokolov, Langmuir 15 (1999) 3486.
[5] S. Saito, T. Arai, H. Fukuda, D. Hisamoto, R. Tsuchiya, S. Kimura, and T. Onai, Solid State Devices and Materials (2004), to be published.

* Contact author: t-arai@crl.hitachi.co.jp

A New Ultrasonic Cavitation approach for the Synthesis of zinc ferrite Nanocrystals

Manickam Sivakumar,* Kyuichi Yasui, Atsuya Towata, Toru Tuziuti and Yasuo Iida
Advanced Manufacturing Research Institute (AMRI), National Institute of Advanced Industrial Science and Technology (AIST), 2266-98 Anagahora, Shimoshidami, Moriyama-ku, Nagoya 463-8560, Japan.

Much effort is currently being devoted to the study of magnetic ferrites in nanometer scale mainly due to their applications in magnetic data storage, ferrofluids, medical imaging, drug targeting and catalysis. Particularly, zinc ferrite nanoparticles have generated a large research effort because of their magnetic properties which differ markedly from those of their counterpart. Many different approaches have been applied to the fabrication of this nanomagnetic ferrite entity, such as co-precipitation, microemulsion, supercritical sol-gel processing, hydrothermal synthesis, or high energy ball milling. Directed to the problems of these conventional methods, new synthetic methods have received increased attention in recent years.

Ultrasonic cavitation chemistry, an approach for synthesizing a variety of compounds at milder conditions is already the rage in materials technology. Over the last few years, the technique has also started to catch on in the materials science community as a way to speed the discovery of everything in this area. The major advantage of this new method is that it affords a reliable and facile route for the control of both the synthetic process and nanostructure in advanced materials. Also, this process provides chemical homogeneity and reactivity through atomic level mixing within the precursor system, and phase pure crystalline materials can be prepared by annealing at reduced temperatures [1].

In this work, we present for the first time fabrication of zinc ferrite nanocrystals (3-5 nm) using ultrasonic cavitation. Our present synthesis approach is based on sonochemically dispersing an aqueous solution of Zn^{+2} and Fe^{+2} cations into rapeseed oil to form well dispersed W/O emulsion droplets, without using a surfactant. Again, by ultrasound mediated hydrolysis, zinc acetate as well as iron acetate present in the aqueous droplets is then directly converted to their oxides without using any precipitant and without subjecting it to any vigorous calcination conditions. Finally, the ultrasonic cavitation events occurring during sonication provide high temperature conditions or in-situ calcination environment, which facile the reaction of sonochemically generated precursors or the oxides in the formation of zinc ferrite nanocrystals. The method, we report, herewith has the advantage of avoiding the cumbersome conditions that exists in the conventional methods; usage of necessary additive components (stabilizers or surfactants, precipitants) and calcination requirements. In addition, rapeseed oil as an oil phase has been used for the first time, replacing the toxic and troublesome organic nonpolar solvents.

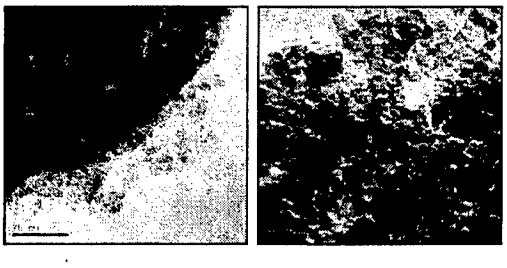

Figure 1 *Transmission electron micrographs of as-prepared zinc ferrite nanocrystals*

The surprising ability of achieving the formation of nanosized zinc ferrite utilizing the present ultrasonic cavitation approach by avoiding the usage of all of the additives and necessary conditions not only provide a simple route but also open a new avenue for the synthesis of various advanced ferrites. Further studies show that the synthesis is not limited to simple ferrite nanoparticles but can be extended to mixed ferrite nanoparticles as well and research is underway to develop a variety of nanoferrite materials.

References

1. K.S. Susklick, Ultrasound: in *Applications to Materials chemistry. In Encyclopedia of Materials science and Engineering*; edited by R.W. Cahn (Pergamon press, Oxford, 1993), 3rd Suppl., pp 2093-2098

* Contact author: manickam-sivakumar@aist.go.jp

All Authors Index